IDENTIFICATION AND CORRELATION OF THE F-4E STALL/POST-STALL AERODYNAMIC STABILITY AND CONTROL CHARACTERISTICS FROM EXISTING TEST DATA

Bernard J. Eulrich
Norman C. Weingarten

FOREWORD

This report was prepared by Calspan Corporation (formerly Cornell Aeronautical Laboratory, Inc.) Buffalo, New York, for the Air Force Flight Dynamics Laboratory, Wright-Patterson Air Force Base, Ohio. The work was performed under Contract No. F33615-72-C-1248, Project No. 8219, "Correlation of High-Angle-of-Attack Data for Various Testing Techniques for Fighter Type Aircraft", Task No. 821902. The Air Force Project Engineer was initially Mr. F. Thomas and later Mr. R. Quaglieri (AFFDL/FGC). Mr. B.J. Eulrich was the principal investigator for Calspan. McDonnell Aircraft Company (MCAIR), under subcontract number CAL S-73-1, performed reduction of raw flight test data from Flight Number 165 in the stall/near stall investigation of the F-4E aircraft. This report covers research performed from March 1972 to June 1973.

The authors wish to express their appreciation to many members of the Flight Research Department of Calspan. In particular, Messrs. C. L. Mesiah, C. M. Poppenberg and M. M. Moore who performed the necessary computer programming for this study; Mr. D. Andrisani who was responsible for the thrust calculations; and Mr. J. V. Lebacqz for his contributions to Appendix V and the recommendation subsection of this report.

Acknowledgement is also due to Mrs. J. Martino for her assistance in the preparation of this report and to Mr. E. G. Rynaski for his many valuable suggestions and discussions during the course of this work.

This report was submitted by the authors in August 1973, and is being published as Calspan Report No. BM-3054-F-1.

This technical report has been reviewed and is approved.

C. B. WESTBROOK
Chief, Control Criteria Branch
Air Force Flight Dynamics Laboratory

ABSTRACT

This report documents the results of a study performed for the United States Air Force Flight Dynamics Laboratory to identify the high-angle-of-attack post stall aerodynamic stability and control characteristics of the F-4 aircraft from existing full scale and radio-controlled drop model test data and to correlate these results with similar characteristics obtained from wind tunnel tests. A parameter identification procedure was set up to extract these nonlinear characteristics from flight test records using a nonlinear iterated Kalman filter/fixed-point smoother algorithm and a least square equation error method. Model form is established from wind tunnel data by representing the aerodynamic coefficients by Taylor's series expansions for selected ranges of angle of attack. Although the best flight test data available at high angles of attack were used, aircraft excitation and record length of the flight data were insufficient to enable the extraction of completely accurate and consistent coefficients from the data. Where there were adequate data and consistent instrumentation, the results were good. The results of this study demonstrated feasibility and applicability of the identification approach and techniques utilized, to obtain meaningful results at high angles of attack. Recommendations for future flight test programs are included in this report. Recommendations for the improvements of the identification procedures for the high-angle-of-attack flight regime are also included.

TABLE OF CONTENTS

TABLE OF CONTENTS (CONT.)

LIST OF ILLUSTRATIONS

LIST OF ILLUSTRATIONS (CONT.)

LIST OF ILLUSTRATIONS (CONT.)

LIST OF ILLUSTRATIONS (CONT.)

LIST OF TABLES

LIST OF TABLES (CONT.)

LIST OF SYMBOLS

b	wing span, ft
$\bar{c}$	mean aerodynamic chord of wing, ft
$E\{\ \}$	expectation operator
F_x	longitudinal force acting along x body axis, lb
F_y	lateral force acting along y body axis, lb
F_z	normal force acting along z body axis, lb
$f(\ )$	nonlinear dynamic system function
g	gravitational constant, 32.2 ft/sec^2
h	altitude, ft
h_{e_x}	angular momentum of engines along x body axis, slug-ft^2/sec
$h(\ )$	nonlinear measurement system function
I_x, I_y, I_z	moments of inertia about x, y, and z body axes respectively, slug-ft^2
I_{xy}, I_{xz}, I_{yz}	products of inertia in body axes, slug-ft^2
ℓ_x	distance along aircraft x axis from c.g.
ℓ_y	distance along aircraft y axis from c.g.
ℓ_z	distance along aircraft z axis from c.g.
m	mass of airplane, slug
M	Mach number
M_x	rolling moment acting about x body axis, ft-lb
M_y	pitching moment acting about y body axis, ft-lb
M_z	yawing moment acting about z body axis, ft-lb
n_x, n_y, n_z	linear accelerations in body axes, g's
p, q, r	angular velocities about x, y, and z body axes respectively, deg/sec
P_o	initial estimate of error covariance matrix

P_f	final error covariance matrix
p	vector of parameters to be identified
Q	process noise covariance matrix
$\bar{q}$	$\frac{1}{2}\rho V^2$, dynamic pressure, lb/ft^2
R	measurement error covariance matrix
S	wing area, ft^2
T_L, T_R	left and right engine thrust, lb
u, v, w	linear velocities along x, y, and z body axes respectively, ft/sec
u	vector of control inputs
V	free-stream velocity, ft/sec
v	vector of measurement noise
$w(t)$	vector of process noise
x, y, z	body axes
x	vector of aircraft states
y	vector of aircraft measurements
α	angle of attack, deg
β	angle of sideslip, deg
δ_{a_L}	left aileron deflection, positive when trailing edge down, deg ($-2^o \leq \delta_{a_L} \leq 30^o$)
δ_{a_R}	right aileron deflection, positive when trailing edge up, deg ($-30^o \leq \delta_{a_R} \leq 2^o$)
δ_a	$\delta_{a_L} + \delta_{a_R}$, effective roll controller, positive right wing down, deg
δ_e or δ_s	horizontal tail deflection, positive when trailing edge is up, deg
δ_r	rudder deflection, positive when trailing edge is to right, deg

θ	angle of pitch, deg
ρ	air density, slugs/ft^2
σ	standard deviation
ϕ	angle of bank, deg
Φ	transition matrix
ψ	angle of yaw, deg
ψ	gain matrix of Kalman filter
$\dot{(\ )}$	time rate of change of ( ), per sec

Coefficients and Derivatives

$C_\ell = \frac{M_x}{\bar{q}Sb}$, rolling-moment coefficient

$C_m = \frac{M_y}{\bar{q}Sc}$, pitching-moment coefficient

$C_n = \frac{M_z}{\bar{q}Sb}$, yawing-moment coefficient

$C_x = \frac{F_x}{\bar{q}S}$, longitudinal-force coefficient

$C_y = \frac{F_y}{\bar{q}S}$, side-force coefficient

$C_z = \frac{F_z}{\bar{q}S}$, normal-force coefficient

All static derivatives have the following form:

$C_{i_j} = \frac{\partial C_i}{\partial j}$ where $i = \ell, m, n, x, y, z$

$j = \alpha, \alpha^2, \beta, \beta^3, \alpha\beta, \ldots$

$\delta_e, \alpha\delta_e, \delta_a, \alpha\delta_a, \ldots$ etc.

All dynamic derivatives have the following form:

$$C_{i_j} = \frac{\partial C_i}{\partial \frac{jb}{2V}} \quad \text{where } i = y, \ell, n$$

$$j = p, q, r, \dot{\alpha}, \alpha p, \alpha^2 p, \alpha q, \text{etc.}$$

$$C_{k_j} = \frac{\partial C_k}{\partial \frac{j\bar{c}}{2V}} \qquad k = x, z, m$$

Subscript and Superscripts

$()_b$	bias parameter
$()_{PS}$	value at pilot station
$()_{cg}$	value at center of gravity
$()_{i \text{ or } k}$	definition implied by context
$()_0$	initial value
$()_f$	final value
$()_m$	measured value
$()_n$	noise or error term
$()_r$	reference value
$()_s$	scale factor parameter
$\hat{()}$	estimates value
$()^{-1}$	matrix inverse
$()^T$	matrix transposition

Abbreviations

c.g.	center of gravity
P.S.	pilot station
LS	least squares identification technique
IKF/FP	iterated Kalman filter/fixed-point smoother

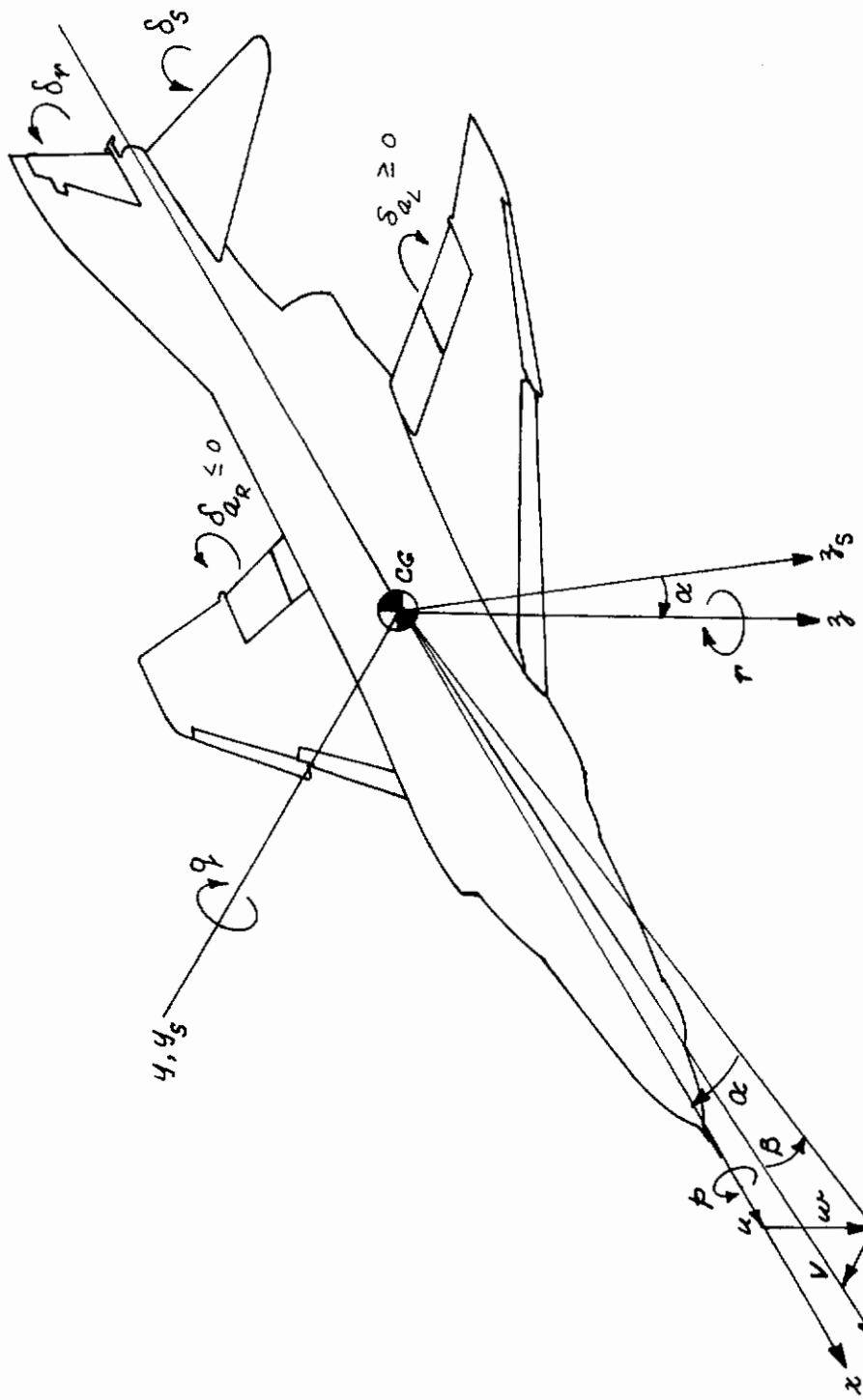

BODY-FIXED AXIS SYSTEMS

Section I

INTRODUCTION

One of the most important areas of research currently being investigated concerns the identification of aircraft aerodynamic characteristics at high angles of attack from flight data. This research is occasioned by the inadequacy of wind tunnel data to properly predict the loss of aircraft control in the post-stall/departure flight regimes, and the disastrous consequences of this loss of control. For example, 194 stall/spin major accidents occurred in the USAF inventory between 1965 and 1970, resulting in an annual loss of approximately $40,000,000. To alleviate this situation, a better understanding of the dynamics and kinematics of control loss is needed; fundamental to this required understanding is an accurate description of the aerodynamic forces and moments on the actual airplane in these flight regimes. If such a description can be made available, the problem becomes amenable to solution; for, as stated in the Ad Hoc Team Report on the F-111 Stall/Post-Stall/Spin Prevention Program (Reference 1): "The mathematics and computing equipment are more than adequate to predict the behavior of the aircraft from the stall to the spin if accurate aerodynamics can be obtained."

This report documents the results of a study performed for the United States Air Force Flight Dynamics Laboratory which had the following general objectives:

(1) To identify the force and moment aerodynamics as well as possible from existing flight data at high angles of attack.

(2) To correlate to the best extent possible identified results from both full scale and drop model flight data with wind tunnel data so as to help develop techniques for more accurately using scaled model data and theoretical methods to predict departure characteristics for new airplanes.

(3) From the results of (1) and (2), to recommend improvements in flight testing and data processing techniques which are necessary to extend the capabilities to extract the aerodynamics.

To meet these objectives, the study consisted of the following series of steps.

First, the existing post stall and departure flight records of three aircraft -- the F-5, the F-111 and the F-4 -- were examined to determine which flight test records were most suitable for identification, for an adequate data base is critical to any identification/correlation program. The existing data were examined for: completeness of instrumentation; documentation and calibration records of the instrumentation; adequacy of the time histories and control inputs applied with respect to motion amplitude and type; length of data for selected ranges of angle of attack; and digital sample rates. Although the original intent was to analyze data from all three aircraft so as to encompass a broad spectrum of aerodynamic shapes, the F-4 data base offered the best possibility for obtaining accurate results, and hence was chosen for investigation.

With the data set chosen, a procedure was set up using parameter estimation techniques to extract the nonlinear aerodynamics of the aircraft during the departure region of flight from flight test records. The parameter identification techniques used were a nonlinear iterated Kalman filter/fixed-point smoother algorithm (IKF/FP) and a least squares (LS) equation error method. As with any identification problem, the four key ingredients are: (1) flight maneuvers and instrumentation, (2) model structure, (3) identification algorithms, and (4) verification of results. The goal of the identification procedure is to reduce the dimensionality of the problem through attention to these ingredients. It can be summarized by the following five steps:

(i) Model form is initially determined from wind tunnel data by representing the nondimensional force and moment coefficients by Taylor's series expansions for selected ranges of angle of attack, sideslip angle and Mach number. The constant coefficients in these expansions represent the unknown parameters to be identified.

(ii) The six-degree-of-freedom (DOF) aircraft kinematic equations and measurement system model are used in the IKF/FP to identify instrumentation errors to determine aircraft initial conditions, and to generate more accurate state estimates of aircraft air data and attitudes. The purposes of this procedure are to separate the identification of instrumentation errors from the identification of aerodynamic parameters, and to improve the accuracy of the LS results.

(iii) The results obtained in (ii) are used to compute the six total nondimensional aerodynamic forces and moments exerted on the aircraft using the corrected rate and acceleration measurements and computed thrust and engine gyroscopic characteristics. The LS method is used to identify the parameters of the aerodynamic model forms; these results provide the initial parameter and covariance estimates for the IKF technique.

(iv) To reduce the number of unknown parameters, the initial estimates are refined using the IKF with the six DOF equations of motion separated into two four DOF systems; one for the extraction of the longitudinal coefficients and the other for the extraction of the lateral-directional coefficients.

(v) Model verification is done with the aid of the residual time histories from the IKF and by predictions of the flight responses from other flight data in the same flight regime.

Analytical models were formulated from wind tunnel data to approximate the aerodynamic coefficients for selected ranges of angle of attack and in a 6 DOF simulation to predict flight test time histories. The wind tunnel data did not accurately predict the flight responses, but the analytical forms served as a starting point to define the form of the aerodynamic model for identification purposes.

Nondimensional force and moment coefficients were extracted from the full scale aircraft flight records for the angle of attack ranges from approximately 12 to 23 degrees and 20 to 40 degrees at Mach numbers around .4 and at altitudes of approximately 32,000 feet. Limited instrumentation on the drop model precluded estimation of the force coefficients, but moment coefficients were extracted for the angle of attack range from 30 to 55 degrees using the LS technique.

The results are mixed. Although the best flight test data available at high angles of attack were used, aircraft excitation and record length of the flight data were insufficient to enable the extraction of completely accurate and consistent coefficients from the data. For the lower range of angle of attack (12 to 20 degrees), where the instrumentation is adequate and the data record length appears sufficient, the model form and complexity used appeared adequate, but the flight records did not permit consistent extraction of these parameters. Above 25 degrees angle of attack, definite conclusions about adequacy and complexity of the coefficients could not be firmly established. Most of the coefficients extracted from the drop model data showed good correlation with wind tunnel tests, but here too, the limited data provided inconclusive results.

In general, the results of this study demonstrated feasibility and applicability of the identification approach and techniques utilized. Where there was adequate data and consistent instrumentation, the results were good. It is clear, however, that to obtain meaningful results at high angles of attack when the aircraft is unstable and in uncontrolled flight, a very carefully planned flight test program must be devised and performed to provide the necessary data base. Such a flight test program is described in Section VI of this report. Recommendations are also given for improvement of the identification procedures for the high angle of attack flight regime.

This study took the first significant and definitive steps toward the identification of the nonlinear aerodynamic characteristics of a high-performance aircraft in the high angle of attack flight regime. The problem is nonlinear, complex and of a very high dimension. Many of the problem areas have been defined and a few have been solved. There is every reason to believe that a carefully controlled flight test program with a properly instrumented aircraft will yield the data required for adequate and accurate results at any angle of attack.

This report is organized as follows. Section II briefly describes the data collection efforts on the F-4, F-5 and F-111 aircraft. A discussion of the identification techniques and procedures is given in Section III.

Section IV describes the development of an analytical model to approximate the F-4E wind tunnel data. The identification and correlation of the results are presented in Section V, including both the identification of instrumentation errors and the extraction of the nonlinear aerodynamic stability and control coefficients from full scale and drop model data. Finally, conclusions and recommendations are given in Section VI. Illustrations and tables are presented at the end of each section for the reader's convenience.

Section II

DATA COLLECTION

2.1 INTRODUCTION

The primary goal of this investigation was to identify and to correlate high angle-of-attack stall/post-stall aerodynamic stability and control characteristics using available data from three sources:

a. Full scale flight test data

b. Radio-controlled free-flight drop model test data

c. Wind tunnel test data.

It is clear that the success of this investigation depended, to a great extent, on both an accurate parameter identification technique for the extraction of the nonlinear aerodynamic parameters from flight test data and, more importantly, upon an adequate data base on which to extract and compare such characteristics. Consequently, the first phase of this contract was associated with the collection and assessment of existing test data which could be made available and was suitable for this program. The F-4, F-5 and F-111 were initially considered as possible study aircraft.

The quality and type of full scale flight test data available on these three aircraft was of major concern. Early in the program it became apparent that very little data currently existed on the F-5 and the full scale flight test data available on the F-111 was sparse. The only high angle-of-attack flight test data on the F-5 (or T-38) are preserved in References 2 and 3; the original oscillograph records were destroyed. Although NASA Langley Research Center (NASA/LRC) was conducting high angle-of-attack wind tunnel tests and free flight drop tests on an F-5 model, the data could not be made available soon enough for use in this program.

A description of the test data available on the F-111 is given in Reference 4. Flight test data at high angles of attack were obtained during a short program, Reference 5, and a stall/post-stall gyration investigation and spin avoidance program was being conducted at Edwards Air Force Base. However, only a small amount of this data could be made available through Convair Aerospace Division of General Dynamics from their F-111A Simulator and Stall Inhibitor Program. This data formed a very incomplete flight test data base for this aircraft. Consequently, the F-5 and F-111 were dropped from further consideration since the F-4 aircraft did have a better spectrum of flight test, drop model, and wind tunnel data available. The data used in this program is briefly described in the following section.

2.2 DATA COLLECTION ON THE F-4E

2.2.1 Full Scale Flight Test Data

There were three possible sources of high-angle-of-attack flight test data for the F-4. These data were obtained during the stall/near stall investigation of the F-4E aircraft at Edwards Air Force Base, References 6 and 7; the evaluation of the spin and recovery characteristics of the F-4B airplane at the Naval Air Test Center (NATC), Reference 8; and the slatted aircraft currently being tested at McDonnell-Douglas. After discussion with personnel from the Air Force Flight Test Center, McDonnell-Douglas (McAIR), and NATC, the latter two sources were dropped from further consideration. Analog data tapes on which the flight data were recorded with the F-4B were available at NATC, but the calibration records were lost and the data preserved in Reference 8 is of rather poor quality because of resolution problems. Although wind tunnel and model drop test data were available on the slatted F-4, the angle of attack excursions were being limited to approximately 30 degrees and it was considered to be difficult to obtain data while the flight test program was currently in progress.

The stall/near stall investigation of the F-4E consisted of a total of 57 flights to investigate the stall/near stall properties of the F-4E aircraft with various external store loadings and aircraft configurations. These tests were conducted at the Air Force Flight Test Center at Edwards Air Force Base (EAFB), California with engineering and maintenance support provided by McAIR. After completion of the program, instrumentation calibration records, various flight logs and records, and the on-board raw flight data tapes were stored at the McAIR/EAFB facility.

The original reduced flight test data were preserved in References 6 and 7 in plot form, and therefore, represented the only available flight data on the F-4. However, the reduced flight data contained in these reports are limited and of inadequate quality for further data reduction required for identification purposes. Hence, in order to get the full scale flight test data needed, McAIR was subcontracted to re-reduce the raw flight test data from flight number 165 of the stall/near stall investigation and provide the data on a digital tape. The details are reported in Reference 9 and the time history plots of the pertinent flight variables, instrumentation and aircraft characteristics are given in Appendix I.

Because budgetary constraints precluded the reduction of more than one flight of the 57-flight investigation[1], the available records were scrutinized to determine their suitability. Flight 165 was selected over the others for the following specific reasons.

---

[1] Because of no requirements to save the raw data tapes, the first thirteen flight tapes were already erased.

1. Low Mach number, stall/post-stall flight maneuvers available, not necessarily time histories of spins.

2. Near clean loading, so as to be compatible with the wind tunnel/free flight model. Loading in flight 165 is 1B-inboard pylons and aft AIM-7 missiles.

3. All instrumentation operational.

4. Switching type control inputs in the angle of attack range of interest were used during some of the maneuvers.

As shown in Appendix I, a total of eight flight records from flight number 165 were provided which cover the angle of attack(α) range from approximately 12 to 45 degrees. Three records in the low α range with Mach number (M) below .5, called 9, 10, 11, have pulse type control inputs separately applied in stabilator, aileron and rudder, respectively. Two rolling departures from a normal stall entry, records 14 and 20, provide data for M $\leq$ .5 in the higher α ranges. The latter three records are rolling departures from an accelerated stall entry, records 15, 17 and 19. These data were not used because the large Mach number and angle of attack range traversed during a relatively short time span precluded a simple representation of the aerodynamic coefficients which could possibly be extracted from this data. In all records, the sideslip angle remained below 15 degrees.

2.2.2 Model Test Data

The majority of low speed wind tunnel data at high angles of attack was obtained from References 10 and 11. Data tabulations from the tests reported in these references were also obtained from the NASA Langley Research Center (NASA/LRC) and other corroborating data came from References 12, 13, and 14. For comparison purposes, two McAIR reports, References 15 and 16, were also used. Reference 15 yielded additional high angle of attack data from an Ames series of tests. These wind tunnel data are plotted in coefficient form in Appendix IV of this report.

Radio controlled free flight drop model data on the F-4 were obtained in the form of tabular listings from the NASA/LRC. The data were obtained from six drop tests with the identical model used in the wind tunnel test series in the clean configuration. The results of these drop tests were not as yet in report form. Also provided were instrumentation calibrations, physical characteristics of the model and the transformation equations to correct the air data measurements to the center of gravity. Since attitude and acceleration measurements were not available, only the moment stability and control coefficients could be extracted from the data. Two of the six records used for identification purposes are shown in Appendix I.

The above data base, although lacking in full scale and free flight model test data, represents the best available spectrum of tests currently available.

Section III

TECHNICAL APPROACH AND MATHEMATICAL PRELIMINARIES

This section briefly describes the general problem of aircraft parameter identification as related to the estimation of stability and control parameters from flight test measurements. Specific problems associated with identification at high angles of attack are cited and the detailed approach taken in this investigation to alleviate some of these problems is discussed. A description of the identification algorithms and mathematical models is given, followed by other necessary data reduction procedures.

3.1 AIRCRAFT IDENTIFICATION PROBLEM AT HIGH ANGLES OF ATTACK

As is well known, the ability to extract stability and control parameters from flight test data depends upon many elements related to both the theory of identification and the very practical matter of flight test experience, but four major ingredients predominate. These four ingredients are:

1. Mathematical modeling
2. Instrumentation
3. Maneuvers or experiment design
4. Identification techniques

The first three are illustrated in Figure 1, which is a conceptual block diagram of the actual aircraft and the general model used for parameter identification purposes. The equations of motion of the aircraft are written in the conventional, but general form:

$$\dot{x} = f(x, p, u) + w(t), \quad x(t_0) = x_0$$
$$y_i = h(x_i, p, u_i) + v_i, \quad i = 1, \ldots, N \tag{3-1}$$

where

x = state vector for the aircraft

p = unknown parameters vector

u = control inputs, such as δ_s, δ_a, δ_r

y_i = measurement vector of sensor outputs at discrete time points

$f(), h()$ = functional form of aircraft and measurement system model

and $\omega(t)$ and v_i are zero mean, Gaussian white noise vectors which represent errors in formulating the model (that is, missing terms, unknown inputs, etc.) and the inherent random error in the instrumentation, respectively. The first equation in equation (3-1) is commonly referred to as the dynamical model of the system to be identified, or the equations of motion of the aircraft if sensor/control system dynamics are neglected, and the second equation the measurement system. The unknown constant parameter vector to be identified from the control inputs and noisy sensor outputs satisfies

$$\dot{p} = 0 \tag{3-2}$$

where p can contain unknown aircraft initial conditions, aerodynamic parameters, and instrumentation errors such as constant biases, for example. Given the first three ingredients -- that is, the model, the instrumentation and the proper maneuvers (e.g., control inputs) to insure that the unknown parameters are identifiable from the measurements -- then the identification technique(s) can be successfully used to obtain these unknowns. In fact, if the instrumentation is complete, very accurate and noise-free, if the model form can adequately represent the motions of the aircraft without significant error and if all the degrees of freedom of motion of the aircraft are properly excited to allow for unique identifiability of the unknown parameters, then some of the simplest, straightforward identification techniques can be used to accurately obtain the stability and control parameters of the vehicle. Before outlining the specific problems and our approach associated with identification at high angles of attack, the identification techniques used will first be discussed.

3.1.1 Identification Algorithm

The identification algorithms used during this program were a classical least squares (LS) linear regression method and a locally iterated Kalman filter/fixed-point smoothing algorithm (IKF/FP). These techniques are explained more fully in Appendix V of this report and a more complete documentation is available in References 17 and 18.

The LS method is used to provide a set of initial parameter estimates and a set of approximate variances of these estimates for initializing the IKF. Once the model form (f( )) is chosen, this method minimizes the error in satisfying the equations with respect to the unknown parameter vector (p) in the equation. That is, $\omega(t)$ in equation (3-1) is minimized with respect to p and consequently, it is called an equation error method. This method also provides an indication as to the adequacy of the model form and the identifiability of the parameters representing the model.

The restrictions are that:

1. All measurements of $\dot{x}$ (aircraft accelerations) and x must be available.

2. The estimates are biased if the state measurements (x) are noisy; that is, $v_i \neq 0$ in equation (3-1).

To account for both equation error (process noise $w(t)$) and instrumentation error (v_i), the identification problem is transformed to a nonlinear filtering problem by augmenting the aircraft state equations with the parameter vector model, equation (3-2).

The nonlinear filter used is a form of an extended Kalman filter utilizing a "local iteration" scheme between successive measurements to reduce the errors in linearizing the $f(x, p, u)$ and $h(x, p, u)$ functions by improving the reference trajectory. This improvement is accomplished by smoothing each measurement data point backwards in time one point and re-linearizing. In addition, the outputs of the filter at each data point can be used in a fixed-point smoothing algorithm to produce a better smoothed estimate of the aircraft initial condition. The mathematical details and selection of the initializing inputs are given in Appendix V. The residuals or innovation sequences (measurement data minus predicted measurements) and the final covariance matrix in the Kalman filter serve as additional checks on the adequacy of the model form and accuracy and uniqueness of the parameter estimates.

3.1.2 Specific Problems and Technical Approach

In relation to the major ingredients for successful identification outlined above, there are four additional problems which increase the difficulties in identifying nonlinear stability and control characteristics in the post-stall high angle of attack flight regime. These are associated with:

1. The complexity and uncertainty of the aerodynamic model(s) required,
2. the gross or large maneuver requirements,
3. the instrumentation, and
4. the short time duration of maneuvers where one particular model is applicable.

The first three items lead to a very high dimensional (and, therefore, a computationally demanding) identification problem because of the large number of unknown parameters needed to represent the model accurately. The fourth item further compounds the problem because the relatively unstable and uncontrollable nature of the aircraft in this flight regime could force the aircraft to traverse the angle of attack range of interest rather quickly, thereby providing only short time-duration records if the aircraft maneuvers are not first carefully planned. This latter problem was not considered in this investigation but recommendations for future flight testing are given in Section VI. The approach taken in this investigation was to reduce the dimensionality of the identification problem by separating the overall problem into separate lower dimensional problems, the solutions of which are computationally practical. The three areas of concern and the approach taken are discussed below.

First, the aircraft model (that is, the functional forms of f ( ) and h ( ) in equation (3-1)) must be selected that adequately represents the aircraft motions to be measured. The model should contain all of the terms of significance that contribute to the forces and moments on the airframe. This includes kinematic terms, inertia coupling, gravitational, thrust, engine gyroscopic effects and aerodynamic forces and moments. The aerodynamic forces and moments in this flight regime are highly nonlinear functions of several variables and a Taylor's series representation of the aerodynamics, where the constant coefficients in these expansions are the unknown parameters to be identified, can contain a large number of terms that can be candidates for logical inclusion in the model.

In order to reduce the number of terms, three approaches can be taken to the problem of identification of high angle of attack (α) aerodynamics. They can be described as:

- fixed point identification
- complete range identification
- limited range identification

Fixed point identification, where the small perturbation equations of motion about a trim or reference flight condition may be applicable, has the favorable feature of using simple linear models with a small number of parameters to identify. However, its major drawback for high angle of attack identification is that the model is good only for very short periods of time, too short to get meaningful identification results. Stability derivatives change very rapidly at high angles of attack so a fixed point identification would only be good for a very small range of α. Compounded with this drawback is the fact that the airplane is highly unstable at high angles of attack so that the airplane cannot be held at a particular α for any significant length of time.

The complete angle of attack range approach to identification overcomes the problems of using a linear model at fixed points to describe a highly nonlinear system. Using the complete range approach, an analytical aerodynamic model complex enough to describe the aircraft at all angles of attack can be developed. There would be no need to try to hold an unstable airplane at a constant angle of attack. However, there is the problem of having too complex a model. To adequately define the complete aerodynamics of an aircraft from normal cruise α through post stall maneuvers may require more than 150 parameters. The practicalities and economics of enabling an identification technique to handle such a large model precluded the possibility of taking this approach.

A limited range of angle of attack identification, where the model is applicable for a selected range of angle of attack, for example, is a practical compromise between the above two approaches. With this approach an analytical model is chosen to adequately represent the aerodynamics for selected ranges

of angle of attack, sideslip angle, Mach number, and altitude. The ranges are selected on the basis of wind tunnel data and the available flight test data within the candidate ranges. Hopefully, enough data will be available in each range so that the unknown parameters can be accurately extracted and that only the parameter values change for different ranges of Mach number and altitude, not the model form. After interaction of the aerodynamics at different ranges of angle of attack, a complete model can be pieced together to define the aerodynamics of the aircraft for the full range of α .

The latter approach was considered the only one feasible for this program because of the flight data base available. The aerodynamics to be identified were expressed in aircraft body axis, nondimensional form instead of stability axes for two reasons:

1. The extracted coefficients could be compared directly to the wind tunnel data which was presented in the body axis system, and

2. the force coefficients (C_x , C_y and C_z) in the body axis system are directly related to the individual body fixed linear acceleration measurements (n_x , n_z and n_y).

Taylor's series expansion were used to represent these nondimensional coefficients, where the coefficients of the expansion are the unknown parameters to be identified, because the resulting analytical forms are readily amenable for use in the present identification algorithms.

The following assumptions were also made:

1. Power effects were included in the aerodynamic coefficients to be estimated.

2. The mass, moments of inertia, and center of gravity of the aircraft are known precisely.

3. The aircraft is rigid and no turbulence or wind effects are present.

4. Mach effects for $M < .5$ and hysteresis effects due to flow separation are negligible.

5. Angle of attack and sideslip angle rate effects are included in the appropriate rotary derivatives.

6. Control surface deflections are measured perfectly.

7. The actual complexity of the aerodynamics (that is, the number of terms and the functional dependence of the variables) is no greater than the wind tunnel data indicates, especially for the static coefficients.

The other two areas which increase the dimensionality of the problem are the instrumentation system and the modeling of gross maneuvers which requires a complete six degree of freedom representation of the aircraft. Even with the limited range identification approach, the number of unknown parameters to be concurrently identified is still extremely large. The measurement system, $h(x, p, u)$ in equation (3-1), must be modeled and if instrumentation inconsistencies or bias errors are present in addition to the random error, v_i, these errors will degrade the accuracy of the estimated aerodynamic parameters if not taken into consideration (References 17, 18 and 19). If these effects are modeled and identified simultaneously with the aerodynamic parameter, it will be extremely difficult to separate errors in the instrumentation from errors caused by incorrectly representing the aerodynamics.

This consideration is especially important for high angle of attack testing, since the large full scale ranges required of the instrumentation and large aircraft maneuvers accentuate these errors. To alleviate this difficulty, and consequently reduce the number of parameters to be concurrently identified, instrumentation consistency checks and error estimation were first performed using the aircraft kinematic equation and measurement system model with the iterated Kalman filter/fixed-point smoother. The equations, which are given in Table I and discussed in Section 3.2.1 below, are the six-degree-of-freedom kinematic equations of the aircraft with the body-fixed airframe linear accelerometers and rate gyros used in the manner of a strapped-down inertial measuring unit. This mechanization allows for the extraction of instrumentation biases from the flight data and the optimal state estimation of the aircraft trajectory ($V, \alpha, \beta, \phi, \theta$) using the Kalman filter to further reduce the effects of measurement noise. In addition, an automatic procedure is thereby provided to optimally transform angle of attack and sideslip angle measurements at the boom to those at the center of gravity of the aircraft (using the equations derived in Reference 20) and to estimate the aircraft initial conditions. It should be noted that if angular acceleration sensors ($\dot{p}, \dot{q}, \dot{r}$) are available, which was not the case in this program, than an optimal estimate of the aircraft rotational rates (p, q, r) can also be easily obtained by simply expanding the instrumentation consistency check equations to model these additional measurements.

To further reduce the computational burden, when employing the iterated Kalman filter, the six-degree-of-freedom equations of motion of the aircraft were separated into two separate four-degree-of-freedom systems; one for extracting the longitudinal coefficients (C_L, C_{y_β} and C_m) and the other for the lateral-directional coefficients (C_l , C_n and C_y). These equations and a discussion on the choice of coordinate system used are given in Section 3.2, page 15.

In summary, the overall identification procedure is illustrated in block diagram form in Figure 2. It can be summarized by the following five steps:

1. Model form is initially determined from wind tunnel data by representing the nondimensional aerodynamic force and moment coefficients by Taylor's series expansion for selected ranges of angle of attack, Mach number, and sideslip angle. The constant coefficients in these expansions represent the unknown parameters to be extracted from the flight data.

2. The six-degree-of-freedom aircraft kinematic equations and measurement system model are mechanized in the iterated Kalman filter/fixed-point smoother (IKF/FP) to identify instrumentation errors in the form of biases, aircraft initial conditions, and generate an optimal state estimate of the aircraft trajectory ($V, \alpha, \beta, \phi, \theta$). This procedure separates the identification of instrumentation errors from the identification of aerodynamic parameters and reduces the effects of measurement noise contaminating the air data and attitude measurements.

3. The results of step 2 are used to compute the six total nondimensional aerodynamic forces and moments exerted on the aircraft using the corrected rate and acceleration measurements and computed thrust and engine gyroscopic characteristics. Angular accelerations ($\dot{p}, \dot{q}, \dot{r}$) are obtained from angular rate measurements (p, q, r). Candidate model forms selected from step 1 above are used in the least squares (LS) identification technique to identify the parameters in the aerodynamic model forms by minimizing the error in satisfying the aerodynamic equations with respect to the unknown parameters in the equations. The error in the fit and the normalized regressor in the technique provide an approximate indication as to the adequacy of the candidate models and identifiability of the unknown parameters from the flight data.

4. The results from step 3, tempered with the values for the coefficients from the wind tunnel data, provide "a priori" estimates of the model form and initial parameters and covariance estimates for the IKF identification technique. Model structure verification is done with the aid of the residual sequences in the Kalman filter. If the model is accurate, and the instrumentation errors are truly zero mean, these residuals are zero mean and random. The final covariance matrix serves as a check

on the accuracy and uniqueness of the resulting parameter estimates.

5. Model verification, the last step, is performed by building up an aerodynamic model base which can be used in a simulation to predict the time histories of flight data in the flight regimes of applicability. This, of course, represents the true test as to the accuracy of the extracted parameters.

3.2 SYSTEM MODELS FOR IDENTIFICATION

A total of three models were used in the iterated Kalman filter/fixed-point smoother identification algorithm. These were the aircraft kinematic equations and measurement system for the identification of instrumentation errors and generation of state estimates of the aircraft trajectory and two separate four DOF systems: one for extracting the longitudinal coefficients (C_x , C_z and C_m) and the other for extracting the lateral-directional coefficients (C_ℓ , C_n and C_y). The representation of the aerodynamic coefficients used in the least squares technique is given in Appendix II.

3.2.1 Aircraft Kinematic Equations

The six-degree-of-freedom aircraft kinematic equations and measurement systems used for the identification of instrumentation errors are given in Table I with appropriate definitions. The kinematic equations are written in the aircraft body axes systems with three linear inertial velocities (u , v , w), one linear position (h) and the three Euler angles (θ , ϕ , ψ) as state variables. Forcing inputs to these equations are measured time histories of the linear accelerations (n_x , n_y , n_z corrected to the c.g.) and the rotational rates (p , q , r). Errors in these measurements are modeled as constant biases (for example, n_{x_b} , n_{y_b} , n_{z_b} , p_b , q_b , r_b) to be identified. Since the linear accelerations and rate gyro measurements are contaminated with random measurement noise, the use of these measurements in the kinematic equation introduces process noise or equation error into the dynamical system and consequently makes the system model stochastic. These noise inputs are accounted for by the w_i , $i = 1, \cdots, 6$ noise terms in the equation.

Seven parameters are modeled in the measurement system. These include true airspeed (V_m), boom vane angle of attack (α_{V_m}) and sideslip angle (β_{V_m}) (with the appropriate corrections as derived in Reference 20), altitude (h_m) and the three Euler angles (ϕ_m , θ_m , ψ_m). Bias errors are included in all measurements to be identified in addition to scale factor errors in the air data measurements to model possible airflow effects. Auxiliary equations are included to generate optimal state estimates of V , α , β (at the c.g.) for use during the identification of the aerodynamic coefficients. All common sources of sensor errors, such as time lags in h_m , for example, were not modeled completely but were accounted for in the bias parameters and random noise terms. The units used are self-explanatory.

Note that all the instrumentation is assumed perfectly aligned to the aircraft reference body axis and that the major source of errors are treated as biases in the measurements in addition to the random noise terms. The rectangular body axis coordinate system (u, v, w) was used instead of the nonorthogonal system (V, α, β) because the accelerometer biases appear linearly in the dynamical system and the α, β vane measurement models are less complicated in the u, v, w system.

The instrumentation consistency check equations as given in Table I contain two approximations. These are associated with neglecting the effects of random errors (noise) in the rate gyro measurements in accounting for airplane rotation rates in the α_{V_m} and β_{V_m} measurement models and the linear acceleration corrections to the center of gravity. Modeling these noise terms would make the process and measurement noise statistics correlated and the measurement noise nonstationary and extremely complex. Errors in neglecting these effects were never fully investigated, but they are small for reasonable levels of rate gyro measurement noise.

However, if angular acceleration sensors are available, the errors caused by the above approximations can be eliminated by simply including three angular acceleration equations in the dynamical model and adding the rate gyro measurements to the measurement system. This will also eliminate the modeling of rate biases (p_b, q_b, r_b) and the w_4, w_5, and w_6 process noise terms in the dynamic model. In addition, an optimal estimate can now be generated for the aircraft rotational rates, p, q, and r. The additions required to the equations of Table I when angular acceleration measurements are available are given in equation (3-3) below.

Dynamical Model:

$$\begin{aligned} \dot{p} &= \dot{p}_m + \dot{p}_b + w_7 \\ \dot{q} &= \dot{q}_m + \dot{q}_b + w_8 \\ \dot{r} &= \dot{r}_m + \dot{r}_b + w_9 \end{aligned} \tag{3-3a}$$

Measurement System:

$$\begin{aligned} p_m &= p + p_b + v_8 \\ q_m &= q + q_b + v_9 \\ r_m &= r + r_b + v_{10} \end{aligned} \tag{3-3b}$$

$\dot{p}_b$, $\dot{q}_b$ and $\dot{r}_b$ are the unknown angular acceleration bias parameters and w_7, w_8, and w_9 the random component of noise on the respective measurements.

3.2.2 Four-Degree-of-Freedom Longitudinal and Lateral-Directional Models

As indicated above, the representation of the aircraft characteristics in the post-stall flight regime when large maneuvers are encountered for identification purposes requires a six-degree-of-freedom (DOF) nonlinear equations-of-motion model and at least two kinematic relationships to describe the evolution of the roll and pitch Euler angles. Further, the use of Taylor series expansions to adequately represent all six aerodynamic force and moment coefficients over a large enough range of angle of attack (as dictated by the flight data being used), leads to a very high-dimensional, and therefore, a computationally demanding identification problem.

To circumvent the high degree of dimensionality, the identification problem was reduced by separating the equations of motion into two systems, one for extracting the longitudinal coefficients (C_x, C_z and C_m) and the other for extracting the lateral-directional coefficients (C_ℓ, C_n and C_y), with cross-coupling turns entering similarly to the control inputs. The systems of equations used are given in Tables II and III respectively, along with appropriate definitions.

The force equations in both systems are written in the nonorthogonal coordinate system (V, α, β), instead of the rectangular body axis system (u, v, w), because the dynamic equations and the measurement system are the most linear with respect to the state variables for this system. This is the case because the time history responses of V, α, β are measured directly (α and β at the c.g. are available as state estimates from the instrumentation consistency checks) and more importantly because the aerodynamic forces and moments are expressed as functions of α and β , so that auxiliary calculations are not required. Both systems are also four-degree-of-freedom, instead of the conventional three. The lift and side force degrees of freedom are included in both sets of equations because the aerodynamic forces and moments are strong functions of both α and β ; particularly α . Due to large attitude maneuvers, the roll and pitch Euler angles are also included in both systems. All aerodynamic coefficients are in the body axis reference system.

The equations are fairly general and no simplifying assumptions, such as small angle approximations, for example, have been made to limit their range of applicability, except that $|\theta| < 90^\circ$. In addition, to further reduce the number of parameters to be concurrently identified, the n_x linear accelerometer measurement can be used to account for the x-force contribution (C_x) to the longitudinal equations and similarly the n_y accelerometer measurement can account for the y-force contribution (C_y) in the lateral-directional model. The analytical representations of the C_x , C_z , C_m , C_ℓ , C_n and C_y coefficients for parameter identification are given in Appendix II. The $\dot{\alpha}$ and $\dot{\beta}$ effects are lumped with the rotary derivatives due to their linear dependency. That is, the effects or sensitivity of the measured responses of the airplane to a variation in C_{m_q} or $C_{m_{\dot{\alpha}}}$, for example, would be almost identical.

In both models, the linear acceleration measurements are first corrected to the c.g. using the appropriate transformation. Forcing inputs to the longitudinal model (Table II) include the stabilator control (δ_s), effective roll control (δ_a)[2], thrust (T_x, T_z), thrust moment (m_{y_T}) and air density (ρ). Cross-coupling inputs are measured roll and yaw rate (p_m, r_m) and side acceleration ($n_{y_{c.g.}}$). For the lateral-directional model (Table III), forcing inputs are the rudder control (δ_r), effective roll control δ_a , thrust (T_y), thrust moment (m_{x_T} , m_{y_T}) and the cross-coupling inputs are measured pitch rate (q_m), airspeed (V_m), and linear accelerations ($n_{x_{cy}}$, $n_{z_{cy}}$). Although the F-4E did have a redundant set of linear accelerometers at the pilot station, these were not used (and therefore only one set of accelerometer measurements are mechanized in these equations) because of their rather poor quality due to noise pickup of structural vibrations.

It should also be noted that by including the cross-coupling and other forcing terms in the dynamic equations (thru the use of the measured time histories of the linear accelerations and the rotational rates) inherently leads to the introduction of process noise into the model. That is, these inputs are in error by an amount equal to the measurement noise on their sensor outputs and consequently, this error is introduced into the dynamical system model as process noise. The identical situation occurs with the kinematic equations used for instrumentation consistency checking as described in the preceding subsection.

The process noise introduced this way is lumped into the ω_i , i = 1, . . . 6 noise terms which are assumed zero-mean, white Gaussian uncorrelated stationary noise processes. An approximate lower bound for the variances of ω_i can be calculated as follows:

For the longitudinal model, let

$$\begin{aligned} n_{x_m} &= n_x + n_{x_n} \\ p_m &= p + p_n \\ r_m &= r + r_n \\ n_{y_m} &= n_y + n_{y_n} \end{aligned} \tag{3-4}$$

where n_{x_n} , p_n , r_n and n_{y_n} are zero-mean white Gaussian measurement noise.

---

[2] The roll controllers on the F-4 are interconnected ailerons and spoilers whose control effects could therefore not be identified separately. Consequently, an effective roll control defined as the sum of the right and left hand ailerons was used to be consistent with the wind tunnel model.

Substituting equation (3-4) into the dynamical model equations given in Table II, assuming $\cos\beta \approx 1$ and eliminating terms of second order (for example $p_n r_n \approx 0$), it can be shown that

$$
\begin{aligned}
\omega_1 &= n_{x_n} \cos\alpha + n_{y_n} \sin\beta \\
\omega_2 &= I_3 (rp_n + pr_n) + 2I_4 (pp_n - rr_n) - \frac{hl_x}{I_y} r_n \\
\omega_3 &= \left(\frac{57.3}{V}\right) \sin\alpha \; n_{x_n} - \tan\beta \, (p_n \cos\alpha + r_n \sin\alpha) \\
\omega_4 &= -\left(\frac{57.3}{V}\right) \cos\alpha \sin\beta \; n_{x_n} + p_n \sin\alpha - r_n \cos\alpha + \frac{57.3}{V} n_{y_n} \\
\omega_5 &= p_n + \cos\phi \tan\theta \, r_n \\
\omega_6 &= -\sin\phi \, r_n
\end{aligned}
\qquad (3\text{-}5)
$$

if all other possible equation error is assumed equal to zero. From equation (3-5) it can be readily seen that ω_i, $i = 1, \ldots 6$ are correlated and nonstationary even though n_{x_n}, p_n, r_n and n_{y_n} are uncorrelated and stationary. However, two additional approximations were made:

1. ω_i, $i = 1, \ldots 6$, were made stationary by choosing constant reference values for α, β, V, r and p. The reference values are, of course, dependent upon the flight record being analyzed.

2. Neglect all cross correlations between ω_i, $i = 1, \ldots 6$.

With the above approximations, equation (3-5) can now be used to calculate the variances for ω_i given the noise statistics for n_{x_n}, p_n, r_n and n_{y_n}. A similar set of equations can be derived for the lateral-directional model.

The errors introduced by the addition of process noise into the dynamical model and the above approximations are small in comparison to other possible error sources, such as model form, for example. Of course, the smaller the measurement errors in these sensors, the more accurate the approximations.

3.3 MISCELLANEOUS DATA REDUCTION PROCEDURES

A few miscellaneous data reduction procedures not directly related to the previous discussions are presented in this subsection. They deal with the time deskewing of data, correction of bad data points, digital filtering of flight data, thrust calculation, generation of aerodynamic forces and moments from flight test data, and some calculations used to obtain correct air data for the radio controlled model.

Ninety aircraft and flight parameters were measured and recorded onboard the test aircraft by a Pulse Duration Modulation (PDM) type data system at a constant sample rate of ten measurements per second. Therefore, there could be a time skew in the data of up to .1 second if the first and last parameters measured in the series happened to be used. To time deskew this data, a common time point was chosen and all of the data parameters were referenced to this point by linear interpolation between the two measured points.

Some bad data points were observed in the air data. These were easily detected and corrected by hand. Specific parameters were also digitally filtered to eliminate high frequency noise. The angular rates (p , q , r) were first processed by a two-pass Butterworth filter with a cutoff frequency of 2 hertz. The data is initially filtered in one direction, reversed in time, and refiltered to eliminate undesirable phase shift. This filtering technique is more fully described in Reference 21. These filtered rates were then processed with a modified spline computer program, Reference 22, which further smoothed the data. The spline functions were differentiated so that angular accelerations ($\dot{p}$, $\dot{q}$, $\dot{r}$) could be obtained. Mach number, dynamic pressure, air density, free air temperature, and engine rpm's were also processed by the two pass Butterworth filter with a cutoff frequency of 1.0 hertz. This gave smooth data for the calculation of thrust.

All flight data available from the radio controlled drop model were also filtered. However, the filter characteristics were first adjusted to allow for the dynamic scaling requirements of the model.

Two techniques were available for the estimation of nominal thrust forces produced by the two aircraft engines. Both techniques are applicable for only low angle-of-attack level flight, so consequently thrust changes as functions of α and β are included in the aerodynamic forces and moments. The primary objective was to calculate, as accurately as possible, the differential thrust forces between engines so that gross yawing moments produced by this difference could be approximately accounted for in the equations of motion.

The first technique involved a computer program written by General Electric (Reference 23) which described the output of the J-79-17 engines given many different combinations of input data. After studying the data required for this computer program and the flight and engine data which were available, it was decided to utilize the engine rpm, altitude, Mach number and free air temperature as inputs. It is believed that this combination of inputs produces the best estimate of uninstalled net thrust for the available data.

The second thrust calculation technique utilizes the generalized performance data contained in Figures 186 and 179 of Reference 24. This technique involves the following approximate calculation.

$$\frac{F_N}{\delta_{t_2}} = 7.59 \frac{N}{\sqrt{\theta_{t_2}}} - 46200$$

where

$$\delta_{t_2} = \frac{P_{t_2}}{P_{t_0}} \left(1 - \frac{H}{145{,}000}\right)^{5.26} (1 + .2M^2)^{3.5}$$

$$\theta_{t_2} = \left(\frac{FAT + 273.16}{288.16}\right)(1 + .2M^2)$$

N	=	engine rpm
FAT	=	free air temperature (^{o}c)
P_{t_2}/P_{t_0}	=	inlet recovery factor
F_N	=	net thrust (lbs)
M	=	Mach number
H	=	altitude (feet)

The assumptions utilized in this technique include: 1) there is a linear relationship between corrected net thrust, F_N/δ_{t_2}, and corrected rpm, $N/\sqrt{\theta_{t_2}}$; 2) this one linear relationship is valid for all data runs; and 3) standard atmospheric conditions existed for each data run. Figure 179 of Reference 24 indicates that assumptions 1 and 2 are reasonable approximations. The value of P_{t_2}/P_{t_0} was obtained from Figure 186 of the above reference.

Comparison of the GE computer program and the generalized performance calculations were made for 44 seconds of run 14 and showed that the methods agreed to within 5%. Since the generalized performance technique was computationally much more efficient and gave adequate answers it was decided to utilize that method for all thrust calculations.

The aerodynamic forces and moments were calculated from the flight test data by the following set of equations.

The total force equations in the body axes are:

$$F_x = mg\, n_{x_*} - m\left[-X_x(r^2+q^2) + Y_x(p\cdot q - \dot{r}) + Z_x(r\cdot p + \dot{q})\right]$$

$$F_y = mg\, n_{y_*} - m\left[X_y(p\cdot q + \dot{r}) - Y_y(r^2+p^2) + Z_y(r\cdot q - \dot{p})\right]$$

$$F_z = mg\, n_{z_*} - m\left[X_z(r\cdot p - \dot{q}) + Y_z(r\cdot q + \dot{p}) - Z_z(p^2+q^2)\right]$$

(3-6)

where "*" refers to the position of the accelerometers, either at the approximate c.g., pilot station, or some intermediate position.

The distances $\begin{Bmatrix} x_x, y_x, z_x \\ x_y, y_y, z_y \\ x_z, y_z, z_z \end{Bmatrix}$ in feet, are the distances

between the actual center of gravity for the specific record and the accelerometer position; i.e., x_y is the length along the x body axis between the c.g. and the n_y accelerometer.

The aerodynamic forces are obtained by subtracting the thrust forces from the total forces:

$$\begin{aligned} F_{x_a} &= F_x - \cos \lambda_T (T_L + T_e) \\ F_{y_a} &= F_y - \sin \lambda_T \cos \phi_T (T_L - T_e) \\ F_{z_a} &= F_z + \sin \lambda_T \sin \phi_T (T_L + T_e) \end{aligned} \tag{3-7}$$

where the thrust orientation angles

$$\begin{aligned} \lambda_T &= 5.25^\circ \\ \phi_T &= 87.28^\circ \end{aligned}$$

were obtained from McDonnell-Douglas. As defined in Reference 15, λ_T is the angle between the thrust vector and a line parallel to the x body axis measured in the plane parallel to the x axis and containing the thrust vector. ϕ_t is the angle between the x-y plane and the plane parallel to the x axis and containing the thrust vector.

The nondimensional aerodynamic forces are:

$$\begin{aligned} C_x &= F_{x_a} / (\bar{q} S) \\ C_y &= F_{y_a} / (\bar{q} S) \\ C_z &= F_{z_a} / (\bar{q} S) \end{aligned} \tag{3-8}$$

where

$$\bar{q} = \frac{1}{2} \rho V^2$$

The total moment equations in the body axes are:

$$\begin{aligned} M_x &= I_x \dot{p} - I_{xz} (\dot{r} + qp) + (I_z - I_y) r \cdot q + h_{e_z} q - h_{e_y} r \\ M_y &= I_y \dot{q} + (I_x - I_z) pr + I_{xz} (p^2 - r^2) + h_{e_x} r - h_{e_z} p \\ M_z &= I_z \dot{r} - I_{xz} (\dot{p} - qr) + (I_y - I_x) p \cdot q + h_{e_y} p - h_{e_x} q \end{aligned} \tag{3-9}$$

The aerodynamic moments are obtained by subtracting the moment due to thrust from the total moments:

$$
\begin{aligned}
M_{x_a} &= M_x - (Y_T \sin\lambda_T \sin\phi_T - Z_T \sin\lambda_T \cos\phi_T)(T_L - T_e) \\
M_{y_a} &= M_y - (Z_T \cos\lambda_T + X_T \sin\lambda_T \sin\phi_T)(T_L + T_e) \\
M_{z_a} &= M_z - (X_T \sin\lambda_T \cos\phi_T + Y_T \cos\lambda_T)(T_L + T_e)
\end{aligned}
\qquad (3\text{-}10)
$$

where the approximate moment arms are: X_T = .608 - (c.g. -.33) $\bar{c}$ ft

Y_T = 1.985 ft

Z_T = -.391 ft

The nondimensional aerodynamic moments are:

$$
\begin{aligned}
C_\ell &= M_{x_q} / (\bar{q} S b) \\
C_m &= M_{y_a} / (\bar{q} S \bar{c}) \\
C_n &= M_{z_a} / (\bar{q} S b)
\end{aligned}
\qquad (3\text{-}11)
$$

where

$$\bar{q} = \frac{1}{2}\rho V^2$$

Some additional computations were necessary to obtain the true velocity, angle of attack, and angle of sideslip at the center of gravity on the radio controlled model. This was due to the location of the sensors on the nose boom. To transfer α_m, β_m, and V_m as measured at the nose boom to corresponding α_{cg}, β_{cg}, and V_{cg} at the center of gravity (33.1% $\bar{c}$) the following equations were used:

$$
\begin{aligned}
u_{cg} &= V_m \cos\beta_m \cos\alpha_m - q\Delta Z \\
v_{cg} &= V_m \sin\beta_m - r\Delta X + p\Delta Z \\
w_{cg} &= V_m \cos\beta_m \sin\alpha_m + q\Delta X \\
V_{cg} &= \sqrt{u_{cg}^2 + v_{cg}^2 + w_{cg}^2} \\
\alpha_{cg} &= \tan^{-1}\left(\frac{w_{cg}}{u_{cg}}\right) \\
\beta_{cg} &= \sin^{-1}\left(\frac{v_{cg}}{V_{cg}}\right)
\end{aligned}
\qquad (3\text{-}12)
$$

ΔX and ΔZ are the distances from the center of gravity to the nose boom sensors:

ΔX = 5.22 ft

ΔZ = .46 ft

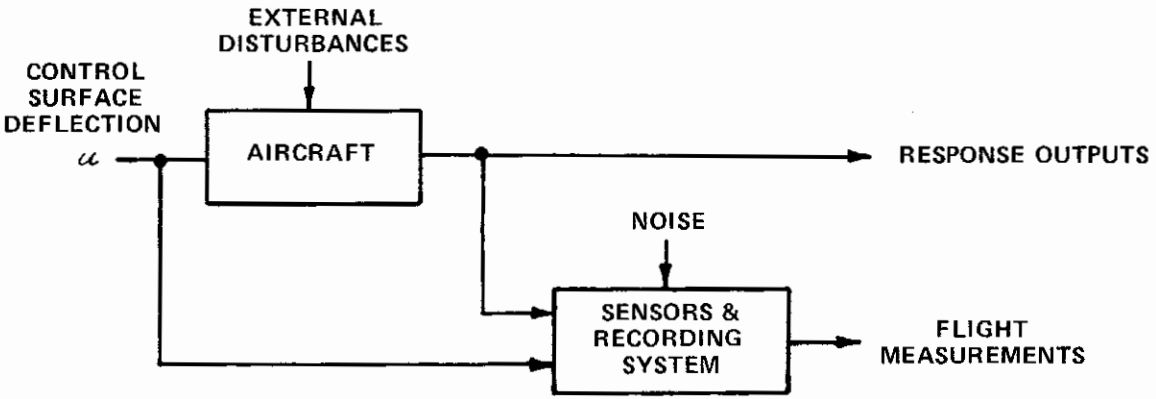

(a) ACTUAL AIRCRAFT

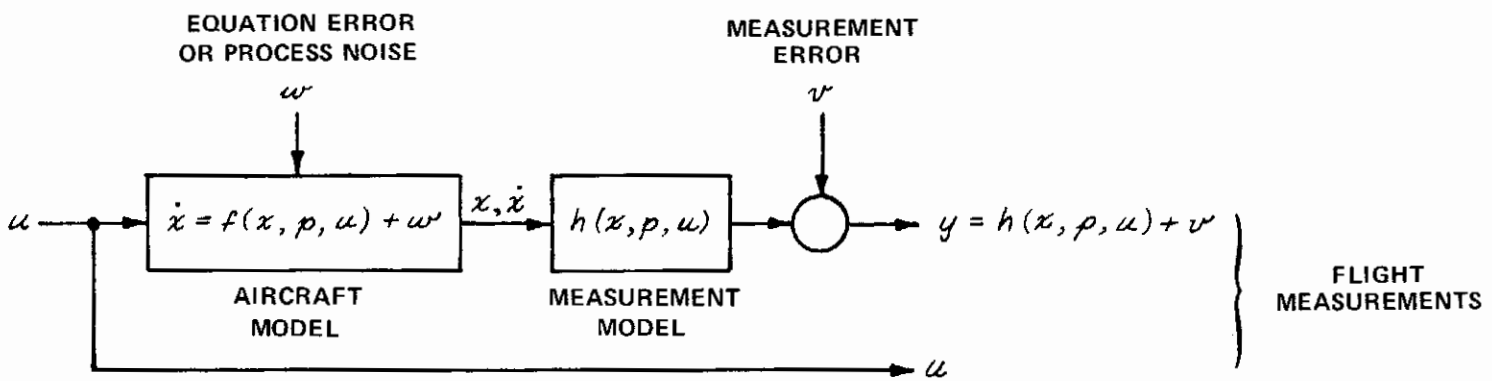

(b) MODEL FOR PARAMETER IDENTIFICATION

Figure 1 BLOCK DIAGRAM OF ACTUAL AIRCRAFT SYSTEM AND MODEL FOR PARAMETER IDENTIFICATION

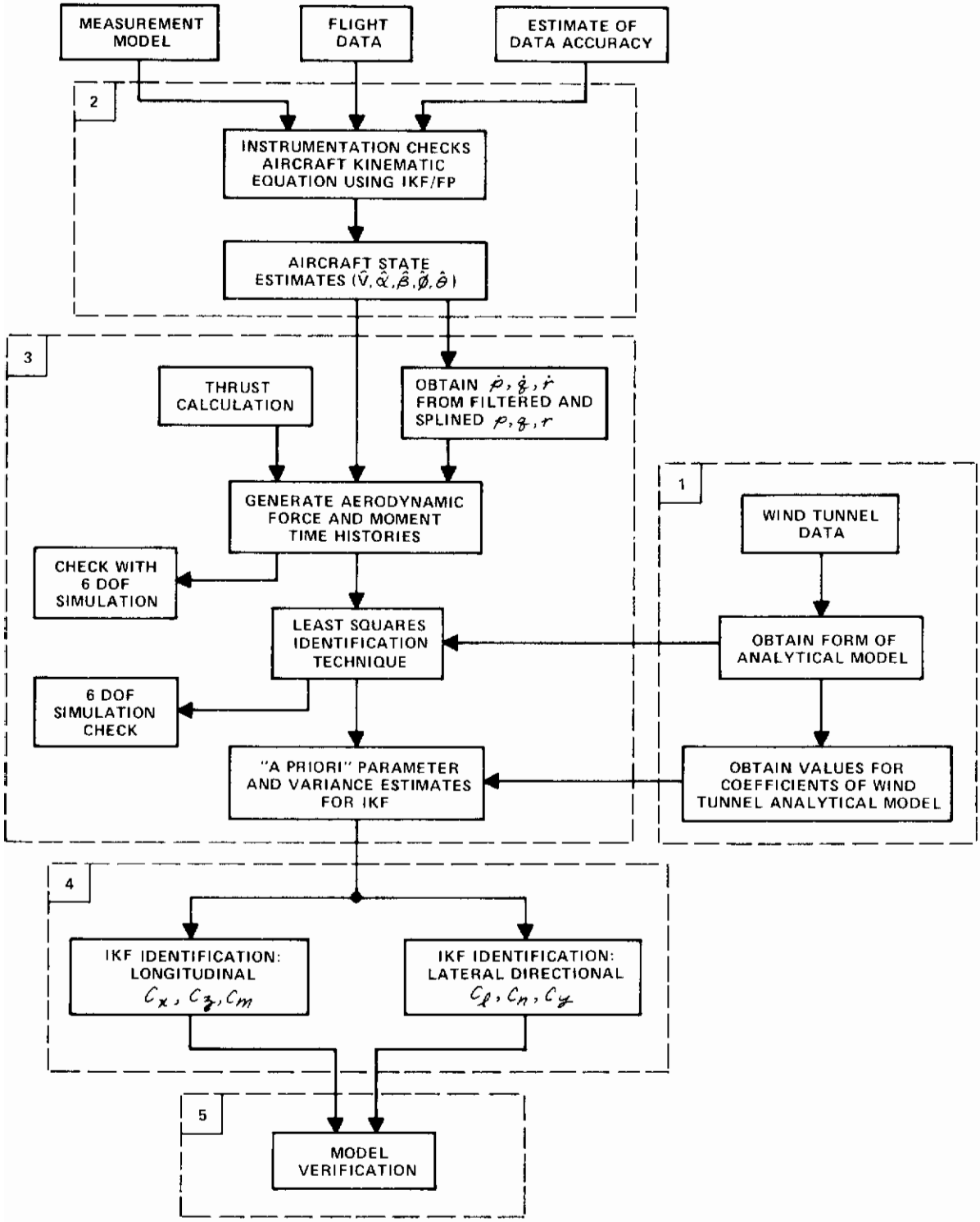

Figure 2 BLOCK DIAGRAM OF GENERAL IDENTIFICATION PROCEDURE

TABLE I

KINEMATIC EQUATIONS FOR INSTRUMENTATION CONSISTENCY CHECKS

Dynamical Model:

$$\begin{bmatrix} \dot{u} \\ \dot{v} \\ \dot{w} \\ \dot{h} \end{bmatrix} = \begin{bmatrix} 0 & \frac{r+r_b}{57.3} & -\frac{q+q_b}{57.3} & 0 \\ -\frac{r+r_b}{57.3} & 0 & \frac{p+p_b}{57.3} & 0 \\ \frac{q+q_b}{57.3} & -\frac{p+p_b}{57.3} & 0 & 0 \\ \sin\theta & -\sin\phi\cos\theta & -\cos\phi\cos\theta & 0 \end{bmatrix} \begin{bmatrix} u \\ v \\ w \\ h \end{bmatrix} + g \begin{bmatrix} -\sin\theta & + n_x \\ \cos\theta\sin\phi & + n_y \\ \cos\theta\cos\phi & + n_z \\ 0 & \end{bmatrix} + \begin{bmatrix} n_{x_b} \\ n_{y_b} \\ n_{z_b} \\ 0 \end{bmatrix}$$

$$+ \frac{1}{57.3} \begin{bmatrix} 0 & -w & v \\ w & 0 & -u \\ -v & u & 0 \\ 0 & 0 & 0 \end{bmatrix} \underbrace{\left[\begin{bmatrix} \omega_4 \\ \omega_5 \\ \omega_6 \end{bmatrix} + \begin{bmatrix} \omega_1 \\ \omega_2 \\ \omega_3 \\ 0 \end{bmatrix} \right]}_{\text{Inherent Process Noise}} + \begin{bmatrix} \text{c.g.} \\ \text{corrections} \\ \text{for} \\ n_x, n_y, n_z \end{bmatrix}$$

$$\begin{bmatrix} \dot{\phi} \\ \dot{\theta} \\ \dot{\psi} \end{bmatrix} = \begin{bmatrix} 1 & \sin\phi\tan\theta & \cos\phi\tan\theta \\ 0 & \cos\phi & -\sin\phi \\ 0 & \frac{\sin\phi}{\cos\theta} & \frac{\cos\phi}{\cos\theta} \end{bmatrix} \underbrace{\begin{bmatrix} p + p_b + \omega_4 \\ q + q_b + \omega_5 \\ r + r_b + \omega_6 \end{bmatrix}}_{\text{Inherent Process Noise}}$$

Measurement System:

$$V_m = (1 + V_S)\left(u^2 + v^2 + w^2\right)^{1/2} + V_b + v_1$$

$$\alpha_{V_m} = 57.3\,(1 + \alpha_S)\,\tan^{-1}\left(\frac{w - 1/57.3\,(q+q_b)\,l_{x_\alpha}}{u}\right) + \alpha_{V_b} + v_2$$

TABLE I Cont.

$$\beta_{V_m} = 57.3\,(1+\beta_S)\tan^{-1}\left(\frac{v + 1/57.3\,(r+r_b)\,l_{x_\beta} - 1/57.3\,(p+p_b)\,l_{y_\beta}}{u}\right) + \beta_{V_b} + v_3$$

$$h_m = h + h_b + v_4$$

$$\phi_m = \phi + \phi_b + v_5$$

$$\theta_m = \theta + \theta_b + v_6$$

$$\psi_m = \psi + \psi_b + v_7$$

Auxiliary Equations:

$$\alpha_{c.g.} = 57.3\,\tan^{-1}\frac{w}{u}$$

$$\beta_{c.g.} = 57.3\,\sin^{-1}\frac{v}{V}$$

$$V = (u^2 + v^2 + w^2)^{1/2}$$

Forcing Inputs:

p, q, r, n_x, n_y and n_z measurements

Definitions and Notes:

Subscripts b - Bias parameters to be identified

Subscripts S - Scale factor parameters to be identified

w_1, w_2, w_3 - Zero mean, white Gaussian process noise, introduced because of measurement noise contaminating n_x, n_y, n_z measurements

w_4, w_5, w_6 - Zero mean, white Gaussian process noise, introduced because of measurement noise contaminating p, q, r measurements

v_i - Zero mean, white Gaussian measurement noise

$l_{x_\alpha}, l_{x_\beta}, l_{y_\beta}$ - Locations of α and β vanes from the c.g. along x, y, z body axes

Accelerometer c.g. corrections are similar to those given in equation (3-6), page 21, but include bias parameters p_b, q_b, r_b.

TABLE II

FOUR-DEGREE-OF-FREEDOM LONGITUDINAL MODEL

Dynamical Model:

$$\dot{V} = \left[\left(b_3 V^2 C_{x_s} + b_4 V C_{x_d} + \frac{T_x}{m}\right)\cos\alpha + \left(b_3 V^2 C_{y_s} + b_4 V C_{y_d} + \frac{T_y}{m}\right)\sin\alpha\right]\cos\beta - g\sin\gamma + g\, n_{y_m}\sin\beta + \omega_1$$

$$\dot{q} = b_1 V^2 C_{m_s} + b_2 V C_{m_d} + I_3\, p_m \cdot r_m + I_4\left(r_m^2 - p_m^2\right) - \frac{h_{I_x}}{I_y} r_m + 57.3\,\frac{m_{y_T}}{I_y} + \omega_2$$

$$\dot{\alpha} = \frac{57.3}{\cos\beta}\left\{\left(b_3 V C_{y_s} + b_4 C_{y_d} + \frac{1}{V}\frac{T_y}{m}\right)\cos\alpha - \left(b_3 V C_{x_s} + b_4 C_{x_d} + \frac{1}{V}\frac{T_x}{m}\right)\sin\alpha\right\} + q + \frac{57.3}{\cos\beta}\,\frac{g}{V}\left(\sin\theta\sin\alpha + \cos\theta\cos\phi\cos\alpha\right) - \left(p_m\cos\alpha + r_m\sin\alpha\right)\tan\beta + \omega_3$$

$$\dot{\beta} = -57.3\sin\beta\left\{\left(b_3 V C_{x_s} + b_4 C_{x_d} + \frac{1}{V}\frac{T_x}{m}\right)\cos\alpha + \left(b_3 V C_{y_s} + b_4 C_{y_d} + \frac{1}{V}\frac{T_y}{m}\right)\sin\alpha + \frac{g}{V}\left(\sin\theta\cos\alpha - \cos\theta\cos\phi\sin\alpha\right)\right\} + 57.3\,\frac{g}{V}\left(n_{y_m} + \cos\theta\sin\phi\right)\cos\beta + p_m\sin\alpha - r_m\cos\alpha + \omega_4$$

$$\dot{\phi} = p_m + \left(q\sin\phi + r_m\cos\phi\right)\tan\theta + \omega_5$$

$$\dot{\theta} = q\cos\phi - r_m\sin\phi + \omega_6\,, \quad \text{for } |\theta| < 90^\circ$$

where $\sin\gamma = \left(\cos\alpha\sin\theta - \sin\alpha\cos\phi\cos\theta\right)\cos\beta - \sin\phi\cos\theta\sin\beta$

Measurement System:

$$V_m = V + v_1$$

$$q_m = q + v_2$$

$$\alpha_m = \alpha + v_3$$

TABLE II Cont.

$$\beta_m = \beta + v_4$$

$$\phi_m = \phi + v_5$$

$$\theta_m = \theta + v_6$$

$$n_{z_m} = \frac{1}{g}\left(b_3 V^2 C_{z_s} + b_4 V C_{z_d} + \frac{T_z}{m}\right) + v_7$$

$$\dot{q}_m = b_1 V^2 C_{m_s} + b_2 V C_{m_d} + I_3 p_m \cdot r_m + I_4 (r_m^2 - p_m^2) - \frac{h_{ex}}{I_y} r_m + 57.3 \frac{m_{y_T}}{I_y} + v_8$$

$$n_{x_m} = \frac{1}{g}\left(b_3 V^2 C_{x_s} + b_4 V C_{x_d} + \frac{T_x}{m}\right) + v_9$$

Control or Forcing Inputs: δ_s, δ_a, T_x, T_z, m_{y_T}, ρ

Cross-Coupling Inputs: p_m, r_m, n_{y_m} (at c.g.)

Definitions:

$$b_1 = \frac{S\bar{c}}{2I_y}\rho$$

$$b_2 = \frac{1}{2}\bar{c}\, b_1$$

$$b_3 = \frac{1}{2}\frac{S}{m}\rho$$

$$b_4 = \frac{\bar{c}}{2} b_3$$

$$I_3 = \frac{I_z - I_x}{57.3\, I_y}$$

$$I_4 = \frac{I_{xz}}{57.3\, I_y}$$

$C_{x_s}, C_{z_s}, C_{m_s}$ - Static Force or Moment Aerodynamic Coefficient; functions of parameters to be identified

$C_{x_d}, C_{z_d}, C_{m_d}$ - Dynamic or Rotary Aerodynamic Coefficients; functions of parameters to be identified

w_i, v_i - Zero mean, white Gaussian process and measurement noise

T_x, T_z - Thrust force along x and z body axes

m_{y_T} - Thrust moment around y axis

TABLE III

FOUR-DEGREE-OF-FREEDOM LATERAL-DIRECTIONAL MODEL

Dynamical Model:

$$\dot{p} = d_1 V^2 C_{\ell_\delta} + d_2 V C_{\ell_d} + d_3 V^2 C_{n_\delta} + d_4 V C_{n_d} + I'_{g} m_{x_T} + I'_{xg} m_{g_T} + (I_1 r + I_2 p + I'_{xg} h_{\ell_x}) q_m + \omega_1$$

$$\dot{r} = d_3 V^2 C_{\ell_\delta} + d_4 V C_{\ell_d} + d_5 V^2 C_{n_\delta} + d_6 V C_{n_d} + I'_{xg} m_{x_T} + I'_{x} m_{g_T} + (I_6 p - I_2 r + I'_{x} h_{\ell_x}) q_m + \omega_2$$

$$\dot{\beta} = \frac{57.3 g}{V} \left\{ \left[(\sin\theta - n_{x_m}) \cos\alpha - (\cos\theta \cos\phi + n_{g_m}) \sin\alpha \right] \sin\beta + \cos\theta \sin\phi \cos\beta \right\} + 57.3 \cos\beta \left(d_7 V C_{y_\beta} + d_8 C_{y_d} + \frac{1}{V} \frac{T_y}{m} \right) + p \sin\alpha - r \cos\alpha + \omega_3$$

$$\dot{\alpha} = \frac{57.3 g}{V \cos\beta} \left\{ (\sin\theta - n_{x_m}) \sin\alpha + (\cos\theta \cos\phi + n_{g_m}) \cos\alpha \right\} - (p \cos\alpha + r \sin\alpha) \tan\beta + q_m + \omega_4$$

$$\dot{\phi} = p + (q_m \sin\phi + r \cos\phi) \tan\theta + \omega_5$$

$$\dot{\theta} = q_m \cos\phi - r \sin\phi + \omega_6 , \quad \text{for } |\theta| < 90°$$

Measurement System:

$$p_m = p + v_1$$

$$r_m = r + v_2$$

$$\beta_m = \beta + v_3$$

$$\alpha_m = \alpha + v_4$$

$$\phi_m = \phi + v_5$$

$$\theta_m = \theta + v_6$$

TABLE III CONT.

$$\dot{p}_m = d_1 V^2 C_{\ell_\delta} + d_2 V C_{\ell_d} + d_3 V^2 C_{n_\delta} + d_4 V C_{n_d} + I'_{\ell} m_{\ell_T} + I'_{\ell n} m_{n_T} + (I_1 r + I_2 p + I'_{\ell n} h_{\ell_\ell}) q_m + v_7$$

$$\dot{r}_m = d_3 V^2 C_{\ell_\delta} + d_4 V C_{\ell_d} + d_5 V^2 C_{n_\delta} + d_6 V C_{n_d} + I'_{\ell n} m_{\ell_T} + I'_{\ell} m_{n_T} + (I_6 p - I_2 r + I'_{\ell} h_{\ell_\ell}) q_m + v_8$$

$$n_{y_m} = \frac{1}{g}\left(d_7 V^2 C_{y_\delta} + d_8 V C_{y_d} + \frac{T_y}{m}\right) + v_9$$

Control or Forcing Inputs: δ_r, δ_a, δ_s, T_y, ρ, m_{ℓ_T}, m_{n_T}

Cross-Coupling Inputs: q_m, V, n_{ℓ_m}, n_{y_m} (at c.g.)

Definitions:

$$d_1 = \frac{1}{2} S b I'_n \rho \qquad d_5 = \frac{1}{2} S b I'_{\ell} \rho$$

$$d_2 = \frac{1}{2} b d_1 \qquad d_6 = \frac{1}{2} b d_5$$

$$d_3 = \frac{1}{2} S b I'_{\ell n} \rho \qquad d_7 = \frac{1}{2} \frac{S}{m} \rho$$

$$d_4 = \frac{1}{2} b d_3 \qquad d_8 = \frac{1}{2} b d_7$$

$$I_1 = \frac{I_n (I_y - I_n) - I_{\ell n}^2}{I_\ell \cdot I_n - I_{\ell n}^2} \frac{1}{57.3}$$

$$I_2 = \frac{I_{\ell n} (I_n + I_\ell - I_y)}{I_\ell \cdot I_n - I_{\ell n}^2} \frac{1}{57.3}$$

$$I_6 = \frac{I_\ell (I_\ell - I_y) + I_{\ell n}^2}{I_\ell \cdot I_n - I_{\ell n}^2} \frac{1}{57.3}$$

$$I'_\ell = \frac{I_\ell}{I_\ell I_n - I_{\ell n}^2}$$

$$I'_n = \frac{I_n}{I_\ell I_n - I_{\ell n}^2}$$

$$I'_{\ell n} = \frac{I_{\ell n}}{I_\ell I_n - I_{\ell n}^2}$$

TABLE III CONT.

$C_{l_s}, C_{n_s}, C_{y_s}$ - Static Aerodynamic Coefficients; function of parameters (and states) to be identified

$C_{l_d}, C_{n_d}, C_{y_d}$ - Dynamic or Rotary Aerodynamic Coefficients; functions of parameters (and states) to be identified

T_y - Thrust force along y-body axis

m_{x_T}, m_{z_T} - Thrust moment around x, z body axes

w_i, v_i - Zero mean, white Gaussian process and measurement noise

Section IV

DEVELOPMENT OF THE ANALYTICAL WIND TUNNEL MODEL

For identification purposes, it is necessary to have a description of the system to be identified which is amenable for use in the identification algorithms to be used. Consequently, an analytical representation of the wind tunnel data was developed to model the aerodynamics of the F-4. These models served to establish an initial model form for use in the identification algorithms and to ascertain how well a simulation using wind tunnel test data exclusively could predict the actual responses of the F-4.

This section describes the development of this analytical model. The model derived is given and comparisons between the flight data and the responses generated with the analytical model using the measured aircraft control surface deflections as inputs are presented.

4.1 DATA SOURCES

The majority of the wind tunnel data was obtained from two NASA reports (References 10 and 11) and accompanying data tabulations from a series of tests in the Langley Full-Scale Wind Tunnel. TN-6425 dealt with the static coefficients and TN-6091 with the dynamic coefficients. These reports were chosen because they gave a fairly complete description of the F-4's aerodynamic coefficients. Both sets of tests were consistent with each other because they were conducted on the same model at identical Reynolds number in the same wind tunnel. Other corroborating data came from a few additional NASA reports on the F-4 at high angles of attack (References 12, 13, 14). Two McDonnell-Douglas reports were also used to obtain some full scale data for comparison (References 15 and 16). Reference 15 also yielded additional wind tunnel data from an Ames series of wind tunnel tests for the static coefficients and a Langley set of tests for the rotary derivatives. However, these tests were conducted in different wind tunnels, with different models and at different Reynolds numbers. The models used were a 1/15th scale model of an F-4D and 1/11th scale model of an F-4B. Consequently, the data from Reference 15, which will hereinafter be referred to as the Ames data, were used only for comparison purposes.

Since this study was concerned with only post-stall characteristics and not fully developed spins, full scale flight data and radio controlled drop model data were obtained with angles of attack of less than fifty-five degrees and magnitudes of sideslip of less than twenty degrees. Therefore, analytical models were only developed for this range of interest.

4.2 ANALYTICAL REPRESENTATION

The analytical representations of the wind tunnel nondimensional aerodynamic coefficients were chosen over other representations, such as trigometric and exponential functions, for example, for the following reasons:

- There were computer programs available to fit polynomial expansions to tabulated data as functions of two variables.

- The polynomial representations were easily inserted into our parameter identification computer programs, especially the least squares technique which requires that the representation be linear in the unknown parameters.

To determine the form and order of the polynomial fit that was to be used for each coefficient, the tabulated wind tunnel data were first cross plotted versus angle of attack and sideslip separately. By looking at the shapes of these curves it could be approximately determined what form the polynomial expansion should take. That is, does the data look independent of β and at least cubic in α ? From these engineering judgements a least squares polynomial fit program was used to determine the values of the coefficients. The order of the polynomial was increased until it appeared that the extra terms added did not significantly improve the fit to the data. All data is referenced to the body axes system.

If one expansion were to be used for each coefficient for the entire range of angle of attack, some coefficients would need fifth order expansions. This would become unwieldy and some of the higher order terms would be very difficult to identify in this form. Therefore some simplifications were made.

First of all the data was broken up into three ranges of angles of attack and separate analytical models were obtained for each range. Natural breaks in the data seemed to appear at 15 degrees and 30 degrees. Therefore, three ranges were chosen as:

$$0^{\circ} \leq \alpha \leq 15^{\circ}$$
$$15^{\circ} \leq \alpha \leq 30^{\circ}$$
$$30^{\circ} \leq \alpha \leq 55^{\circ}$$

In this way, the polynomial expansions could be limited to α^2 and β^3 terms as the highest order terms, to adequately define the wind tunnel model's characterisitcs. It should be noted that this work preceded the detailed analysis of the full scale flight test data. It was initially believed that the flight data available, although limited, were consistent with these chosen ranges of model applicability. Later in the program it was determined this was not the case and the ranges were subsequently changed to:

$$10^{\circ} \leq \alpha \leq 20^{\circ}$$
$$20^{\circ} \leq \alpha \leq 40^{\circ}$$

for identification purposes.

Modeling the wind tunnel data in this way did not limit the identification of the flight data to these specific ranges. The

form of the models would be the same for different ranges of angle of attack as long as the range was not too large. The specific values of the identified coefficients, such as $C_{n_{\alpha^2\beta}}$, of course could not be compared directly to the wind tunnel values. However, the shape of the lumped parameter [e.g.: $C_{n_\beta}(\alpha) = C_{n_\beta} + (C_{n_{\alpha\beta}})\alpha + (C_{n_{\alpha^2\beta}})\alpha^2$] could be plotted against the wind tunnel derived curves in the appropriate range of angle of attack for comparison.

Another simplification was to eliminate all aerodynamic asymmetries in the analytical model, that is, all β^0 and β^2 terms were dropped in the lateral-directional coefficients and β^1 terms in the longitudinal coefficients. The physical wind tunnel model was supposed to be symmetrical and there was no way of determining the full scale aircraft's asymmetries, a priori. In fact, Reference 15 states that two supposedly identical F-4's exhibited different spin characteristics that could be due to different aerodynamic asymmetries in the aircraft. Therefore, when computer integrations were run with the wind tunnel values to match flight test time histories, no asymmetries were used. However, lateral-directional asymmetries at zero sideslip (i.e.: C_{y_o}, C_{ℓ_o}, and C_{n_o}) were not deleted from the identification schemes and these characteristics could be extracted from the flight data. In the following paragraphs, examples are given to the above procedure.

Figure 3, taken from Reference 10, shows the static longitudinal coefficients plotted versus α at $\beta = 0^o$. Figure 4 shows C_m plotted versus β at various values of α. Looking at the C_m versus α curve in the ranges of 0 to 15, 15 to 30, and 30 to 55 degrees it appeared that C_m could be defined as a linear function of α in each range. Also it appears that at a constant angle of attack C_m is quadratic in β up to $\alpha \cong 30^o$ and looks independent of β beyond $\alpha \cong 30^o$. This was borne out when least squares polynomial fits were obtained for these data.

Similarly, the lateral-directional static coefficients are shown in Figure 5(a) versus β at $\alpha = 30^o$. Similar curves are presented in Reference 10 for other angles of attack. It appeared that C_n, for example, was a cubic function of β for $|\beta| < 20^o$. The curves at other values of α showed the same trends. Figure 5(b), C_η versus α at various values of β indicated independence of α in the low α range, and perhaps linear in α in the other ranges. This also was verified with the least squares polynomial fits, where more complex representations did not significantly improve the fit error.

The polynomial fits for the rotary derivatives were calculated in the same manner. However, there was no data taken at any other values of β than zero, so no relationship with β could be determined. Figure 6 shows some of the major rotary derivatives as a function of α. The data available in the wind tunnel reports were taken at various values of frequency and amplitudes in the oscillation tests. For the polynomial fits, only the lowest frequency and amplitude test values were used, as it was felt that these values were closer to the true rotary derivatives than the test points taken at higher frequencies and amplitudes.

The analytical representation for the control derivatives were obtained from data taken for small positive surface deflections around the neutral position. There was some data available that gave surface effectiveness at full deflections. This data indicated that the surface effectiveness did fall off somewhat at large deflections. However, since most of the flight data available for analysis did not have large control deflections, it was decided to use the small deflection values without any changes. Figure 7 shows $C_{l_{\delta_a}}$ versus α and β . The extreme data point scatter is readily apparent, especially due to β . Similar polynomial representations were obtained to approximate all of the wind tunnel data.

Because of the inability to separate $\dot{\alpha}$ and $\dot{\beta}$ effects from the rotary derivatives, the following approximations were made:

$$C_{m_q} = C_{m_q} + C_{m_{\dot{\alpha}}}$$

$$C_{z_q} = C_{z_q} + C_{z_{\dot{\alpha}}}$$

$$C_{x_q} = C_{x_q} + C_{x_{\dot{\alpha}}}$$

$$C_{y_p} = C_{y_p} + C_{y_{\dot{\beta}}} \sin\alpha$$

$$C_{n_p} = C_{n_p} + C_{n_{\dot{\beta}}} \sin\alpha$$

$$C_{l_p} = C_{l_p} + C_{l_{\dot{\beta}}} \sin\alpha$$

$$C_{y_r} = C_{y_r} - C_{y_{\dot{\beta}}} \cos\alpha$$

$$C_{n_r} = C_{n_r} - C_{n_{\dot{\beta}}} \cos\alpha$$

$$C_{l_r} = C_{l_r} - C_{l_{\dot{\beta}}} \cos\alpha$$

where the terms on the right hand side of the above equations are the actual coefficients.

The results of this analysis are the following analytical models for the aerodynamics of the F-4 (all states are in degrees and the moment data re-referred to a center-of-gravity position of .33 $\bar{c}$). Note that for simulation purposes, the lumped C_{m_q} derivative was separated into a C_{m_q} and $C_{m_{\dot{\alpha}}}$ derivative.

α-Range: $0° \leq \alpha \leq 15°$

$$C_{x_{Aero}} = -.0434 + 2.39 \times 10^{-3}\alpha + 2.53 \times 10^{-5}\beta^2 - 1.07 \times 10^{-6}\alpha\beta^2$$
$$- 9.5 \times 10^{-4}\delta_e + 8.5 \times 10^{-7}\delta_e\beta^2$$
$$+ \bar{c}/(2V)\left\{8.73 \times 10^{-3}q + .001q\alpha - 1.75 \times 10^{-4}q\alpha^2\right\}$$

$$C_{y_{Aero}} = -.012\beta - 1.55 \times 10^{-3}\delta_r + 8. \times 10^{-6}\delta_r\alpha$$
$$+ b/(2V)\left\{2.25 \times 10^{-3}p + .0117r - 3.67 \times 10^{-4}r\alpha\right.$$
$$\left. - 1.75 \times 10^{-4}r\delta\right\}$$

$$C_{z_{Aero}} = -.131 - .0538\alpha + 4.76 \times 10^{-3}\delta_e + 3.3 \times 10^{-5}\delta_e\alpha$$
$$- 7.5 \times 10^{-5}\delta_a^2$$
$$+ \bar{c}/(2V)\left\{-.111q + 5.17 \times 10^{-3}q\alpha - 1.1 \times 10^{-3}q\alpha^2\right\}$$

$$C_{l_{Aero}} = -5.98 \times 10^{-4}\beta - 2.83 \times 10^{-4}\alpha\beta + 1.51 \times 10^{-5}\alpha^2\beta$$
$$+ 6.1 \times 10^{-4}\delta_a + 2.5 \times 10^{-5}\delta_a\alpha - 2.6 \times 10^{-6}\delta_a\alpha^2$$
$$- 2.3 \times 10^{-4}\delta_r + 4.5 \times 10^{-6}\delta_r\alpha$$
$$+ b/(2V)\left\{-4.12 \times 10^{-3}p - 5.24 \times 10^{-4}p\alpha + 4.36 \times 10^{-5}p\alpha^2\right.$$
$$\left. + 4.36 \times 10^{-4}r + 1.05 \times 10^{-4}r\alpha - 5.24 \times 10^{-5}r\delta_e\right\}$$

$$C_{m_{Aero}} = -6.61 \times 10^{-3} - 2.67 \times 10^{-3}\alpha - 6.48 \times 10^{-5}\beta^2$$
$$- 2.65 \times 10^{-6}\alpha\beta^2 + 6.54 \times 10^{-3}\delta_e + 8.49 \times 10^{-5}\delta_e\alpha$$
$$- 3.74 \times 10^{-6}\delta_e\beta^2 - 3.5 \times 10^{-5}\delta_a^2$$
$$+ \bar{c}/(2V)\left\{-.0473q - 1.57 \times 10^{-3}q\alpha - .0273\dot{\alpha}\right.$$
$$\left. - .87 \times 10^{-3}\dot{\alpha}\alpha\right\}$$

$$C_{n_{Aero}} = 2.28 \times 10^{-3}\beta + 1.79 \times 10^{-6}\beta^3 - 1.4 \times 10^{-5}\delta_a - 7. \times 10^{-6}\delta_a\alpha + 9. \times 10^{-4}\delta_r - 4. \times 10^{-6}\delta_r\alpha + b/(2V)\left\{-6.63 \times 10^{-5}p - 1.92 \times 10^{-5}p\alpha + 5.06 \times 10^{-6}p\alpha^2 - 6.06 \times 10^{-3}r + 8.73 \times 10^{-5}r\delta_e - 8.7 \times 10^{-6}r\delta_e\alpha\right\}$$

α-Range: $15° \leq \alpha \leq 30°$

$$C_{x_{Aero}} = .141 - .0154\alpha + 2.96 \times 10^{-4}\alpha^2 - 3.72 \times 10^{-4}\beta^2 + 4.14 \times 10^{-5}\alpha\beta^2 - 9.12 \times 10^{-7}\alpha^2\beta^2 - 1.82 \times 10^{-3}\delta_e + 7.3 \times 10^{-5}\delta_e\alpha + \bar{c}/(2V)\left\{-.0602q + 2.04 \times 10^{-3}q\alpha\right\}$$

$$C_{y_{Aero}} = -2.08 \times 10^{-2}\beta + 6.07 \times 10^{-4}\alpha\beta + 2.37 \times 10^{-6}\beta^3 - 3.64 \times 10^{-7}\alpha\beta^3 - 2.3 \times 10^{-3}\delta_r + 5.9 \times 10^{-5}\delta_r\alpha + b/(2V)\left\{-1.62 \times 10^{-3}p + 3.32 \times 10^{-4}p\alpha + .0311r - 1.4 \times 10^{-3}r\alpha - 1.75 \times 10^{-4}r\delta_e\right\}$$

$$C_{z_{Aero}} = -.608 - .022\alpha + 6.77 \times 10^{-3}\delta_e - 9.7 \times 10^{-5}\delta_e\alpha - 7.5 \times 10^{-5}\delta_a^2 + \bar{c}/(2V)\left\{1.136q - .1418q\alpha + 3.11 \times 10^{-3}q\alpha^2\right\}$$

$$C_{\ell_{Aero}} = -1.29 \times 10^{-2}\beta + 1.04 \times 10^{-3}\alpha\beta - 2.02 \times 10^{-5}\alpha^2\beta + 1.36 \times 10^{-5}\beta^3 - 1.13 \times 10^{-6}\alpha\beta^3 + 2.01 \times 10^{-8}\alpha^2\beta^3 + 7.74 \times 10^{-4}\delta_a - 1.9 \times 10^{-5}\delta_a\alpha - 2. \times 10^{-4}\delta_r + 5. \times 10^{-6}\delta_r\alpha + b/(2V)\left\{2.78 \times 10^{-3}p - 2.79 \times 10^{-4}p\alpha - 6.81 \times 10^{-3}r + 6.46 \times 10^{-4}r\alpha - 5.24 \times 10^{-5}r\delta_e\right\}$$

$$C_{m_{Aero}} = .0549 - 6.08 \times 10^{-3}\alpha - 1.69 \times 10^{-4}\beta^2 + 5.64 \times 10^{-7}\alpha\beta^2 + 8.14 \times 10^{-3}\delta_e - 1.1 \times 10^{-4}\delta_e\alpha - 3.5 \times 10^{-5}\delta_a^2 + \bar{c}/(2V)\left\{-.0951q + 1.4 \times 10^{-3}q\alpha - .0479\dot{\alpha} + 6.9 \times 10^{-4}\dot{\alpha}\alpha\right\}$$

$$C_{n_{Aero}} = 1.02 \times 10^{-2}\beta - 5.12 \times 10^{-4}\alpha\beta - 5.27 \times 10^{-6}\beta^3 + 3.79 \times 10^{-7}\alpha\beta^3 - 9.1 \times 10^{-5}\delta_a - 3. \times 10^{-6}\delta_a\alpha + 1.37 \times 10^{-3}\delta_r - 3.8 \times 10^{-5}\delta_r\alpha + b/(2V)\left\{.0236p - 2.5 \times 10^{-3}p\alpha + 6.25 \times 10^{-5}p\alpha^2 + 6.2 \times 10^{-4}r - 4.89 \times 10^{-4}r\alpha + 8.73 \times 10^{-5}r\delta_e - 8.7 \times 10^{-6}r\alpha\delta_e\right\}$$

α-Range: $30° \leq \alpha \leq 55°$

$$C_{x_{Aero}} = -.0326 - 2.16 \times 10^{-3}\alpha + 4.89 \times 10^{-5}\alpha^2 - 1.24 \times 10^{-4}\beta^2 + 1.076 \times 10^{-5}\alpha\beta^2 - 1.54 \times 10^{-7}\alpha^2\beta^2 - 7.5 \times 10^{-4}\delta_e + 3.9 \times 10^{-5}\delta_e\alpha + \bar{c}/(2V)\left\{-.026q + 8.73 \times 10^{-4}q\alpha\right\}$$

$$C_{y_{Aero}} = -2.095 \times 10^{-3}\beta - 6.36 \times 10^{-5}\alpha\beta - 2.15 \times 10^{-5}\beta^3 + 5.42 \times 10^{-7}\alpha\beta^3 - 1.4 \times 10^{-3}\delta_r + 2.6 \times 10^{-5}\delta_r\alpha + b/(2V)\left\{.196p - 9.27 \times 10^{-3}p\alpha + 1.01 \times 10^{-4}p\alpha^2 + .0326r - 2.55 \times 10^{-3}r\alpha + 3.26 \times 10^{-5}r\alpha^2 - 1.75 \times 10^{-4}r\delta_e\right\}$$

$$C_{z_{Aero}} = -.891 - .01146\alpha - 6.2 \times 10^{-3}\delta_e + 5.4 \times 10^{-3}\delta_e\alpha - 6.2 \times 10^{-6}\delta_e\alpha^2 - 7.5 \times 10^{-5}\delta_a^2 + \bar{c}/(2V)\left\{.589q - .0494q\alpha + 6.11 \times 10^{-4}q\alpha^2\right\}$$

$$C_{l_{Aero}} = 1.18 \times 10^{-2}\beta - 5.29 \times 10^{-4}\alpha\beta + 4.88 \times 10^{-6}\alpha^2\beta - 2.2 \times 10^{-5}\beta^3 + 9.05 \times 10^{-7}\alpha\beta^3 - 9.08 \times 10^{-9}\alpha^2\beta^3 + 5. \times 10^{-5}\delta_a - 9. \times 10^{-5}\delta_r + 1.8 \times 10^{-6}\delta_r\alpha + b/(2V)\left\{-.0428p + 1.82 \times 10^{-3}p\alpha - 1.94 \times 10^{-5}p\alpha^2 + .073r - 3.02 \times 10^{-3}r\alpha + 3.14 \times 10^{-5}r\alpha^2 - 5.24 \times 10^{-5}r\delta_e\right\}$$

$$C_{m_{Aero}} = 7.3 \times 10^{-3} - 5.5 \times 10^{-3}\alpha + 7.93 \times 10^{-3}\delta_e - 8.23 \times 10^{-5}\delta_e\alpha - 3.5 \times 10^{-5}\delta_a^2 + \bar{c}/(2V)\left\{+.16q - .0101q\alpha + 1.05 \times 10^{-4}q\alpha^2 + .08\dot{\alpha} - .005\dot{\alpha}\alpha + 5.2 \times 10^{-5}\dot{\alpha}\alpha^2\right\}$$

$$
\begin{aligned}
C_{n_{Aero}} = & - 9.23 \times 10^{-3}\beta + 1.52 \times 10^{-4}\alpha\beta + 1.62 \times 10^{-5}\beta^3 \\
& - 3.46 \times 10^{-7}\alpha\beta^3 - 1.5 \times 10^{-4}\delta_a + 6.8 \times 10^{-4}\delta_r \\
& - 1.2 \times 10^{-5}\delta_r\alpha + 1.67 \times 10^{-4}\delta_e\beta - 5.56 \times 10^{-6}\delta_e\alpha\beta \\
& - 3.81 \times 10^{-7}\delta_e\beta^3 + 1.27 \times 10^{-8}\delta_e\alpha\beta^3 \\
& + b/(2V)\left\{.0385p - 1.73 \times 10^{-3}p\alpha + 1.92 \times 10^{-5}p\alpha^2\right. \\
& - .0202r + 3.67 \times 10^{-4}r\alpha - 2.58 \times 10^{-3}r\delta_e \\
& \left. + 1.31 \times 10^{-4}r\delta_e\alpha - 1.69 \times 10^{-6}r\delta_e\alpha^2\right\}
\end{aligned}
$$

Figures 6 and 7 are typical examples of the accuracy to which these analytical expressions approximate the wind tunnel data points. Hand faired reference plots of the wind tunnel data, compared to the actual data points, are given in Appendix IV for restricted conditions. Also shown for comparison are the hand faired plots of the wind tunnel data from Reference 15 (Ames data). The major physical difference in these sets of tests and the radio controlled drop model and full scale flight test data are given below.

	Langley	Ames		Drop Model	Aircraft**
		Static	Rotary		
Model Size	13%*	7%	9%	13%*	100%
Reynolds No.	1.4×10^6	4.0×10^6	$.45 \times 10^6$	$\approx 3.0 \times 10^6$	$\approx 17.0 \times 10^6$
Mach No.	.1	.2	.07	.14 - .22	.32 - .47

* Same model.
** Not clean loading.

4.3 ERROR SOURCES IN ANALYTICAL MODEL

Although a fairly complete analytical model of the F-4's aerodynamic characteristics was developed from the wind tunnel data, there are some possible sources of errors to be noted when comparing time histories developed from it to flight test data.

First of all, the Reynolds number in the wind tunnel test was 1.4×10^6 while in the radio controlled drop model tests it was approximately $3. \times 10^6$ and in the full-scale flight tests it averaged about $17. \times 10^6$.

Figure 8, from Reference 13, shows that there are differences in the Langley wind tunnel test results between Reynolds numbers of .5 x 10^6 and 4.3 x 10^6; especially in C_{n_β}. Reference 15 also indicates the critical Reynolds number for the Ames series of tests is near 4.0 x 10^6. Consequently, the flight test results may differ appreciably from those from the wind tunnel tests, due to Reynolds number effects alone.

Another source of error could be Mach effects. The wind tunnel data was taken at relatively low speed where the flow could be assumed to be incompressible. Most of the flight test data was also obtained at less than Mach .5 before compressibility or Mach effects start taking place. There were, however, some flight data up to Mach .7 where some differences could develop between the wind tunnel and full-scale coefficients.

Physical differences between the wind tunnel models and the full-scale aircraft can be a significant source of errors. It has been noted that small irregularities on the model or full-scale aircraft can result in completely different spin characteristics (References 15 and 25). There most likely are some physical asymmetries on the full-scale aircraft that the analytical model cannot possibly describe. This may hinder the accurate time history matching of flight data with the analytical model. Other physical differences between the models and full-scale aircraft are the stores loading, spin chute modification to the aft fuselage, and mass flow effects through the engines.

Uncertainties in the actual flight vehicle itself may cause problems in matching time histories. The weight, inertias, and center of gravity location are all important parameters that can cause errors if not known accurately.

Deficiencies in the wind tunnel data also exist which can cause some inaccurate modeling. There was not enough information to obtain a complete description of the interference effects of one control surface on another. Some data was available with full pro-spin or anti-spin control on the aircraft but none with smaller deflections like those which exist in the flight data. Although they probably are small, there was no wind tunnel data available on longitudinal effects of aileron and rudder, except for some lift and pitching moment effects due to aileron control. In addition, the dynamic derivatives were only given as functions of angle of attack. Therefore, there was no way to model these coefficients as functions of sideslip or nonlinear functions of the angular rates themselves.

4.4 RESPONSE COMPARISONS

The analytical model derived from the Langley wind tunnel data was used to generate responses to match the flight data responses. The six-degree-of-freedom simulation computer program described in Appendix III was used along with the control inputs and thrust calculated from the flight data. Initially very poor response matches were obtained. When trying to trim the airplane to the initial condition on the flight tape, large increments in forces and mo-

ments were found necessary. From preliminary identification runs, it was discovered that there were consistent offsets in the static C_x, C_y and C_m coefficients. In addition, the elevator effectiveness was shown to be higher in the Ames test and some of the identification runs. There also appeared to be a consistent C_{l_o} offset at the low angles of attack but not at the higher values. These offsets were approximated by:

$$\Delta C_{x_o} = +0.05$$

$$\Delta C_{y_o} = +0.15$$

$$\Delta C_{n_o} = +0.05$$

Responses were again generated with the above offsets and the results are shown in Figures 9 through 13. The response matches were much better than before, but they still could be considered as poor comparisons to the flight data. It can be concluded that the wind tunnel data by itself is not enough to predict in-flight high angle of attack responses.

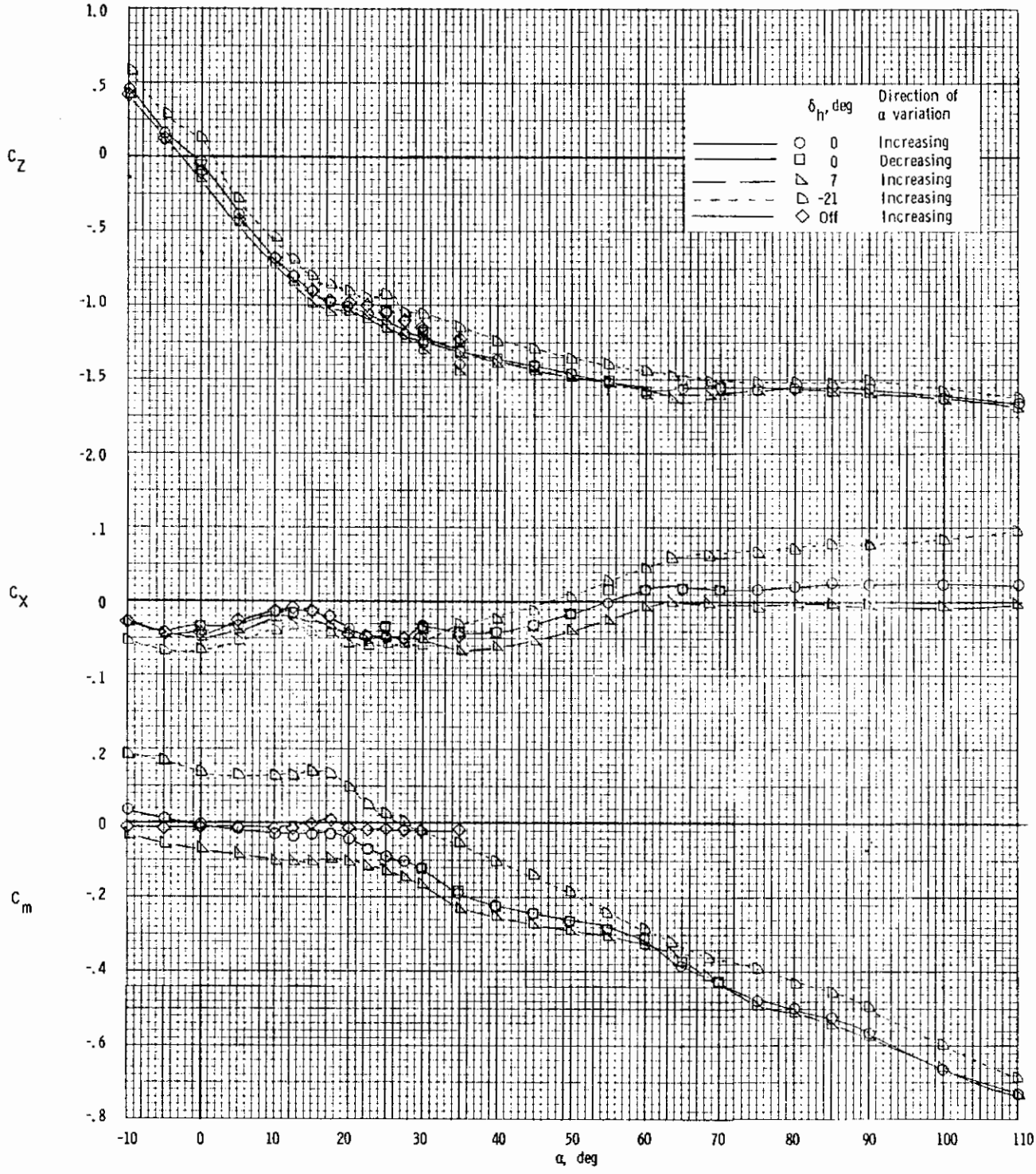

Figure 3 F-4 LONGITUDINAL COEFFICIENTS vs α ($\beta = 0^o$)

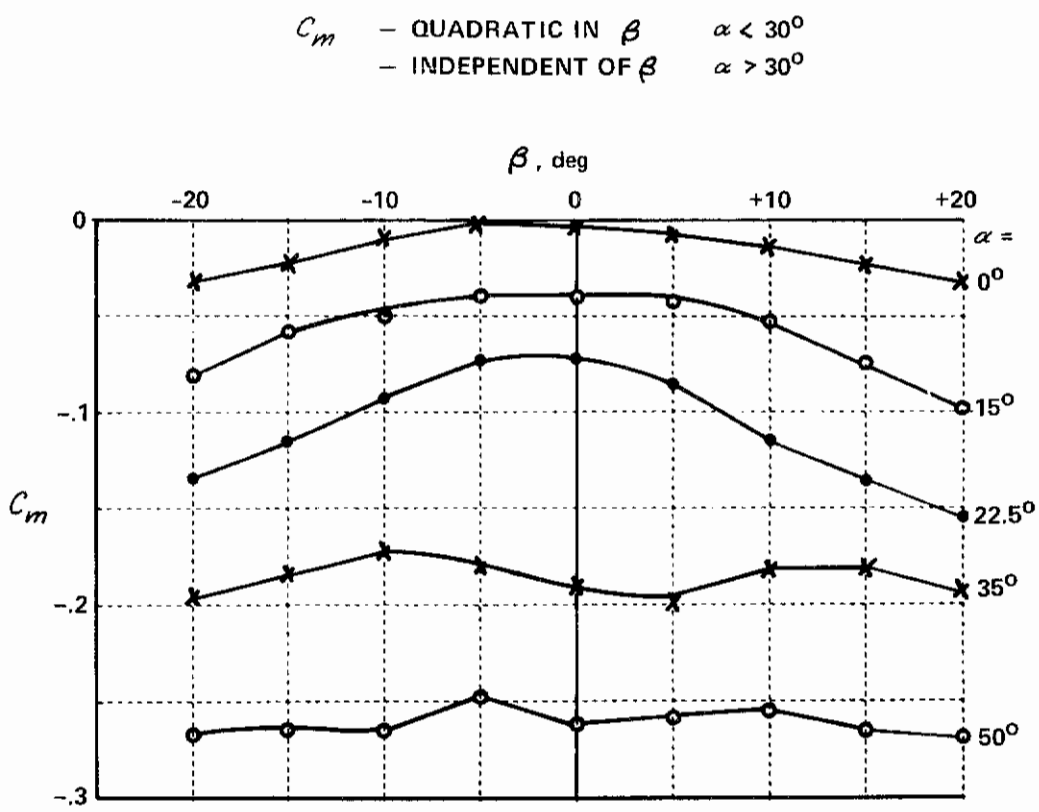

Figure 4 F-4 C_m vs β AT VARIOUS α
REF: NASA-TN-6425

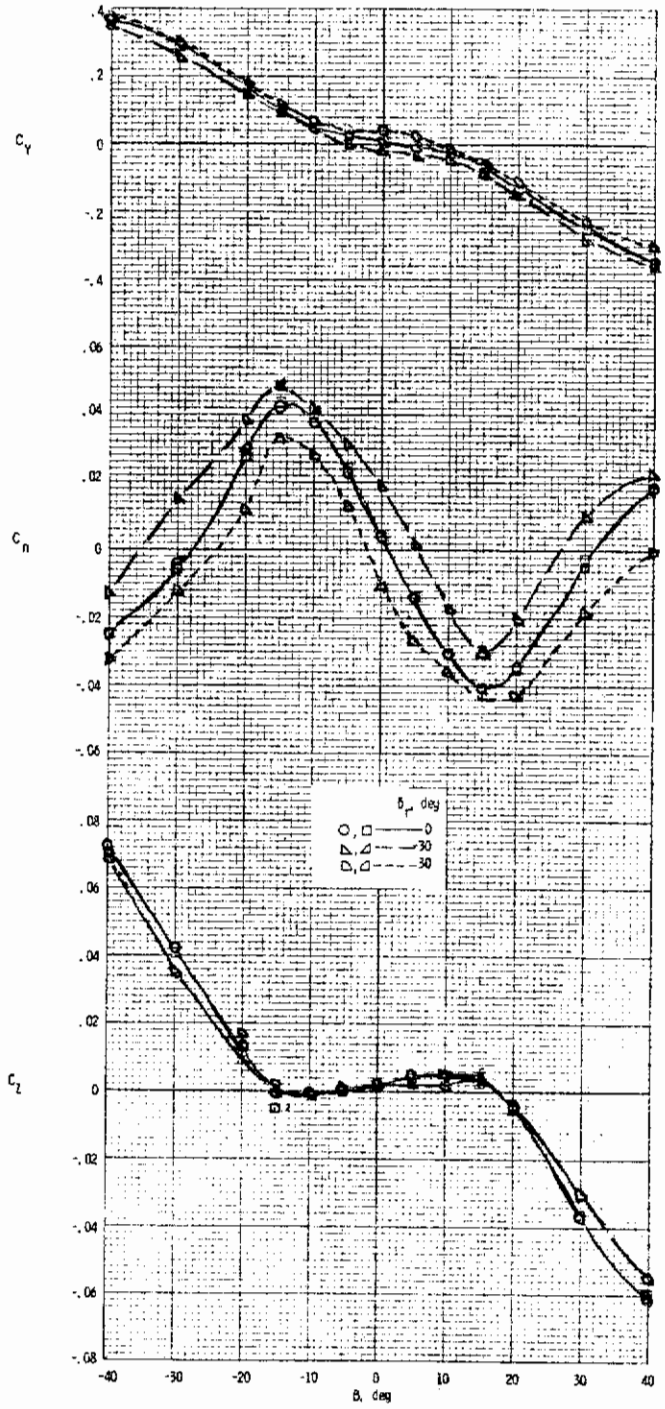

Figure 5 F-4 LATERAL-DIRECTIONAL COEFFICIENTS
(a) Lateral-Directional Coefficients vs β (α = 30°)

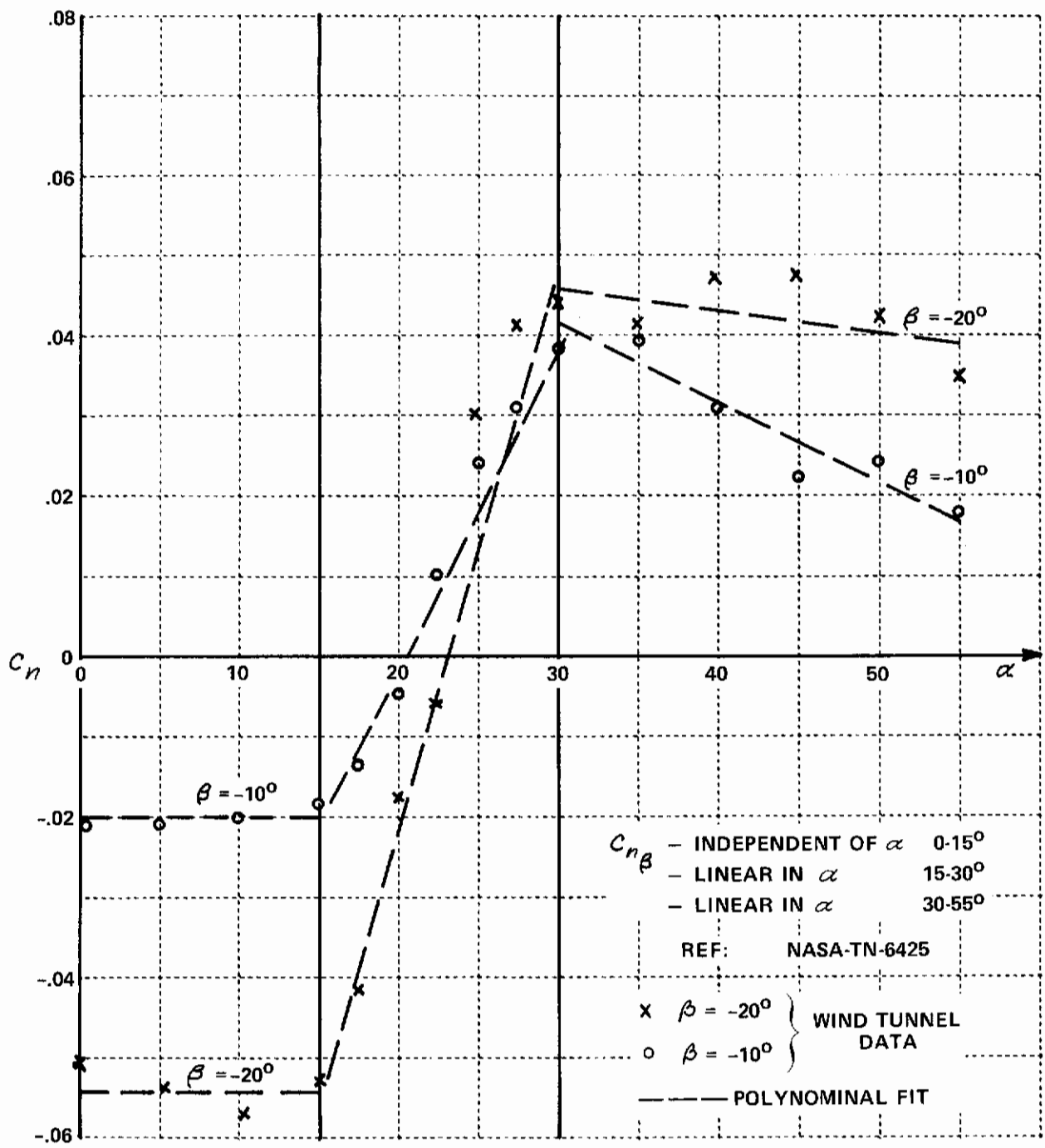

Figure 5 F-4 LATERAL-DIRECTIONAL COEFFICIENTS
(b) F-4 C_n vs α AT VARIOUS β

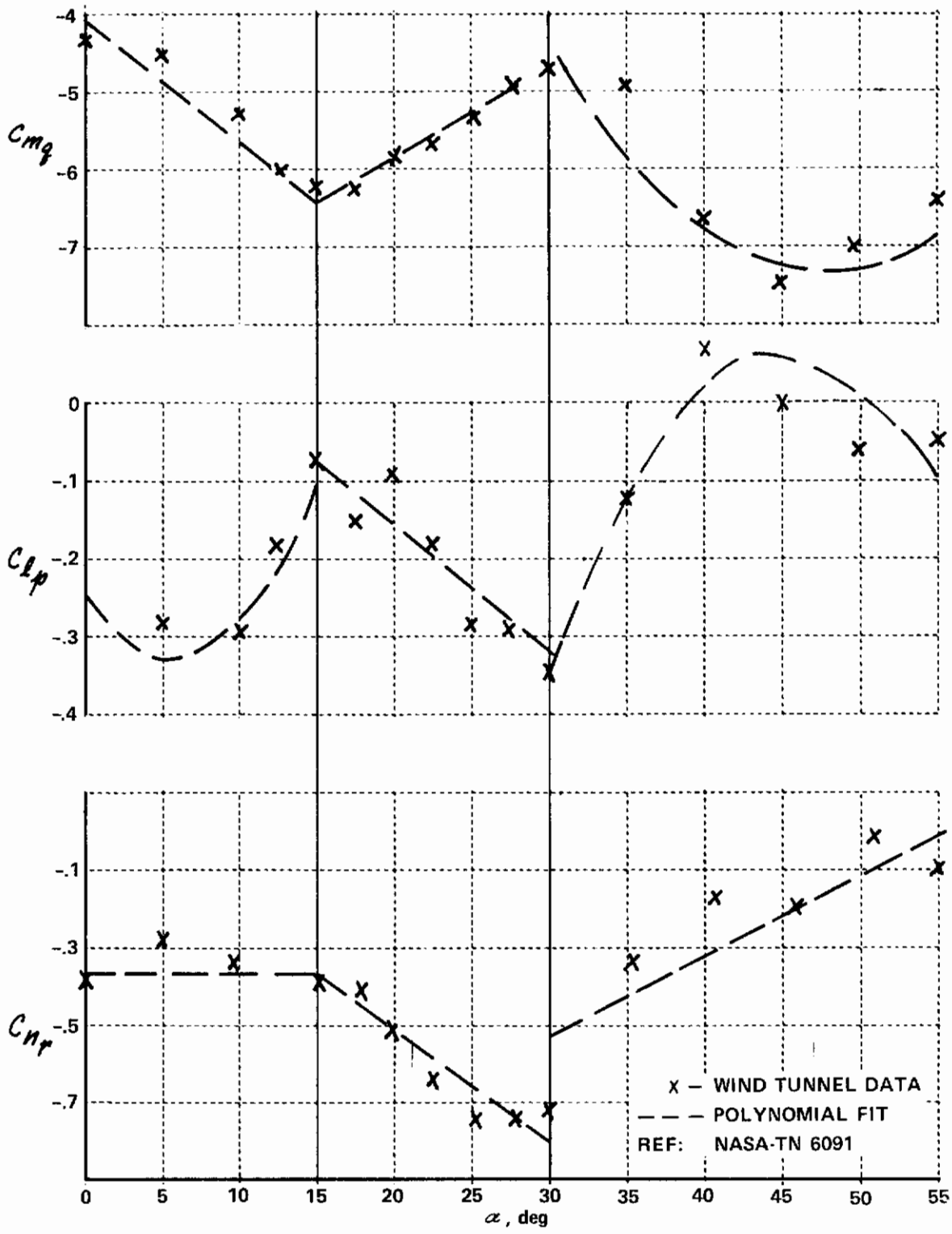

Figure 6 F-4 MAJOR DYNAMIC DERIVATIVES vs α

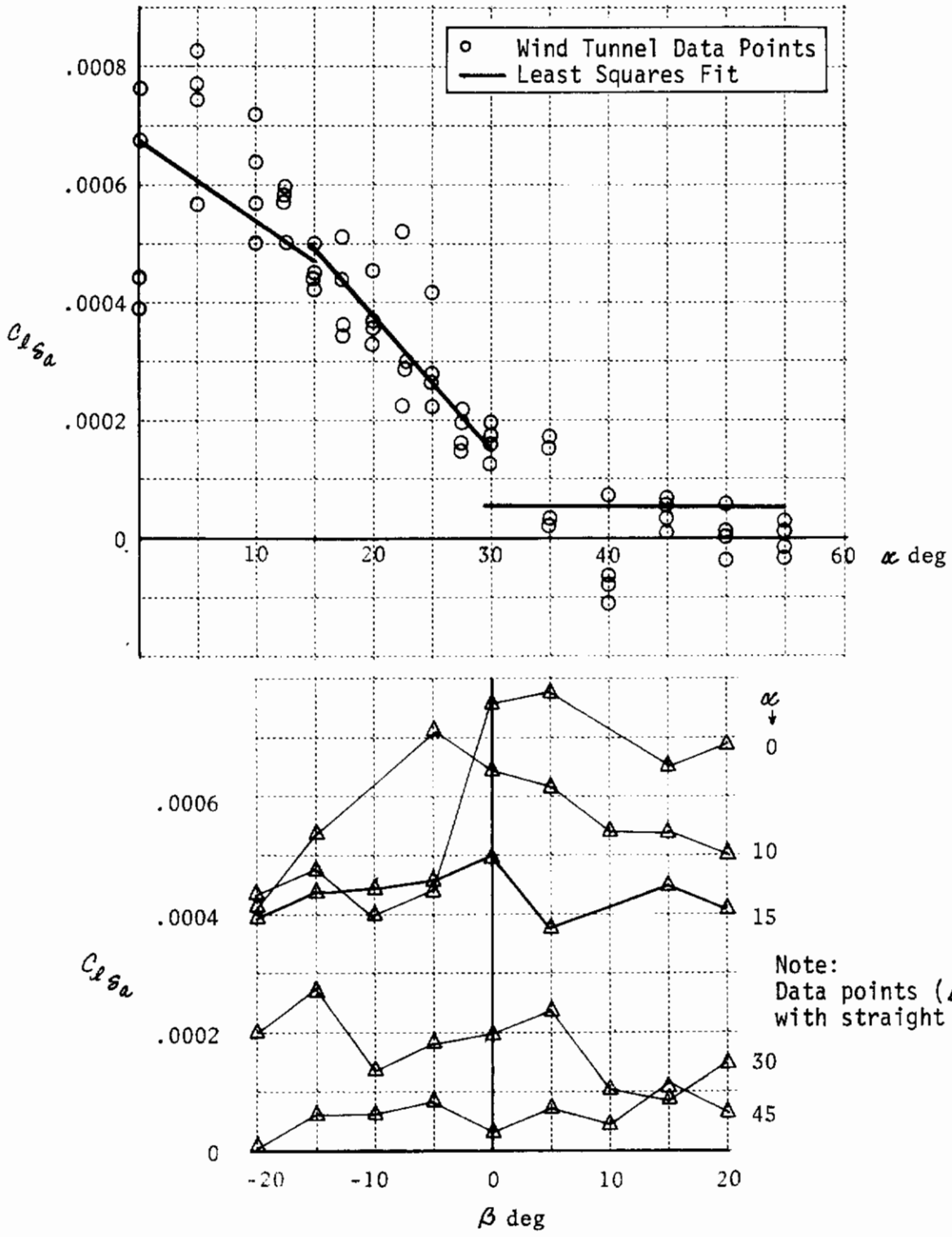

Figure 7 $C_{l_{\delta_a}}$ vs α and β

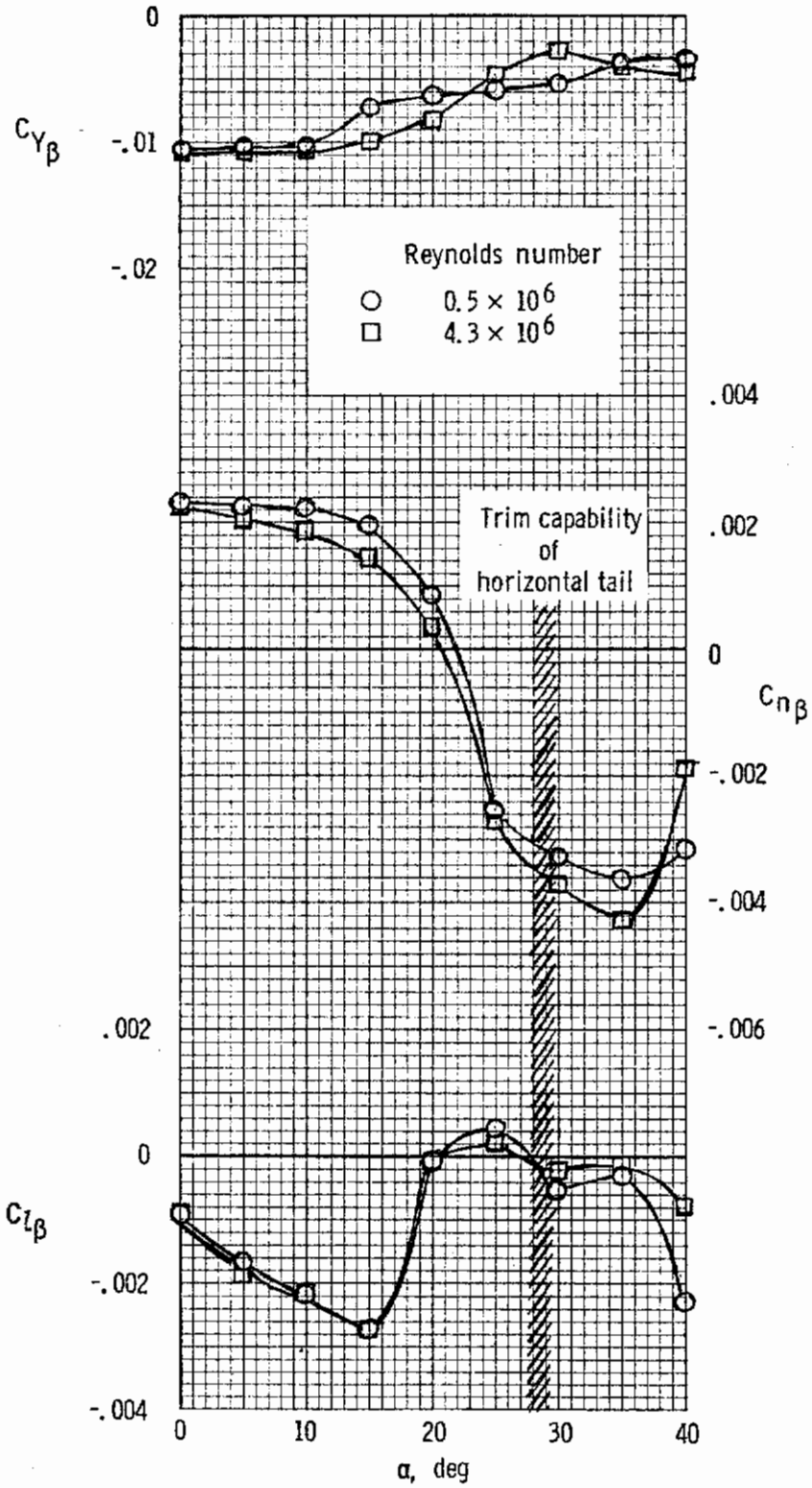

Figure 8 Variations of F-4 Static Lateral-Directional Stability Derivatives with Reynolds Number

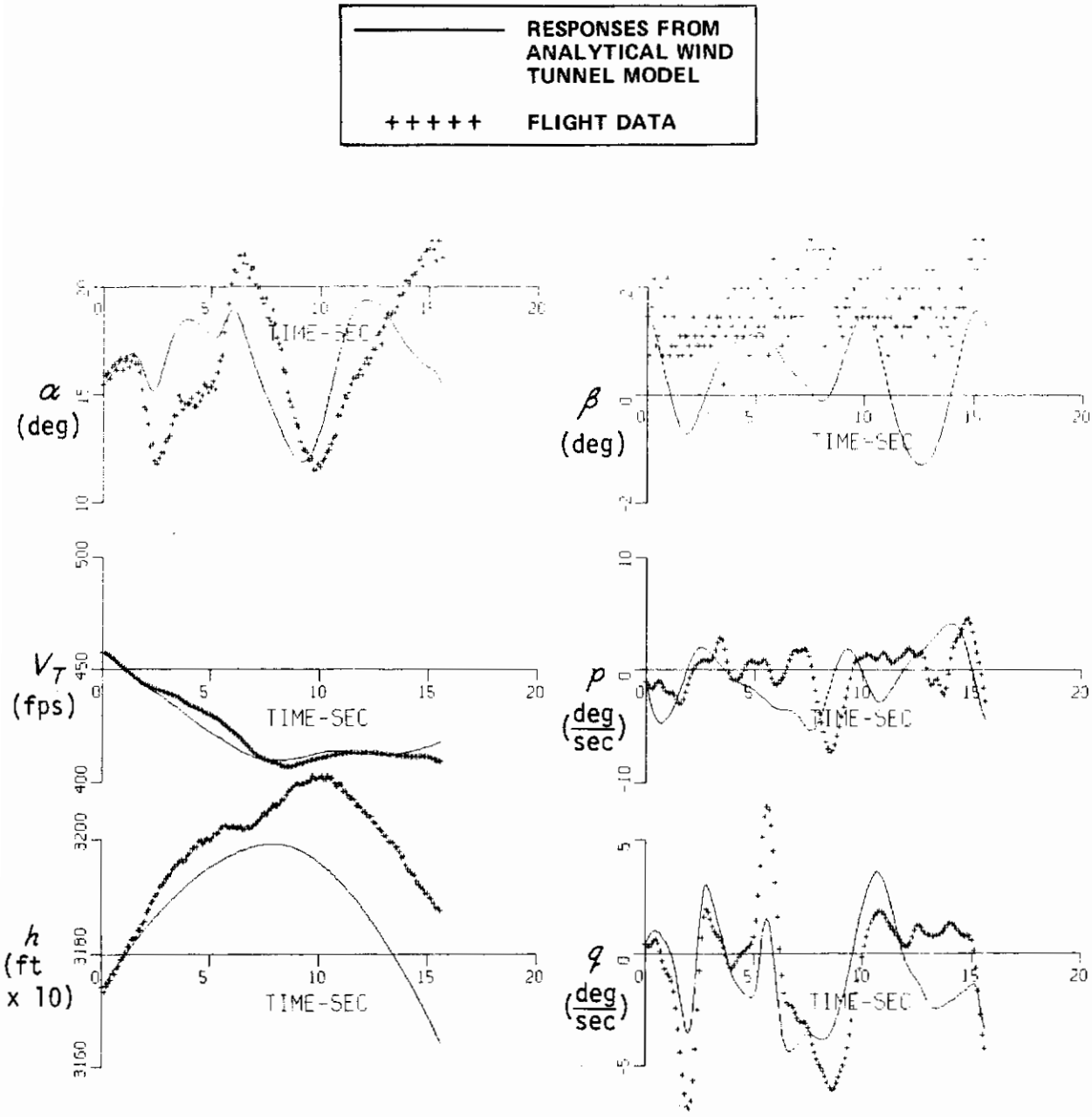

Figure 9 COMPARISON OF RESPONSES FROM WIND TUNNEL ANALYTICAL MODEL AND FLIGHT DATA – RECORD 9

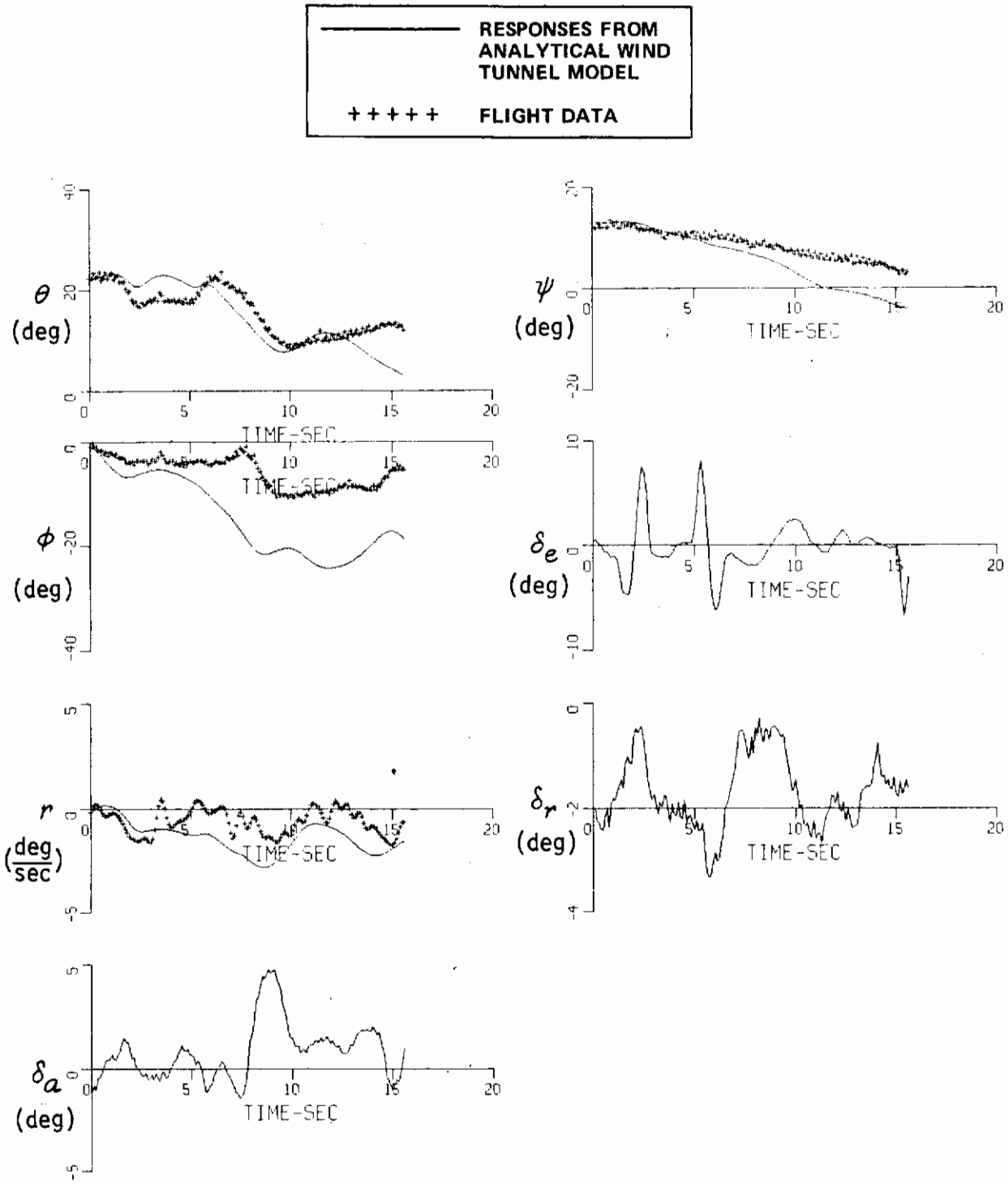

Figure 9 (Concluded) COMPARISON OF RESPONSES FROM WIND TUNNEL ANALYTICAL MODEL AND FLIGHT DATA -- RECORD 9

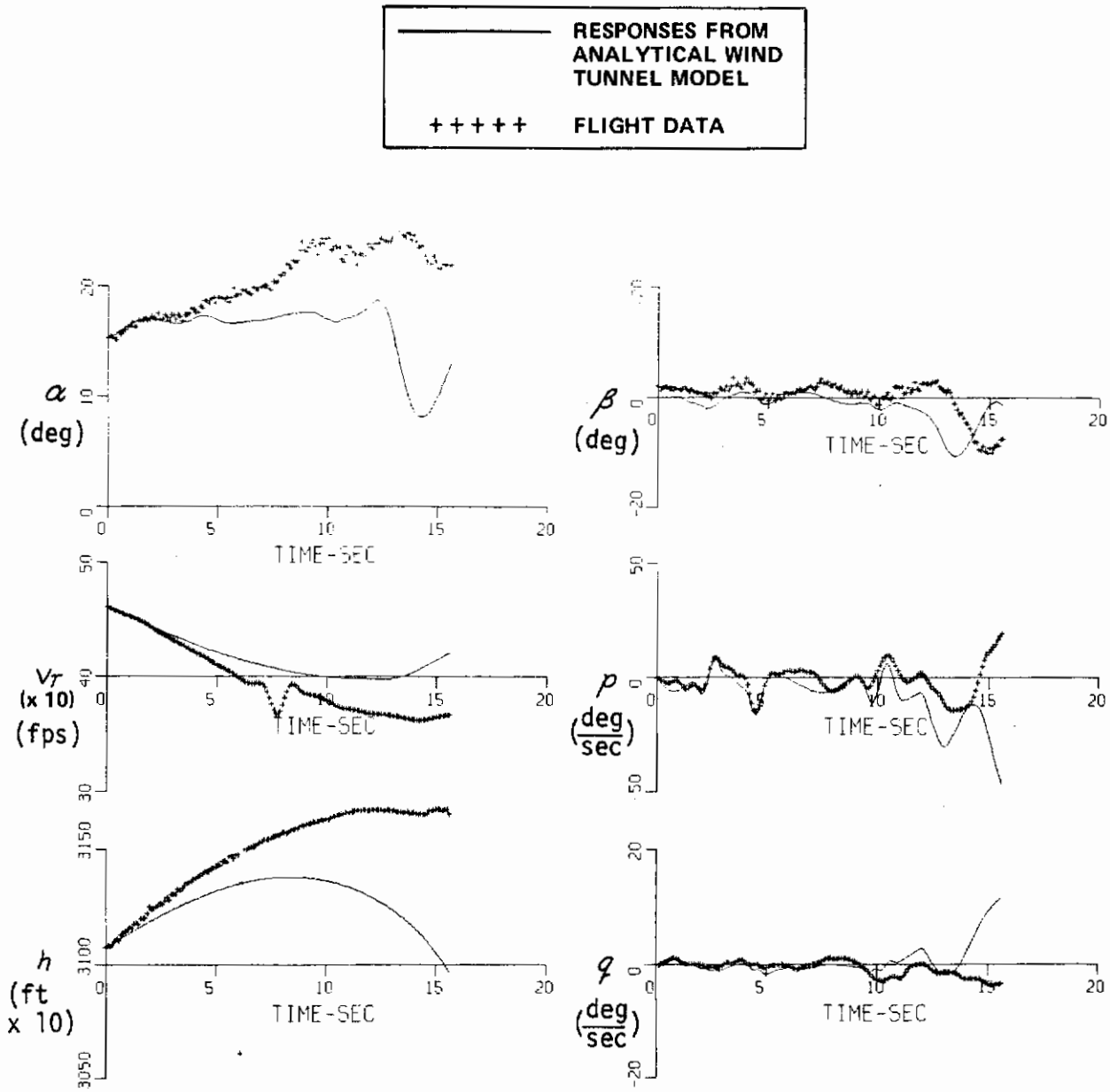

Figure 10 COMPARISON OF RESPONSES FROM WIND TUNNEL ANALYTICAL MODEL AND FLIGHT DATA – RECORD 10

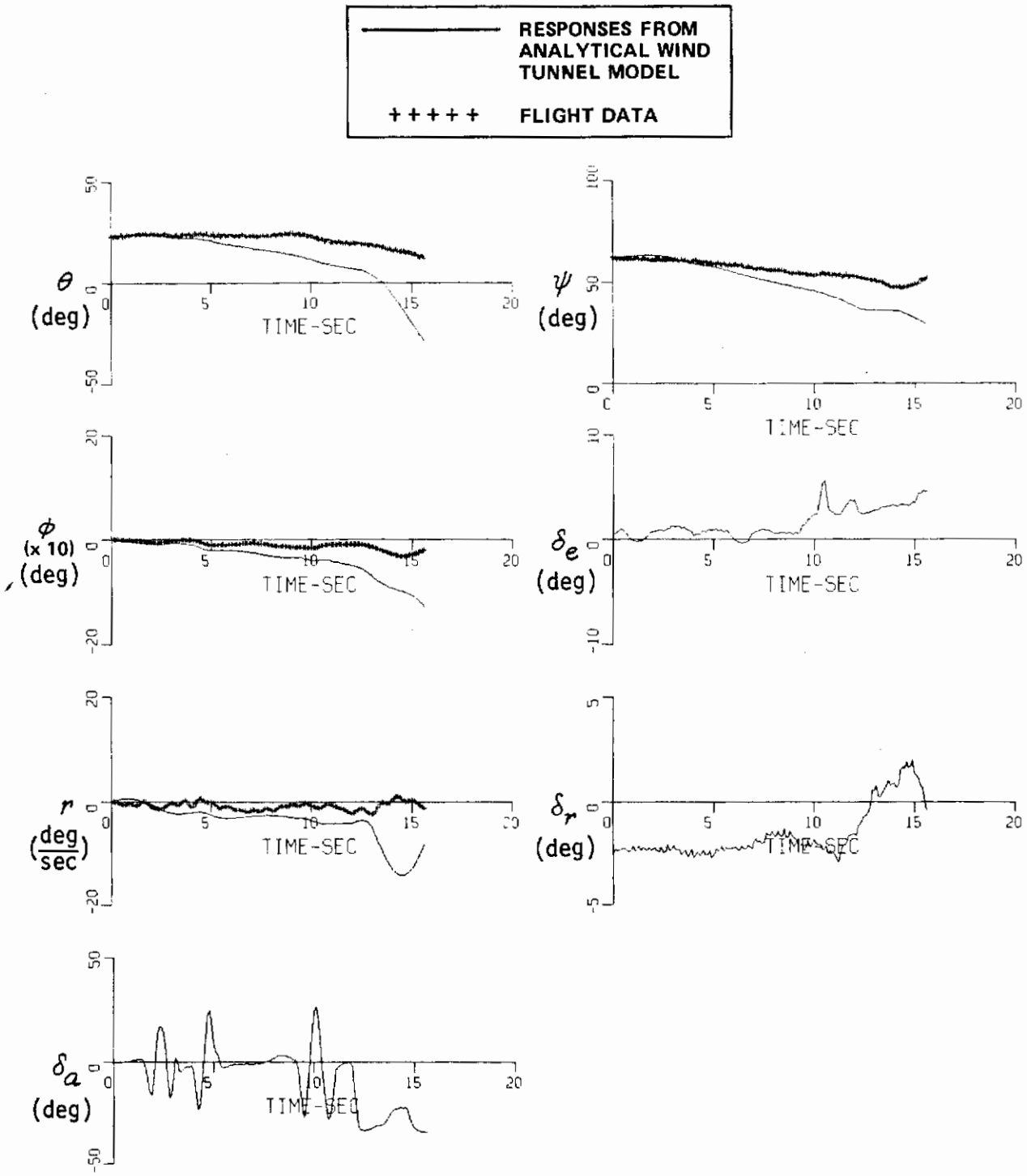

Figure 10 (Concluded) COMPARISON OF RESPONSES FROM WIND TUNNEL ANALYTICAL MODEL AND FLIGHT DATA – RECORD 10

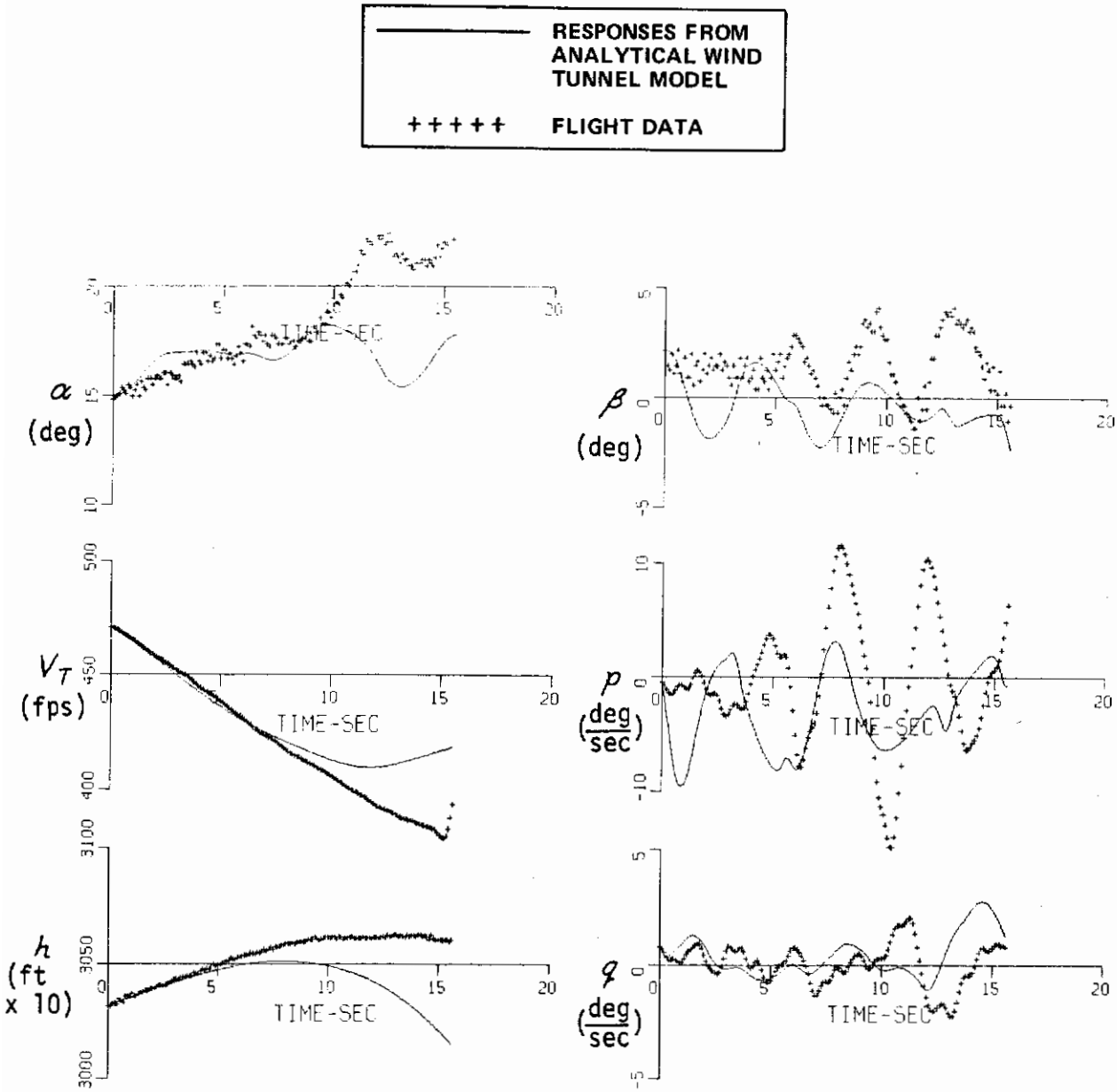

Figure 11 COMPARISON OF RESPONSES FROM WIND TUNNEL ANALYTICAL MODEL AND FLIGHT DATA – RECORD 11

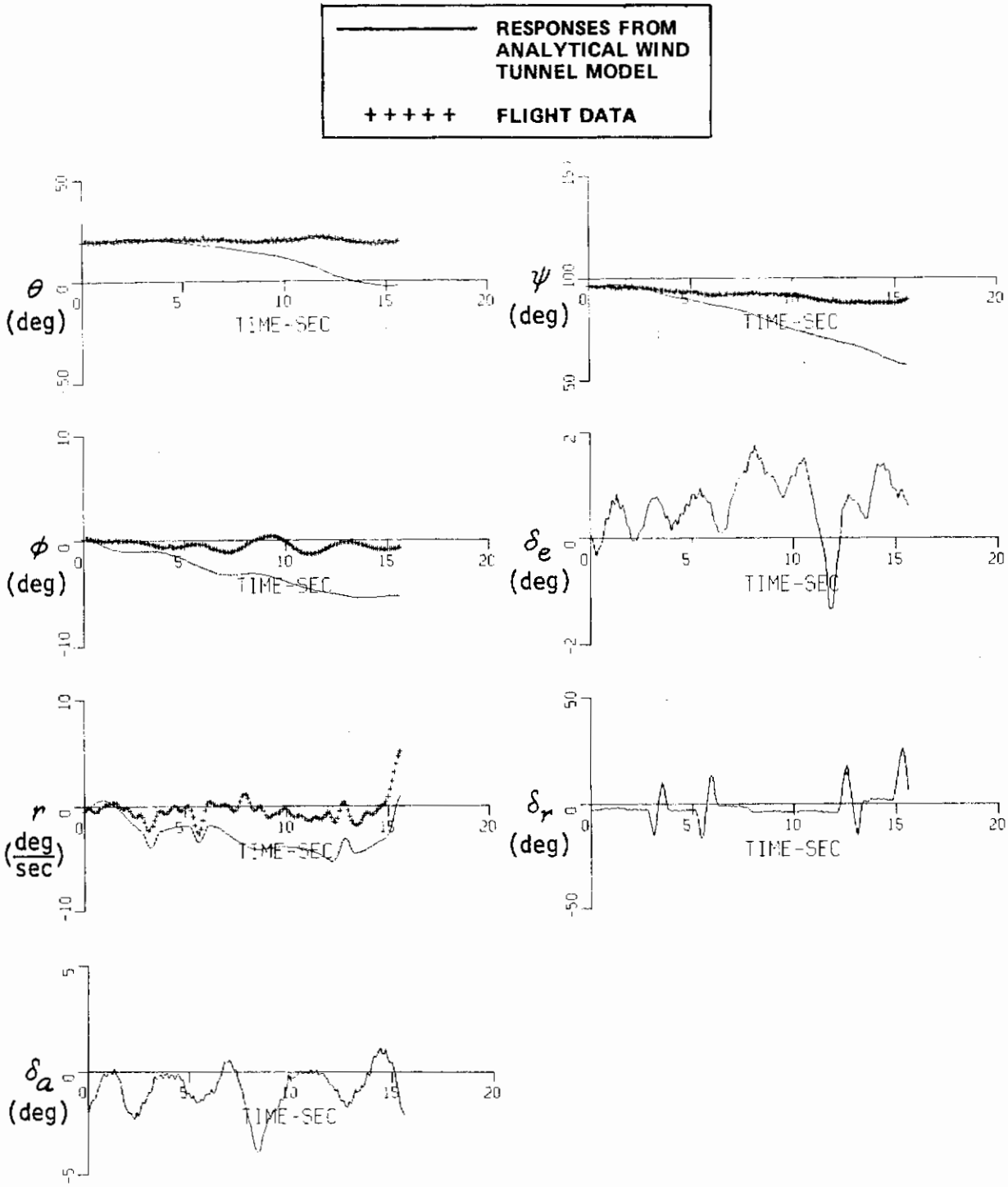

Figure 11 (Concluded) COMPARISON OF RESPONSES FROM WIND TUNNEL ANALYTICAL MODEL AND FLIGHT DATA – RECORD 11

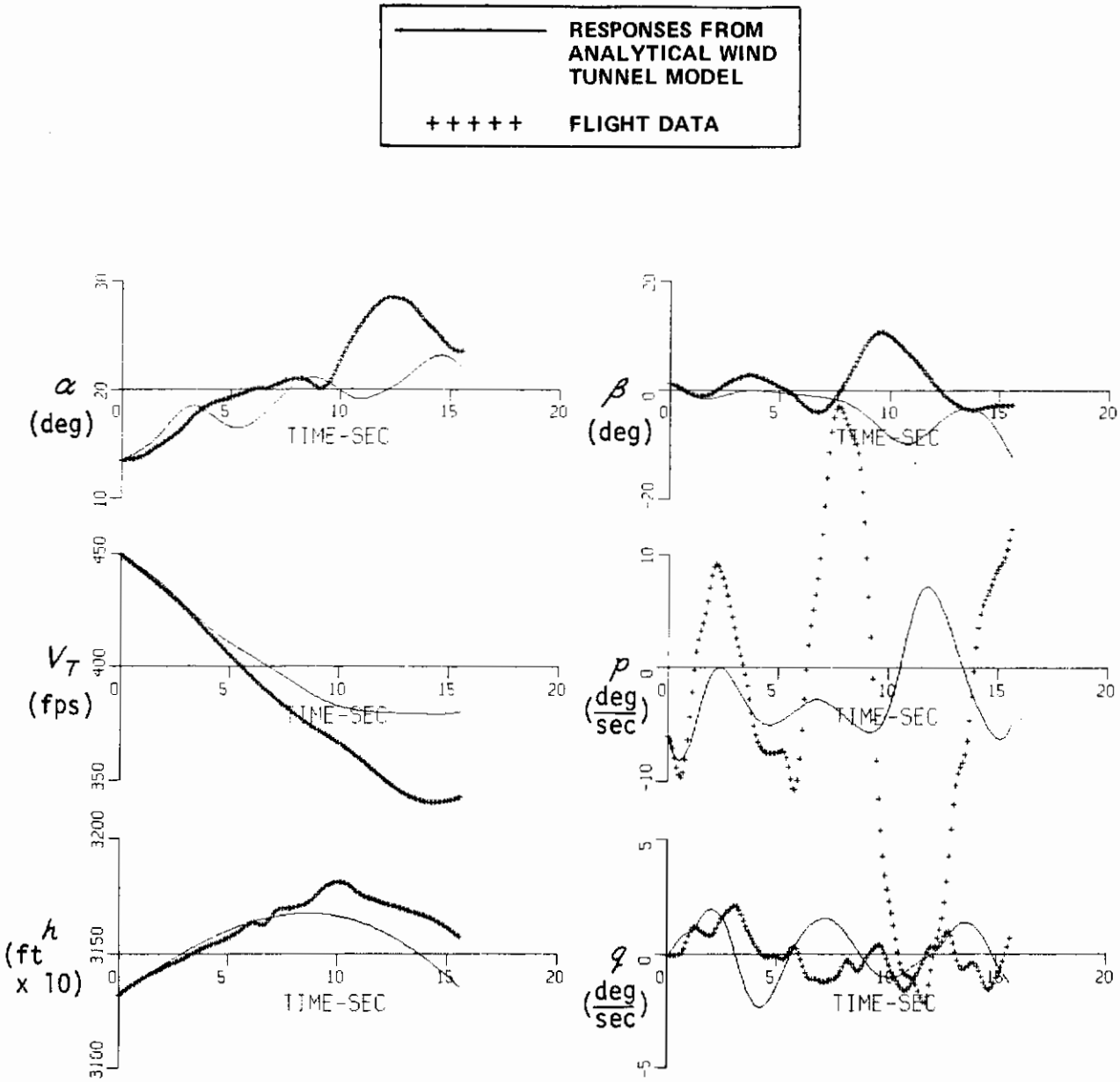

Figure 12 COMPARISON OF RESPONSES FROM WIND TUNNEL ANALYTICAL MODEL AND FLIGHT DATA – RECORD 14

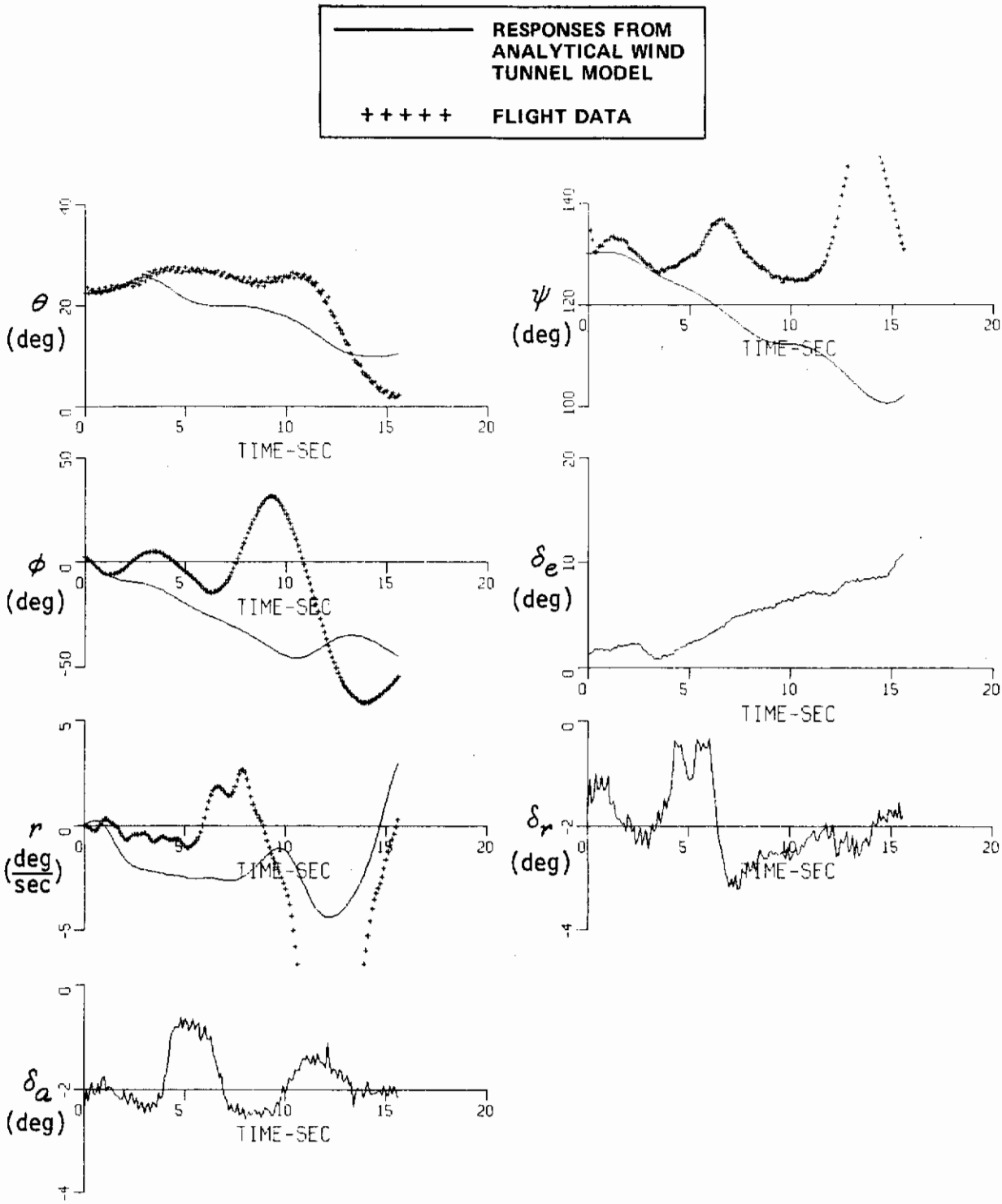

Figure 12 (Concluded) COMPARISON OF RESPONSES FROM WIND TUNNEL ANALYTICAL MODEL AND FLIGHT DATA – RECORD 14

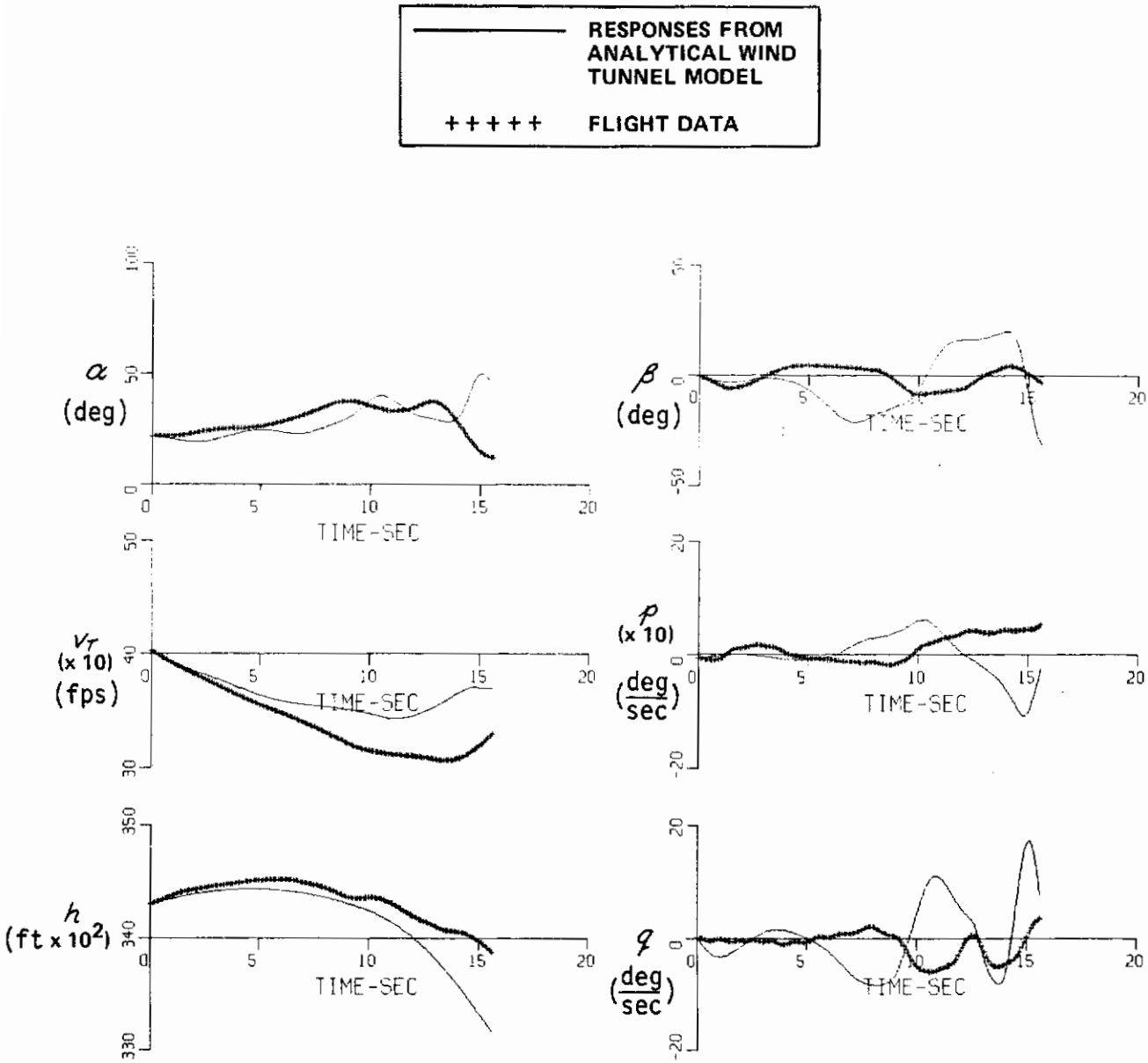

Figure 13 COMPARISON OF RESPONSES FROM WIND TUNNEL ANALYTICAL MODEL AND FLIGHT DATA – RECORD 20

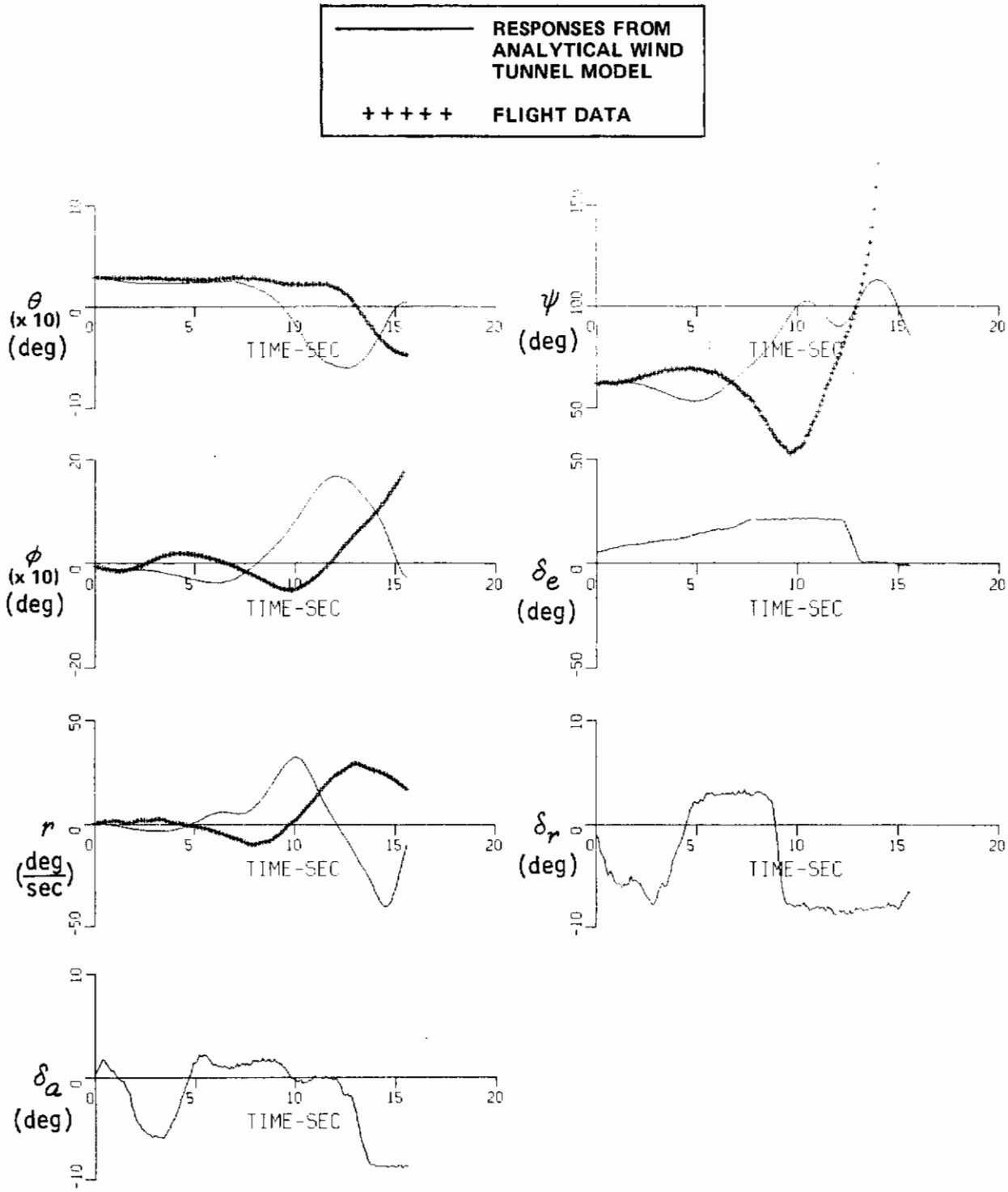

Figure 13 (Concluded) COMPARISON OF RESPONSES FROM WIND TUNNEL ANALYTICAL MODEL AND FLIGHT DATA – RECORD 20

Section V

IDENTIFICATION RESULTS

This section deals with the identification results of the full scale and radio controlled model data. The instrument consistency testing and state estimation are first discussed. Then the identification results from the full scale flight test data are discussed. This includes both least squares and Kalman results. The analysis of the radio controlled flight data is presented next. Only the least squares technique was used with this data, due to the lack of Euler angle measurements on the model. Finally, a summary correlation of identification results with the coefficient values extracted from the wind tunnel data is presented.

5.1 CONSISTENCY OF THE FLIGHT INSTRUMENTATION AND AIRCRAFT STATE ESTIMATION

As briefly discussed in Section III, one of the major ingredients for successful and reliable extraction of aircraft characteristics from flight test data is the instrumentation used and its quality. That is, the accuracy and consistency (or data compatibility) of the flight measurements used. Although no control could be exercised over selection and calibration of the instrumentation used at this time, data compatibility checks were made to ascertain significant discrepancies and are the subject of this subsection.

Two types of instrument compatibility checks are possible and these are classified here as static and dynamic checks. The static checks are a subclass of the dynamic checks and are essentially a set of algebraic relationships which must exist between the instrument readings under restricted equilibrium flight conditions. If these relationships are satisfied, then relative consistency between some particular measurements are satisfied. Since these checks are very restrictive and can be used on only a limited number of flight measurements (linear accelerations and attitude measurements, in particular), the more demanding dynamic checks are necessary.

The dynamic checks, which were also explained in Section 3.2, use the standard six-degree-of-freedom aircraft kinematic differential equations with linear inertial velocities (u , v , w), one linear position (altitude or h), and the three Euler angles (ϕ , θ , ψ) as state variables. Inputs to the kinematic equations are measured time histories of the linear accelerations (n_x , n_y , n_z corrected to the c.g.) and the rotational rates (p , q , r). Integrating these equations from a specified initial condition produces computed time histories of the aircraft states (u , v , w, h , ϕ , θ , ψ) and V , α and β when using the appropriate transformations. These predicted responses are then compared with the measured flight data to ascertain the degree of consistency which exists. Inconsistencies in the form of inaccurate initial conditions and biases in the measured flight variables, for example, will show up in poor response comparisons.

These unknown initial conditions and biases can, of course, be treated as unknown parameters to be identified from the flight measurements using the iterated Kalman filter/fixed-point smoother identification technique. Two approaches are now readily apparent.

1. The identification of these measurement inconsistencies and the aerodynamic parameters can be combined as one problem and all parameters extracted together.

or

2. The measurement inconsistencies can be identified separately using the aircraft kinematic equations and the appropriate measurement system model. This approach also provides the added feature of generating an estimate of the aircraft states (V , α , β , ϕ, θ) for use in the identification of the aerodynamic coefficients, once the measurement inconsistencies are determined.

The latter approach was followed and the kinematic equations and measurement system model used are given in Table I (page 26). The only type of errors considered were measurement biases, except for the air data measurements which also include scale factor errors to account for possible air flow effects.

In summary, the purposes and assumptions made are given as follows:

Purposes and Reasons:

1. Determination of significant instrumentation errors and limitations and also provide a tentative selection of measurement accuracy levels for identification of the aerodynamic parameters.

2. Estimation of aircraft initial conditions and the generation of more accurate V , α_{cg} , β_{cg} , ϕ , θ time histories via nonlinear Kalman filtering.

3. Separation of the instrumentation errors from the aerodynamic modeling errors and consequently reduce the error caused by separating the six-degree-of-freedom equation of motion into two four DOF systems for aerodynamic parameter identification.

Assumptions:

1. Major sources of errors can be treated as biases in the measurements. Errors caused by instrumentation misalignments to the reference axis of the airframe, scale factor nonlinearities, sensor cross-coupling errors and rate limits, for example, are assumed negligible compared to bias error.

5.1.1 Instrumentation

The instrumentation used is well documented in References 6 and 9 and a list of the instrumentation of importance is given in Table XXVI of Appendix I. Table I-3 lists the full scale ranges of the various sensors and an estimate of the final accuracy of the data as a root sum square value using vendor accuracy specification for all system components involved in the measurement and reduction process. Angular accelerometers were not used. The instrumentation was aligned with the body axis, and the angle-of-attack and angle-of-sideslip vanes were mounted on a nose boom which also contained a pitot-static head for measurement of airspeed and altitude. Because of the high angle of attack attained during these flights, an empirical relationship between the ratio of measured impact pressure and measured impact pressure corrected for total pressure error as a function of angle of attack was derived in Reference 6 and used in the calculation of Mach number and consequently true airspeed. These total pressure corrections are essentially zero for angles of attack less than twenty degrees.

Additionally, a two-degree-of-freedom cageable vertical gyro was used to sense aircraft roll and pitch attitude. This was a free gyro and consequently, it was caged and erected to the local vertical prior to the initiation of each flight maneuver. Also, the inner gimbal had precession pins located at $\pm$ 85° to prevent gimbal lock, which therefore invalidated readings of roll and pitch at pitch attitudes greater than $\pm$ 85°.

Besides the instrumentation listed in Table XXVI, the F-4E has a pilot's cockpit angle-of-attack indicator, called the production angle of attack (α_p). This indicator is calibrated in units, has a full scale capability of approximately twenty-six degrees true angle of attack and requires corrections due to sideslip angle. However, it serves as a useful source of angle of attack for comparison purposes at angles of attack less than 26 degrees.

5.1.2 Static Data Compatibility Checks

Prior to initiating the dynamic consistency checks, static checks were made in the flight data where possible. If the airplane is in equilibrium flight, then all linear accelerations ($\dot{u}$, $\dot{v}$, $\dot{w}$) and angular rates and accelerations (p , q , r , $\dot{p}$, $\dot{q}$, $\dot{r}$) are equal to zero and it is readily seen from the kinematic equations that the relationships in equations (5-1) should hold.

$$n_x = \sin\theta$$
$$n_z = -\cos\theta \quad \text{for } \phi \approx 0 \tag{5-1}$$

Further, if also $\beta \approx 0$ and $\dot{h} \approx 0$, then flight path angle (γ) is zero or since

$$\gamma = \theta - \alpha$$

we have

$$\theta = \alpha \,, \quad (\gamma = 0) \tag{5-2}$$

Such checks could not be performed using the data from flight number 1 65 (Appendix I) because the conditions of equilibrium flight were not met. However, other flight records taken during the Stall/Near Stall Investigation of the F-4E aircraft which are documented in Appendix I of Reference 6 and record 9 of Flight 171, which was obtained from McDonnell-Douglas during the data collection effort as a candidate flight for analysis, did have flight conditions under which equations (5-1) and (5-2) were valid. In particular, Flight 195, record 12 and Flight 184, record 25, Figures 19 and 33 in Reference 6 respectively, had near-equilibrium wings-level flight for the first three to four seconds of recorded data. Also, Flight 171, record 9, provided seven seconds of data at similar conditions.

The results in all three cases were that the boom vane angle-of-attack reading was approximately three to four degrees higher than pitch attitude when $\gamma \approx 0$. Hence, a 3 to 4 degree inconsistency was indicated between α and θ . Poor resolution of the plots of the responses from Flight 195 and 184 precluded the accurate use of equation (5-1), however $n_{x_{PS}}$ and θ appeared to be consistent to within one degree of pitch attitude for Flight 171, record 9.

In addition, comparisons were made between the pilot's cockpit production indicator (α_{PP}) and the boom angle-of-attack reading (α_V) using the conversion from α_{PP} in units to α of the fuselage reference line in degrees as given in Reference 26 and Reference 16. Various data points were checked in the flight records in Reference 6 and all the records in Flight 165 at $\beta \approx 0$ conditions. The readings between α_P and α_V were within .2 to 1.1 degrees with α_V always reading higher.

The readings from the linear accelerations at the c.g. and the pilot station (p.s.) were also compared on Flight 165 under conditions of near zero angular rates and accelerations. In all cases, the mean readings of n_x and n_y at both stations were very consistent, being within .01 g's of each other. However, the $n_{z_{PS}}$ reading was offset from the $n_{z_{cg}}$ by approximately .16 g's.

Consequently, although the above checks are only relative checks between instrumentation and by no means absolute since we do not have an absolute standard, the following conclusions can be drawn:

1. An inconsistency of 3 to 4 degrees exists between the θ and α_V measurements, with either α_V reading too high, θ too low or a combination of both.

2. α_{PP} and α_V are consistent to within approximately one degree at low α . Hence, if α_V is incorrect by the amount indicated in (1) above, then so is α_P .

3. The linear accelerometers at the c.g. and p.s. are very consistent (within their accuracy levels) except for $n_{y_{cg}}$ and $n_{y_{ps}}$ which are different by approximately .16 g's.

4. θ and $n_{x_{ps}}$ (which also implies $n_{x_{cg}}$) appeared consistent on one flight record, but the bad resolution on the plots precludes an accurate judgment.

5.1.3 Dynamic Data Compatibility Checks

The dynamic checks were initiated by using the kinematic equations and predicting the measured flight variables with the rate and linear accelerometer measurements at the c.g. used as inputs. The resulting comparisons between the flight data and predicted responses, starting with the first data point of the record as the initial conditions and including no biases, are shown for flight records 9, 10, 11, 14 and 20 in Figures 14 through 18, respectively. Crosses represent flight data and solid traces are predicted responses.

In all five records the results are similar. Apparent biases in the rate measurements produce bad attitude responses which in turn give bad air data comparisons. Also noted are minor anomalies in the V and h measurements due to scale factor changes of the sensors in all records and pitch attitude gyro limiting at approximately minus 85 degrees in record 14, Figure 17, which could be causing a bad roll attitude reading. Heading angle (ψ) was also generated and comparisons made which are not included in these figures. ψ was bad at large roll angles and consequently was not used in Records 14 and 20.

As indicated in the preceding paragraph, bad attitude responses could be causing bad air data and altitude matches. Therefore, the iterated Kalman filter was used on a subset of the kinematic equations, the Euler equations, to identify offsets in p , q , r to match attitudes more accurately.

The extracted biases, whose values are essentially equal to the extracted rate biases when using the complete kinematic equations, are described below. The resulting comparisons when including the rate biases are shown in Figures 19 to 21 for records 9, 10, and 11, respectively. Similar results hold for records 14 and 20 except that an anomaly is present in record 14 when θ approaches -85°.

From these figures the following observations are readily apparent:

1. Lateral-directional flight variables (β , ϕ) compare very well, indicating that errors in ϕ , β and n_y are small for these flight records.

2. The predicted altitude measurement is low and airspeed is high, thus indicating a low predicted flight path angle and therefore, an error in α_v or θ which is consistent with the static checks. Also any significant lags in the altimeter are not apparent.

3. Low predicted α, coupled with the observation in (2) above, indicates possible bias errors in n_z and/or n_x.

5.1.4 Identification of Bias Errors in the Measurements

The checks cited in the aforementioned subsections clearly show a large inconsistency between pitch attitude and angle of attack, but unfortunately, it was not possible to determine exactly which measurement was in error. Consequently, these errors were identified using the iterated Kalman filter with the kinematic equations as the dynamical model.

Various experimental identification runs on most of the flight records with different combinations of bias parameters to be extracted were performed. These were done to verify if indeed the lateral-directional measurements contain small errors (which they did) and to tune the identification technique by selecting the measurement and process noise statistics and the variances of the initial estimates (P_0). The identification results reported below are the ones from which major conclusions were drawn. Prior to presenting these results, the selection of the noise statistics (weighting matrices in the identification techniques) is discussed.

The measurement and process noise statistics were initially obtained by visual examination of the flight records. Generally, the "hash" on the records is assumed to equal the variance of the random noise. These estimates were then checked by comparing plots of the actual residual or innovation sequences from the Kalman filter and the calculated statistical values for these residuals, and readjusting the statistics if required. The final values selected are those given in Table IV. In all cases, the initial state estimates for u, v, w were determined from equation (5-3).

$$\begin{aligned} u &= V_T \cos\alpha_T \cos\beta_T \\ v &= V_T \sin\beta_T \\ w &= V_T \sin\alpha_T \cos\beta_T \end{aligned} \qquad (5\text{-}3)$$

where V_T, α_T, β_T are the initial measured values. The initial covariances for u, v, w were obtained by linearizing equation (5-3) about the initial V_T, α_T and β_T and using this relationship to calculate the variance of u, v, w (σ_u^2, σ_v^2, σ_w^2) given the variance of the measurement noise (σ_V^2, σ_α^2, σ_β^2) including bias uncertainties. The result is given in equation (5-4).

$$\sigma_u^2 \approx \cos^2 \alpha_r \, \sigma_v^2 + (V_r/57.3)^2 \sin^2 \alpha \, \sigma_\alpha^2$$

$$\sigma_v^2 \approx (V_r/57.3)^2 \, \sigma_\beta^2$$

$$\sigma_w^2 \approx \sin^2 \alpha \, \sigma_v^2 + (V_r/57.3)^2 \cos^2 \alpha \, \sigma_\alpha^2 \qquad (5\text{-}4)$$

The initial bias parameter estimates were set equal to zero and their initial standard deviation set to .5% of the full scale measurement reading. These "a priori" bias variances were then multiplied equally by a constant factor (PK) to remove any effect of the "a priori" weighting on the final bias parameter values extracted. PK was determined experimentally by increasing its value until changes between the extracted bias parameters and their final covariances for contiguous identification runs were small. A value of $PK = 10$ was found adequate.

The immediate objective now was to ascertain which measurement (α_v or θ) was in error. Since the aerodynamic force and moment coefficients are strong functions of α , an error of three to four degrees in α_v could lead to erroneous identification results and consequently invalidate any correlation efforts.

It is clear that the extraction of these errors depend, to a large extent, on the accuracy of the altitude and airspeed measurements. Since these measurements are considered more accurate at the lower angles of attack, the identification results from records 9, 10, 11 are presented first.

The extracted biases from records 9, 10, and 11 are given in Tables V, VI, and VII respectively. In these tables, three identification cases, labeled 1, 2 and 3, are presented for each record. For Case 1, all seven bias parameters (n_{x_b} , n_{y_b} , α_{v_b} , θ_b , p_b , q_b , r_b) are identified, while Case 2 assumes no bias in Θ and Case 3 assumes no bias in α_v . In both the latter two cases, the p_b , q_b and r_b biases are fixed at the values extracted in Case 1. Also shown are the smoothed normalized covariance matrix of errors for the parameters from the iterated Kalman filter/fixed point smoother, and the initial (σ_o) and final (σ_f) standard deviation for each parameter. The off-diagonal terms in the normalized covariance matrix, which are the correlation coefficients between the parameter estimates, indicate the degree of linear dependence (or non-uniqueness) of the parameters extracted. In all cases, a smoothed estimate of the initial condition was also obtained.

The comparison of the responses generated from the kinematic equation to the flight data for Case 1 of records 9, 10, and 11 are given in Figures 22a, 23a, and 24a, respectively. Similarly, the residuals from the Kalman filter and a time history of the bias parameter estimates are given in Figures 22b, 23b, and 24b. On the residual plots, the solid lines represent the calculated $\pm 2\sigma$ values and the zeros represent the residuals. Although different biases were identified, these figures are representative of all three cases for each flight record.

The rate biases extracted were consistently negative and within the accuracy specified for the rate gyros. However, it is seen that the α_{v_b} and θ_b biases still cannot be uniquely separated from these flight records because of the relatively small motion in roll angle (ϕ). This is indicated by the high correlation between α_{v_b} and θ_b and n_{x_b} and θ_b and the fact that the biases can be included in α or θ (or both) and the response comparisons are similar. However, the magnitude of the error is approximately the same as determined from the static checks. These results were not unexpected, since upon examinng the kinematic equations under small motion assumption in θ, ϕ and β, then the following approximations are valid.

$$\gamma \approx \theta - \alpha$$
$$\cos\theta \approx \cos\phi \approx 1$$
$$\sin\theta \approx \theta, \sin\phi \approx \phi \qquad (5\text{-}5)$$

Substituting these approximations into the kinematic equation, and comparing relative magnitudes of various terms, it can be shown that it would be difficult to uniquely identify α_{v_b} and θ_b or θ_b and n_{x_b} under the measurement noise levels here, because the sensitivities of the measurements to changes in these parameters are similar. Nevertheless, it is apparent from the results of these nine identification runs that the larger the value of θ_b extracted (in the negative sense) the more positive the value of n_{x_b} extracted, which is consistent with the large negative correlation coefficient between these two parameters. This observation can be used to ascertain the relative consistency between the n_{x_m} and θ_m measurements in the following way.

Transforming certain terms to the left hand side, the x force equation of the kinematic equations can be written as equation (5-6)

$$\frac{\dot{u} - rv + qw}{g} = n_{x_m} + n_{x_b} - \sin\theta + w_1 \qquad (5\text{-}6)$$

where n_{x_m} is the x-axis accelerometer measurement and w_1 random noise. Letting $\theta = \theta_m - \theta_b$, which is the model used for the pitch gyro measurement, and making use of the approximations in equation (5-5), equation (5-7) can be written:

$$\frac{\dot{u} - rv + qw}{g} = n_{x_m} - \frac{\theta_m}{57.3} + \frac{1}{57.3}\left[\theta_b + 57.3\, n_{x_b}\right] + w_1 \qquad (5\text{-}7)$$

Now, under the modeling assumption imposed above, equation (5-7) is exact except for the random term w_1 (zero mean or $E\{w_1\} = 0$). Consequently, the relative consistency between the n_x and θ measurements can be determined by examining the magnitude of the $\theta_b + 57.3\, n_{x_b}$ term. For example, if θ_b and n_{x_b} are truly zero, but a value of θ_b was extracted because it could not be identified uniquely from the data, then n_{x_b} would adjust to force $\theta_b + 57.3\, n_{x_b} \approx 0$. Note that this check is similar to a static check, except that the identification technique was used to establish the relationship. This term was computed for each of the nine cases and the results are presented in

Table VIII. Although scatter in the results is evident, a fair degree of consistency is indicated between the pitch attitude gyro and the $n_{x_{cg}}$ accelerometer, as was previously suspected from the static checks, indicating that most of the error is in the α_V measurement.

To reinforce the above results, three additional identification runs were made using data at the ends of flight records 15, 17, and 20 where large attitudes were present and α remained below twenty degrees. The results are given in Table IX. For all three records, the correlation between α_{V_b} and α_b was small (less than .3) and the α_{V_b} bias parameter exhibited convergence asymptotically to its final estimate - a good indication of accurate identification. A representative example of the time histories of the bias parameter estimates from flight record 15 is given in Figure 25. The response comparisons to the flight data using the extracted biases were very good for all three records. Note that the extracted α_{V_b} bias from all six records, 15, 17, and 20 (Table IX) and 9, 10, and 11 (Case 2) were consistently around three degrees.

Measurement biases were also extracted from flight records 14 and 20. These are the high angle-of-attack rolling departures where large lateral-directional motions are present and hence would surely allow the unique identification of the measurement biases. It turned out for these records that, although consistent biases were extracted in the rate measurements, the biases in the α_V and n_z measurements were unrealistically high - for example, α_{V_b} ranged from 3 to 8 degrees. It also appeared that the angle-of-attack error could not be modeled as a consistent time invariant bias since the bias parameter extracted increased as a function of α. This increasing α_{V_b} bias was initially contributed to boom bending due to air and/or inertia loading and possibly air flow effects on the vanes at high angles of attack. Assuming boom bending due to air loading and possibly air flow effects, attempts to model the above effect with a quadratic scale factor proved futile. It was therefore reasoned that although the error of approximately three degrees is present in the α_V measurement, the additional error is caused by inaccurate attitude measurement at the high attitude angles. Accordingly, the errors in θ (and ϕ) cannot be modeled as a constant time invariant bias at large attitudes, especially when pitch attitude nears 85 degrees.

Results of identifying measurement biases from the first portion of flight records 14 and 20 are given in Table X, and the resulting response comparisons to the flight data and time histories of bias parameter estimates are shown in Figures 26 and 27, respectively. The extracted rate biases from these identification runs were used in further analysis.

To summarize, the results of the instrumentation consistency checks, which gave relative consistency but not absolute accuracy, were as follows:

1. Rate Gyros

   Consistent and easily identifiable biases in the rate measurements were determined. Although different bias values were extracted from each record, the biases were within the accuracy of the sensor/recording system. Two explanations are possible for the differences.

(i) Statistical uncertainty or (ii) misalignment of the instrument axes to the airframe or scale factor nonlinearities. In the latter case, it was considered better to approximate the errors by constant biases than not to include them at all, even though they were slightly different for each record.

2. Linear Accelerometers

Bias errors in the n_x and n_y accelerometer measurements at the c.g. were small, but a bias error was determined to exist in n_z of approximately .03 g's. Differences could exist for the same reasons that the rate gyros exhibit differences.

3. Angle of Attack and Sideslip Vanes

The angle-of-attack vane measurement is reading approximately 3 degrees too high and this offset was used for subsequent data analysis. The offset is attributed mostly to an offset in the calibration or an electrical offset in the sensor/recording system. Consequently, a similar offset also existed in the production indicator. Boom bending was present but a quantitative estimate of its magnitude was not made. No apparent offset was found to exist in the β -vane measurement.

4. Attitude Gyros

No significant offsets were determined for the roll and pitch attitude measurements at low attitudes. However, cross-coupling errors appear to be present at the large attitude angles so that these errors could not be modeled with constant biases. A small (less than one degree) gyro misalignment to the airframe appears to be present which is variable for each record due to gyro erection prior to each maneuver. This misalignment, however, is not large enough to invalidate the Euler angle equations.

5. Airspeed

Empirical total pressure corrections appear good but produce very noisy airspeed measurements. Calibration factor changes also cause jumps in the measurements, but these can be smoothed with the Kalman filter.

5.1.5 Aircraft State Estimation

From the results of the instrumentation checks, a uniform three degree offset was determined to be present in the boom vane angle of attack reading for all five flight records. Fixing the α_{V_b} at 3 degrees and the rate biases at their specific values extracted previously, each flight record was reprocessed through the iterated Kalman filter/fixed point smoother to: (i) estimate the aircraft initial conditions for each record and (ii) update the n_{x_b} and θ_b biases. Note that only the first portion of flight records 14 and 20 were used for this purpose.

The resulting initial conditions (and their indicated variances) and bias parameters were then used as initializing inputs to generate aircraft state estimates ($\hat{V}$, $\hat{\alpha}$, $\hat{\beta}$, $\hat{\phi}$, and $\hat{\theta}$) with the iterated Kalman filter.

A special problem, however, had to be considered for flight records 14 and 20. As previously stated, these were rolling departures with large excitation in pitch and roll attitude which led to time varying errors in these measurements. Therefore, these errors could not be modeled as constant biases.

To circumvent this problem during state filtering of these records, the θ_b and ϕ_b bias parameters were modeled as random (not time invariant constants) parameters by the inclusion of state noise to these biases. That is, these parameters were modeled as

$$\dot{\phi}_b = \omega_1$$
$$\dot{\theta}_b = \omega_2 \qquad (5\text{-}8)$$

where ω_1, ω_2 are assumed zero mean, white Gaussian process noise. The noise statistics were adjusted by experiment and the model was considered adequate when $\sigma_{\omega_1} = \sigma_{\omega_2} = 1.5$ deg/sec.

A summary of the biases used in the generation of the aircraft state estimates is given in Table XI. The time history plots of the aircraft state estimates appear in Figures 48 through 52 of Appendix I for flight records 9, 10, 11, 14 and 20, respectively. Only the first 29 seconds of data from record 14 could be used because the large pitch attitude at that time invalidated the Euler angle representation.

The resulting biases given in Table XI were removed from the appropriate flight data and the nondimensional aerodynamic force and moment time histories were computed for each flight record as described in Section 3.3 of the report. The resulting time history plots for both the dimensional aerodynamic force and moments, and the respective nondimensional coefficients, are also given in Figures 48 and 55 of Appendix I. These nondimensional aerodynamic time histories provide the data to be fit with an appropriate aerodynamic representation (model), for extraction of the aerodynamic characteristics using the least squares (LS) technique.

Since the LS technique uses as its criterion the minimization of "equation error" and not "response error", it is instructive to check the accuracy of the data used, for example, the pitching moment coefficient, $C_m(t)$, time history.

A simple check was made for each flight record by predicting the flight measurements with the 6 DOF simulation (Appendix III) using as forcing inputs the nondimensional aerodynamic force and moment time histories previously computed. The response comparison for record 10, which is representative of the other records, is shown in Figure 28. Perfect matches here, of course, do not necessarily imply more accurate LS results, but they do give greater confidence in the accuracy of these computed time histories.

5.1.6 Categorization of Full Scale Flight Test Data

Upon completion of the instrumentation consistency checks, the flight records and wind tunnel data were re-examined to ascertain the most suitable ranges of angle of attack over which to model the aerodynamics. This was necessary since the three degree offset uncovered in the α_v measurement invalidated the previously selected ranges of approximately 15 to 30 and 30 to 55 degrees angle of attack. From the analysis of the wind tunnel data these ranges appeared the most suitable, but the segments of continuous flight data available where any one of the models would be applicable were considered too short for identification purposes. The idea, of course, is to select the range of angle of attack so as to allow for the simplest of models (fewest parameters), for which characteristics can be extracted from the available flight data. The results of this re-examination are summarized for the low Mach number records ($M < .5$) in Table XII.

It was decided to use two aerodynamic models: one for the 12 to 20 degrees angle-of-attack range, the other for the 20 to 40 degree range. These will subsequently be referred to as the low-α and high-α models. From Table XII, it is seen that flight records 9, 10, and 11 provide data for extraction of the low-α model parameters and records 14 and 20 for the high-α model parameters.

The higher Mach number flight records (15, 17, 19) were not considered useable for identification purposes because of the large variation in Mach number encountered and the small record length over which one analytical aerodynamic model would be applicable.

5.2 DISCUSSION OF THE IDENTIFICATION RESULTS FROM THE LEAST SQUARES TECHNIQUES

This subsection describes the identification results using the least squares technique on the full scale flight test data. This type of identification is performed primarily in order to determine initial model forms and to provide initial parameter and covariance estimates for the iterated Kalman filter technique. From the preceding subsection and Appendix I, five flight records are available for identification purposes which cover the range of α from approximately 10 to 45 degrees. Flight records 9, 10, and 11 are used to identify the low - α models and records 14 and 20 the high - α models.

It should be noted that record 9 has very good aircraft excitation and control input (δ_s) for identification of the longitudinal coefficients but very little lateral-directional excitation. Records 10 and 11 provide data for identification of only the lateral-directional coefficients. Record 10 has δ_a pulse type inputs with small δ_r inputs and record 11 has the opposite. In both records, yaw rate motions are extremely small. Records 14 and 20 provide mostly lateral-directional motions but with very small δ_a and δ_r control inputs.

Accordingly, a discussion of the results is presented in the following order:

Longitudinal - low α

Longitudinal - high α

Lateral-Directional - low α

Lateral-Directional - high α

Various candidate model forms were tried for each of these using the wind tunnel data as a guide, to determine the functional relationships and the number of unknown parameters needed to represent each total aerodynamic coefficient in the equations of motion. The analytical representations which provided both: (1) reasonable fits to the force and moment time histories, and (2) extracted coefficient values that agreed qualitatively with the wind tunnel data are shown in Table XIII for all records. An asterisk signifies the particular parameters that were included in the model representation to be identified. Note that some parameters were fixed at the wind tunnel values.

Figures 43 and 44 present these identified coefficients overlayed on the wind tunnel coefficients for comparison. The wind tunnel data (Langley and Ames) are presented in the form of hand faired plots to the actual test data points for convenience and are representative for $-15^{o} \leq \beta \leq 15^{o}$. A comparison of the hand faired plots to the wind tunnel data points for the Langley data is given in Appendix IV for reference and the differences between the two series of tests are discussed in Section IV. Parameter values for coefficients held fixed at the Ames wind tunnel data, which are not provided below, are also given in Appendix IV.

In Figures 43 and 44, the least squares results are referened to the nominal .33 $\bar{c}$ center of gravity position. The Kalman results which are presented in the following subsection are also shown on these figures. A comparison of the nondimensional force and moment time histories computed from the flight data with those computed using the estimated coefficients are presented for records 9, 10, 11, 14 and 20 in Figures 29 through 33, respectively.

5.2.1 Longitudinal - Low Angle of Attack

The longitudinal - low α least squares identification was done mainly with record 9. Although results were obtained with records 10 and 11, the small longitudinal excitation in these records precluded very meaningful results. However, the results for record 9 were very good. Comparisons between the flight data and the computed data with the estimated coefficients, as shown in Figure 29, are very good for the C_{y}, C_{m} and C_{x} time histories. The form of the model used is given in Table XIII.

The identified statics compared favorably with the wind tunnel data as shown in Figure 43. The identified C_{z} versus α curve was almost identical to the wind tunnel data and the offsets in the C_{x} and C_{m} curves were not unreasonable; these effects were later shown to be in fact present. The $C_{y_{\delta e}}$ control derivative was closer to the Ames wind tunnel data while $C_{m_{\delta e}}$ was around the Langley results. The identified dynamic derivatives C_{x_q} and C_{m_q}, however, were unrealistic. This is not too surprising since C_{x_q} is extremely hard to identify and the least squares technique has been known from past experience to give inaccurate dynamic derivatives in some cases. The identified values did pass through the values indicated from the wind tunnel data but at the end points of the α range, near 10 and 20 degrees, the values appeared poor.

Simpler aerodynamic models were briefly investigated but the equation matches were not as good and consequently, the fit errors were increased. More complex models reduced the magnitude of the fit error, but the identified coefficients were unreasonable. In these latter cases, high correlations existed between the extracted parameter estimates representing a lumped coefficient (e.g. C_{m_q}); these high correlations indicate the onset of an ill-conditioned (near singular) regressor or identifiability matrix in the least squares algorithm. Round-off and measurement errors, however, usually prevent this matrix from becoming singular and consequently, it can only serve as an approximate indicator.

Therefore, the model form given in Table XIII appears to be adequate to describe the aircraft characteristics in this range of α. Comparisons between the flight data and computed data with the estimated coefficients using the same model form as on record 10 and 11 are also given in Figures 30 and 31, respectively.

5.2.2 Longitudinal - High Angle of Attack

For reasons similar to those given above, the best model forms provided the data comparisons for C_{x}, C_{z} and C_{m} as shown in Figures 32 and 33 for records 14 and 20, respectively. Unfortunately, excitation of the pitch degree of freedom occurs mostly toward the end of the record and hence very little information is provided for identification purposes. The identified static coefficients continued to show the same trends as those extracted in the low α records, Figure 43. For example, C_{z} versus α was close to the wind

tunnel values until past 30 degrees. C_X , C_m and $C_{Y\delta_e}$ versus α were all higher than the wind tunnel data. The dynamic derivatives were poor while most of the control derivatives appeared reasonable. An adequate model form is not readily apparent from these results, although the major characteristics appear to be adequately modeled. Possibly C_m and $C_{m_{\delta_e}}$ should be approximated to third or fourth order in α for such a large range of α , but this approach was not tried.

5.2.3 Lateral-Directional - Low Angle of Attack

Since record 9 contained very little lateral-directional motion, only records 10 and 11 were analyzed for meaningful least squares results. The comparisons of flight data with those computed using the extracted coefficients are shown in Figures 30 and 31, respectively. The comparisons are good. The static C_{y_β} , C_{l_β} and C_{n_β} versus α curves identified showed good correlation with the wind tunnel results. However, the dynamic coefficients and cross-coefficients were impossible to extract with any repeatability between records because of the relatively low yaw rate and the type of control inputs applied. For example, Figure 44 shows the different C_{n_β} coefficients extracted from records 10 and 11 respectively. The identified coefficients did show the same trends and relative magnitudes, which indicates the model form may be adequate, but the exact values cannot be accurately determined with the least squares method. The aileron derivatives extracted on record 10 were reasonable, but the rudder coefficients were poor as was expected because of the small rudder inputs. On record 11, only the rudder control coefficient was included as an unknown to be identified. The aileron coefficients were held fixed at the wind tunnel values.

In general, the model form appears adequate for this angle of attack range and flight data used.

5.2.4 Lateral-Directional - High Angle of Attack

Both records 14 and 20 had significant lateral-directional motions but little δ_r and δ_a control excitation. Consequently, all the δ_a and δ_r control coefficients had to be fixed at the "best guess" values - the wind tunnel values; otherwise unrealistic coefficients were extracted, which is due to the high correlations between these parameter estimates and others, and because of the low sensitivity of the flight data to changes in these parameters. The "best guess" values were taken from the Ames data since preliminary Kalman identification results and other sources (Reference 27) indicate the Ames results appear closer to the full scale aircraft for these control derivatives (Appendix IV). Comparisons between the flight data and the estimated data are shown in Figures 32 and 33 for records 14 and 20, respectively. The large or gross variations compare very well, but the smaller variations do not, thus indicating possible missing terms in the aerodynamic representation. These small variations could, of course, be within the accuracy of the force and moment time histories computed from the flight data, but it is

possible the model was not sufficiently complex. More complex models were tried, except for the static C_{l_p} and C_{n_p} coefficients, but the extracted coefficients were unreasonable.

The extracted coefficients shown in Figure 44 are not consistent between records, especially the dynamic coefficients. For example, at approximately 20 degrees of α, C_{l_β} on both records was consistent with the values identified from the low α records, in that both seemed to be shifted a little to the right. However, as the curves went beyond 25 degrees they became different. C_{l_β} from record 14 stayed relatively flat, but on record 20 C_{l_β} had a more discernible maximum. The C_{y_β} and C_{n_β} versus α curves were similar for each record and correlated fairly well with the wind tunnel results. The C_{y_p} derivatives were identified as constants and went through the average wind tunnel value on both records. The identified C_{n_p} and C_{l_p} coefficients were very different from each record but generally these curves passed through the wind tunnel data. In summary, the model form cannot be firmly established from these flight records.

5.2.5 Choice of Initial Estimates for Kalman Identification

The choice of initial estimates for the parameter values and their variances for the Kalman identification technique is now discussed. It was originally intended that the identified values of the parameters and their variances from the least squares results would be used directly in the Kalman method. For the following reason, this approach was not used.

Many of the values for the coefficients from the least squares results were unrealistic. This is especially true for the dynamic derivatives. Also, some of the control derivatives were difficult to identify because of their small movements on most records. However, most of the static coefficients were identified realistically close to the wind tunnel values. Therefore, since a consistent set of identified coefficients was not available, it was felt that it was best to use all of the wind tunnel values for the initial estimates of parameters. The model forms obtained by the least squares results were essentially similar to those derived from the wind tunnel data.

It should also be noted that the values for the identified standard deviations of individual terms of the coefficients from the least squares results were approximately equal in size to the parameter itself. However, since there were cross-correlations between terms, the true standard deviation or variance of the full coefficient was not a simple weighted sum of the individual variances. Therefore, the standard deviations on the full coefficients were not as high as would be given by the individual terms. This fact is extremely important when representing lumped coefficients (e.g. $C_{m_q}(\alpha)$) as a polynomial expansion in α for identification purposes where the number of terms to include in the expansions is not known. That is, the estimated accuracy of the results should be determined by computing the variance of the coefficient taking into consideration the cross-correlation between the parameter estimates representing

the coefficients, and not by observing the individual variance of the parameter estimates themselves. Usually, the inclusion of an additional unknown parameter in the expansion will result in increased variances for the individual parameter estimates, but the variance of the lumped coefficient is reduced.

For example, consider the evaluation of a hypothetical coefficient ($y(\alpha)$) which is an n'th order function of α . That is, let

$$y(\alpha) = p_0 + p_1 \alpha + \cdots + p_n \alpha^n \tag{5-9}$$

where $p_0, p_1, \ldots, p_n$ are the unknown parameters to be estimated from the flight data. The estimates of these parameters have assumed known statistics and covariance matrix, P . Defining z and p as

$$\begin{aligned} z &= (1 \;\; \alpha \;\; \alpha^2 \cdots \alpha^n)^T \\ p &= (p_0 \;\; p_1 \cdots p_n)^T \end{aligned} \tag{5-10}$$

$y(\alpha)$ can be expressed as:

$$y(\alpha) = z^T p = p^T z \tag{5-11}$$

Since y is a linear function of p , the variance of y is given by

$$\sigma_y^2(\alpha) = E\left\{ \left[y - E(y) \right]^2 \right\} = z^T P z \tag{5-12}$$

where P is the $n+1$ by $n+1$ covariance matrix of the parameter estimates, p . For $n = 2$ and $p = (a \;\; b \;\; c)^T$, equation (5-12) reduces to:

$$\begin{aligned} \sigma_y^2(\alpha) = {} & \sigma_a^2 + \alpha^2 \sigma_b^2 + \alpha^4 \sigma_c^4 \\ & + 2\alpha \sigma_a \sigma_b \gamma_{ab} + 2\alpha^2 \sigma_a \sigma_c \gamma_{ac} \\ & + 2\alpha^3 \sigma_b \sigma_c \gamma_{bc} \end{aligned} \tag{5-13}$$

where $\gamma_{i,j}$ - are the correlation coefficients between individual terms of the expansion

σ_i - standard deviations of individual terms of the expansion

$i, j \in \{ a, b, c \}$

As an example, the results from the least squares method on record $C_{z}(\alpha)$ are:

C_{z_o}	= .0106	$\sigma_{C_{z_o}}$	= .0342	$r_{C_{z_o} C_{z_\alpha}}$	= -.99
C_{z_α}	= -.0905	$\sigma_{C_{z_\alpha}}$	= .00499	$r_{C_{z_o} C_{z_\alpha^2}}$	= .98
$C_{z_{\alpha^2}}$	= .001903	$\sigma_{C_{z_{\alpha^2}}}$	= .000176	$r_{C_z C_{z_{\alpha^2}}}$	= -1.00

α	$\sigma_{C_z}^2$	σ_{C_z}	$C_z(\alpha)$
10	.000014	.00368	-.704
15	.000002	.00135	-.919
20	.000005	.00228	-1.038

If the correlation coefficients are neglected, the answers would be:

α	$\sigma_{C_z}^2$	σ_{C_z}	$C_z(\alpha)$
10	.00397	.063	-.704
15	.00834	.091	-.919
20	.01609	.127	-1.038

Similarily for $C_{m_q}(\alpha)$:

C_{m_q}	= -51.696	$\sigma_{C_{m_q}}$	= 12.56	$r_{C_{m_q} C_{m_{\alpha q}}}$	= 1.00
$C_{m_{\alpha q}}$	= 7.787	$\sigma_{C_{m_{\alpha q}}}$	= 1.93	$r_{C_{m_q} C_{m_{\alpha^2 q}}}$	= .99
$C_{m_{\alpha^2 q}}$	= -.3015	$\sigma_{C_{m_{\alpha^2 q}}}$	= .0712	$r_{C_{m_{\alpha q}} C_{m_{\alpha^2 q}}}$	= -1.00

α	$\sigma^2_{C_{mq}}$	$\sigma_{C_{mq}}$	$C_{mq}(\alpha)$
10	1.64	1.28	-3.98
15	3.89	1.97	-2.73
20	1.20	1.09	-16.56

or with the cross correlations neglected:

α	$\sigma^2_{C_{mq}}$	$\sigma_{C_{mq}}$	$C_{mq}(\alpha)$
10	581.	24.1	-3.98
15	1252.	35.4	-2.73
20	2459.	49.6	-16.56

The iterated Kalman identification technique as presently programmed has the capability of accepting only initial variances of individual parameters and does not take into account the cross-correlations between parameters representing a total coefficient. That is, the "a priori" weighting matrix, P_o , is diagonal. Therefore, to limit the variances on the full coefficients to reasonable values a multiplier (PK) was used on the inputted variances. The variances were read in as approximately the value of the individual initial parameter estimates squared. Then the PK multiplier was set at some value like .04 to 1.0 to get more realistic values for P_o . For example, multiplying the variance by .04 brings the standard deviation down to 20% of its original value. The value of PK is easily "tuned" to eliminate the effect of "a priori" weighting on the final parameter estimates, if the aircraft is sufficiently excited to be able to uniquely identify all the unknown parameters accurately. If not, these problems are easily determined by comparing the size of the diagonal elements of the final covariance matrix with the diagonal elements of the initial covariance matrix and by denoting the size of the normalized off-diagonal coefficients.

5.3 DISCUSSION OF THE IDENTIFICATION RESULTS FROM THE ITERATED KALMAN FILTER TECHNIQUE

This subsection presents a chronology of the identification results employing the iterated Kalman filter technique on the full scale flight test data. The initial aerodynamic model forms used were those established from the least squares results and the wind tunnel data. As described in Section III, the identification of the longitudinal and lateral-directional coefficients were separated by employing the two four-degree-of-freedom equation of motion

models and measurement systems given in Tables II and III of Section III, respectively. Similar to the preceding subsection, the results are discussed in the following order:

Longitudinal - Low α

Longitudinal - High α

Lateral-Directional - Low α

Lateral-Directional - High α

In all cases, a lower bound on the process noise statistics was computed using the procedure described in Section III and the measurement noise statistics were adjusted using the residual sequences of the filter as a guide (Appendix V) along with the results from the instrumentation consistency checks. These statistics are:

Measurement Noise Statistics

Standard Deviation		Record 9, 10, 11	Record 14, 20
σ_V	ft/sec	.3	.5
σ_α	deg	.1	.2
σ_β	deg	.13	.2
σ_p	^{o}/sec	.4	.5
σ_q	^{o}/sec	.2	.2
σ_r	^{o}/sec	.5	.5
σ_ϕ	deg	.1	.3
σ_θ	deg	.1	.2
$\sigma_{\dot{p}}$	^{o}/sec^2	2.	2.
$\sigma_{\dot{q}}$	^{o}/sec^2	1.	1.
$\sigma_{\dot{r}}$	^{o}/sec^2	1.6	2.
σ_{n_y}	ft/sec^2	.75	.75
σ_{n_x}	ft/sec^2	.3	-

Process Noise Statistics

Standard Deviation	Longitudinal Model		Lateral-Directional Model	
	Record 9, 10, 11	Record 14, 20	Record 9, 10, 11	Record 14, 20
σ_{w_1} -	.14 ft/sec^2	.2 ft/sec^2	.01 deg/sec^2	.01 deg/sec^2
σ_{w_2} deg/sec^2	.1	.15	.04	.06
σ_{w_3} deg/sec	.02	.03	.02	.025
σ_{w_4} deg/sec	.5	.5	.15	.16
σ_{w_5} deg/sec	.5	.5	.02	.07
σ_{w_6} deg/sec	.1	.2	.12	.12

The time history comparisons between the flight data measurements and the predicted responses using the extracted coefficients in the model are given in Figures 34 through 43 for the identification results presented. Crosses represent flight data and solid traces the predicted responses. Also shown in part (b) of these figures are the residual sequences (actual measurements minus the predicted measurements) from the Kalman filter and selected time histories of the parameter estimates during an identification run. On the residual plots, the solid lines represent the calculated $\pm 2\sigma$ values from the identification algorithm and the zeros the residuals. Tables XIV through XXII list the initial and final parameter estimates along with their standard deviations. Also included in each table is the normalized final covariance. The extracted coefficients are compared to the wind tunnel data in Figures 43 and 44. Note that the identification results presented in Tables XIV through XXII are referenced to the actual c.g. position during which the record was taken, while the results in Figures 43 and 44 are normalized to the .33 $\bar{c}$ c.g. position. Significant differences are only discernible for records 14 and 20.

5.3.1 Preliminaries

Before presenting the identification results, however, a short review of the mechanics of identification will be presented to provide a better appreciation and understanding of possible problems which can occur with poorly conditioned data and to discuss the indicators available in the identification algorithm to identify these potential problems.

Most problems caused by poorly conditioned data are those related to the identifiability of the resulting parameter set (model) extracted from the available data. Stated formally (Reference 17) a nonstochastic system, linear or nonlinear, is identifiable if and only if the sensitivity vector functions of the measurements with respect to the unknown parameters representing the system are nontrivial (nonzero) and linearly independent. This, of course, is equivalent to saying that small changes in each parameter must produce a change in the measured responses of the aircraft and these changes

must be a different type for each parameter. If these conditions are met, the accuracy of the parameter estimates are also functions of the level of measurement noise present and the data record length, i.e., the signal to noise ratio in the output measurements.

In practice, unrealistic parameter estimates are usually obtained whenever the sensitivity of the output measurements to changes in these parameters is small (low signal to noise ratio) or else there is strong dependency between the sensitivities of several parameters. These problems are readily identified in the Kalman identification algorithm by comparing the size of the diagonal elements in the final covariance matrix (P_f) with the size of the diagonal elements of the initial covariance matrix (P_0) and by observing the size of the off-diagonal correlation coefficients in the normalized P_f matrix; large values, for example greater than .8, indicate potential problems. Two possible solutions to these problems are to use "a priori" weighting with P_0 or to fix one or more of the parameters in the group which show high correlation at the "best guess" values (e.g. wind tunnel values). "A priori" weighting is accomplished by reducing the magnitude of the initial parameter variance in P_0 so as to reflect a more accurate initial parameter estimate and hence weight the initial estimate more heavily. Other solutions are to use penalty functions in a cost functional which can easily be incorporated into the measurement system with the Kalman technique. In any event, all these solutions are "ad hoc", and usually done on a trial and error basis using good engineering judgment. Generally with short or finite record lengths, "a priori" weighting is always present (or must be used) if large correlations exist between parameter estimates. However, if the model form is adequate, the parameters which exhibit high sensitivity in the measurements and are not correlated with other parameters, usually are extracted relatively accurately even if other groups of parameters are highly correlated. Model adequacy is easily determined from the residual sequences of the iterated Kalman filter (Appendix V).

For the nonlinear aircraft identification problem, it was observed that relatively large correlation usually existed between the parameter estimates making up a particular lumped coefficient (e.g. $C_{m_q}(\alpha)$). If large correlation did not exist between the parameter estimates representing different lumped coefficients, this "internal correlation" did not appear to be a particular problem. It should be realized that the correlation coefficient is a measure of the degree of linearity between two parameter estimates in question. A correlation coefficient close to zero only indicates the absence of a linear relationship between the parameter estimates. It does not preclude the possibility of some nonlinear relationship. If the number of terms in the Taylor's series representing a particular coefficient is not adequate for the range of angle of attack being considered, the resulting extracted coefficient tends to match the actual coefficient only in the range of angle of attack where most of the data and excitation occurs. An additional difficulty occurs when the data record length in which the aircraft excitation occurs is short, as an asymptotically convergent solution is then not possible. In this case, extremely unrealistic coefficient values in certain ranges of angle of attack may be obtained. Consequently, the comparisons between the flight data and predicted responses, which are used as one criteria of goodness for the resulting

extracted coefficients, could be extremely bad. This same problem can also occur when a coefficient whose parameters exhibit low sensitivity in the output measurements are identified grossly in error. In this case, the parameter fix solution works the best. Both problems are cited in the results.

When comparing the estimated coefficients with the wind tunnel data such as given in Figures 43 and 44, it should be noted that the estimated curves represent the mean value of the coefficient. Associated with each estimated coefficient are their second central moments or variances which can be computed from equation (5-12) using the final covariance matrix from the iterated Kalman filter. This band of uncertainty associated with each coefficient should be taken into consideration when comparing the extracted curves to wind tunnel data or when combining estimates from different flight records. However, these variances are only approximately accurate if the model being used is correct. If not, the final covariance from the iterated Kalman filter is in error as explained in Appendix K of Reference 17. Consequently, the residual sequences in the iterated Kalman filter are of added importance, since they serve as an indication of model adequacy.

The coefficient variances were not calculated for all flight records and therefore are not presented. The identification results follow.

5.3.2 Longitudinal - Low Angle of Attack

The majority of the longitudinal low angle of attack identification was done using record 9. Initially, 14 unknown parameters representing C_z and C_m were identified with the x-force contribution to the equations of motion supplied by the $n_{x_{cg}}$ measurement. The initial estimates were taken as the Langley wind tunnel values except for the $C_{z_{\delta e}}$ and $C_{m_{\delta e}}$ coefficients. These were initialized at the Ames wind tunnel values which showed the higher effectiveness that was consistent with the values identified with the least squares method and other flight test results (Reference 27). These coefficients were identified quite accurately, and so they were then held fixed at their estimated values while the six unknown parameters representing the C_x coefficients were identified separately. In each case, the $C_{z_{|\delta a|}}$ and $C_{m_{|\delta a|}}$ parameters were held fixed at their wind tunnel estimates because of the small δ_a inputs. These parameters obviously have very little effect on the responses of the aircraft but they were included for completeness. In fact, these parameters were held fixed at the wind tunnel values and included in all identification runs.

The resulting extracted parameter values are given in Table XIV and the response comparisons between flight data and computed time histories using the 4 DOF longitudinal equations of motion are given in Figure 34(a). The comparisons can be seen to be excellent. As seen in Figure 34(b), the residuals and selected parameter variations indicate adequate model form for this flight record and asymptotic convergence for most parameters. These results were expected, since this record is considered good for identification purposes.

Comparisons of the extracted coefficients to the wind tunnel are given in Figure 43. The static C_z versus α curve agrees almost exactly with the wind tunnel data. C_m showed a positive .03 shift from the wind tunnel

data which is consistent with the least squares results and the positive increment in the extracted $C_{Z_{\delta_e}}$. It is possible C_m could have been expanded to a cubic term in α but this was not done. The static C_x versus α curve showed a positive .05 shift or approximately 2300 pounds less drag or more thrust than the wind tunnel data indicated. Less damping in pitch, C_{m_q}, was also obtained. In general, all coefficients identified were very reasonable. An attempt was also made to identify a cubic C_{m_q} versus α derivative, to see if the form of C_{m_q} would more closely approximate the wind tunnel data. The result was a $C_{m_{\alpha^3 q}}$ term that was almost zero.

These extracted values on record 9 were then used to "predict" the responses from records 10 and 11, which are mainly lateral-directional maneuvers and therefore have very little longitudinal motion. The predicted responses did not match the flight data very well, but the disparity can be attributed to the small longitudinal motions present in these records and also to the slightly higher angle of attack range. Record 10 was then used to identify the static C_m and C_Z coefficients, holding the other coefficients fixed at the values extracted from record 9. All 14 C_Z and C_m parameters were identified on record 11. The resulting response comparisons to the flight data are given in Figures 35 and 36, respectively, and the extracted parameter values are given in Tables XV and XVI. The response comparisons are better than those obtained by using the estimates from record 9 but still not perfect. Small longitudinal motions precluded the accurate extraction of the longitudinal characteristics from these records. Nonetheless, as can be seen from Figure 43, the extracted C_m, C_{Z_q}, $C_{Z_{\delta_e}}$, C_{m_q} and $C_{m_{\delta_e}}$ coefficients are relatively consistent between the records. Note also the change in the C_m versus α curve for record 10, which is a slightly higher angle of attack record. This difference indicates that the form of the wind tunnel data from 10 to 23 degrees is probably accurate but possibly more terms should be added to represent the C_m coefficient for the complete 10 to 23 degree range.

5.3.3 Longitudinal - High Angle of Attack

Records 14 and 20, which have primarily lateral-directional motions, provided the only longitudinal motions in the high angle of attack range. Two problems with these records are readily apparent. First, the record length (time duration) over which the aircraft is excited in the pitch degree of freedom for useful identification is relatively small. Second, the angle of attack response is similar to the slowly monotonically increasing δ_e control input, which, of course, is expected for this type of control input. Consequently, since $\alpha \sim \delta_e$, estimated parameters like $C_{m_{\alpha\delta_e}}$ and $C_{m_{\alpha^2}}$ would be expected to be highly correlated.

Various model forms were tried on these records with the initial parameter estimates set at the wind tunnel values. The best results in terms of the response comparisons with the flight data are given in Tables XVII and XVIII and Figures 37 and 38, for records 14 and 20, respectively.

For record 20, thirteen parameters in C_Z and C_m were identified. The response comparisons are fair, Figure 38(a); however, the parameter esti-

mates have not converged or else model errors are present as indicated by the α , V and n_z residuals. Poor results were obtained when attempting to identify all the C_Z and C_m parameters from record 14. High correlation existed between parameters from C_m and $C_{m_{\delta_e}}$ because of the type of δ_e control input and C_{m_q} was unreasonable.

Consequently, the parameters were held fixed at the values extracted from record 20 except for six parameters in the C_Z , C_m and $C_{m_{\delta_e}}$ coefficients. The extracted parameter estimates are given in Table XVII and the response comparisons in Figure 37. Note that only the constant parameter of the static C_m coefficient was identified because the other two parameters were highly correlated with the $C_{m_{\delta_e}}$ and $C_{m_{\alpha\delta_e}}$ parameters. Similar to record 20, the residuals indicate modeling errors, especially the α residual, Figure 37(b).

The divergence of the α residuals in both records occurred at approximately the same time that the large inconsistencies in the α_V measurement were noted during the instrumentation consistency checks, Section 5.1. These α_V inconsistencies were attributed to large errors in the attitude measurements and were treated accordingly. However, the possibility now exists that the measurement is indeed in error at the high angles of attack or else, of course, the aerodynamic model is incorrect and errors are accentuated at the high angle of attack. The poorly conditioned data precluded further investigation of this potential problem. Consequently, the results are inconclusive.

Comparisons between the identified coefficients and the wind tunnel data are shown for records 14 and 20 in Figure 43. The static C_m and $C_{m_{\delta_e}}$ coefficients are very consistent between records and they exhibit trends similar to the low α results.

5.3.4 Lateral-Directional - Low Angle of Attack

All the low - α lateral-directional identification was done on data from records 10 and 11, since record 9 was primarily a longitudinal maneuver with extremely small lateral-directional motions. However, these records were poorly conditioned for extracting all lateral-directional parameters simultaneously. Recall that record 10 contained aileron pulse type inputs but little rudder movement, while record 11 had rudder pulse type inputs and little aileron movement. One drawback to both records is that yaw rate is extremely small. This implies that the sensitivity of the measurements to changes in all the parameters representing the r derivatives will be extremely small and therefore difficult to extract accurately.

Various identification attempts were made with different model complexities, using the wind tunnel data for initial parameter estimates. For example, these attempts included identifying all coefficients, holding some control coefficients fixed at the wind tunnel values, and also using different complexities to describe the static coefficients and the dynamic coefficients and cross-coefficients. As expected, when attempting to identify all coefficients simultaneously from these records, high correlation existed between the parameters representing the control derivatives which were lightly excited

(e.g. $C_{n_{\delta_r}}$ and $C_{l_{\delta_r}}$ for record 10) and the static coefficients. As a result, unrealistic values were identified for these coefficients. In addition, all the yaw rate derivatives and dynamic cross-derivatives were impossible to extract with any repeatability between records because of the low excitation of the yaw degree of freedom. For all identification tries, the n_y measurement was used as the y-force contribution in the equations of motion.

The best results were obtained on record 10 when the $C_{l_{\delta_r}}$, $C_{n_{\delta_r}}$ and C_{l_r} derivatives were held fixed at the wind tunnel values and only constant parameters were used to model C_{n_p} and C_{n_r}. Response comparisons and the extracted parameter values are given in Figures 39 and Table XIX, respectively. Although the residuals do indicate slight modeling errors, the response comparisons are fair. C_{n_r} was identified as an extremely low value and is highly correlated with C_{n_0}, the parameter modeling yawing moment asymmetries.

Results for record 11 are given in Table XV and Figure 40 shows the response comparison to flight data. Fifteen parameters were identified, with $C_{l_{\delta_a}}$, $C_{n_{\delta_a}}$ and $C_{l_{\delta_r}}$ derivatives held fixed at the wind tunnel values and the C_{l_r}, C_{n_r} and C_{n_p} modeled as constants. Again, the response matches are fair.

Comparisons of the extracted aerodynamics to the wind tunnel curves are presented in Figure 44. The C_{l_β} versus α curves for both records were very consistent and show a shift of approximately 2 degrees to the right of the wind tunnel curves. The aileron derivative extracted from record 10 shows less effectiveness than the Langley wind tunnel but the rudder derivative ($C_{n_{\delta_r}}$) identified from record 11 was more consistent with the Ames data. The values of C_{n_β} were not consistent possibly because of low yaw degree of freedom excitation.

Consistent rolling moment asymmetries were extracted, possibly due to actual aerodynamic asymmetries or else the roll controller (δ_a) was rigged (or its response recorded) with an offset.

In general, the model form and complexity used appeared to be adequate, but further analysis with better conditioned data is required.

5.3.5 Lateral-Directional - High Angle of Attack

Records 14 and 20 were rolling departures from a normal stall entry and had relatively large amplitude, low frequency, motions in roll and yaw rate, and sideslip angle. However, the aileron and rudder control inputs were relatively small and initial attempts to identify these control coefficients therefore led to identified values for the coefficient which were both unrealistic and had high correlations with the static coefficient parameters. Consequently, the $C_{l_{\delta_a}}$, $C_{n_{\delta_a}}$, $C_{l_{\delta_r}}$ and $C_{n_{\delta_r}}$ control derivatives were held fixed at the wind tunnel values for all subsequent identification tries.

Various model complexities were tried with the wind tunnel data serving as initial estimates for the C_ℓ and C_n coefficients; the C_y coefficients were not identified. The time duration of these records is such that the aerodynamic models postulated must be complex enough to describe the characteristics exhibited by the aircraft from approximately 20 to 40 degrees angle of attack. Identification over a lesser angle of attack range, and therefore the use of a simpler model, was not possible, since there was not a long enough time slice in the records where a simple model could be used and identified.

The simpler models tended to give the better response comparison to the gross motions, but they were inadequate in describing the salient characteristics exhibited in the aircraft responses. In all cases, some of the residuals became large and divergent when angle of attack approached 30 to 33 degrees, hence indicating the onset of modeling errors. This problem occurred at approximately the same time within the flight records that the inconsistency in the angle of attack measurement was noted during the instrumentation consistency checks and the longitudinal high α identification, Section 5.3.3. Consequently, subsequent identification tries were limited to the angle of attack ranges of approximately 20 to 30 degrees for record 14, and 20 to 33 degrees for record 20. This limitation provided only 10 and 7 seconds of data, respectively.

Response comparisons to the flight data for these short record lengths are given in Figures 41 and 42 for records 14 and 20, respectively. The model forms used and the identified parameter values are presented in Tables XXI and XXII. More complex models tended to give unrealistic coefficient values, especially for the dynamic derivatives, because of the high correlation between particular sets of parameters for these short record lengths.

However, as shown in Figure 44, some trends are apparent. The identified static C_ℓ and C_n coefficients seemed to be consistent with the lower α coefficients. At approximately 20 degrees α, the C_{ℓ_β} coefficients seemed to confirm the shift observed in the lower α runs. The C_{n_β} versus α curve appeared to follow the same trends as that of wind tunnel values. C_{n_β} seemed to reach a negative maximum at a higher α but at about the same value of C_{n_β}. The dynamic derivatives appeared to be in the same area as the wind tunnel values but no conclusive statements can be made about them.

Definite conclusions as to the adequacy of the model forms could not, of course, be established. However, it is believed the C_{ℓ_β} and C_{n_β} curves would more adequately be represented by cubic to fourth order polynomials for this angle of attack range. Further analysis is clearly needed with "well conditioned" flight data, which can only be made available from carefully planned, future flight test programs at high angles of attack.

5.4 ANALYSIS OF RADIO CONTROLLED DROP MODEL DATA

One of the objectives of this study was the investigation of the correlation between the wind tunnel data and the radio controlled drop model (RC) data. Data were obtained from six drop tests made with the identical

model used in the Langley wind tunnel tests. Of the six records available, two of the runs (RC1 and RC3) were chosen for analysis. Time histories of these runs are shown in Figures 56 and 57 of Appendix I. These were the only runs where step control inputs were not applied concurrently. The analysis of the other records would not separate the effects of the individual controllers.

Approximately twenty seconds of real time model data are available on each of the two runs at a sample rate of twenty samples per second. This corresponds to about fifty-five seconds of data at a sample rate of 7.22 samples per second when dynamically scaling the model data to full scale.[3] Both runs involved control surface deflections of the full throw verity; full aft elevator followed by full rudder and aileron deflections. These types of inputs put the model into the high angle of attack range in less than one-half a second (real time). The angle of attack oscillated between thirty and fifty degrees and the sideslip between plus and minus fifteen degrees. This continued for approximately ten seconds on both runs until the elevator was abruptly reversed and then brought back to full aft again. This reduced the angle of attack to less than zero, then back to thirty to fifty degrees. As a result, very little data in the ranges of angle of attack less than thirty degrees exists, and therefore it was decided to identify parameters only from the data above this value.

Since attitude and acceleration measurements were not available, instrument consistency checks could not be made and only the moment stability and control derivatives could be identified. Also, because of the limited measurements, only the least squares equations-of-motion parameter identification scheme was used, and no time history integrations could be made.

Moment time histories were generated from the RC flight data and an analytical model which adequately defined the wind tunnel model in this 30-50 degree range was chosen, which had 28 coefficients including nonlinear effects due to angle of attack. Table XXIII lists the parameters that were identified for each run. Figure 45 shows the extracted identified parameters from the two runs, RC1 and RC3, plotted with the wind tunnel model parameters. Figures 46 and 47 show the moment time history matches between the least squares results evaluating the moment equations and the radio controlled model flight data.

As seen from Figure 45, most of the coefficients identified showed good correlation with the wind tunnel data. These included:

---

[3] The scaling ratio between the full scale (f.s.) and model (m) time is (Reference 28):

$$\frac{t_{fs}}{t_m} = \left(\frac{\ell_{fs}}{\ell_m}\right)^{1/2} = \left(\frac{1}{.13}\right)^{1/2} = 2.77$$

$$\left[C_{m_o} + C_{m_\alpha}(\alpha)\right], \quad \left[C_{m_q} + C_{m_{q\alpha}}(\alpha) + C_{m_{q\alpha^2}}(\alpha^2)\right],$$

$$\left[C_{m_{\delta_e}} + C_{m_{\delta_e\alpha}}(\alpha)\right] - RC\,3\ only, \quad \left[C_{l_{\delta_a}} + C_{l_{\delta a\alpha}}(\alpha)\right],$$

$$\left[C_{l_{\delta_r}} + C_{l_{\delta_r\alpha}}(\alpha)\right], \quad \left[C_{n_p} + C_{n_{p\alpha}}(\alpha) + C_{n_{p\alpha^2}}(\alpha^2)\right] - RC3\ only$$

$$\left[C_{n_r} + C_{n_{r\alpha}}(\alpha)\right], \quad \left[C_{n_{\delta_a}}\right], \quad \left[C_{n_{\delta_r}} + C_{n_{\delta_r\alpha}}(\alpha)\right] - RC3\ only$$

The wind tunnel data had shown that a few terms were highly nonlinear with respect to angle of attack near 30 degrees. However, due to insufficient flight data near 30 degrees the identified coefficients did not indicate this large nonlinearity and only matched the wind tunnel data past 35 to 40 degrees. These terms included:

$$\left[C_{l_p} + C_{l_{p\alpha}}(\alpha) + C_{l_{p\alpha^2}}(\alpha^2)\right], \left[C_{l_r} + C_{l_{r\alpha}}(\alpha) + C_{l_{r\alpha^2}}(\alpha^2)\right]$$

There was a third set of terms which did not match the wind tunnel derived values as well as the others. The identified functions of angle of attack matched the wind tunnel data fairly well in part of the 30 to 50 degree range. However, the functional relationship with angle of attack was opposite that of the wind tunnel derived coefficients, so that one or both ends of the range near 30 or 50 degrees were poorly matched. This discrepancy could be due to the small amount of RC flight data at the extremes of the α range and the low overall effect of angle of attack on these coefficients. Additionally, the covariance matrix from the least squares estimation indicated a high correlation for these coefficients between the constant and angle of attack terms. These coefficients included:

$$\left[C_{m_{\delta_e}} + C_{m_{\delta_e\alpha}}(\alpha)\right] - RC1\ only, \quad \left[C_{l_\beta} + C_{l_{\beta\alpha}}(\alpha)\right]$$

$$\left[C_{n_\beta} + C_{n_\alpha}(\alpha)\right], \quad \left[C_{n_p} + C_{n_{p\alpha}}(\alpha) + C_{n_{p\alpha^2}}(\alpha^2)\right] - RC1_{only},$$

$$\left[C_{n_{\delta_r}} + C_{n_{\delta_r\alpha}}(\alpha)\right] - RC\,1\ only$$

In addition to the identification of parameters described above, the coefficients derived from the wind tunnel data were used to see if a better match to the moment time histories was possible. This involved using the least squares identification method with all of the coefficients fixed at the wind tunnel values, except for the constant terms C_{ℓ_0}, C_{m_0} and C_{n_0}. This approach was taken to see if the wind tunnel model would accurately describe the moments developed on the RC model. The resulting time history comparisons were good, but the variances of the fits to the moments were much lower using the extracted coefficients.

Conclusions which can be drawn from this analysis are as follows:

1. Good correlation appears to exist between some of the identified parameters from the radio controlled drop model data and the wind tunnel data. The use of the same model in both sets of tests contributes to this good correlation, and, furthermore, the implication is that the instruments used on this model may very well be adequate for extraction of the moment coefficients. However, no integrated time history comparisons were possible.

2. Better maneuvers can be defined. Due to the types of inputs (constant steps) and developed motions (steady oscillations in all of the states), many of the estimated parameters showed a high degree of correlation with each other. If a more judicious set of switching type inputs was applied that kept the model in the range of interest without steady oscillations developing in all the states, some of the fine effects due to angle of attack could possibly be identified.

5.5 CORRELATION OF RESULTS

This subsection summarizes the correlation between the identified coefficients from full scale flight test data and those derived from the wind tunnel data. Also presented are the correlations between the coefficients obtained from the radio controlled model flight data and the wind tunnel. Refer to Figures 43 through 45 for the plots of these coefficients. It is worth observing that, in several cases, the correlation or lack thereof is inconclusive as a result of the poor data quality for identification purposes. Nonetheless, trends are generally apparent even in these cases and will be delineated. In most cases, the forms of the coefficients (versus α) identified are in good agreement with the wind tunnel data and their values usually fall within the range of the two wind tunnel data sets. However, since the identified coefficients provide a much better match to the flight responses, it is thus concluded that they are in general more accurate than the wind tunnel data.

C_Y versus α (page 159) - Most of the lower angle of attack identification runs with the least squares and Kalman methods indicate very good correlation with both sets of wind tunnel data. However, as the angle of attack increases beyond 30 degrees the identified C_Y generally indicates higher lift than the wind tunnel data. As was discussed in Section 5.3.3, the quality of the data and of the instrumentation in the higher angle of attack range precluded good identification results. Therefore, the accuracy of the wind tunnel data in this range could not be ascertained.

C_X versus α (page 159) - The results for both identification techniques generally indicate that the C_X coefficient is approximately .05 higher than that shown by the Langley wind tunnel results, which corresponds to 2300 pounds less drag or more thrust. The difference is somewhat less for the Ames data. The identification results are consistent with some available full scale drag polars which indicate similar C_X values. Inaccuracies in the calculation of C_X coefficients from wind tunnel data can be due to a number of factors. First, the wind tunnel model is not an exact replica of the full scale airplane. Estimation of drag due to stores and the effect of mass flow through the engines cannot be determined very accurately. Secondly, the Reynolds number is also very different for the two vehicles: for example, 1.4×10^6 for the Langley wind tunnel and around 17×10^6 for the full scale vehicle. Third, the precise calculation of installed thrust on the aircraft is very hard to accomplish. Therefore, although it appears that the identification techniques are giving an accurate C_X coefficient, the correlation of these results with wind tunnel and computed values is inconclusive.

C_m versus α (pages 159 and 167) - Both the lower and high angle of attack coefficients identified from the full scale data indicate a more positive C_m than the wind tunnel does. Since the calculated responses match the flight data fairly well on the lower α, record 9, the .03 C_{m_o} offset from the Langley data appears to be correct. The identification of the actual slope along the curve, or C_{m_α}, is much harder to obtain and little confidence can be given to any of the actual shapes of the curves, especially at the high α values. Even between 10 and 20 degrees where C_m versus α is known to be relatively flat, the identified α curve was sometimes slightly concave or convex, depending upon initial estimates for parameters and variances. At the higher angles of attack the accurate determination of C_m is hampered by the fact that the record lengths are not long enough and do not include enough α motions. However, the identified C_m is closer to the Ames wind tunnel data than the Langley data. The least squares identification of C_m versus α from the radio controlled model data matches the Langley wind tunnel values fairly well, due to the many α oscillations and because the same physical model was used in both tests.

C_{Yq} versus α (page 160) - Since this is a very minor term in the equations of motion and therefore would be very difficult to identify, this coefficient was approximated by a constant for identification purposes. The identification results were generally in the same area as the wind tunnel values. However, if values two or three times their size were used for C_{Yq}, the responses would not change greatly. Therefore, little confidence can be held in the actual identified values.

C_{L_q} versus α (page 160) - This term is also very hard to identify with any confidence. Values for identified from the full scale flight data fell generally in the same order of magnitude as the wind tunnel values, but sometimes looked unrealistic.

C_{m_q} versus α (pages 160 and 168) - The C_{m_q} coefficients extracted from full scale flight data show good correlation with the Langley wind tunnel results. Although on some records poor least squares results were obtained, the Kalman method seemed to extract reasonable values for C_{m_q} and yielded good response matches to the flight test data. Also using the C_{m_q} derived from the wind tunnel data along with static coefficients from the Kalman technique yielded good response matches indicating that the wind tunnel values for C_{m_q} are fairly good. The results from the radio controlled model also indicate good correlation with this wind tunnel coefficient at the higher angles of attack.

$C_{\eta_{\delta_e}}$ versus α (page 161) - This coefficient was consistently identified as being much higher than what the Langley wind tunnel had shown and closer to the Ames data. This consistency and the good longitudinal response matches indicate that the higher effectiveness is actually present in the full scale aircraft.

$C_{L_{\delta_e}}$ versus α (page 161) - This parameter is relatively minor and could not be identified with any consistency from the flight data and therefore, no correlations could be determined about this coefficient.

$C_{m_{\delta_e}}$ versus α (pages 161 and 169) - For the low angles of attack the identified moment effectivenss of the elevator was higher than the Langley wind tunnel value, similar to and consistent with the lift effectiveness. This was also shown in the Ames wind tunnel data. However, in the higher angles of attack records this feature was not as certain. In these higher α records there was less repeatability or consistency with the results. The identified values for $C_{m_{\delta_e}}$ appeared to go through the wind tunnel derived values at some angle of attack in the range of interest, but the shape could not be determined with any certainty. The radio controlled model results also show this inconsistency with a positive slope identified on one record and a negative slope on the other. The reason for all this uncertainty is probably the elevator inputs applied. In the full scale tests at the high angles of attack they usually were gradually increasing deflections that were highly correlated with angle of attack. The radio controlled model inputs were just full deflection steps. These types of inputs do not allow the identification of the angle of attack effects on $C_{m_{\delta_e}}$.

C_{y_β} versus α (page 162) - This coefficient was identified with the least squares method only, primarily because the data quality precluded obtaining very good response matches with the Kalman method when identifying just the C_l and C_n coefficients, and if the C_y coefficients had been identified with the Kalman method too, the results would be expected to be poor. The C_{y_β} obtained from the least squares method was fairly close to both wind tunnel values until about $\alpha \approx 30^\circ$, where it then followed the Langley data. Therefore, at least for this aircraft, the wind tunnel results appeared to accurately predict the full scale C_{y_β}.

C_{l_β} versus α (pages 162 and 170) - One fact must be noted about this and the rest of the lateral-directional coefficients. Generally, the time response matches to the full scale flight data from the identification were only fair as a result of badly conditioned data. Therefore, the quantitative results are inconclusive. The static coefficients did show some consistent trends, but little could be said about the dynamic derivatives.

The identified C_{l_β} versus α curves showed a consistent shift of approximately two degrees to the right of the wind tunnel derived curves and also seemed to remain more negative than the wind tunnel values. Though no conclusive statements can be made because of the poor response matches, this shift in C_{l_β} could be due to the larger tail surface on the full scale airplane giving rise to a larger rolling moment with sideslip. Past an angle of attack of 30 degrees the results were inconsistent, and no correlation can be attempted. The extracted values from both runs of the radio controlled model flight data were very consistent, but correlated poorly with the Langley data.

C_{n_β} versus α (pages 162 and 170) - For the low angle of attack records inconsistent results for C_{n_β} were obtained. This inconsistency is likely due to poor β, r and α excitation in these records. The values for C_{n_β} appeared to approximate those indicated from the wind tunnel results, but accurate shapes and positions of the true full scale C_{n_β} could not be determined. Small differences in slopes and maximum amplitude between the full scale identified values and the wind tunnel results could be due to the larger tail on the full scale airplane. The results from the radio controlled model flight data were similar to the C_{l_β} results; consistency between runs but poor correlation with the Langley wind tunnel values.

C_{y_p} versus α (page 163) - Identification of this parameter was attempted with the least squares method only. Very inconsistent results were obtained. The only statement that can be made about the value of C_{y_p} is that its order of magnitude is the same as that shown in the wind tunnel results.

C_{n_p} versus α (pages 163 and 171) - This cross derivative was very hard to identify accurately, and, in fact, it was even difficult to model accurately in the angle of attack ranges of interest. The two wind tunnel test results also gave completely different looking curves. Most of the time in the identification runs, C_{n_p} was identified as a constant or linear function of angle of attack and its resulting values came out near the average value of C_{n_p} from the wind tunnel results. A similar result was obtained with the radio controlled model.

C_{l_p} versus α (pages 163 and 171) - The identified results for the coefficient were somewhat consistent for the lower angle of attack range. They generally appeared to follow the same magnitudes and shapes as those derived from the wind tunnel values but conclusive results could not be established. The radio controlled model derived values also were consistent and fairly close to the wind tunnel data.

C_{y_r} versus α (page 164) - Again, as with the identification of C_{y_p}, very poor results were obtained for this coefficient. The least squares results were only close to the wind tunnel value for C_{y_r} over a limited portion of the angle of attack range of interest.

C_{n_r} versus α (pages 168 and 172) - The most reasonable results for this coefficient were obtained when it was identified as a constant. The difficulty in the identification of the r coefficients was due to the small amount of r excitation in the records, and in some of the identification runs C_{n_r} was simply set equal to the wind tunnel values. The C_{n_r} derived from the radio controlled model tests did approximate the wind tunnel values very closely for most of the angle of attack range, but in these records there were many r and α oscillations.

C_{l_r} versus α (pages 164 and 172) - The identification results for C_{l_r} were similar to those for C_{n_r}. Usually only constant values could be realistically identified, but often very poor response matches were obtained. The results from the radio controlled model did indicate that the model had a C_{l_r} similar to that obtained in the wind tunnel. Again, there seemed to be enough r motion in these records. Since the C_{n_r} and C_{l_r} from the radio controlled model results appeared to be the same as the Langley wind tunnel values, it was considered to be reasonable to use these wind tunnel values as known values when identifying static coefficients with some of the full scale flight data.

$C_{n_{\delta_a}}$ versus α (pages 165 and 173) - Generally, fairly good correlation was obtained between the identified values for $C_{n_{\delta_a}}$ and the wind tunnel values for low angles of attack, record 10. On the other records there was not enough aileron motion to extract these derivatives. The radio controlled model derived coefficient also matched the wind tunnel data fairly well. Again, because of the good radio controlled model parameter matches, it was reasonable to use the wind tunnel aileron derivatives as known values in the other identification runs.

$C_{l_{\delta_a}}$ versus α (pages 165 and 173) - The same thing that was said about $C_{n_{\delta_a}}$ can be said of $C_{l_{\delta_a}}$. Only record 10 could be used to get realistic values for $C_{l_{\delta_a}}$ and the extracted value was lower than the wind tunnel data. The results from the radio controlled model flight data were fairly close to the wind tunnel values, but there was no consistency between identification runs.

$C_{y_{\delta_r}}$ versus α (page 166) - Only record 11 had enough rudder movement to identify $C_{y_{\delta_r}}$ derivatives and the $C_{y_{\delta_r}}$ extracted with the least squares technique from this record passed through the wind tunnel data fairly close. However, the results are inconclusive, since there was not enough rudder excitation in the other flight records to establish consistency.

$C_{n_{\delta_r}}$ versus α (pages 166 and 174) - The least squares results for $C_{n_{\delta_r}}$ were inconclusive. An attempt was made to identify this derivative with the Kalman technique on record 11 to obtain more definitive results. The best Kalman identification obtained indicated that $C_{n_{\delta_r}}$ was slightly higher than the Langley wind tunnel results and closer to the Ames results. However, since the response matches were only fairly good, no conclusive statement can be made. Values obtained for $C_{n_{\delta_r}}$ from the radio controlled model data were also slightly higher than the Langley wind tunnel results.

$C_{l_{\delta_r}}$ versus α (pages 166 and 174) - The least squares results for $C_{l_{\delta_r}}$ on record 11 were similar to those obtained with $C_{y_{\delta_r}}$ and $C_{n_{\delta_r}}$. It appeared that there was enough rudder motion to get an average value for $C_{l_{\delta_r}}$ for the α range of interest but not enough δ_r and α to get a good estimation on the variation with α. The values extracted from both runs of the radio controlled model were very consistent and slightly lower than the Langley wind tunnel values.

Concluding Remarks

This subsection has discussed the correlation of full scale flight data and radio controlled model flight data with wind tunnel data. An additional correlation, which was not performed, would have been between identified flight data derivatives and those that can be computed using the Air Force Stability and Control DATCOM techniques. This additional correlation was felt to be unnecessary, and was therefore not performed for the following reasons. The results obtained in this program indicate the need for improved flight test techniques at high angles of attack to obtain data suitable for identification. Specifically, the identification results for $\alpha \geq 30^{\circ}$ were severely compromised by the poor data quality of the flight tests. As has been discussed in this section, correlation of the full scale identified parameters with wind tunnel data was frequently inconclusive as a result. Therefore, attempting an additional correlation with DATCOM computations would have been equally inconclusive. Although there is no question that the accuracy of DATCOM methods must be investigated, such an investigation should be accomplished in the future when better conditioned flight data is available.

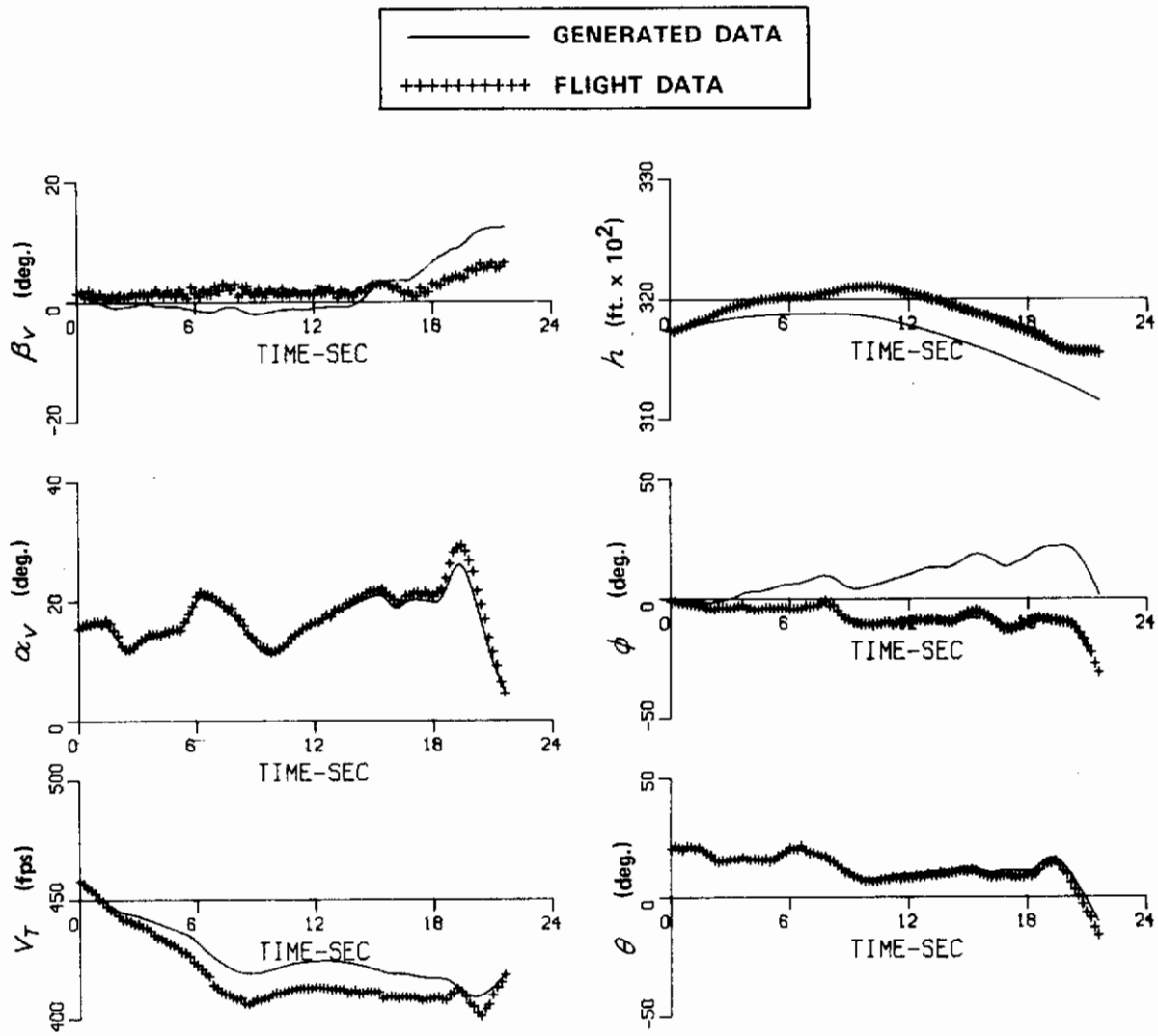

Figure 14 COMPARISON OF FLIGHT DATA WITH RESPONSES GENERATED FROM THE KINEMATIC EQUATIONS WITH NO BIASES – RECORD 9

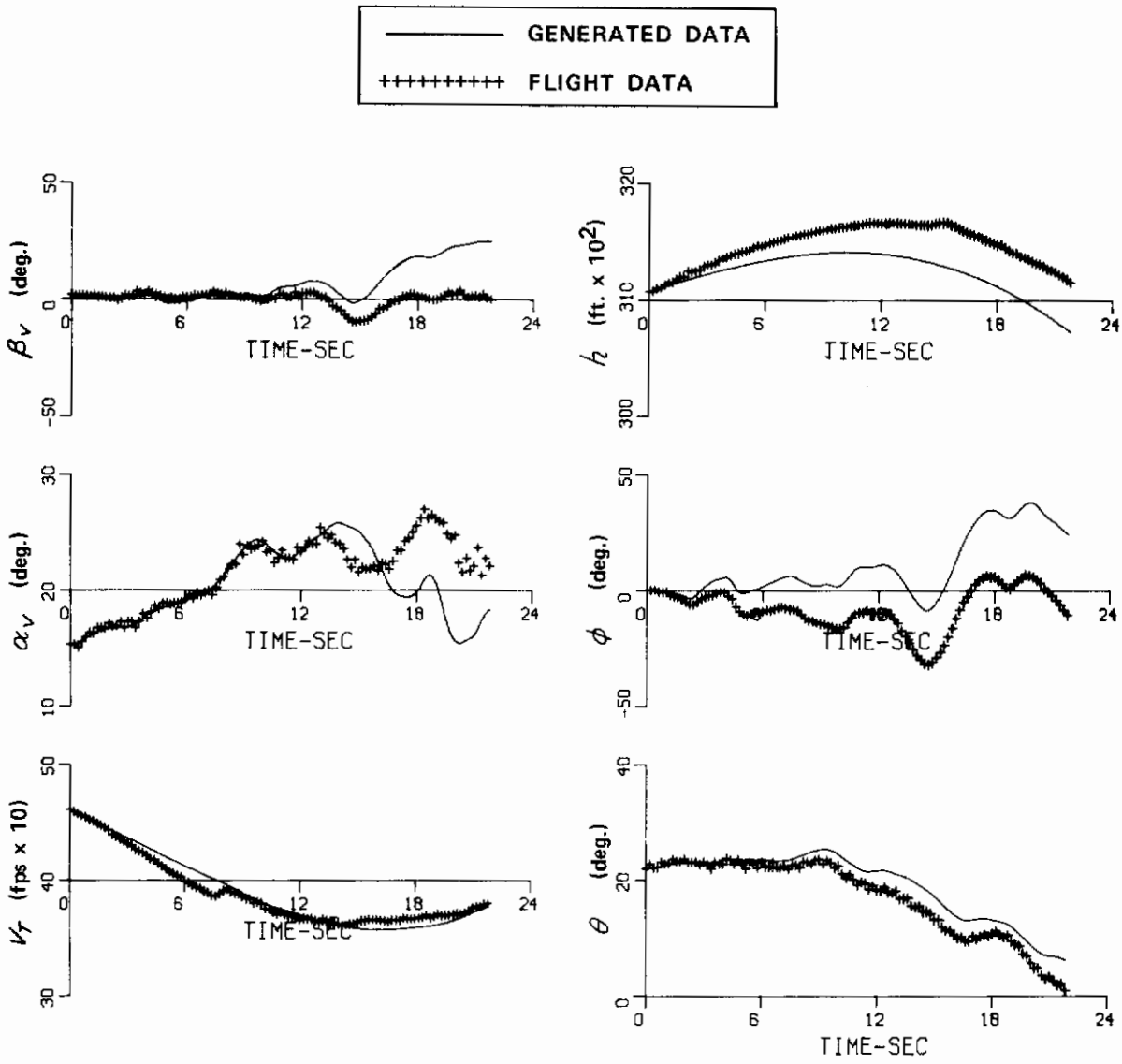

Figure 15 COMPARISON OF FLIGHT DATA WITH RESPONSES GENERATED FROM THE KINEMATIC EQUATIONS WITH NO BIASES – RECORD 10

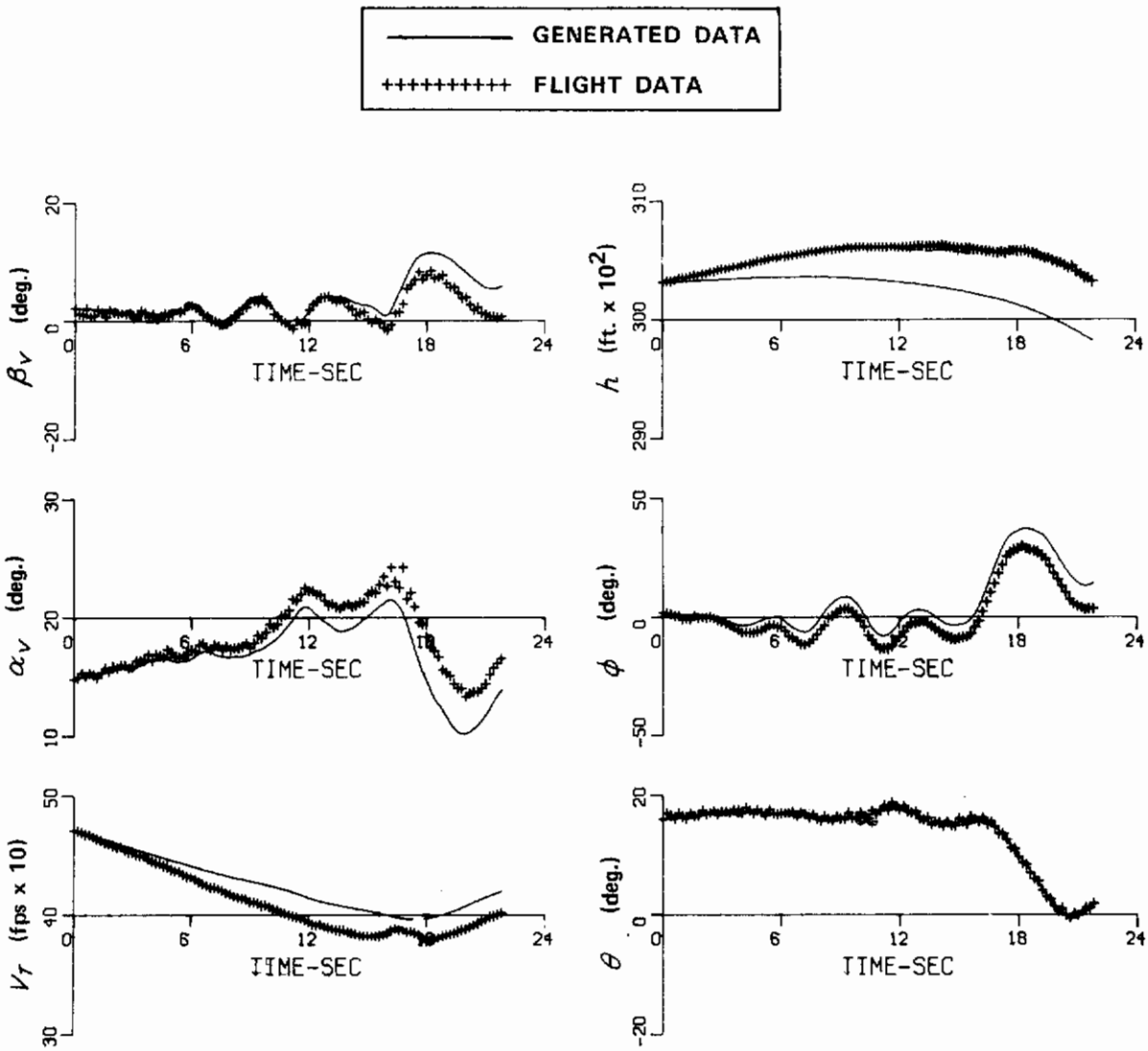

Figure 16 COMPARISON OF FLIGHT DATA WITH RESPONSES GENERATED FROM THE KINEMATIC EQUATIONS WITH NO BIASES – RECORD 11

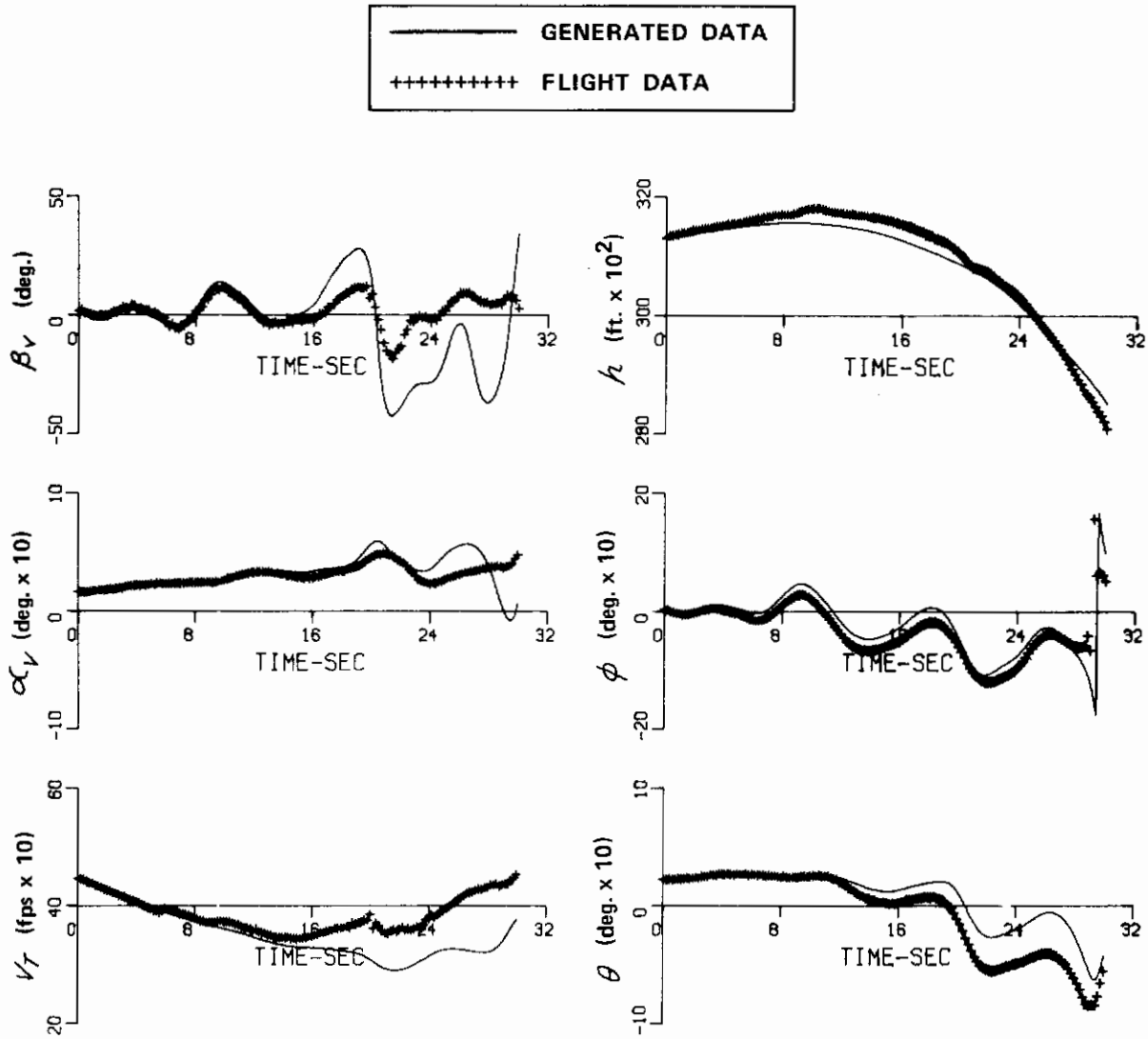

Figure 17 COMPARISON OF FLIGHT DATA WITH RESPONSES GENERATED FROM THE KINEMATIC EQUATIONS WITH NO BIASES – RECORD 14

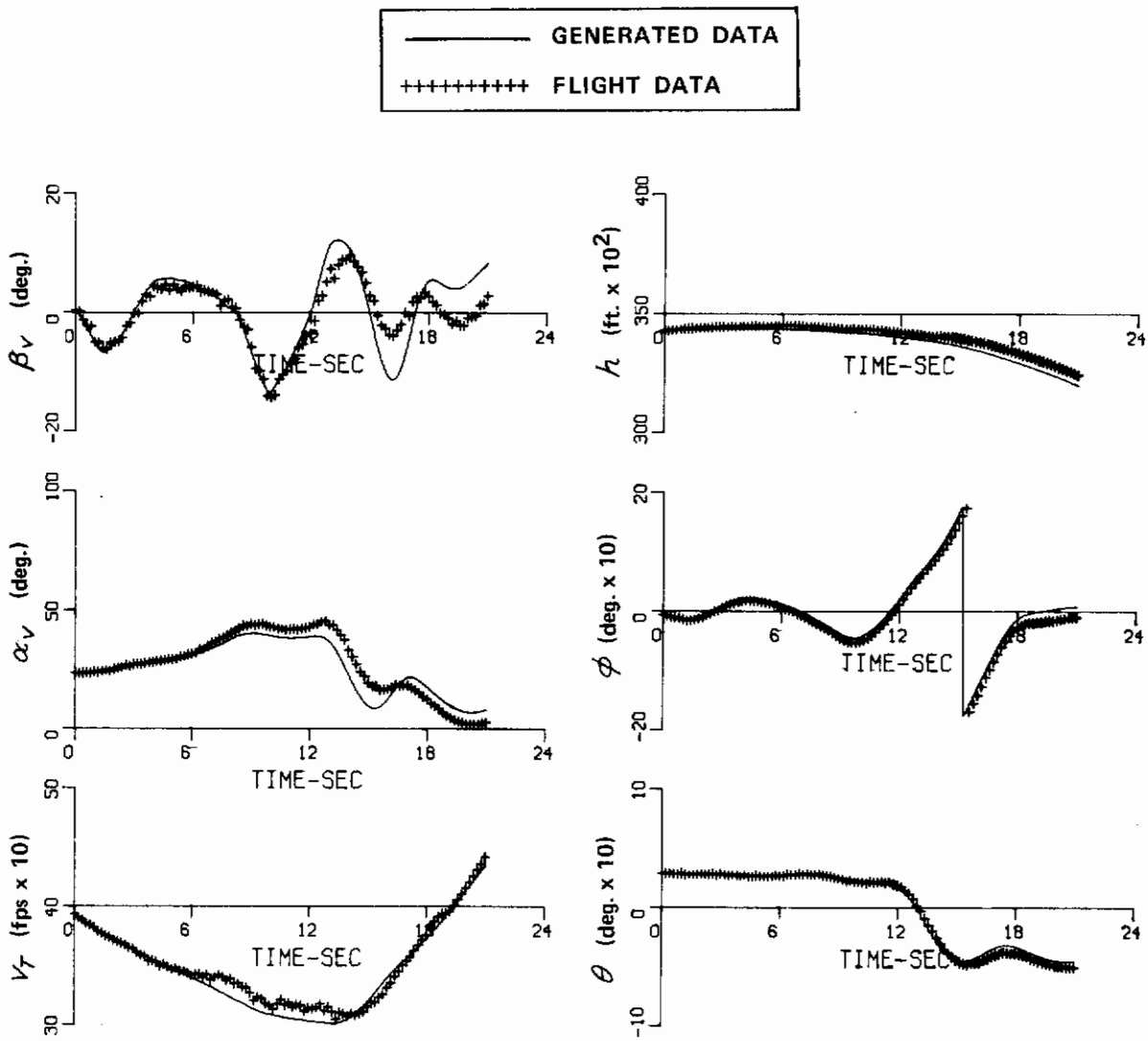

Figure 18 COMPARISON OF FLIGHT DATA WITH RESPONSES GENERATED FROM THE KINEMATIC EQUATIONS WITH NO BIASES – RECORD 20

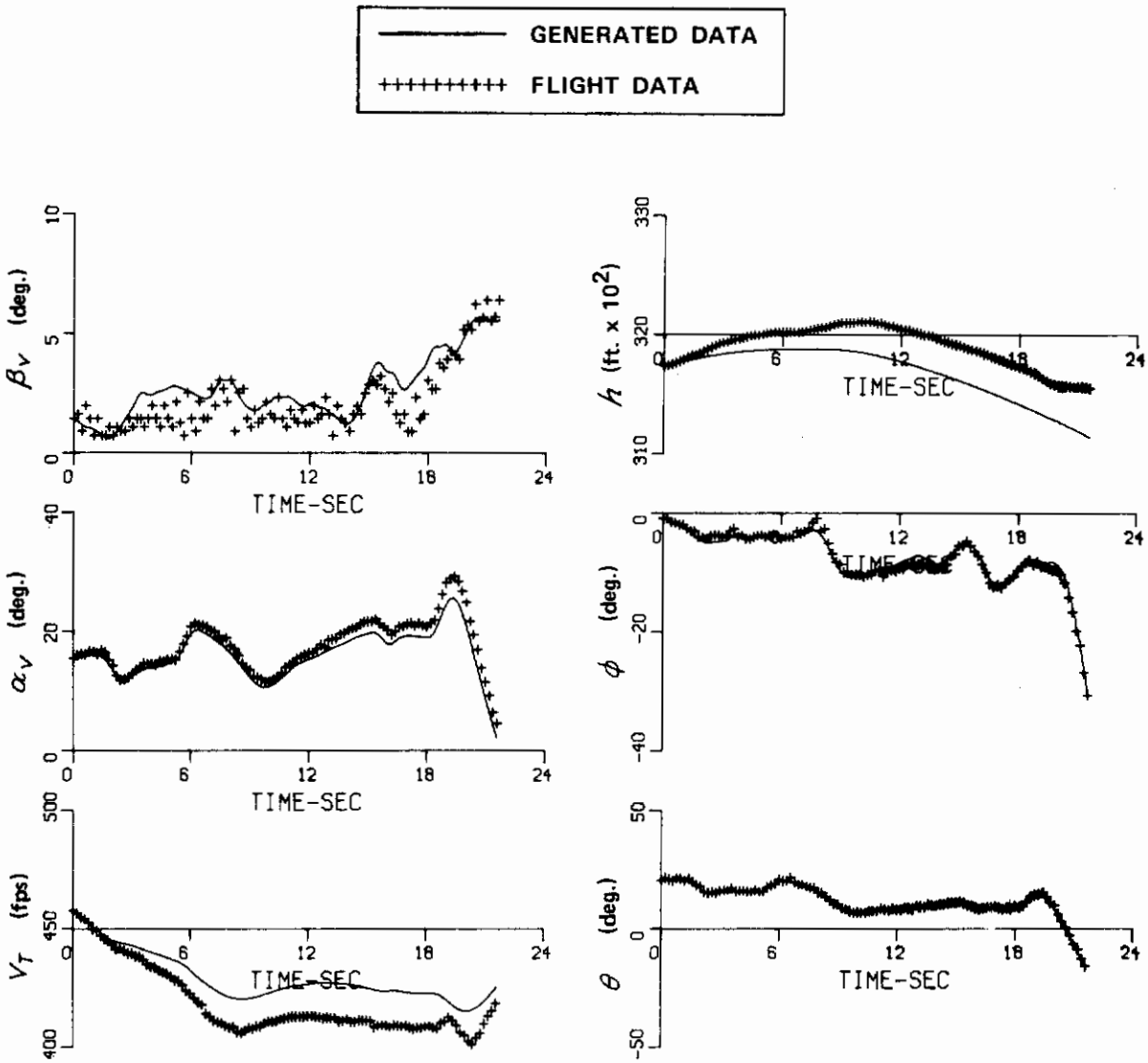

Figure 19 COMPARISON OF FLIGHT DATA WITH RESPONSES GENERATED FROM THE KINEMATIC EQUATIONS WITH IDENTIFIED p_b, q_b AND r_b BIASES – RECORD 9

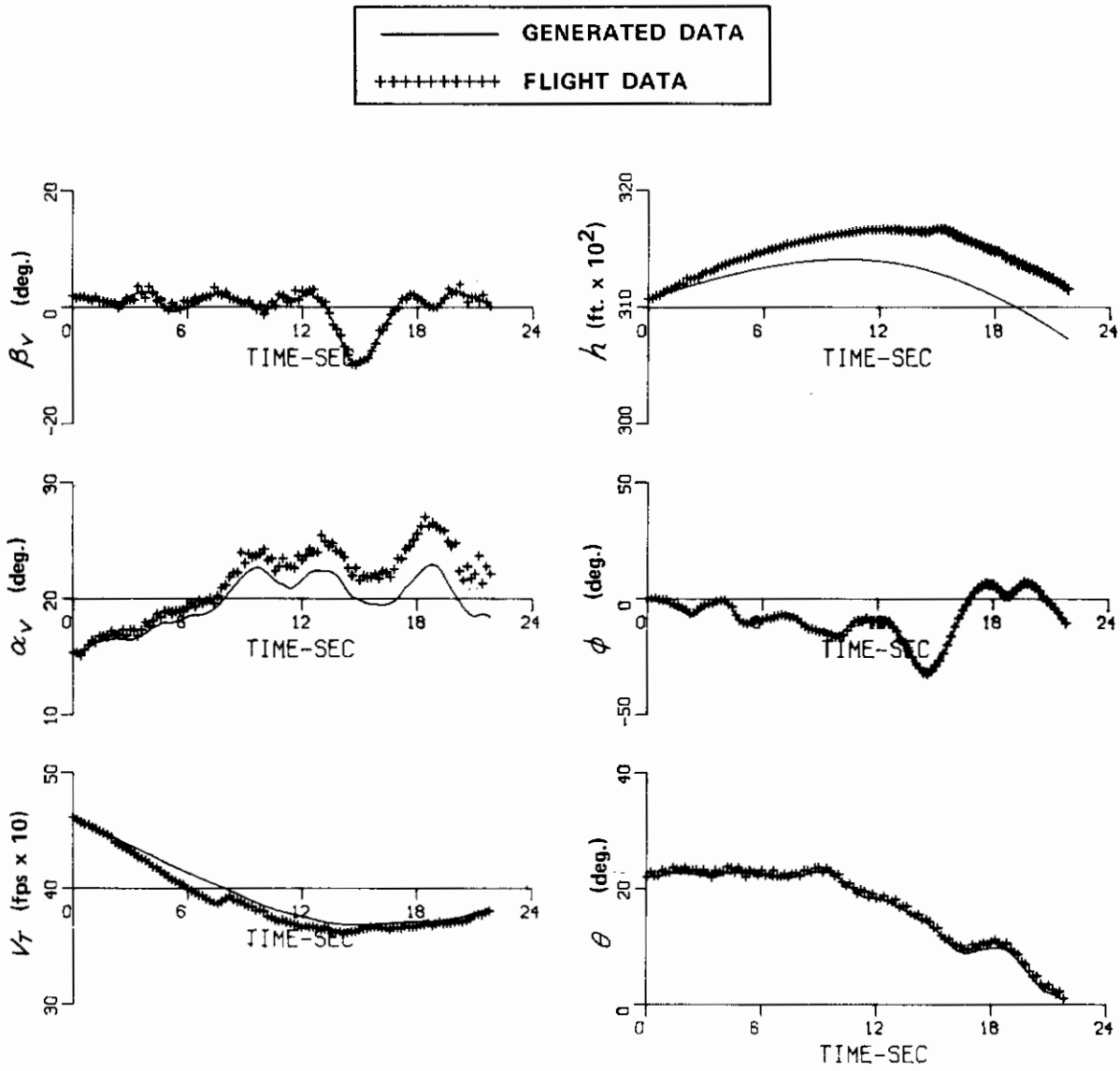

Figure 20 COMPARISON OF FLIGHT DATA WITH RESPONSES GENERATED FROM THE KINEMATIC EQUATIONS WITH IDENTIFIED p_b, q_b AND r_b BIASES – RECORD 10

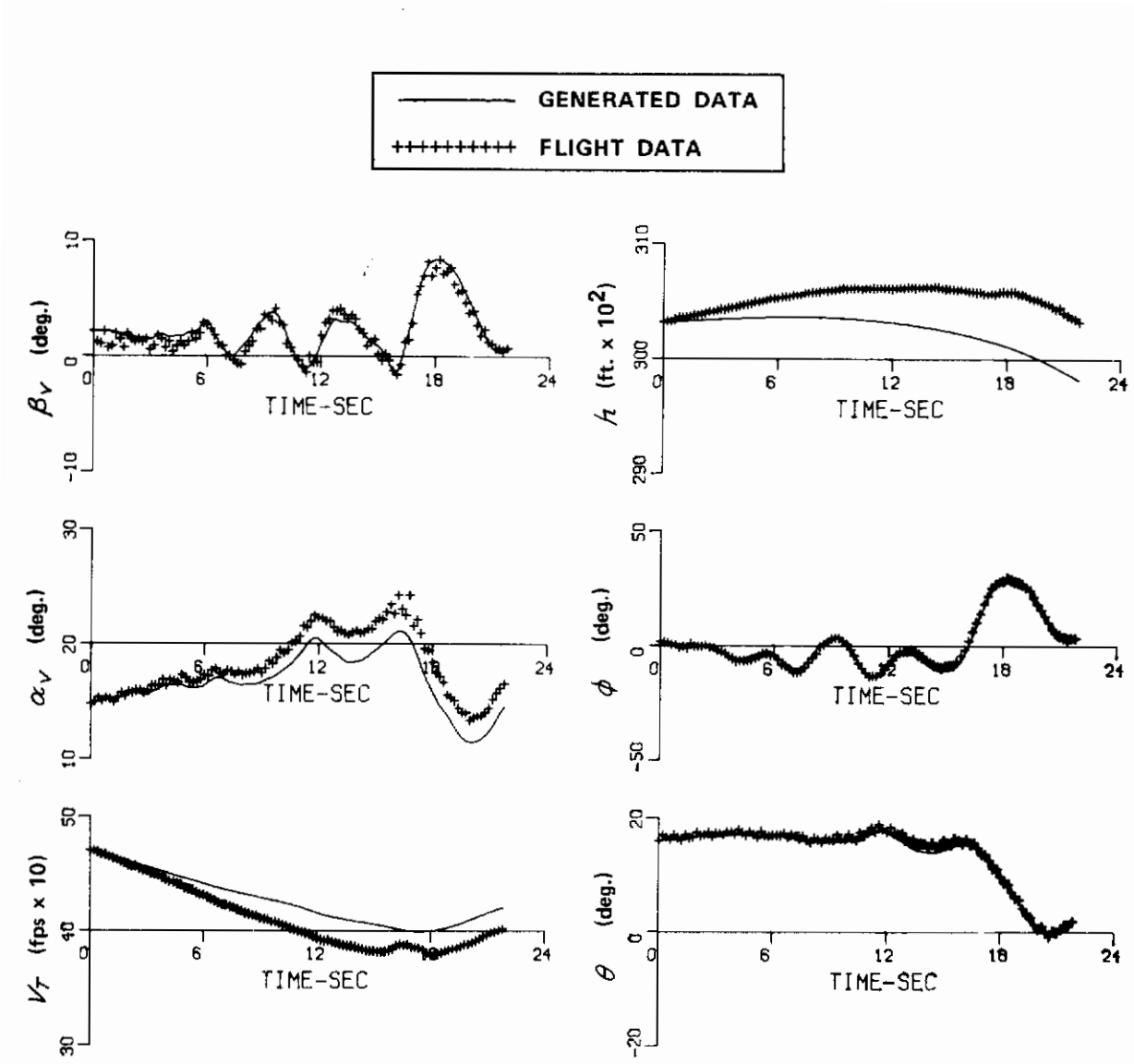

Figure 21 COMPARISON OF FLIGHT DATA WITH RESPONSES GENERATED FROM THE KINEMATIC EQUATIONS WITH IDENTIFIED p_b, q_b AND r_b BIASES – RECORD 11

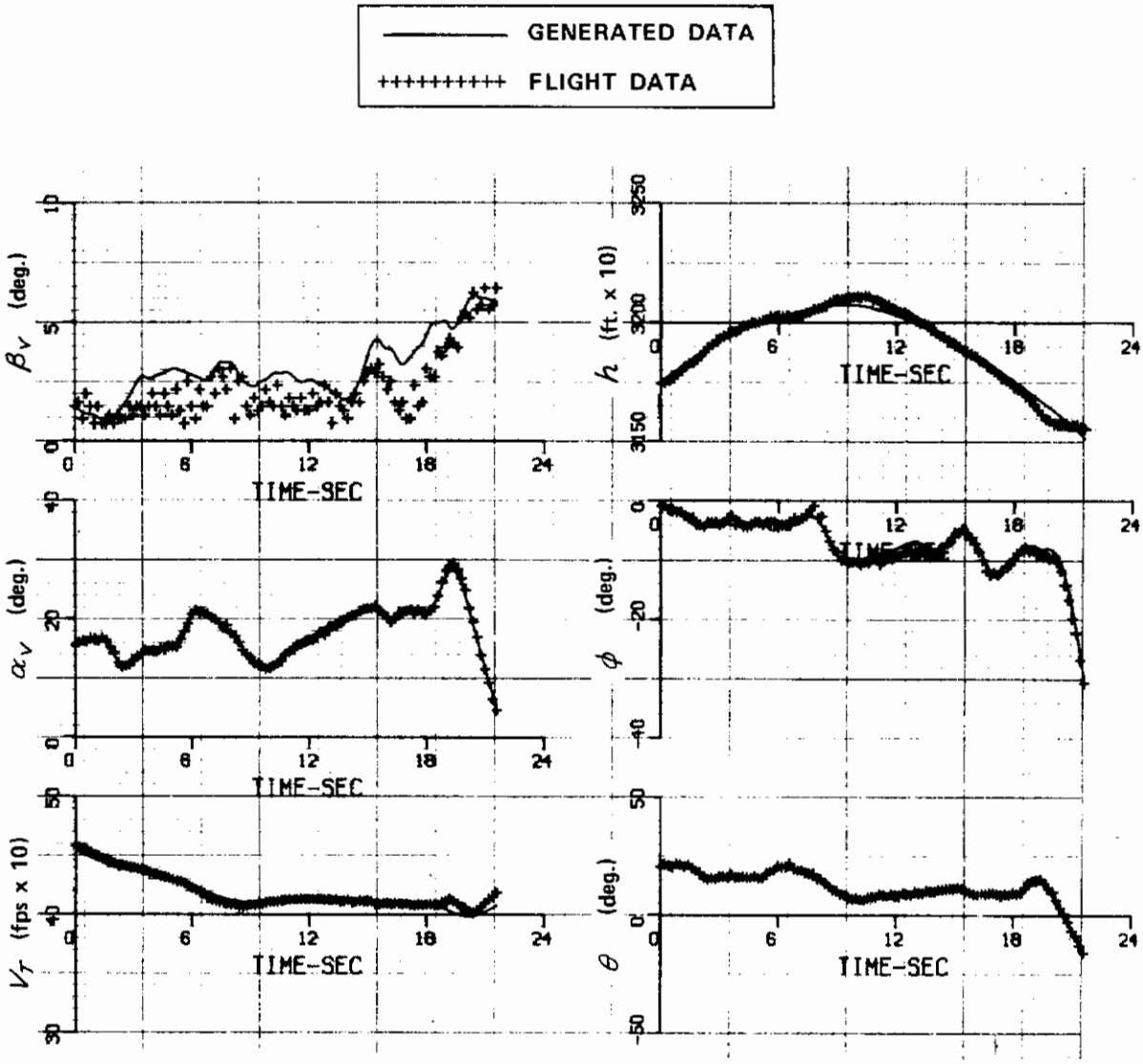

Figure 22 (a) COMPARISON OF FLIGHT DATA WITH RESPONSES GENERATED FROM THE KINEMATIC EQUATIONS WITH IDENTIFIED n_{x_b}, n_{z_b}, p_b, q_b r_b, α_{v_b}, θ_b BIASES – RECORD 9

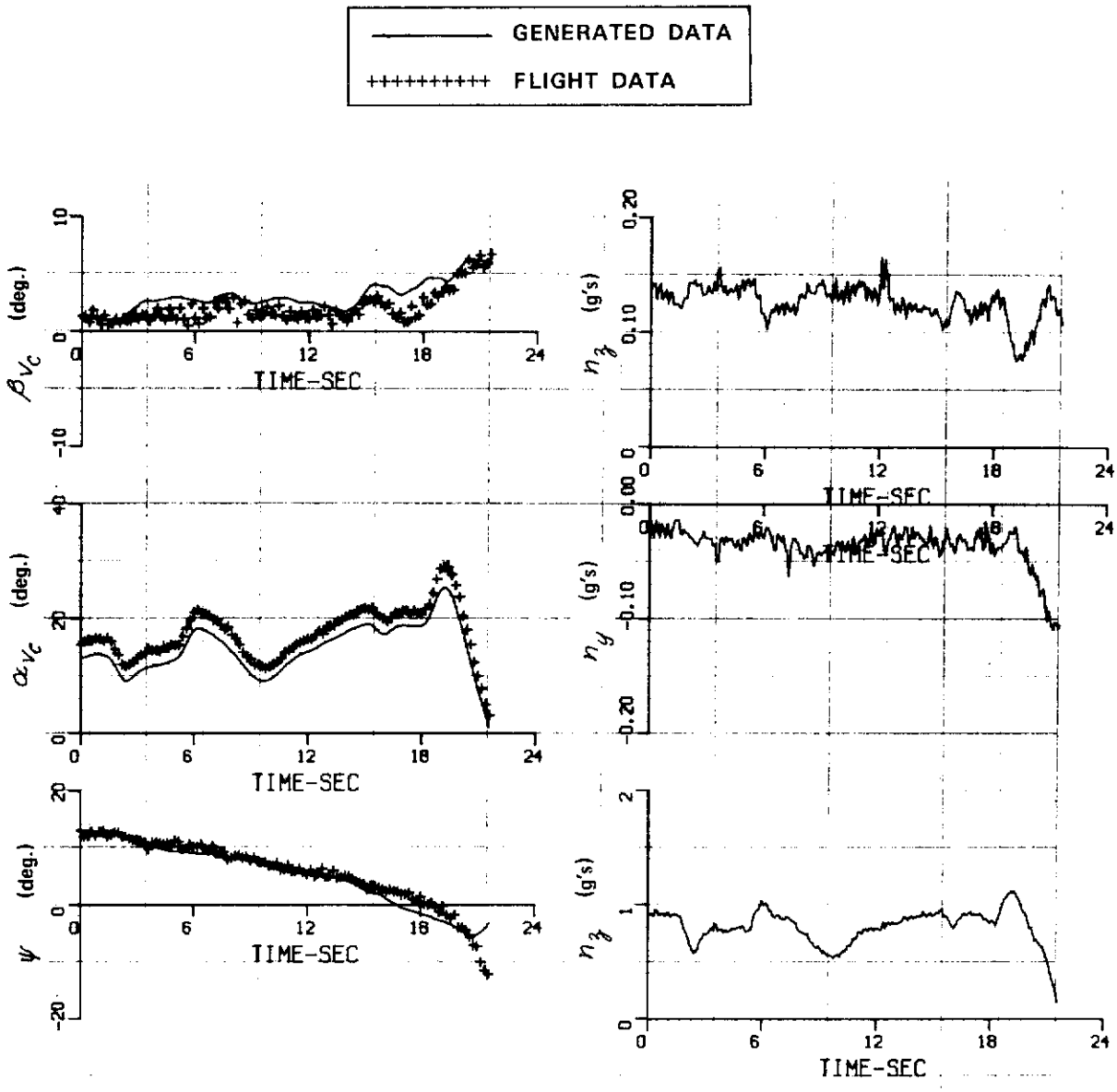

Figure 22 (a) (Concluded) COMPARISON OF FLIGHT DATA WITH RESPONSES GENERATED FROM THE KINEMATIC EQUATIONS WITH IDENTIFIED n_{x_b}, n_{z_b}, p_b, q_b, r_b, α_{V_b}, θ_b BIASES – RECORD 9

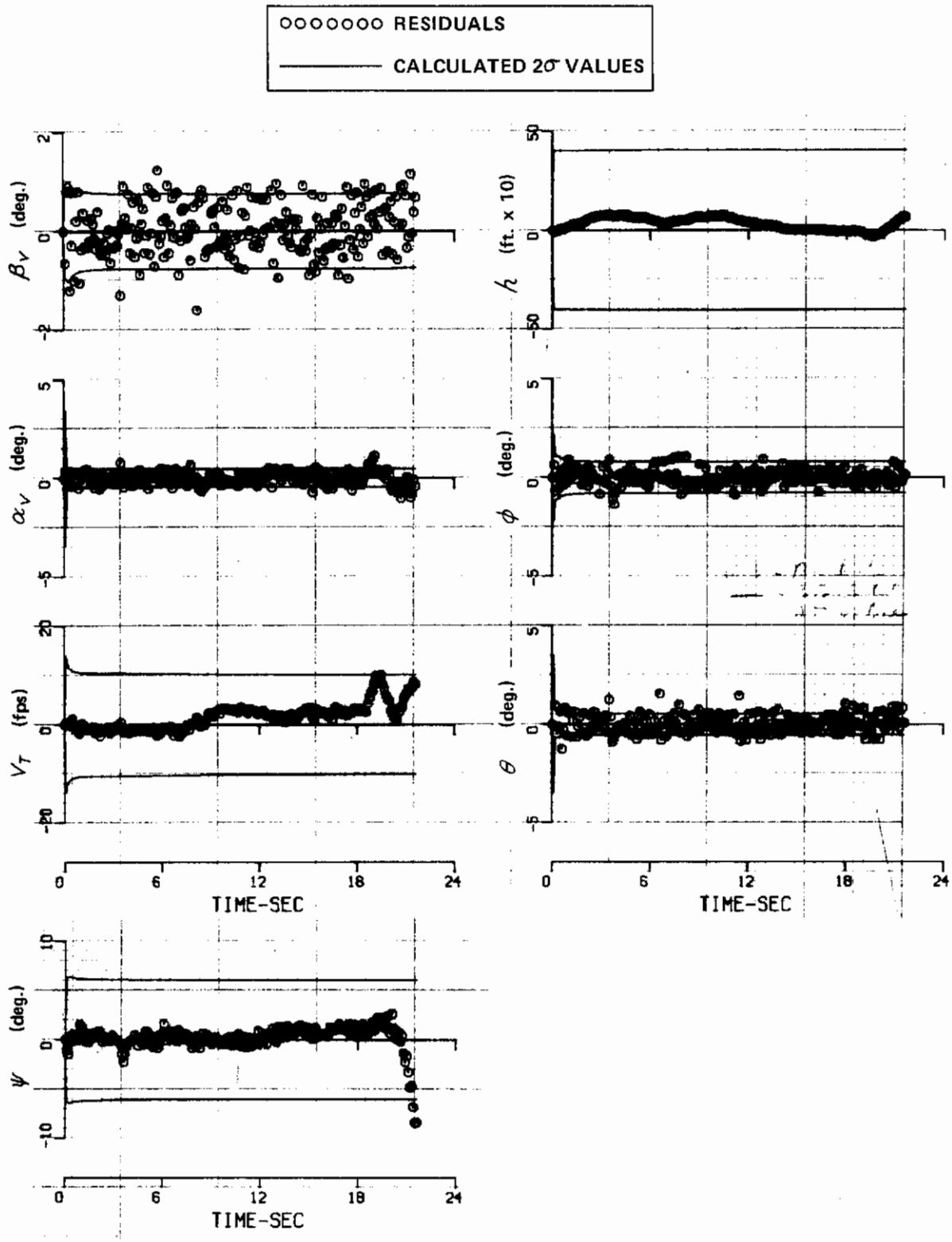

Figure 22 (b) RESIDUALS FROM THE ITERATED KALMAN FILTER AND TIME HISTORIES OF BIAS PARAMETER ESTIMATES – RECORD 9

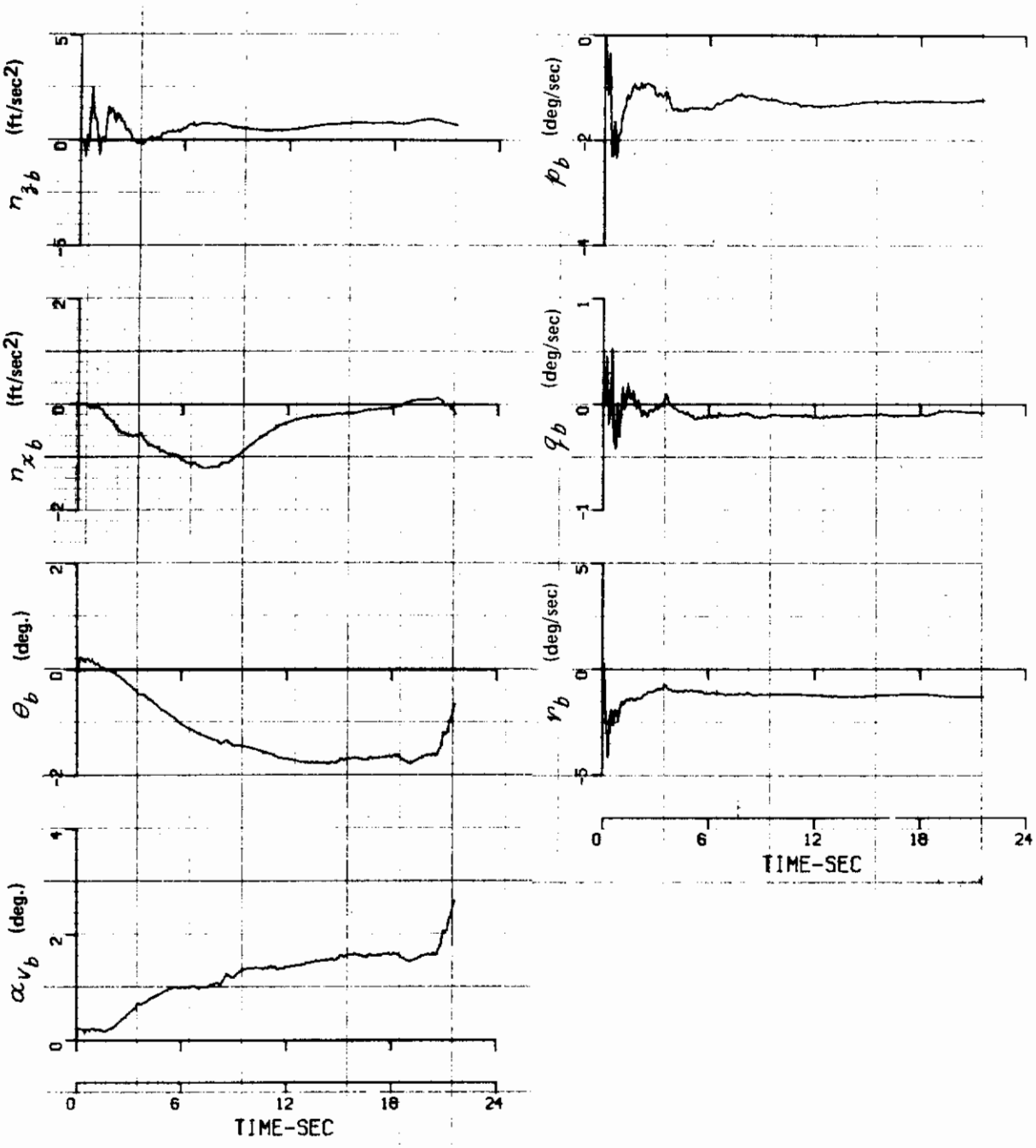

Figure 22 (b) (Concluded) RESIDUALS FROM THE ITERATED KALMAN FILTER AND TIME HISTORIES OF BIAS PARAMETER ESTIMATES – RECORD 9

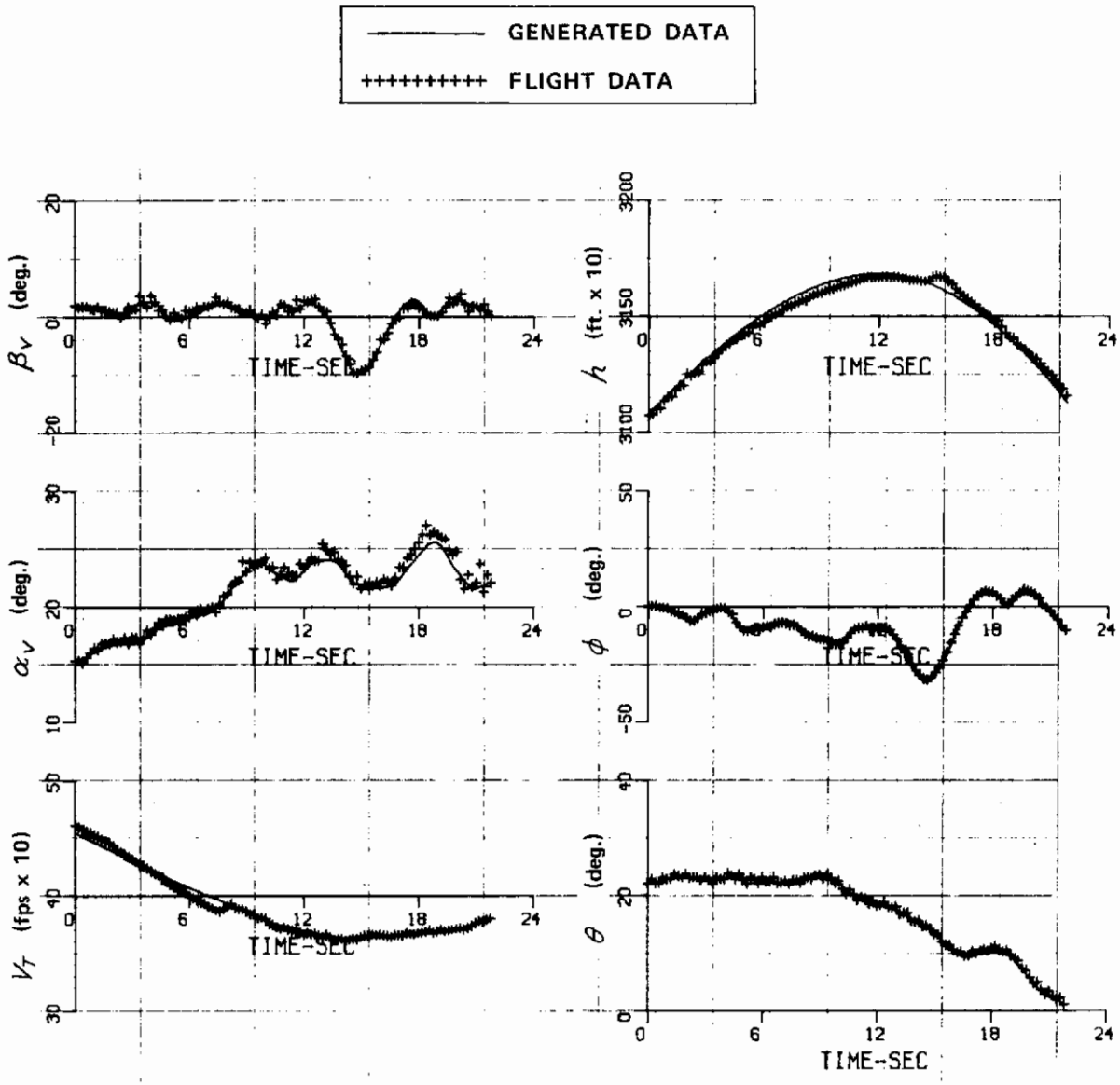

Figure 23 (a) COMPARISON OF FLIGHT DATA WITH RESPONSES GENERATED FROM THE KINEMATIC EQUATIONS WITH IDENTIFIED n_{x_b}, n_{z_b} p_b, q_b, r_b, α_{v_b}, θ_b BIASES – RECORD 10

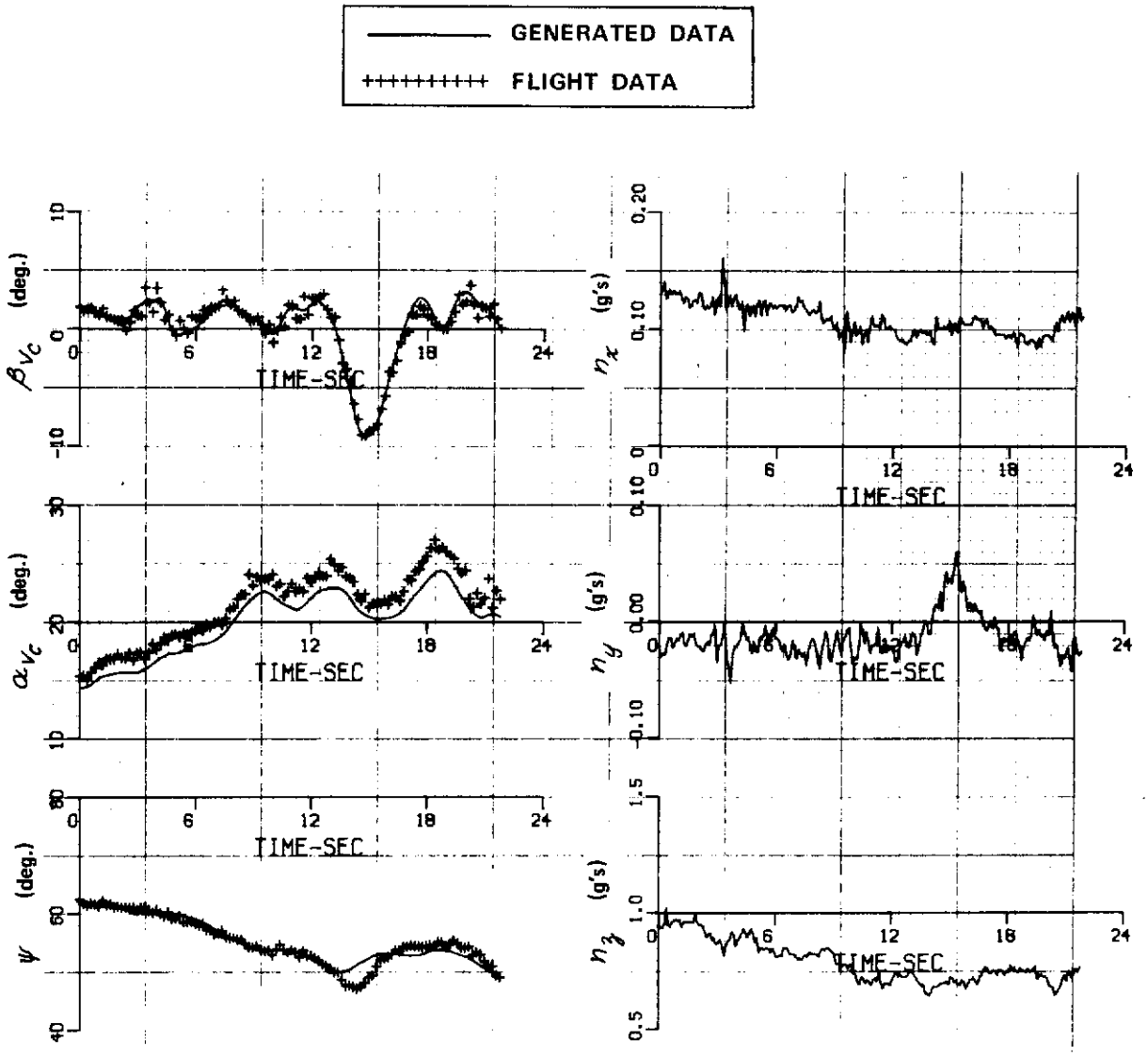

Figure 23 (a) (Concluded) COMPARISON OF FLIGHT DATA WITH RESPONSES GENERATED FROM THE KINEMATIC EQUATIONS WITH IDENTIFIED n_{x_b}, n_{z_b}, p_b, q_b, r_b, α_{V_b}, θ_b BIASES – RECORD 10

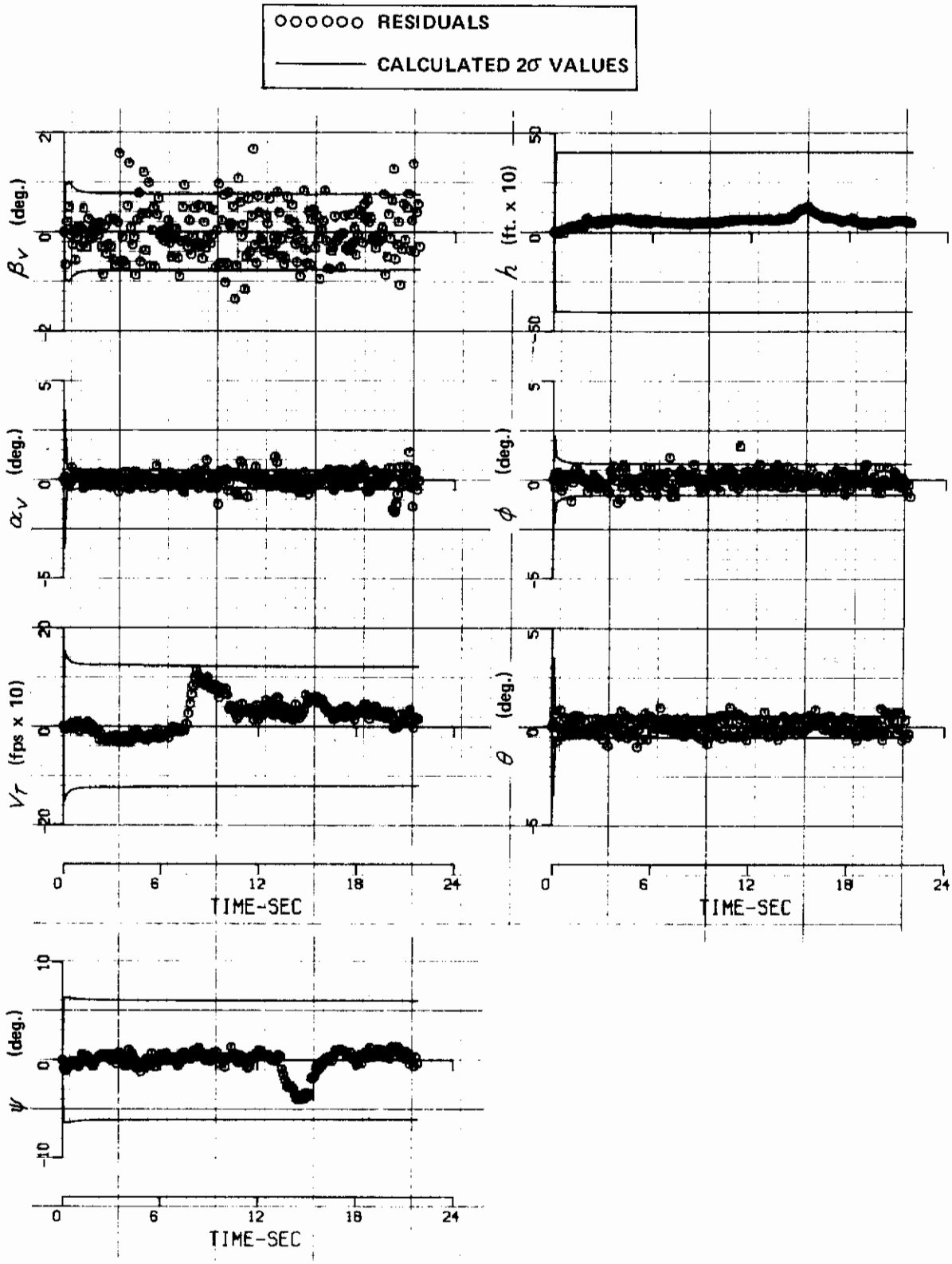

Figure 23 (b) RESIDUALS FROM THE ITERATED KALMAN FILTER AND TIME HISTORIES OF BIAS PARAMETER ESTIMATES – RECORD 10

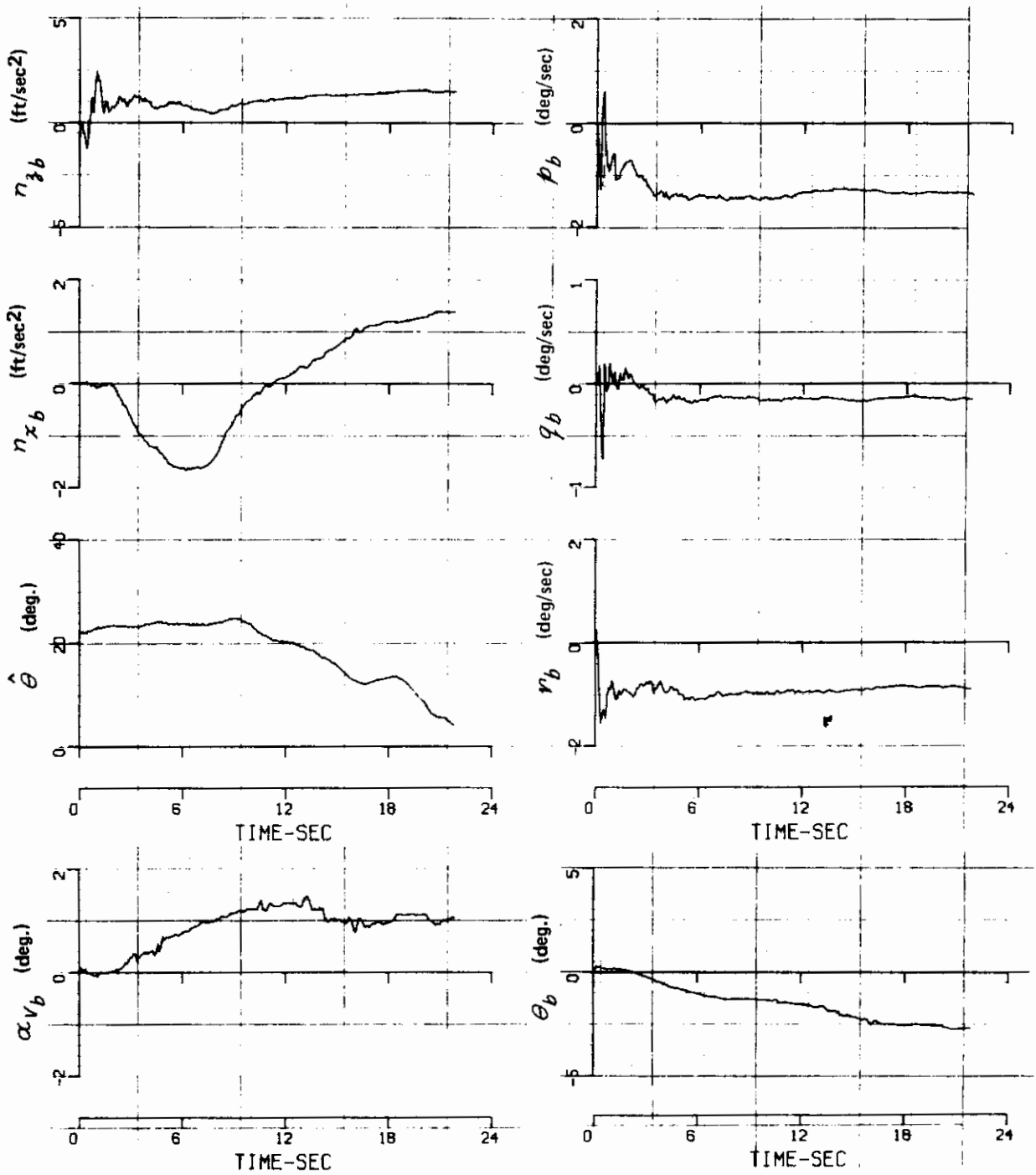

Figure 23 (b) (Concluded) RESIDUALS FROM THE ITERATED KALMAN FILTER AND TIME HISTORIES OF BIAS PARAMETER ESTIMATES – RECORD 20

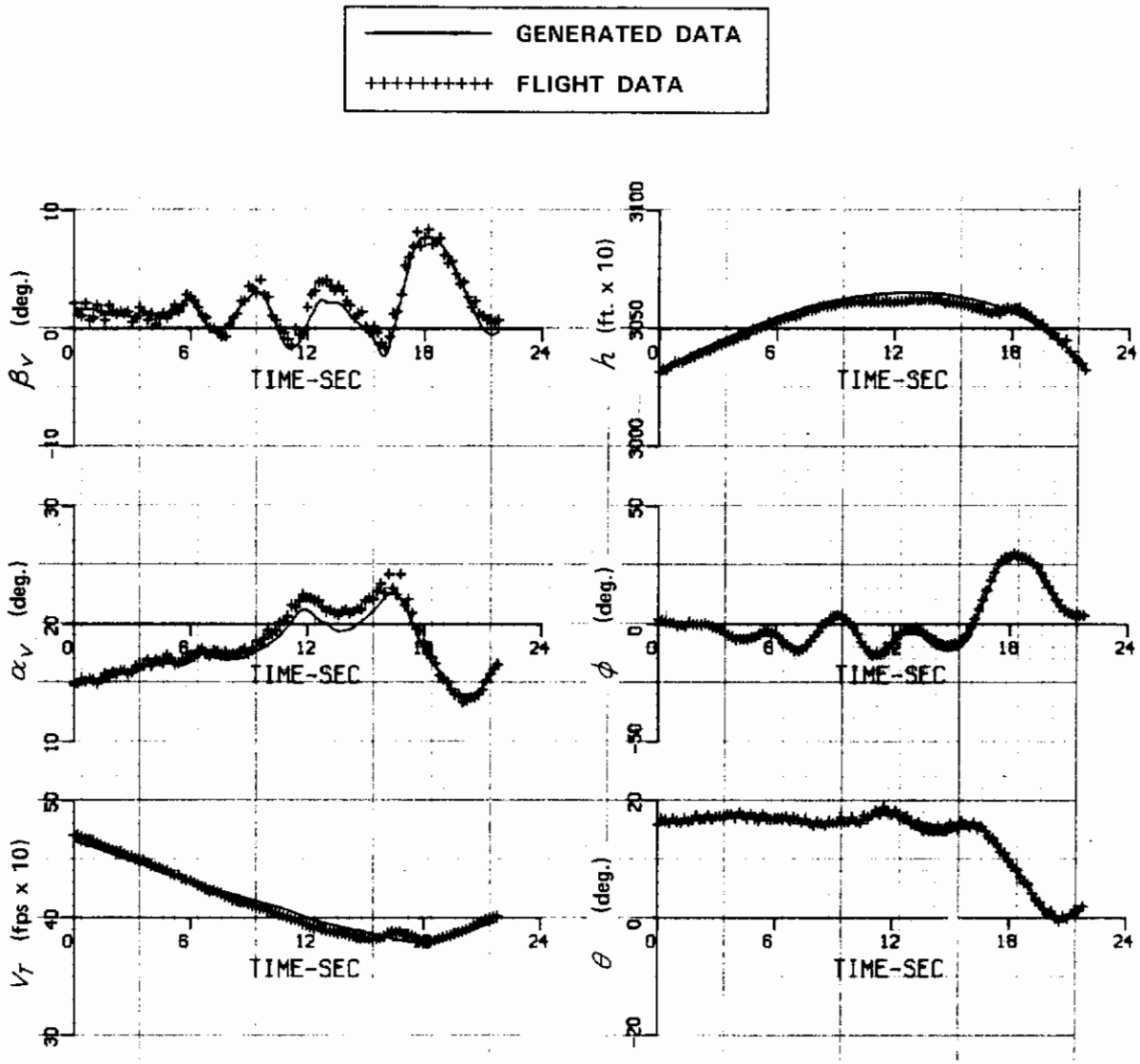

Figure 24 (a) COMPARISON OF FLIGHT DATA WITH RESPONSES GENERATED FROM THE KINEMATIC EQUATIONS WITH IDENTIFIED n_{x_b}, n_{z_b}, p_b, q_b, r_b, α_{V_b}, θ_b BIASES – RECORD 11

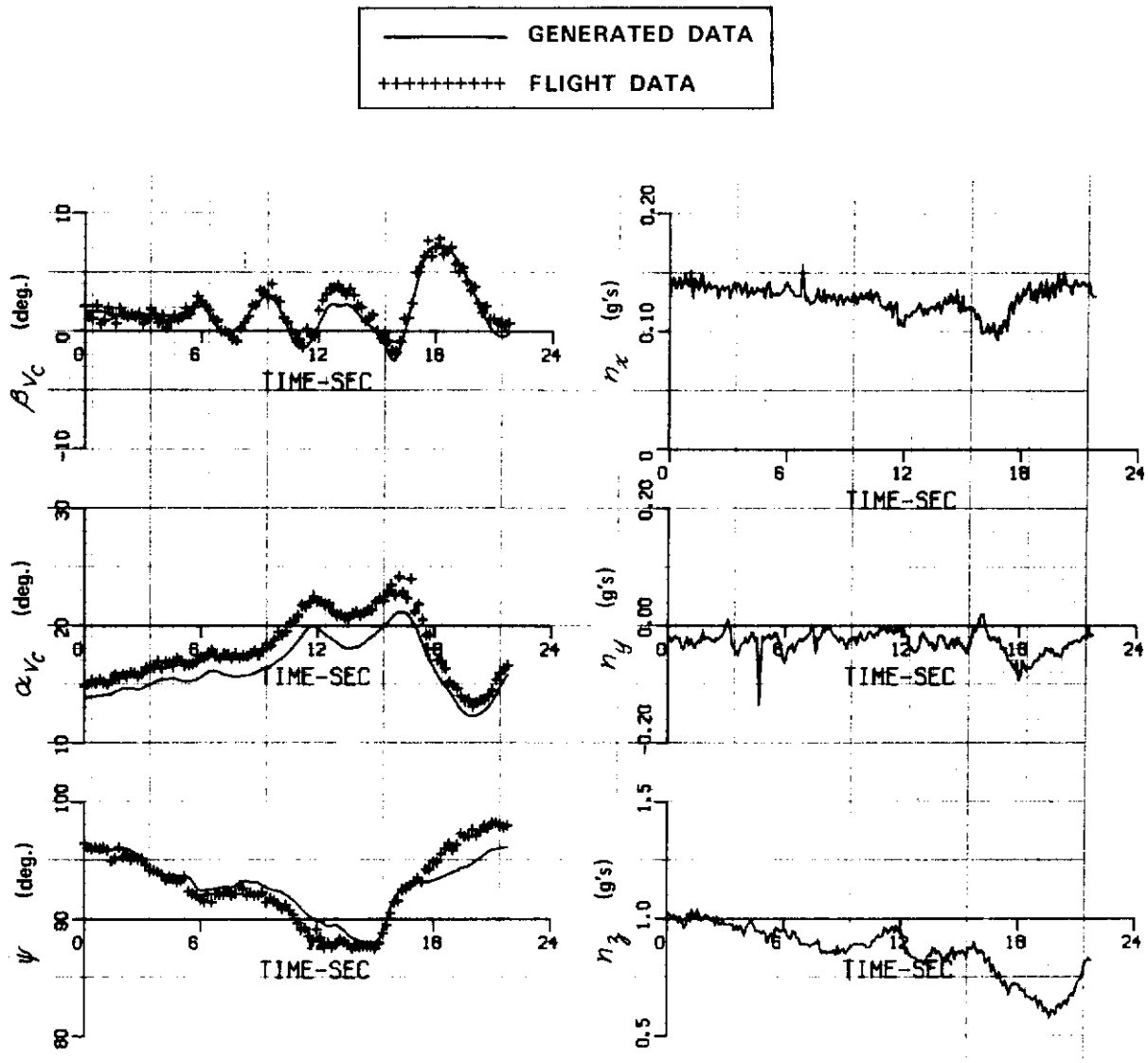

Figure 24 (a) (Concluded) COMPARISON OF FLIGHT DATA WITH RESPONSES GENERATED FROM THE KINEMATIC EQUATIONS WITH IDENTIFIED n_{x_b}, n_{z_b}, p_b, q_b, r_b, α_{V_b}, θ_b BIASES – RECORD 11

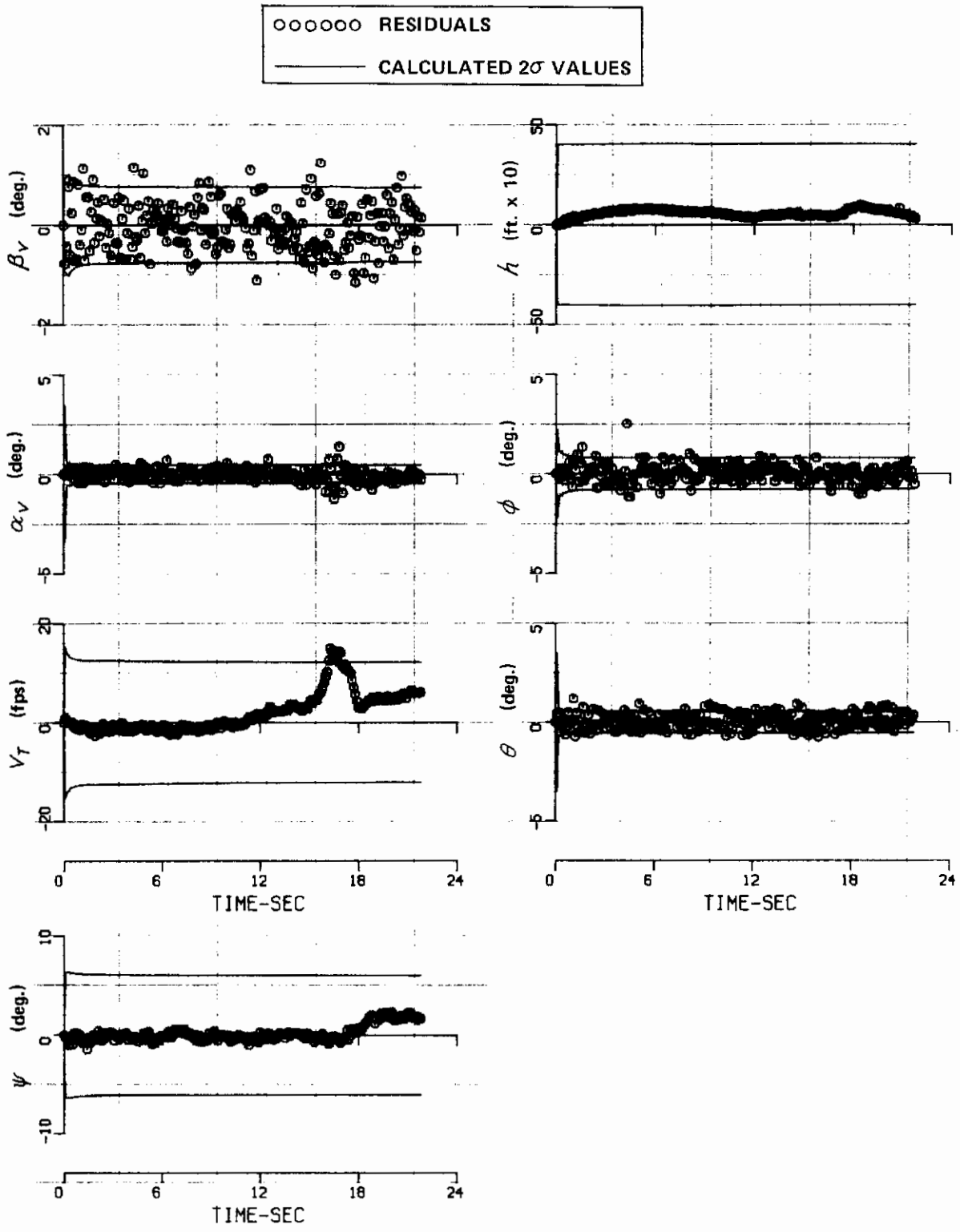

Figure 24 (b) RESIDUALS FROM THE ITERATED KALMAN FILTER AND TIME HISTORIES OF BIAS PARAMETER ESTIMATES – RECORD 11

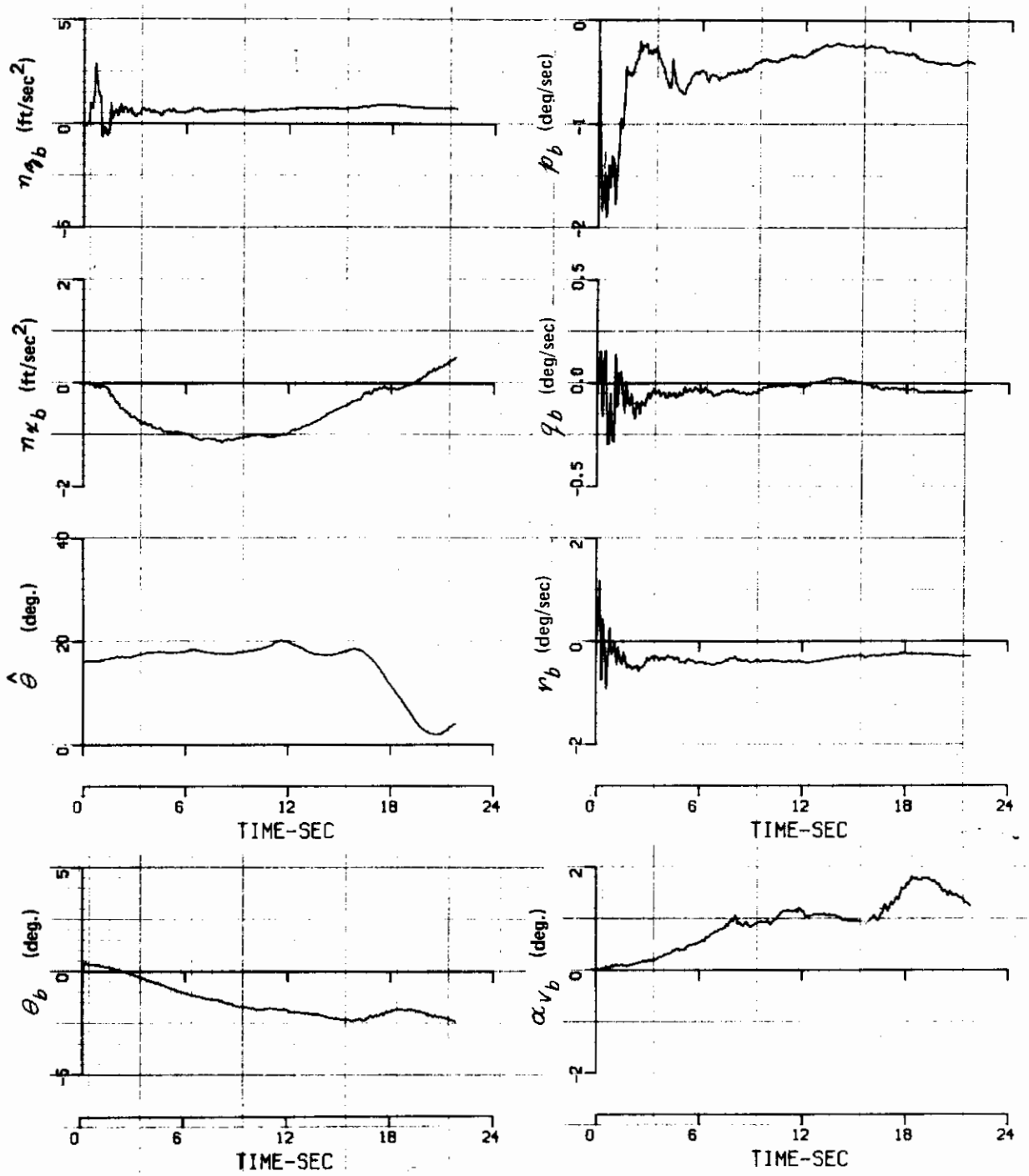

Figure 24 (b) (Concluded) RESIDUALS FROM THE ITERATED KALMAN FILTER AND TIME HISTORIES OF BIAS PARAMETER ESTIMATES – RECORD 11

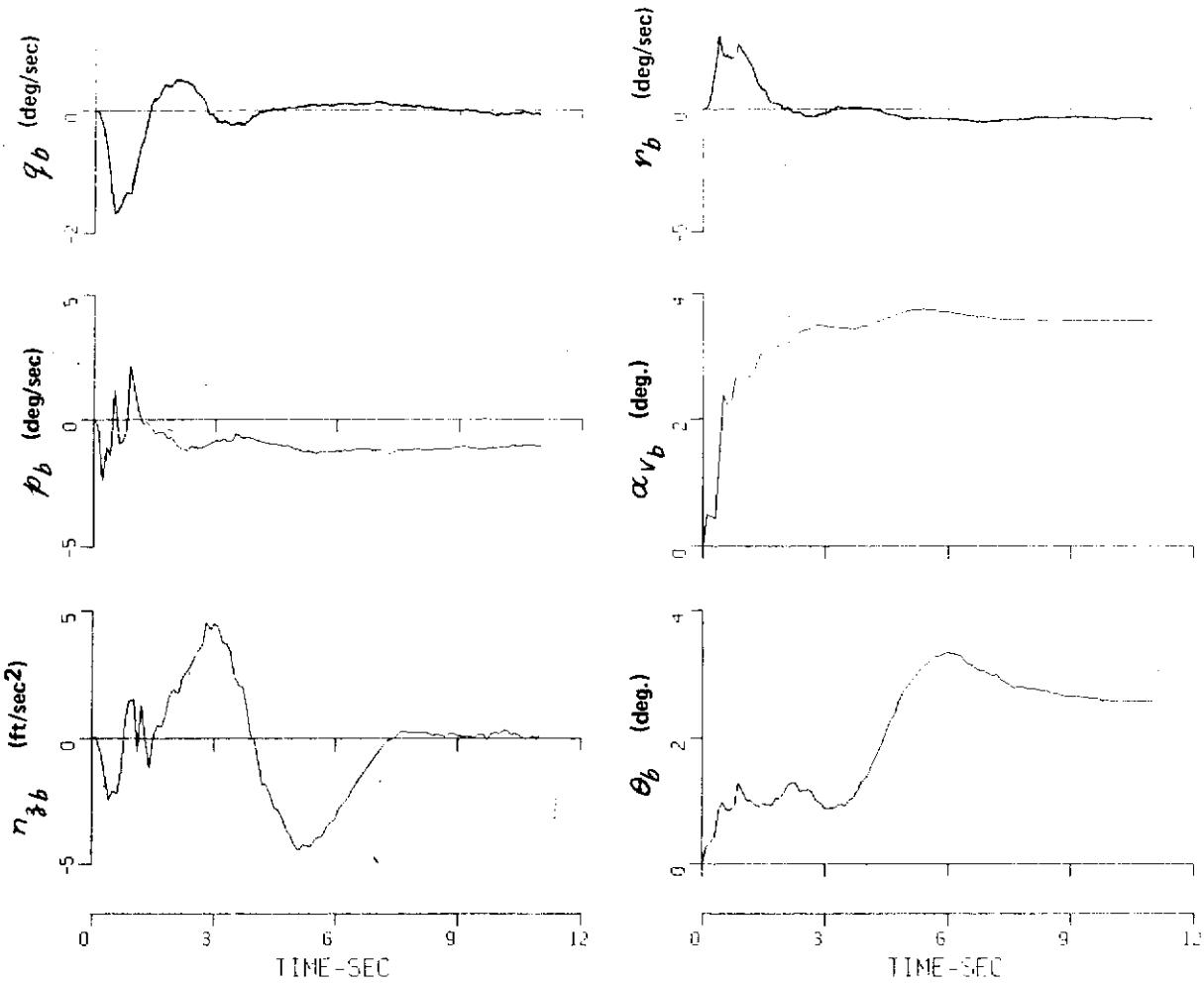

Figure 25 TIME HISTORIES OF BIAS PARAMETER ESTIAMTES USING END PORTION OF FLIGHT RECORD – RECORD 15

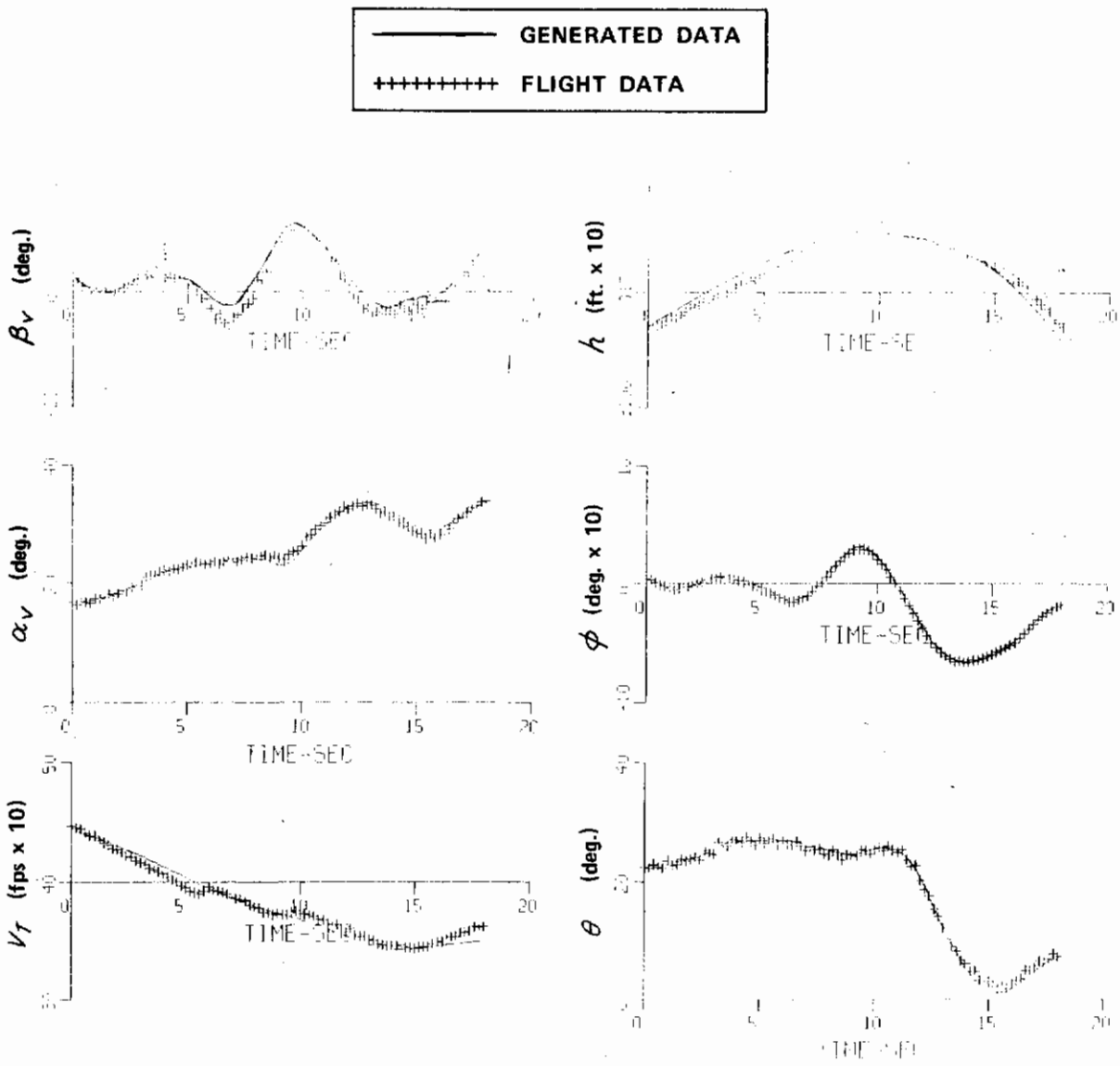

Figure 26 (a) COMPARISON OF FLIGHT DATA WITH RESPONSES GENERATED FROM THE KINEMATIC EQUATIONS WITH IDENTIFIED n_{z_b}, p_b, q_b, r_b, α_{v_b}, θ_b BIASES – RECORD 14

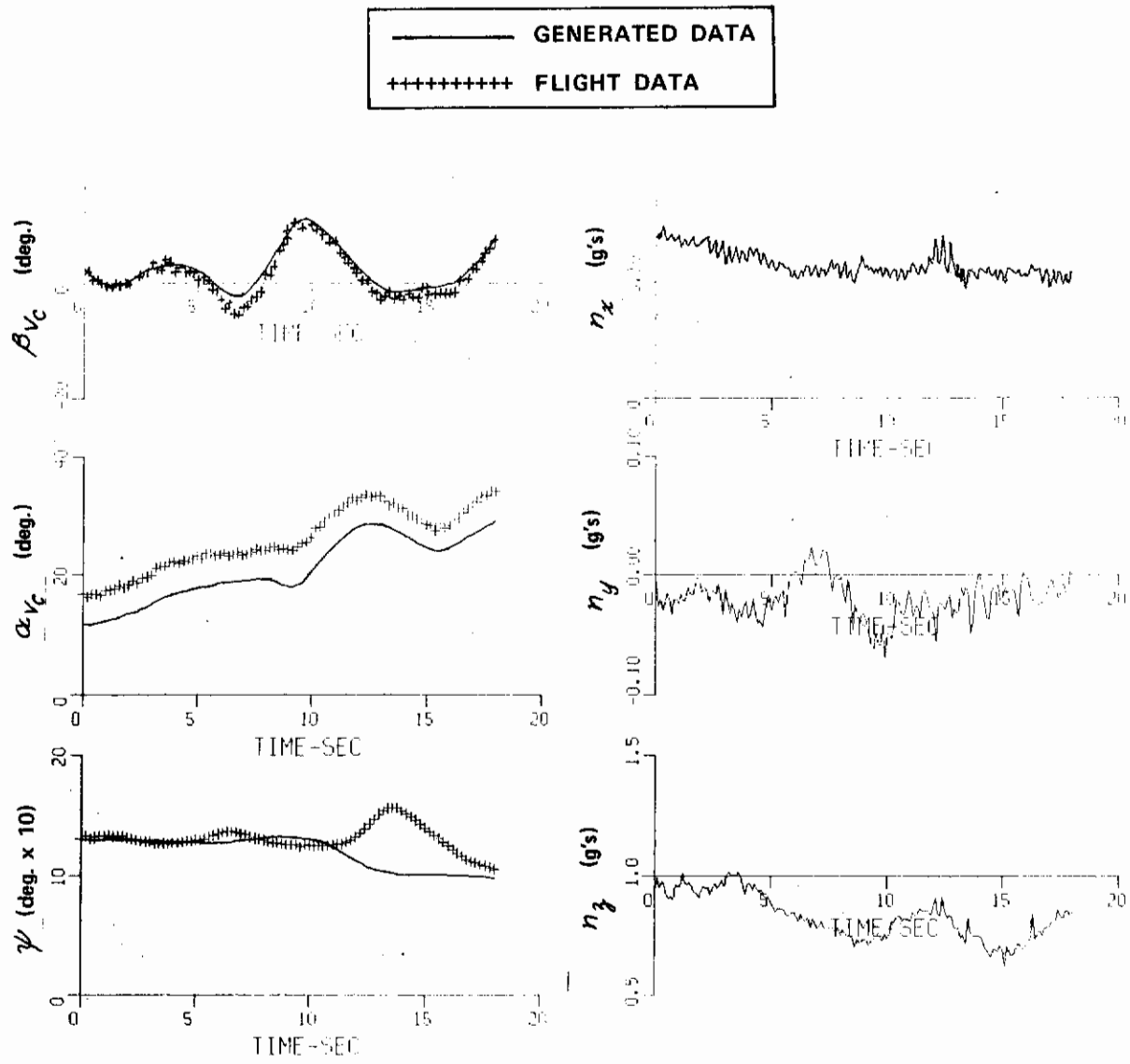

Figure 26 (a) (Concluded) COMPARISON OF FLIGHT DATA WITH RESPONSES GENERATED FROM THE KINEMATIC EQUATIONS WITH IDENTIFIED n_{z_b}, p_b, q_b, r_b, α_{V_b}, θ_b BIASES – RECORD 14

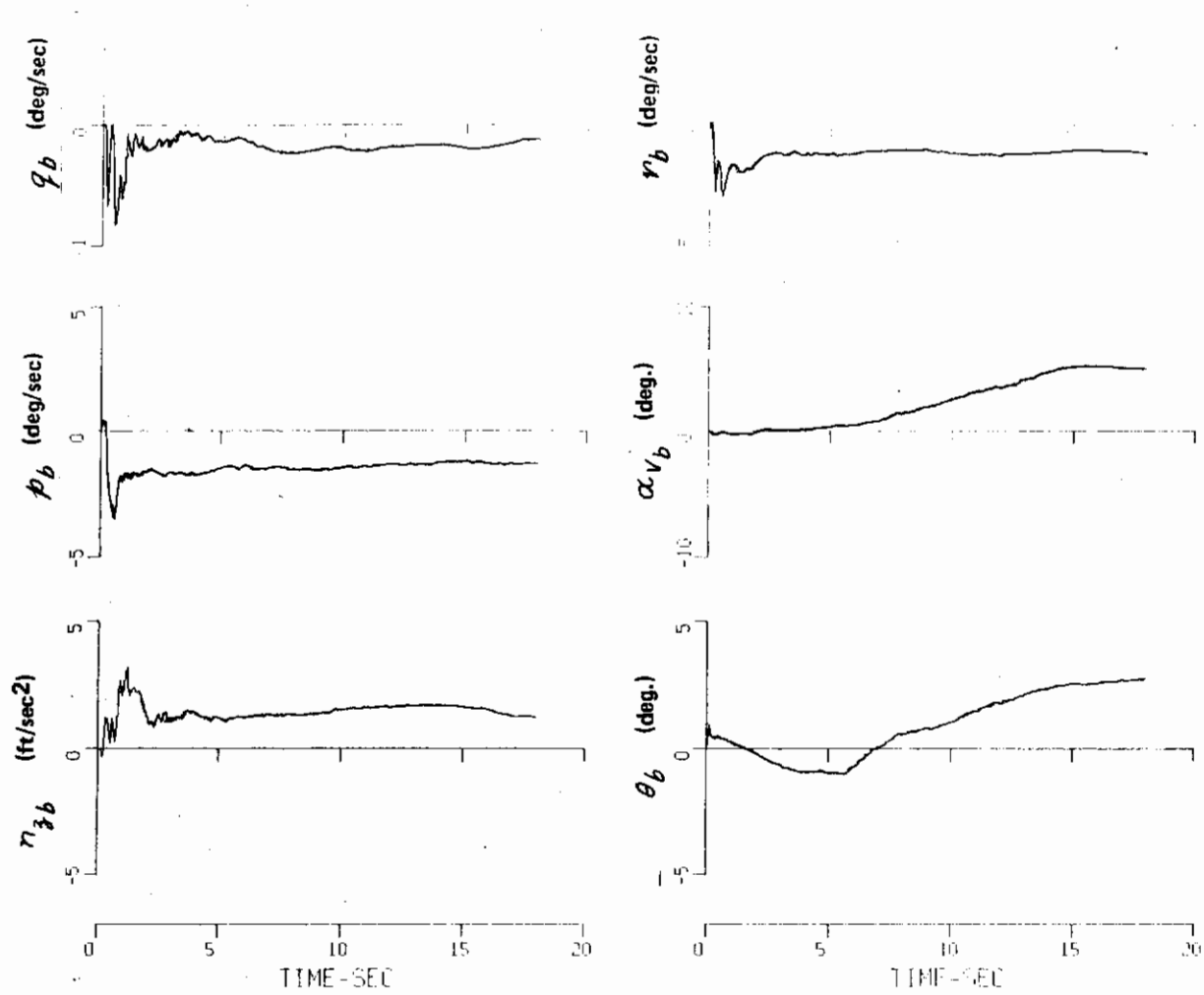

Figure 26 (b) TIME HISTORIES OF BIAS PARAMETER ESTIMATES – RECORD 14

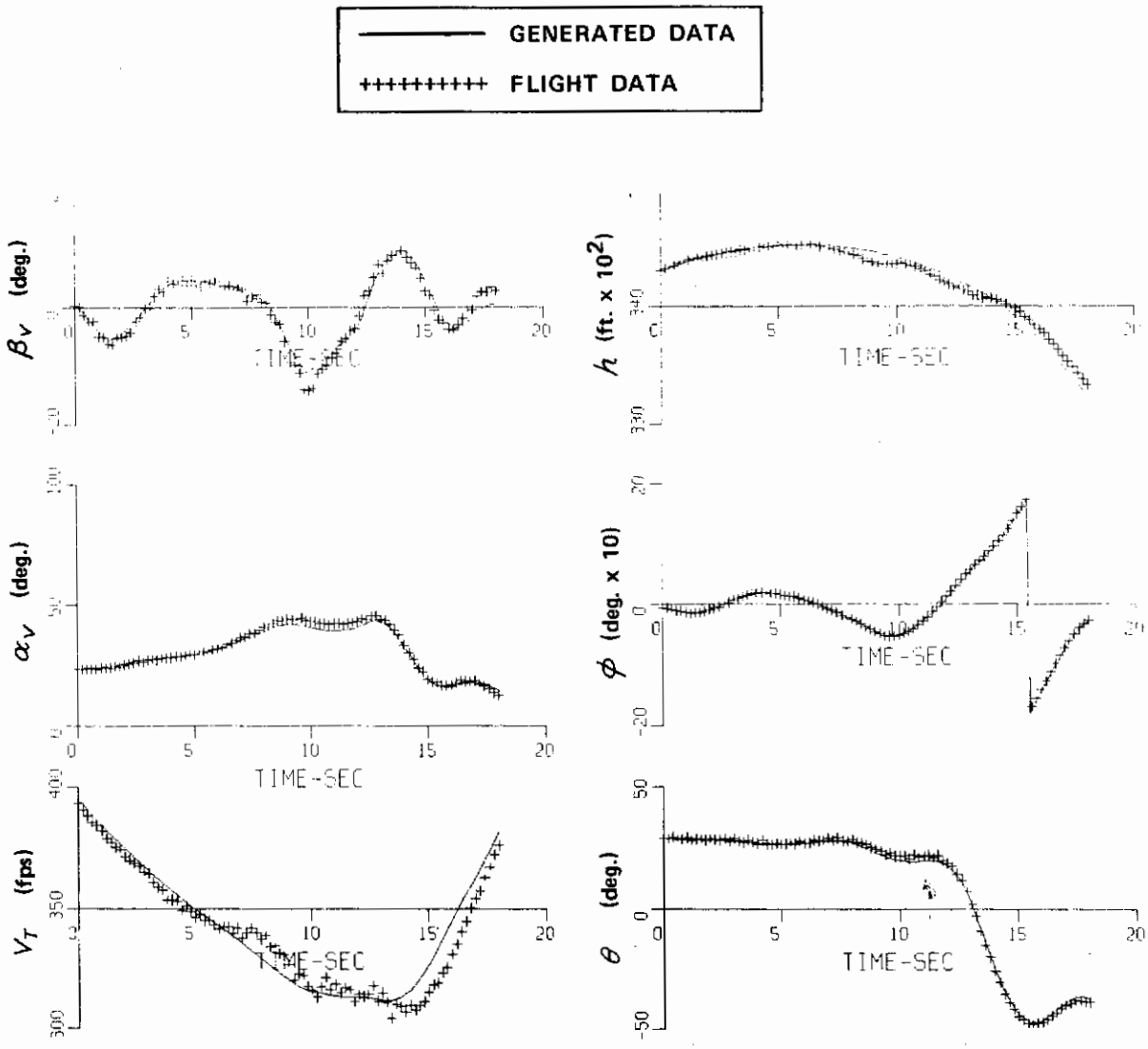

Figure 27 (a) COMPARISON OF FLIGHT DATA WITH RESPONSES GENERATED FROM KINEMATIC EQUATIONS WITH IDENTIFIED n_{z_b}, p_b, q_b, r_b, α_{v_b}, ϕ_b, θ_b BIASES – RECORD 20

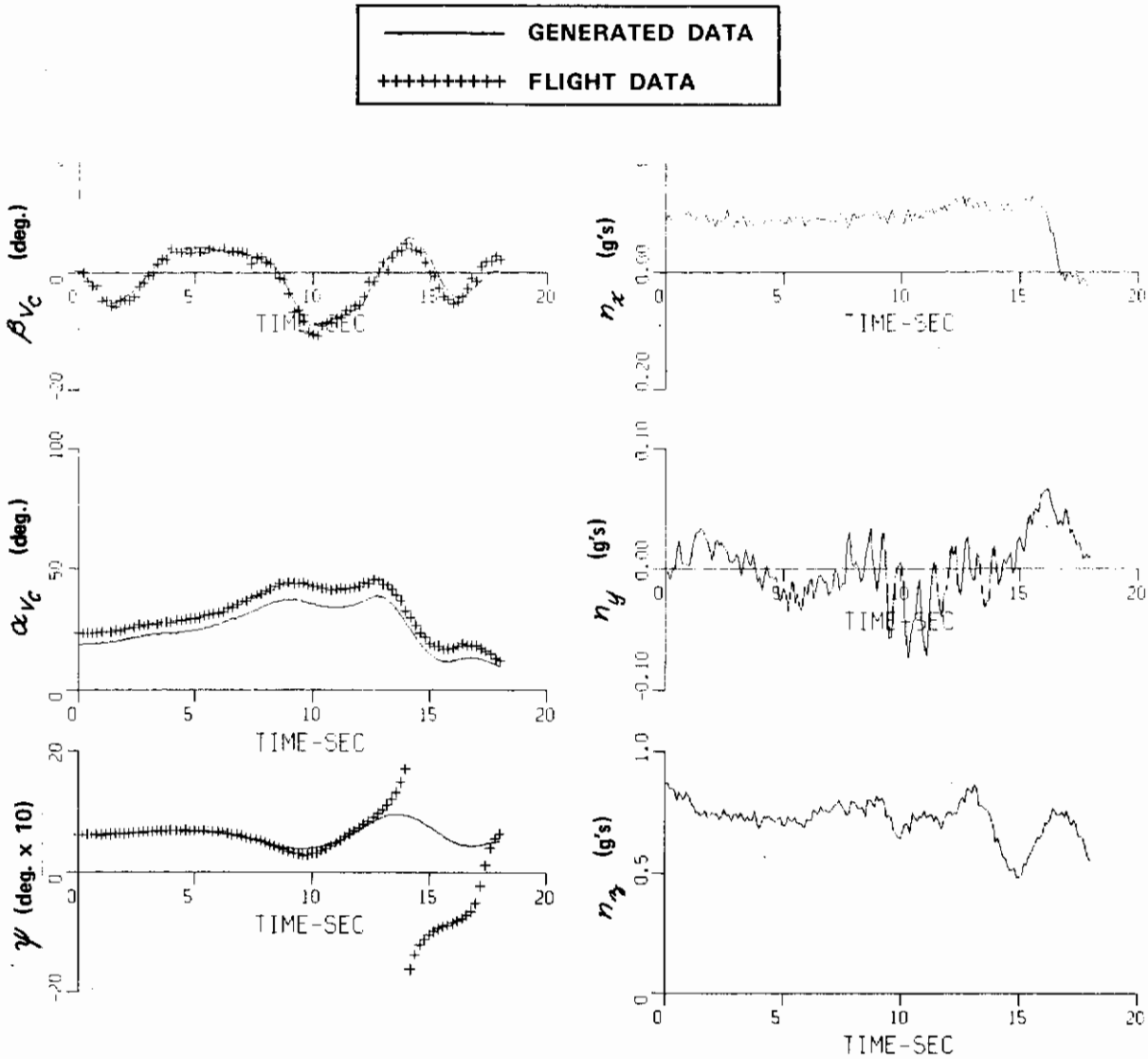

Figure 27(a) (Concluded) COMPARISON OF FLIGHT DATA WITH RESPONSES GENERATED FROM THE KINEMATIC EQUATIONS WITH IDENTIFIED n_{z_b}, p_b, q_b, r_b, α_{V_b}, ϕ_b, θ_b BIASES – RECORD 20

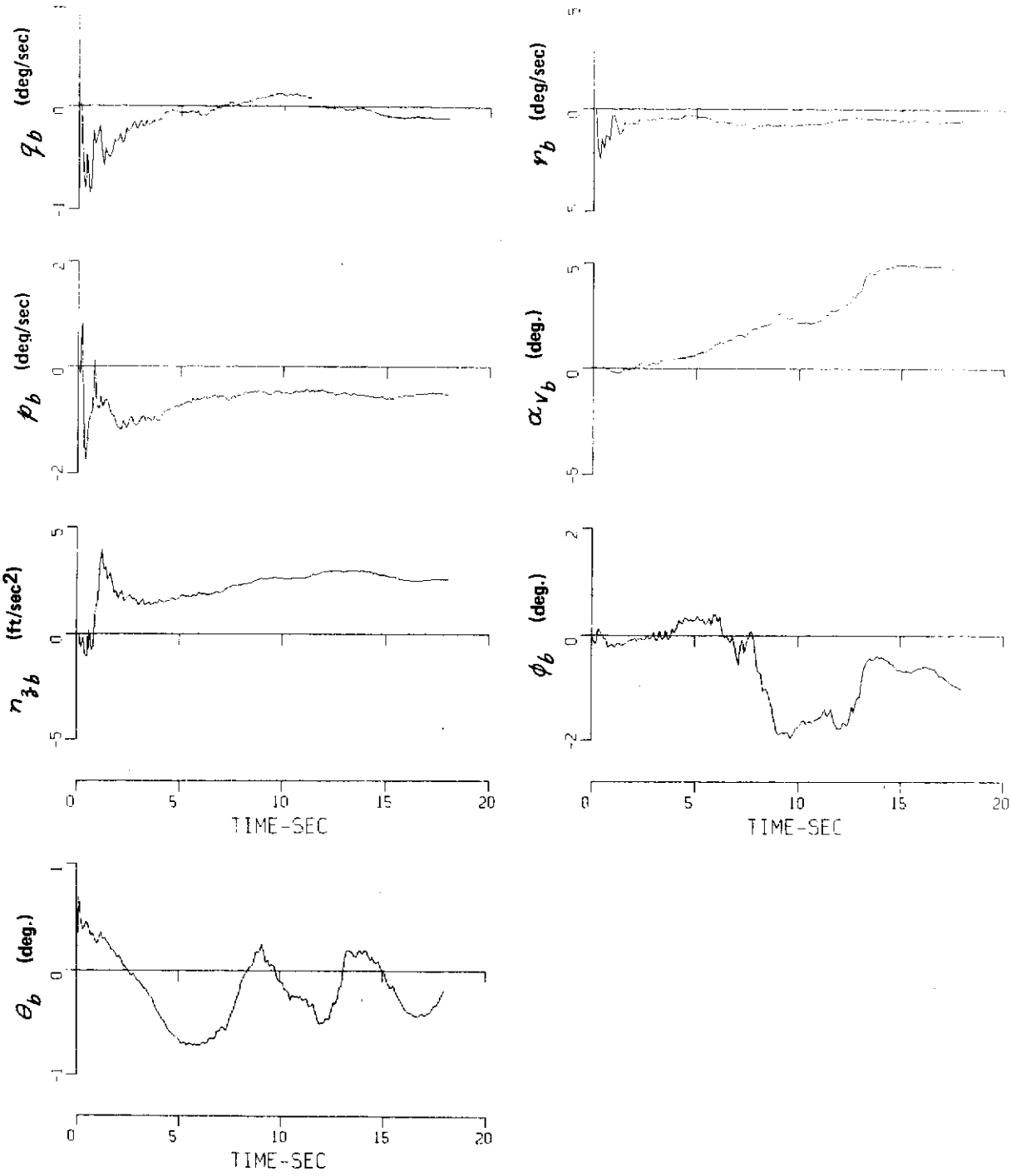

Figure 27 (b) TIME HISTORIES OF BIAS PARAMETER ESTIMATES – RECORD 20

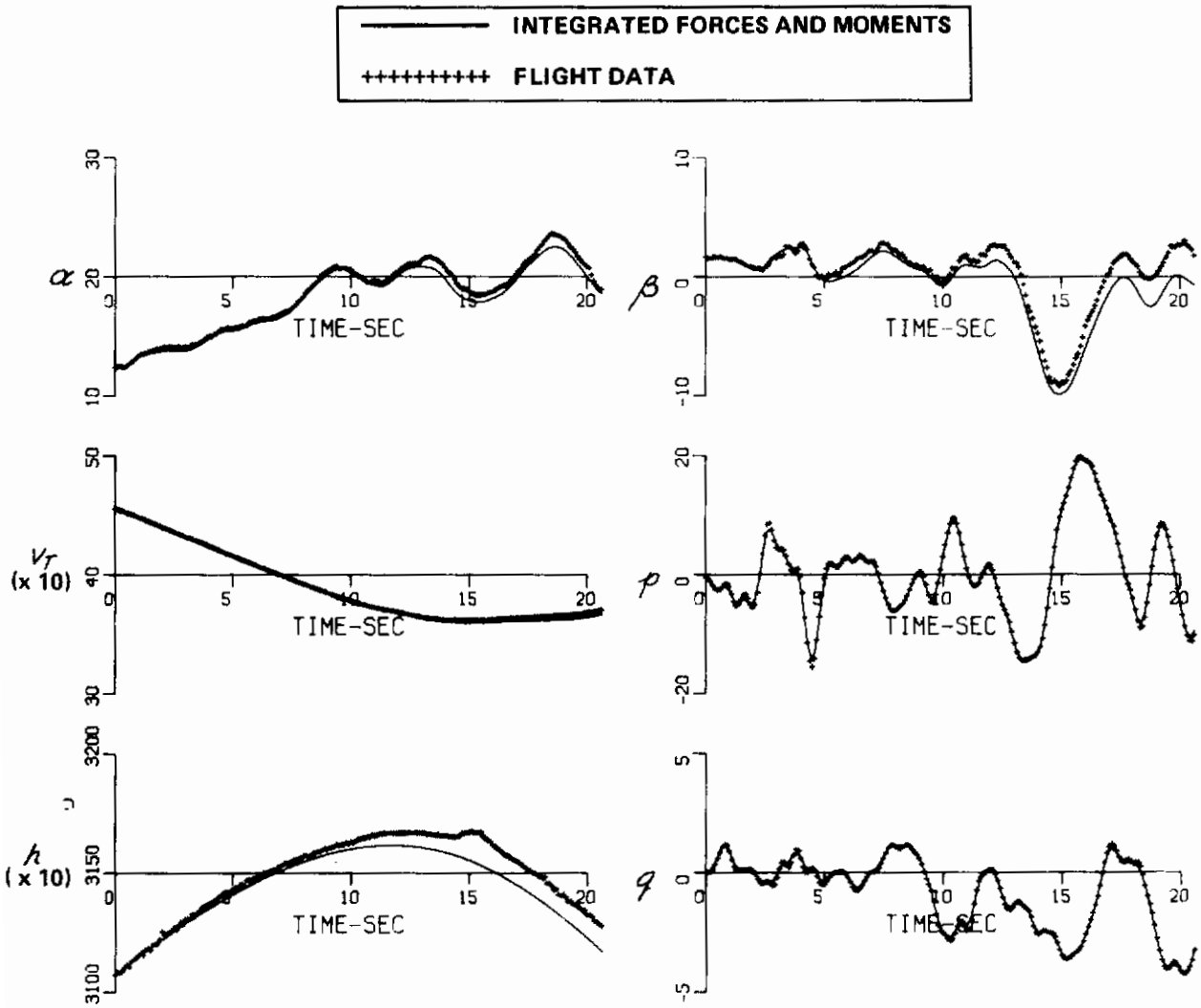

Figure 28 RESPONSE COMPARISONS BETWEEN THOSE GENERATED WITH NONDIMENSIONAL FORCE AND MOMENTS AND FLIGHT DATA - RECORD 10

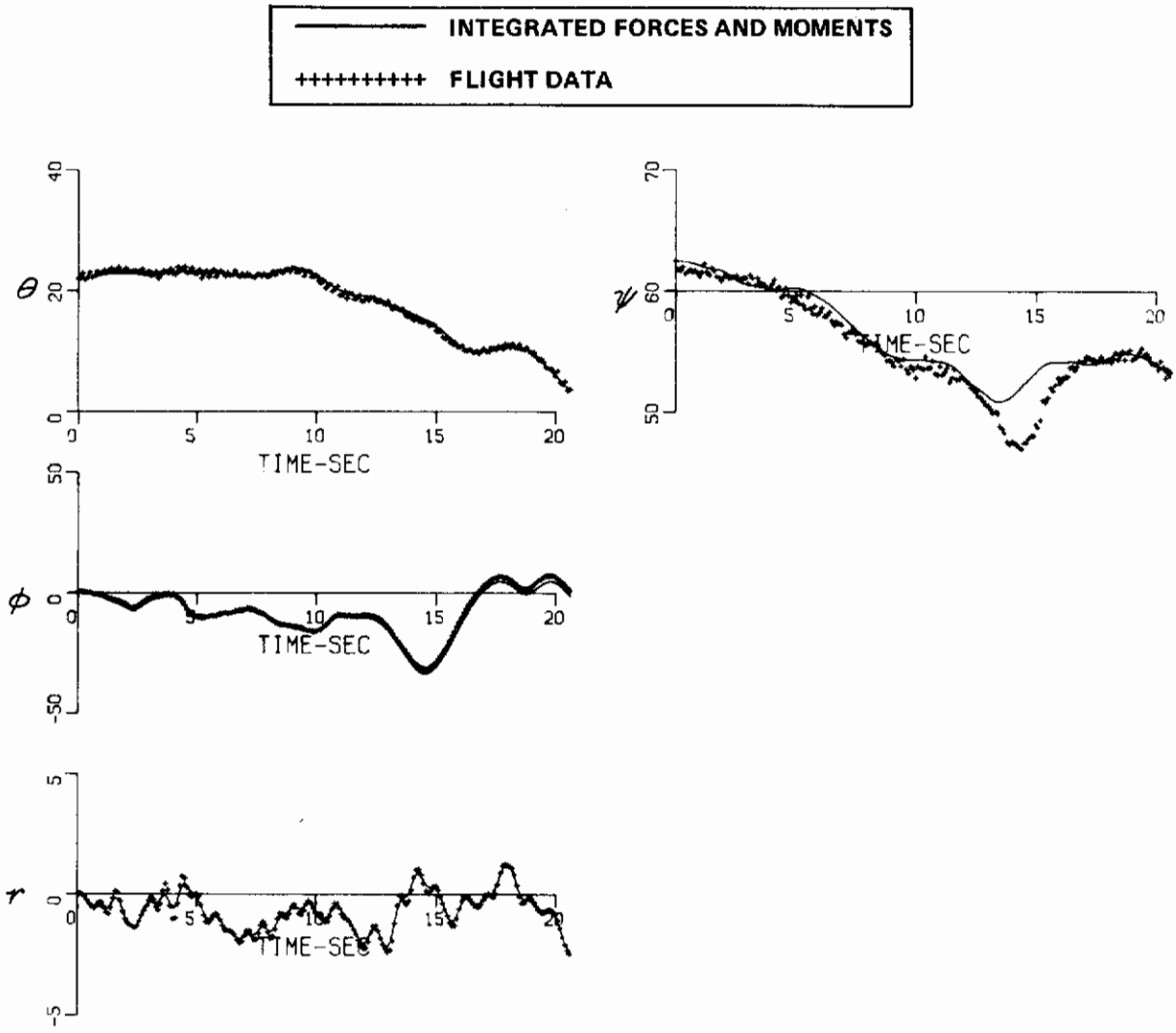

Figure 28 (Concluded) RESPONSE COMPARISONS BETWEEN THOSE GENERATED WITH NONDIMENSIONAL FORCE AND MOMENTS AND FLIGHT DATA - RECORD 10

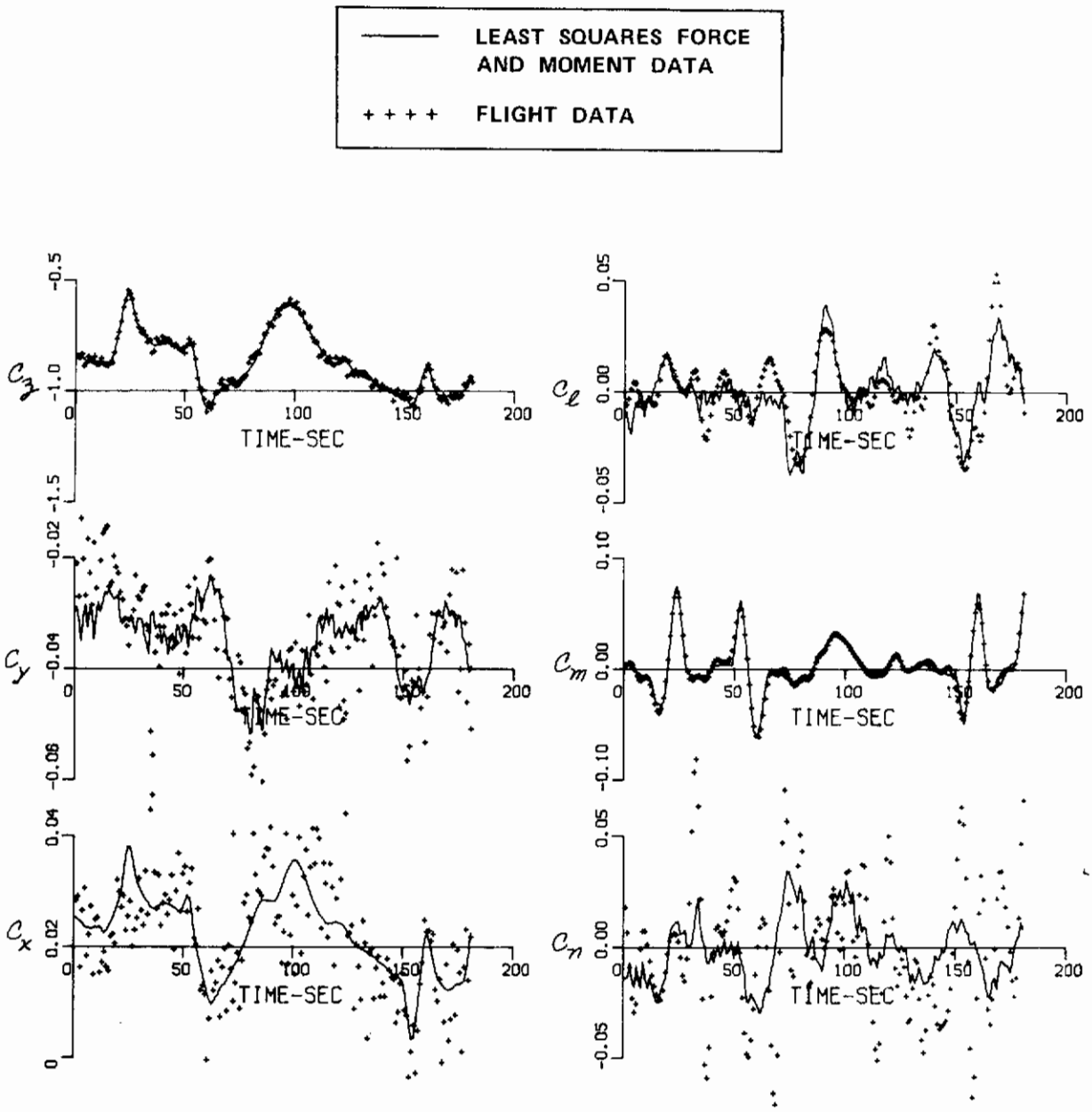

Figure 29 LEAST SQUARES FORCE AND MOMENT COMPARISONS WITH FLIGHT DATA - RECORD 9

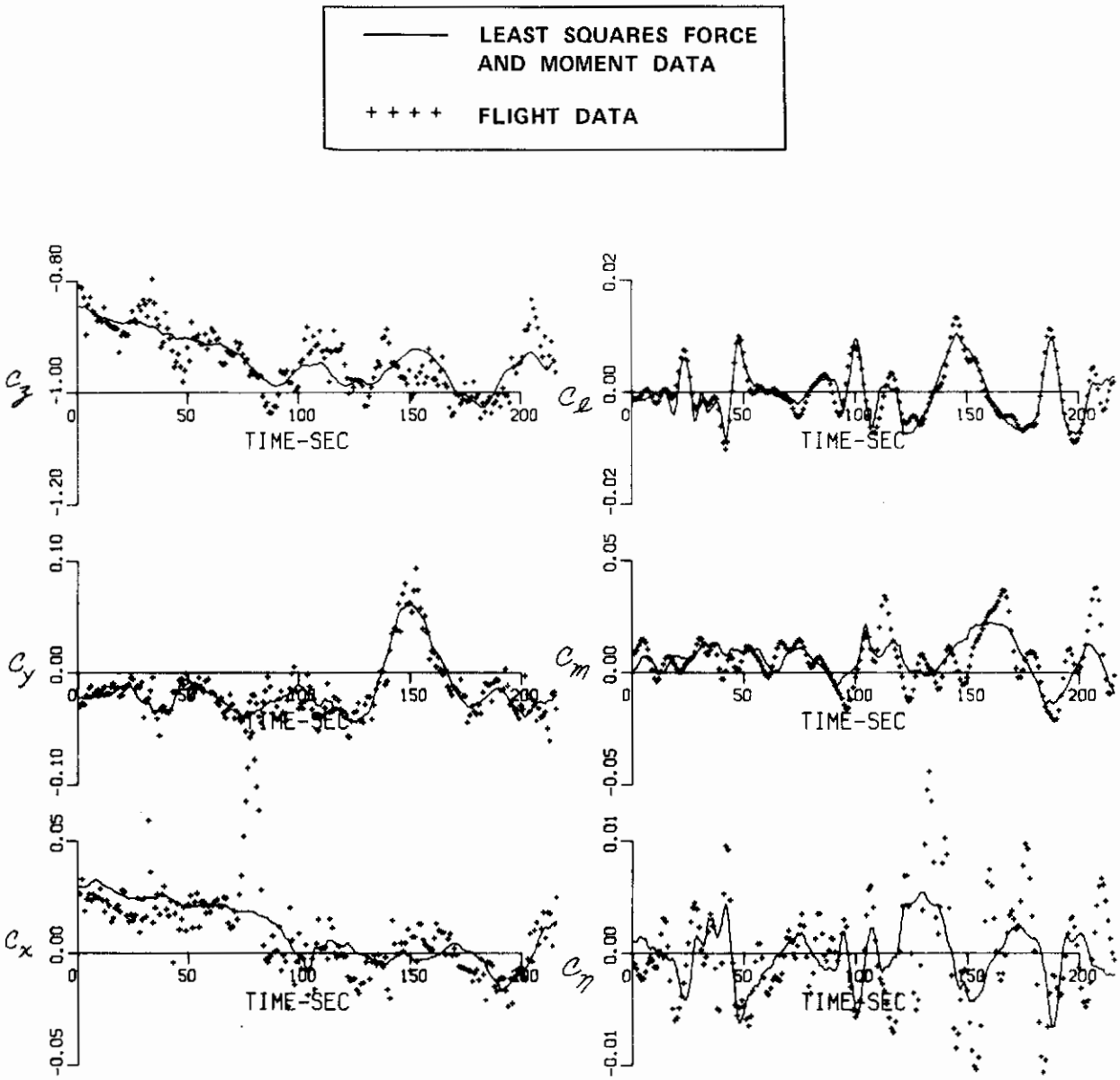

Figure 30 LEAST SQUARES FORCE AND MOMENT COMPARISONS WITH FLIGHT DATA - RECORD 10

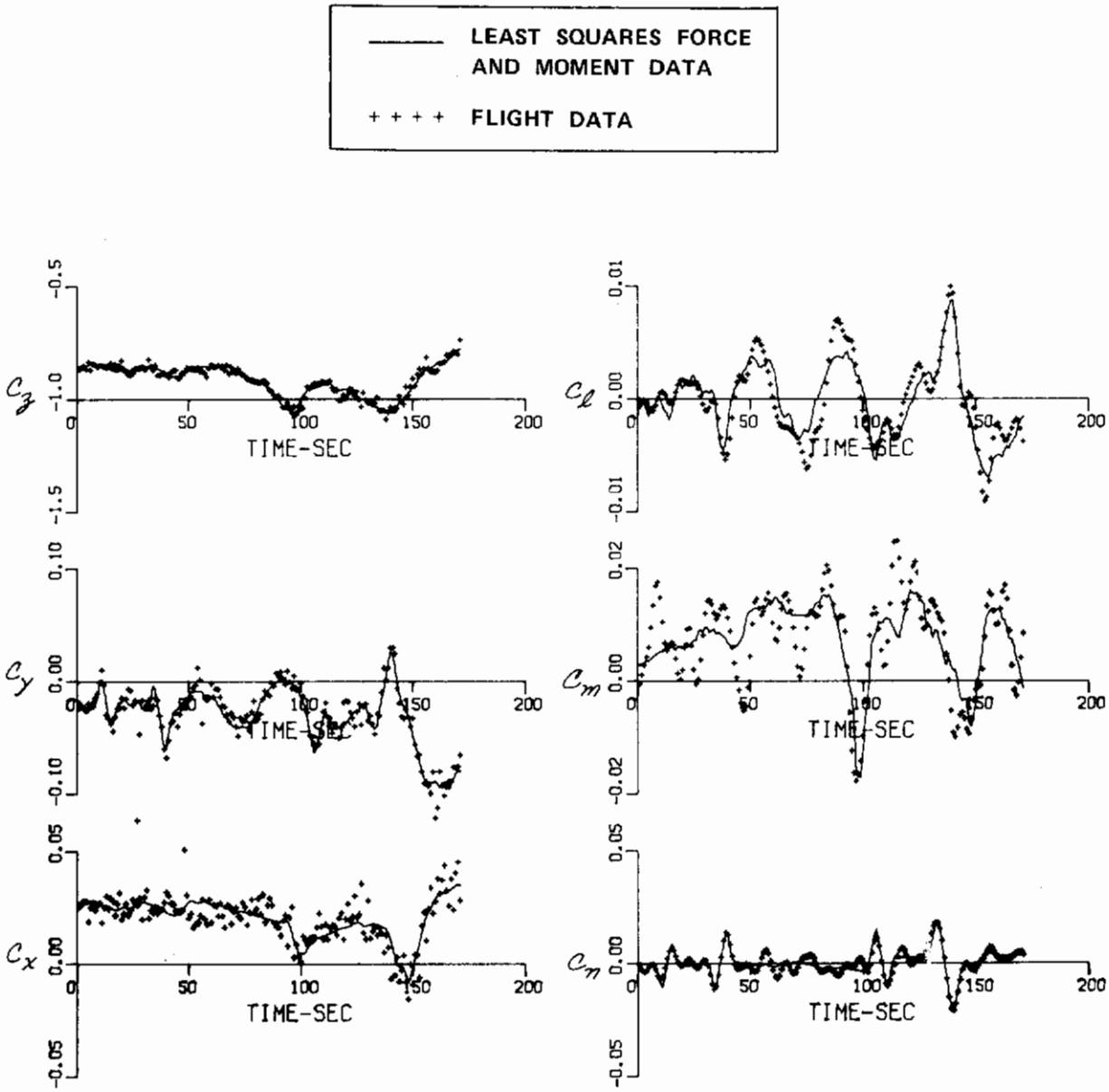

Figure 31 LEAST SQUARES FORCE AND MOMENT COMPARISONS WITH FLIGHT DATA - RECORD 11

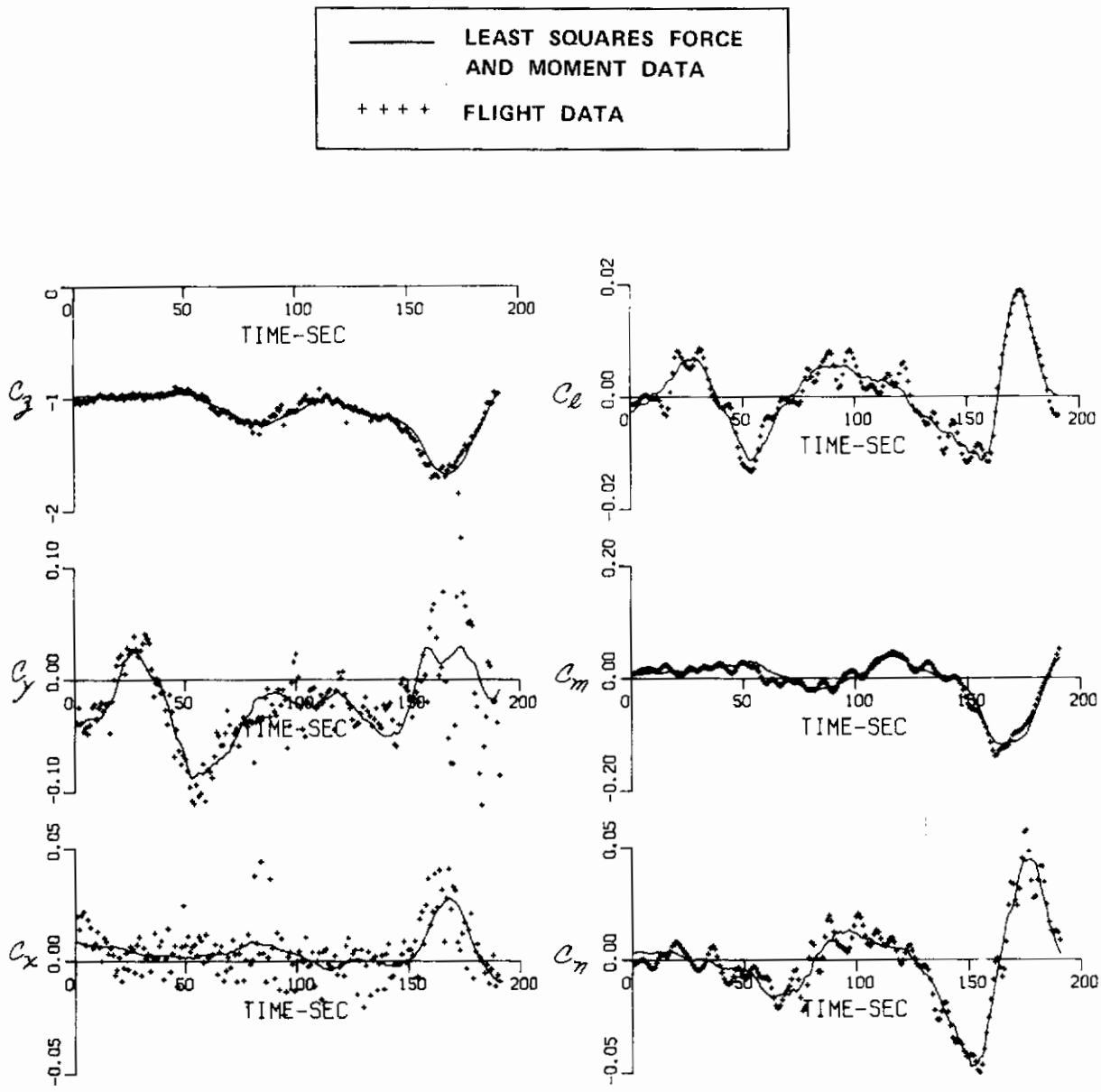

Figure 32 LEAST SQUARES FORCE AND MOMENT COMPARISONS WITH FLIGHT DATA - RECORD 14

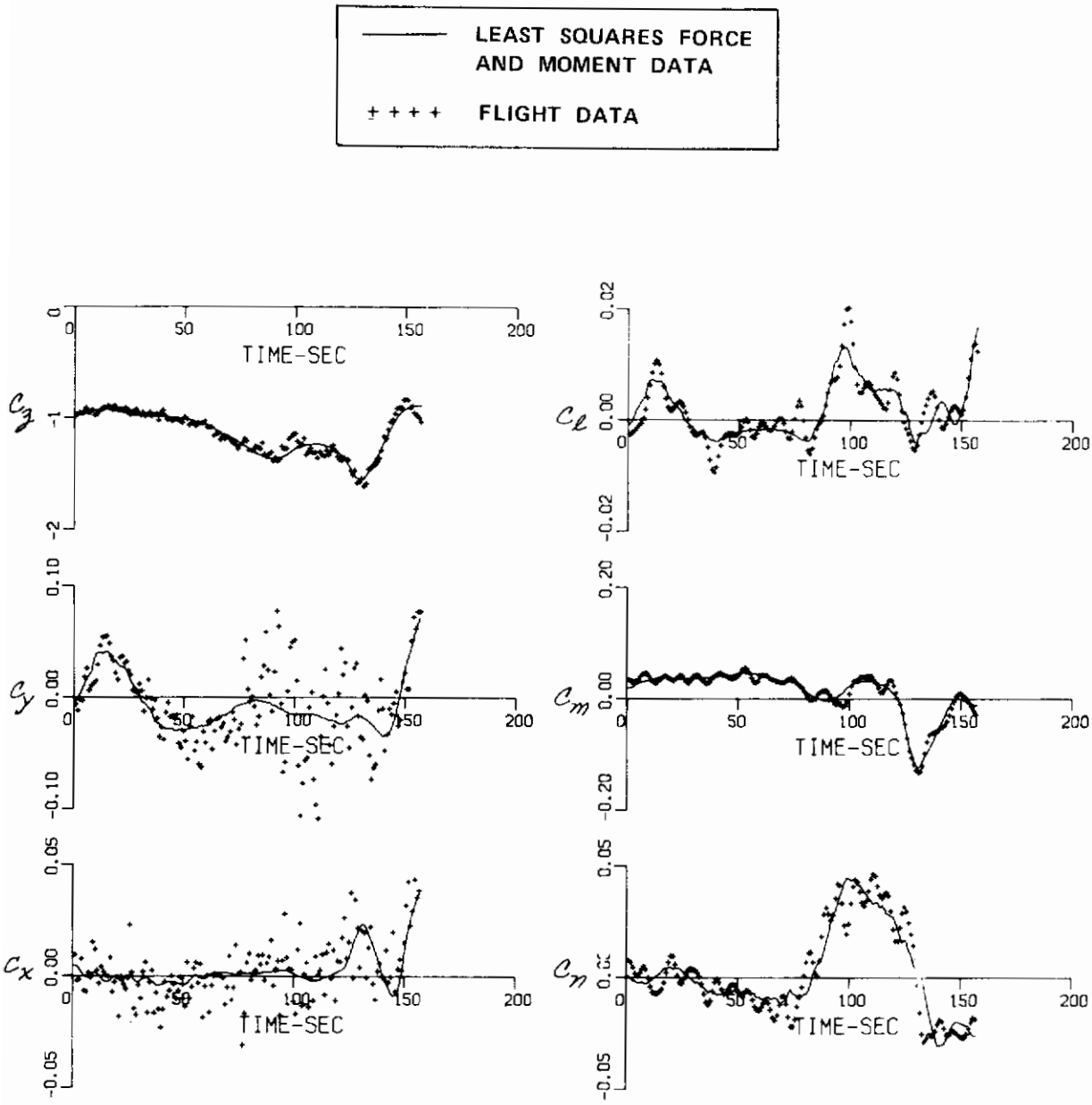

Figure 33 LEAST SQUARES FORCE AND MOMENT COMPARISONS WITH FLIGHT DATA - RECORD 20

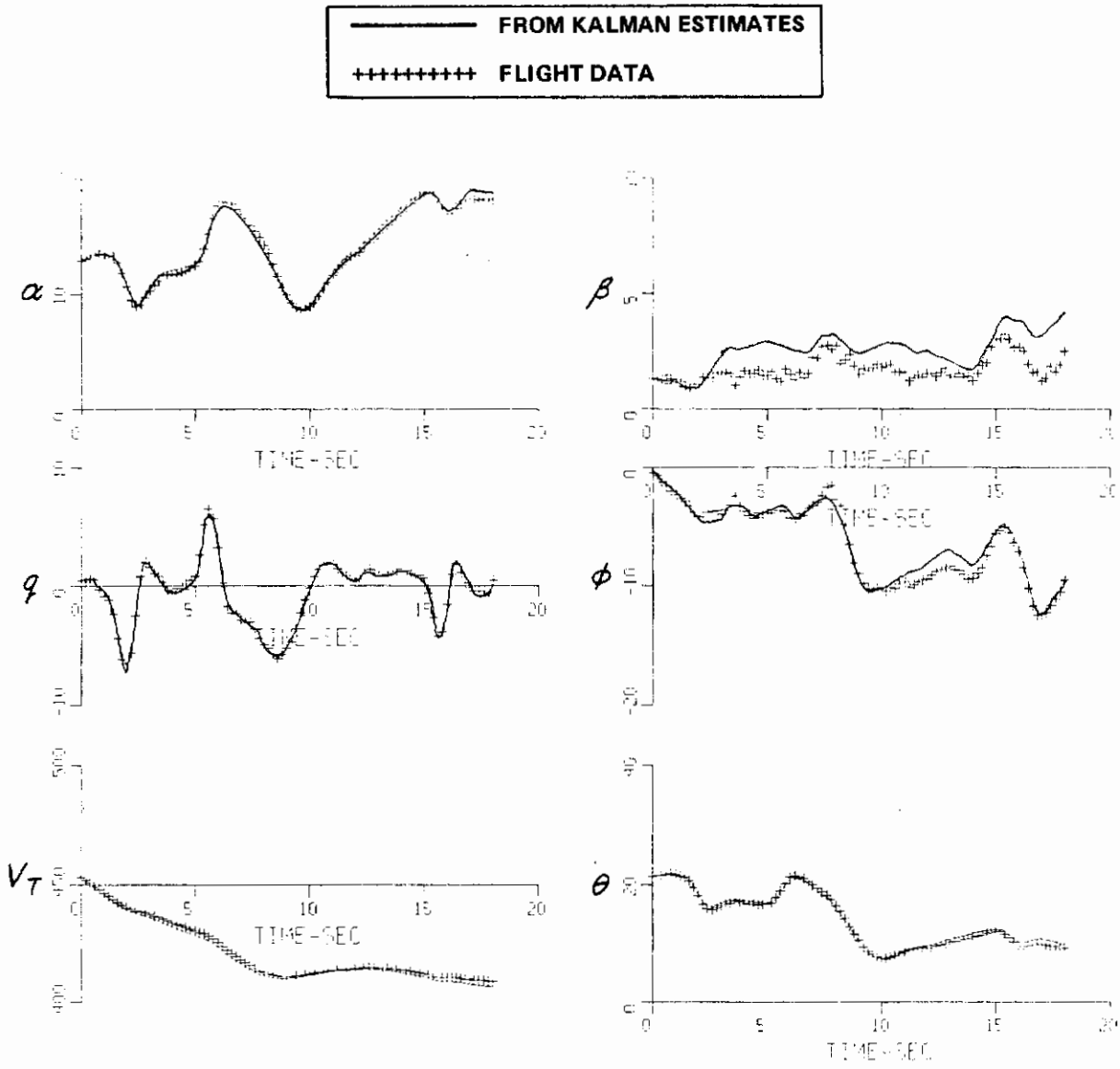

Figure 34 KALMAN RESULTS — RECORD 9, LONGITUDINAL

(a) RESPONSE COMPARISONS WITH FLIGHT DATA

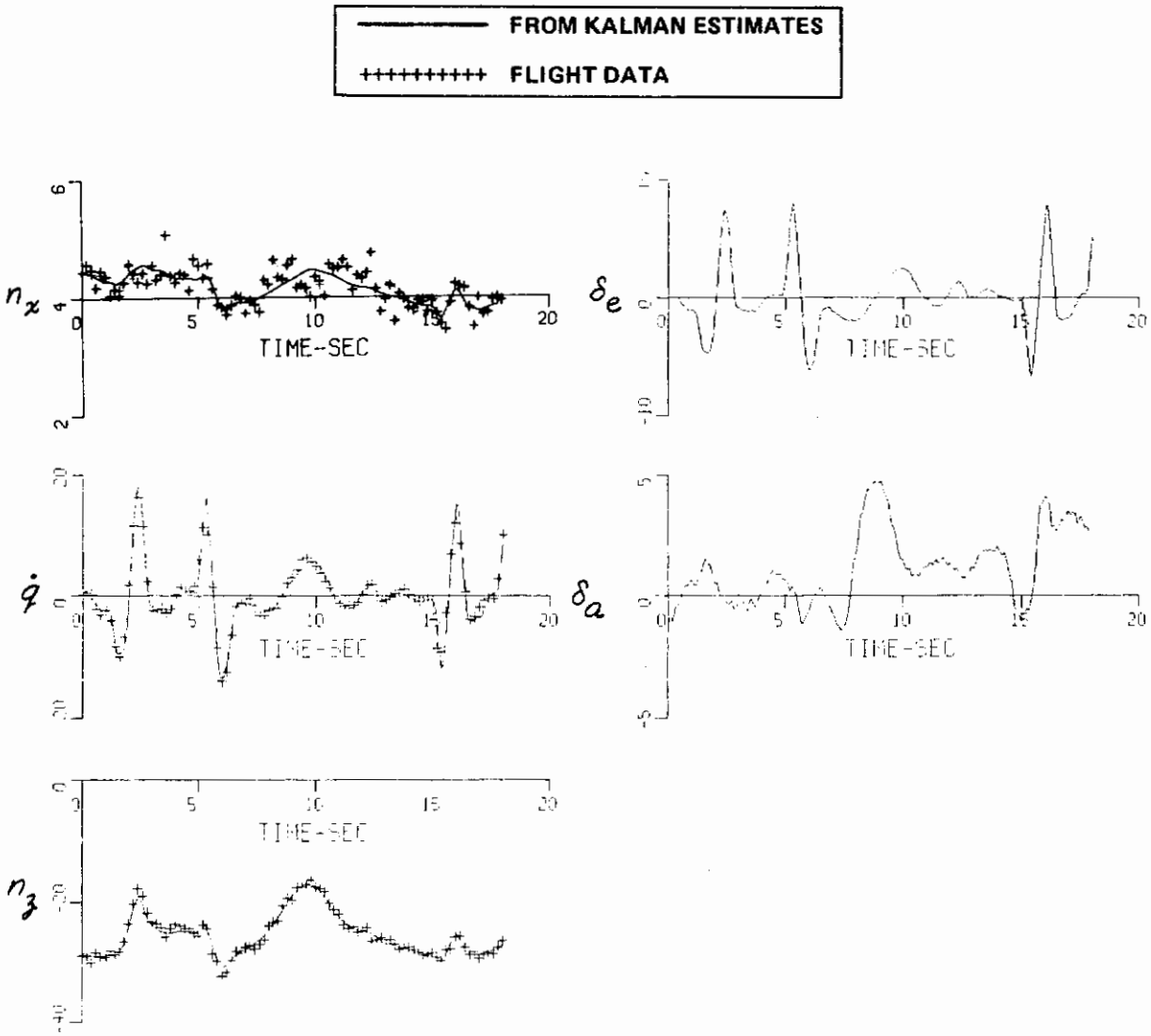

Figure 34 (Continued) KALMAN RESULTS – RECORD 9, LONGITUDINAL
(a) RESPONSE COMPARISONS WITH FLIGHT DATA

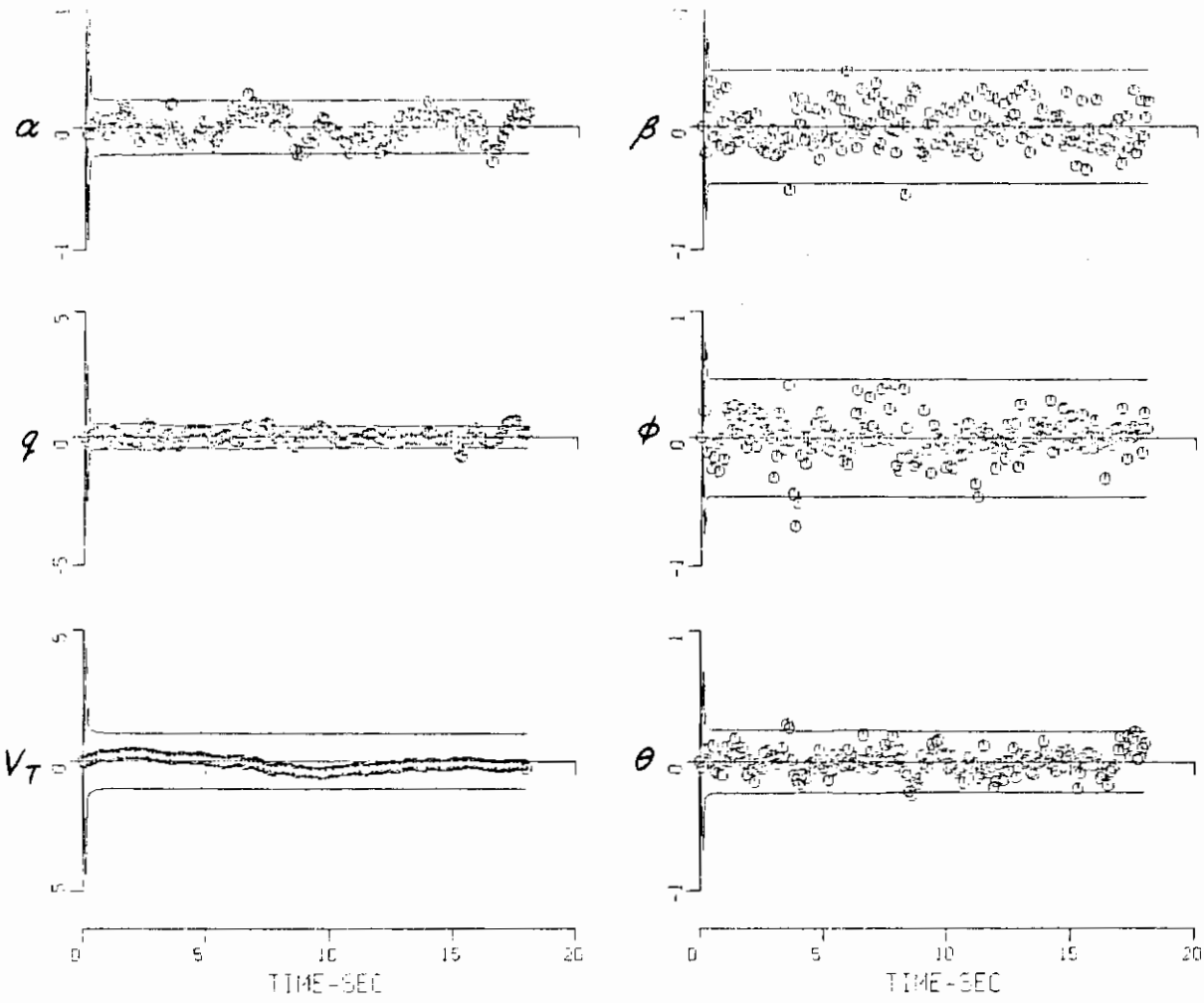

Figure 34 (Continued) KALMAN RESULTS – RECORD 9, LONGITUDINAL
(b) RESIDUALS AND SELECTED PARAMETER VARIATIONS

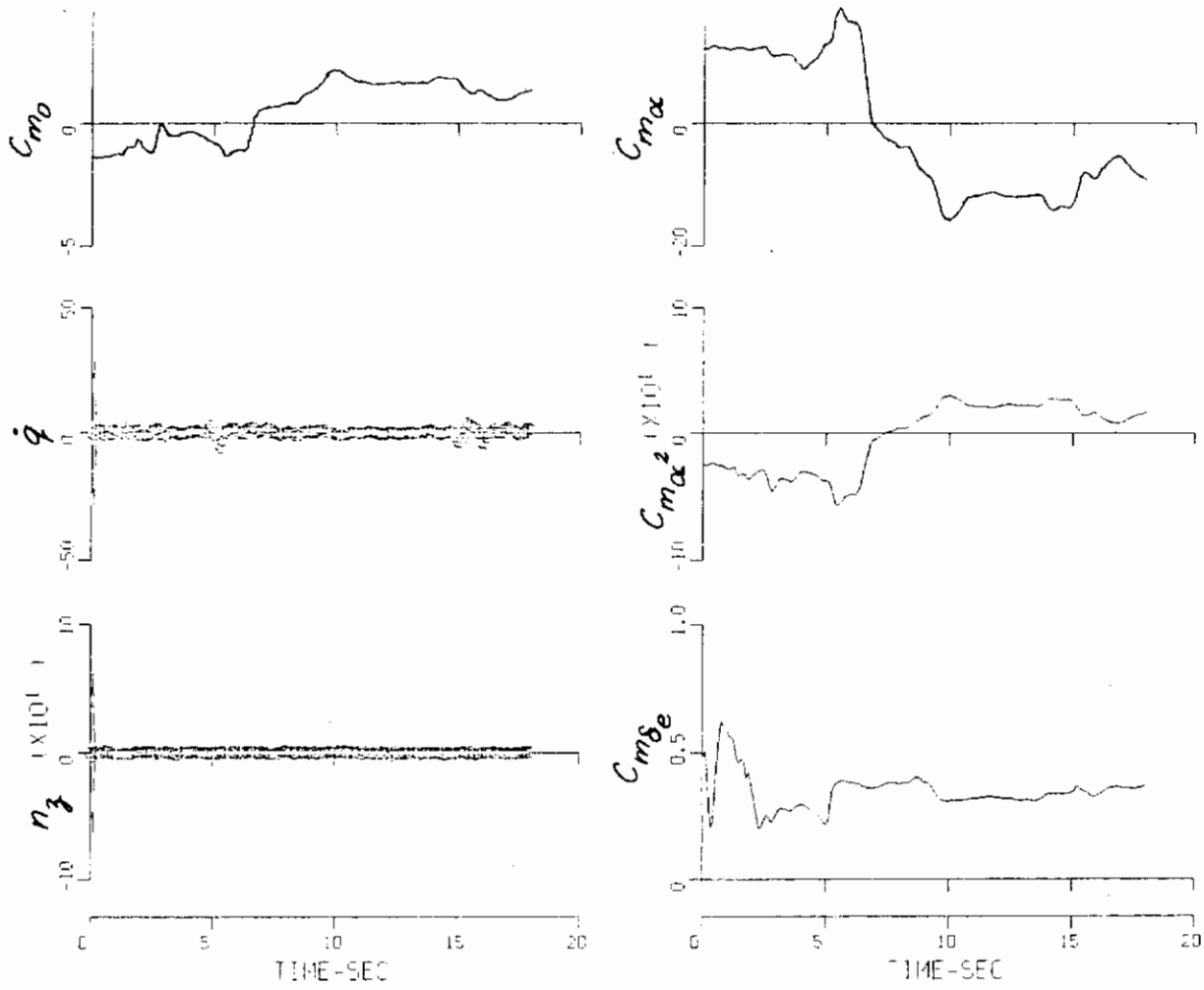

Figure 34 (Continued) KALMAN RESULTS – RECORD 9, LONGITUDINAL
(b) RESIDUALS AND SELECTED PARAMETER VARIATIONS

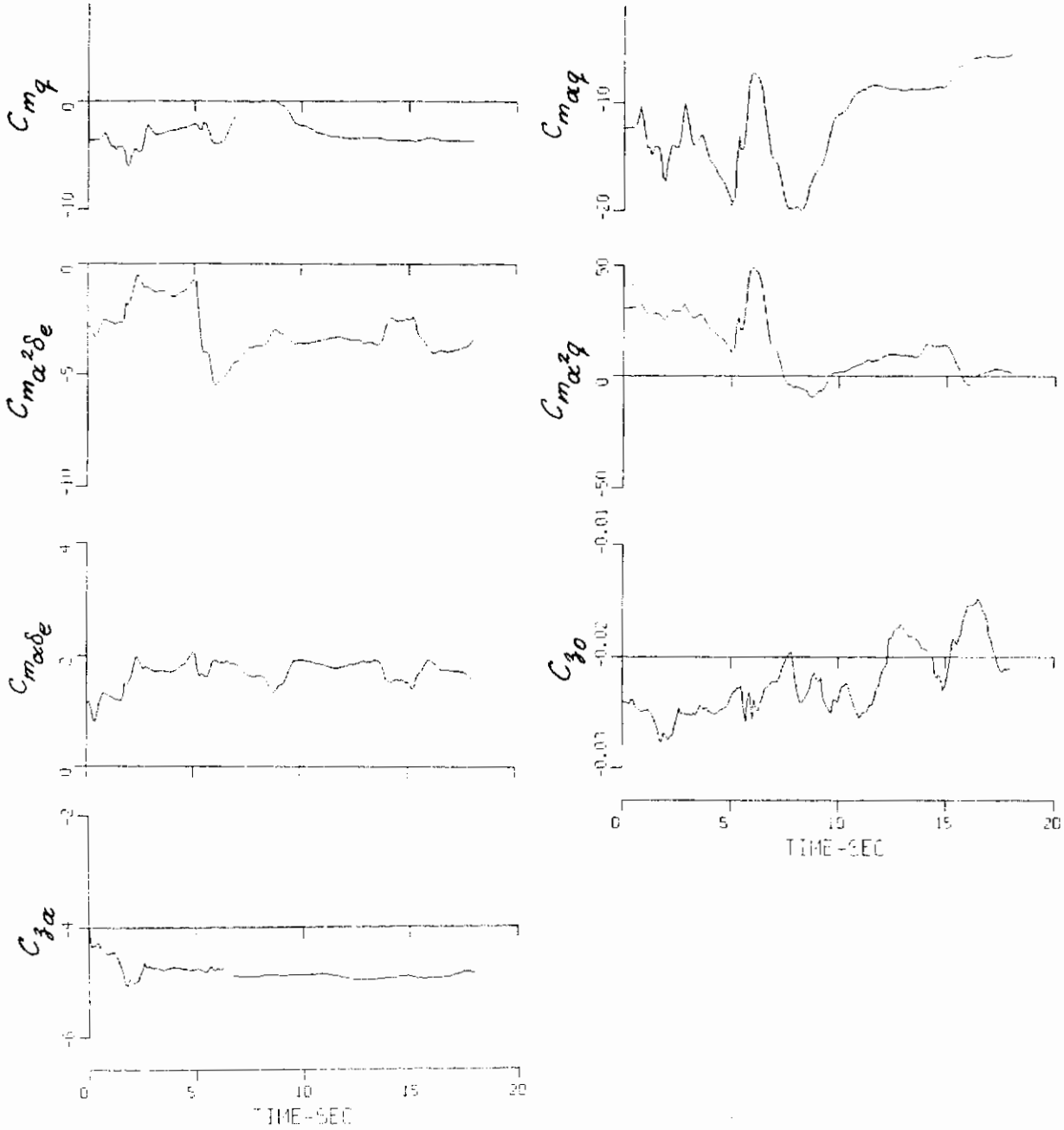

Figure 34 (Concluded) KALMAN RESULTS – RECORD 9, LONGITUDINAL
(b) RESIDUALS AND SELECTED PARAMETER VARIATIONS

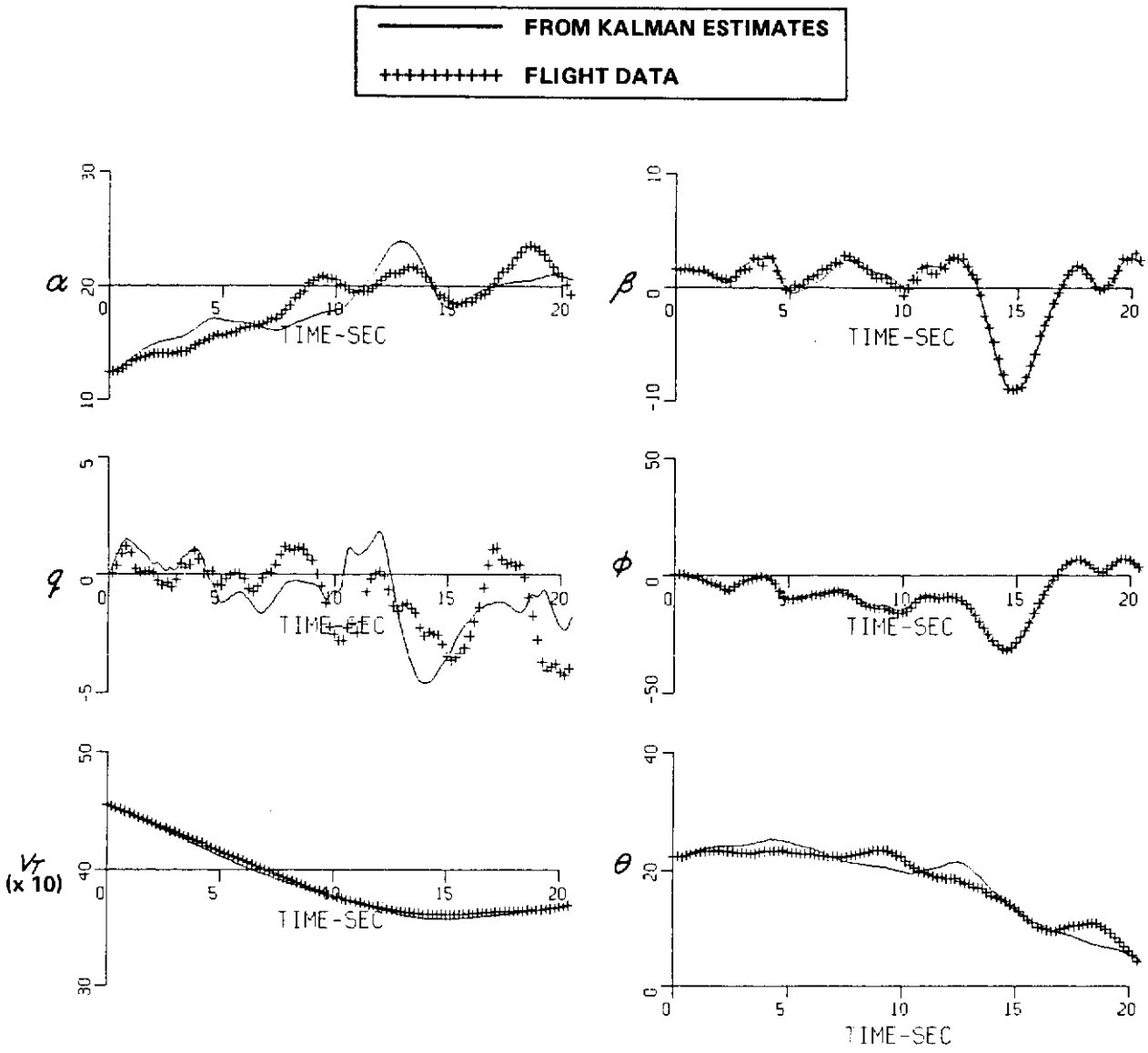

Figure 35 KALMAN RESULTS – RECORD 10, LONGITUDINAL

(a) RESPONSE COMPARISONS WITH FLIGHT DATA

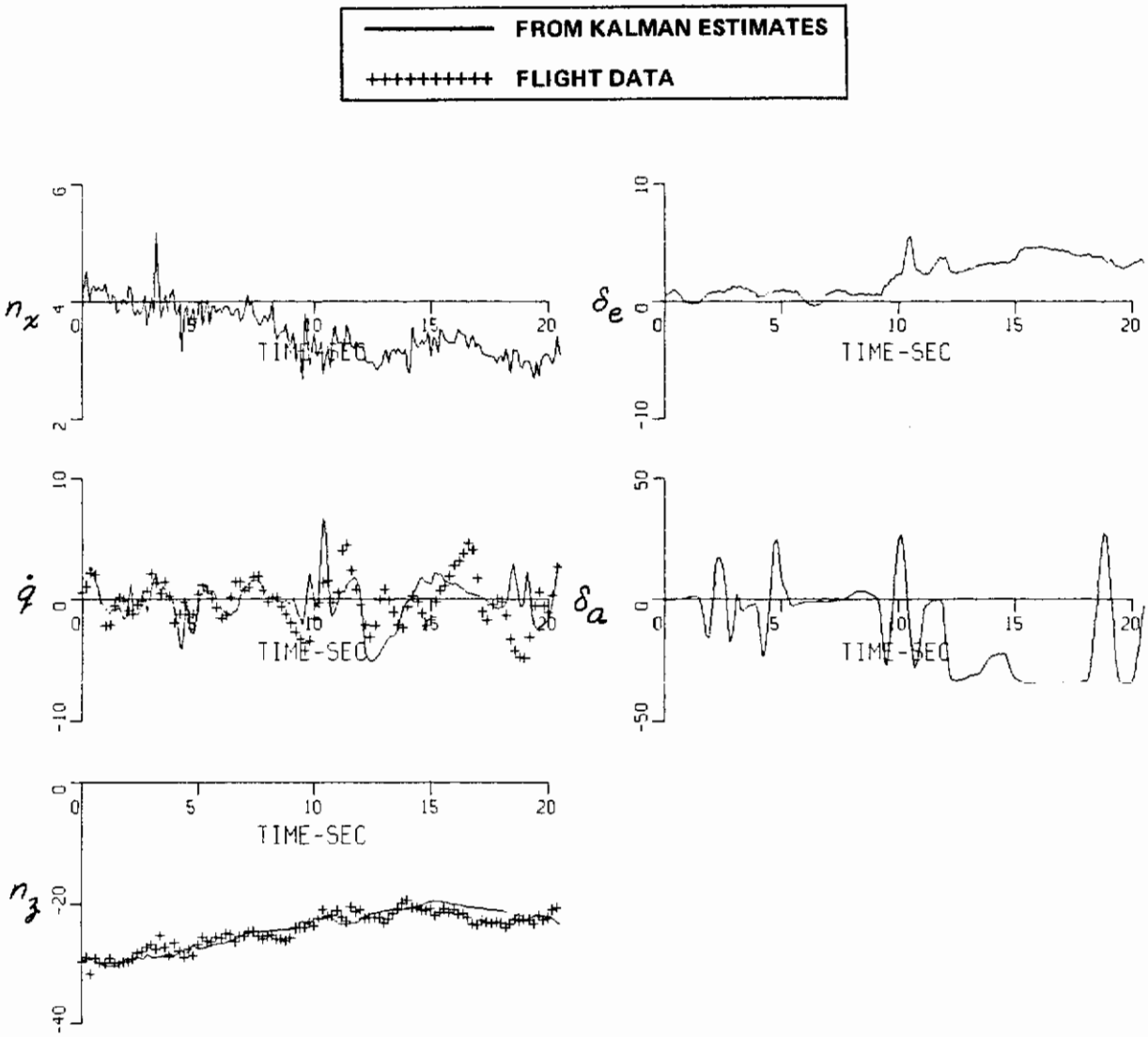

Figure 35 (Continued) KALMAN RESULTS – RECORD 10, LONGITUDINAL
(a) RESPONSE COMPARISONS WITH FLIGHT DATA

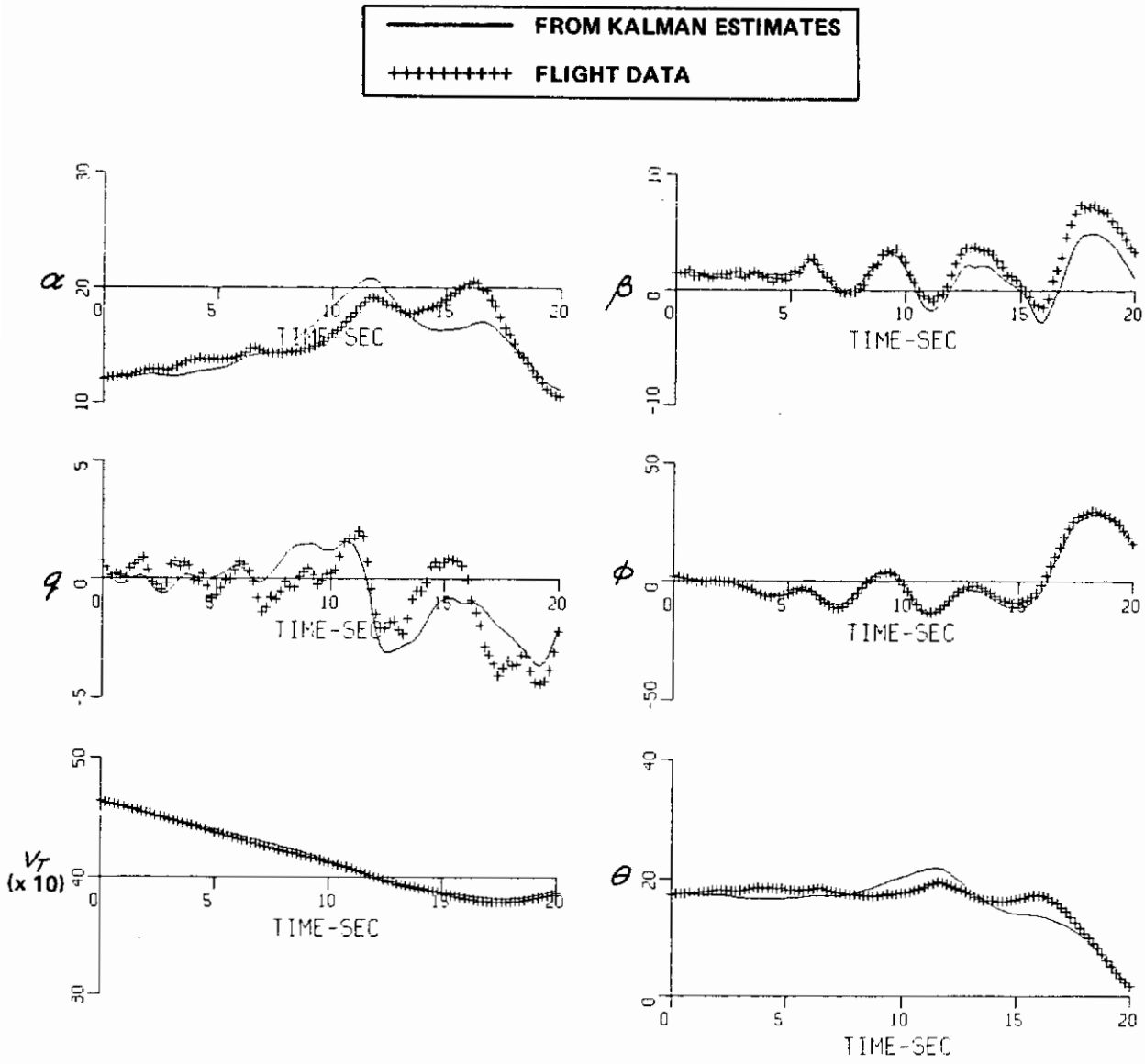

Figure 36 KALMAN RESULTS – RECORD 11, LONGITUDINAL
(a) RESPONSE COMPARISONS WITH FLIGHT DATA

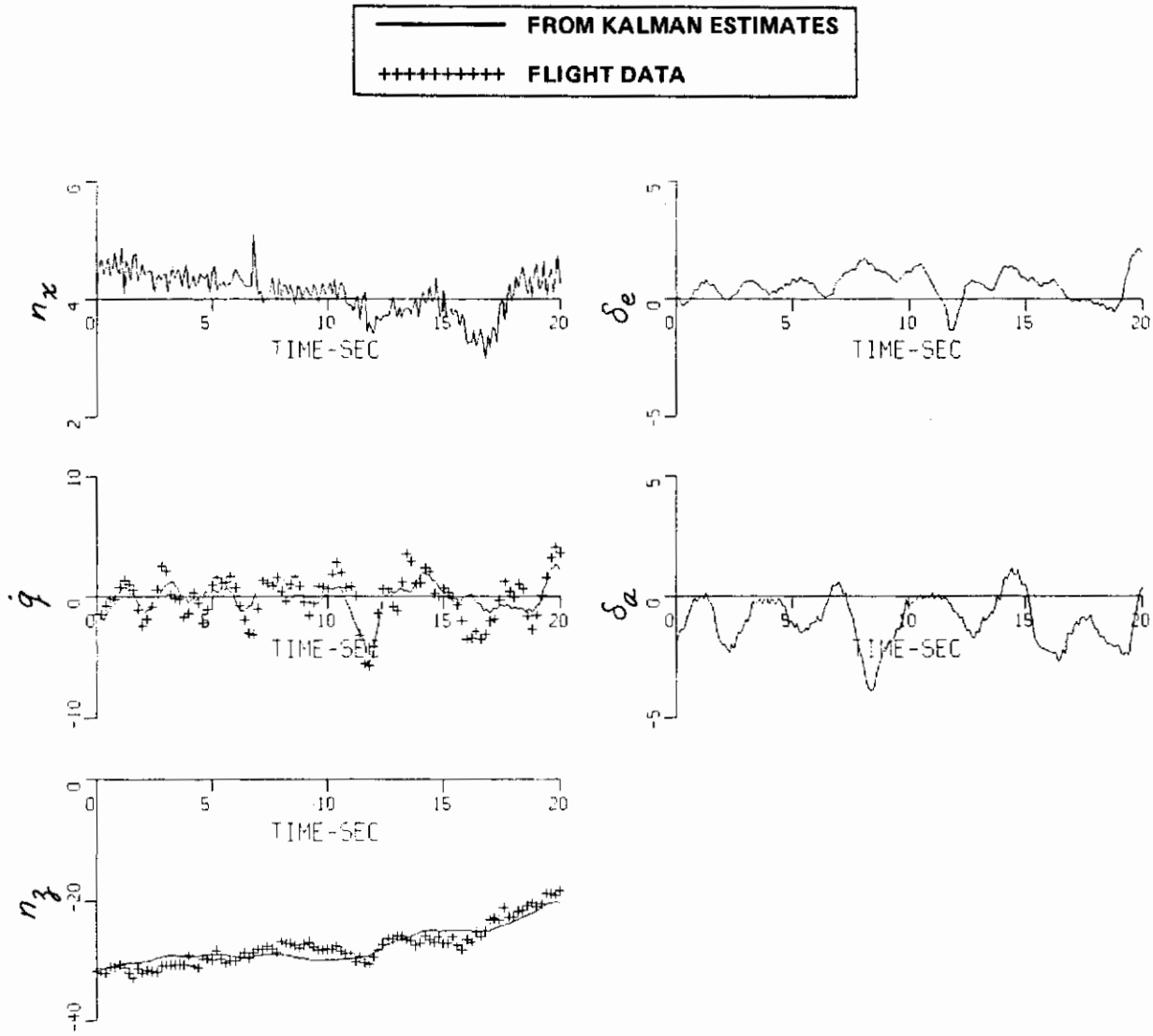

Figure 36 (Continued) KALMAN RESULTS – RECORD 11, LONGITUDINAL
(a) RESPONSE COMPARISONS WITH FLIGHT DATA

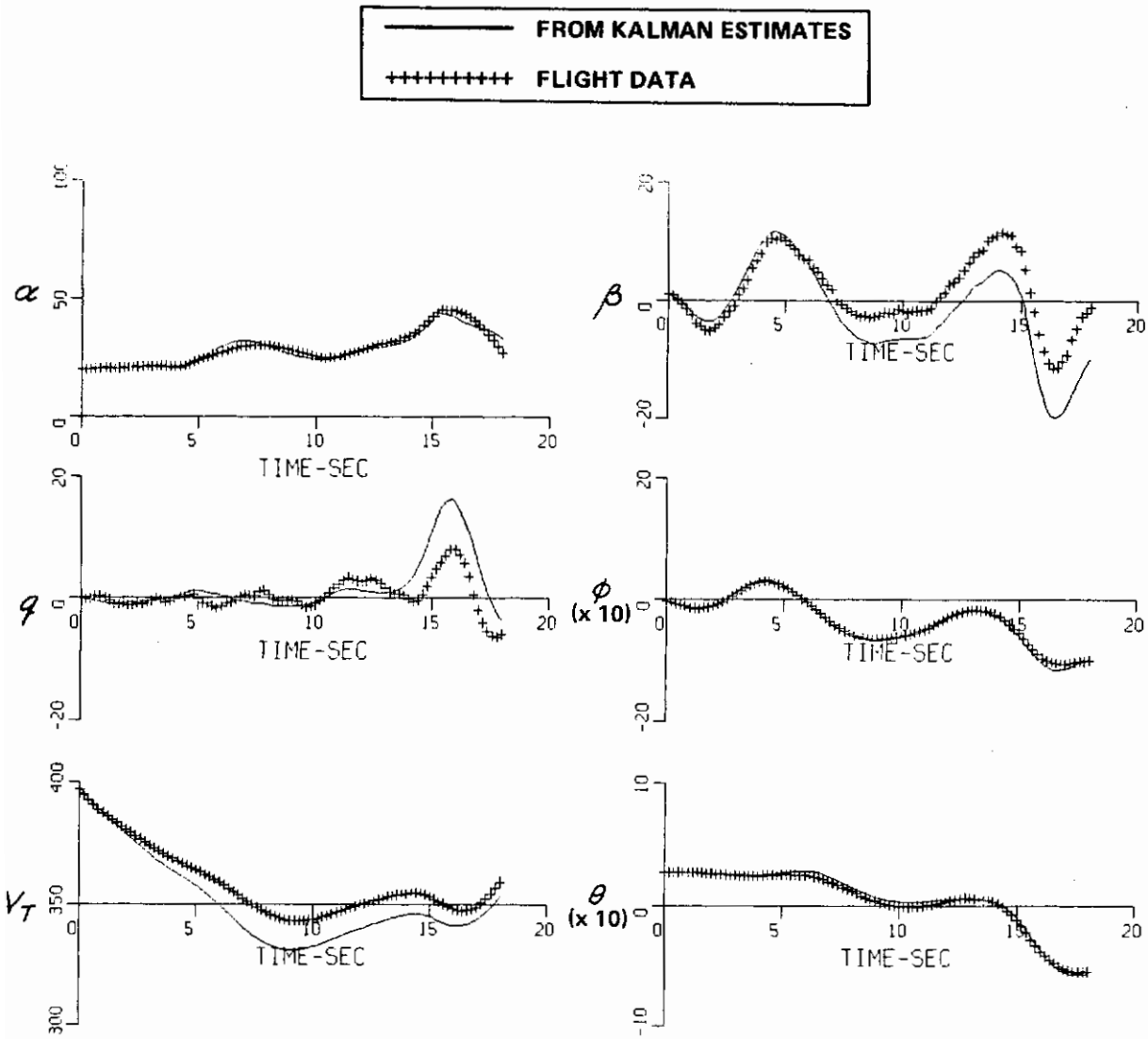

Figure 37 KALMAN RESULTS – RECORD 14, LONGITUDINAL

(a) RESPONSE COMPARISONS WITH FLIGHT DATA

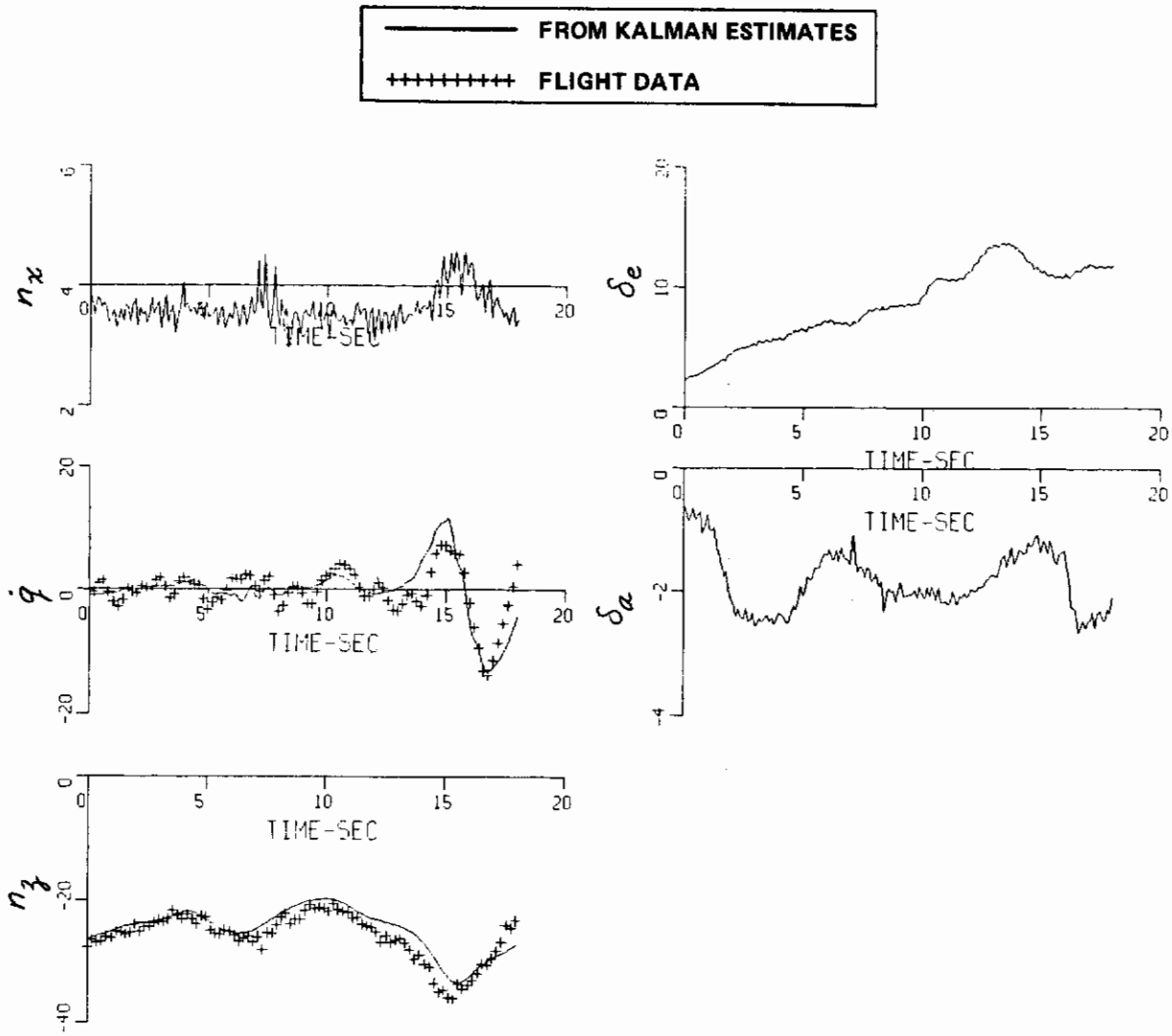

Figure 37 (Continued) KALMAN RESULTS – RECORD 14, LONGITUDINAL
(a) RESPONSE COMPARISONS WITH FLIGHT DATA

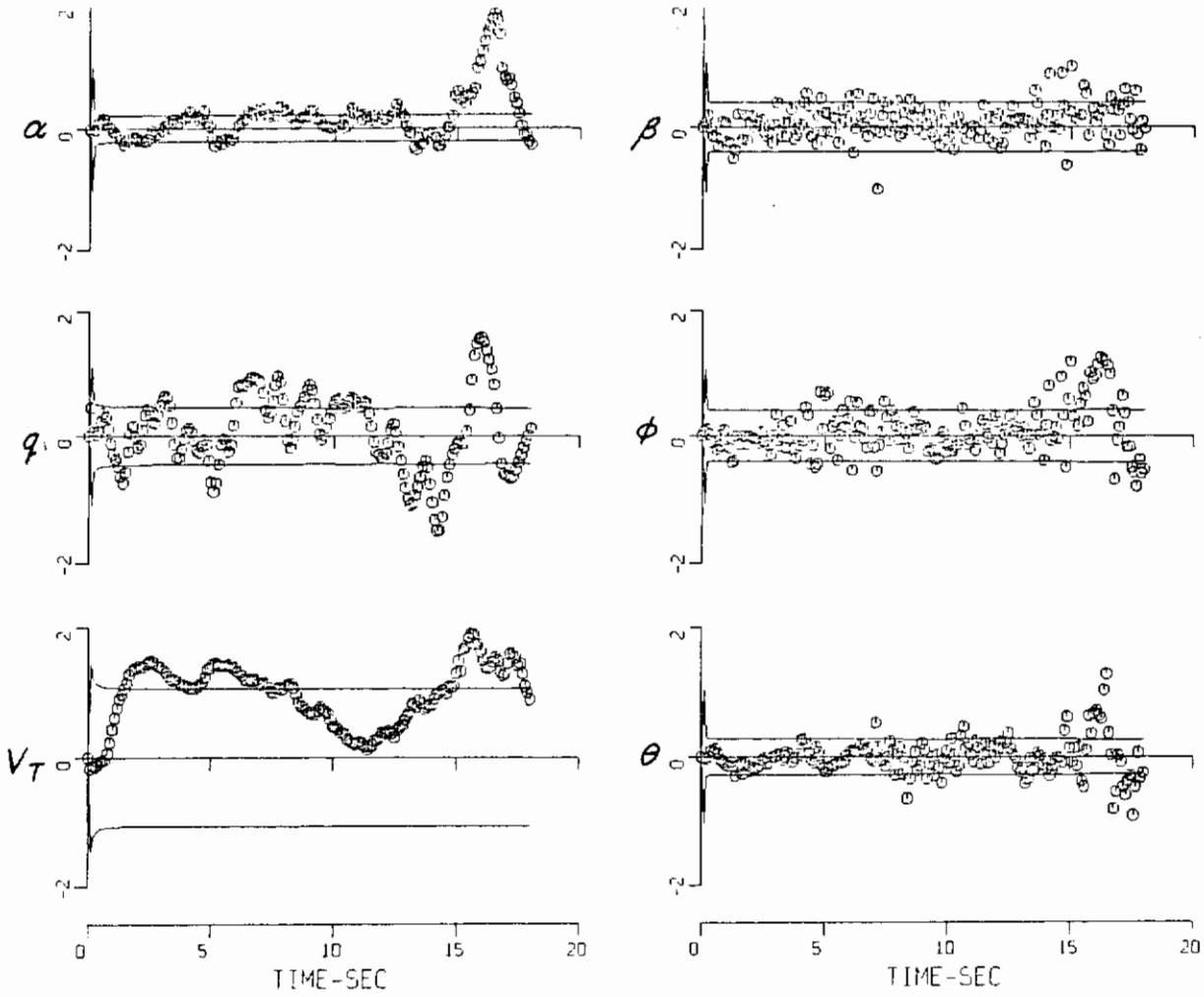

Figure 37 (Continued) KALMAN RESULTS – RECORD 14, LONGITUDINAL
(b) RESIDUALS AND SELECTED PARAMETER VARIATIONS

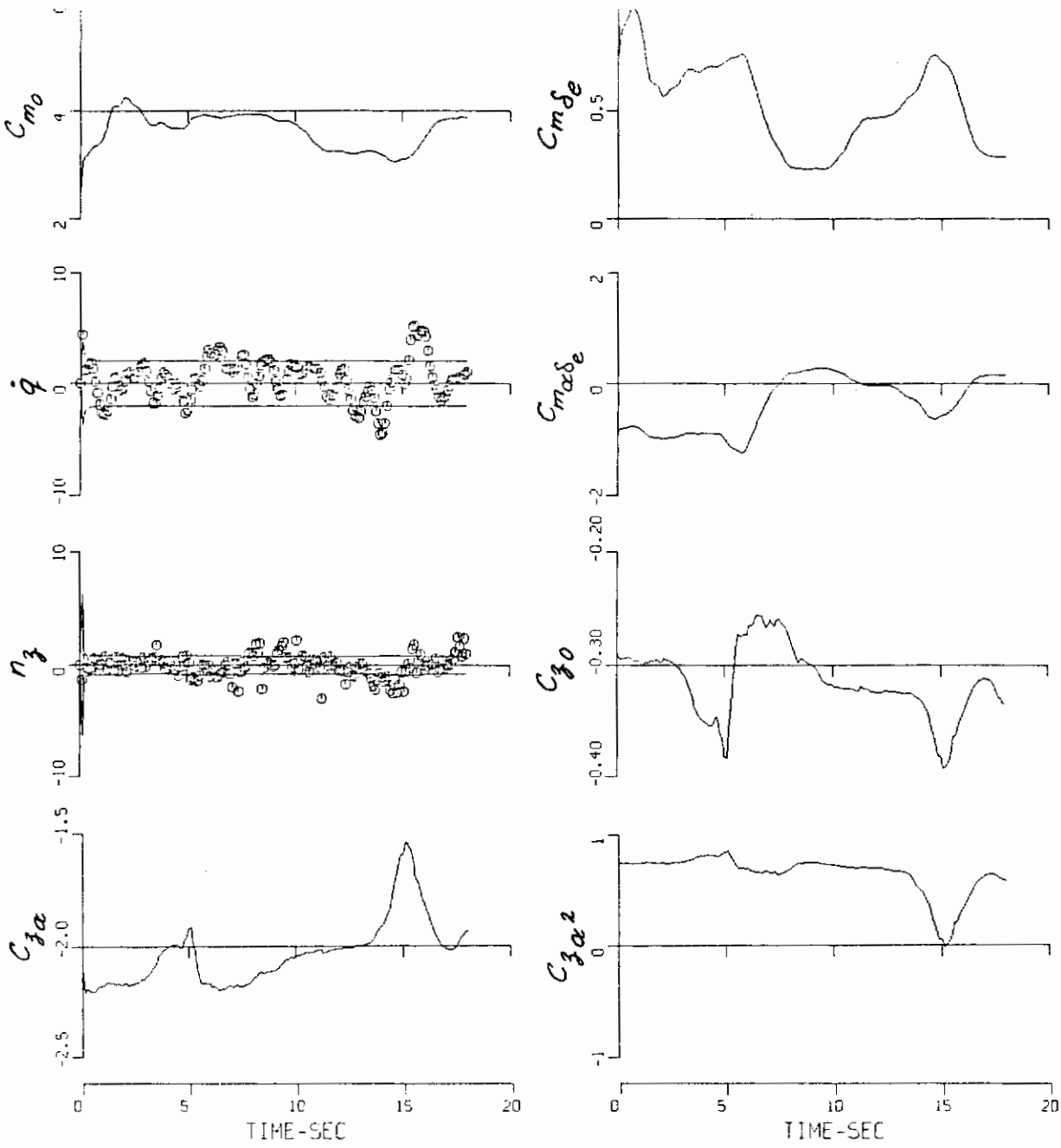

Figure 37 (Concluded) KALMAN RESULTS – RECORD 14, LONGITUDINAL
(b) RESIDUALS AND SELECTED PARAMETER VARIATIONS

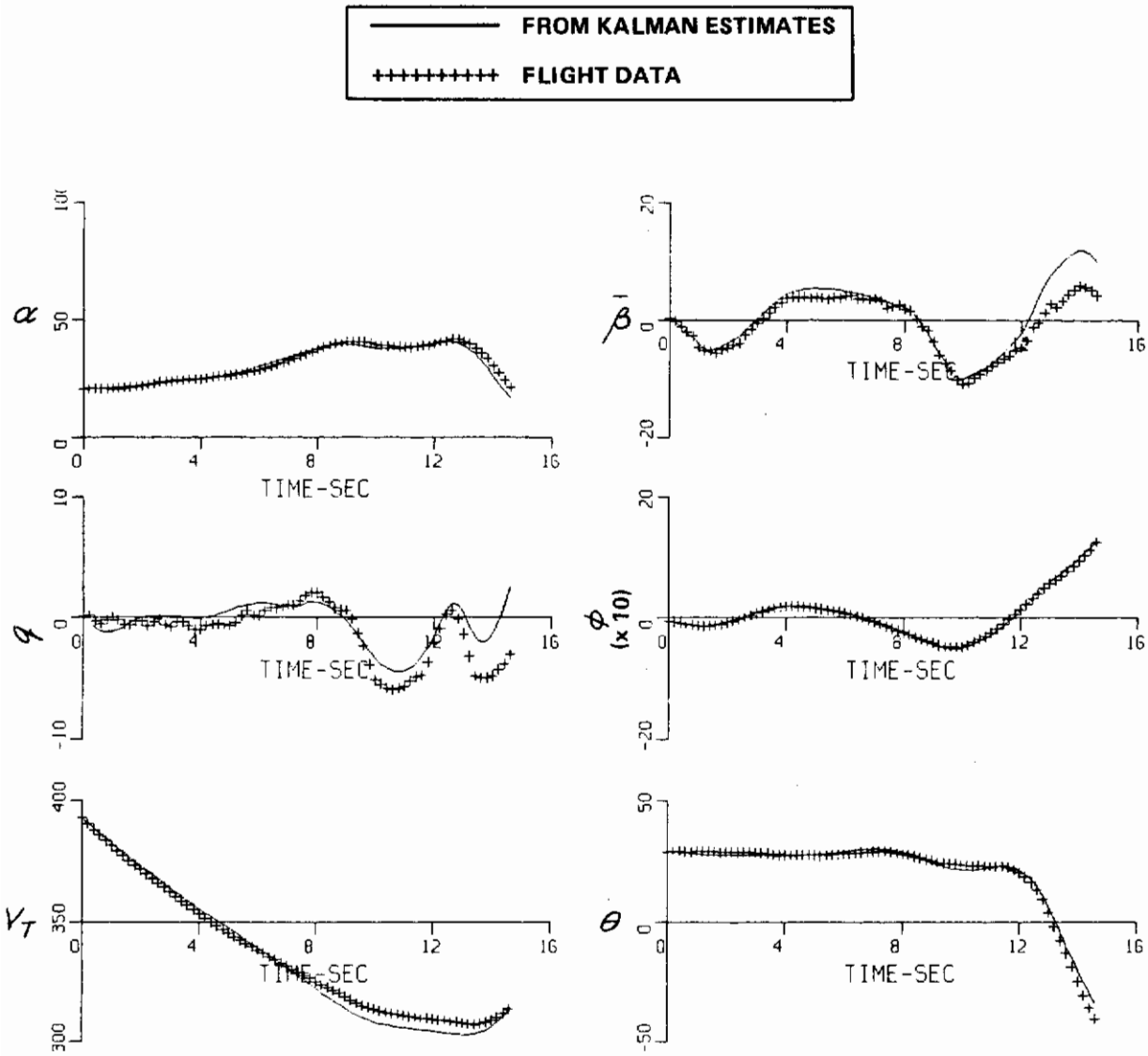

Figure 38 KALMAN RESULTS – RECORD 20, LONGITUDINAL
(a) RESPONSE COMPARISONS WITH FLIGHT DATA

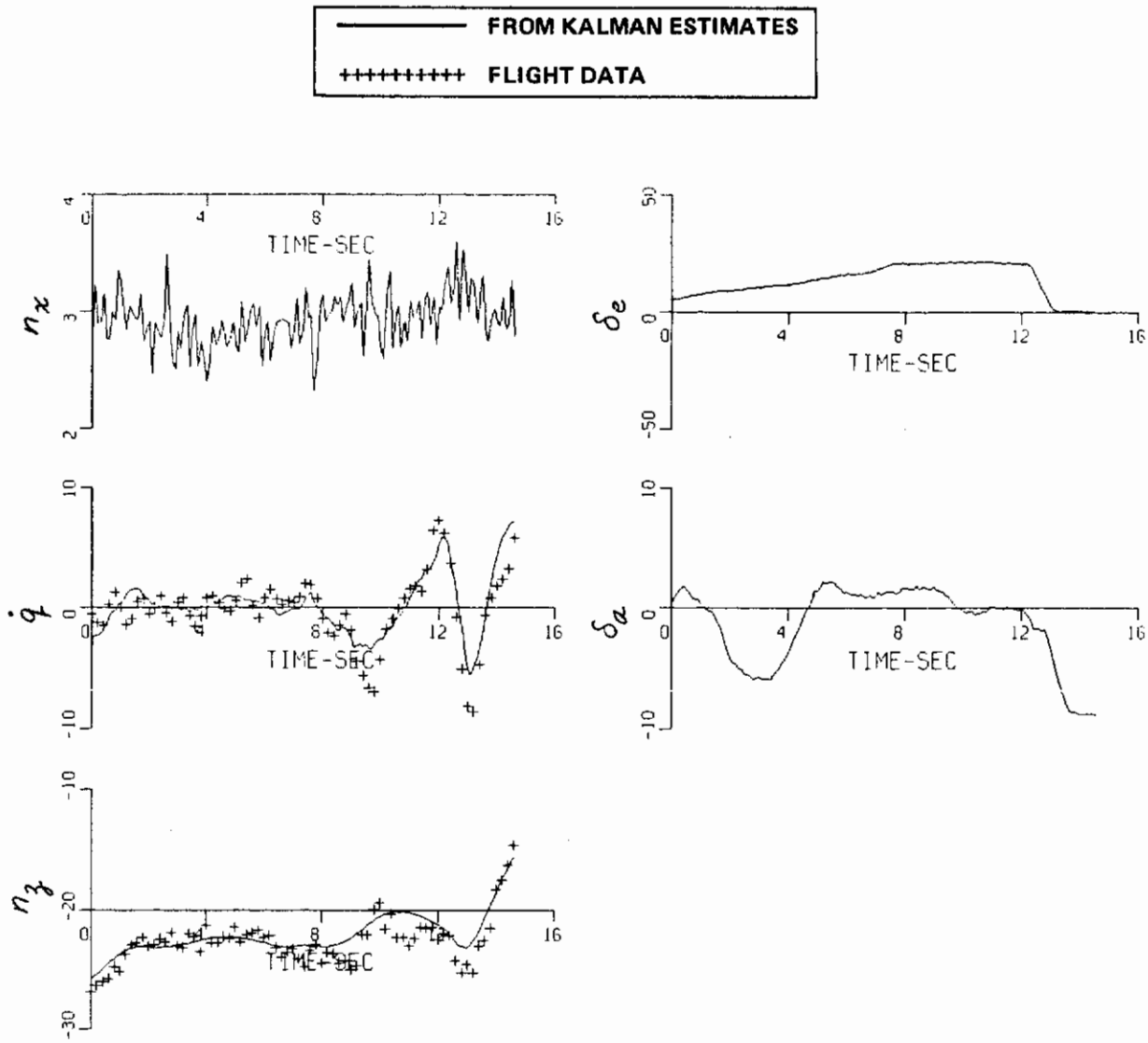

Figure 38 (Continued) KALMAN RESULTS – RECORD 20, LONGITUDINAL

(a) RESPONSE COMPARISONS WITH FLIGHT DATA

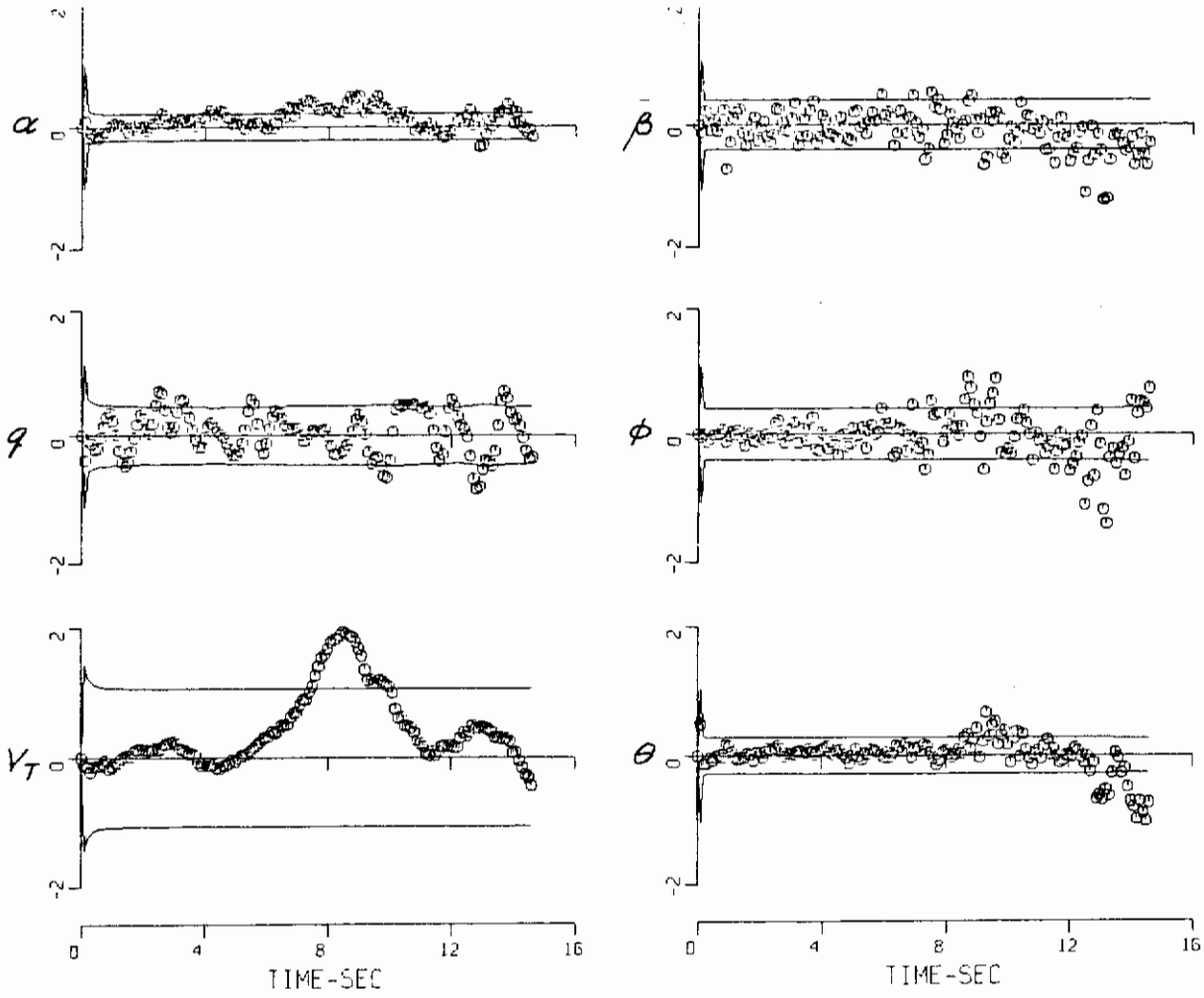

Figure 38 (Continued) KALMAN RESULTS – RECORD 20, LONGITUDINAL
(b) RESIDUALS AND SELECTED PARAMETER VARIATIONS

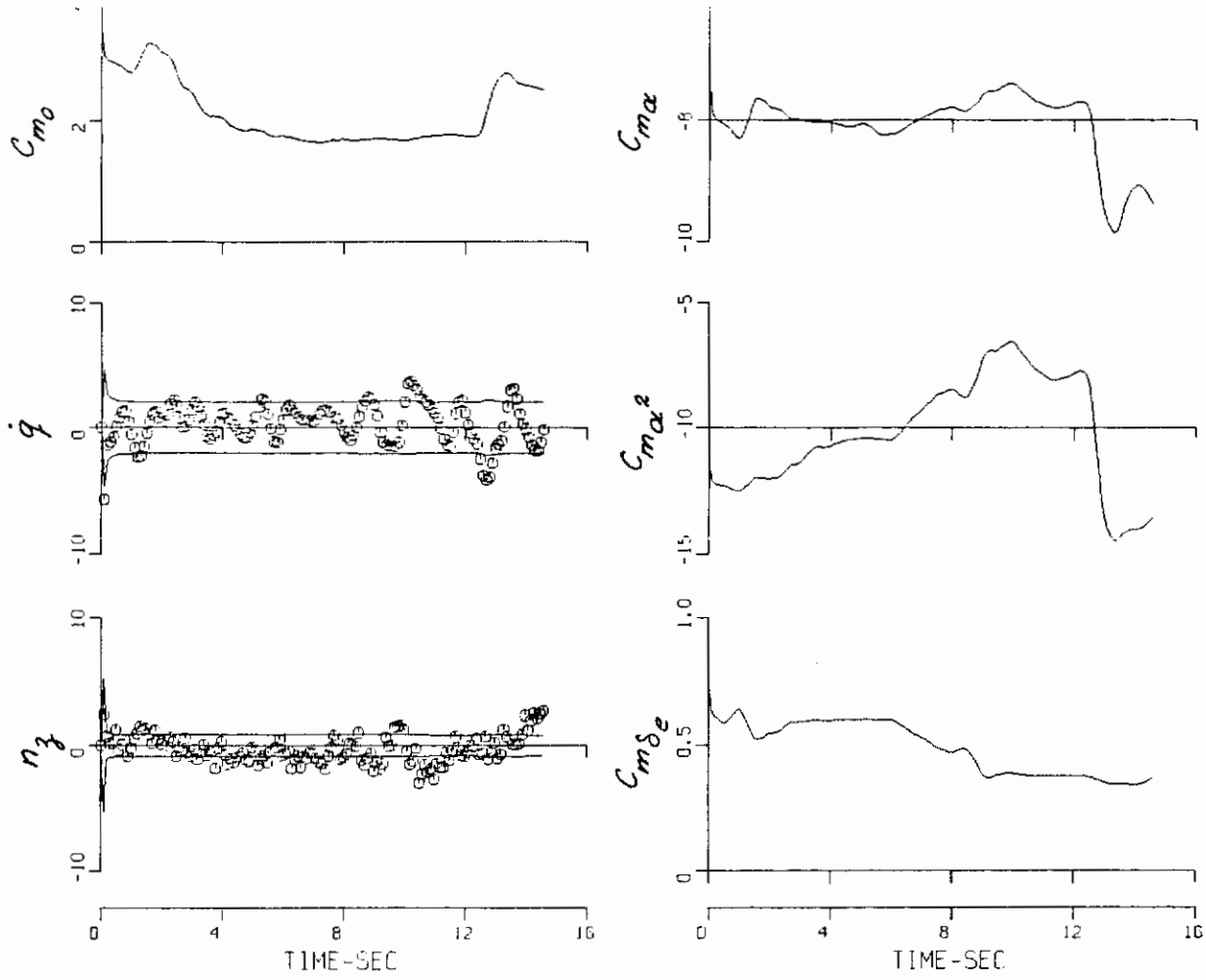

Figure 38 (Continued) KALMAN RESULTS – RECORD 20, LONGITUDINAL
(b) RESIDUALS AND SELECTED PARAMETER VARIATIONS

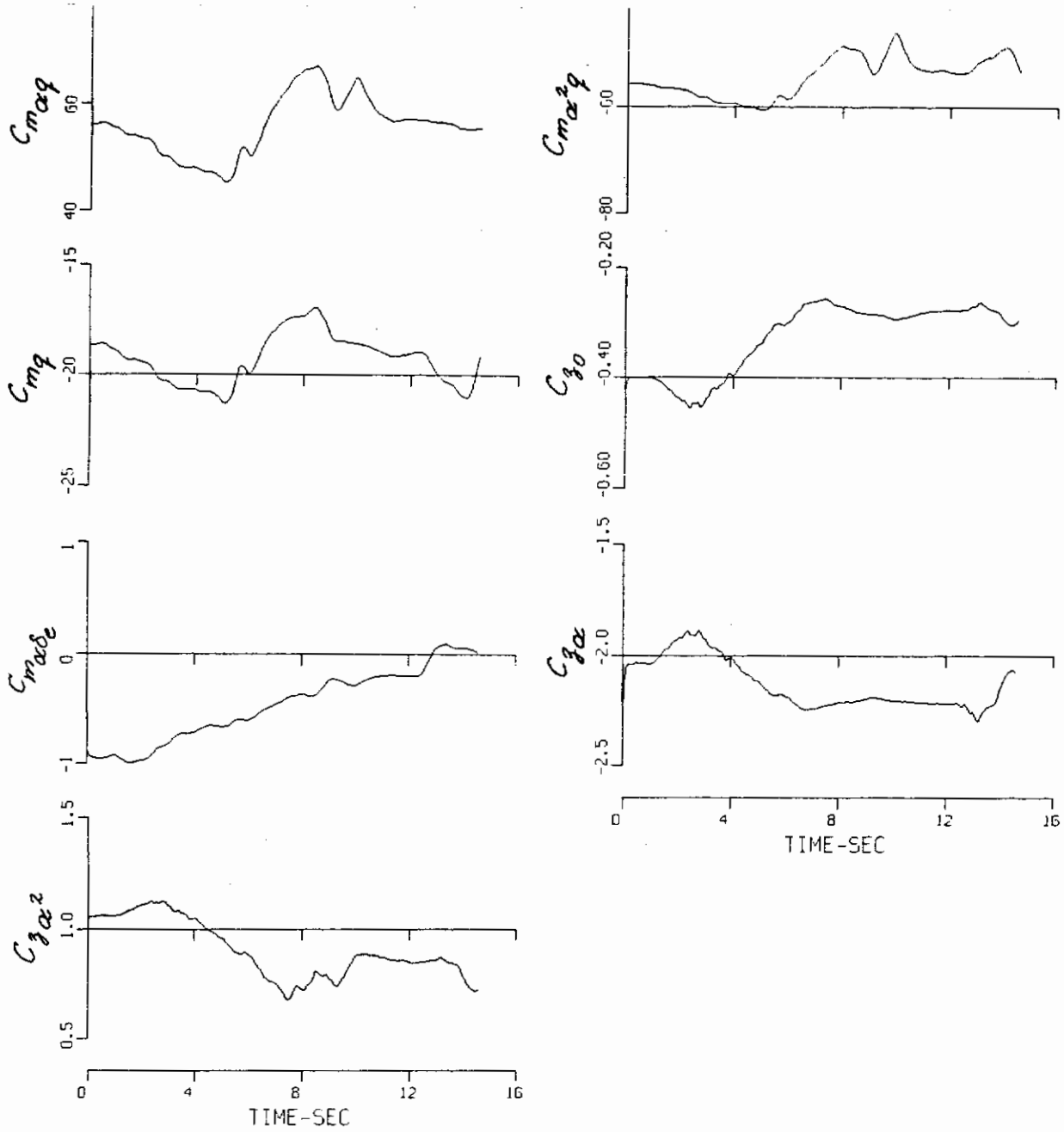

Figure 38 (Concluded) KALMAN RESULTS – RECORD 20, LONGITUDINAL
(b) RESIDUALS AND SELECTED PARAMETER VARIATIONS

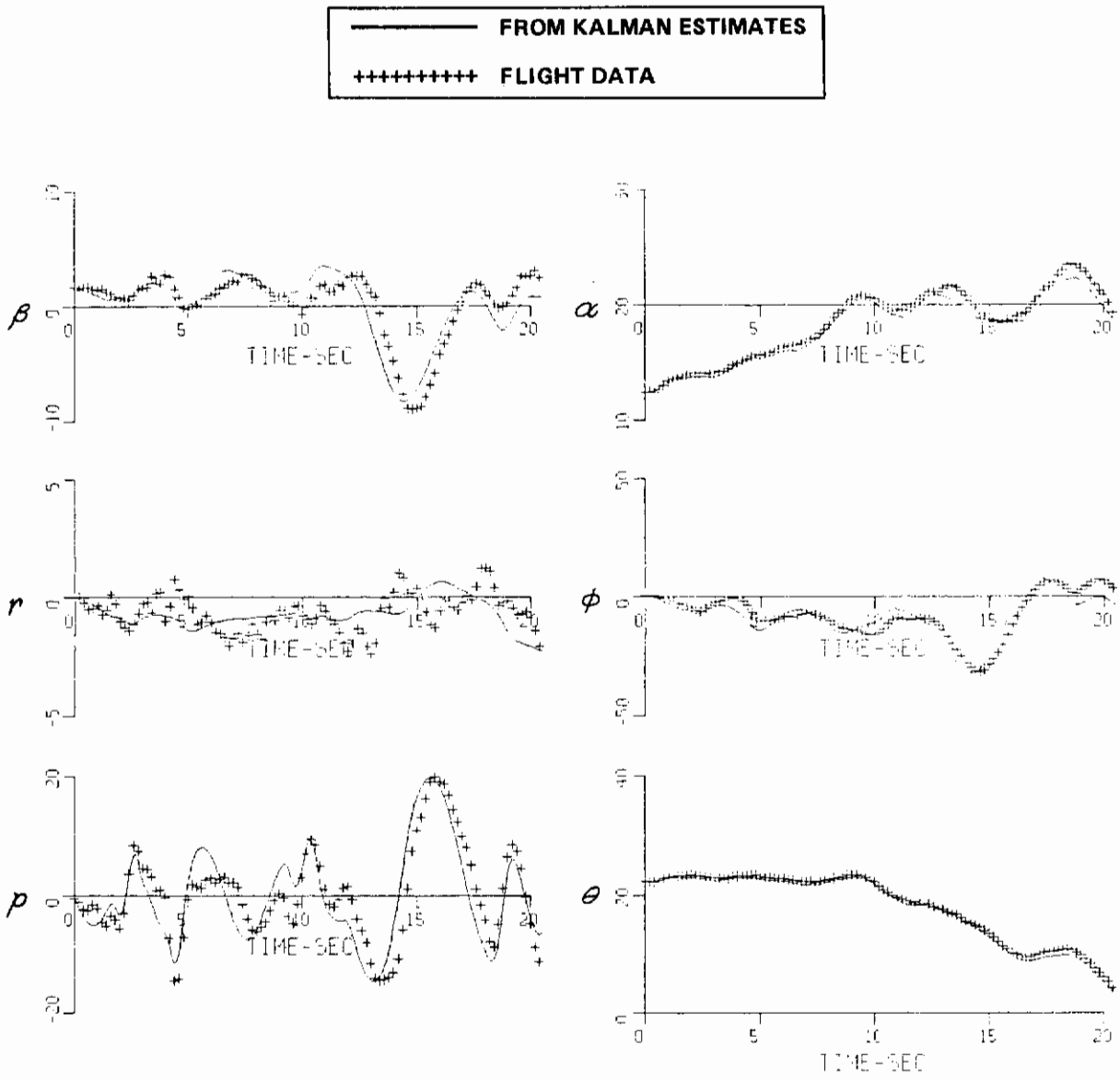

Figure 39. KALMAN RESULTS – RECORD 10, LATERAL-DIRECTIONAL
(a) RESPONSE COMPARISONS WITH FLIGHT DATA

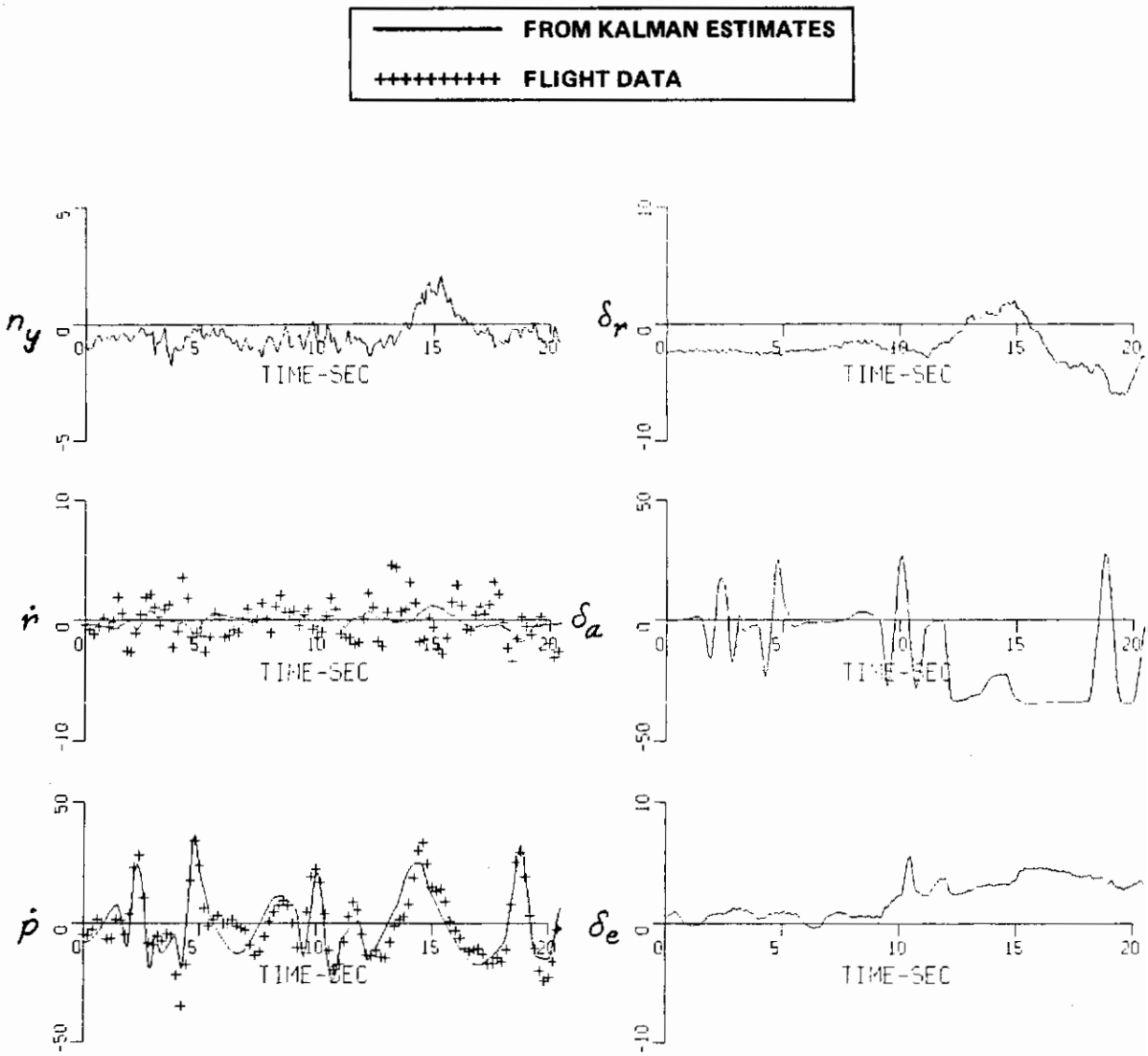

Figure 39 (Continued) KALMAN RESULTS – RECORD 10, LATERAL-DIRECTIONAL

(a) RESPONSE COMPARISONS WITH FLIGHT DATA

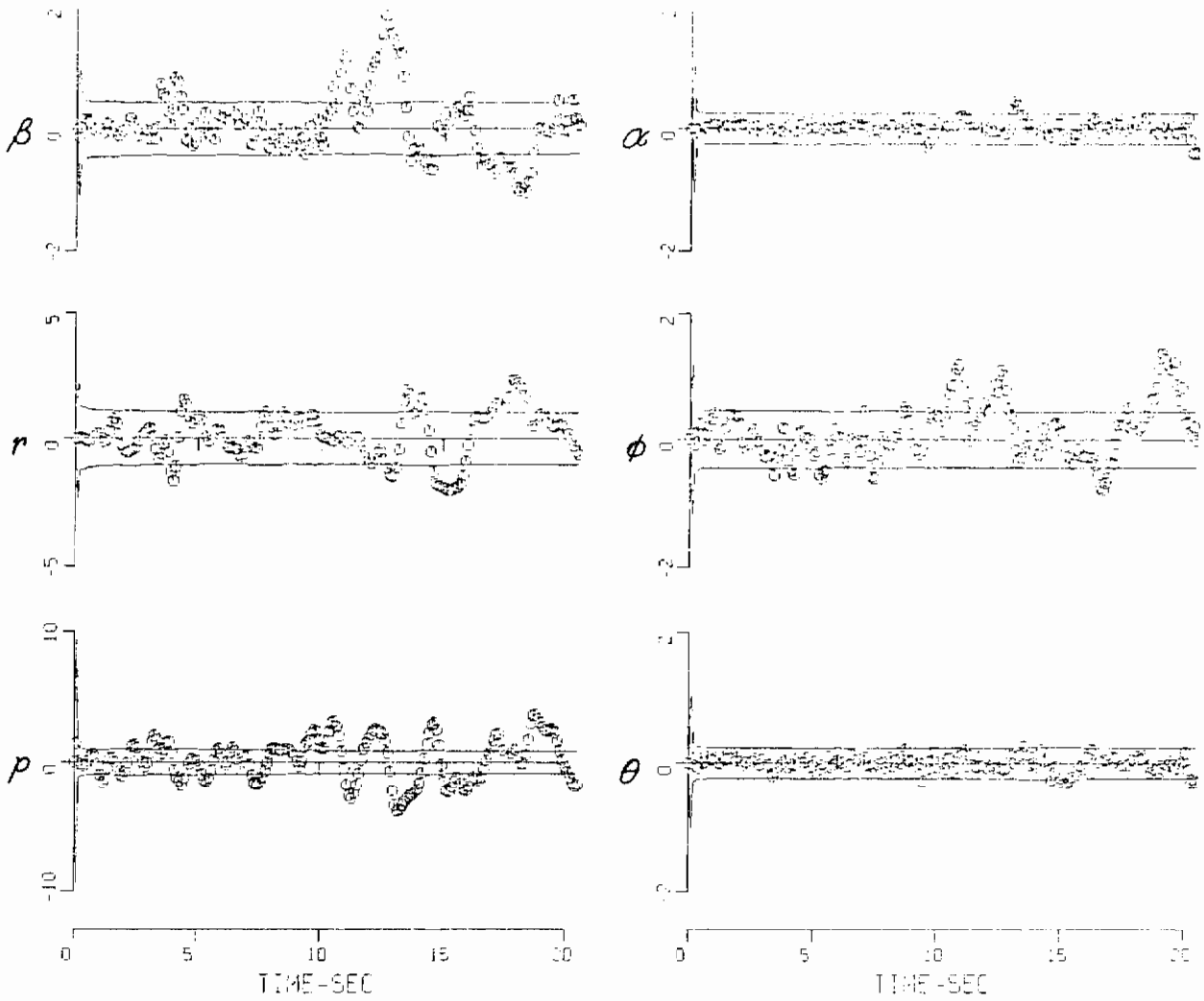

Figure 39 (Continued) KALMAN RESULTS – RECORD 10, LATERAL-DIRECTIONAL
(b) RESIDUALS AND SELECTED PARAMETER VARIATIONS

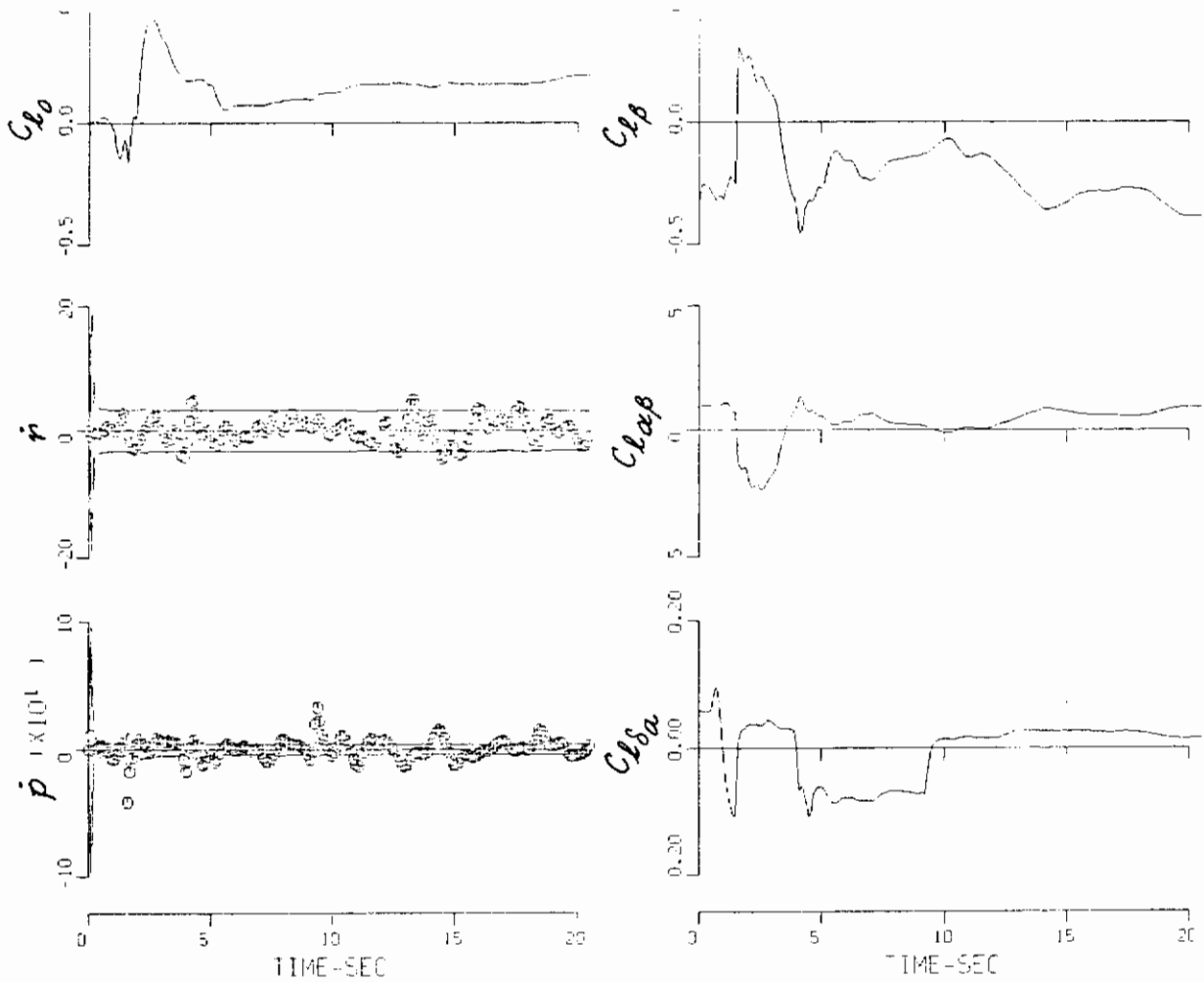

Figure 39. (Continued) KALMAN RESULTS – RECORD 10, LATERAL-DIRECTIONAL
(b) RESIDUALS AND SELECTED PARAMETER VARIATIONS

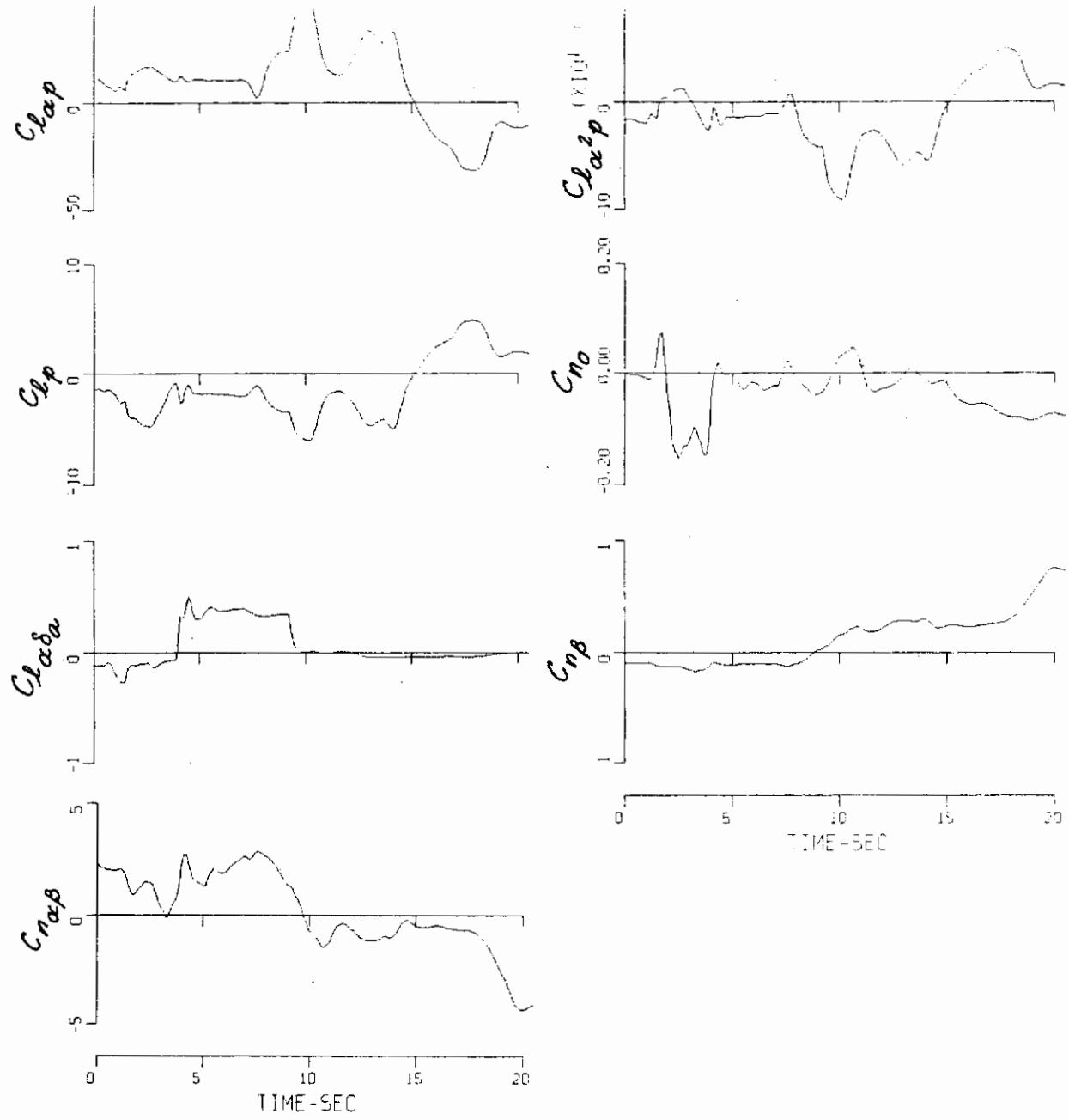

Figure 39 (Concluded) KALMAN RESULTS – RECORD 10, LATERAL-DIRECTIONAL
(b) RESIDUALS AND SELECTED PARAMETER VARIATIONS

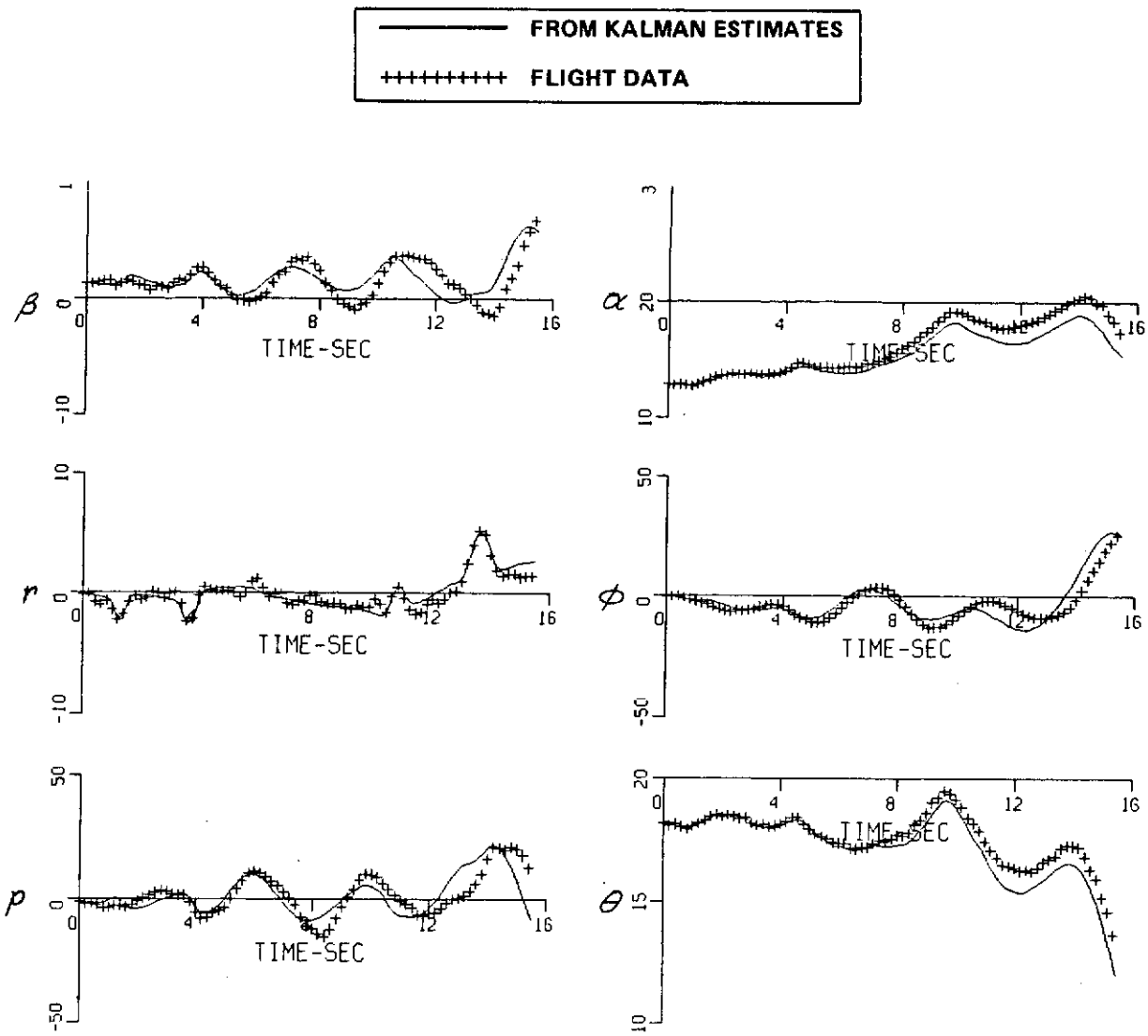

Figure 40 KALMAN RESULTS – RECORD 11, LATERAL-DIRECTIONAL RESPONSE COMPARISONS WITH FLIGHT DATA

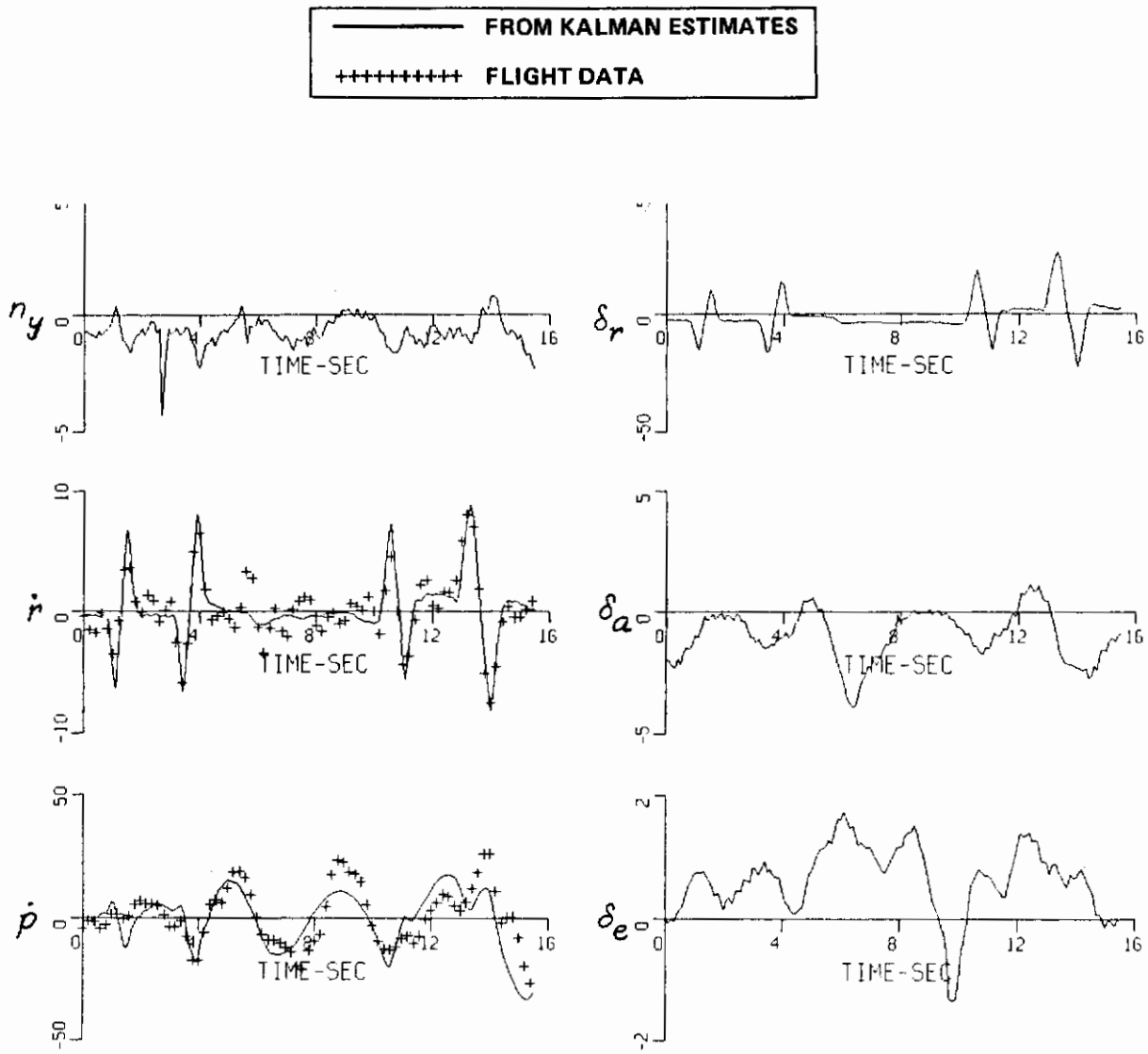

Figure 40 (Concluded) KALMAN RESULTS – RECORD 11, LATERAL-DIRECTIONAL RESPONSE COMPARISONS WITH FLIGHT DATA

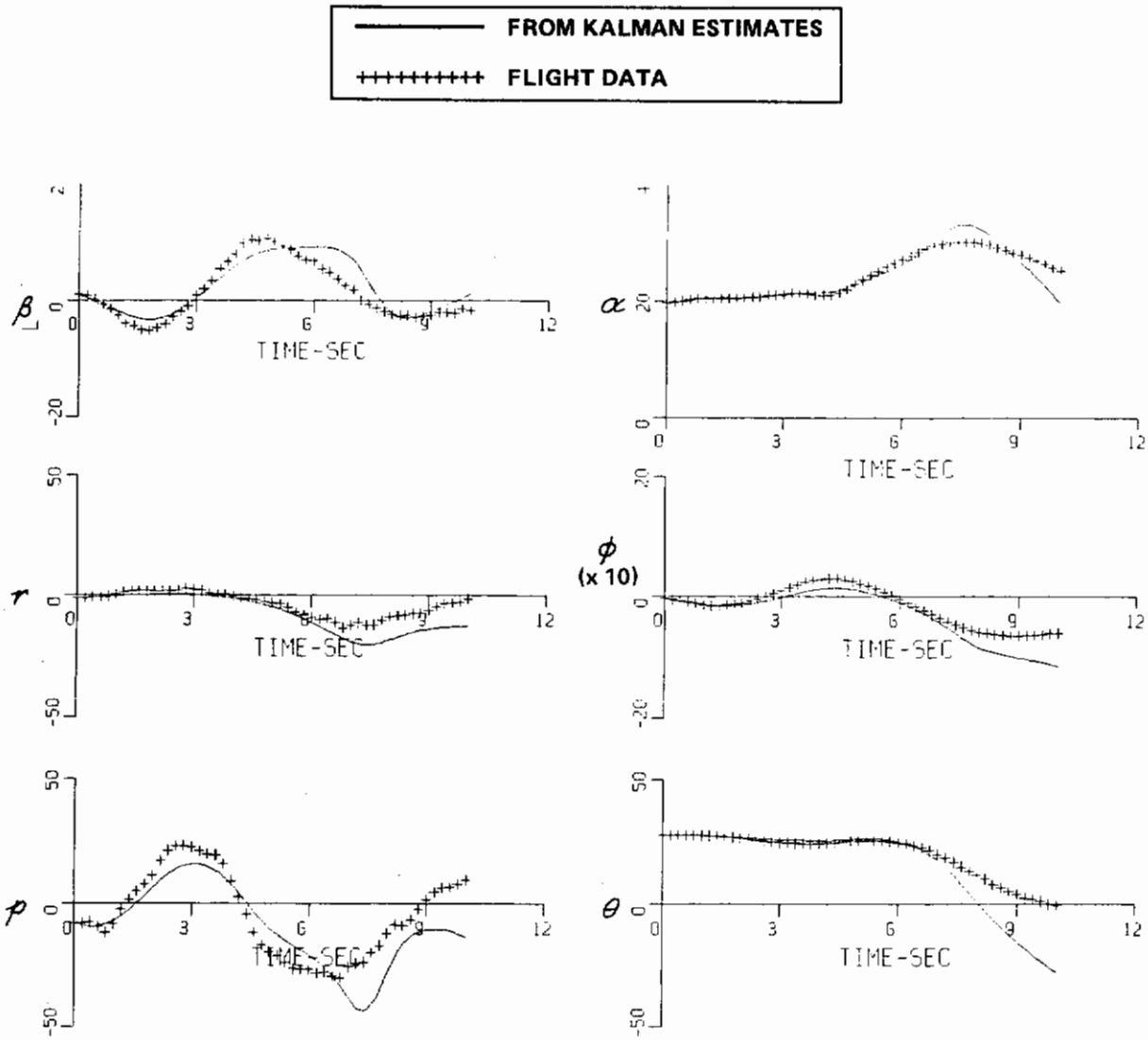

Figure 41 KALMAN RESULTS – RECORD 14, LATERAL-DIRECTIONAL RESPONSE COMPARISONS WITH FLIGHT DATA

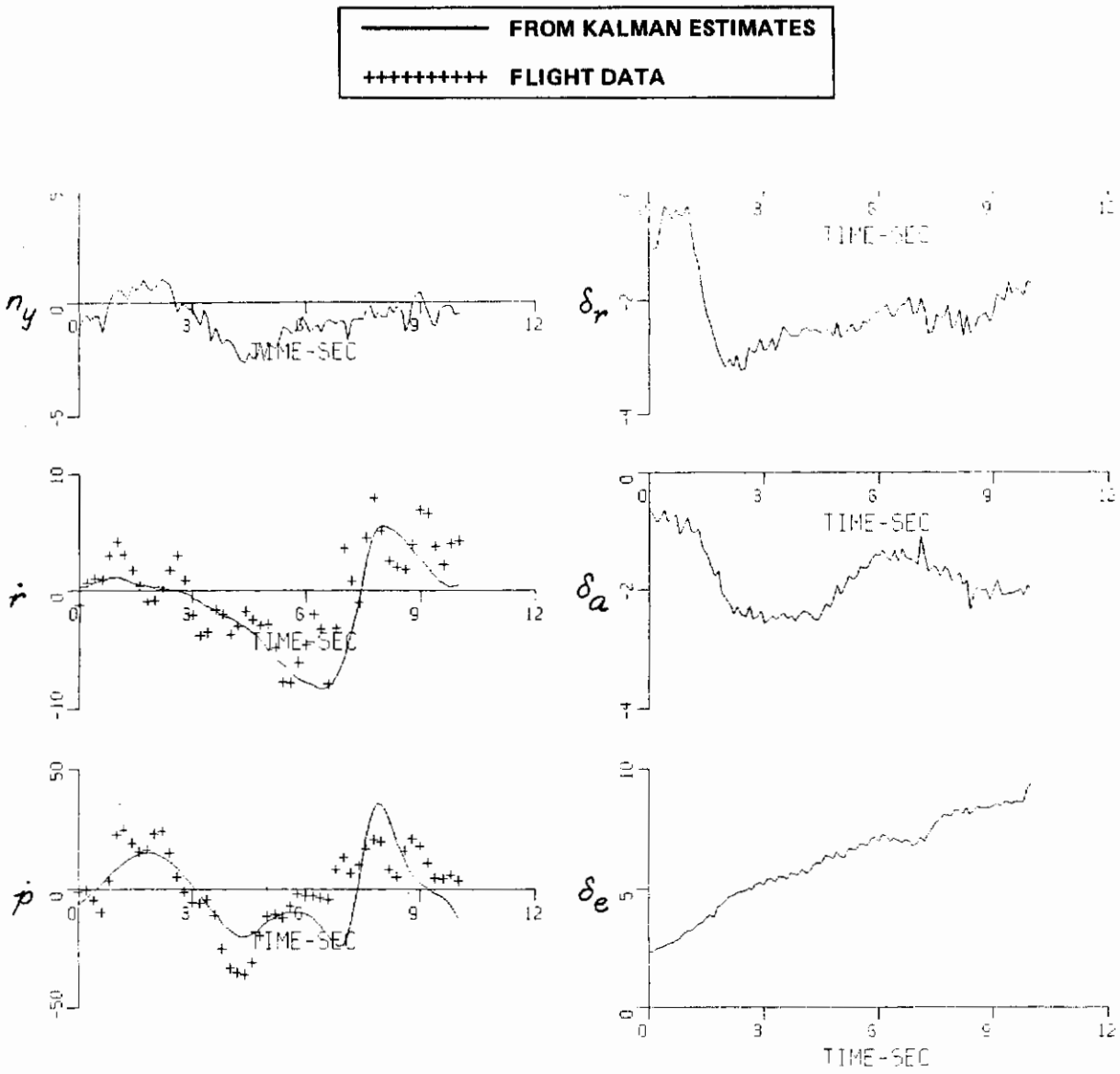

Figure 41 (Concluded) KALMAN RESULTS – RECORD 14, LATERAL-DIRECTIONAL RESPONSE COMPARISONS WITH FLIGHT DATA

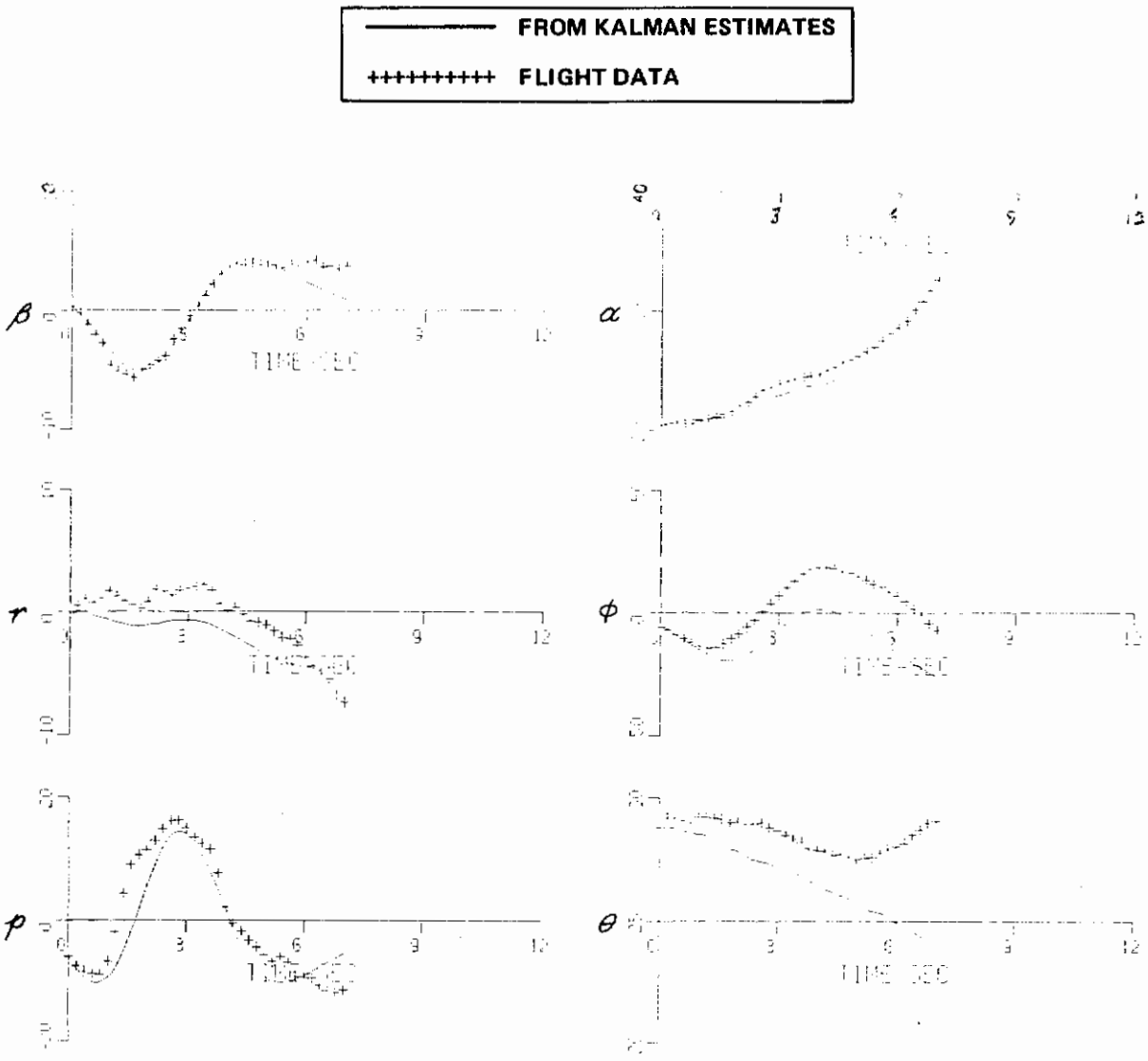

Figure 42 KALMAN RESULTS – RECORD 20, LATERAL-DIRECTIONAL

(a) RESPONSE COMPARISONS WITH FLIGHT DATA

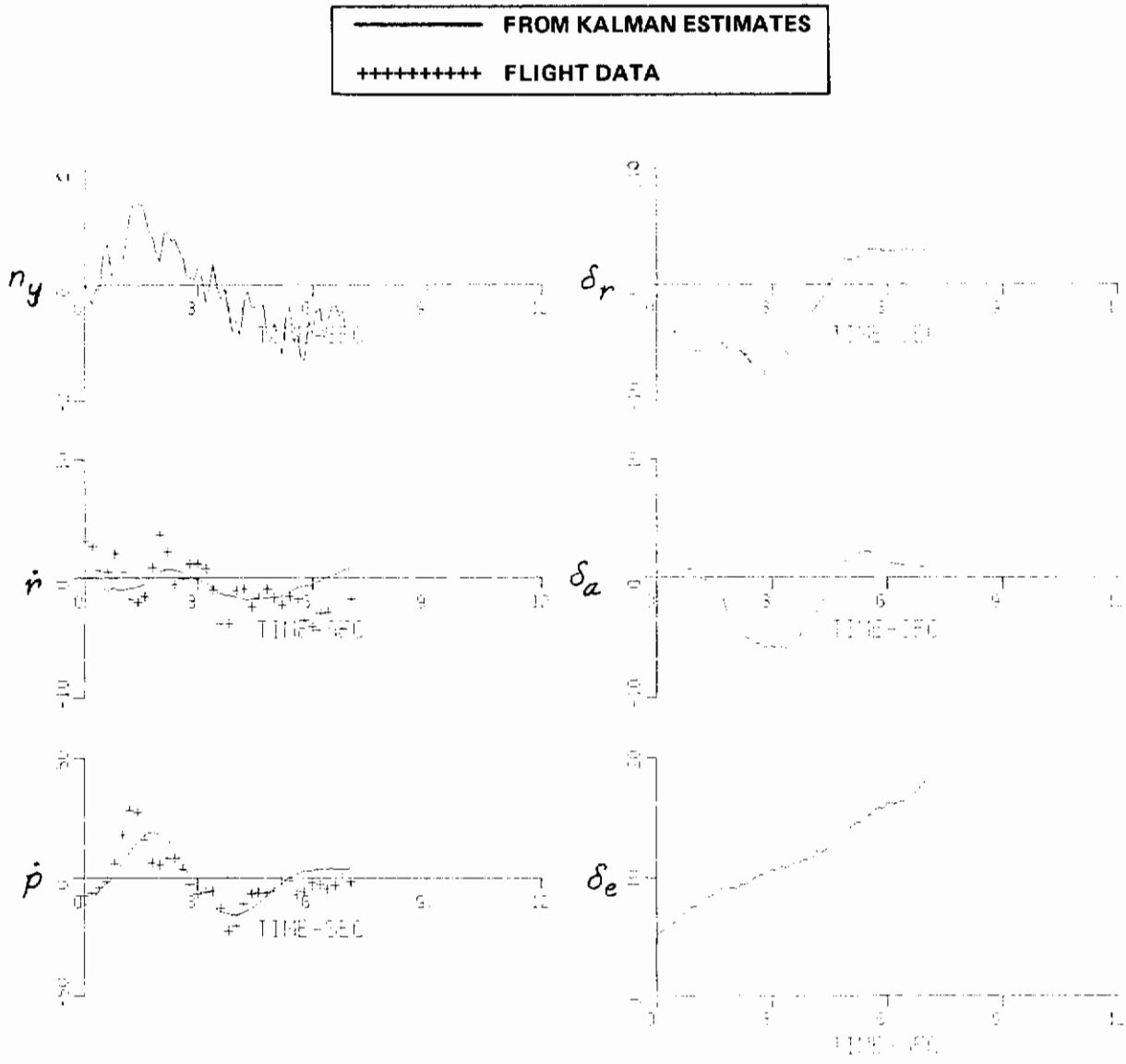

Figure 42 (Continued) KALMAN RESULTS – RECORD 20, LATERAL-DIRECTIONAL
(a) RESPONSE COMPARISONS WITH FLIGHT DATA

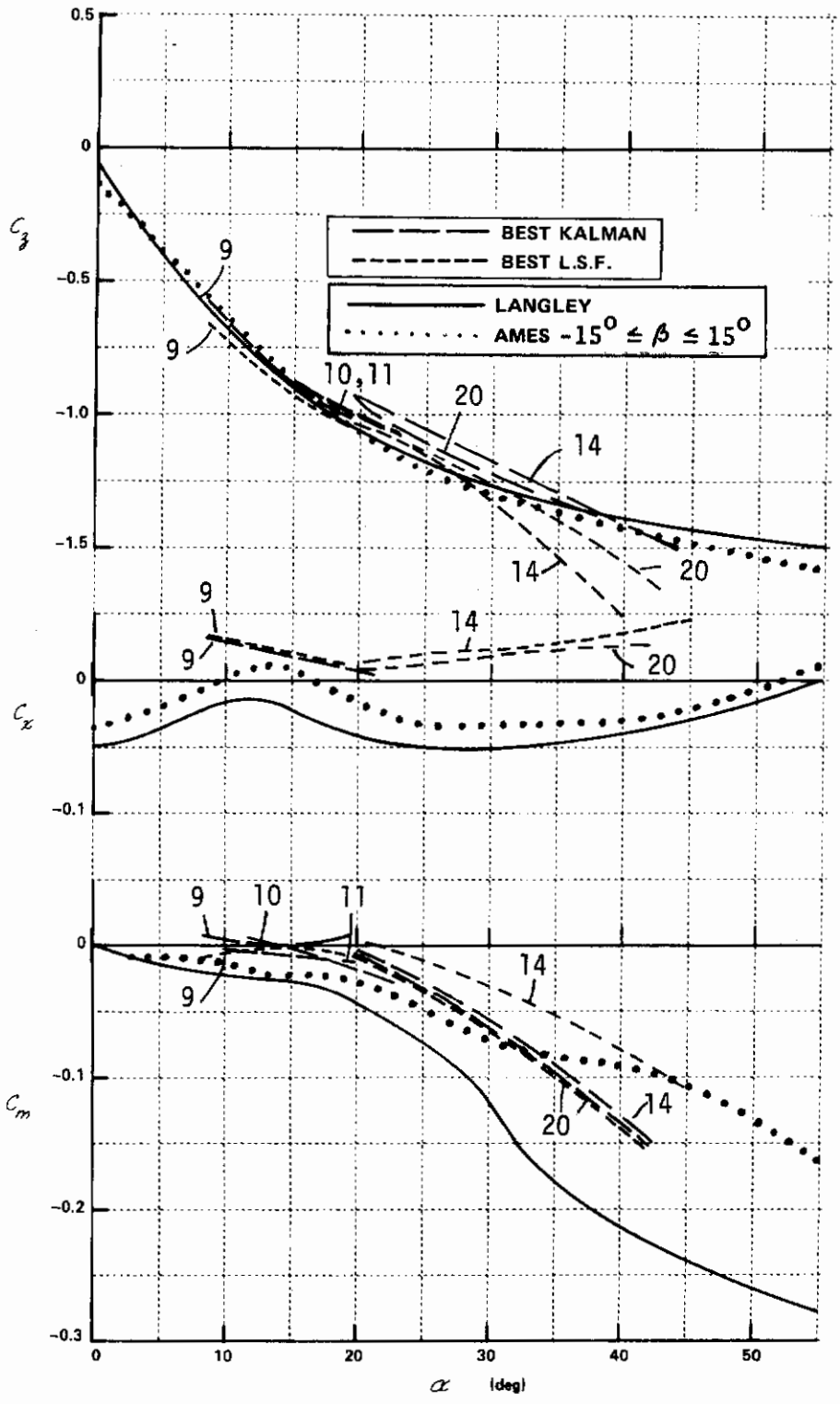

Figure 43 IDENTIFIED COEFFICIENTS VERSUS WIND TUNNEL VALUES - LONGITUDINAL

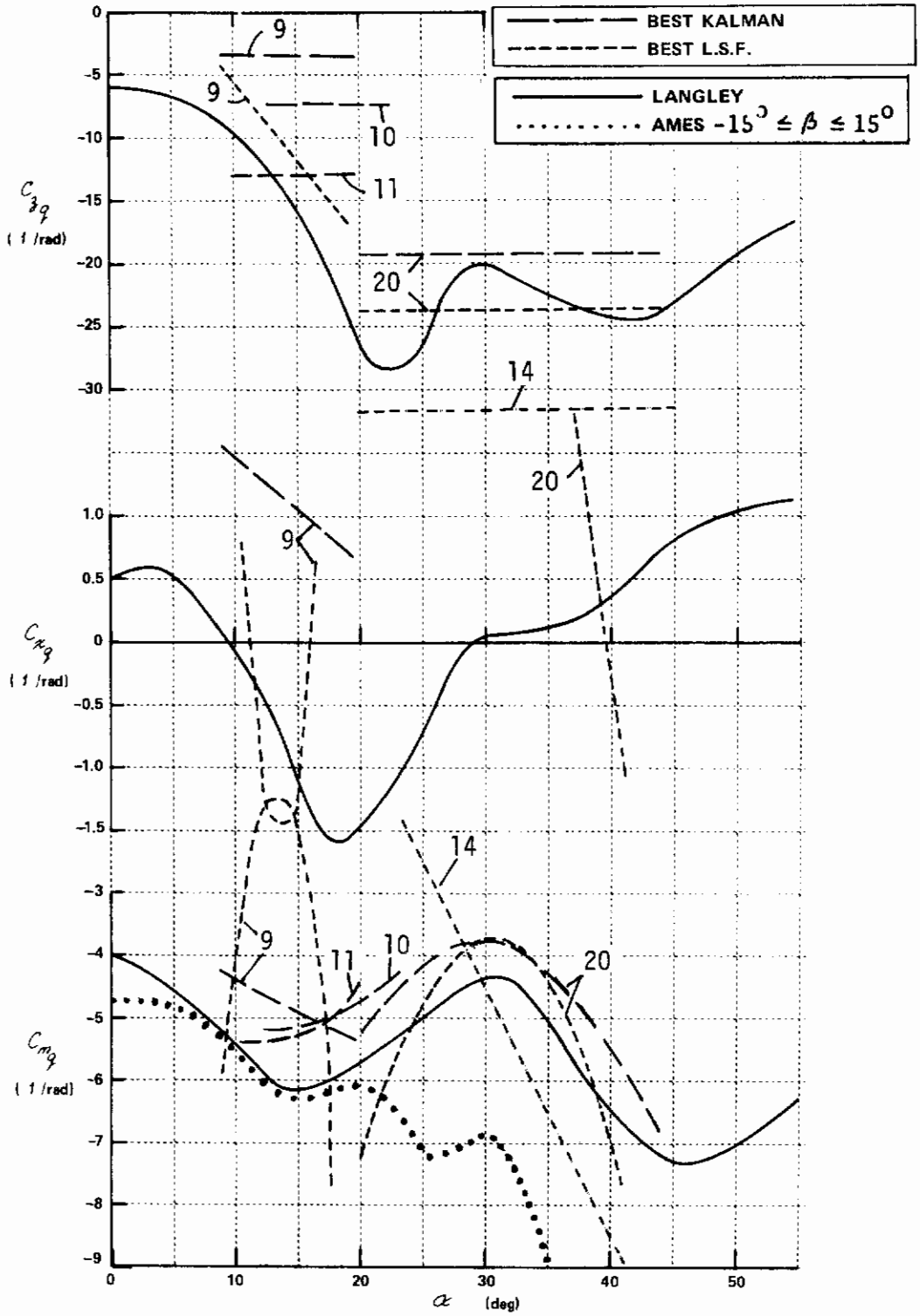

Figure 43 (Continued) IDENTIFIED COEFFICIENTS VERSUS WIND TUNNEL VALUES - LONGITUDINAL

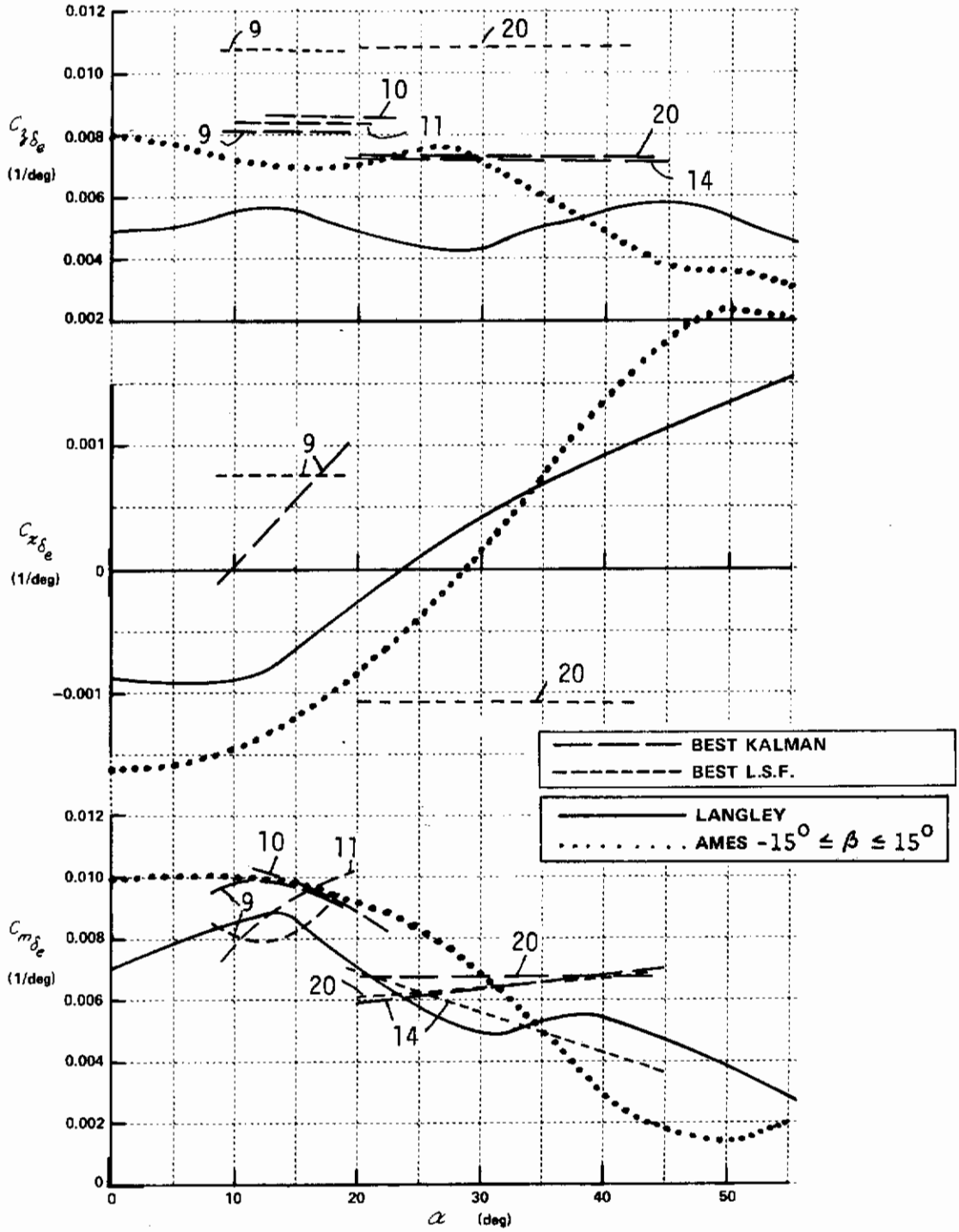

Figure 43 (Concluded) IDENTIFIED COEFFICIENTS VERSUS WIND TUNNEL VALUES - LONGITUDINAL

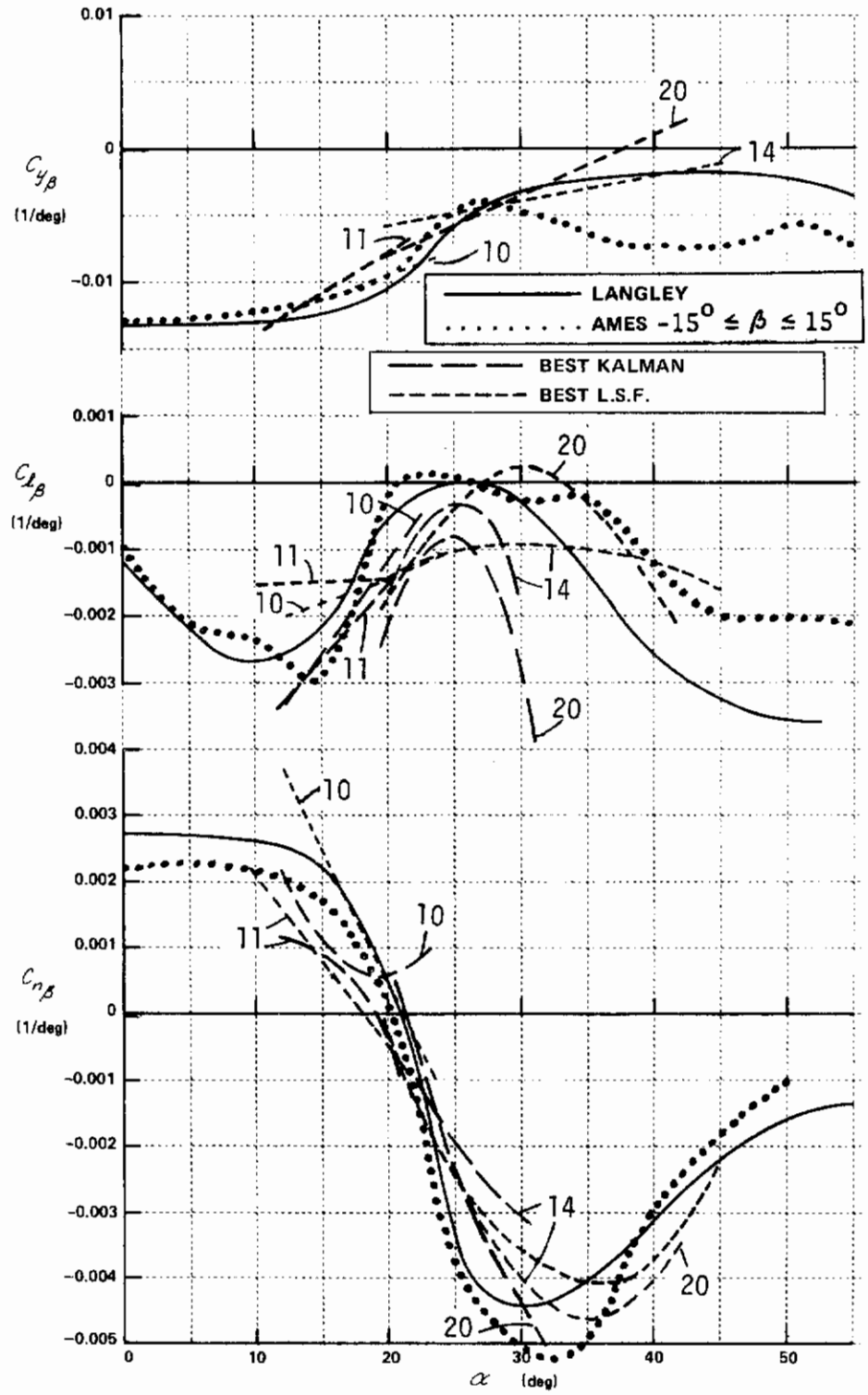

Figure 44 IDENTIFIED COEFFICIENTS VERSUS WIND TUNNEL VALUES - LATERAL - DIRECTIONAL

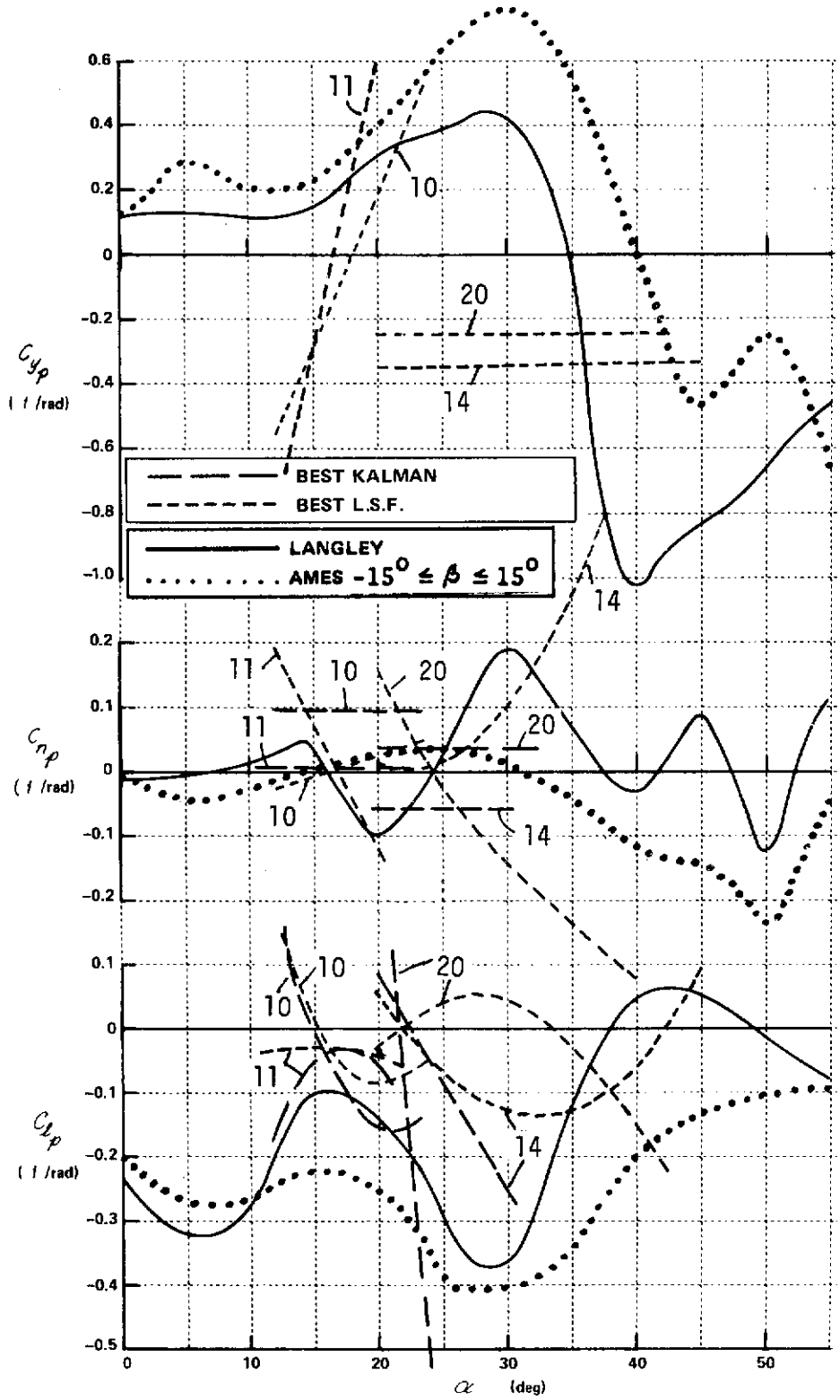

Figure 44 (Continued) IDENTIFIED COEFFICIENTS VERSUS WIND TUNNEL VALUES - LATERAL - DIRECTIONAL

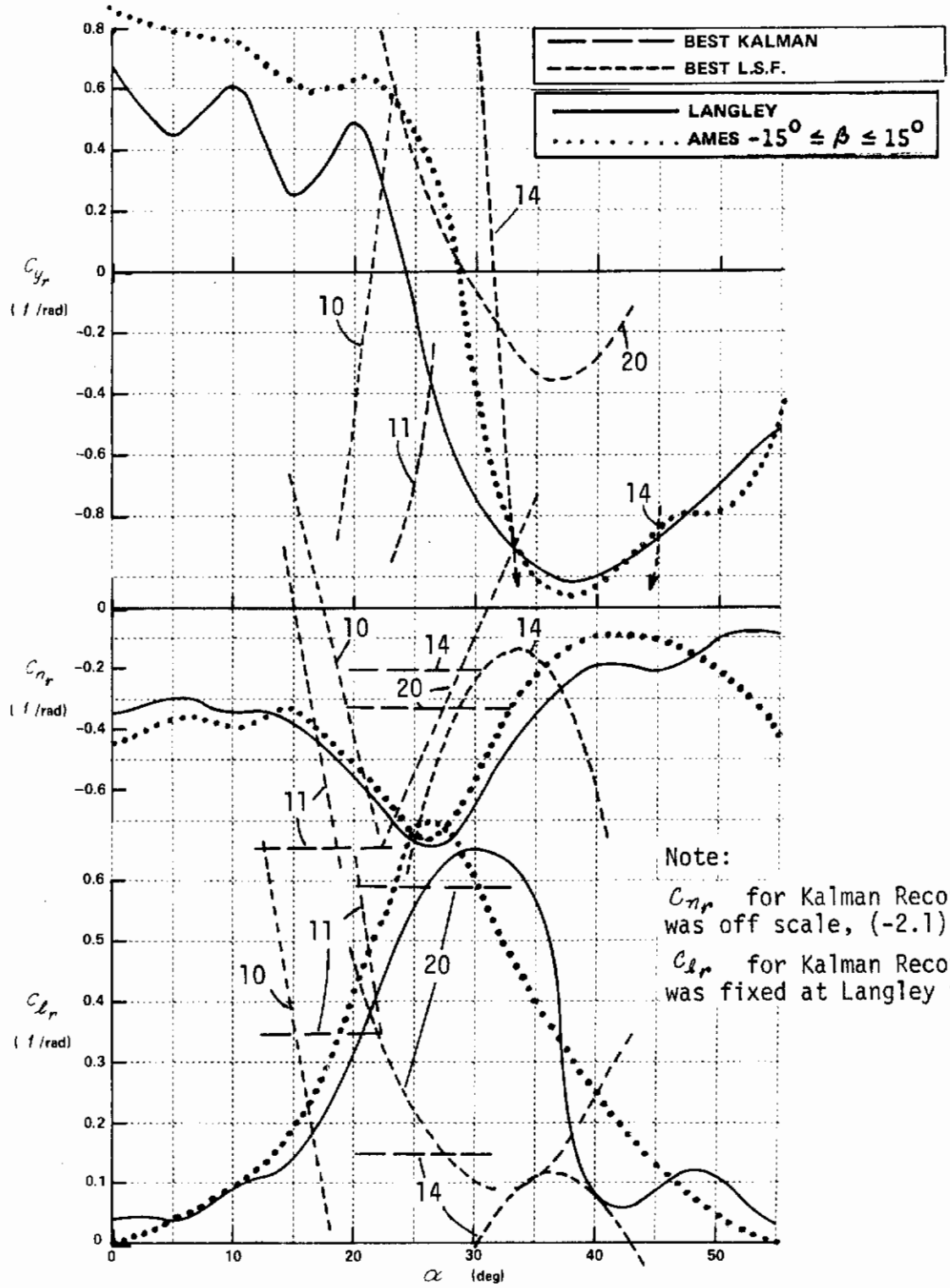

Figure 44 (Continued) **IDENTIFIED COEFFICIENTS VERSUS WIND TUNNEL VALUES - LATERAL - DIRECTIONAL**

Note: $C_{n_{\delta_a}}$ and $C_{\ell_{\delta_a}}$ fixed at Ames values when not shown

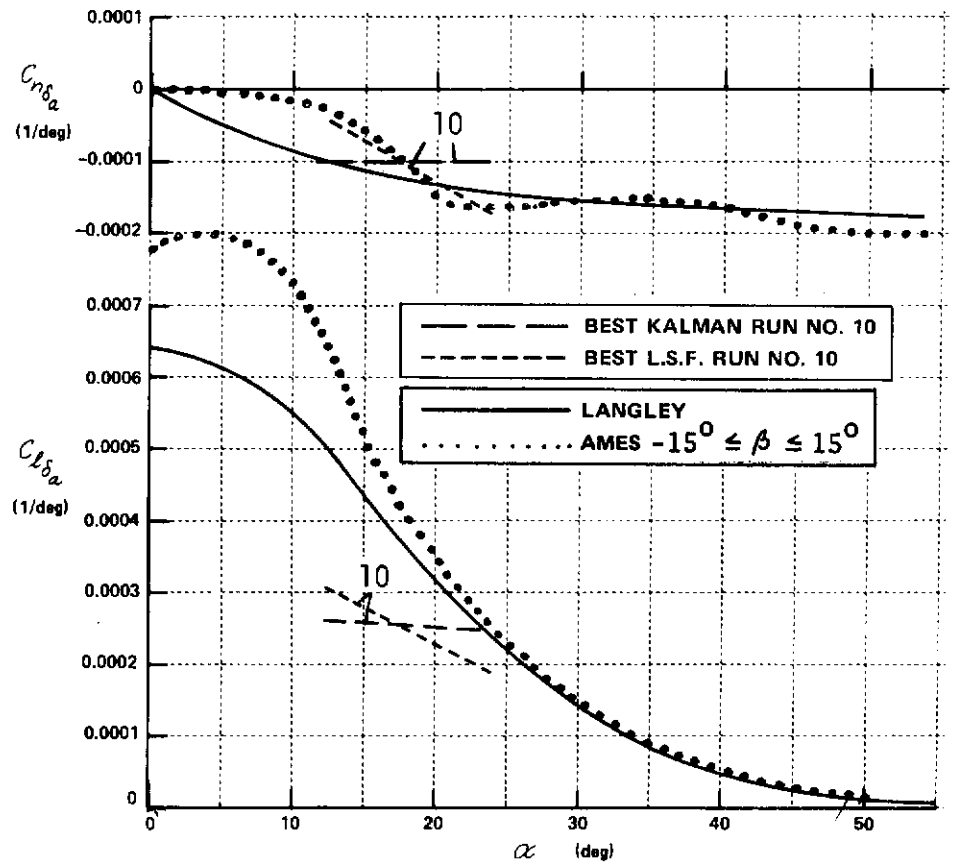

Figure 44 (Continued) **IDENTIFIED COEFFICIENTS VERSUS WIND TUNNEL VALUES - LATERAL - DIRECTIONAL**

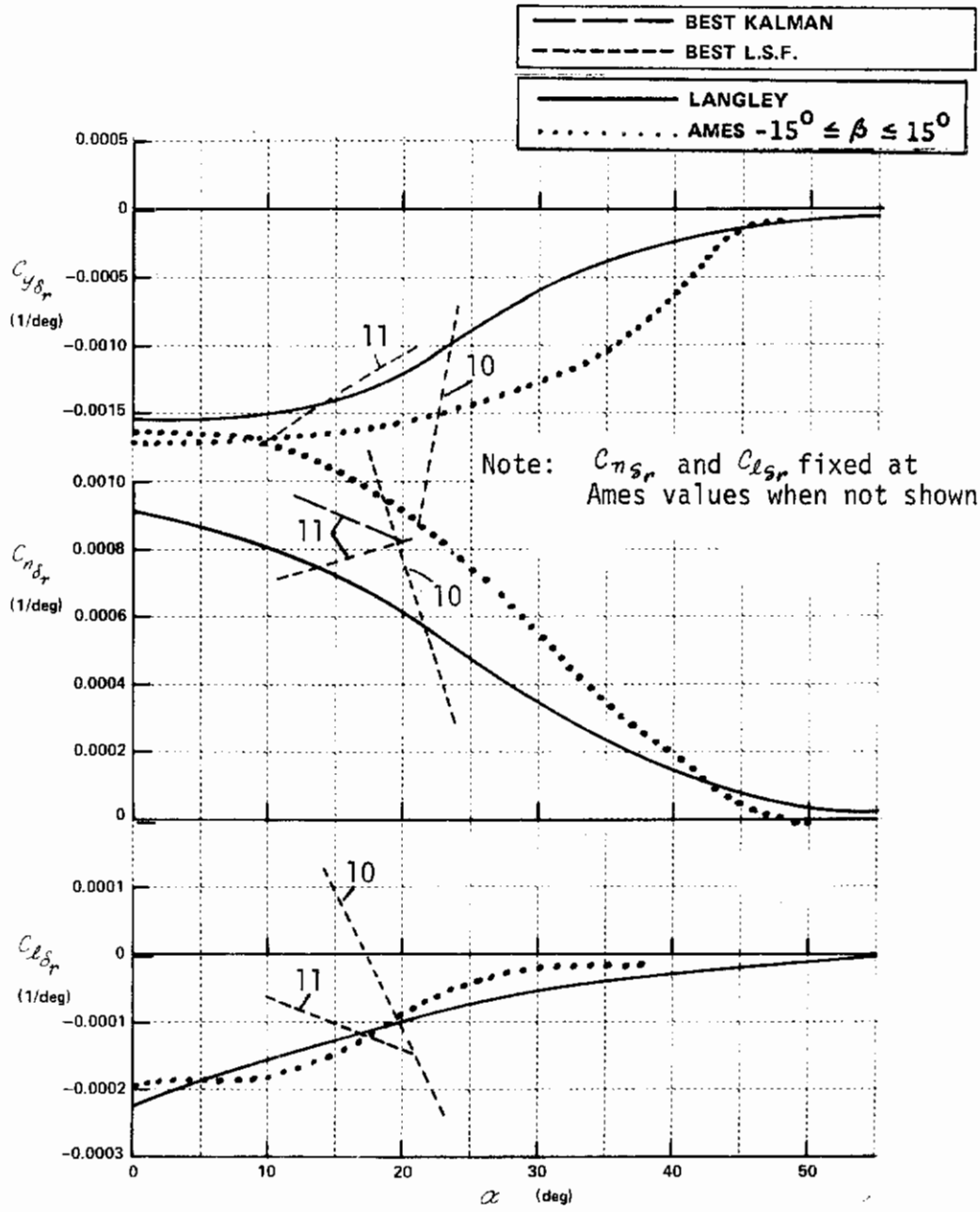

Figure 44 (Concluded) IDENTIFIED COEFFICIENTS VERSUS WIND TUNNEL VALUES - LATERAL - DIRECTIONAL

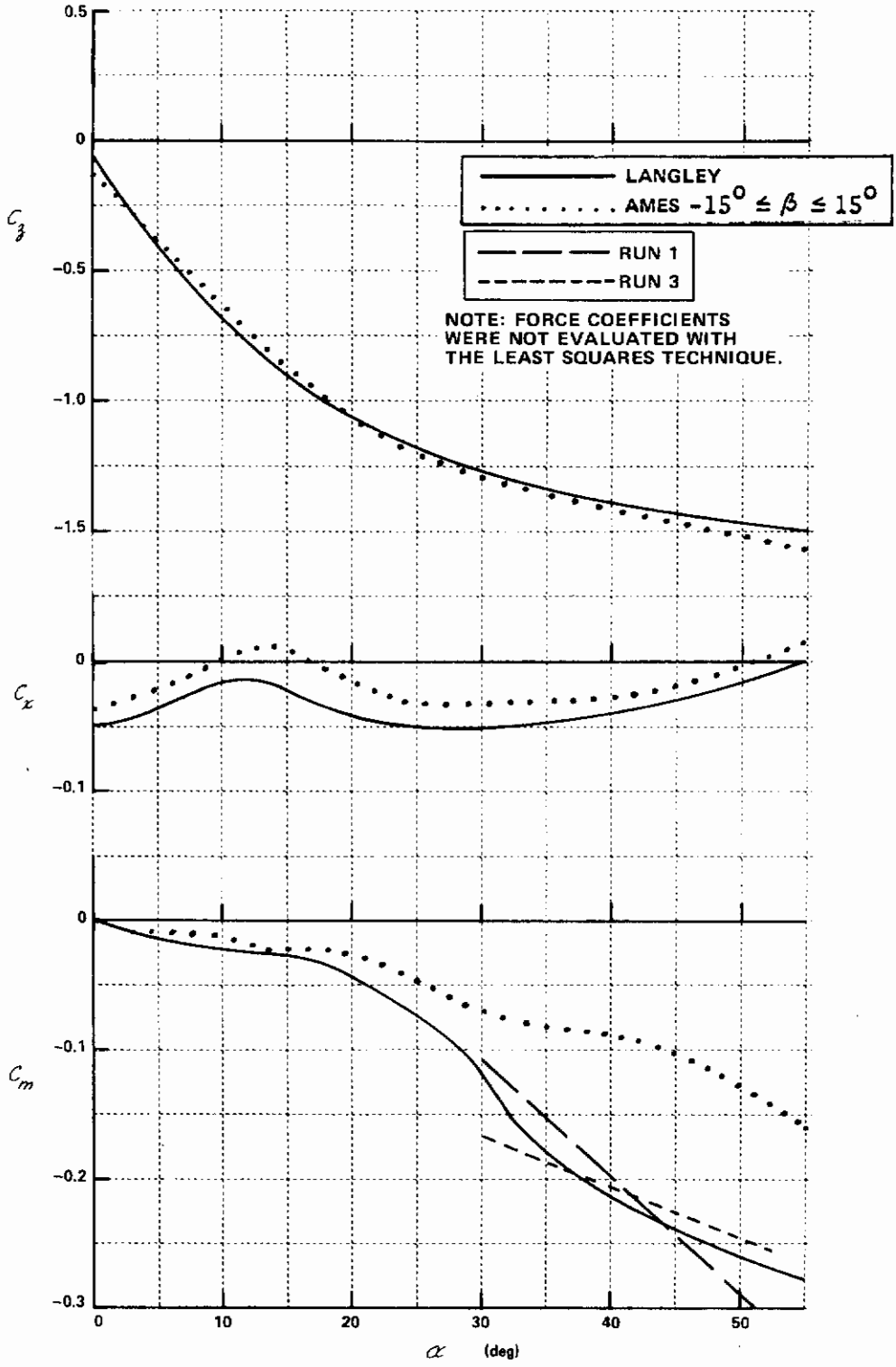

Figure 45 RADIO CONTROLLED MODEL COEFFICIENTS IDENTIFIED WITH LEAST SQUARES ESTIMATOR, PLOTTED ON WIND TUNNEL VALUES

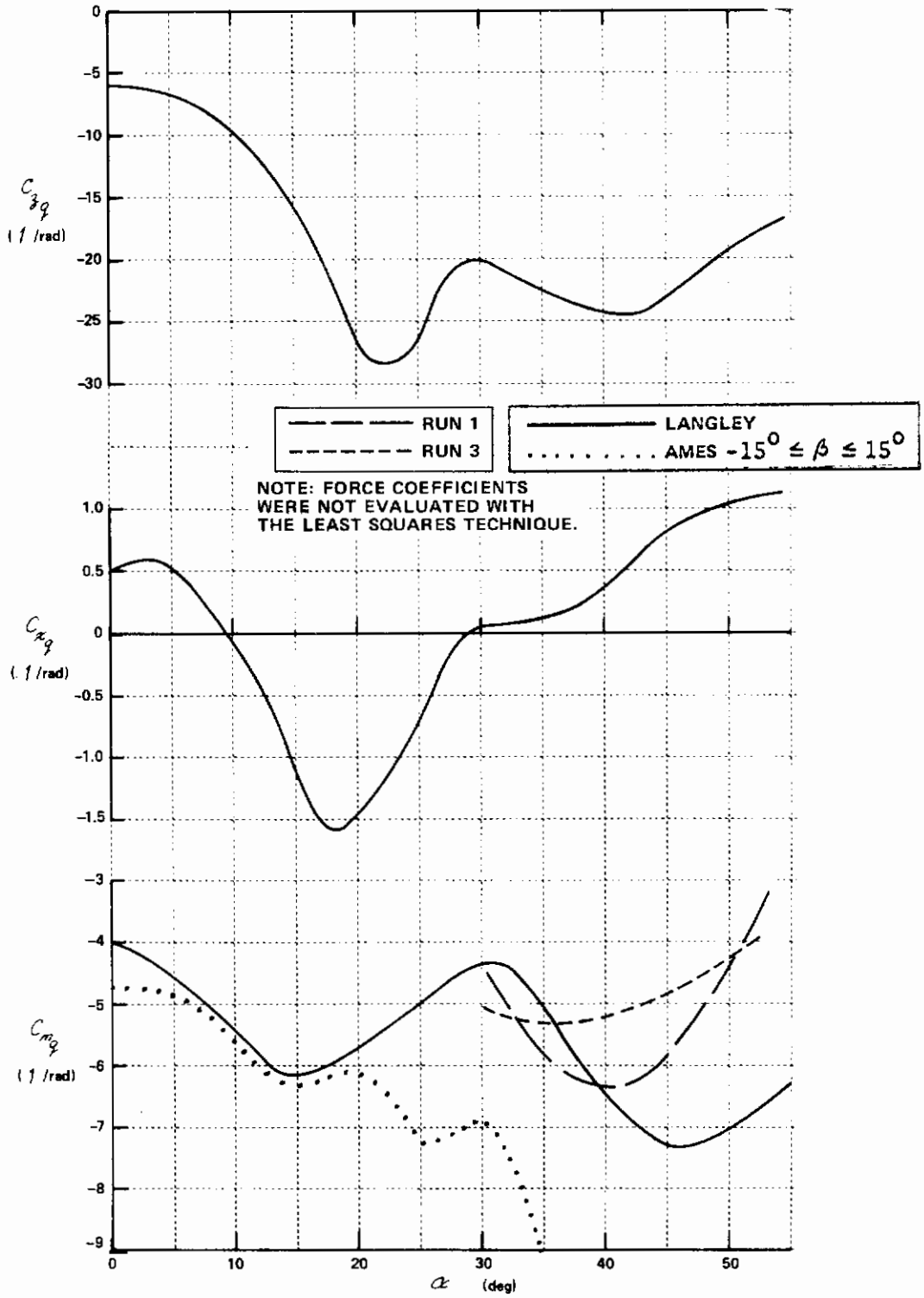

Figure 45 (Continued) RADIO CONTROLLED MODEL COEFFICIENTS IDENTIFIED WITH LEAST SQUARES ESTIMATOR, PLOTTED ON WIND TUNNEL VALUES

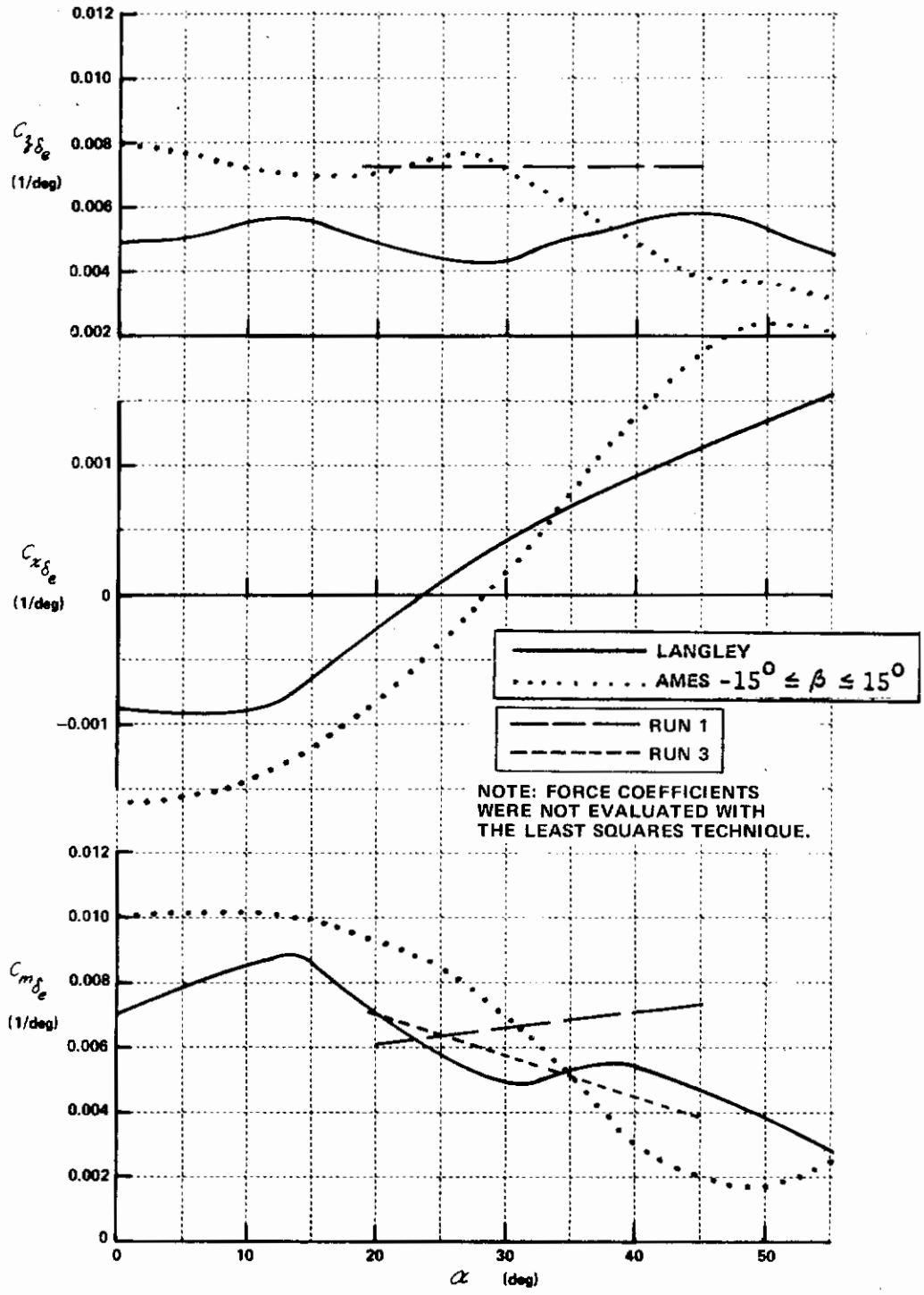

Figure 45 (Continued) RADIO CONTROLLED MODEL COEFFICIENTS IDENTIFIED WITH LEAST SQUARES ESTIMATOR, PLOTTED ON WIND TUNNEL VALUES

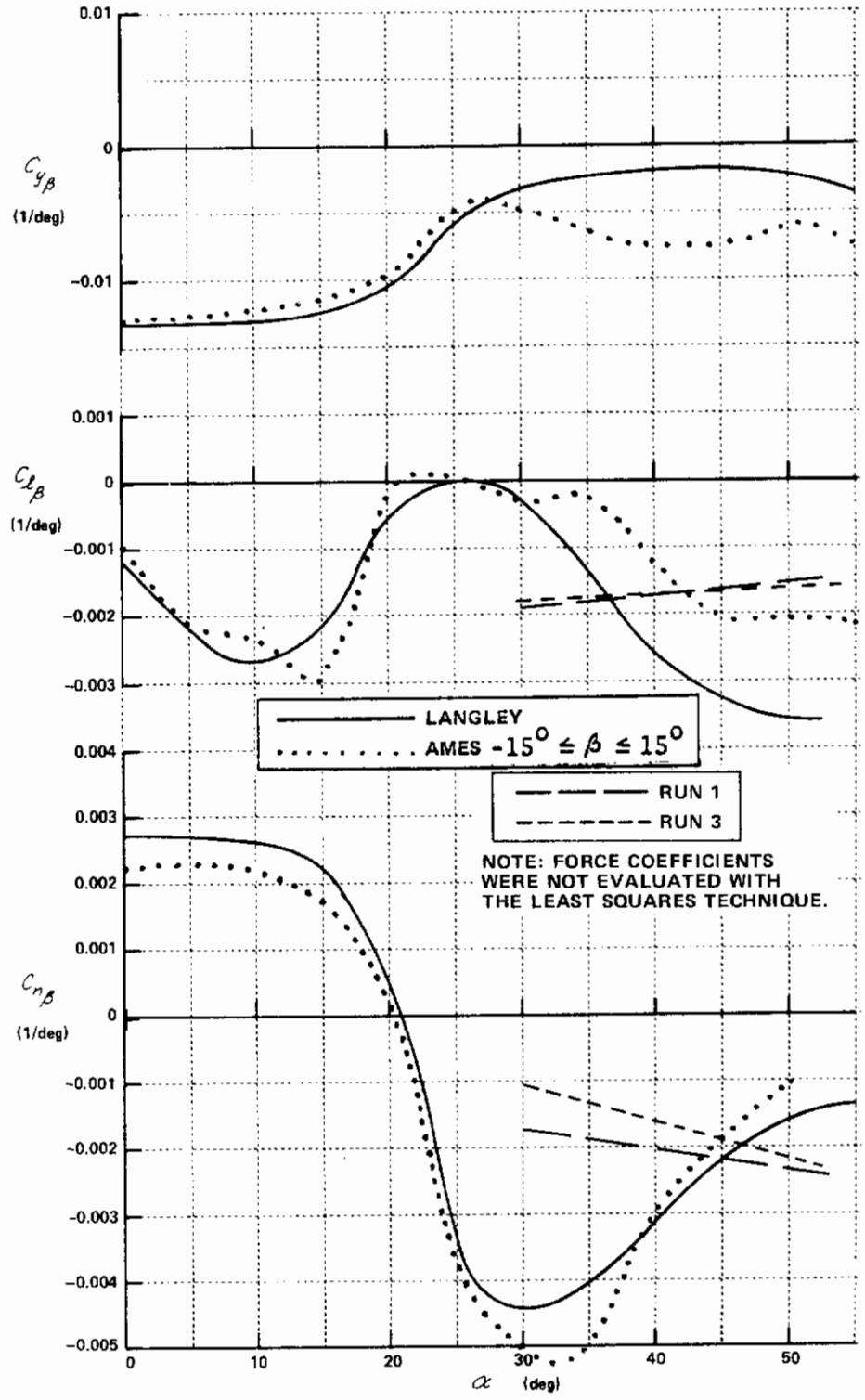

Figure 45 (Continued) RADIO CONTROLLED MODEL COEFFICIENTS IDENTIFIED WITH LEAST SQUARES ESTIMATOR, PLOTTED ON WIND TUNNEL VALUES

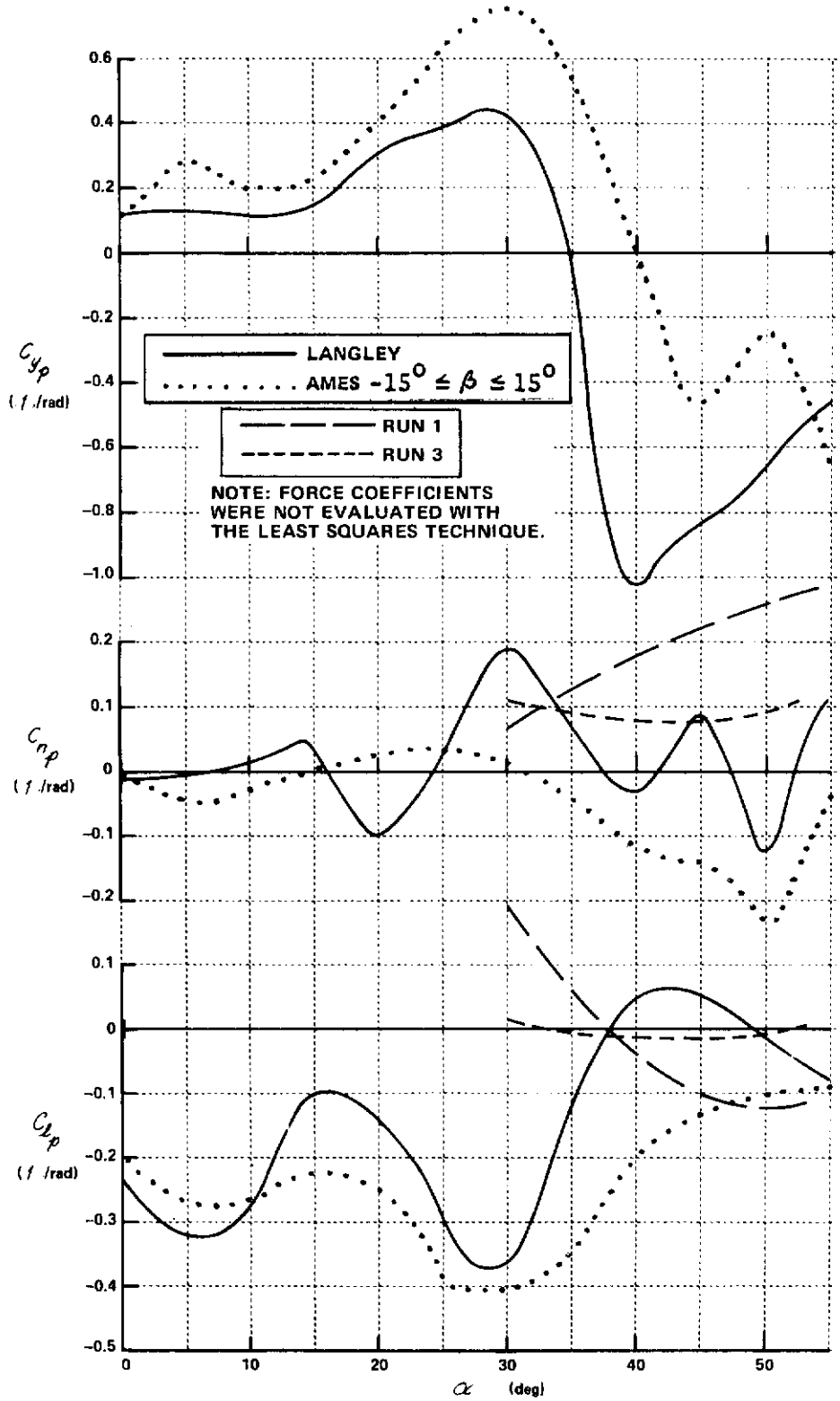

Figure **45** (Continued) RADIO CONTROLLED MODEL COEFFICIENTS IDENTIFIED WITH LEAST SQUARES ESTIMATOR, PLOTTED ON WIND TUNNEL VALUES

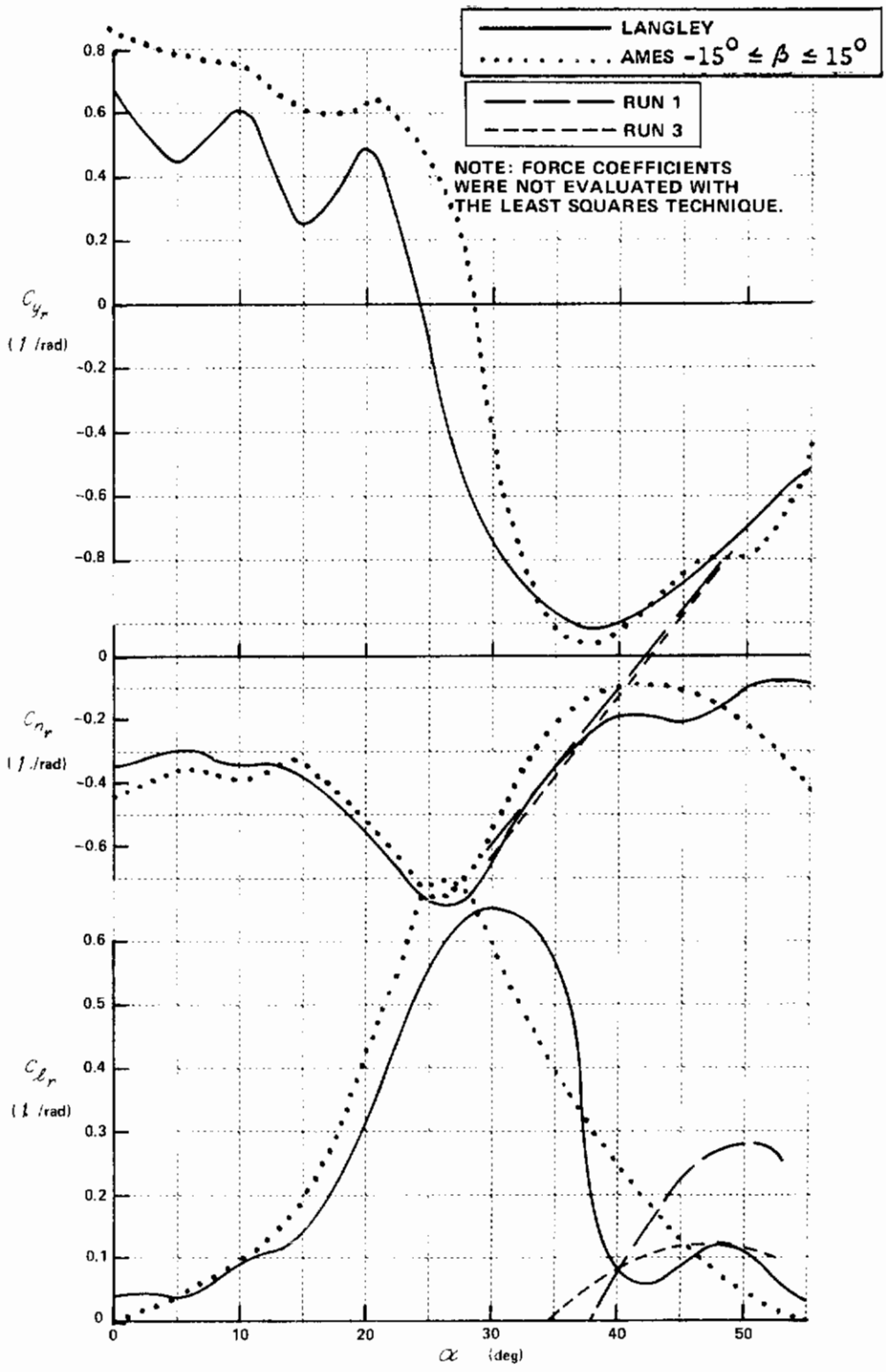

Figure 45 (Continued) RADIO CONTROLLED MODEL COEFFICIENTS IDENTIFIED WITH LEAST SQUARES ESTIMATOR, PLOTTED ON WIND TUNNEL VALUES

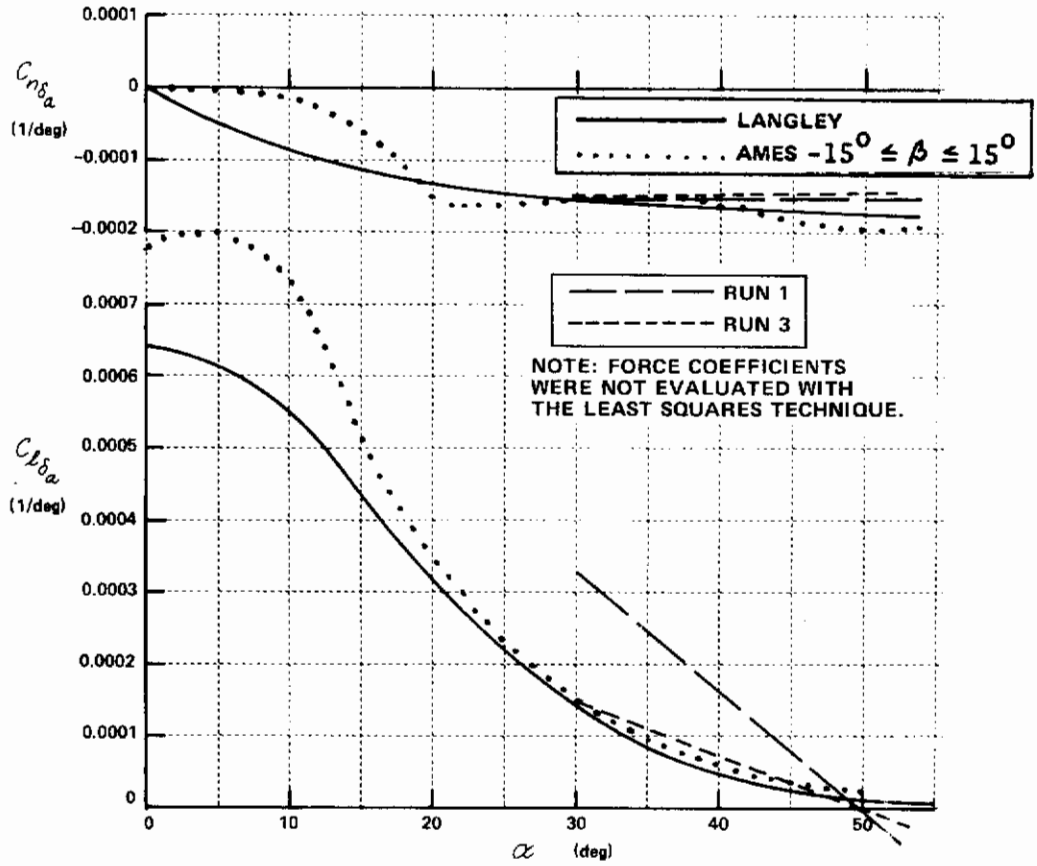

Figure 45 (Continued) RADIO CONTROLLED MODEL COEFFICIENTS IDENTIFIED WITH LEAST SQUARES ESTIMATOR, PLOTTED ON WIND TUNNEL VALUES

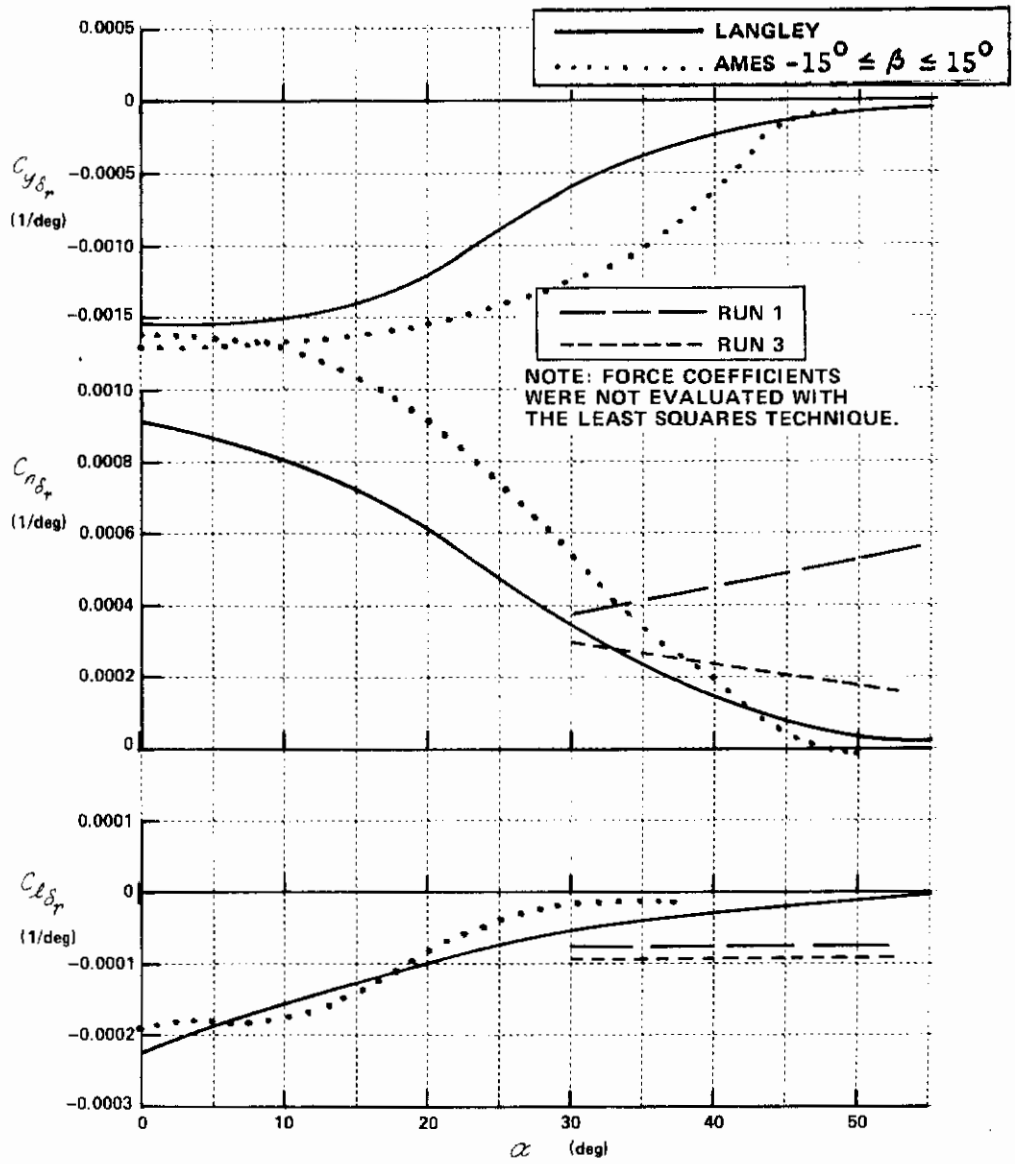

Figure 45 (Concluded) RADIO CONTROLLED MODEL COEFFICIENTS IDENTIFIED WITH LEAST SQUARES ESTIMATOR, PLOTTED ON WIND TUNNEL VALUES

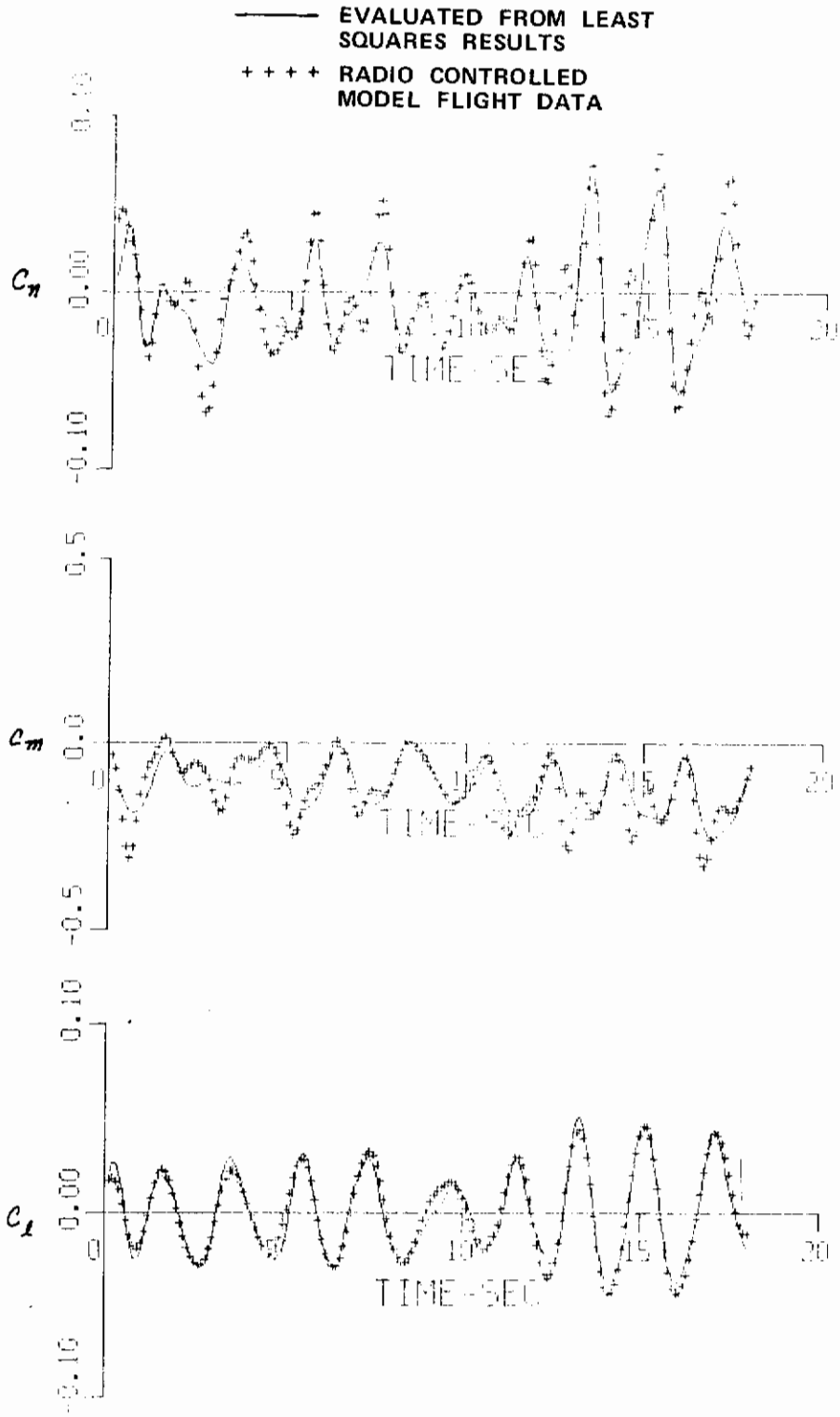

Figure 46 COMPARISON OF AERODYNAMIC MOMENTS EVALUATED WITH LEAST SQUARES RESULTS AND MODEL FLIGHT DATA - RUN 1

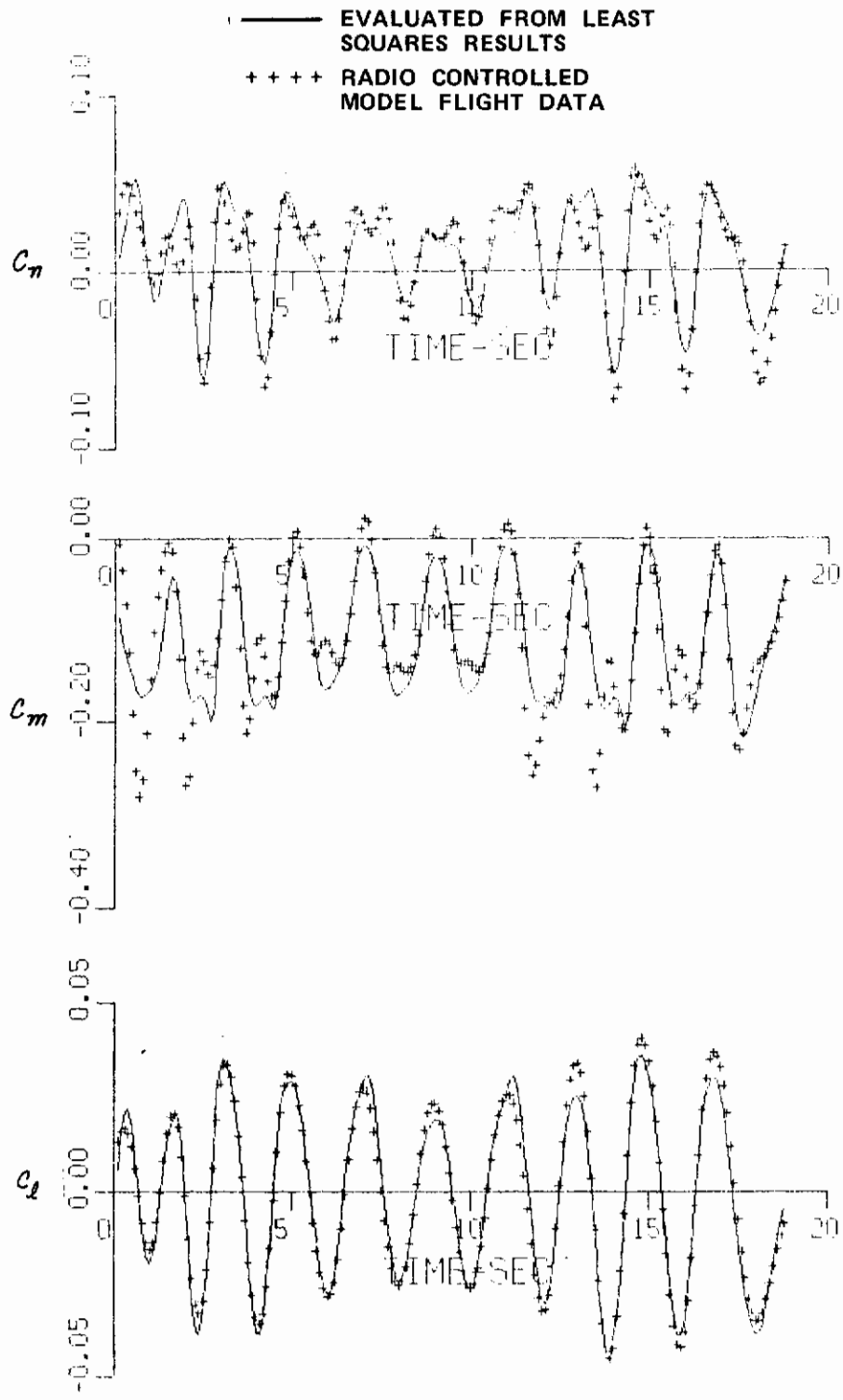

Figure 47 COMPARISON OF AERODYNAMIC MOMENTS EVALUATED WITH LEAST SQUARES RESULTS AND MODEL FLIGHT DATA - RUN 3

Table IV

NOISE STATISTICS USED FOR INSTRUMENTATION CONSISTENCY CHECKS AND STATE ESTIMATION

MEASUREMENT NOISE STANDARD DEVIATION USED

SENSOR		FLIGHT RECORDS 9, 10, 11	FLIGHT RECORDS 14, 20
V	(fps)	6	8
α_V	(deg)	0.2	0.3
β_V	(deg)	0.3	0.3
h	(ft)	200	200
ϕ	(deg)	0.3	0.8
θ	(deg)	0.25	0.6
ψ	(deg)	3	–

PROCESS NOISE STANDARD DEVIATION

SENSOR		ALL FLIGHT RECORDS
$n_{x_{cg}}$	(g's)	0.004
$n_{y_{cg}}$	(g's)	0.004
$n_{z_{cg}}$	(g's)	0.013
p	(deg/sec)	0.5
q	(deg/sec)	0.125
r	(deg/sec)	0.4

Table V

IDENTIFIED BIAS PARAMETERS AND THEIR STANDARD DEVIATION FROM FLIGHT RECORD 9

BIAS PARAMETER		INITIAL σ_0	CASE 1		CASE 2		CASE 3	
			EXTRACTED VALUE	σ_f	EXTRACTED VALUE	σ_f	EXTRACTED VALUE	σ_f
n_{x_b}	(g's)	0.03	(-0.006)	0.006	(-0.018)	0.002	(0.025)	0.003
n_{z_b}	(g's)	0.11	0.021	0.003	0.023	0.003	0.028	0.003
α_{V_b}	(deg)	1.41	2.7	0.45	3.1	0.13	**	
θ_b	(deg)	1.41	(-0.58)	0.46	(**)		(-3.08)	0.13
p_b	(deg/sec)	3.16	-1.24	0.1	*		*	
q_b	(deg/sec)	0.77	-0.082	0.028	*		*	
r_b	(deg/sec)	2.4	-1.31	0.087	*		*	

* FIXED AT CASE 1 VALUE

** NOT IDENTIFIED

NORMALIZED COVARIANCE MATRIX

CASE 1

	n_{x_b}	n_{z_b}	α_{V_b}	θ_b	p_b	q_b	r_b
n_{x_b}	1						
n_{z_b}	0.33	1					
α_{V_b}	(-0.83)	-0.20	1				
θ_b	(-0.96)	-0.30	(0.90)	1			
p_b	0.05	0.02	-0.05	-0.06	1		
q_b	0.04	-0.03	-0.04	-0.04	-0.00	1	
r_b	-0.06	0.00	0.08	0.07	0.00	-0.01	1

CASE 2

	n_{x_b}	n_{z_b}	α_{V_b}
n_{x_b}	1		
n_{z_b}	0.12	1	
α_{V_b}	0.16	0.09	1

CASE 3

	n_{x_b}	n_{z_b}	θ_b
n_{x_b}	1		
n_{z_b}	0.22	1	
θ_b	(-0.75)	-0.19	1

Table VI

IDENTIFIED BIAS PARAMETERS AND THEIR STANDARD DEVIATION FROM FLIGHT RECORD 10

BIAS PARAMETER		INITIAL σ_0	CASE 1		CASE 2		CASE 3	
			EXTRACTED VALUE	σ_f	EXTRACTED VALUE	σ_f	EXTRACTED VALUE	σ_f
n_{x_b}	(g's)	0.03	0.04	0.006	0.004	0.002	0.058	0.003
n_{z_b}	(g's)	0.11	0.045	0.003	0.036	0.003	0.049	0.003
α_{v_b}	(deg)	1.41	1.06	0.34	2.83	0.19	**	**
θ_b	(deg)	1.41	-2.67	0.38	**	**	-3.82	0.136
p_b	(deg/sec)	3.16	-1.36	0.11	*		*	
q_b	(deg/sec)	0.77	-0.158	0.027	*		*	
r_b	(deg/sec)	2.4	-0.92	0.086	*		*	

* FIXED AT CASE 1 VALUE

** NOT IDENTIFIED

NORMALIZED COVARIANCE MATRIX

CASE 1

n_{x_b}	1						
n_{z_b}	0.44	1					
α_{v_b}	-0.71	-0.21	1				
θ_b	-0.93	-0.39	0.83	1			
p_b	0.03	0.02	-0.03	-0.04	1		
q_b	0.01	-0.03	0.00	0.00	0.00	1	
r_b	0.02	0.01	-0.02	-0.03	0.01	0.00	1
	n_{x_b}	n_{z_b}	α_{v_b}	θ_b	p_b	q_b	r_b

CASE 2

n_{x_b}	1		
n_{z_b}	0.24	1	
α_{v_b}	0.26	0.2	1
	n_{x_b}	n_{z_b}	α_{v_b}

CASE 3

n_{x_b}	1		
n_{z_b}	0.30	1	
θ_b	-0.77	-0.26	1
	n_{x_b}	n_{z_b}	θ_b

Table VII

IDENTIFIED BIAS PARAMETERS AND THEIR STANDARD DEVIATION FROM FLIGHT RECORD 11

BIAS PARAMETER		INITIAL σ_0	CASE 1		CASE 2		CASE 3	
			EXTRACTED VALUE	σ_f	EXTRACTED VALUE	σ_f	EXTRACTED VALUE	σ_f
n_{x_b}	(g's)	0.03	(0.016)	0.006	(-0.022)	0.002	(0.036)	0.003
n_{z_b}	(g's)	0.11	0.022	0.003	0.016	0.003	0.025	0.003
α_{v_b}	(deg)	1.41	1.2	0.34	3.02	0.18	**	**
θ_b	(deg)	1.41	(-2.42)	0.38	(—)	**	(-3.73)	0.13
p_b	(deg/sec)	3.16	-0.41	0.1	*		*	
q_b	(deg/sec)	0.77	-0.004	0.028	*		*	
r_b	(deg/sec)	2.4	-0.30	0.086	*		*	

* FIXED AT CASE 1 VALUE

** NOT IDENTIFIED

NORMALIZED COVARIANCE MATRIX

CASE 1

n_{x_b}	1						
n_{z_b}	0.35	1					
α_{v_b}	(-0.78)	-0.17	1				
θ_b	(-0.94)	-0.31	(0.84)	1			
p_b	-0.01	0.00	0.01	0.01	1		
q_b	0.02	-0.04	-0.02	-0.02	0.00	1	
r_b	-0.01	-0.01	0.01	0.01	0.01	0.00	1
	n_{x_b}	n_{z_b}	α_{v_b}	θ_b	p_b	q_b	r_b

CASE 2

n_{x_b}	0		
n_{z_b}	0.18	1	
α_{v_b}	0.08	0.17	1
	n_{x_b}	n_{z_b}	α_{v_b}

CASE 3

n_{x_b}	1		
n_{z_b}	0.25	1	
θ_b	(-0.75)	-0.21	1
	n_{x_b}	n_{z_b}	θ_b

Table VIII

RELATIVE CONSISTENCY BETWEEN $n_{x_{cg}}$ ACCELEROMETER AND PITCH GYRO FROM FLIGHT RECORDS 9, 10, 11

CASE NUMBER	$\theta_b + 57.3\, n_{x_b}$ TERM (degrees)		
	RECORD 9	RECORD 10	RECORD 11
1	-0.92	-0.38	-1.5
2	-1.03	0.23	-1.26
3	-1.6	-0.5	-1.66

Table IX

IDENTIFIED BIAS PARAMETERS FROM THE END OF FLIGHT RECORDS 15, 17 AND 20 WHERE LARGE ATTITUDES ARE ENCOUNTERED; $\alpha < 20^o$

BIAS PARAMETER	IDENTIFIED VALUES		
	RECORD 15	RECORD 17	RECORD 20
n_{3_b}	0.002*	0.038	-0.06*
p_b	-1.04	0.36	-1.27
q_b	-0.06	-0.52	0.2
r_b	-0.4	-0.16	-0.49
α_{V_b}	3.56	3.34	3.18
θ_b	2.59	-2.0	1.7

*Cannot be adequately modeled as constant bias

Table X

IDENTIFIED BIAS PARAMETERS USING FIRST PORTION OF FLIGHT RECORDS 14 AND 20

BIAS PARAMETER		RECORD 14 ESTIMATED VALUE	RECORD 20 ESTIMATED VALUE
n_{zb}	(g's)	0.038	0.08
p_b	(deg/sec)	-1.16	-0.38
q_b	(deg/sec)	-0.08	-0.07
r_b	(deg/sec)	-1.1	-0.72
α_{v_b}	(deg)	5.0	4.9
ϕ_b	(deg)	—	-1.0
θ_b	(deg)	2.8	-1.5

Table XI

SUMMARY OF BIASES USED IN GENERATION OF STATE ESTIMATES OF V, α, β, ϕ AND θ

BIAS PARAMETER		FLIGHT RECORD				
		9	10	11	14	20
n_{zb}	(g's)	0.023	0.035	0.021	0.03	0.03
p_b	(deg/sec)	-1.24	-1.36	-0.41	-1.16	-0.38
q_b	(deg/sec)	-0.082	-0.158	-0.04	-0.08	-0.07
r_b	(deg/sec)	-1.31	-0.92	-0.30	-1.1	-0.72
α_{v_b}	(deg)	3.0	3.0	3.0	3.0	3.0
θ_b	(deg)	-0.70	0.0	-1.1	*	*

*θ_b, ϕ_b MODELED AS RANDOM PARAMETERS

TABLE XII

SUMMARY OF CATEGORIZATION OF FULL SCALE AIRCRAFT FLIGHT TEST DATA INTO SELECTED RANGES OF ANGLE OF ATTACK

Aerodynamic Models	Record Number	Time Integral or Record	α-Range (deg) (Min - Max)	Mach Range	Altitude (Kft)	Dominant Motions	Seconds of Useful Data
Low-α $12 \lessapprox \alpha \lessapprox 20$	9	0. to 18.5	10. to 20.	.41 - .46	$\approx$ 31.9	Longitudinal δ_e -pulse inputs	55.5
	10	0. to 21.5	12.5 to 23.	.37 - .47	$\approx$ 31.3	Lateral-Directional δ_a -inputs	
	11	2. to 17.5	13. to 20.	.38 - .46	$\approx$ 30.5	Lateral-Directional δ_r -inputs	
High-α $20 \lessapprox \alpha \lessapprox 40$	14	5. to 28.	20. to 45.	.35 - .4	29.6 - 31.6	Lateral-Directional δ_r, δ_a Small	32.5
	20	0. to 14.5	20.5 to 40.	.32 - .4	$\approx$ 34.1	Lateral-Directional δ_r, δ_a Small	

Table XIII

TERMS IN ANALYTICAL REPRESENTATION OF AERODYNAMIC COEFFICIENTS FOR LEAST SQUARES MODELS

	RECORD NO.				
	9	10	11	14	20
C_{x_o}	*	*	*	*	*
C_{x_α}	*	*	*	*	*
C_{x_q}	*	*	*	*	*
$C_{x_{\alpha q}}$	*	*	*	*	*
$C_{x_{\alpha^2 q}}$	*	*	*		*
$C_{x_{\delta_e}}$	*	*	*	*	*
C_{y_o}	*	*	*	*	*
C_{y_β}	*	*	*	*	*
$C_{y_{\alpha\beta}}$	*	*	*	*	*
C_{y_p}	*	*	*	*	*
$C_{y_{\alpha p}}$	*	*	*		
C_{y_r}	*	*	*	*	*
$C_{y_{\alpha r}}$	*	*	*	*	*
$C_{y_{\alpha r^2}}$				*	*
$C_{y_{\delta_r}}$	FIXED AT † WIND TUNNEL	*	*	FIXED AT † WIND TUNNEL	FIXED AT † WIND TUNNEL
$C_{y_{\alpha\delta_r}}$	FIXED AT † WIND TUNNEL	*	*	FIXED AT † WIND TUNNEL	FIXED AT † WIND TUNNEL
C_{z_o}	*	*	*	*	*
C_{z_α}	*	*	*	*	*
$C_{z_{\alpha^2}}$	*	*	*	*	*
C_{z_q}	*	*	*	*	*
$C_{z_{\alpha q}}$	*	*	*		
$C_{z_{\delta_e}}$	*	*	*	*	*
C_{ℓ_o}	*	*	*	*	*
C_{ℓ_β}	*	*	*	*	*
$C_{\ell_{\alpha\beta}}$	*	*	*	*	*
$C_{\ell_{\alpha^2\beta}}$				*	*
C_{ℓ_p}	*	*	*	*	*
$C_{\ell_{\alpha p}}$	*	*	*	*	*
$C_{\ell_{\alpha^2 p}}$	*	*	*	*	*
C_{ℓ_r}	*	*	*	*	*
$C_{\ell_{\alpha r}}$	*	*	*	*	*
$C_{\ell_{\alpha^2 r}}$				*	*

† AMES

Table XIII (Cont.)

TERMS IN ANALYTICAL REPRESENTATION OF AERODYNAMIC COEFFICIENTS FOR LEAST SQUARES MODELS

	RECORD NO.				
	9	10	11	14	20
$C_{\ell\delta_a}$	FIXED AT [1] WIND TUNNEL	*	FIXED AT [1] WIND TUNNEL	FIXED AT [1] WIND TUNNEL	FIXED AT [1] WIND TUNNEL
$C_{\ell\alpha\delta_a}$	FIXED AT [1] WIND TUNNEL	*	FIXED AT [1] WIND TUNNEL	FIXED AT [1] WIND TUNNEL	FIXED AT [1] WIND TUNNEL
$C_{\ell\delta_r}$	FIXED AT [1] WIND TUNNEL	*	*	FIXED AT [1] WIND TUNNEL	FIXED AT [1] WIND TUNNEL
$C_{\ell\alpha\delta_r}$	FIXED AT [1] WIND TUNNEL	*	*	FIXED AT [1] WIND TUNNEL	FIXED AT [1] WIND TUNNEL
C_{m_o}	*	*	*	*	*
C_{m_α}	*	*	*	*	*
$C_{m_{\alpha^2}}$	*	*	*	*	*
C_{m_q}	*	*	*	*	*
$C_{m_{\alpha q}}$	*	*	*	*	*
$C_{m_{\alpha^2 q}}$	*	*	*	*	*
$C_{m_{\delta_e}}$	*	*	*	*	*
$C_{m_{\alpha\delta_e}}$	*	*	*	*	*
$C_{m_{\alpha^2\delta_e}}$	*	*	*		
C_{n_o}	*	*	*	*	*
C_{n_β}	*	*	*	*	*
$C_{n_{\alpha\beta}}$	*	*	*	*	*
$C_{n_{\alpha^2\beta}}$				*	*
C_{n_p}	*	*	*	*	*
$C_{n_{\alpha p}}$	*	*	*	*	*
$C_{n_{\alpha^2 p}}$				*	*
C_{n_r}	*	*	*	*	*
$C_{n_{\alpha r}}$	*	*	*	*	*
$C_{n_{\alpha^2 r}}$				*	*
$C_{n_{\delta_a}}$	FIXED AT [1] WIND TUNNEL	*	FIXED AT [1] WIND TUNNEL	FIXED AT [1] WIND TUNNEL	FIXED AT [1] WIND TUNNEL
$C_{n_{\alpha\delta_a}}$	FIXED AT [1] WIND TUNNEL	*	FIXED AT [1] WIND TUNNEL	FIXED AT [1] WIND TUNNEL	FIXED AT [1] WIND TUNNEL
$C_{n_{\delta_r}}$	FIXED AT [1] WIND TUNNEL	*	*	FIXED AT [1] WIND TUNNEL	FIXED AT [1] WIND TUNNEL
$C_{n_{\alpha\delta_r}}$	FIXED AT [1] WIND TUNNEL	*	*	FIXED AT [1] WIND TUNNEL	FIXED AT [1] WIND TUNNEL

[1] AMES

Table XIV

KALMAN FILTER RESULTS – RECORD NO. 9, LONGITUDINAL PARAMETER ESTIMATES

PARAMETER	IDENTIFIED PARAMETER VALUES		STANDARD DEVIATIONS	
	INITIAL ESTIMATE	FINAL VALUE	INITIAL	FINAL
C_{m_o}	-0.02374	0.02382	0.02374	0.00381
C_{m_α}	0.003738	-0.003738	0.003738	0.000547
$C_{m_{\alpha^2}}$	-0.000134	0.000089	0.000134	0.000019
$C_{m_{\delta_e}}$	0.00855	0.00647	0.00855	0.00124
$C_{m_{\alpha\delta_e}}$	0.00035	0.00048	0.00035	0.000181
$C_{m_{\alpha^2\delta_e}}$	-0.000015	-0.000018	0.000015	0.000006
C_{m_q}	-3.600	-3.568	3.600	1.139
$C_{m_{\alpha q}}$	-0.2154	-0.0952	0.2154	0.1561
$C_{m_{\alpha^2 q}}$	0.00932	0.00039	0.00932	0.00592
C_{z_o}	-0.0240	-0.0212	0.0240	0.0206
C_{z_α}	-0.0695	-0.0841	0.0695	0.0031
$C_{z_{\alpha^2}}$	0.00104	0.00171	0.00104	0.00011
$C_{z_{\delta_e}}$	0.0077	0.0080	0.0077	0.0007
C_{z_q}	-14.89	-3.29	14.89	1.99
C_{x_o}	0.0800	0.0548	0.0800	0.0033
C_{x_α}	-0.0080	-0.00231	0.0080	0.00023
$C_{x_{\delta_e}}$	-0.00135	-0.00126	0.00135	0.00059
$C_{x_{\alpha\delta_e}}$	0.0000475	0.0001214	0.0000475	0.0000377
C_{x_q}	1.7475	2.3473	1.7475	1.3831
$C_{x_{\alpha q}}$	-0.1842	-0.0873	0.1842	0.1077

Table XIV (Cont.)

KALMAN FILTER RESULTS – RECORD NO. 9, LONGITUDINAL
NORMALIZED COVARIANCE MATRIX

	C_{m_o}	C_{m_α}	$C_{m_{\alpha^2}}$	$C_{m_{\delta_e}}$	$C_{m_{\alpha\delta_e}}$	$C_{m_{\alpha^2\delta_e}}$	C_{m_q}	$C_{m_{\alpha q}}$	$C_{m_{\alpha^2 q}}$	C_{z_o}	C_{z_α}	$C_{z_{\alpha^2}}$	$C_{z_{\delta_e}}$	C_{z_q}
C_{m_o}	1.00													
C_{m_α}	-1.00	1.00												
$C_{m_{\alpha^2}}$	0.98	-1.00	1.00											
$C_{m_{\delta_e}}$	-0.36	0.33	-0.29	1.00										
$C_{m_{\alpha\delta_e}}$	0.27	-0.23	0.20	-0.99	1.00									
$C_{m_{\alpha^2\delta_e}}$	-0.19	0.16	-0.12	0.96	-0.99	1.00								
C_{m_q}	0.10	-0.08	0.07	0.03	-0.02	0.01	1.00							
$C_{m_{\alpha q}}$	-0.04	0.04	-0.04	0.03	-0.05	0.06	-0.93	1.00						
$C_{m_{\alpha^2 q}}$	0.01	-0.02	0.02	-0.05	0.06	-0.07	0.73	-0.93	1.00					
C_{z_o}	-0.02	0.02	-0.03	-0.00	0.00	-0.00	0.03	-0.01	-0.02	1.00				
C_{z_α}	0.02	-0.02	0.02	0.00	0.00	-0.00	-0.03	0.01	0.02	-0.98	1.00			
$C_{z_{\alpha^2}}$	-0.01	0.02	-0.02	0.00	-0.00	0.00	0.03	-0.01	-0.02	0.93	-0.98	1.00		
$C_{z_{\delta_e}}$	0.02	-0.02	0.02	0.00	-0.01	0.01	0.01	-0.00	0.01	-0.14	0.08	-0.03	1.00	
C_{z_q}	-0.06	0.05	-0.05	0.02	-0.02	0.01	-0.01	0.00	0.00	0.12	-0.06	0.02	-0.25	1.00

Table XV

KALMAN FILTER RESULTS – RECORD NO. 10. LONGITUDINAL PARAMETER ESTIMATES

PARAMETERS	IDENTIFIED PARAMETER VALUES		STANDARD DEVIATIONS	
	INITIAL ESTIMATE	FINAL VALUE	INITIAL	FINAL
C_{m_o}	-0.00632	-0.00854	0.00126	0.00107
C_{m_α}	-0.00153	0.00287	0.00031	0.00013
$C_{m_{\alpha^2}}$	-0.000064	-0.000151	0.000013	0.000004
C_{z_o}	-0.0256	-0.0273	0.00514	0.00507
C_{z_α}	-0.0829	-0.0867	0.0166	0.0008
$C_{z_{\alpha^2}}$	0.00165	0.00191	0.00033	0.00003

NORMALIZED COVARIANCE MATRIX

	C_{m_o}	C_{m_α}	$C_{m_{\alpha^2}}$	C_{z_o}	C_{z_α}	$C_{z_{\alpha^2}}$
C_{m_o}	1.00					
C_{m_α}	-0.95	1.00				
$C_{m_{\alpha^2}}$	0.84	-0.97	1.00			
C_{z_o}	-0.00	0.00	-0.00	1.00		
C_{z_α}	-0.01	-0.01	0.02	-0.74	1.00	
$C_{z_{\alpha^2}}$	0.01	0.01	-0.03	0.50	-0.95	1.00

Table XVI

KALMAN FILTER RESULTS – RECORD NO. 11, LONGITUDINAL
PARAMETER ESTIMATES

PARAMETER	IDENTIFIED PARAMETER VALUES		STANDARD DEVIATIONS	
	INITIAL ESTIMATE	FINAL VALUE	INITIAL	FINAL
C_{m_o}	-0.00632	-0.00681	0.00126	0.00104
C_{m_α}	0.00153	0.00137	0.00031	0.00014
$C_{m_{\alpha^2}}$	-0.000064	-0.000074	0.000013	0.000005
$C_{m_{\delta_e}}$	0.00848	0.00331	0.00171	0.00075
$C_{m_{\alpha\delta_e}}$	0.000324	0.000422	0.000065	0.000054
$C_{m_{\alpha^2\delta_e}}$	-0.000015	-0.0000033	0.0000031	0.0000022
C_{m_q}	-3.650	-4.384	0.729	0.489
$C_{m_{\alpha q}}$	-0.2269	-0.2124	0.0454	0.0348
$C_{m_{\alpha^2 q}}$	0.00838	0.01024	0.00168	0.00146
C_{z_o}	-0.0256	-0.0278	0.00514	0.00510
C_{z_α}	-0.0829	-0.0869	0.0166	0.0009
$C_{z_{\alpha^2}}$	0.00165	0.00196	0.00033	0.00004
$C_{z_{\delta_e}}$	0.0084	0.0082	0.0017	0.0014
C_{z_q}	-7.334	-12.811	1.450	1.289

Table XVI (Cont.)

KALMAN FILTER RESULTS – RECORD NO. 11, LONGITUDINAL

NORMALIZED COVARIANCE MATRIX

	C_{m_o}	C_{m_α}	$C_{m_{\alpha^2}}$	$C_{m_{\delta_e}}$	$C_{m_{\alpha\delta_e}}$	$C_{m_{\alpha^2\delta_e}}$	C_{m_q}	$C_{m_{\alpha q}}$	$C_{m_{\alpha^2 q}}$	C_{z_o}	C_{z_α}	$C_{z_{\alpha^2}}$	$C_{z_{\delta_e}}$	C_{z_q}
C_{m_o}	1.00													
C_{m_α}	-0.93	1.00												
$C_{m_{\alpha^2}}$	0.78	-0.95	1.00											
$C_{m_{\delta_e}}$	-0.08	-0.12	0.25	1.00										
$C_{m_{\alpha\delta_e}}$	0.04	0.01	-0.06	-0.73	1.00									
$C_{m_{\alpha^2\delta_e}}$	0.05	0.09	-0.20	-0.14	-0.53	1.00								
C_{m_q}	0.04	-0.01	-0.02	0.05	-0.03	-0.01	1.00							
$C_{m_{\alpha q}}$	-0.02	0.01	0.01	-0.02	-0.00	-0.00	-0.71	1.00						
$C_{m_{\alpha^2 q}}$	-0.03	0.00	0.03	-0.03	0.00	-0.00	-0.22	-0.41	1.00					
C_{z_o}	-0.00	0.00	-0.00	0.00	-0.00	-0.00	0.00	-0.00	-0.00	1.00				
C_{z_α}	-0.01	-0.01	0.02	0.00	0.00	0.00	-0.01	0.01	0.01	-0.77	1.00			
$C_{z_{\alpha^2}}$	0.01	0.02	-0.03	-0.00	-0.00	-0.01	0.01	-0.01	-0.01	0.52	-0.94	1.00		
$C_{z_{\delta_e}}$	0.00	0.00	0.00	-0.01	-0.00	0.00	0.00	0.01	0.01	0.00	-0.15	0.12	1.00	
C_{z_q}	-0.00	-0.00	0.01	0.00	-0.00	-0.01	-0.00	-0.01	-0.00	0.01	0.02	-0.00	-0.04	1.00

Table XVII

KALMAN FILTER RESULTS – RECORD NO. 14, LONGITUDINAL
PARAMETER ESTIMATES

PARAMETER	IDENTIFIED PARAMETER VALUES		STANDARD DEVIATIONS	
	INITIAL ESTIMATE	FINAL VALUE	INITIAL	FINAL
C_{m_o}	0.04355	0.06747	0.00604	0.00066
$C_{m_{\delta_e}}$	0.0129	0.0051	0.00183	0.00018
$C_{m_{\alpha\delta_e}}$	-0.000267	0.000045	0.000038	0.000004
C_{z_o}	-0.2883	-0.3345	0.0407	0.0159
C_{z_α}	-0.0366	-0.0337	0.0052	0.0011
$C_{z_{\alpha^2}}$	0.000227	0.000176	0.000032	0.000017

NORMALIZED COVARIANCE MATRIX

	C_{m_o}	$C_{m_{\delta_e}}$	$C_{m_{\alpha\delta_e}}$	C_{z_o}	C_{z_α}	$C_{z_{\alpha^2}}$
C_{m_o}	1.00					
$C_{m_{\delta_e}}$	-0.78	1.00				
$C_{m_{\alpha\delta_e}}$	0.54	-0.93	1.00			
C_{z_o}	-0.01	0.01	-0.01	1.00		
C_{z_α}	0.00	-0.01	0.01	-0.99	1.00	
$C_{z_{\alpha^2}}$	-0.00	0.00	-0.00	0.95	-0.99	1.00

Table XVIII

KALMAN FILTER RESULTS – RECORD NO. 20. LONGITUDINAL PARAMETER ESTIMATES

PARAMETER	IDENTIFIED PARAMETER VALUES		STANDARD DEVIATIONS	
	INITIAL ESTIMATE	FINAL VALUE	INITIAL	FINAL
C_{m_0}	0.06144	0.04355	0.006144	0.00281
C_{m_α}	-0.002196	-0.002870	0.000220	0.000169
$C_{m_{\alpha^2}}$	-0.0000612	-0.0000717	0.0000061	0.0000034
$C_{m_{\delta_e}}$	0.0129	0.0065	0.0013	0.0003
$C_{m_{\alpha\delta_e}}$	-0.000267	0.0000049	0.0000267	0.0000084
C_{m_q}	-18.64	-18.93	1.864	1.53
$C_{m_{\alpha q}}$	0.9817	0.9697	0.0982	0.0627
$C_{m_{\alpha^2 q}}$	-0.01699	-0.01639	0.00170	0.00133
C_{z_0}	-0.4214	-0.2883	0.0421	0.0195
C_{z_α}	0.03906	-0.03658	0.00391	0.00134
$C_{z_{\alpha^2}}$	0.000318	0.000227	0.000032	0.000021
$C_{z_{\delta_e}}$	0.0090	0.0072	0.0009	0.0003
C_{z_q}	-22.46	-19.44	2.246	1.398

Table XVIII (Cont.)

KALMAN FILTER RESULTS – **RECORD NO. 20, LONGITUDINAL**

NORMALIZED COVARIANCE MATRIX

	C_{m_0}	C_{m_α}	$C_{m_{\alpha^2}}$	$C_{m_{\delta_e}}$	$C_{m_{\alpha\delta_e}}$	C_{m_q}	$C_{m_{\alpha q}}$	$C_{m_{\alpha^2 q}}$	C_{z_0}	C_{z_α}	$C_{z_{\alpha^2}}$	$C_{z_{\delta_e}}$	C_{z_q}
C_{m_0}	1.00												
C_{m_α}	-0.73	1.00											
$C_{m_{\alpha^2}}$	0.35	-0.87	1.00										
$C_{m_{\delta_e}}$	-0.47	-0.21	0.56	1.00									
$C_{m_{\alpha\delta_e}}$	0.48	0.19	-0.58	-0.98	1.00								
C_{m_q}	0.13	0.08	-0.13	-0.19	0.14	1.00							
$C_{m_{\alpha q}}$	0.01	0.02	-0.01	-0.03	0.02	-0.59	1.00						
$C_{m_{\alpha^2 q}}$	-0.09	-0.07	0.10	0.14	-0.09	-0.07	-0.75	1.00					
C_{z_0}	-0.02	0.00	0.01	0.02	-0.02	-0.00	-0.00	0.00	1.00				
C_{z_α}	0.01	-0.00	-0.01	-0.02	0.02	0.00	0.00	0.00	-0.98	1.00			
$C_{z_{\alpha^2}}$	-0.01	0.00	0.01	0.02	-0.02	-0.00	-0.00	0.00	0.95	-0.98	1.00		
$C_{z_{\delta_e}}$	-0.00	-0.01	0.01	0.00	-0.01	0.02	0.00	-0.01	0.13	-0.21	0.08	1.00	
C_{z_q}	0.00	-0.00	0.00	-0.01	0.01	-0.00	-0.00	-0.00	-0.03	0.04	0.02	-0.25	1.00

Table XIX

KALMAN FILTER RESULTS – RECORD NO. 10, LATERAL-DIRECTIONAL PARAMETER ESTIMATES

PARAMETER	IDENTIFIED PARAMETER VALUES		STANDARD DEVIATIONS	
	INITIAL ESTIMATE	FINAL VALUE	INITIAL	FINAL
C_{l_o}	0.0	0.0034	0.0025	0.00003
C_{l_β}	-0.00576	-0.00673	0.00576	0.000084
$C_{l_{\alpha\beta}}$	0.000265	0.000274	0.000265	0.0000044
$C_{l_{\delta_a}}$	0.00105	0.00027	0.00105	0.000015
$C_{l_{\alpha\delta_a}}$	-0.000035	-0.0000011	0.000035	0.0000007
C_{l_p}	-1.516	1.753	1.516	0.1707
$C_{l_{\alpha p}}$	0.1689	-0.1817	0.1689	0.0187
$C_{l_{\alpha^2 p}}$	-0.00502	0.00438	0.00502	0.00051
C_{n_o}	0.0	-0.00133	0.00247	0.00013
C_{n_β}	-0.00157	0.01274	0.00157	0.00121
$C_{n_{\alpha\beta}}$	0.000743	-0.001246	0.000743	0.000137
$C_{n_{\alpha^2\beta}}$	-0.0000330	0.0000318	0.0000330	0.0000039
$C_{n_{\delta_a}}$	-0.000052	-0.000108	0.000052	0.000005
C_{n_p}	0.0	0.0972	0.0500	0.00953
C_{n_r}	-0.400	-2.135	0.400	0.1253

Table XIX (Cont.)

KALMAN FILTER RESULTS – RECORD NO. 10, LATERAL-DIRECTIONAL
NORMALIZED COVARIANCE MATRIX

	C_{l_o}	C_{l_β}	$C_{l_{\alpha\beta}}$	$C_{l_{\delta_a}}$	$C_{l_{\alpha\delta_a}}$	C_{l_p}	$C_{l_{\alpha p}}$	$C_{l_{\alpha^2 p}}$	C_{n_o}	C_{n_β}	$C_{n_{\alpha\beta}}$	$C_{n_{\alpha^2\beta}}$	$C_{n_{\delta_a}}$	C_{n_p}	C_{n_r}
C_{l_o}	1.00														
C_{l_β}	-0.30	1.00													
$C_{l_{\alpha\beta}}$	0.27	-1.00	1.00												
$C_{l_{\delta_a}}$	0.06	0.46	-0.49	1.00											
$C_{l_{\alpha\delta_a}}$	-0.00	-0.49	0.51	-1.00	1.00										
C_{l_p}	0.18	-0.03	0.02	-0.27	0.25	1.00									
$C_{l_{\alpha p}}$	-0.19	0.04	-0.04	0.26	-0.24	-1.00	1.00								
$C_{l_{\alpha^2 p}}$	0.20	-0.05	0.04	-0.23	0.22	0.99	-1.00	1.00							
C_{n_o}	-0.02	-0.17	0.15	0.05	-0.05	-0.18	0.15	-0.13	1.00						
C_{n_β}	0.06	-0.08	0.08	0.04	-0.03	-0.05	0.04	-0.04	-0.44	1.00					
$C_{n_{\alpha\beta}}$	-0.08	0.10	-0.09	-0.06	0.05	0.07	-0.07	0.06	0.35	-0.99	1.00				
$C_{n_{\alpha^2\beta}}$	0.09	-0.11	0.10	0.08	-0.07	-0.10	0.09	-0.08	-0.26	0.97	-0.99	1.00			
$C_{n_{\delta_a}}$	0.23	-0.25	0.21	0.14	-0.11	-0.12	0.09	-0.07	0.45	0.28	-0.36	0.41	1.00		
C_{n_p}	0.01	0.12	-0.14	-0.02	0.02	0.15	-0.12	0.10	-0.24	-0.19	0.24	-0.27	-0.18	1.00	
C_{n_r}	-0.11	-0.07	0.06	-0.02	0.01	-0.12	0.10	-0.09	0.87	-0.58	0.52	-0.45	0.02	-0.16	1.00

Table XX

KALMAN FILTER RESULTS – RECORD NO. 11, LATERAL-DIRECTIONAL PARAMETER ESTIMATES

PARAMETER	IDENTIFIED PARAMETER VALUES	
	INITIAL ESTIMATE	FINAL VALUE
C_{ℓ_o}	0.0	0.00463
C_{ℓ_β}	-0.00576	-0.00624
$C_{\ell_{\alpha\beta}}$	0.000265	0.000231
C_{ℓ_p}	-1.516	-1.628
$C_{\ell_{\alpha p}}$	0.1689	0.1837
$C_{\ell_{\alpha^2 p}}$	-0.00502	-0.00529
C_{ℓ_r}	0.150	0.349
C_{n_o}	0.0	-0.00006
C_{n_β}	-0.00157	-0.00213
$C_{n_{\alpha\beta}}$	0.000743	0.000559
$C_{n_{\alpha^2\beta}}$	-0.0000330	-0.0000238
$C_{n_{\delta_r}}$	0.00140	0.00112
$C_{n_{\alpha\delta_r}}$	-0.000025	-0.000014
C_{n_p}	0.0	0.00597
C_{n_r}	-0.400	-0.782

Table XXI

KALMAN FILTER RESULTS – RECORD NO. 14, LATERAL-DIRECTIONAL PARAMETER ESTIMATES

PARAMETER	IDENTIFIED PARAMETER VALUES	
	INITIAL ESTIMATE	FINAL VALUE
C_{ℓ_o}	0.0	0.00155
C_{ℓ_β}	-0.0517	-0.0297
$C_{\ell_{\alpha\beta}}$	0.00348	0.00227
$C_{\ell_{\alpha^2\beta}}$	-0.0000576	-0.0000441
C_{ℓ_p}	0.450	0.574
$C_{\ell_{\alpha p}}$	-0.0300	-0.0211
C_{ℓ_r}	0.50	-0.220
C_{n_o}	0.0	-0.00172
C_{n_β}	0.0267	0.0216
$C_{n_{\alpha\beta}}$	-0.001892	-0.001551
$C_{n_{\alpha^2\beta}}$	0.0000288	0.0000238
C_{n_p}	0.0	0.0367
C_{n_r}	-0.70	-0.440

Table XXII

KALMAN FILTER RESULTS – RECORD NO. 20, LATERAL-DIRECTIONAL PARAMETER ESTIMATES

PARAMETER	IDENTIFIED PARAMETER VALUES		STANDARD DEVIATIONS	
	INITIAL ESTIMATE	FINAL VALUE	INITIAL	FINAL
C_{ℓ_o}	0.0	-0.00084	0.00035	0.00021
C_{ℓ_β}	-0.0517	-0.0438	0.00732	0.00218
$C_{\ell_{\alpha\beta}}$	0.00348	0.00348	0.00049	0.00018
$C_{\ell_{\alpha^2\beta}}$	-0.0000576	-0.0000707	0.0000081	0.0000037
C_{ℓ_p}	2.446	4.941	0.3458	0.2132
$C_{\ell_{\alpha p}}$	-0.2021	-0.2279	0.0286	0.0153
$C_{\ell_{\alpha^2 p}}$	0.00361	0.000586	0.000510	0.000364
C_{ℓ_r}	0.450	0.5954	0.0633	0.0604
C_{n_o}	0.0	0.00300	0.00035	0.00023
C_{n_β}	0.0267	0.0254	0.00378	0.00175
$C_{n_{\alpha\beta}}$	-0.001892	-0.001666	0.000268	0.000136
$C_{n_{\alpha^2\beta}}$	0.0000288	0.0000224	0.0000041	0.0000027
C_{n_p}	0.0	0.0304	0.0141	0.0129
C_{n_r}	-0.50	-0.3171	0.0707	0.0680

Table XXII (Cont.)

KALMAN FILTER RESULTS – RECORD NO. 20, LATERAL-DIRECTIONAL

NORMALIZED COVARIANCE MATRIX

	C_{ℓ_o}	C_{ℓ_β}	$C_{\ell_{\alpha\beta}}$	$C_{\ell_{\alpha^2\beta}}$	C_{ℓ_p}	$C_{\ell_{\alpha p}}$	$C_{\ell_{\alpha^2 p}}$	C_{ℓ_r}	C_{n_o}	C_{n_β}	$C_{n_{\alpha\beta}}$	$C_{n_{\alpha^2\beta}}$	C_{n_p}	C_{n_r}
C_{ℓ_o}	1.00													
C_{ℓ_β}	0.16	1.00												
$C_{\ell_{\alpha\beta}}$	-0.03	-0.99	1.00											
$C_{\ell_{\alpha^2\beta}}$	-0.12	0.95	-0.99	1.00										
C_{ℓ_p}	0.38	-0.06	0.11	-0.16	1.00									
$C_{\ell_{\alpha p}}$	-0.11	-0.15	0.15	-0.14	-0.88	1.00								
$C_{\ell_{\alpha^2 p}}$	-0.25	0.30	-0.36	0.42	0.51	-0.85	1.00							
C_{ℓ_r}	-0.14	0.25	-0.26	0.27	0.02	0.01	-0.06	1.00						
C_{n_o}	-0.03	0.03	-0.02	0.02	-0.04	0.02	0.00	-0.01	1.00					
C_{n_β}	-0.02	-0.00	0.00	0.00	0.01	-0.00	0.00	-0.01	0.37	1.00				
$C_{n_{\alpha\beta}}$	0.03	0.00	0.00	-0.01	-0.01	0.01	-0.01	0.01	-0.23	-0.98	1.00			
$C_{n_{\alpha^2\beta}}$	-0.04	-0.00	-0.00	0.01	0.01	-0.01	0.01	-0.01	0.06	0.93	-0.98	1.00		
C_{n_p}	-0.05	0.00	-0.00	0.01	-0.01	0.00	0.01	-0.01	-0.39	-0.08	0.04	0.02	1.00	
C_{n_r}	0.01	0.01	-0.00	0.00	-0.01	0.01	-0.00	0.00	-0.29	0.00	-0.05	0.12	-0.07	1.00

TABLE XXIII

ANALYTICAL REPRESENTATION OF THE AERODYNAMIC COEFFICIENTS IDENTIFIED FOR THE RADIO CONTROLLED MODEL

$$C_l = C_{l_\beta}(\beta) + C_{l_{\alpha\beta}}(\alpha\beta) + C_{l_{\delta_a}}(\delta_a) + C_{l_{\alpha\delta_a}}(\alpha\delta_a)$$
$$+ C_{l_{\delta_r}}(\delta_r) + \frac{b}{2V}\left[C_{l_p}(p) + C_{l_{\alpha p}}(\alpha p) + C_{l_{\alpha^2 p}}(\alpha^2 p)\right.$$
$$\left. + C_{l_r}(r) + C_{l_{\alpha r}}(\alpha r) + C_{l_{\alpha^2 r}}(\alpha^2 r)\right]$$

$$C_m = C_{m_o} + C_{m_\alpha}(\alpha) + C_{m_{\delta_e}}(\delta_e) + C_{m_{\alpha\delta_e}}(\alpha\delta_e)$$
$$+ \frac{\bar{c}}{2V}\left[C_{m_q}(q) + C_{m_{\alpha q}}(\alpha q) + C_{m_{\alpha^2 q}}(\alpha^2 q)\right]$$

$$C_n = C_{n_\beta}(\beta) + C_{n_{\alpha\beta}}(\alpha\beta) + C_{n_{\delta_a}}(\delta_a) + C_{n_{\delta_r}}(\delta_r)$$
$$+ C_{n_{\alpha\delta_r}}(\alpha\delta_r) + \frac{b}{2V}\left[C_{n_p}(p) + C_{n_{\alpha p}}(\alpha p) + C_{n_{\alpha^2 p}}(\alpha^2 p)\right.$$
$$\left. + C_{n_r}(r) + C_{n_{\alpha r}}(\alpha r)\right]$$

Section VI

CONCLUSIONS AND RECOMMENDATIONS

This section presents the conclusions and recommendations which can be drawn based upon the results of this investigation. The results of this program demonstrated the feasibility and applicability of the identification approach and technique utilized, even though they were compromised by the poor data quality available for identification purposes. It is quite clear that a flight test data base at high angles of attack is not currently available to obtain conclusive and meaningful results and consequently, a very carefully planned flight test program should be devised and performed to provide the necessary data base. Recommendations for such a program are presented in this section. The conclusions and recommendations follow.

6.1 CONCLUSIONS

6.1.1 Identification Approach and Techniques

The identification procedure developed in this program, which centers around a straightforward least squares equation error method and an advanced nonlinear iterated Kalman filter/fixed-point smoother algorithm, was shown to be a sufficiently adequate and accurate data reduction procedure for the high angle of attack flight regime. Model definition from wind tunnel data, limited range angle of attack identification, separation of instrumentation error identification and optimal aircraft trajectory estimation from aerodynamic parameter identification, and the partial decoupling of the longitudinal and lateral-directional degrees of freedom of the aircraft, were shown to enhance the accuracy of the identification and to reduce the overall high dimensional problem into separate lower dimensional problems, the solutions of which are computationally feasible. The importance of the other three factors for identification, that is, data conditioning, instrumentation and modeling, were also demonstrated.

With the identification procedure, instrumentation inconsistencies were generally easily determined and identified from the full-scale flight test records. These records provided limited data in the angle of attack (α) range from approximately 12 to 40 degrees. For the low range of α (12 to 23 degrees), where the instrumentation checked well and where the data were properly conditioned for identification purposes (i.e., the longitudinal maneuvers), the results were excellent and the longitudinal characteristics were accurately identified. Poor data conditioning precluded accurate and consistent extraction of the lateral-directional characteristics at this range of α , but these problems were readily detected. In general, the aerodynamic models used appeared adequate to describe the longitudinal and lateral-directional characteristics at the low α range. For angles of attack above 25 degrees, definite conclusions as to the adequacy and complexity of the aerodynamics could not be firmly established because of the short record lengths of usable data, caused, in part, by large instrumentation inconsistencies at angles of attack greater than 30 degrees.

The instrumentation complement used on the full scale aircraft was minimal but adequate for identification purposes. More accurate instruments are currently available. However, the level of accuracy of the data was not within the instrumentation capabilities, because the full scale range on most of the measurements was too large, thereby compromising the accuracy of small variations in the data and accentuating nonlinearities in the calibration. The full scale range should be commensurate with the expected maneuvers. Instrumentation inconsistencies were identified using the aircraft kinematic equation for dynamic instrumentation consistency checking. These checks afford a valuable tool for augmenting current flight testing instrumentation calibration techniques, as well as obtaining the best approximation to all the data using optimal filtering techniques, and could save valuable flight testing time.

Redundant instrumentation is very useful, if economically feasible and practical, to afford additional information for analysis purposes and also to provide cross checks for ascertaining instrumentation consistency. Angular acceleration measurements should be used in the identification algorithm (they are a necessity for the least squares method) to increase the accuracy and speed of convergence of the parameter estimates for a given data length. If individual angular acceleration sensors are not available, digital differentiation of good rate measurements, as was done in this investigation, appears to be adequate. However, angular acceleration sensors afford a more complete and accurate formulation of the dynamic instrumentation consistency checks and therefore, they should be utilized whenever possible. Limited instrumentation on the radio controlled model, missing linear acceleration and attitude measurements, preclude estimations of the force coefficients, but moment coefficients were extracted for the angle of attack range from 30 to 55 degrees using the least squares technique.

6.1.2 Correlation of Test Data

The wind tunnel data by itself was not accurate and complete enough to define an accurate aerodynamic model which would predict full-scale aircraft responses. This problem also precluded predicting the moments acting on the radio controlled model with wind tunnel data. However, the forms of static aerodynamics as a function of angle of attack appear to be accurate, although conclusive results cannot be firmly established because of the poorly conditioned test data.

For the angle of attack range from 10 to 20 degrees where the longitudinal maneuvers were adequate for identification, the results are conclusive. The static pitching moment coefficient, C_m, z-force due to stabilator $C_{z_{\delta_e}}$, and stabilator effectiveness, $C_{m_{\delta_e}}$, were all extracted with values consistently higher than those given by the wind tunnel data. Less damping in pitch, $C_{m_q} + C_{m_{\dot{\alpha}}}$, was also obtained but the static z-force coefficient, C_z, was almost identical to the wind tunnel data. Similar results were obtained for the angle of attack range from 20 to 40 degrees. The reasons for these differences are not readily apparent, although Reynolds number and power effects could be the cause.

For the lateral-directional aerodynamics, consistent rolling moment asymmetries were identified but only very small, and not consistent, yawing moment asymmetries were obtained. The rolling moment asymmetries could be partially aerodynamic, but it is believed that the main cause was that the roll controller (δ_a) was rigged (or its responses recorded) with an offset. Similarly, yaw moment asymmetries could be present, but the results are inconclusive. If the controllers were inaccurately rigged or if the control coefficients from the wind tunnel are incorrect, these errors would affect the asymmetries extracted. In general, the poorly conditioned flight records did not allow for the accurate and consistent extraction of the lateral-directional characteristics, especially the dynamic coefficients and cross-coefficients. However, the static derivatives exhibited similar trends for all flight records.

Most of the moment coefficients extracted from the drop model data showed good correlation with the wind tunnel data, but here too the limited data and instrumentation provided inconclusive results.

6.2 RECOMMENDATIONS

It is readily apparent that no data analysis techniques or procedures, no matter how advanced, can compensate for inadequate instrumentation and improper maneuvers - called "data conditioning." It is therefore recommended that a variety of carefully performed flight test programs, for both full scale aircraft and models, be performed in the stall and post-stall regimes. In addition, the data analysis should be done concurrently with the flight testings in order to insure a complete and adequate enough data base. The aircraft should be completely instrumented with research caliber equipment and the emphasis should be placed on the quality of the results, rather than the quantity. Further recommendations for improvements in flight testing techniques for gathering high angles of attack data for identification pruposes are given in Section 6.2.2.

Section II in this report describes the difficult task associated with acquiring flight test data which would be appropriate for high angle of attack identification. In many ways, this difficulty was the result of inadequate documentation of the basic flight data and the calibration and records associated with the data. It was quite disturbing to observe that the data obtained in major flight test programs was so poorly documented and, in fact, was in some cases destroyed. Storage of this data and its basic supporting documentation should be mandatory for at least the period during which the aircraft is in the inventory.

The following two subsections present detailed recommendations for improving the identification techniques and the quality of the flight data.

6.2.1 Refinements to the Identification Techniques

An improvement which should be made in using both the least squares and iterated Kalman identification techniques is the simultaneous processing of several maneuvers. This additional capability would help eliminate the problem that develops when a relatively complex model is required in an angle of attack range in which the aircraft is very unstable and uncontrollable. Under these conditions, very short data records are usually obtained from these regimes and they do not contain enough information for complete identification. By processing several records simultaneously the amount of data is increased and a model applicable for all records can be more readily identified.

Another area of improvement is a more automatic way to determine model form. The method used in this investigation, although adequate, was a trial and error procedure starting with the wind tunnel data. Terms were added or subtracted until a model was found that adequately defined the aerodynamic forces and moments for the particular flight data, initially by using the least squares technique and then by adding refinements with the iterated Kalman filter. This procedure could be automated using multiple linear regression by initially defining an overly complex model, as indicated from the wind tunnel data, and then, starting with a simplified subset of this model, add terms until further additions do not decrease the equation error by some prespecified criterion. The resulting model is further checked using a "goodness of fit" test to the residuals from the iterated Kalman filter.

6.2.2 Recommendations for High Angle of Attack Flight Testing

The results of the investigation discussed in this report were compromised in some cases by the quality of the flight data. Identification of flight data is strongly affected by what might be called proper "conditioning" of the data, as well as by the obvious effects of instrumentation inaccuracies and poor signal-to-noise characteristics. The debilitating effects on identification capability caused by poor conditioning are exacerbated when the mathematical model is complex and ill-defined, as is the case in high angle-of-attack flight maneuvers, and the determination of an appropriate model therefore becomes difficult. The purpose of this subsection is therefore to discuss specific areas in which improvements to flight test techniques for gathering high angle of attack data for identification purposes should be considered.

The most obvious area needing improvement is in the instrumentation used, particularly with regard to air-sensed variables such as angle of attack, sideslip angle, and airspeed. During this investigation, large inconsistencies in the measured variables with each other were found. While calibration and bias errors of rate and attitude gyros, for example, can be quite easily ascertained via the consistency checks discussed in Section V of this report, errors in air-sensed quantities that are caused by local flow effects and boom bending at high angles of attack are much more difficult to determine, partially due to difficulties in modeling these effects and partially because insufficient redundancies in the measurements exist. It is therefore recommended

that attempts be made to improve the aircraft instrumentation for identification at high angles of attack, particularly:

1) Redundancy in air-measured quantities, or alternate measurements such as accurate rate-of-climb information from which they can be estimated, should be incorporated.

2) Specific flights should be designed and devoted to gathering data to determine instrument consistency over the angle of attack range of interest prior to the flights devoted to identification.

Although improvements in the instrumentation accuracy and consistency are important to increase the identification capability, equally important is careful attention to the "conditioning" of the data obtained. This conditioning involves the selection and constraining of the range of flight variables investigated for a given data record to aid the simplification and validation of the mathematical model used, and the design and implementation of control inputs to enhance the identifiability of the data record. These two aspects of data conditioning are discussed in the following paragraphs.

As has been discussed previously in this report, it is desirable to simplify as much as possible the mathematical model of the aircraft to make the identification process efficient. The approach taken in this investigation was to consider partial decoupling of the longitudinal and lateral-directional degrees of freedom to reduce the order of the equation set, and to separate the ranges considered of important variables, notably angle of attack, in order to simplify the representation of the aerodynamic coefficients in each range. These procedures are analogous to the more highly constrained restrictions placed on the flight conditions and maneuvers in the usual cases which employ linearized equations, and require that the test data meet the assumptions used in obtaining the equations. For identification of high angle of attack test data, then, it is important to know prior to the flight tests the candidate mathematical models which will be used, and then to attempt to constrain the flight conditions to validate the assumptions made. Specific recommendations are:

1) Data records should be obtained over limited ranges of important parametric variables (e.g., $10^{o} < \alpha < 20^{o}$, $15^{o} < \alpha < 25^{o}$, $20^{o} < \alpha < 30^{o}$, etc.). For records which are primarily for longitudinal identification, a monotonic change in the angle of attack with perturbations superposed would be good; for records which are primarily for lateral-directional identification, oscillations over the range of interest would be desirable, but may be very difficult to achieve in practice.

2) Attempts should be made to provide motions which at least partially decouple the aircraft responses.

The final area to be discussed is the design of control inputs to enhance identifiability. For a given mathematical model and set of parameters, the success of any identification technique is highly dependent on the control inputs applied to the airplane. For a given input, the best identification performance possible, in the sense of minimum mean square estimation error, is given by the Cramer-Rao lower bound: that is, the elements of the Cramer-Rao matrix are the lowest variances on the estimates that can be achieved. It is therefore possible, for example, to design inputs based on a minimization of this lower bound. The Cramer-Rao lower bound is the inverse of the Fisher information matrix, the elements of which are the sensitivity functions which are computed to perform the minimizations discussed in the last section, and so maximization of some norm of this matrix may also be used to design inputs, although the two methods are not exactly equivalent. Implementation of such inputs in a flight program, however, is difficult, and hence approximations that provide at least some benefit to identifiability are sought.

In flying qualities experiments, for example, inputs for identification records have historically been simple analytically and chosen to accentuate some particular features of the response. Examples include rudder doublets, for the Dutch roll characteristics, and aileron steps for roll mode time constants and ϕ/δ_{AS} transfer function characteristics. It is easy to demonstrate that these inputs do indeed provide large sensitivities for the stability derivatives which have the primary influence on the characteristics of interest, but the other derivatives may not be identifiable with any accuracy at all. The usual procedure that is followed is to obtain several records with different inputs tailored heuristically to certain characteristics and thereby obtain in a composite fashion the total identification.

The difficulty with using several different inputs, of course, is that it requires additional flight time. On a recent X-22A program, conducted by Calspan (Reference 29), therefore, an attempt was made to provide control inputs that increased many of the sensitivity functions simultaneously. In general, for amplitude-constrained inputs (which are necessary to aid the assumption of linearity made in this flight program), it can be shown that "switching" type inputs increase the sensitivity for most parameters, the frequency of switching being dependent on the dynamic characteristics of the system. It was therefore decided to attempt to have the pilots provide this type of input in both yaw and roll. The advantages of using the pilot, rather than a programmed automatic input, include his capability to maintain the aircraft responses within linear limits and his ability to sense to some degree the characteristic frequencies of the aircraft to provide switching cues. The disadvantages of using pilot inputs is primarily the pilot's tendency to act as a feedback controller; in that case, the inputs become linearly related to at least one aircraft output, which is inimical to good identification. These inputs generally did enhance identifiability of the data records

obtained on the X-22A program, and this approach therefore seems quite desirable.

For systems which are described by nonlinear equations of motion, which is characteristic of the high angle of attack problem, further theoretical work is required, but it is clear that the switching type of input would be beneficial in any case. It is therefore recommended that these types of control inputs be applied to the aircraft in future flight testing, and also that further theoretical work be done to determine the best switching frequencies.

This section has reviewed three areas in which improvements in high angle of attack flight testing are recommended. These areas are:

1. Instrumentation accuracy and consistency.
2. Constrained flight conditions and maneuvers.
3. Type of control inputs applied to the aircraft.

The recommended improvements in all three areas are required to obtain valid identification results in this flight regime. Only through obtaining these better flight data can correlation of identified flight data with wind tunnel data and theoretical predictions be properly performed.

This page left blank intentionally.

Appendix I

FLIGHT TEST DATA AND AIRCRAFT PHYSICAL PROPERTIES

1. F-4E Flight Test Records

This appendix contains the time history plots of the important flight parameters of the eight high-angle-of-attack flight records used in the program. The data is from Flight Number 165 of the Stall/Near Stall Investigation of the F-4E aircraft, Reference 6, which was conducted at the Air Force Flight Test Center at Edwards Air Force Base. The data was obtained from McDonnell Aircraft Company under a subcontract, Reference 9. Additional data, such as aircraft mass, inertia, and geometric characteristics, center of gravity (c.g.) locations and instrumentation characteristics and location from c.g. have also been included. This data appears in Tables XXIV, XXV, and XXVI respectively.

The flight records are shown in Figures 48 through 55. Generation of the aerodynamic force and moment time histories, thrust, angular acceleration ($\dot{p}$, $\dot{q}$, $\dot{r}$), and the Kalman filter state estimates ($\hat{\alpha}$, $\hat{\beta}$, $\hat{V}$, $\hat{\phi}$, and $\hat{\theta}$) are described in Sections III and V of this report. Note that Mach number, dynamic pressure, air density and the angular rate signals (p , q , r) have been filtered with a digital filter having the frequency characteristics of two cascaded fourth order Butterworth filters with no phase shift.

Special calculations for Mach number, airspeed, air density, dynamic pressure and corrected nose-boom angle of attack and sideslip are given in Reference 9.

2. Radio Controlled Drop Model Test Data

Figures 56 and 57 show the time histories of the radio controlled drop model responses on Runs 1 and 3 respectively. These were obtained from computer listings of a NASA F-4 drop model test series. Geometric and mass characteristics of the radio controlled model are presented in Table XXVII. The data was obtained from NASA/LRC, Reference 32.

The following is a list of symbols used in Figures 48 through 55.

C_ℓ, C_m, C_n	AERODYNAMIC MOMENT COEFFICIENTS IN BODY AXES
C_x, C_y, C_z	AERODYNAMIC FORCE COEFFICIENTS IN BODY AXES
F_{x_a}, F_{y_a}, F_{z_a}	AERODYNAMIC FORCE ALONG THE x, y, z BODY AXES, lb
h	ALTITUDE, ft
h_{e_x}	ANGULAR MOMENTUM OF ENGINES ALONG x BODY AXIS, slug-ft^2/ sec
M	MACH NUMBER
M_{x_a}, M_{y_a}, M_{z_a}	AERODYNAMIC MOMENTS ABOUT x, y, z AXES, ft-lb
$n_{x_{cg}}$, $n_{y_{cg}}$, $n_{z_{cg}}$	ACCELEROMETER SIGNALS AT CG ALONG x, y, z BODY AXES, g's
p, q, r	ROLL, PITCH AND YAW GYRO SIGNALS ABOUT x, y, z BODY AXES, deg/sec
$\dot{p}, \dot{q}, \dot{r}$	DIFFERENTIATED p, q, r SIGNALS, deg/sec^2
$\bar{q}$	DYNAMIC PRESSURE, lb/ft^2
T_R, T_L	RIGHT AND LEFT HAND ENGINE THRUST, lb
δ_a	$\delta_{a_r} + \delta_{a_L}$ (SUM OF RIGHT AND LEFT AILERON DISPLACEMENTS), + = RIGHT WING DOWN, deg
δ_r	RUDDER DISPLACEMENT, + = TRAILING EDGE RIGHT, deg
δ_s	STABILATOR DISPLACEMENT, + = AIRCRAFT NOSE UP, deg
α_{V_C}	BOOM VANE ANGLE-OF-ATTACK SIGNAL CORRECTED TO CG, deg
β_{V_C}	BOOM VANE SIDESLIP ANGLE CORRECTED TO CG, deg
V_T	TRUE AIRSPEED, ft/sec
ϕ, θ, ψ	EULER ANGLE ATTITUDE SIGNALS, deg
$\hat{\alpha}$	KALMAN FILTER ESTIMATE OF ANGLE OF ATTACK, deg
$\hat{\beta}$	KALMAN FILTER ESTIMATE OF SIDESLIP ANGLE, deg
$\hat{V}_T$	KALMAN FILTER ESTIMATE OF TRUE AIRSPEED, ft/sec
$\hat{\phi}, \hat{\theta}$	KALMAN FILTER ESTIMATE OF ROLL AND PITCH EULER ANGLES, deg

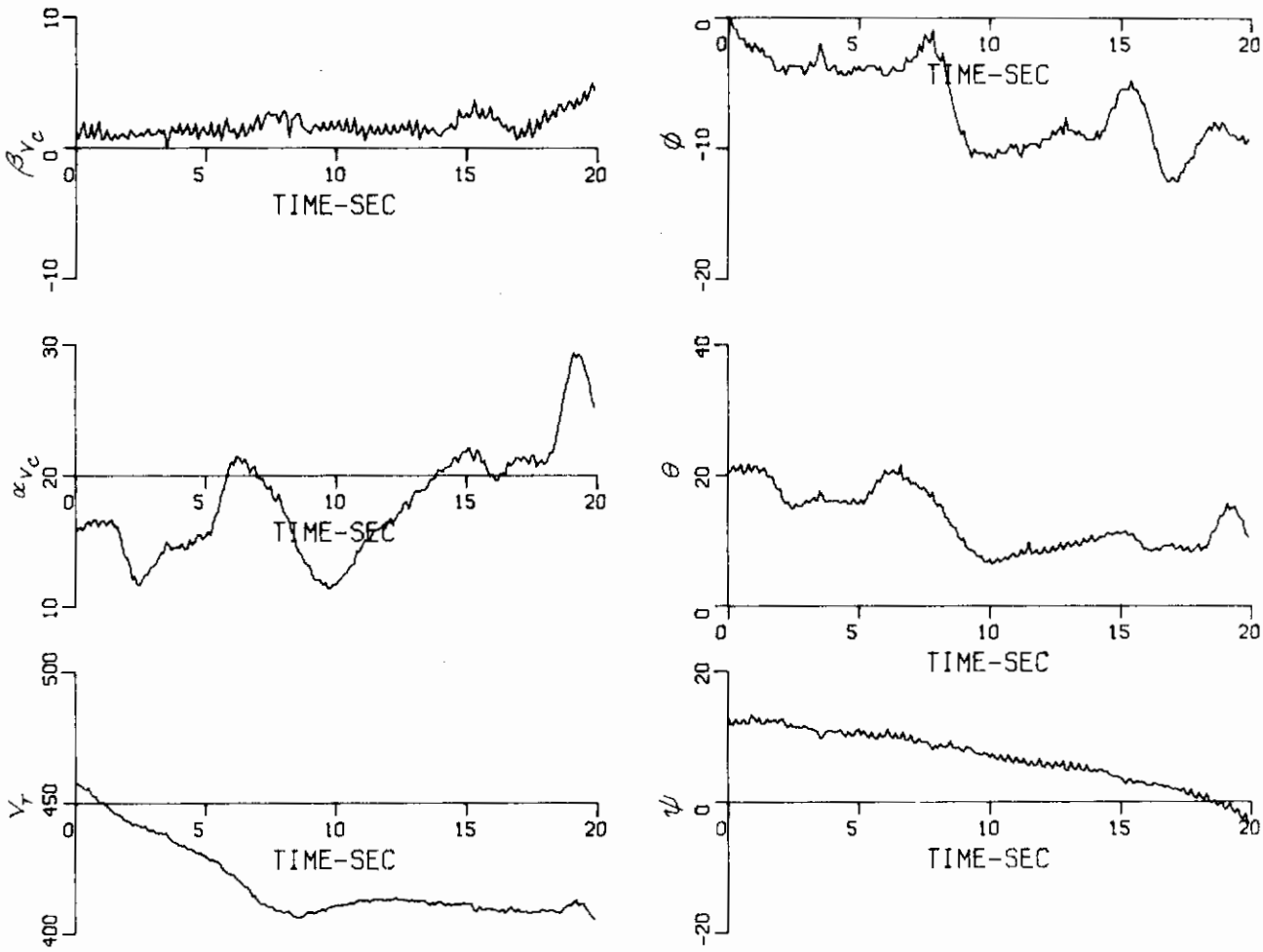

Figure 48 RECORD 9 – STABILATOR INPUTS AT HIGH ANGLES OF ATTACK

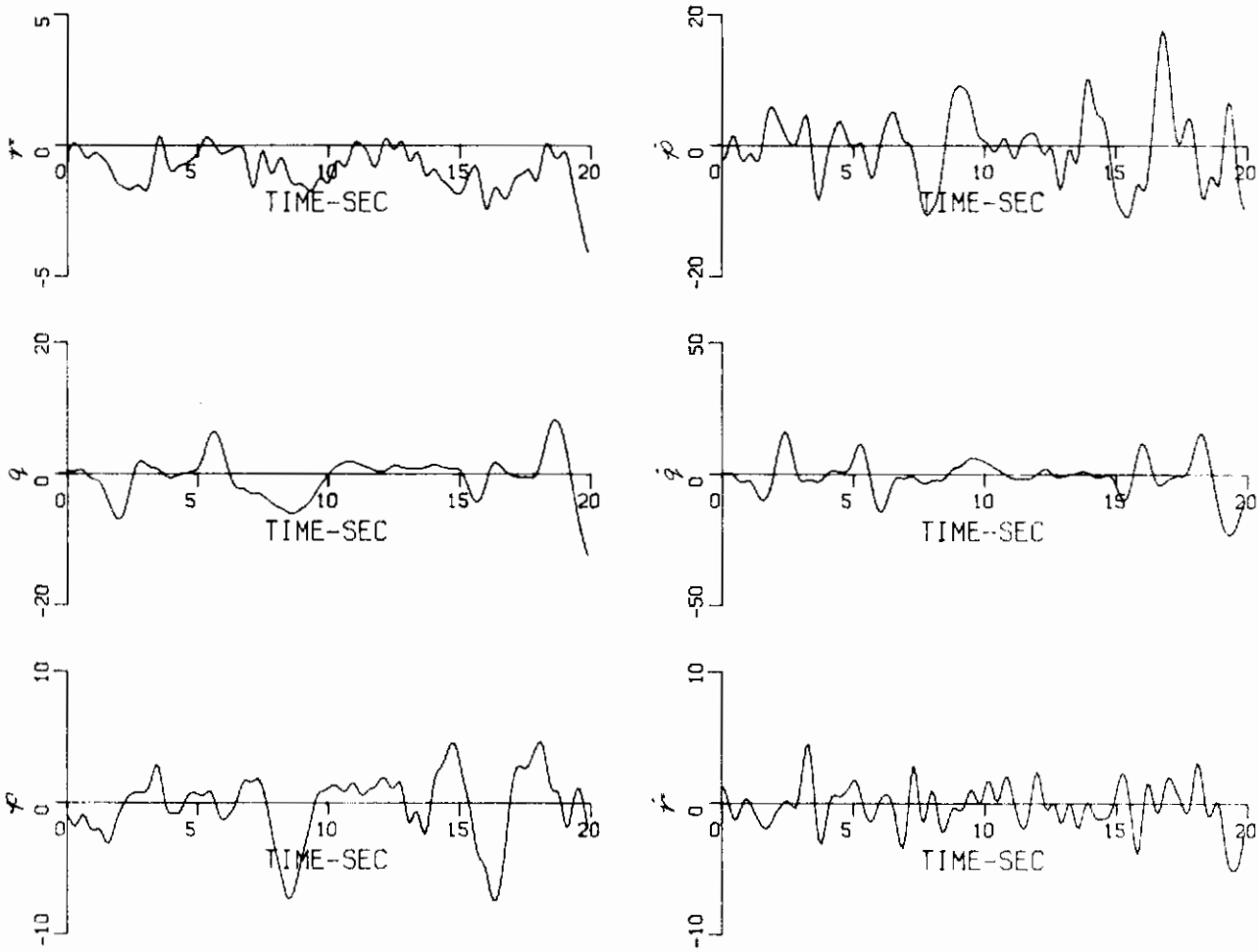

Figure 48 (Continued) RECORD 9 – STABILATOR INPUTS AT HIGH ANGLES OF ATTACK

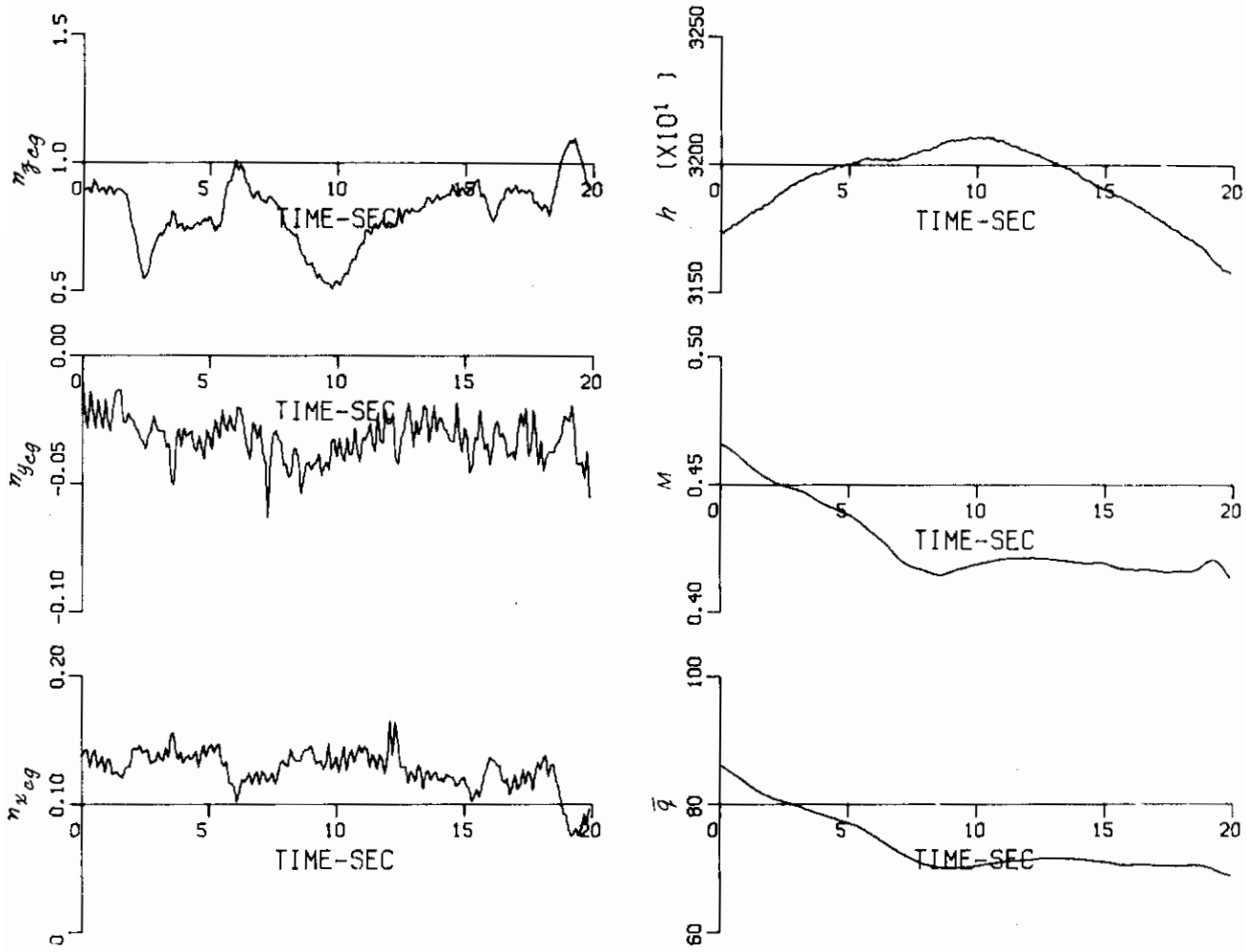

Figure 48 (Continued) RECORD 9 – STABILATOR INPUTS AT HIGH ANGLES OF ATTACK

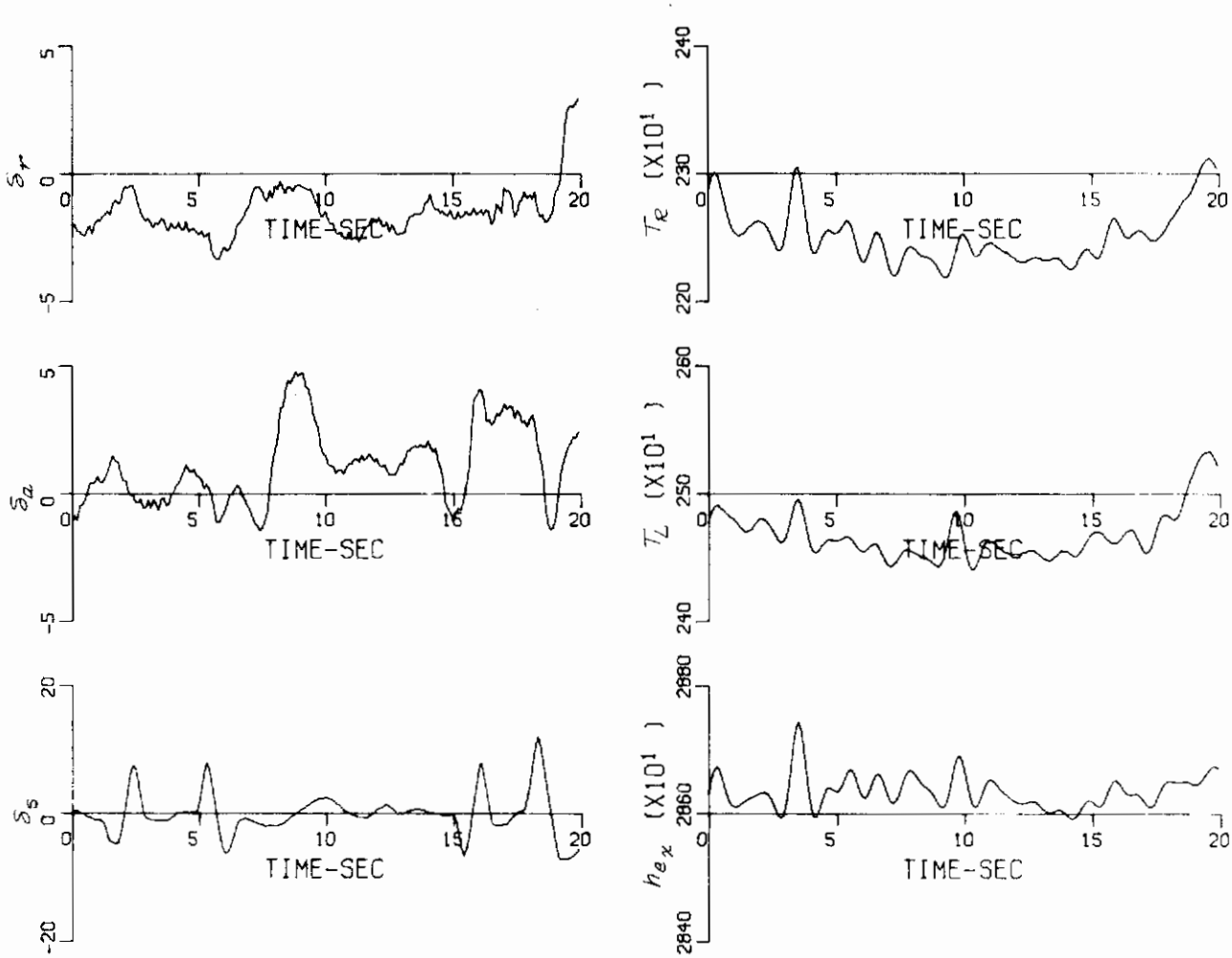

Figure 48 (Continued) RECORD 9 – STABILATOR INPUTS AT HIGH ANGLES OF ATTACK

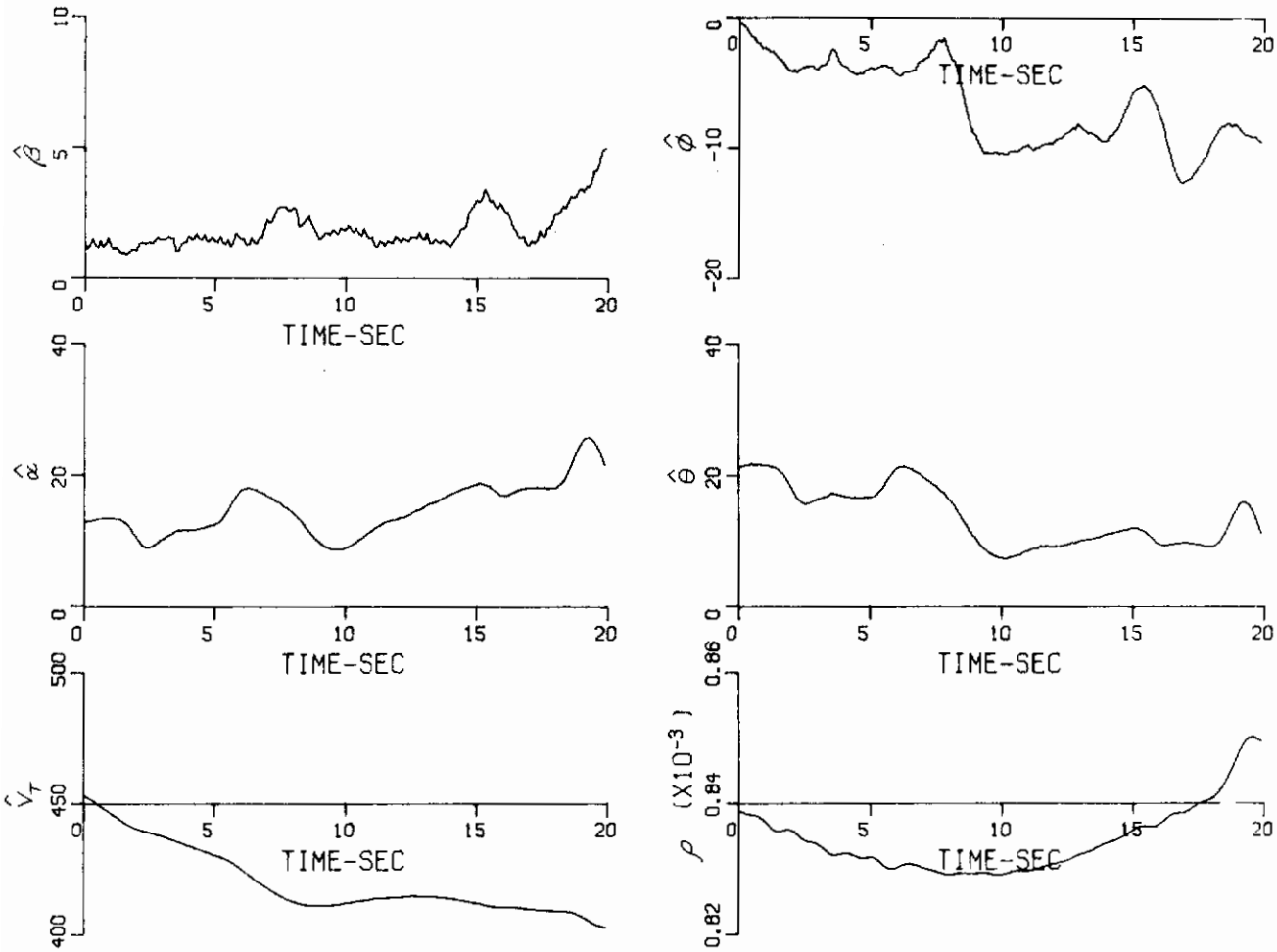

Figure 48 (Continued) RECORD 9 – STABILATOR INPUTS AT HIGH ANGLES OF ATTACK

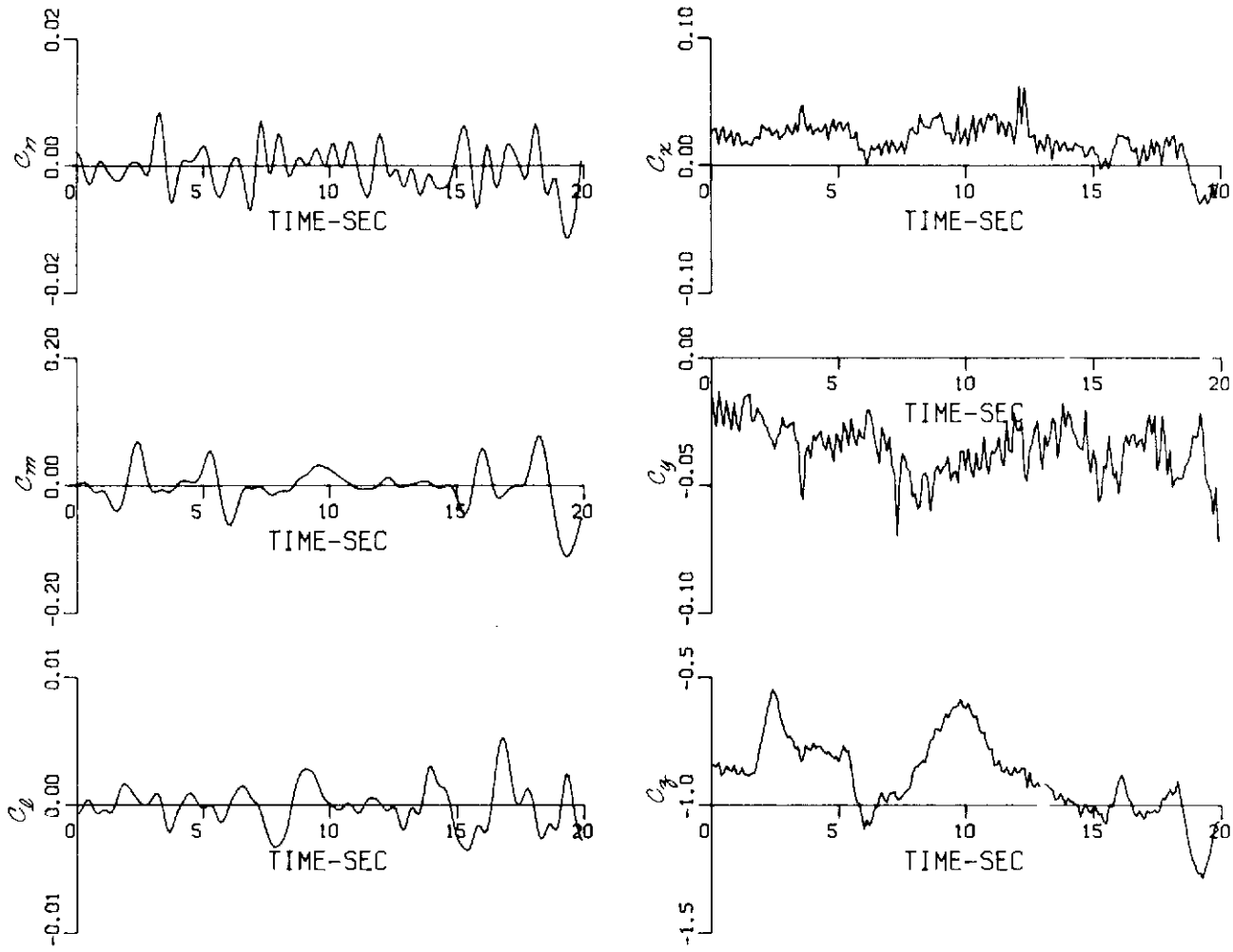

Figure 48 (Continued) RECORD 9 — STABILATOR INPUTS AT HIGH ANGLES OF ATTACK

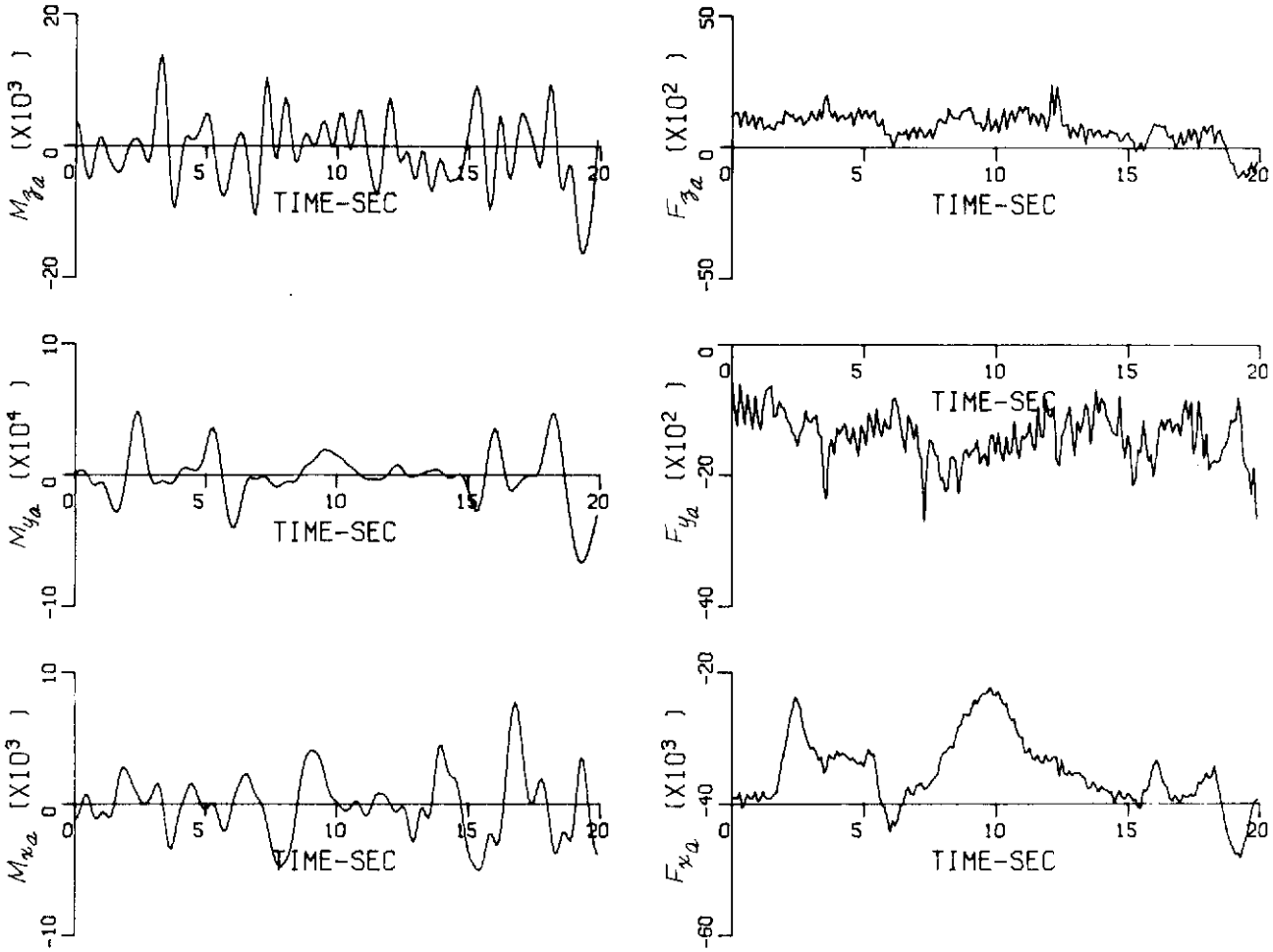

Figure 48 (Concluded) RECORD 9 – STABILATOR INPUTS AT HIGH ANGLES OF ATTACK

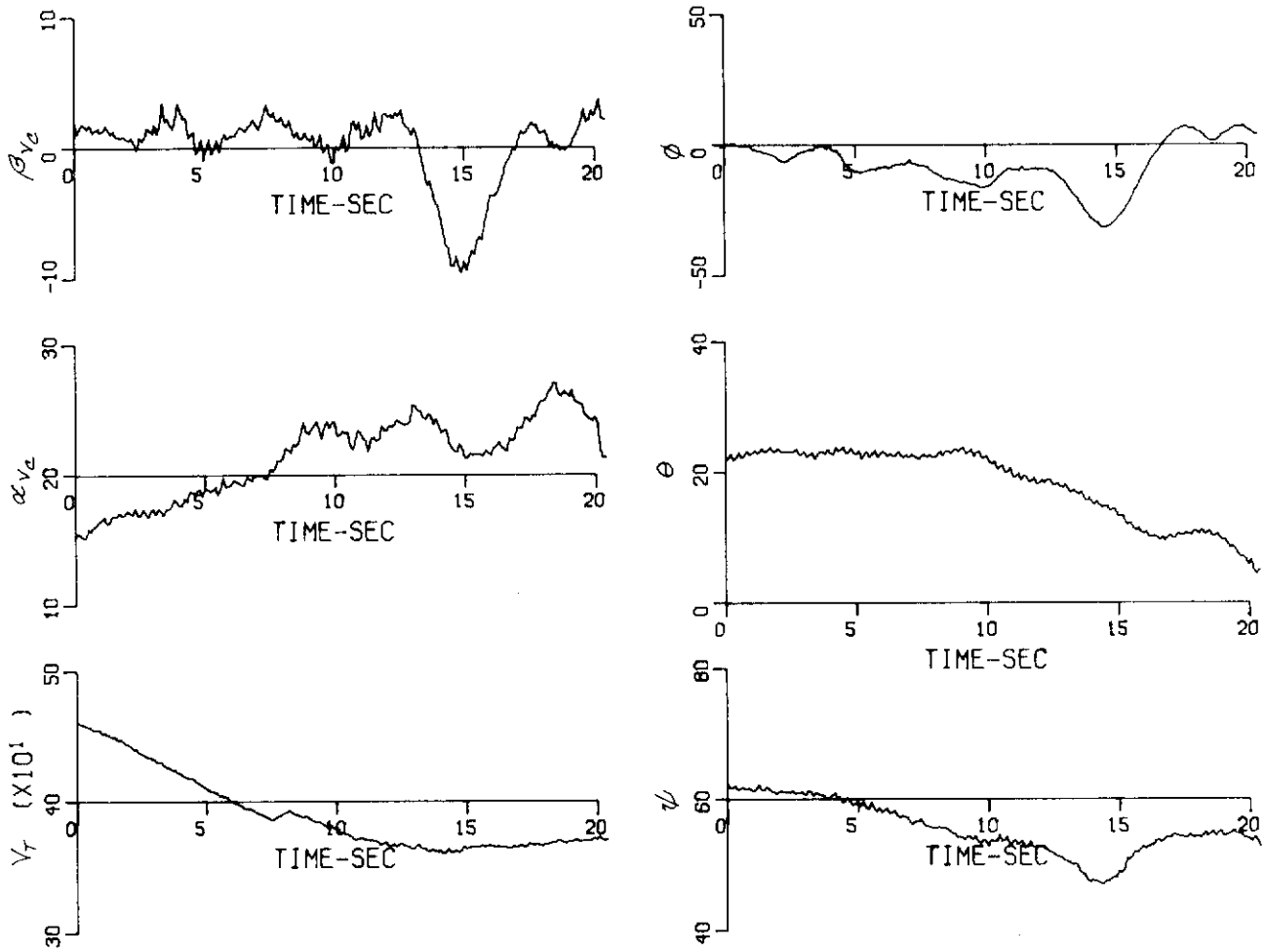

Figure 49 RECORD 10 – AILERON INPUTS AT HIGH ANGLES OF ATTACK

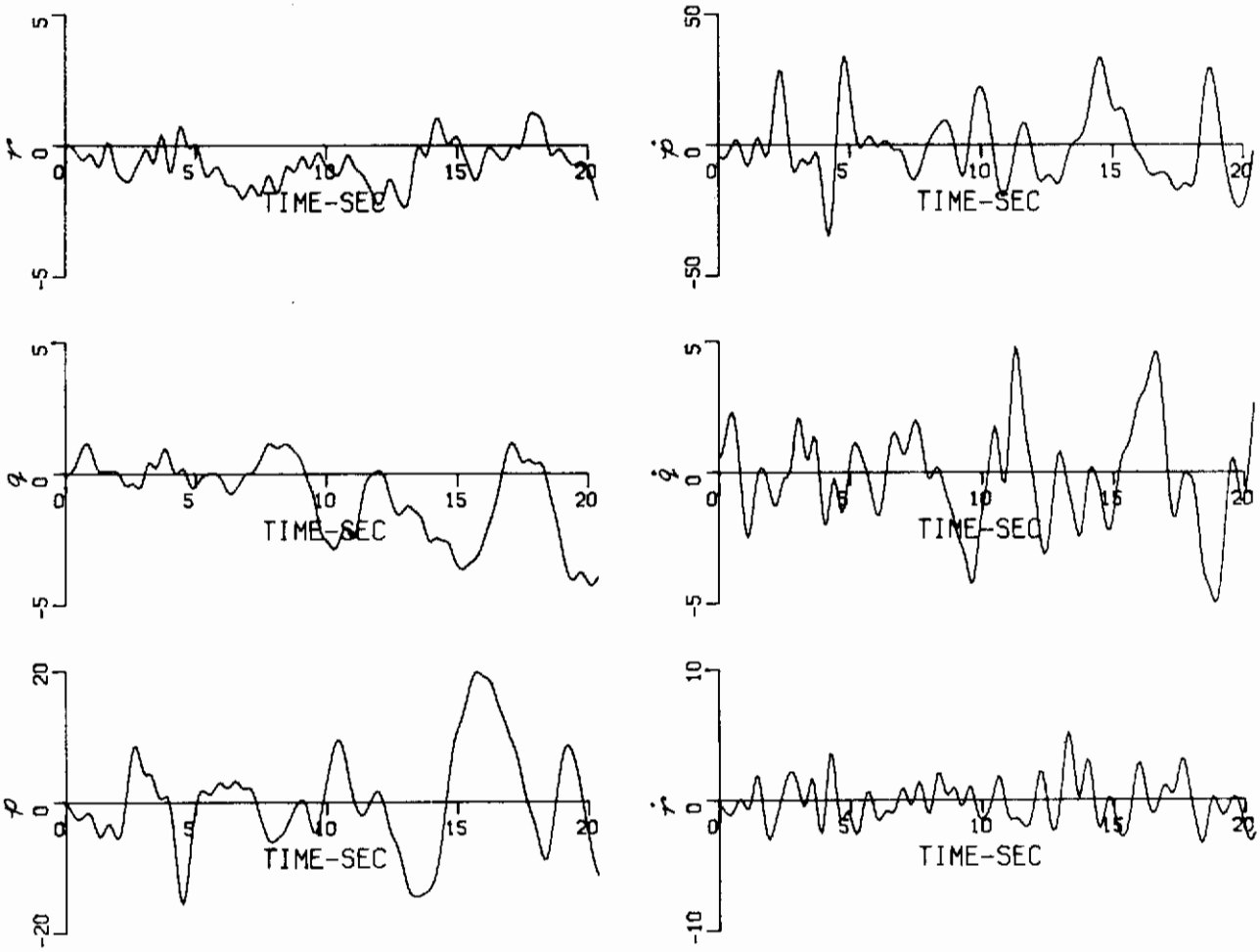

Figure 49 (Continued) RECORD 10 – AILERON INPUTS AT HIGH ANGLES OF ATTACK

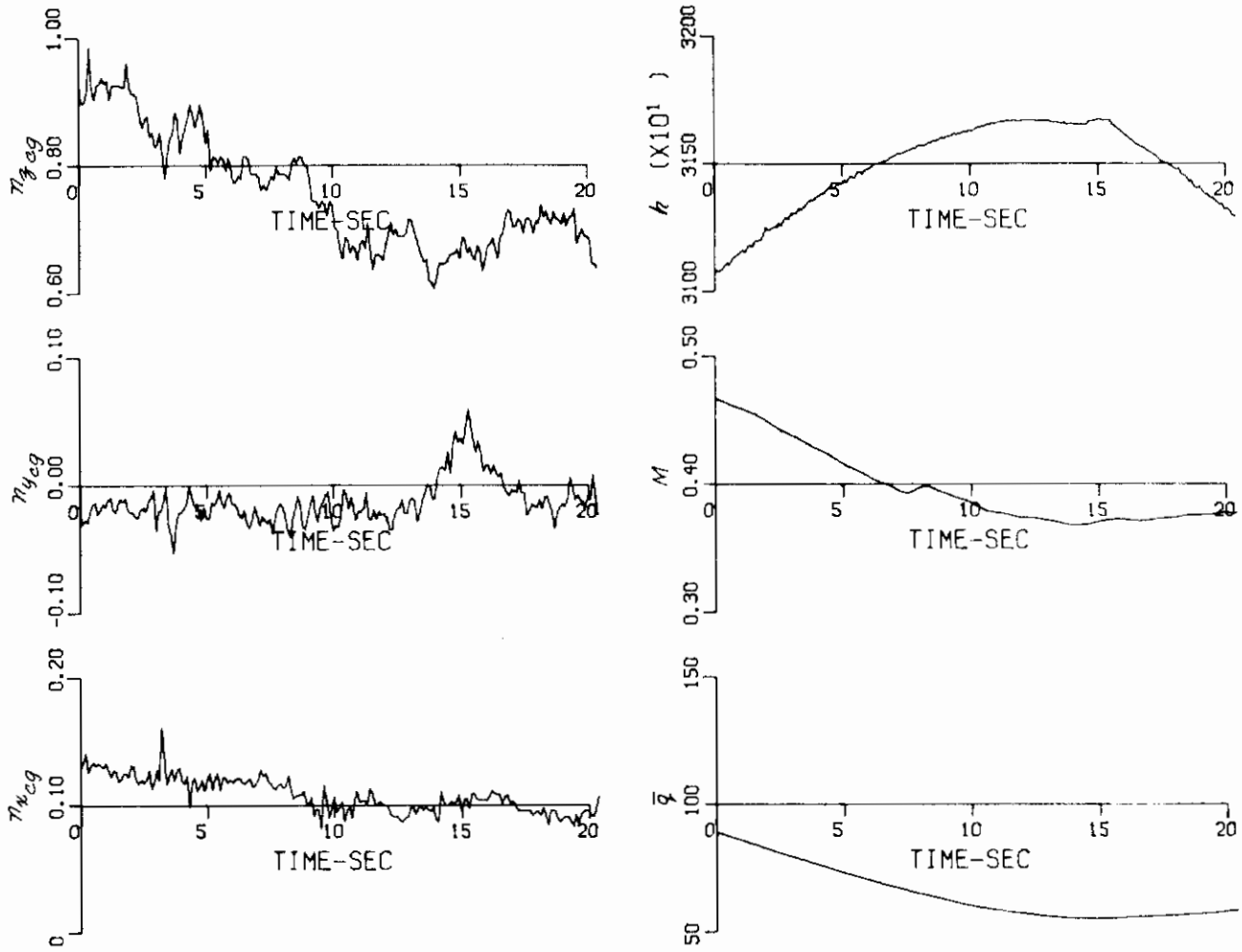

Figure 49 (Continued) RECORD 10 – AILERON INPUTS AT HIGH ANGLES OF ATTACK

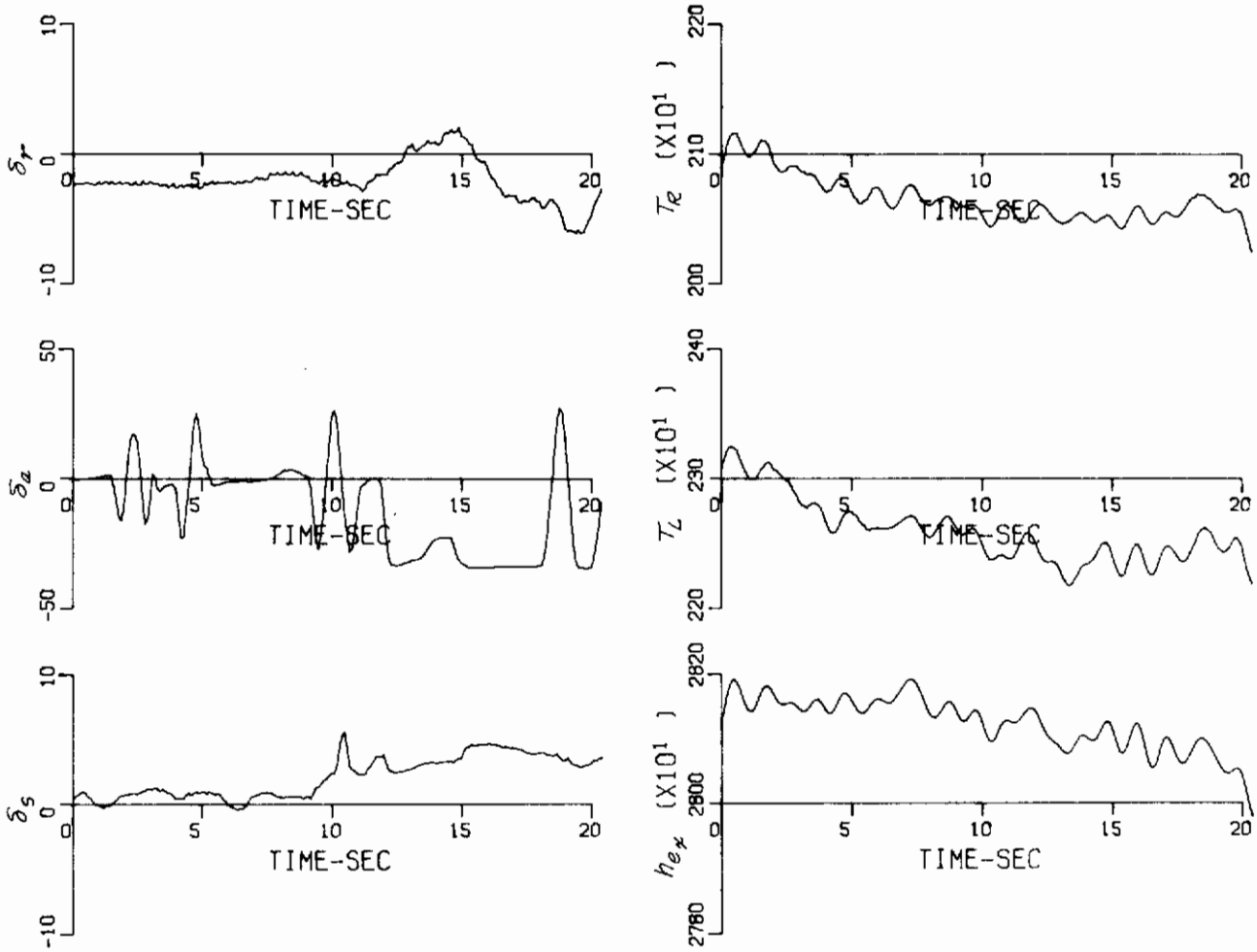

Figure 49 (Continued) RECORD 10 – AILERON INPUTS AT HIGH ANGLES OF ATTACK

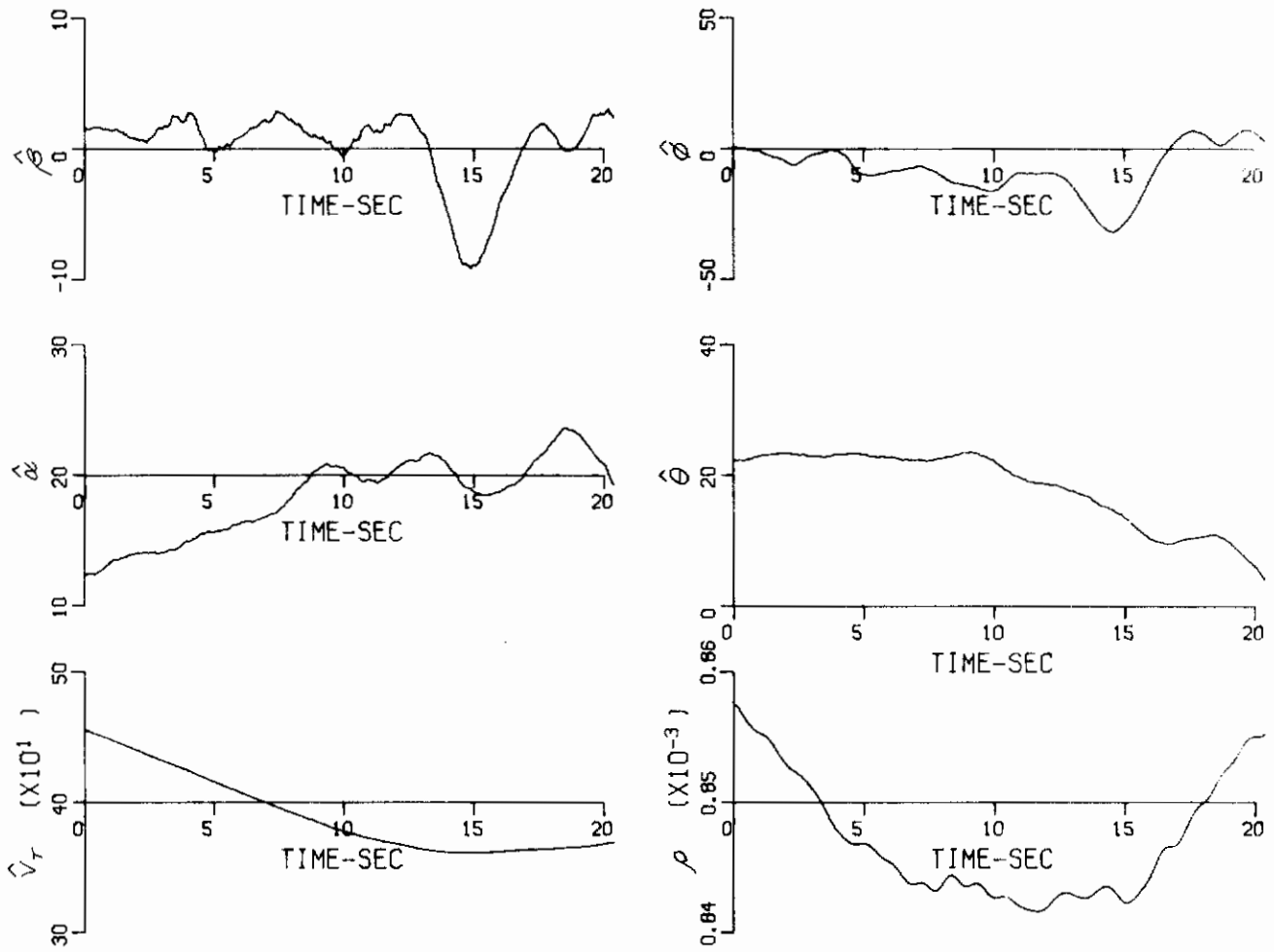

Figure 49 (Continued) RECORD 10 — AILERON INPUTS AT HIGH ANGLES OF ATTACK

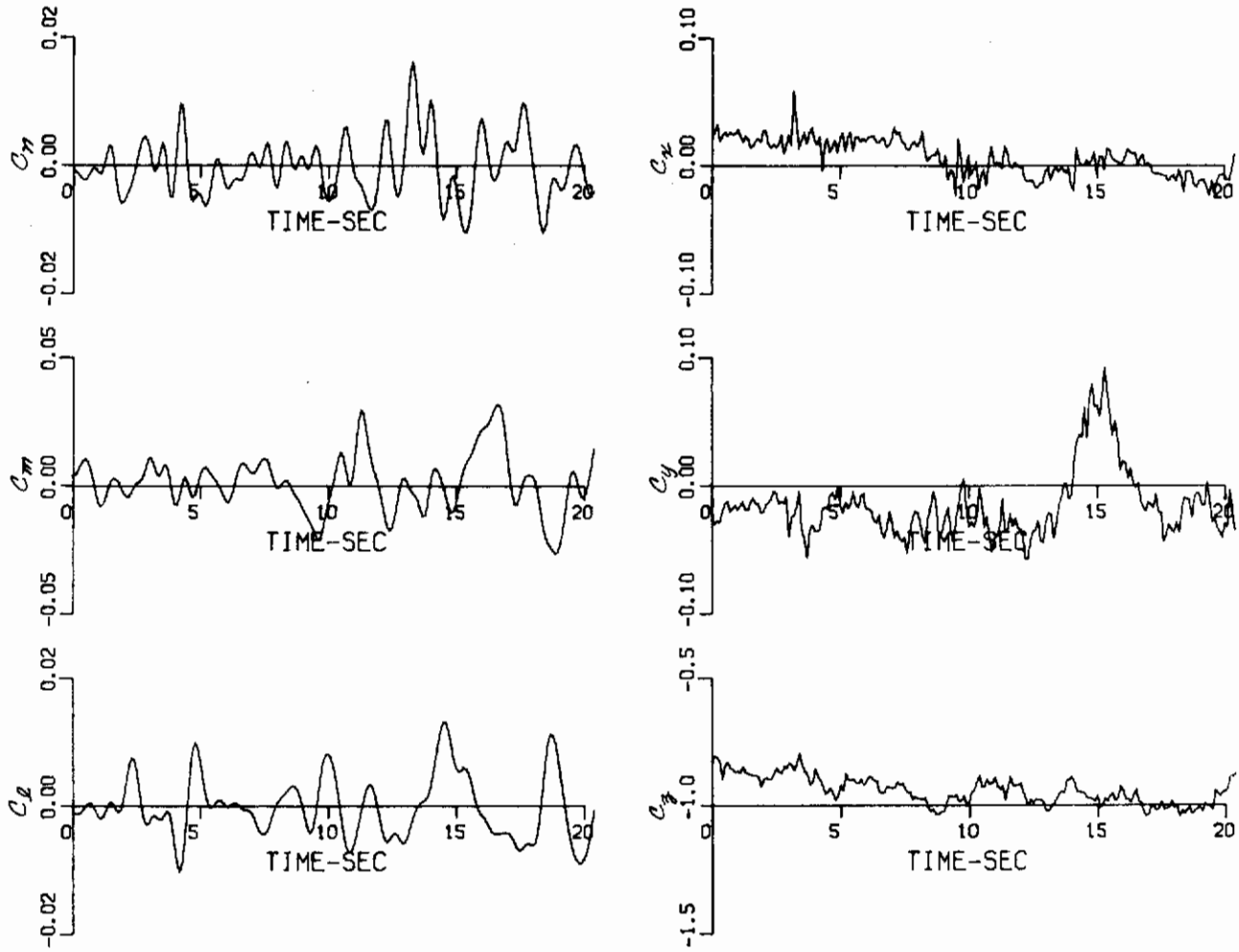

Figure 49 (Continued) RECORD 10 – AILERON INPUTS AT HIGH ANGLES OF ATTACK

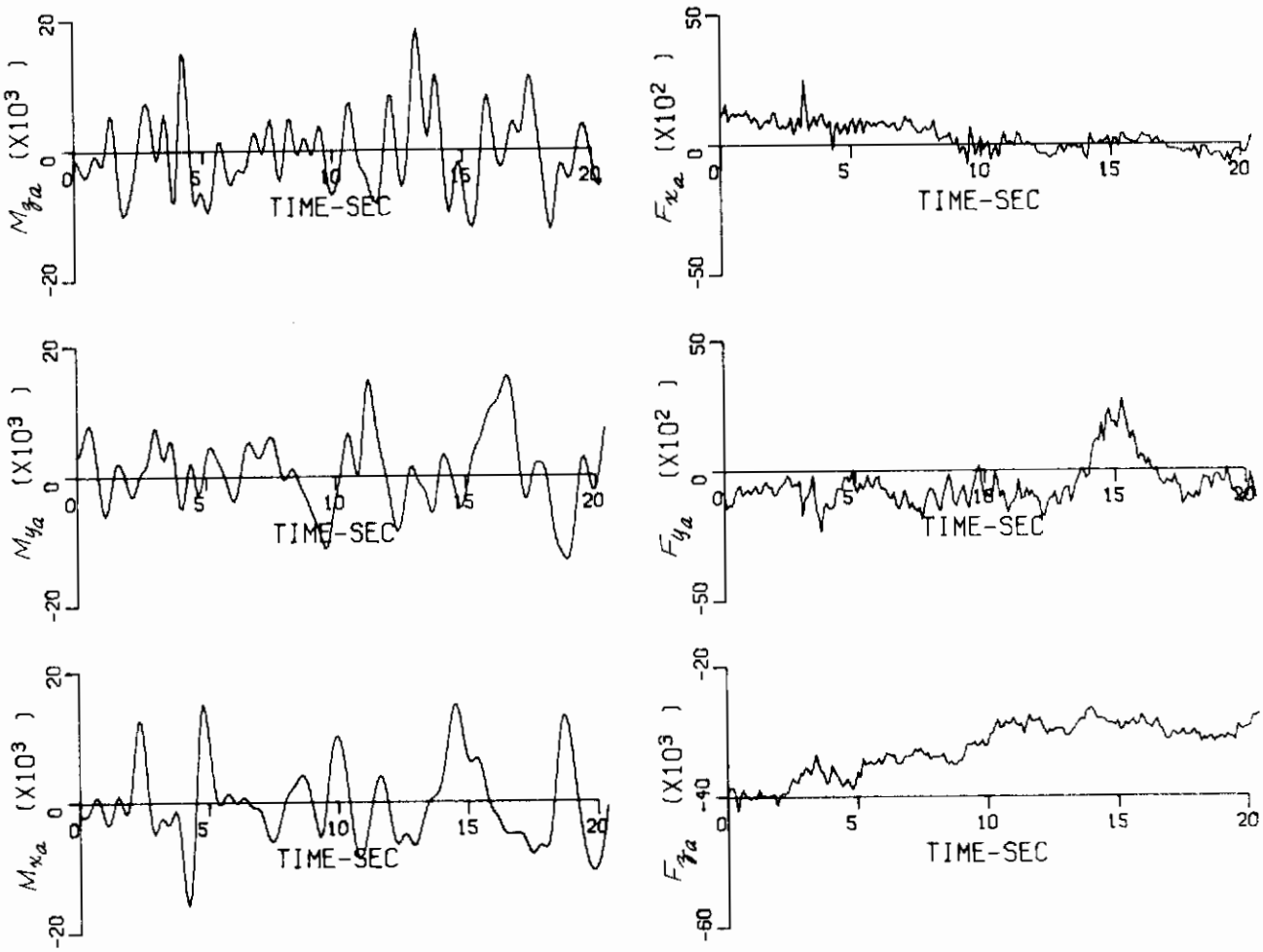

Figure 49 (Concluded) RECORD 10 — AILERON INPUTS AT HIGH ANGLES OF ATTACK

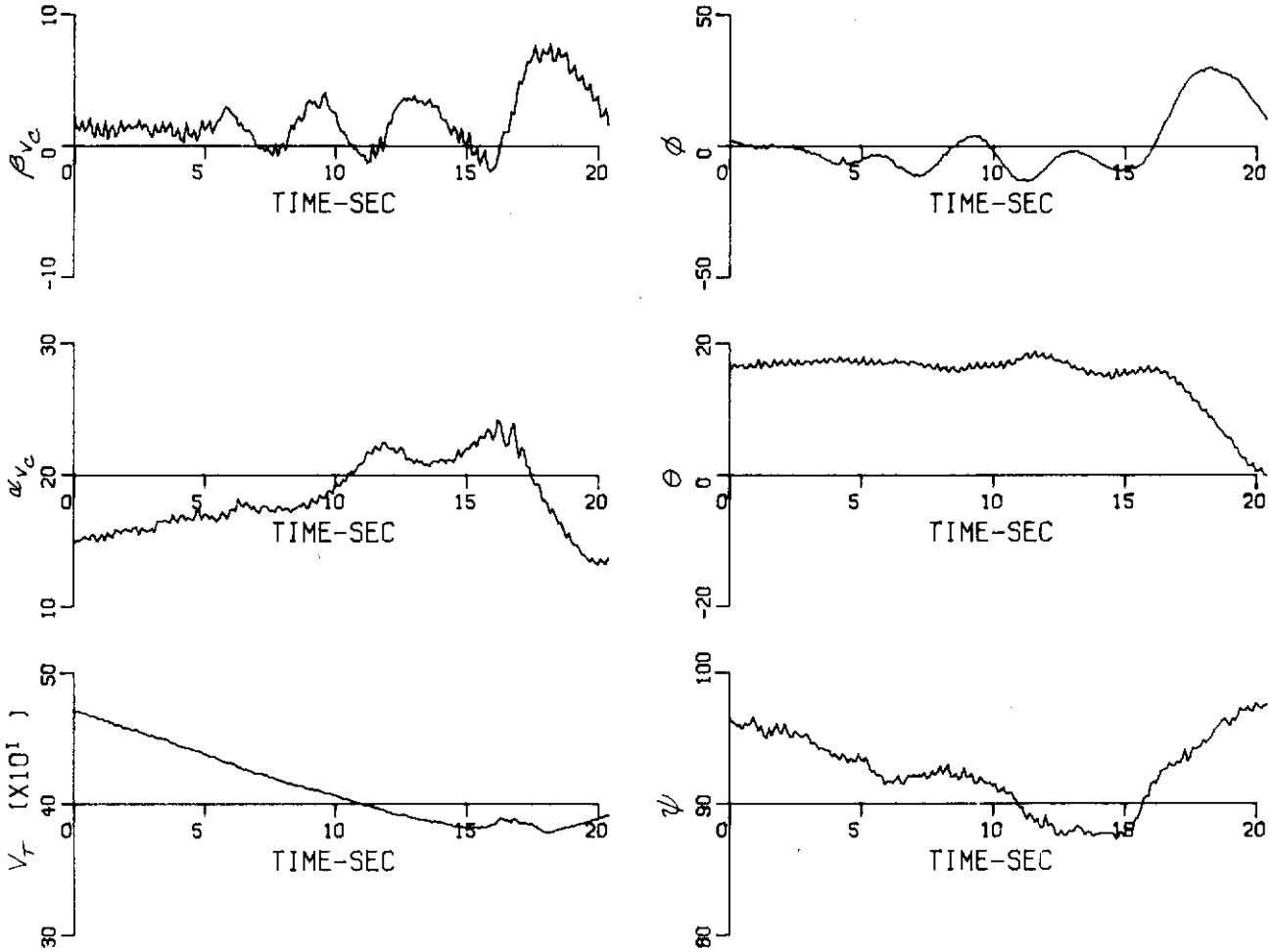

Figure 50 RECORD 11 — RUDDER INPUTS AT HIGH ANGLES OF ATTACK

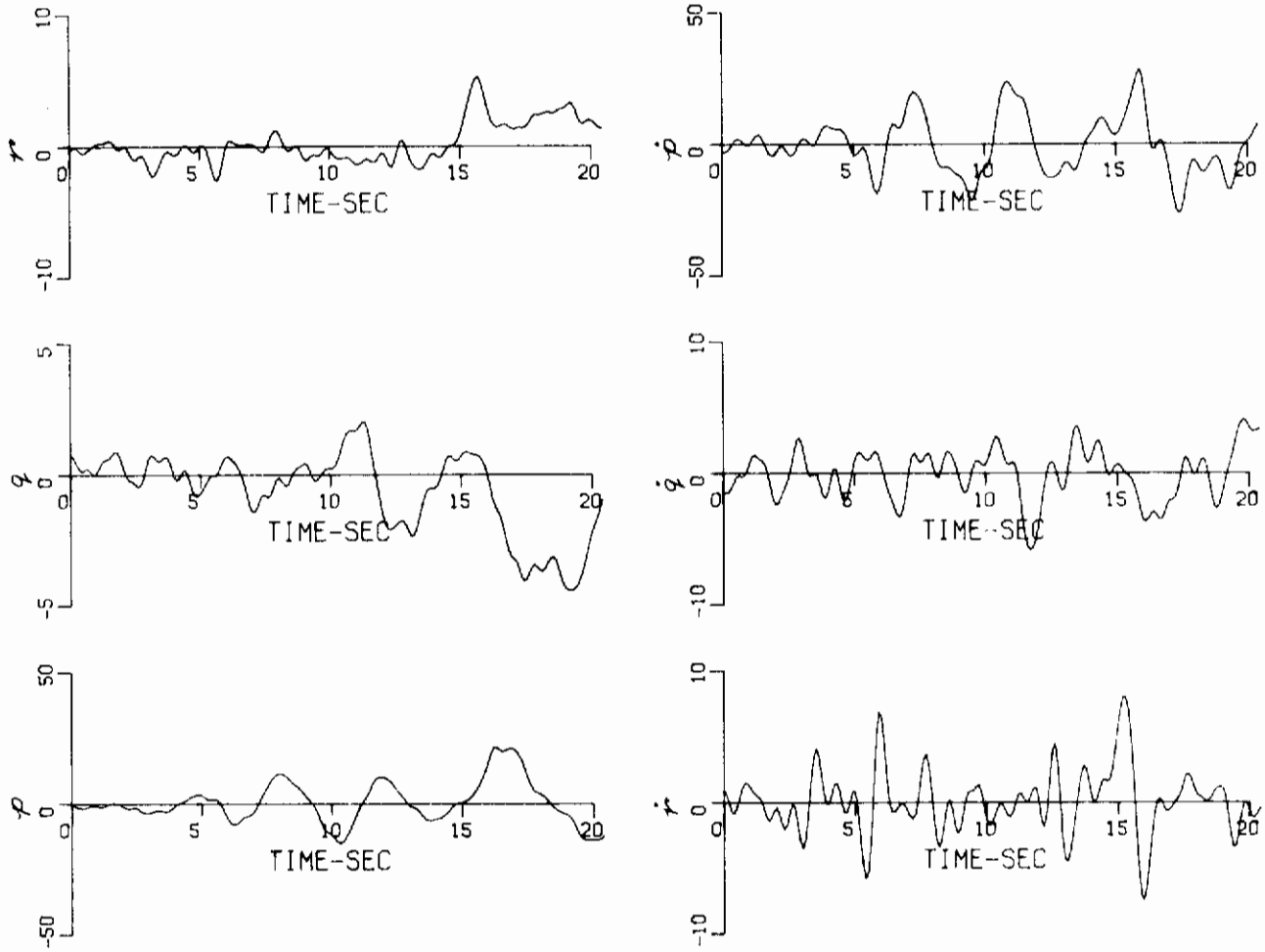

Figure 50 (Continued) RECORD 11 – RUDDER INPUTS AT HIGH ANGLES OF ATTACK

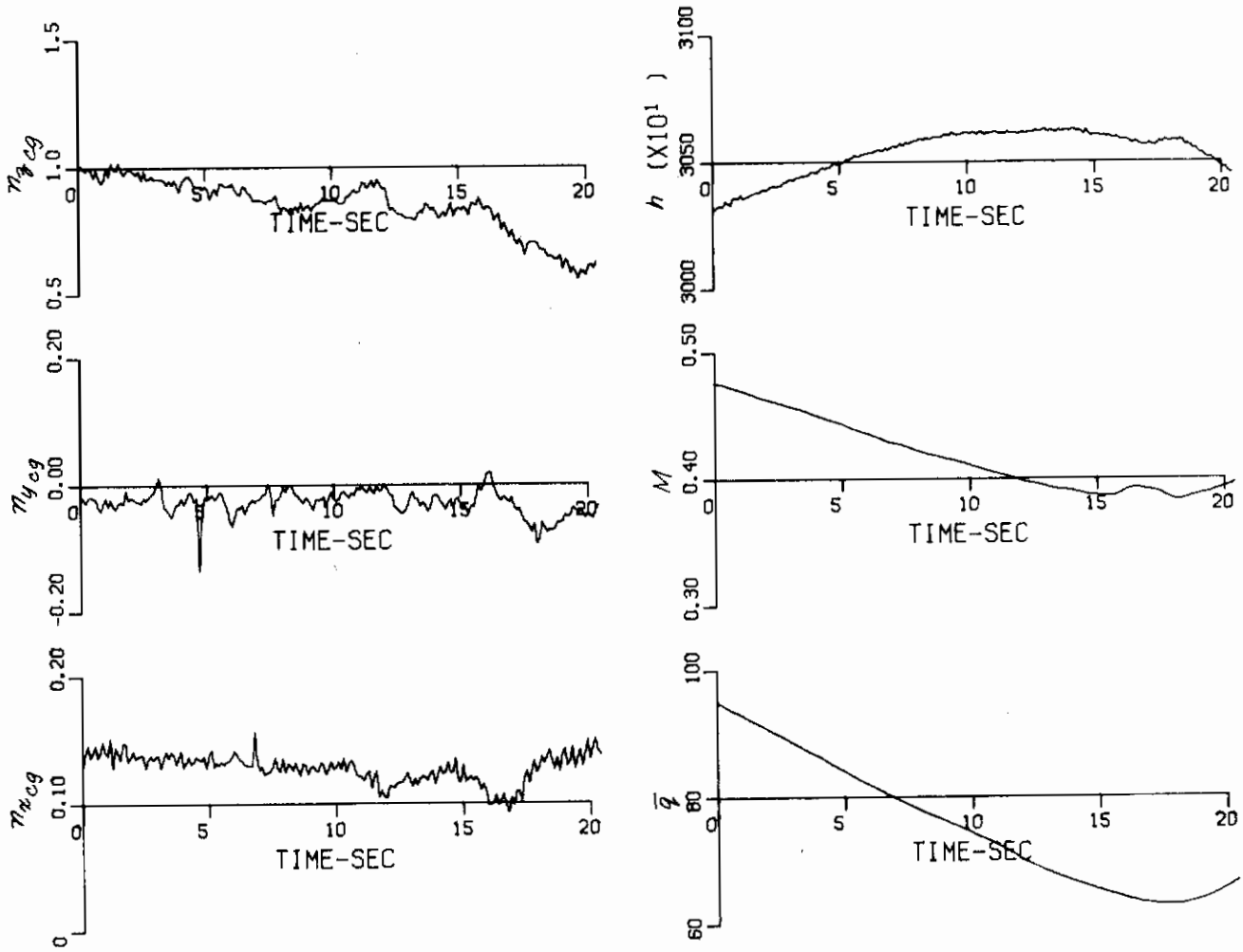

Figure 50 (Continued) RECORD 11 -- RUDDER INPUTS AT HIGH ANGLES OF ATTACK

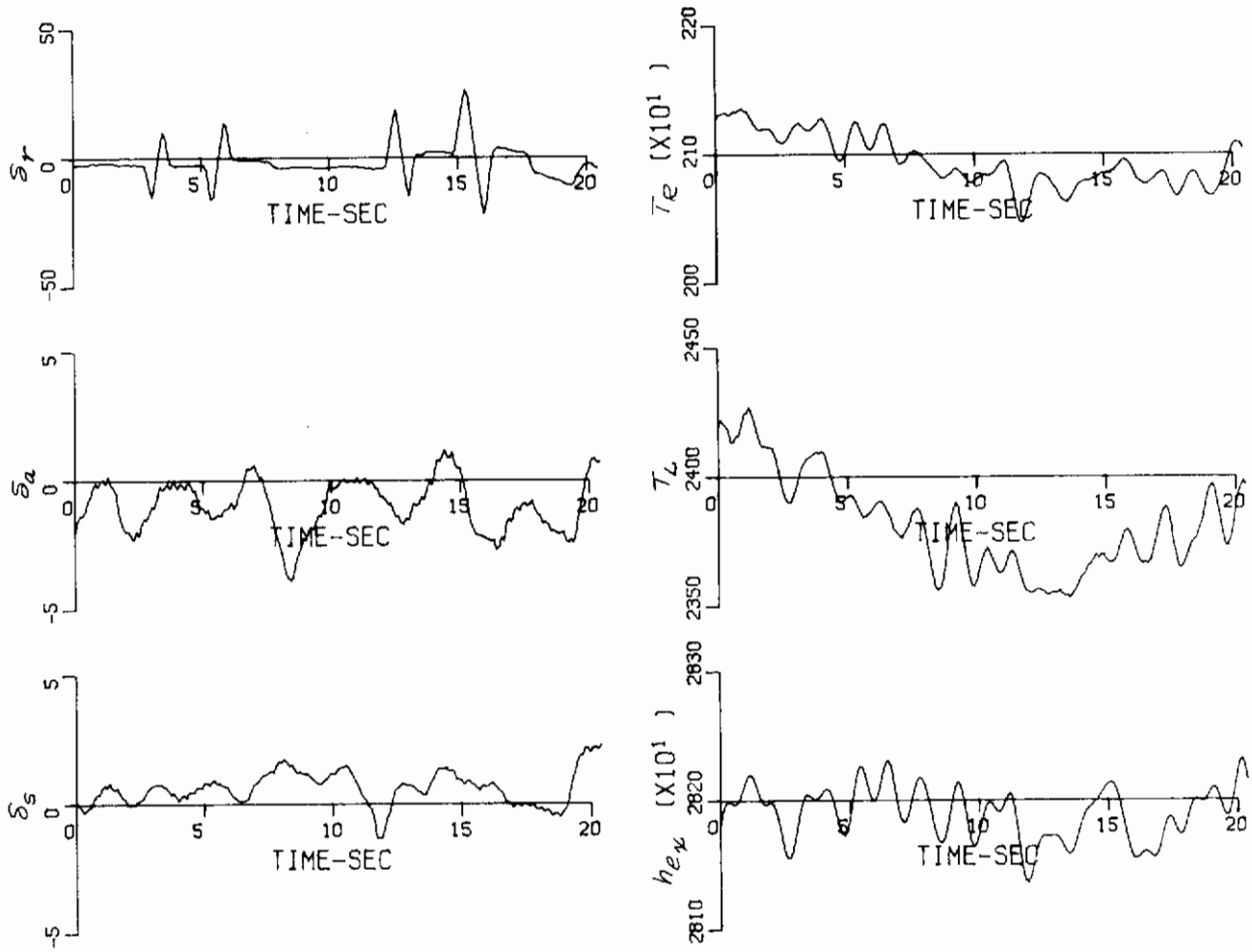

Figure 50 (Continued) RECORD 11 – RUDDER INPUTS AT HIGH ANGLES OF ATTACK

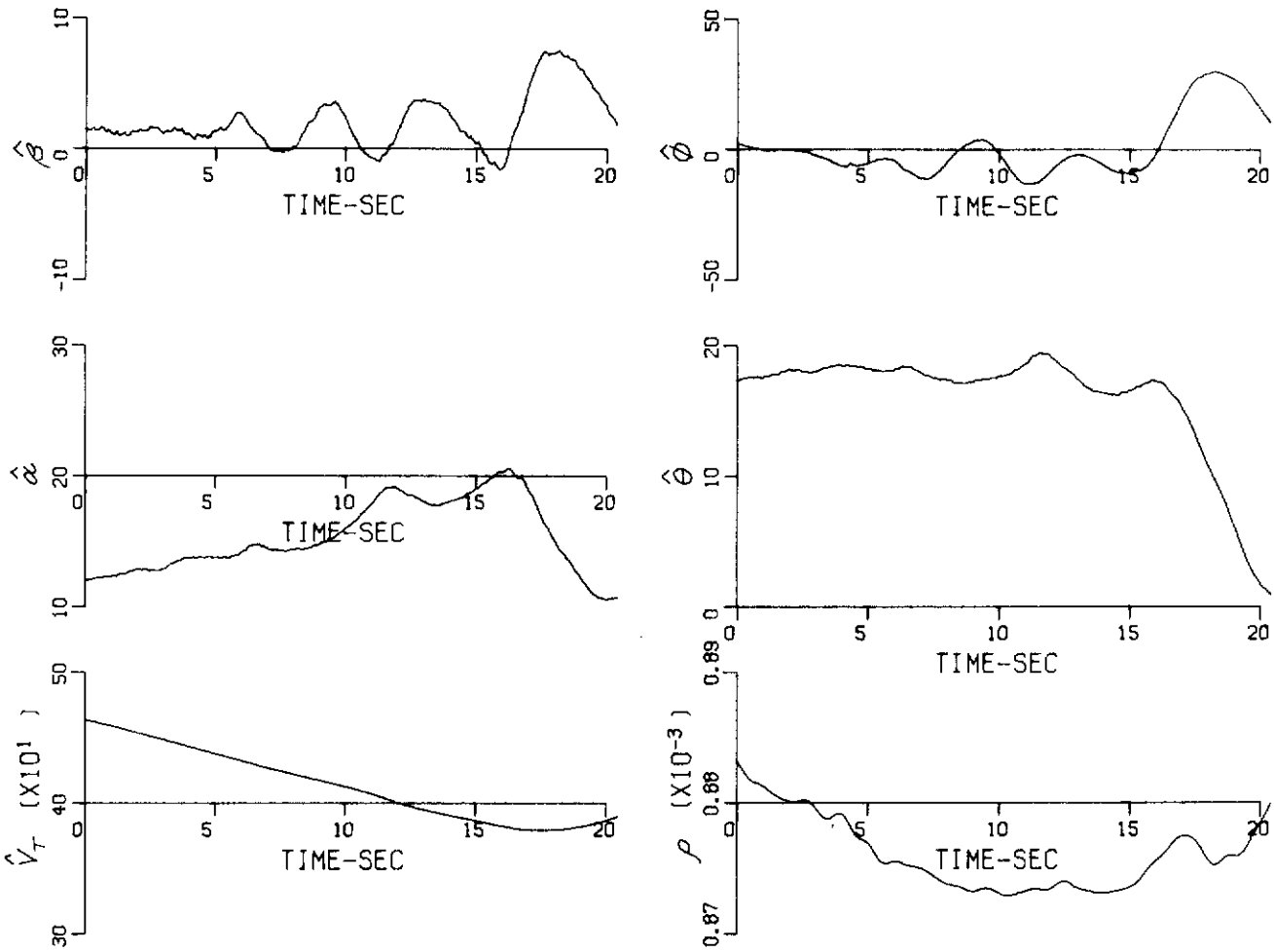

Figure 50 (Continued) RECORD 11 – RUDDER INPUTS AT HIGH ANGLES OF ATTACK

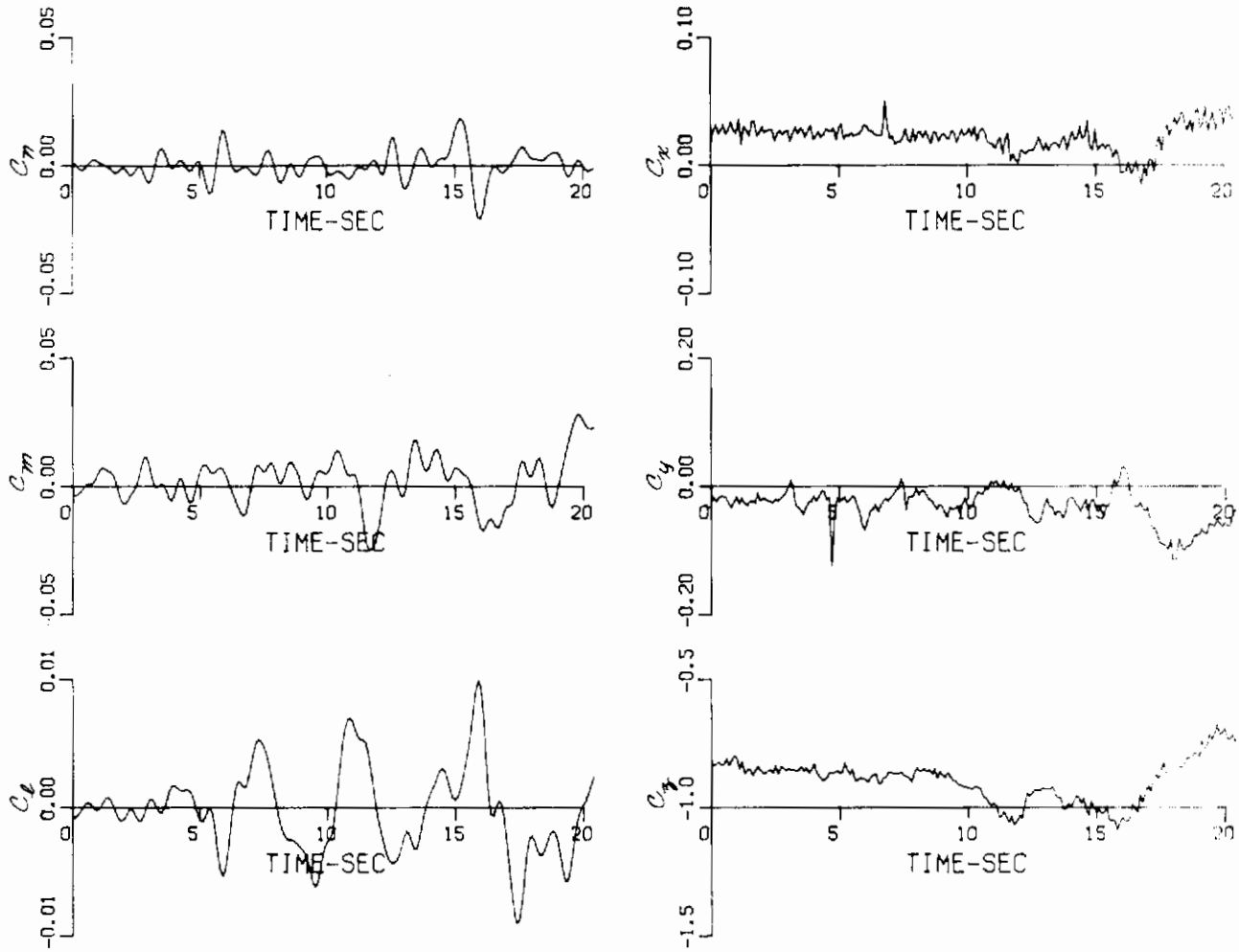

Figure 50 (Continued) RECORD 11 – RUDDER INPUTS AT HIGH ANGLES OF ATTACK

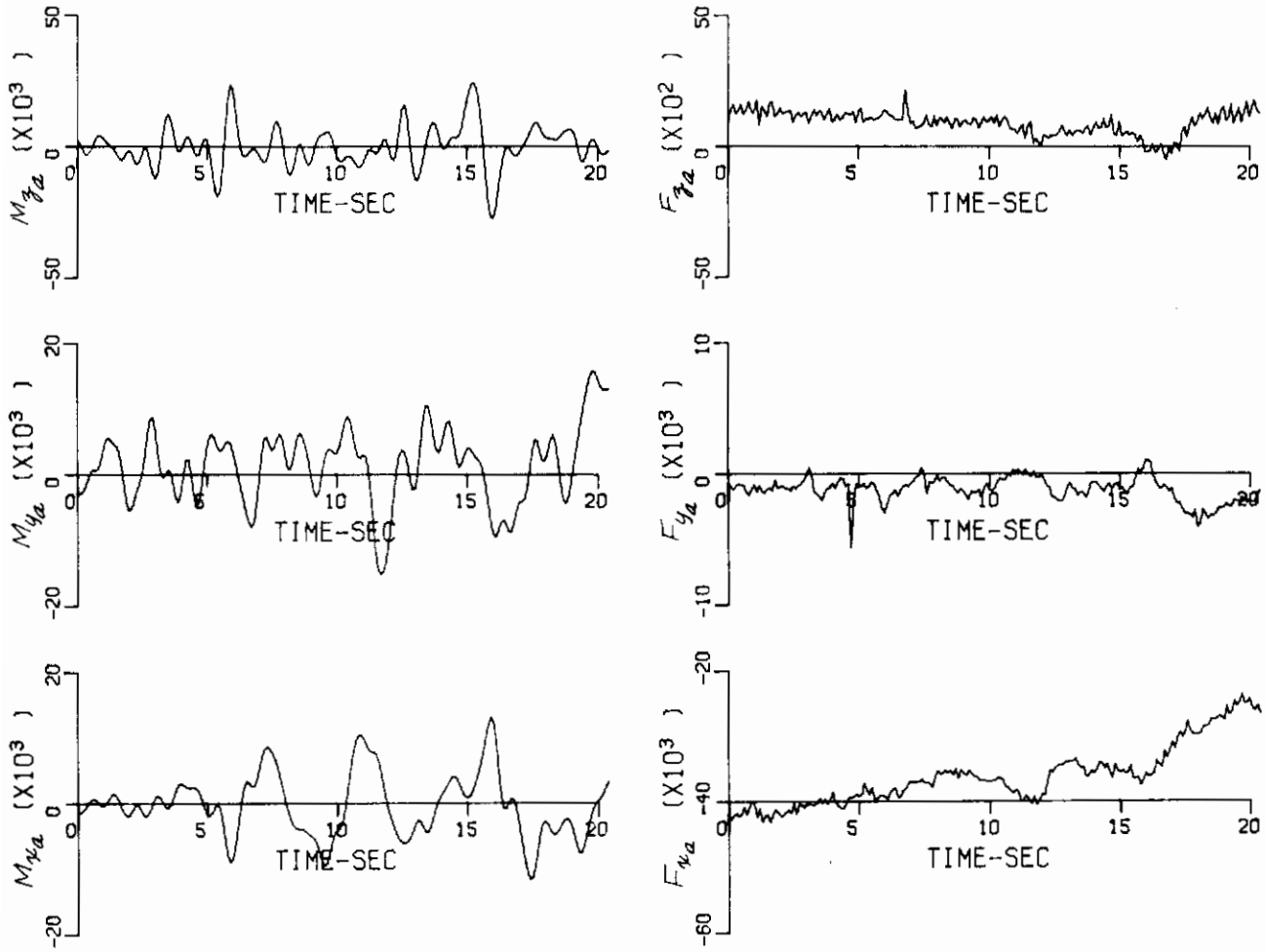

Figure 50 (Concluded) RECORD 11 — RUDDER INPUTS AT HIGH ANGLES OF ATTACK

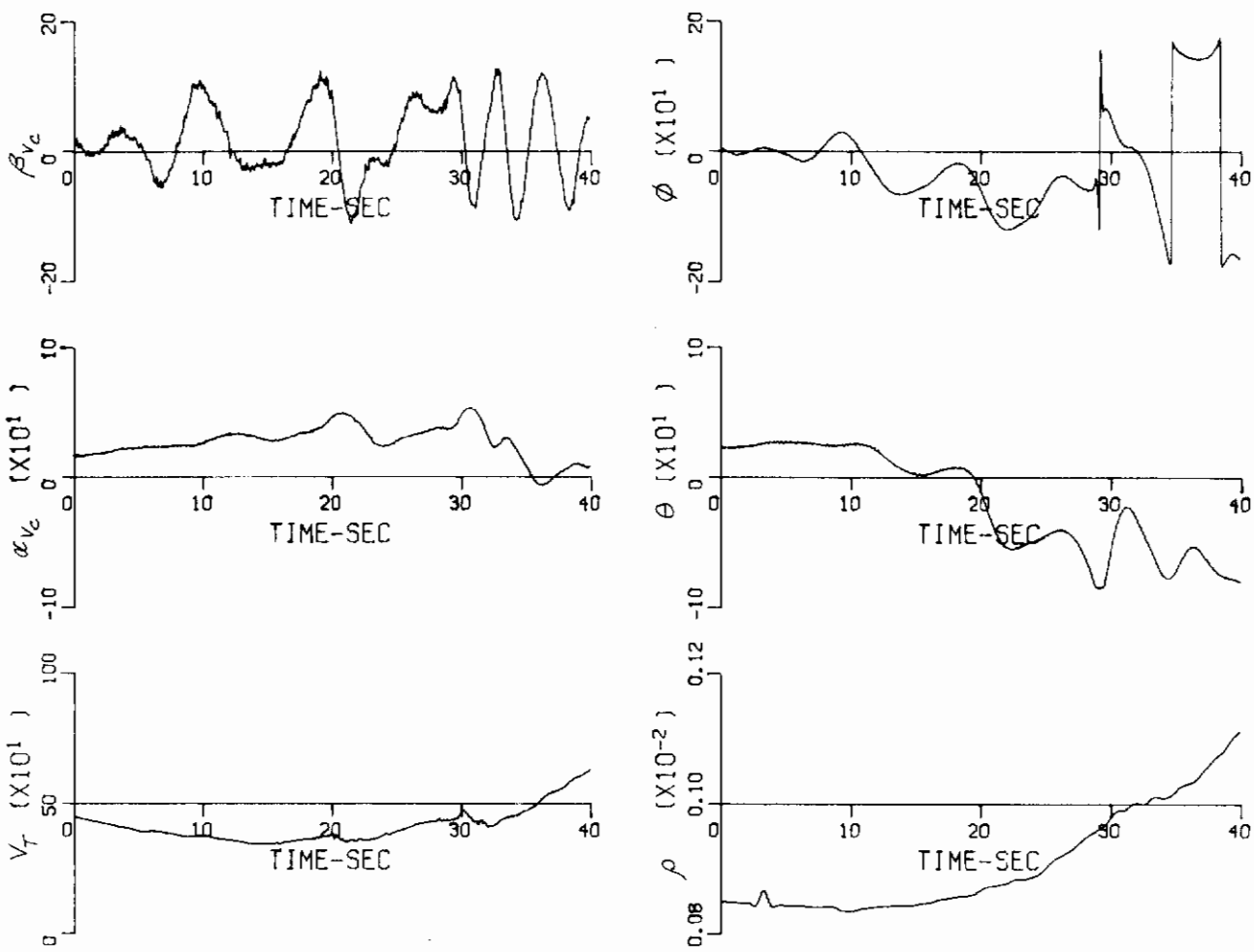

Figure 51 RECORD 14 – ROLLING DEPARTURE FROM A NORMAL STALL ENTRY

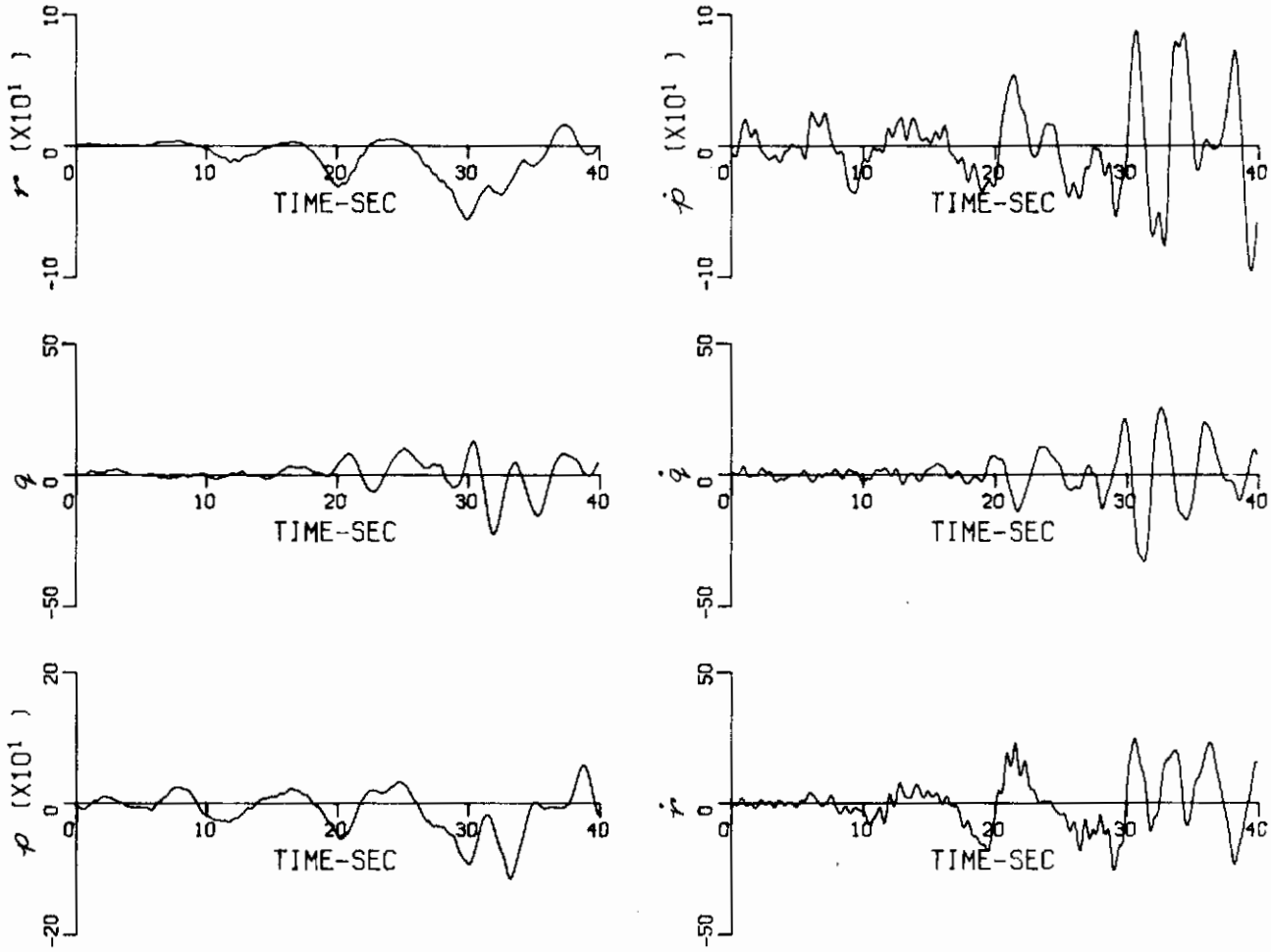

Figure 51 (Continued) RECORD 14 – ROLLING DEPARTURE FROM A NORMAL STALL ENTRY

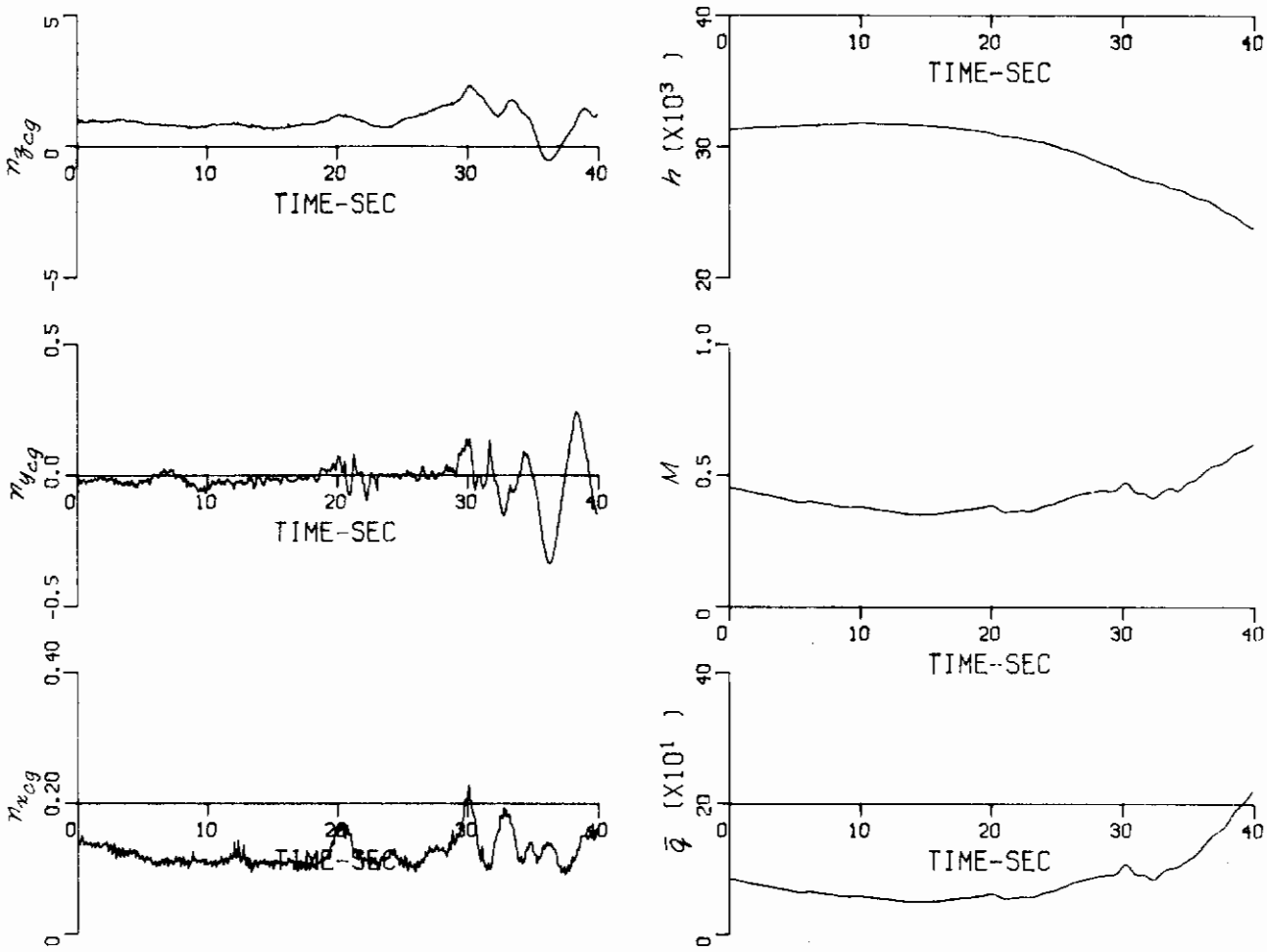

Figure 51 (Continued) RECORD 14 – ROLLING DEPARTURE FROM A NORMAL STALL ENTRY

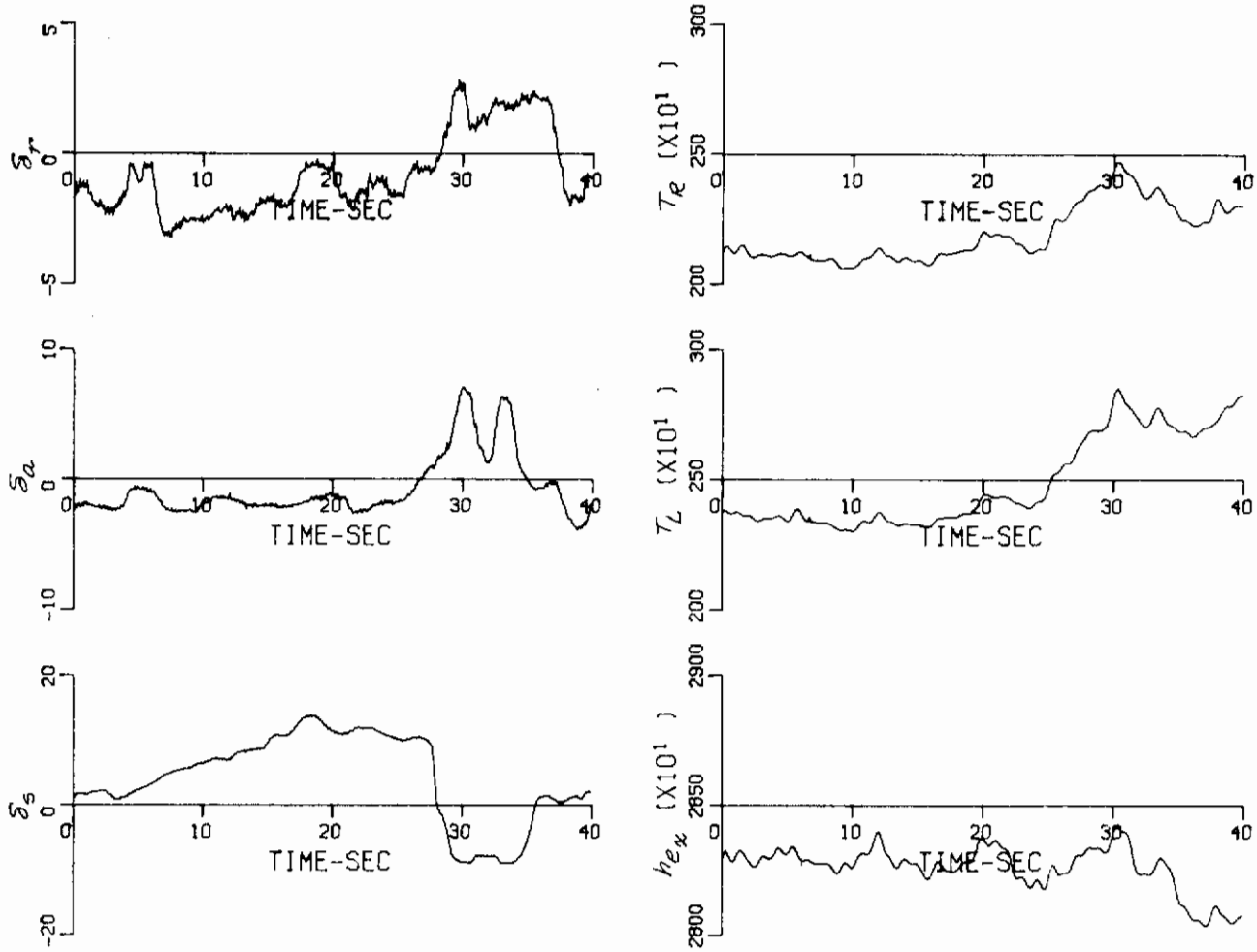

Figure 51 (Continued) RECORD 14 – ROLLING DEPARTURE FROM A NORMAL STALL ENTRY

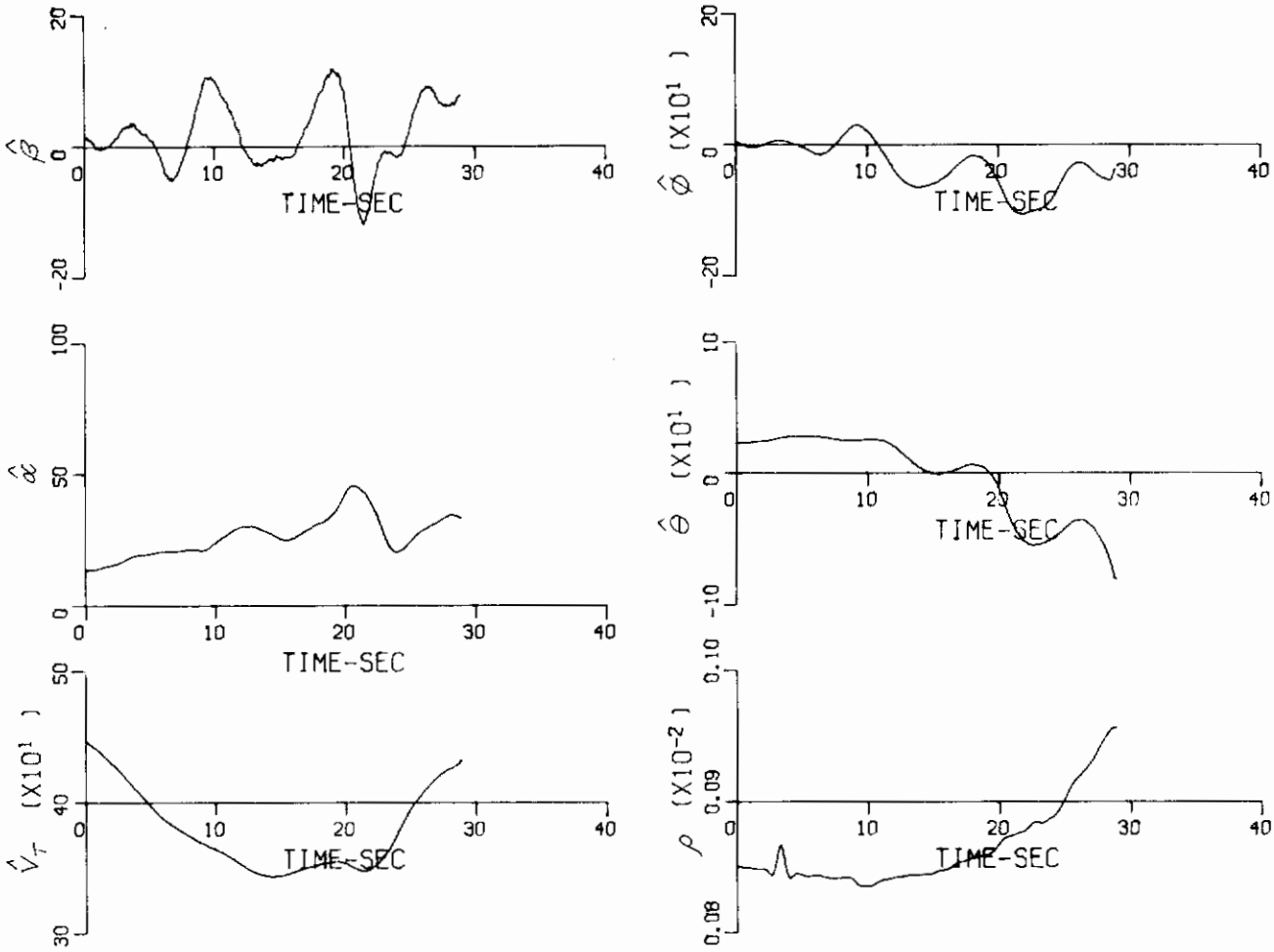

Figure 51 (Continued) RECORD 14 – ROLLING DEPARTURE FROM A NORMAL STALL ENTRY

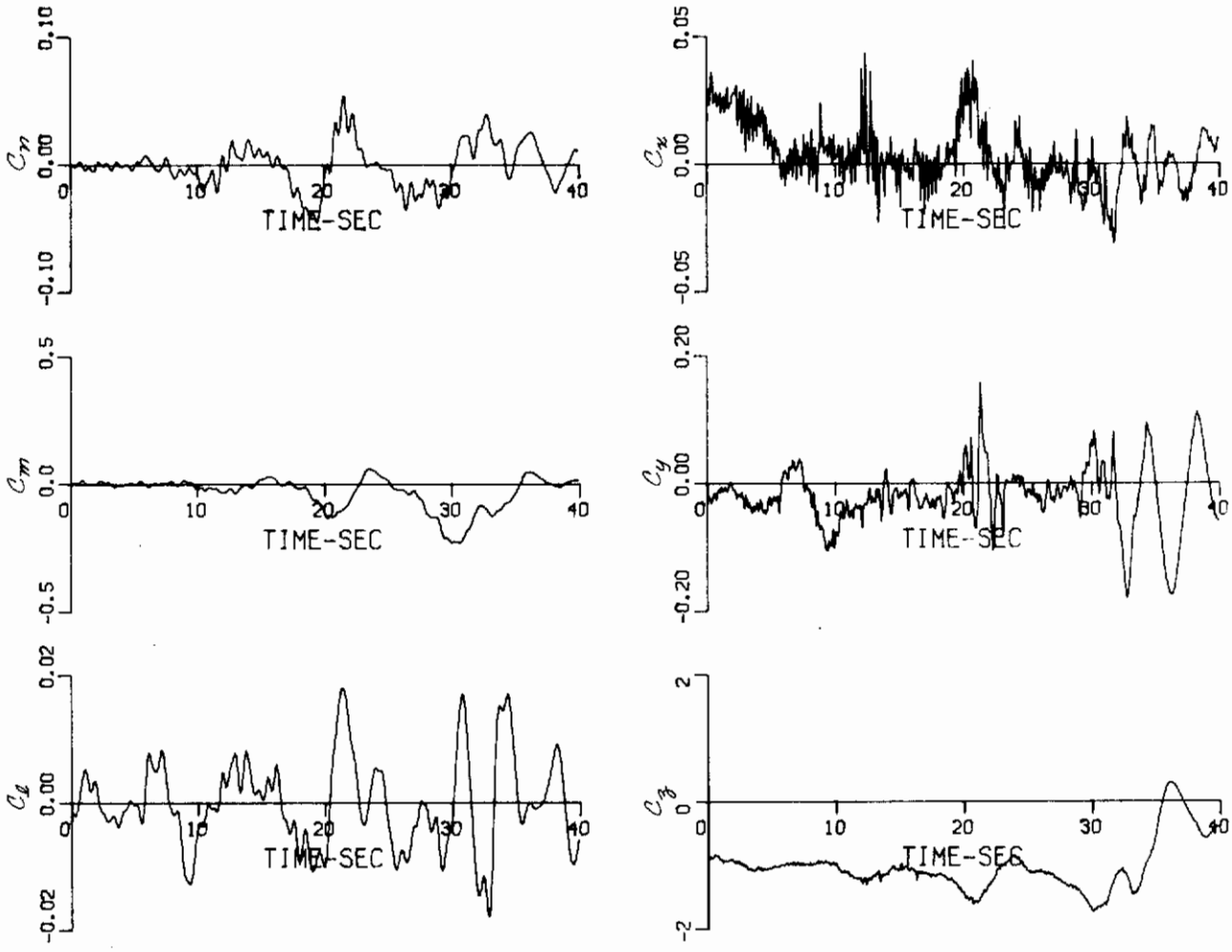

Figure 51 (Continued) RECORD 14 – ROLLING DEPARTURE FROM A NORMAL STALL ENTRY

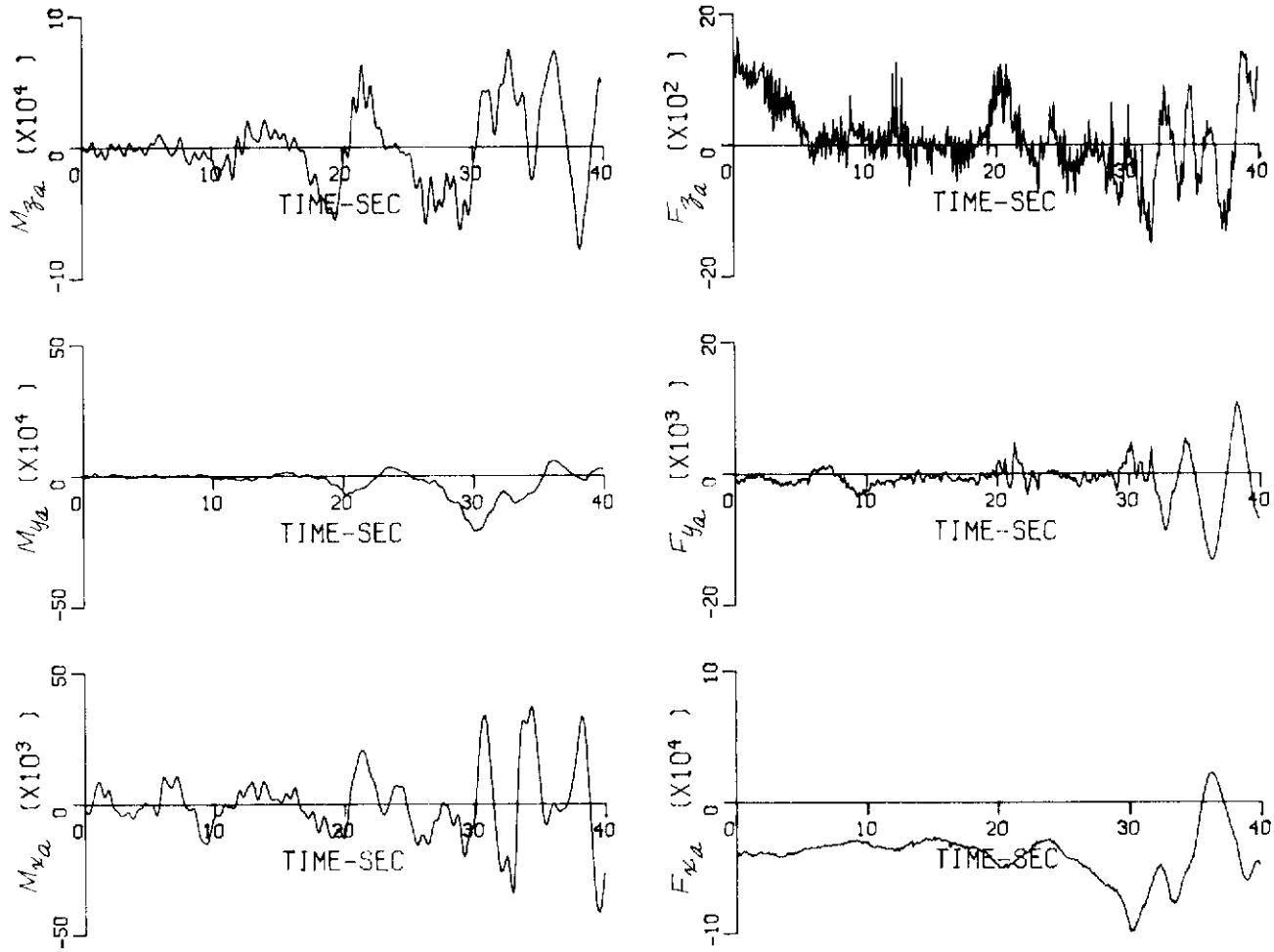

Figure 51 (Continued) RECORD 14 – ROLLING DEPARTURE FROM A NORMAL STALL ENTRY

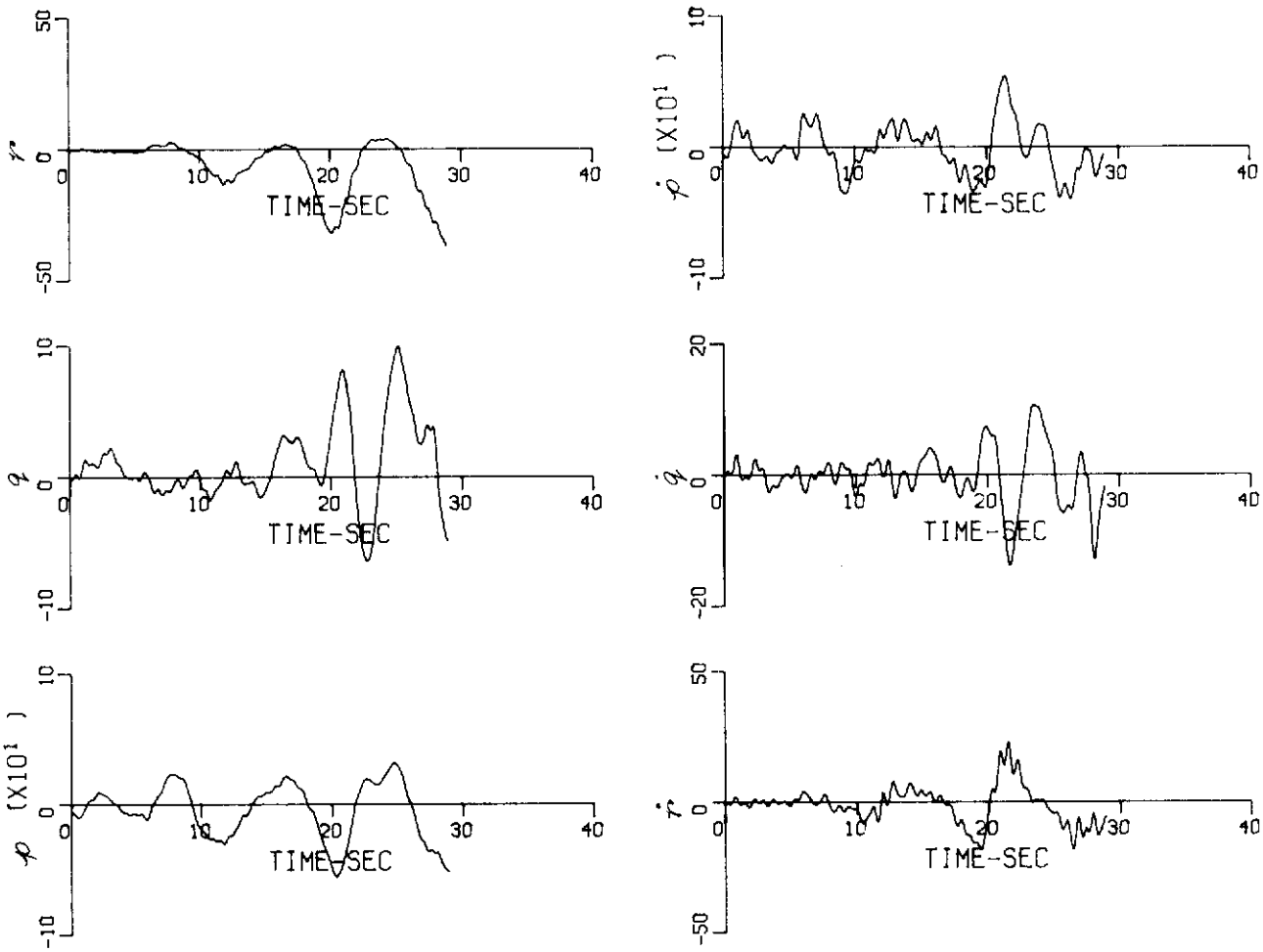

Figure 51 (Continued) RECORD 14 – ROLLING DEPARTURE FROM A NORMAL STALL ENTRY

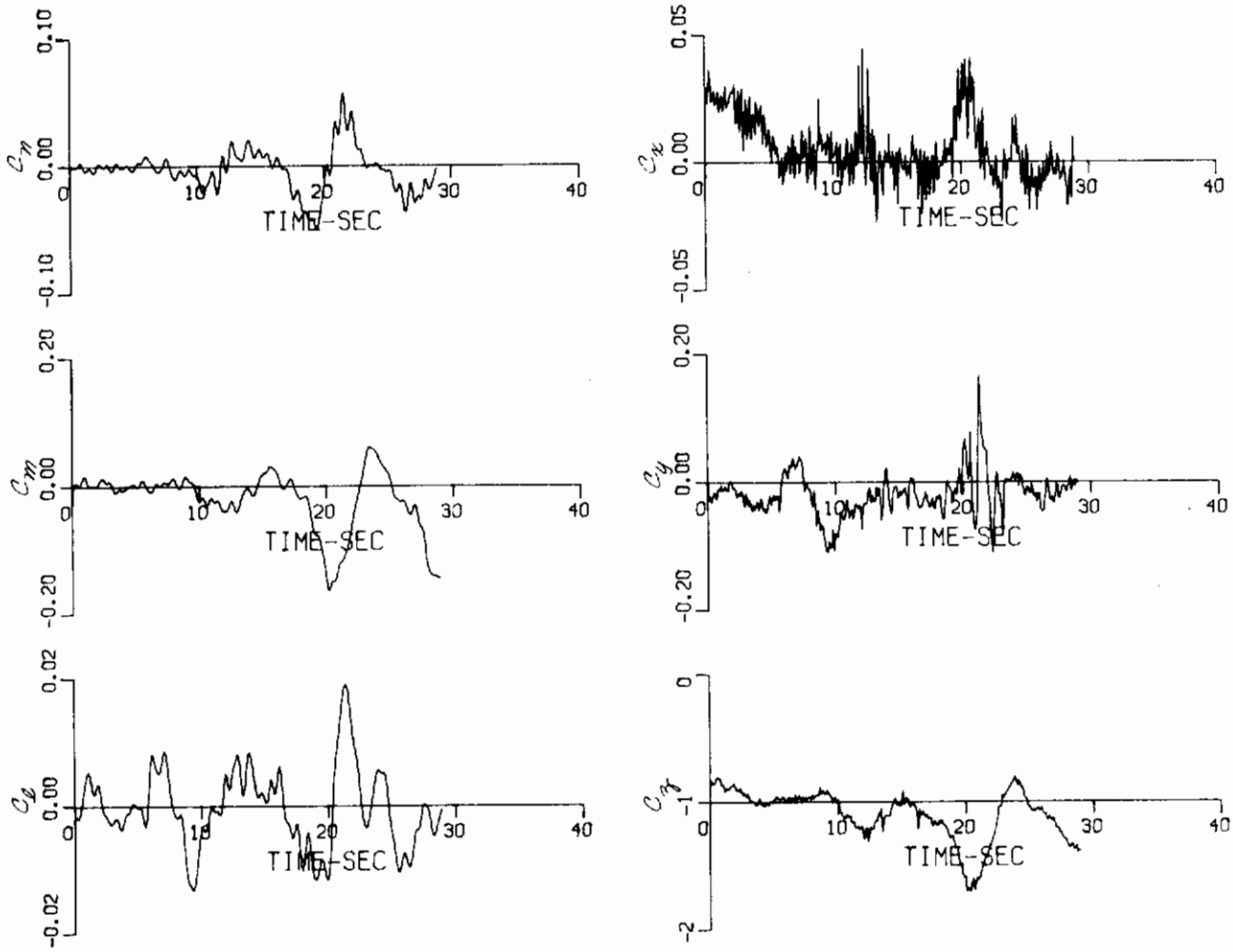

Figure 51 (Continued) RECORD 14 – ROLLING DEPARTURE FROM A NORMAL STALL ENTRY

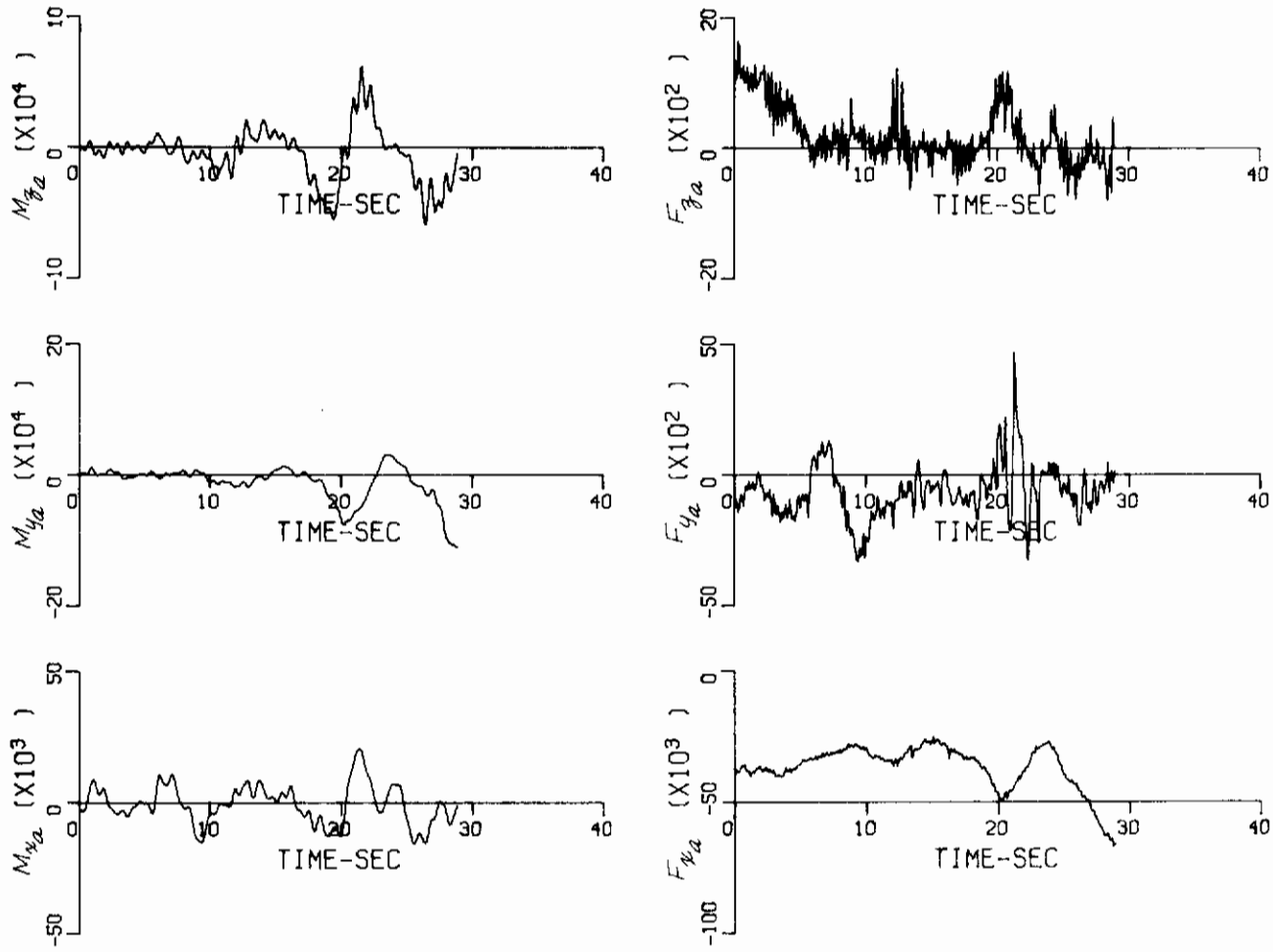

Figure 51 (Concluded) RECORD 14 – ROLLING DEPARTURE FROM A NORMAL STALL ENTRY

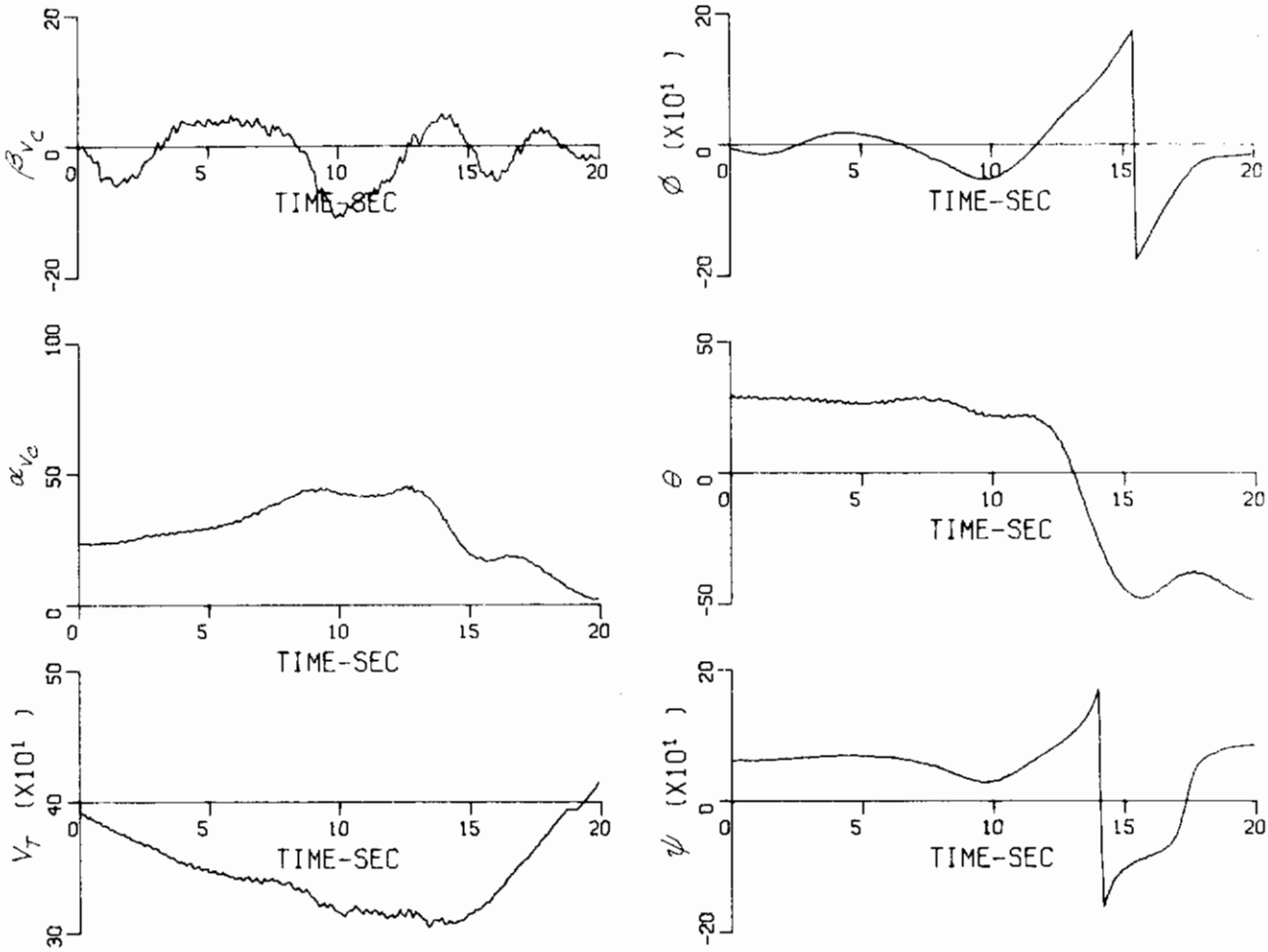

Figure 52 RECORD 20 – ROLLING DEPARTURE FROM A NORMAL STALL ENTRY

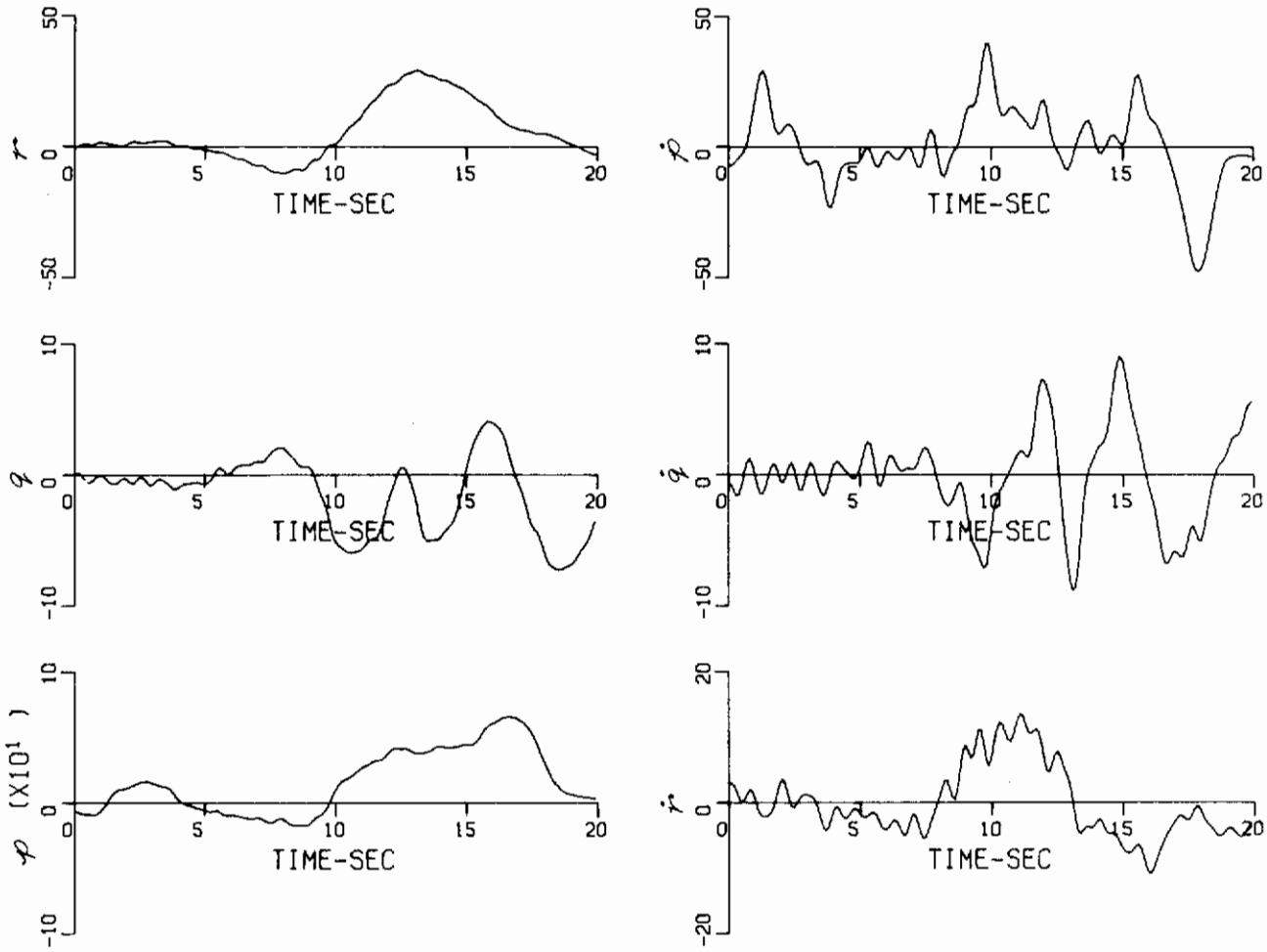

Figure 52 (Continued) RECORD 20 – ROLLING DEPARTURE FROM A NORMAL STALL ENTRY

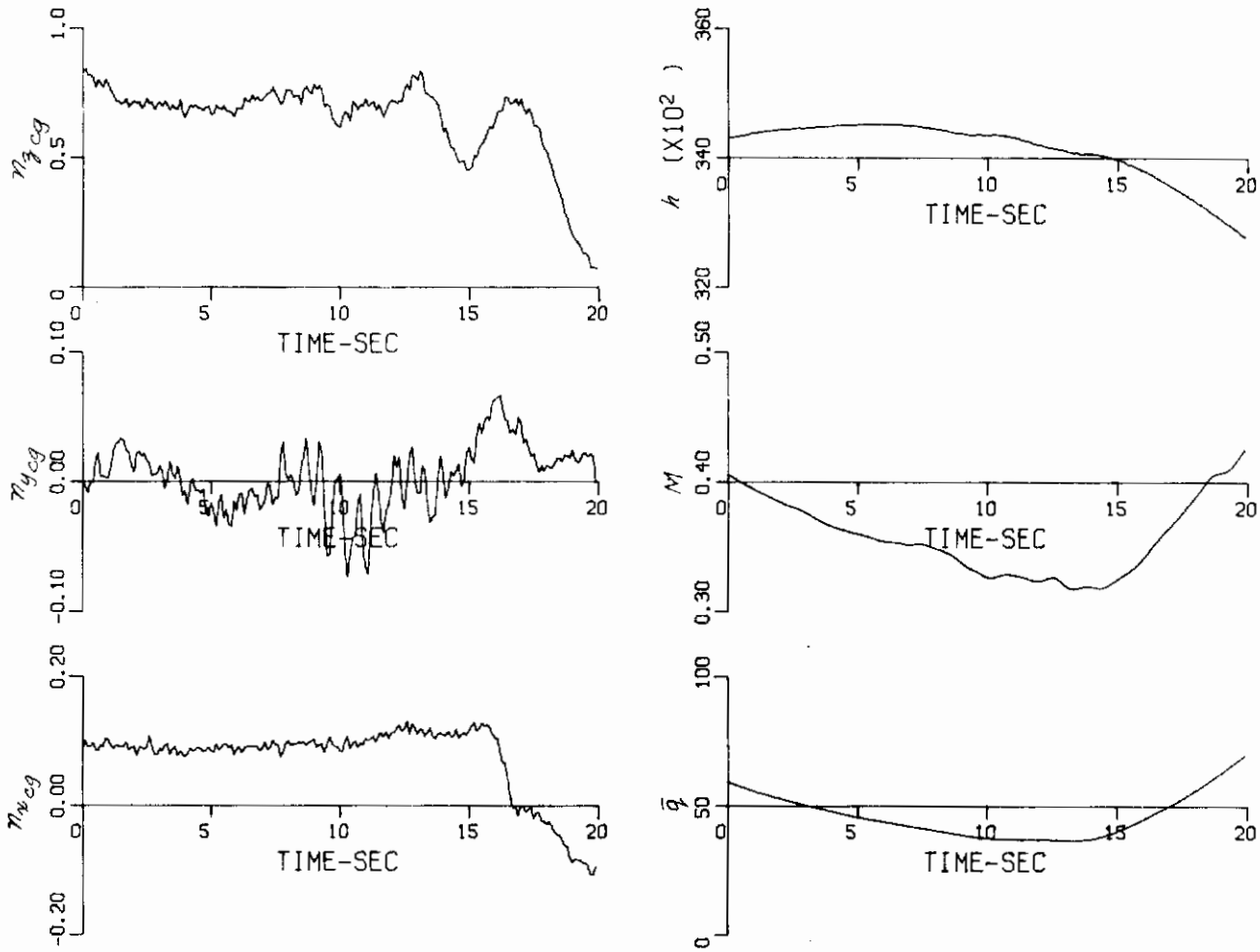

Figure 52 (Continued) RECORD 20 – ROLLING DEPARTURE FROM A NORMAL STALL ENTRY

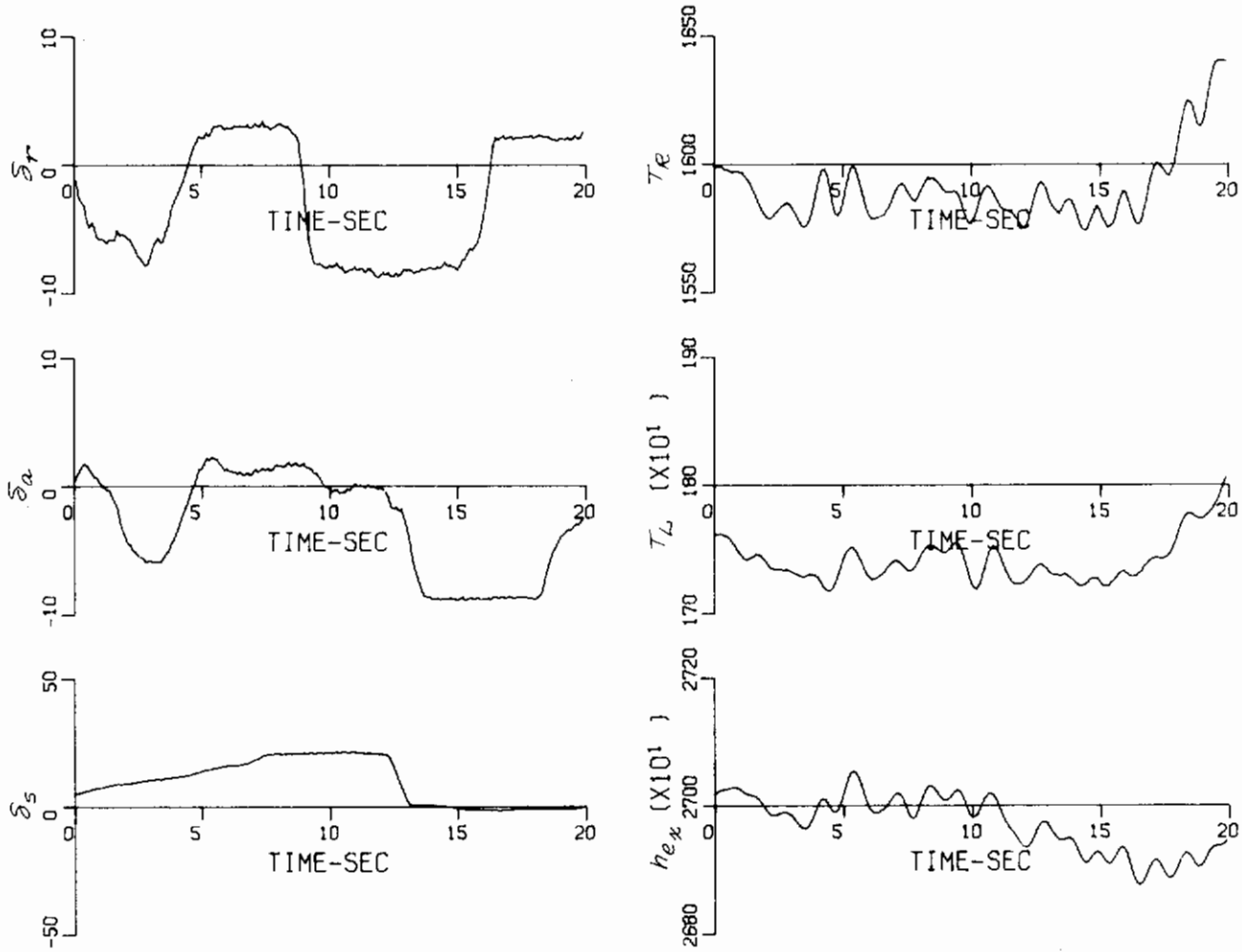

Figure 52 (Continued) RECORD 20 – ROLLING DEPARTURE FROM A NORMAL STALL ENTRY

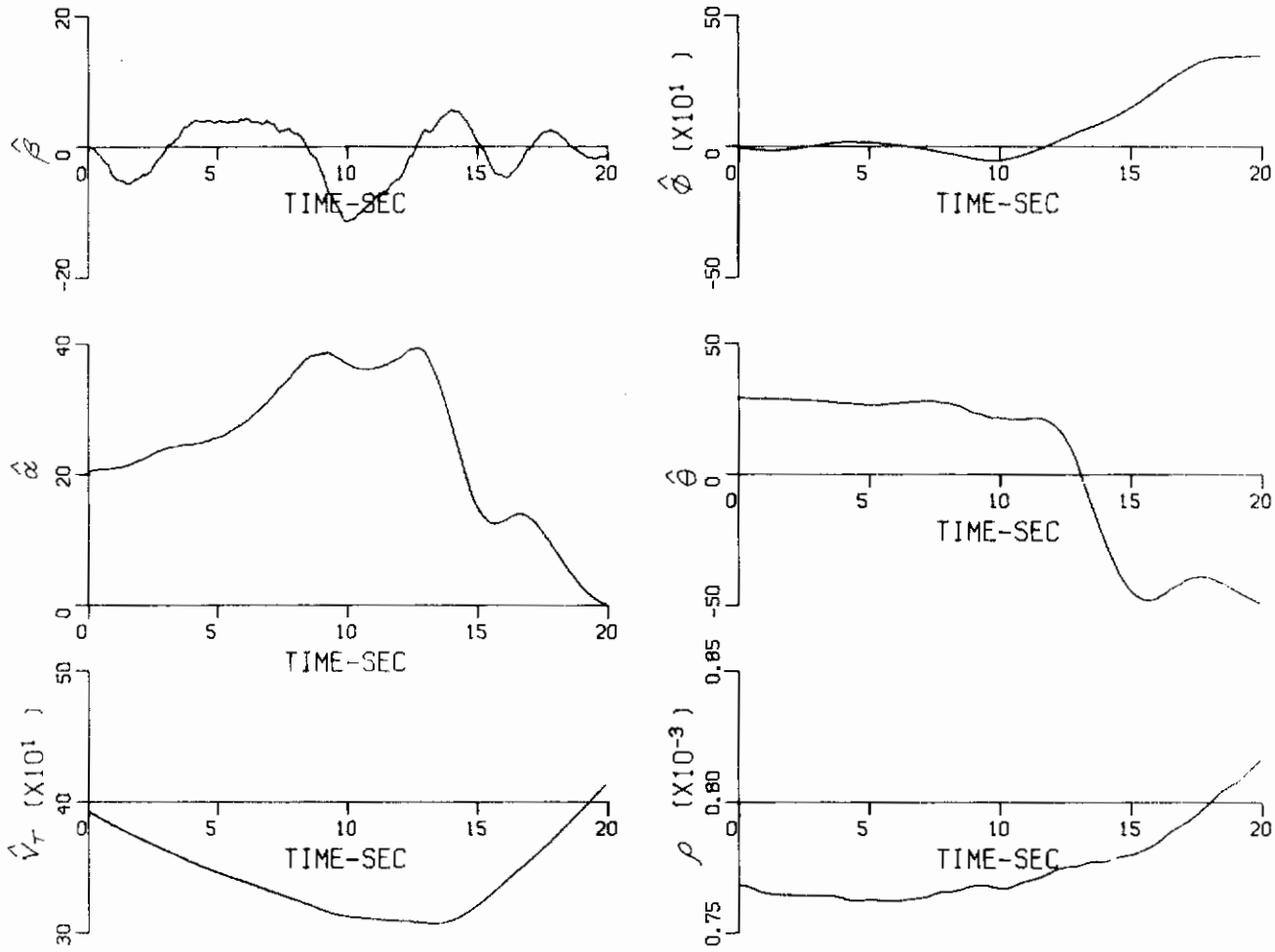

Figure 52 (Continued) RECORD 20 – ROLLING DEPARTURE FROM A NORMAL STALL ENTRY

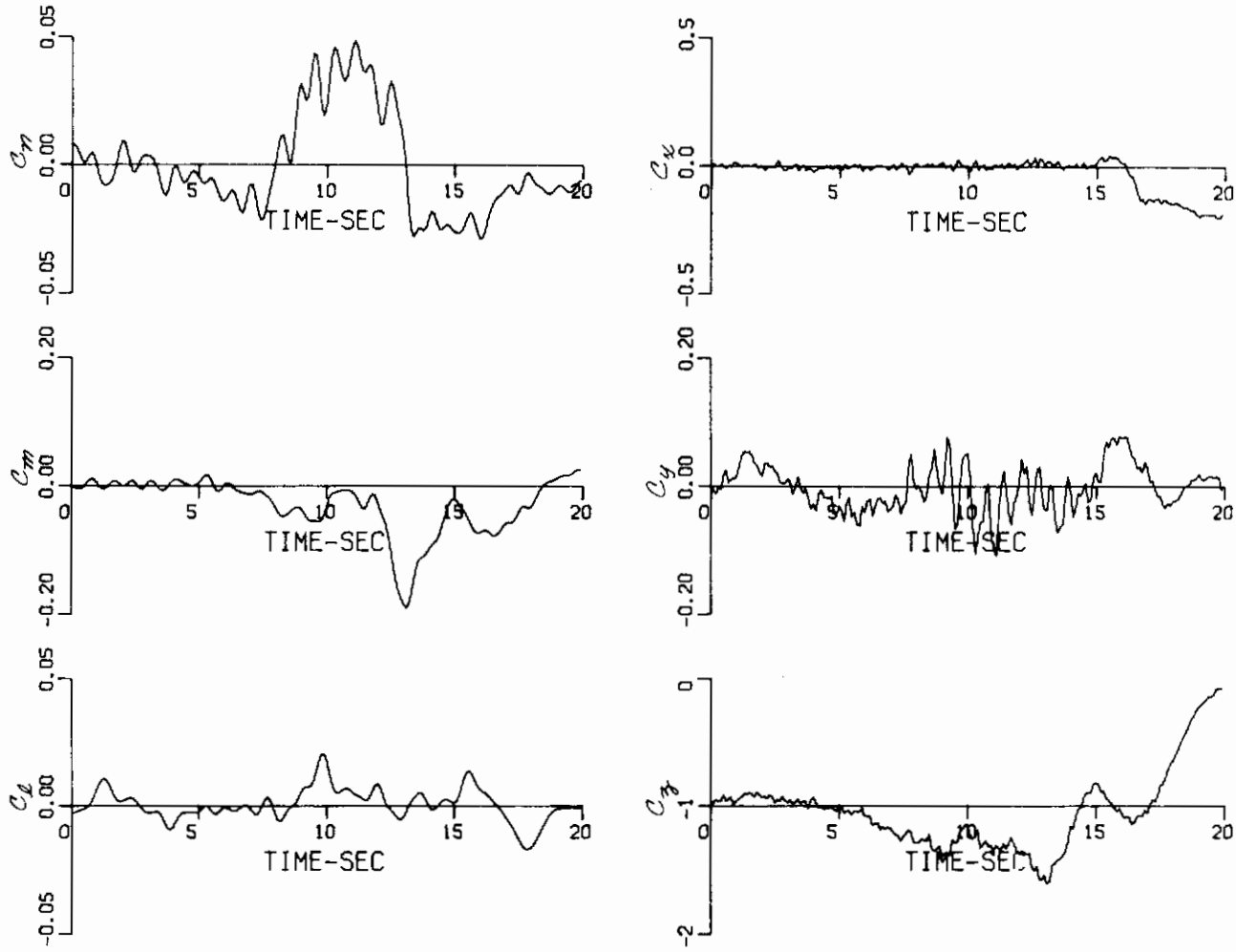

Figure 52 (Continued) RECORD 20 – ROLLING DEPARTURE FROM A NORMAL STALL ENTRY

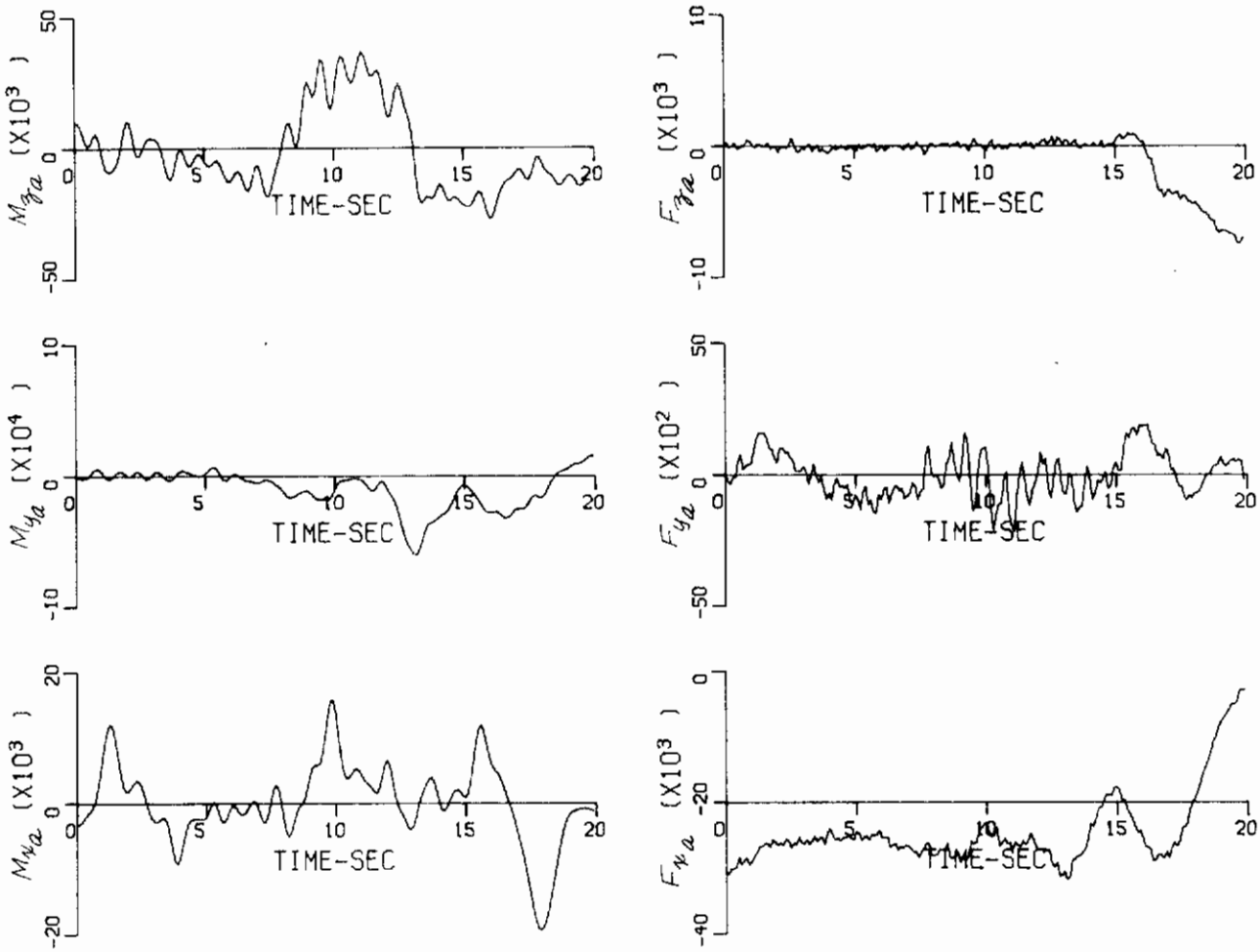

Figure 52 (Concluded) RECORD 20 — ROLLING DEPARTURE FROM A NORMAL STALL ENTRY

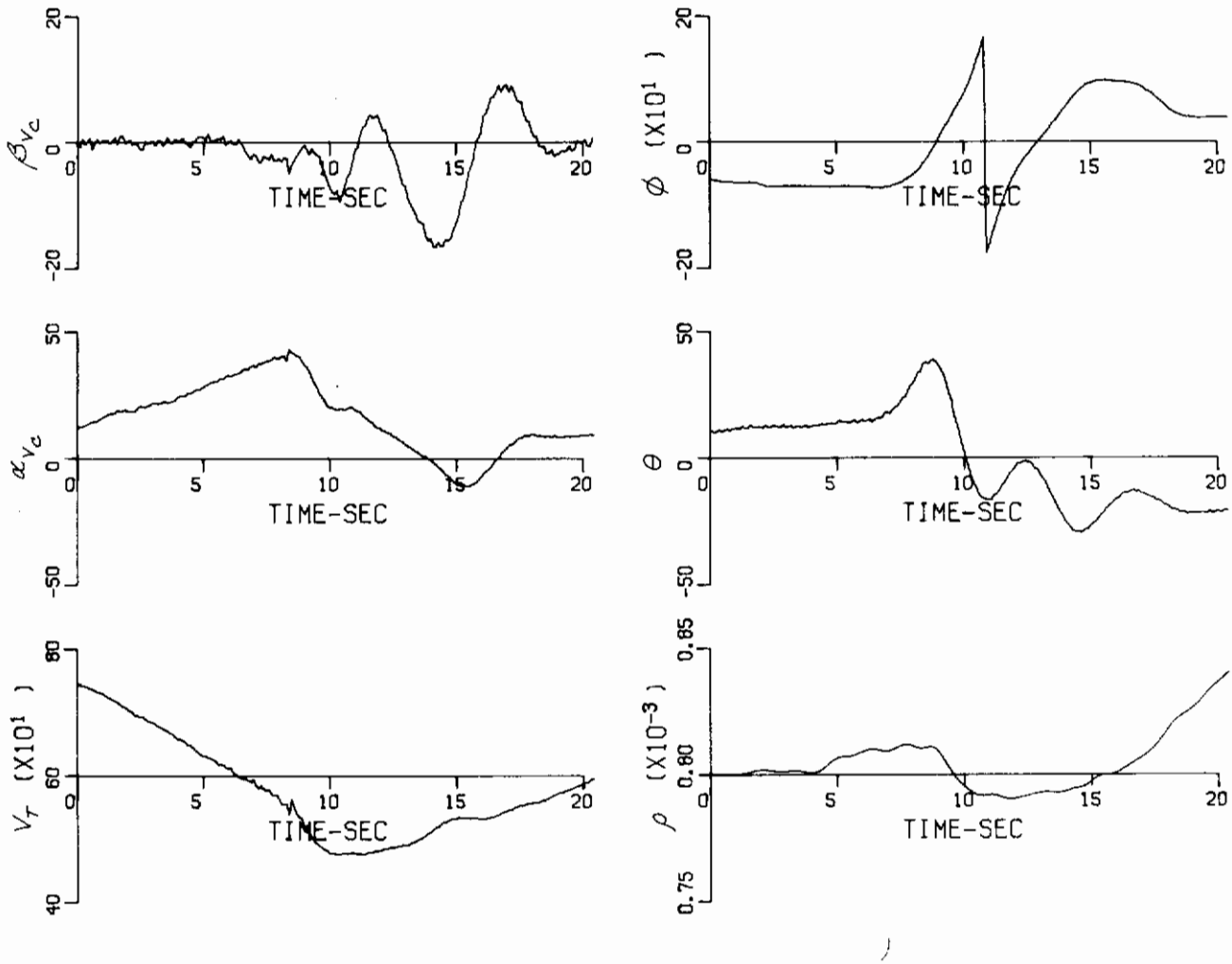

Figure 53 RECORD 15 – ROLLING DEPARTURE FROM AN ACCELERATED STALL ENTRY

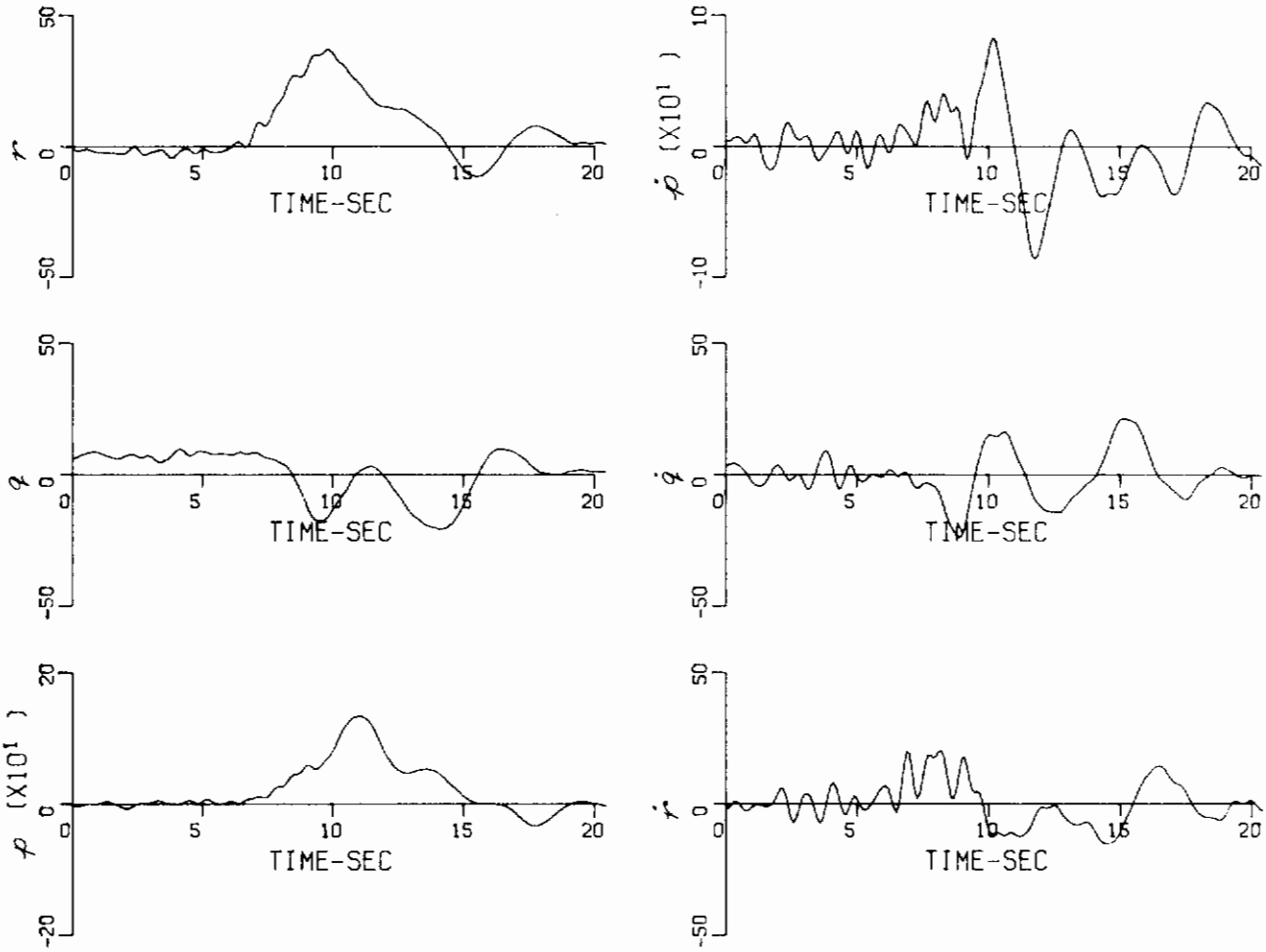

Figure 53 (Continued) RECORD 15 — ROLLING DEPARTURE FROM AN ACCELERATED STALL ENTRY

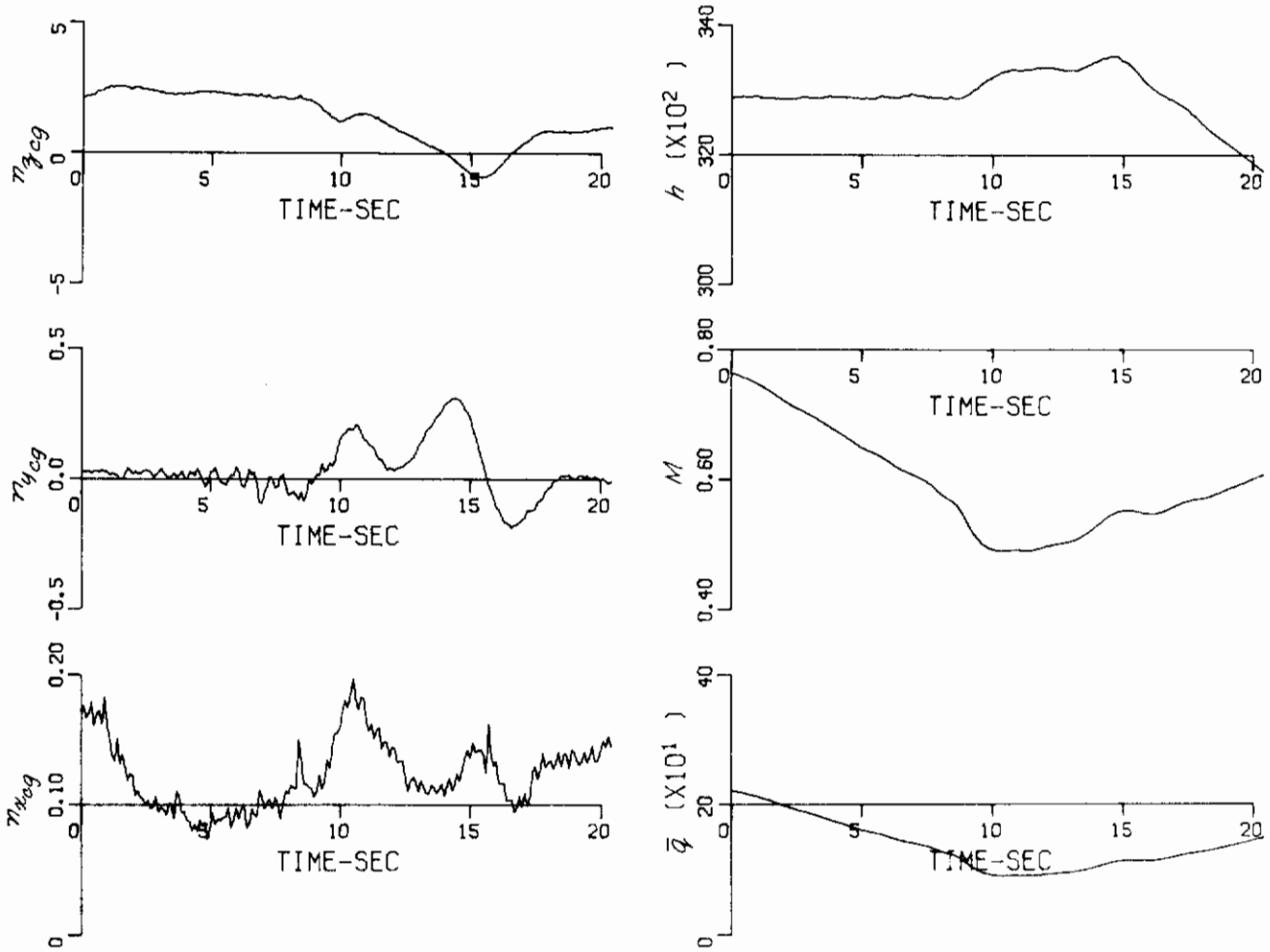

Figure 53 (Continued) RECORD 15 – ROLLING DEPARTURE FROM AN ACCELERATED STALL ENTRY

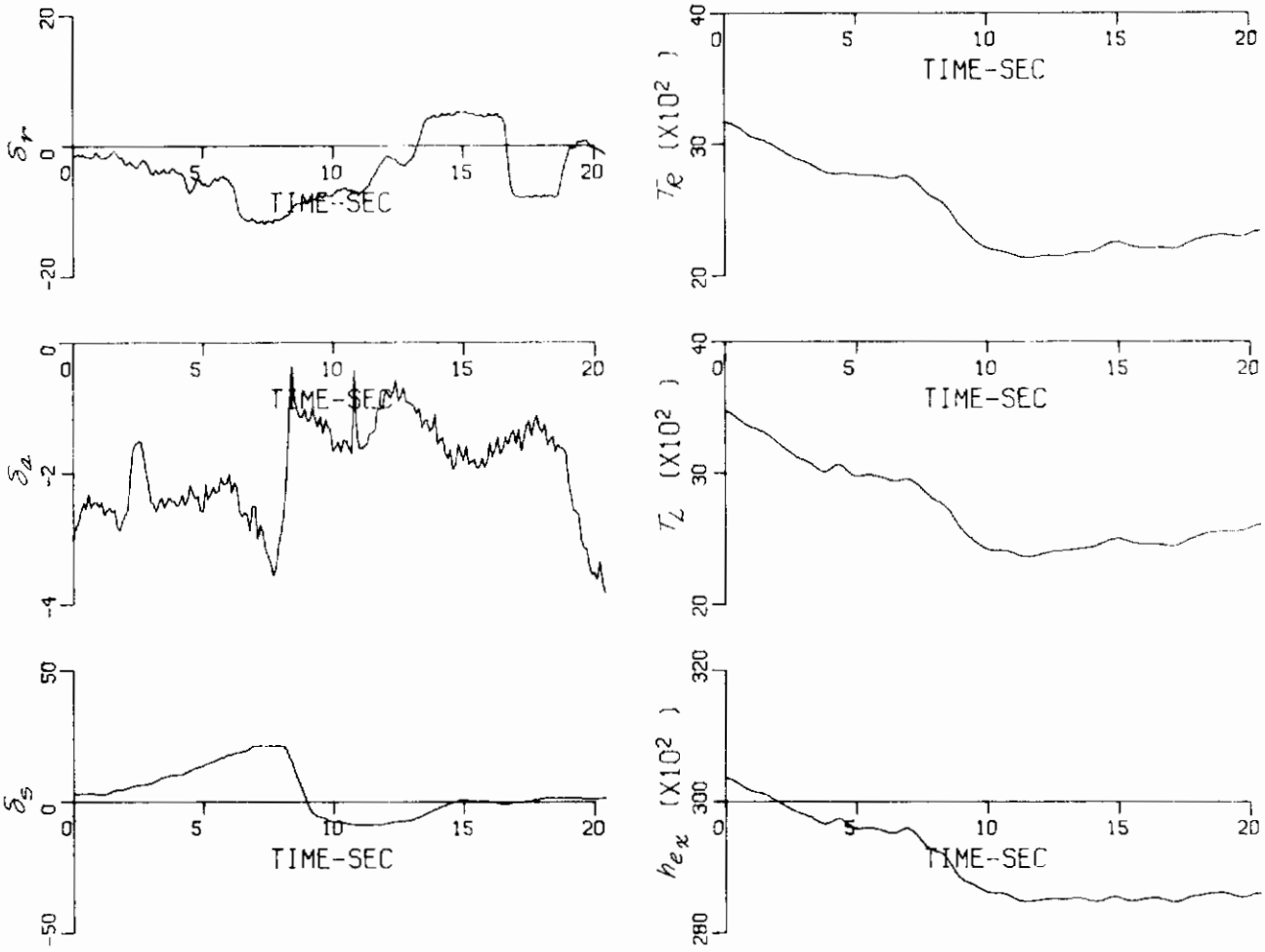

Figure 53 (Continued) RECORD 15 – ROLLING DEPARTURE FROM AN ACCELERATED STALL ENTRY

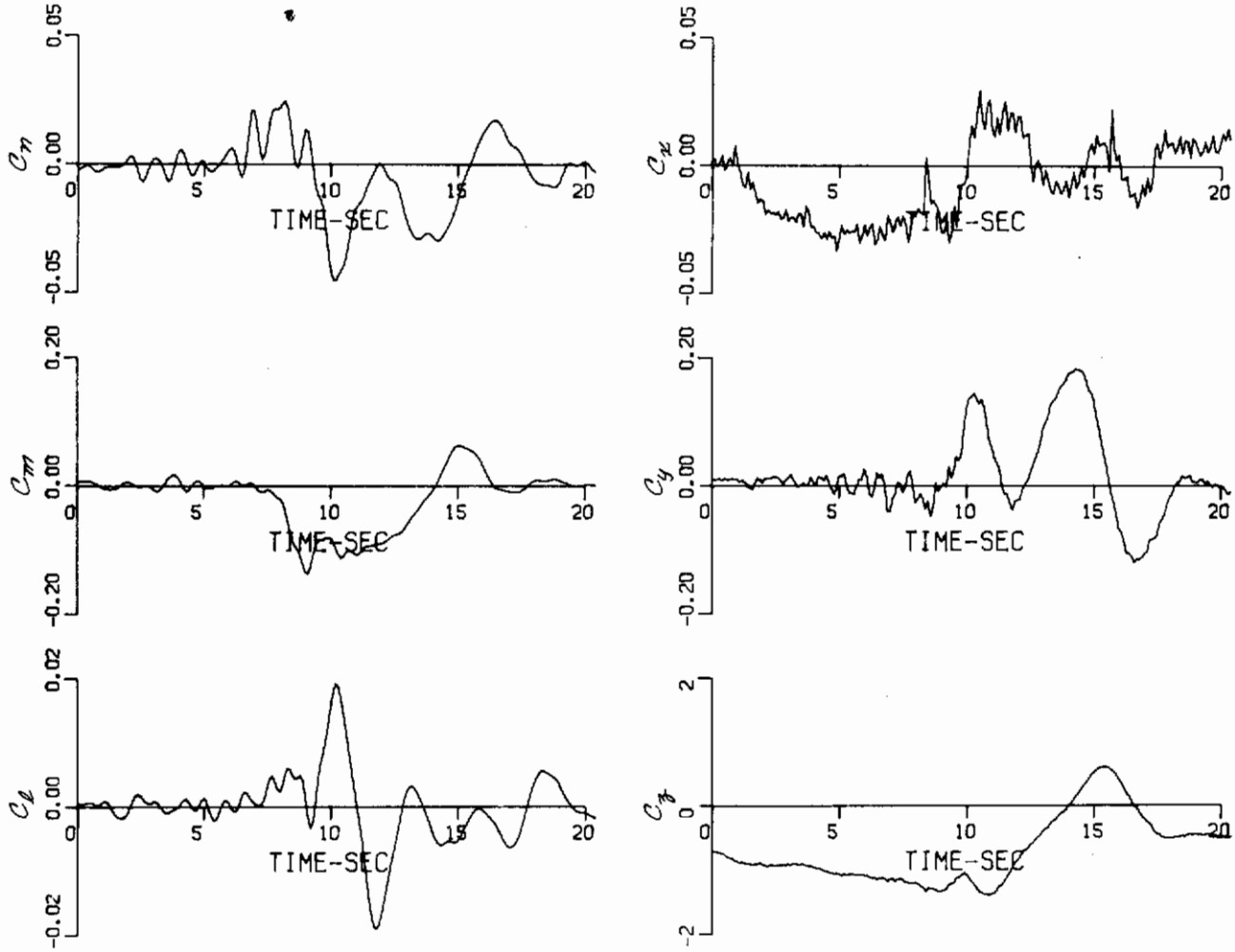

Figure 53 (Concluded) RECORD 15 – ROLLING DEPARTURE FROM AN ACCELERATED STALL ENTRY

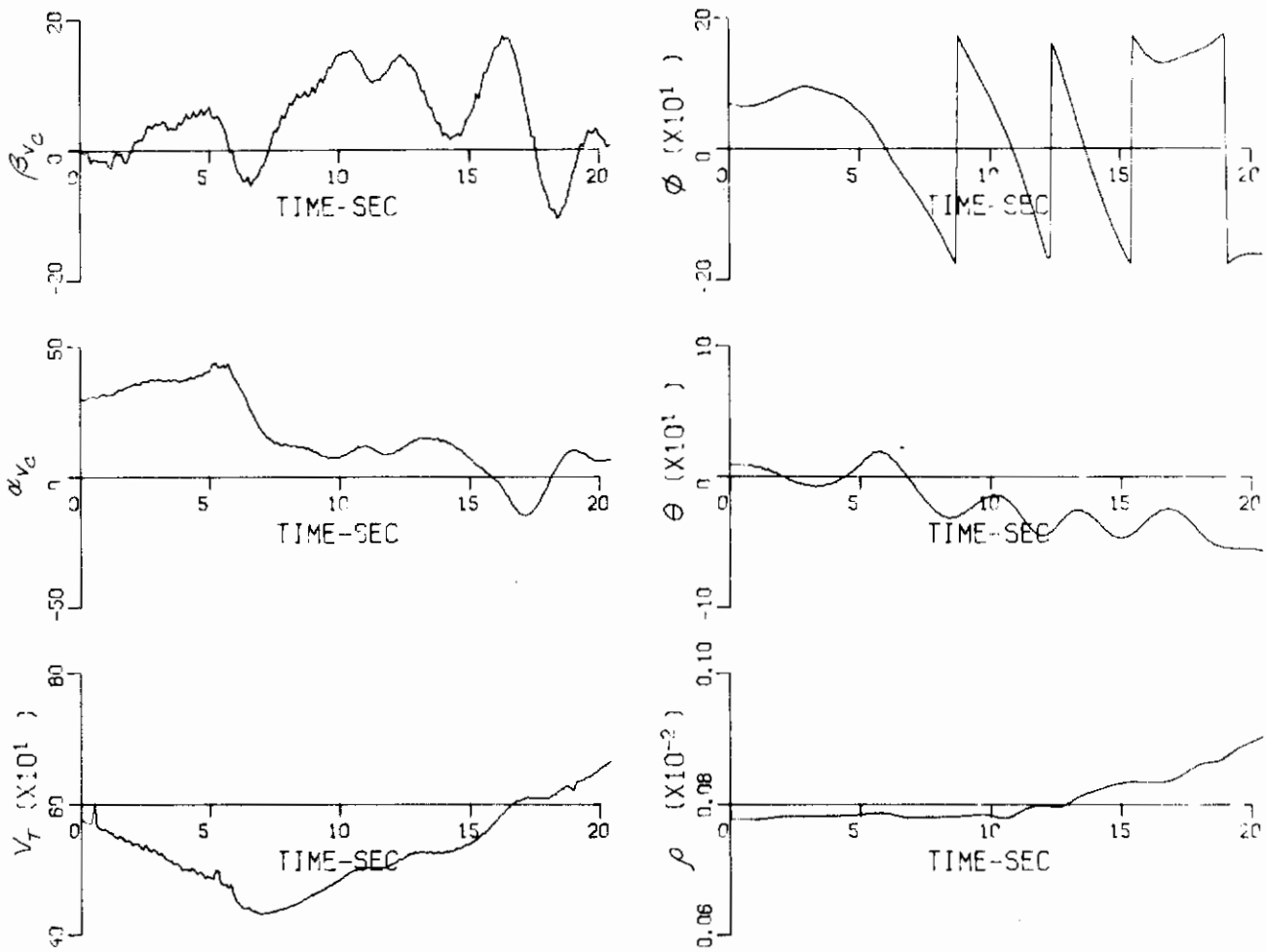

Figure 54 RECORD 17 – ROLLING DEPARTURE FROM AN ACCELERATED STALL ENTRY

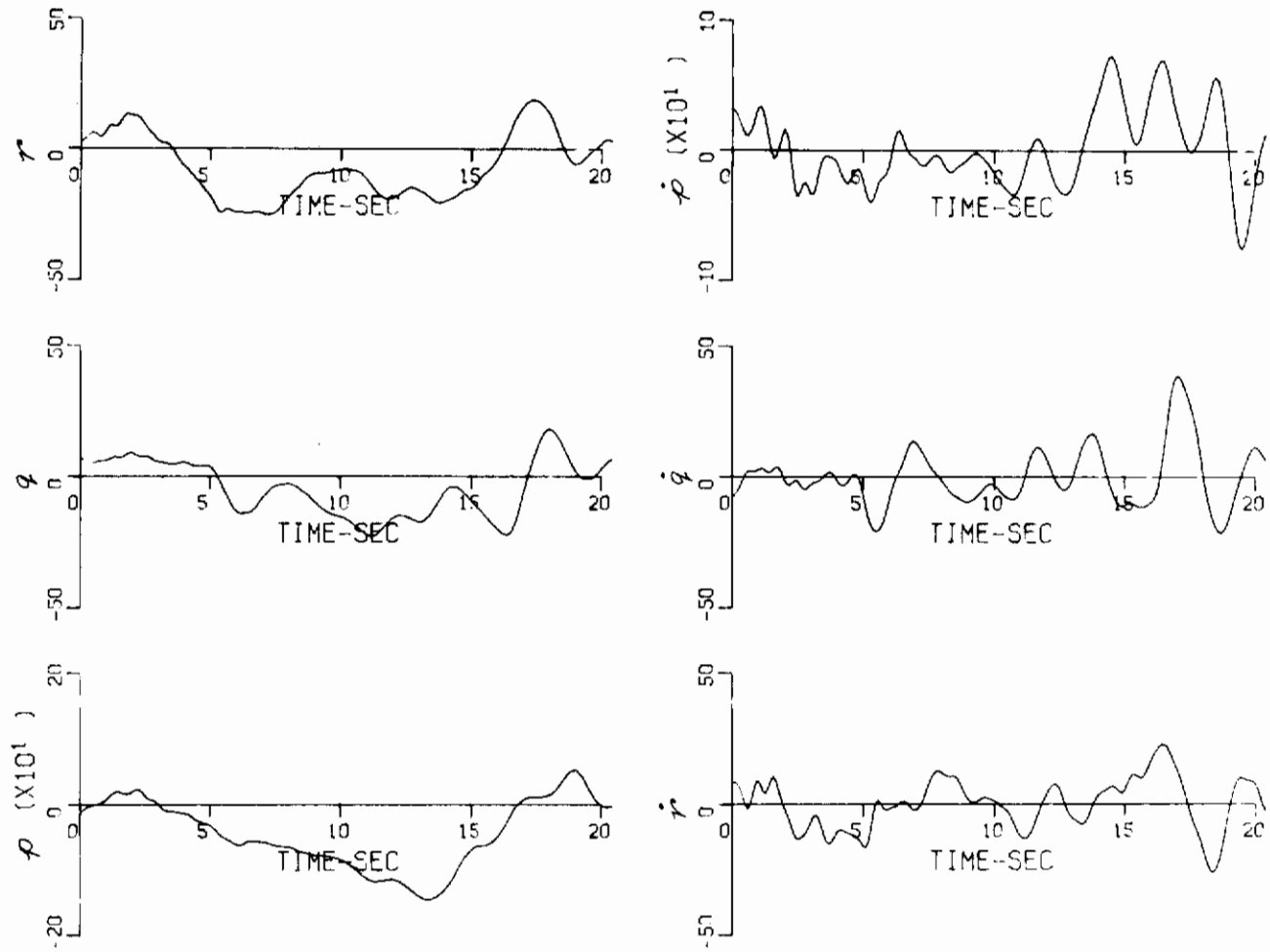

Figure 54 (Continued) RECORD 17 – ROLLING DEPARTURE FROM AN ACCELERATED STALL ENTRY

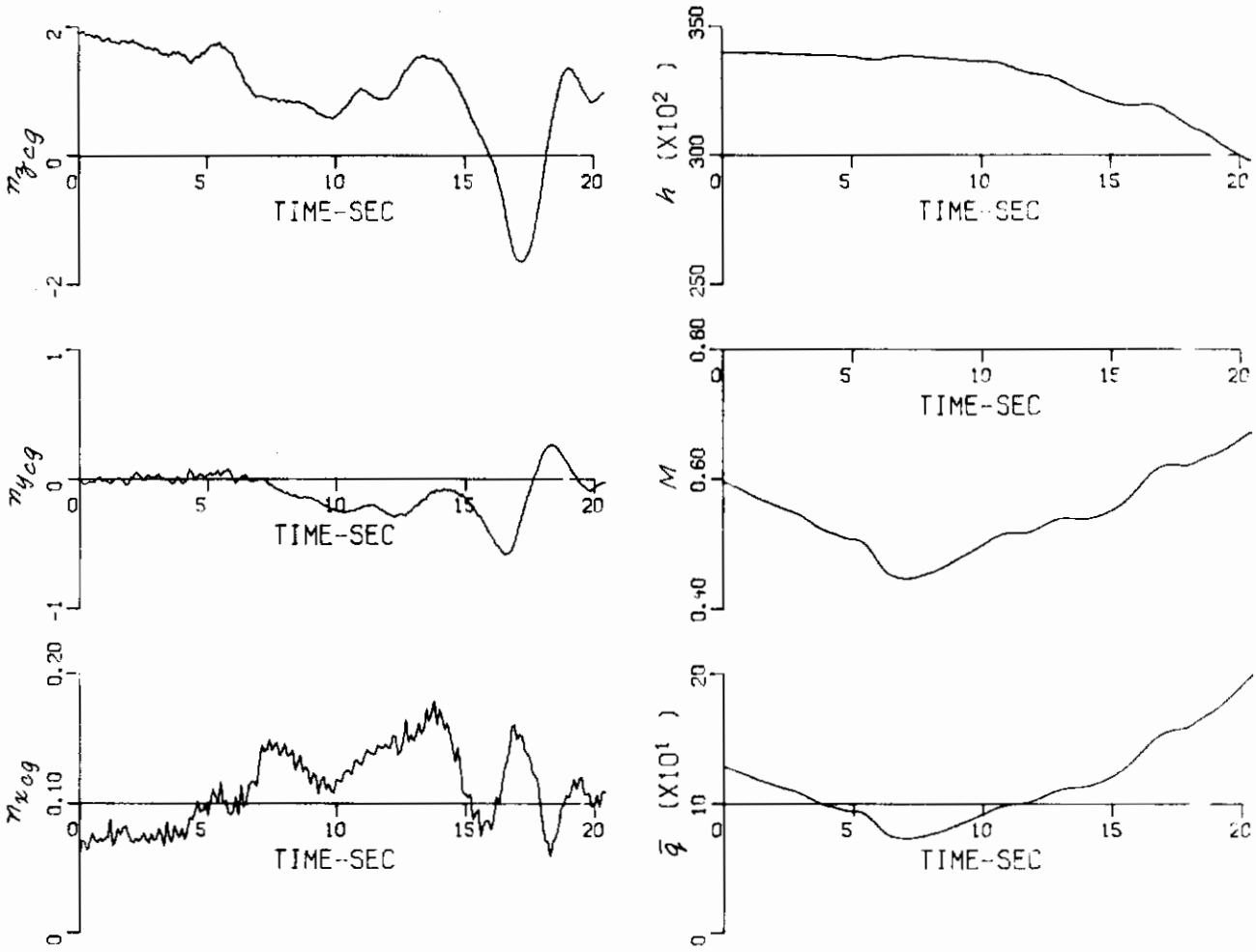

Figure 54 (Continued) RECORD 17 – ROLLING DEPARTURE FROM AN ACCELERATED STALL ENTRY

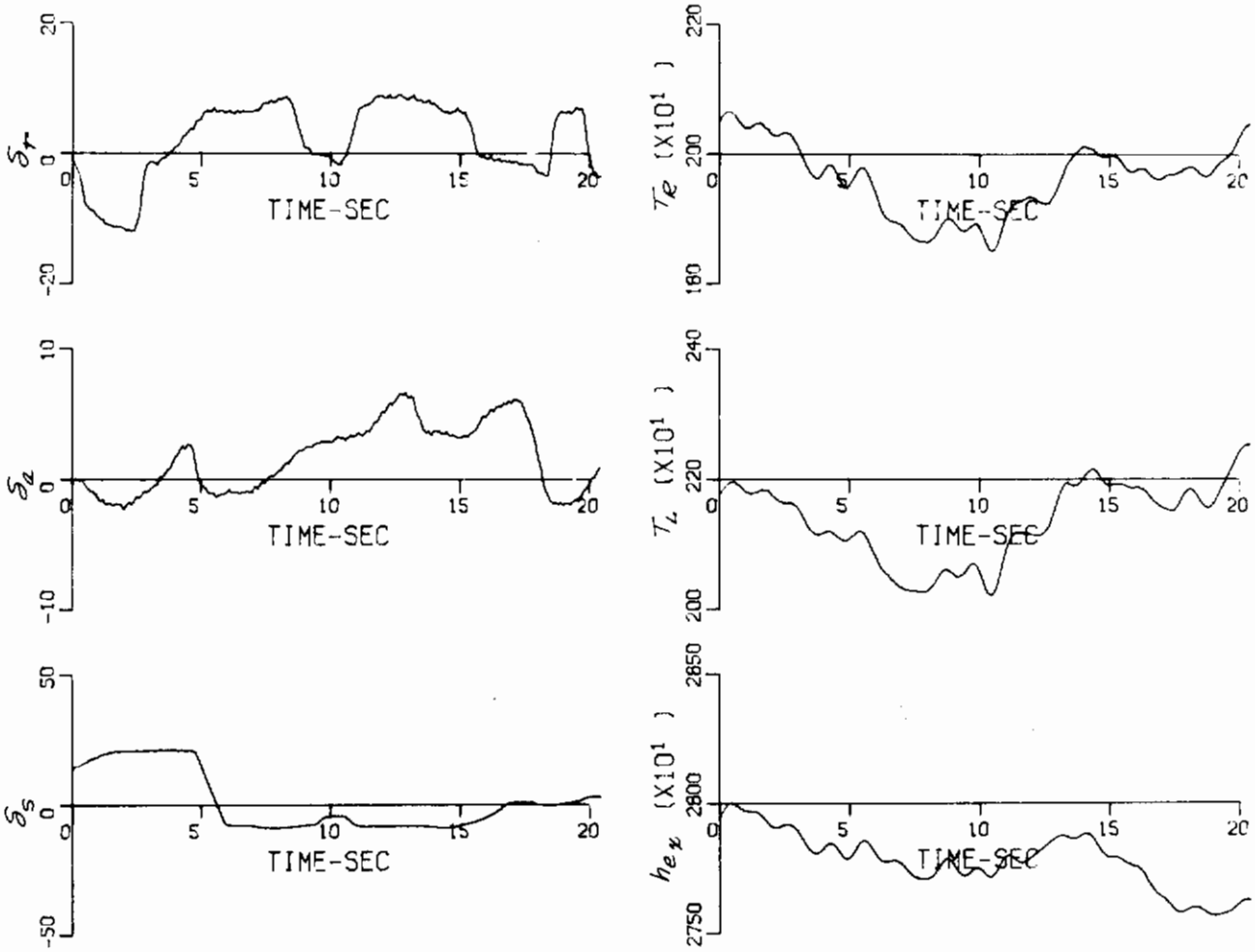

Figure 54 (Continued) RECORD 17 – ROLLING DEPARTURE FROM AN ACCELERATED STALL ENTRY

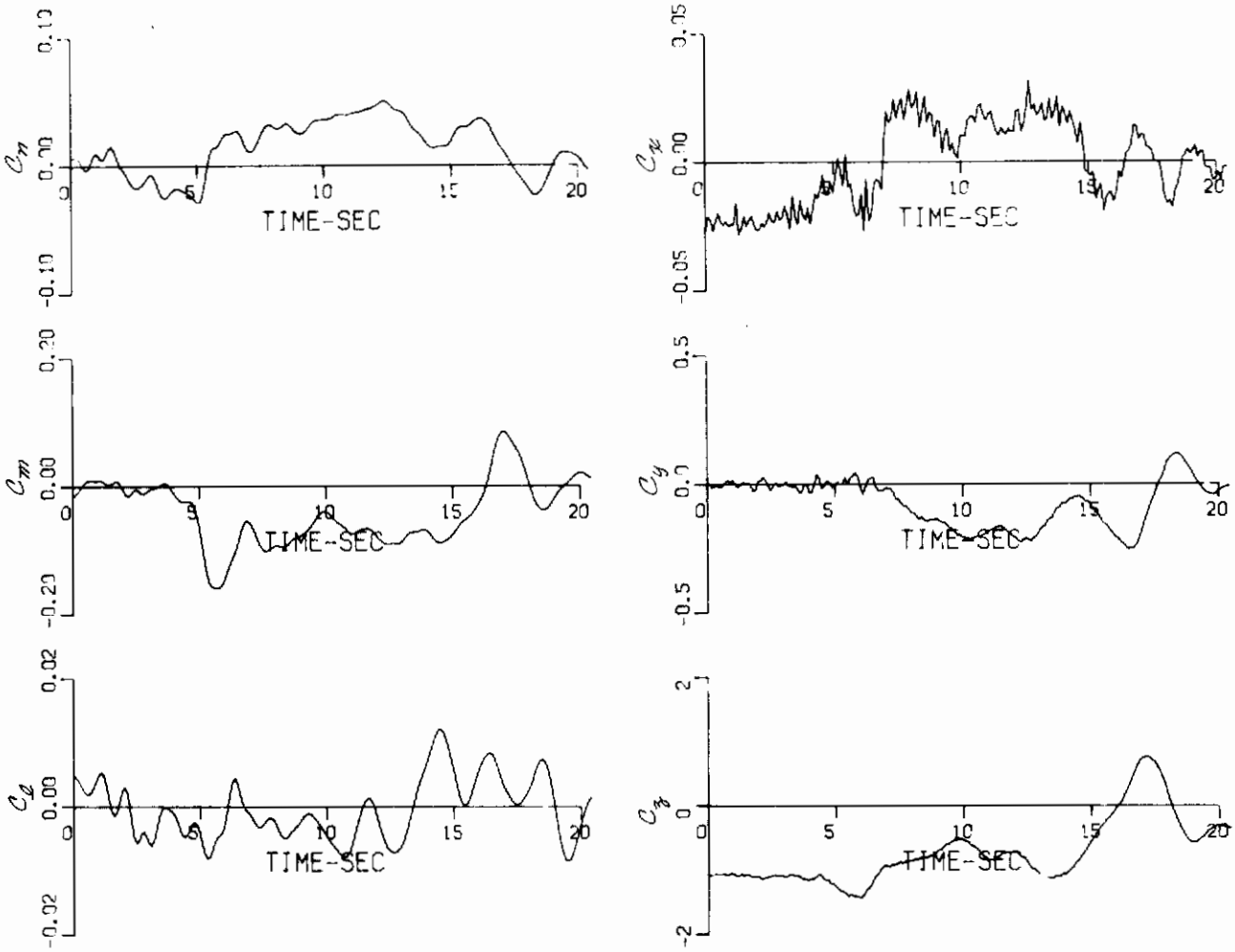

Figure 54 (Concluded) **RECORD 17 – ROLLING DEPARTURE FROM AN ACCELERATED STALL ENTRY**

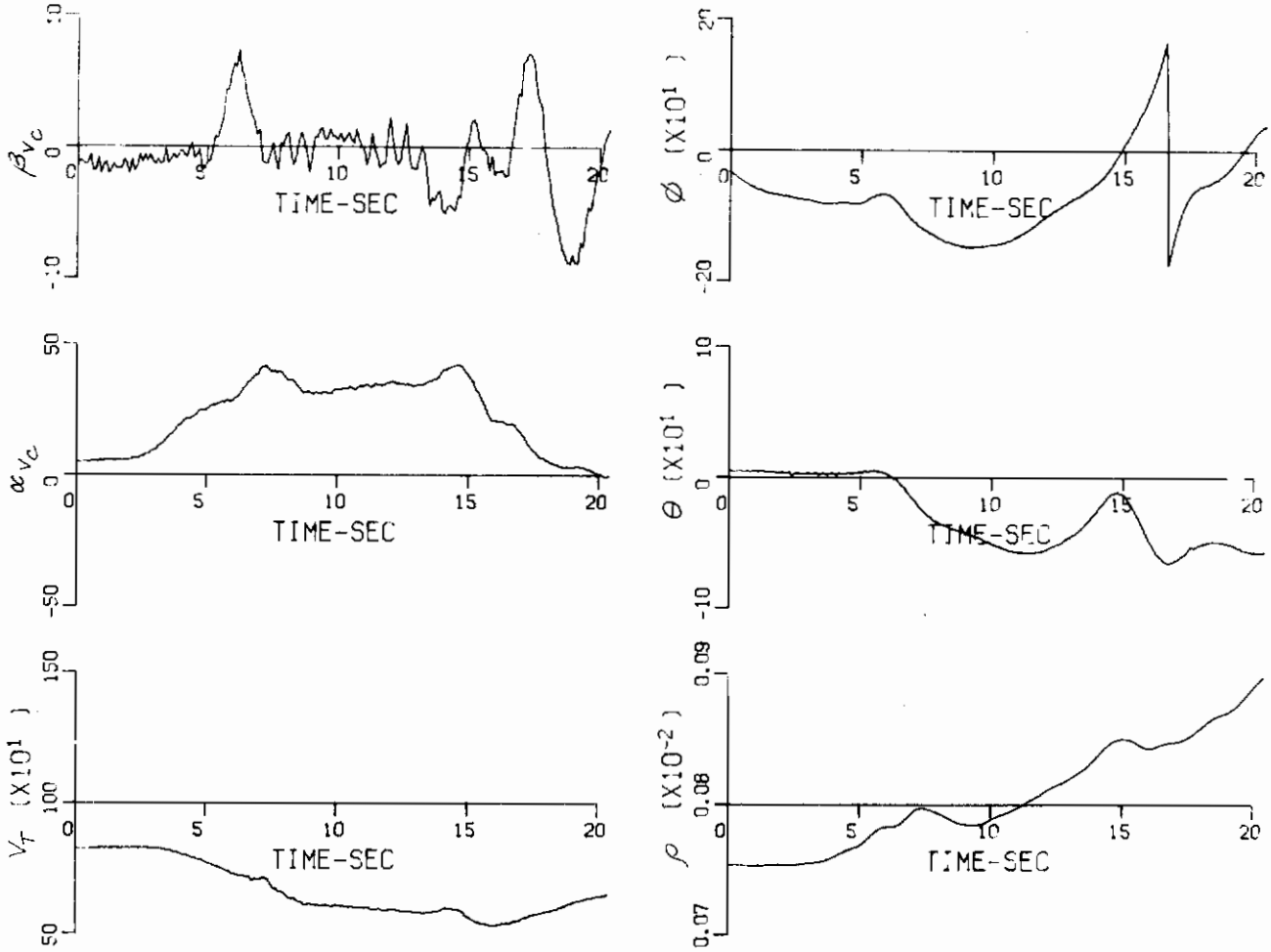

Figure 55 RECORD 19 — ROLLING DEPARTURE FROM AN ACCELERATED STALL ENTRY

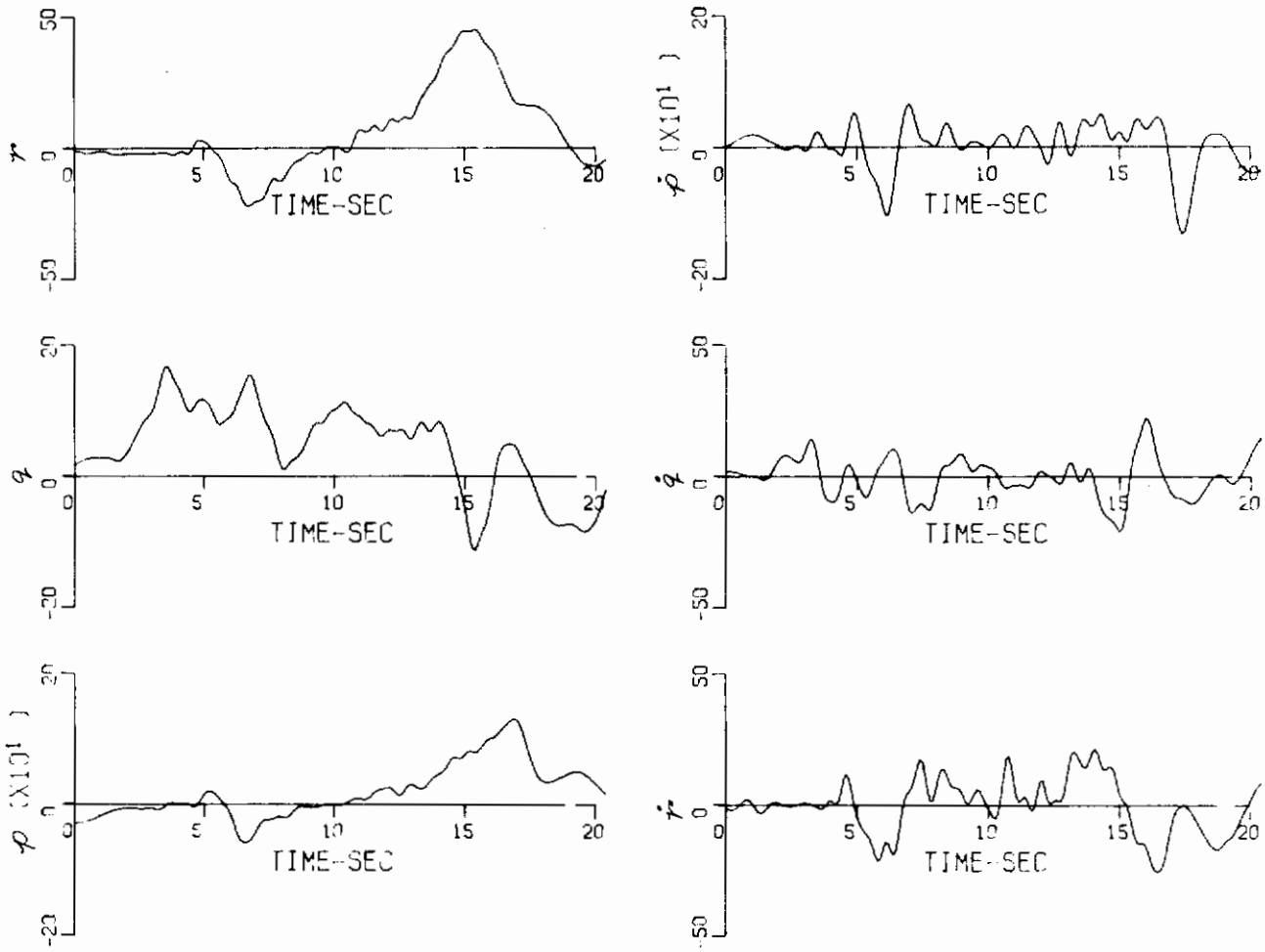

Figure 55 (Continued) **RECORD 19 – ROLLING DEPARTURE FROM AN ACCELERATED STALL ENTRY**

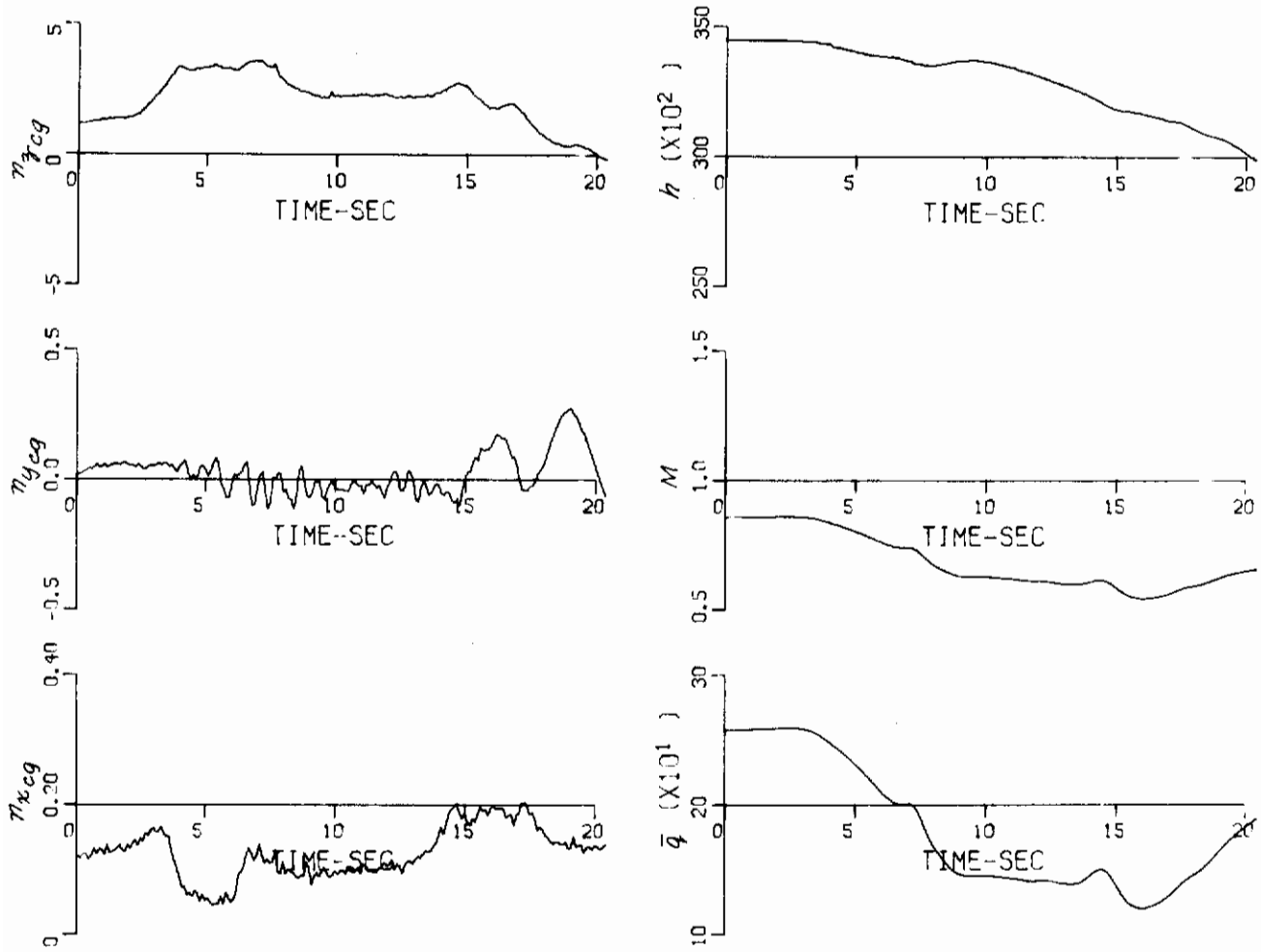

Figure 55 (Continued) RECORD 19 – ROLLING DEPARTURE FROM AN ACCELERATED STALL ENTRY

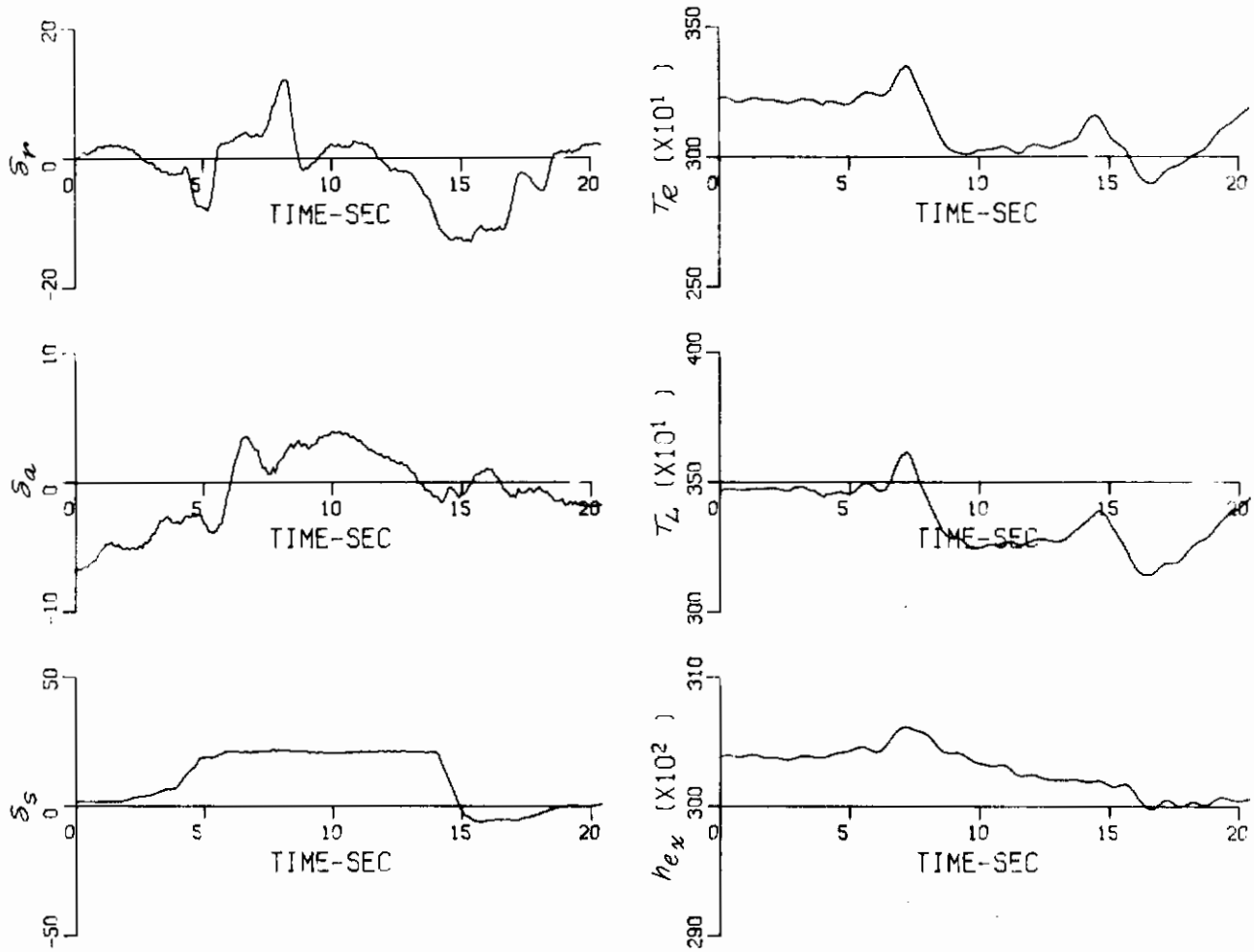

Figure 55 (Continued) RECORD 19 – ROLLING DEPARTURE FROM AN ACCELERATED STALL ENTRY

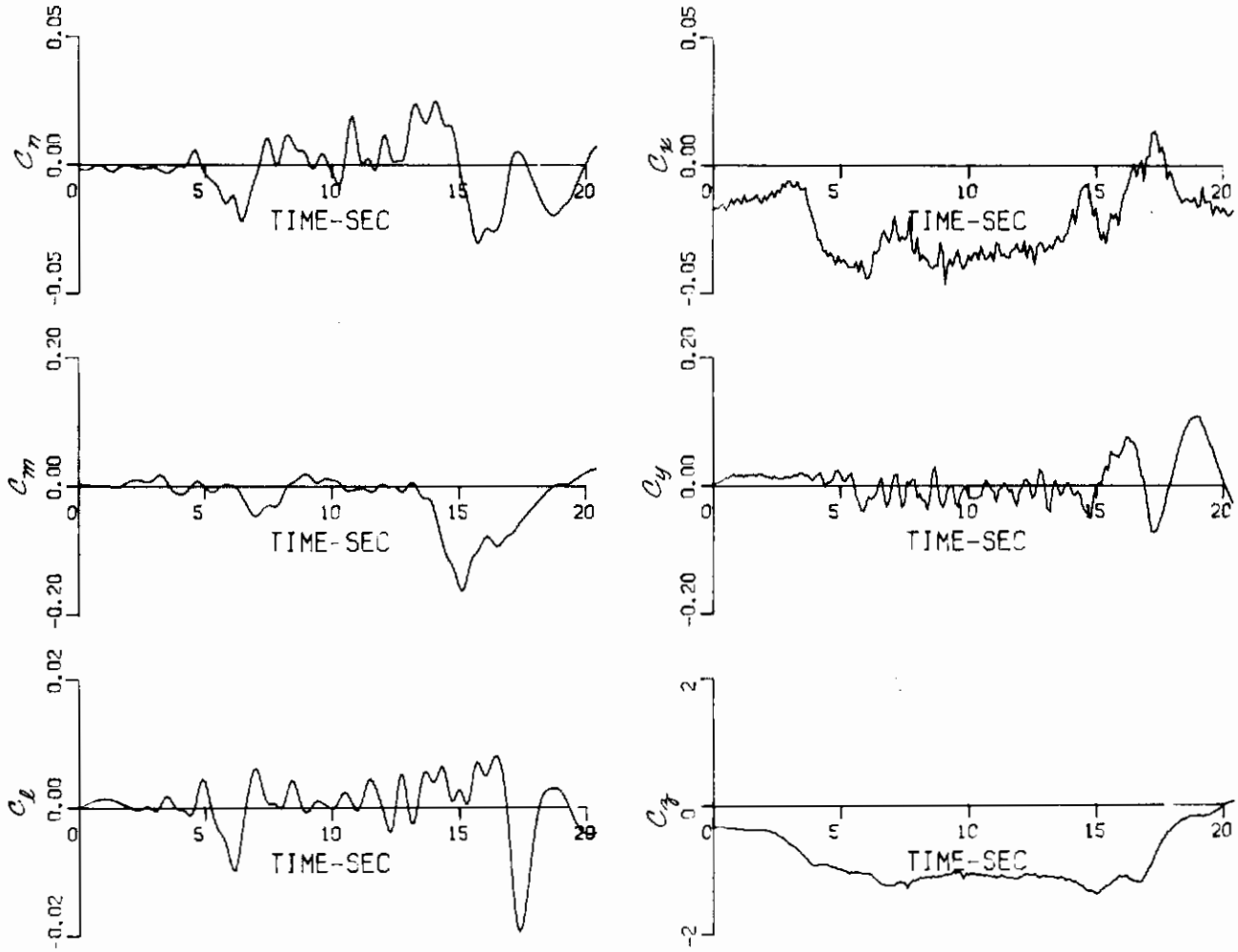

Figure 55 (Concluded) RECORD 19 – ROLLING DEPARTURE FROM AN ACCELERATED STALL ENTRY

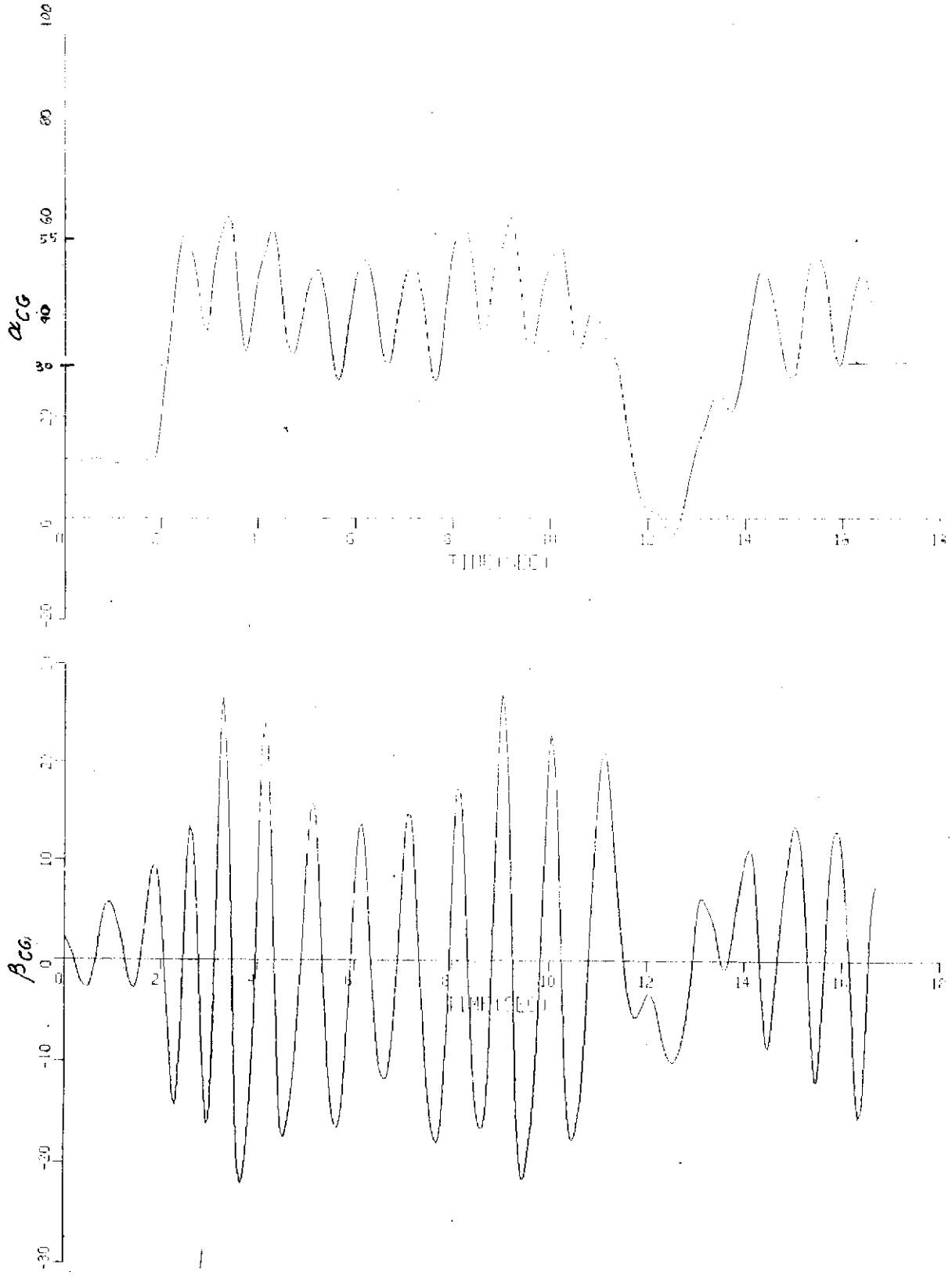

Figure 56 RADIO CONTROLLED MODEL TIME HISTORIES - RUN 1

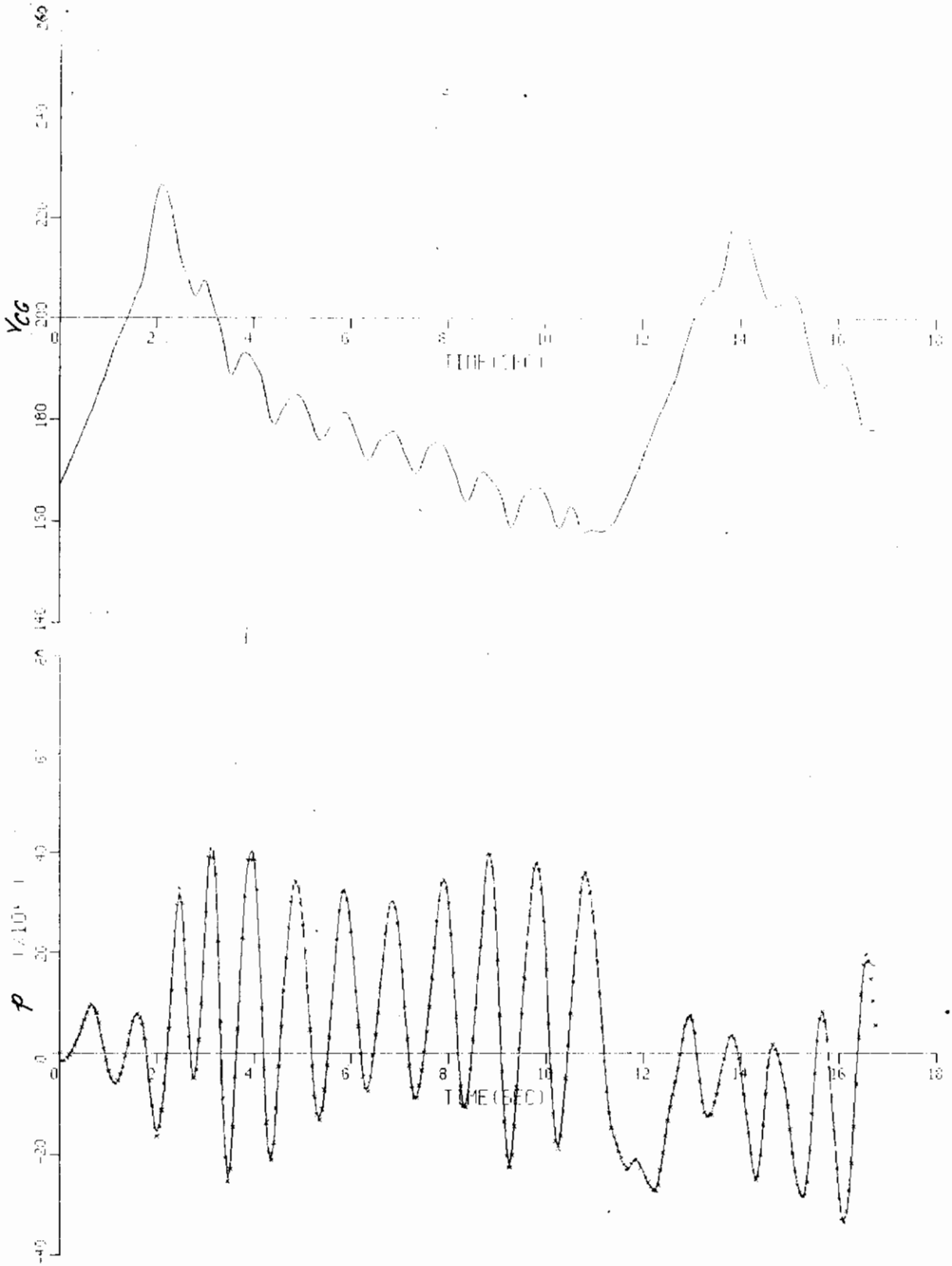

Figure 56 (Continued) RADIO CONTROLLED MODEL TIME HISTORIES - RUN 1

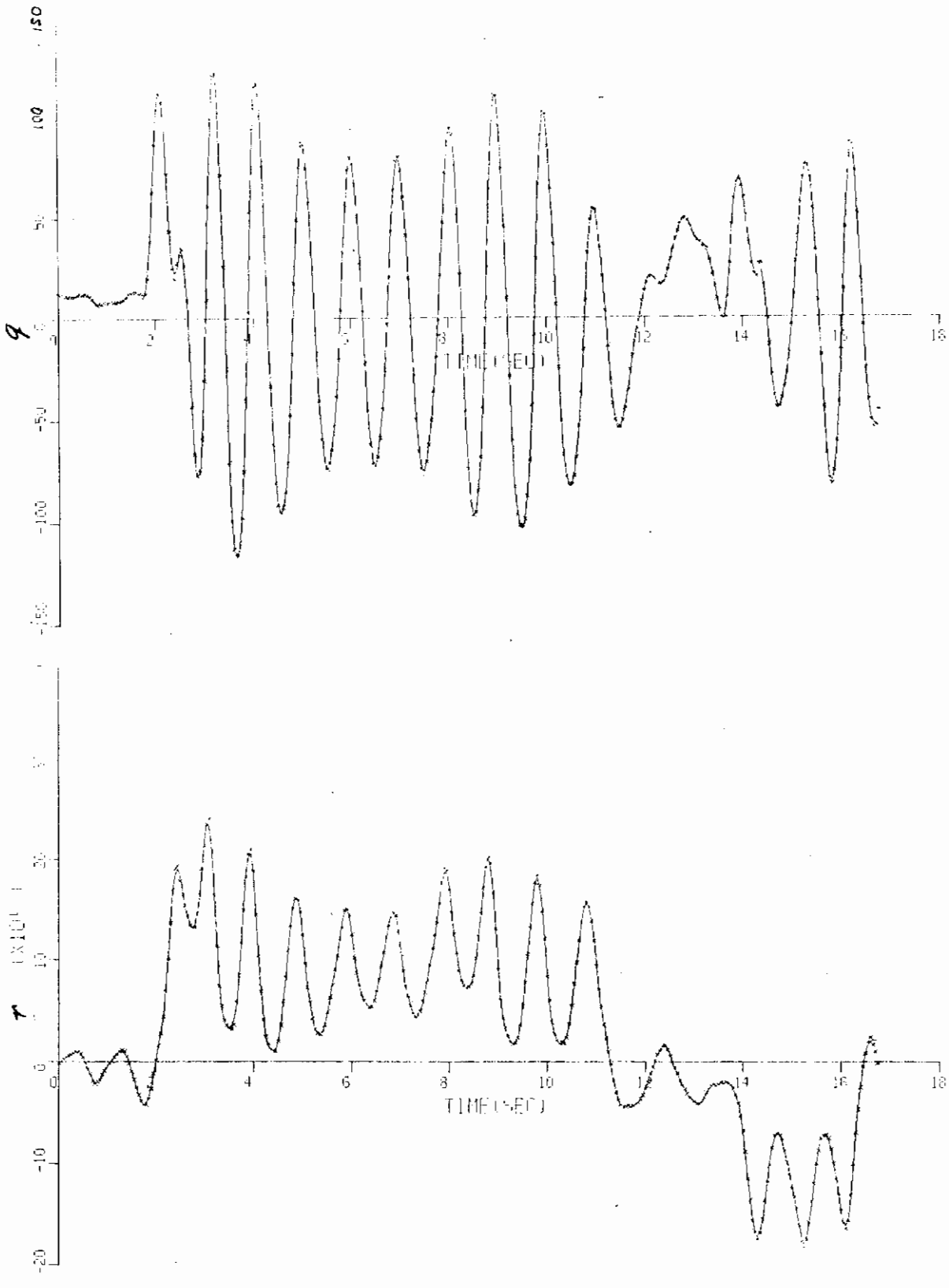

Figure 56 (Continued) RADIO CONTROLLED MODEL TIME HISTORIES - RUN 1

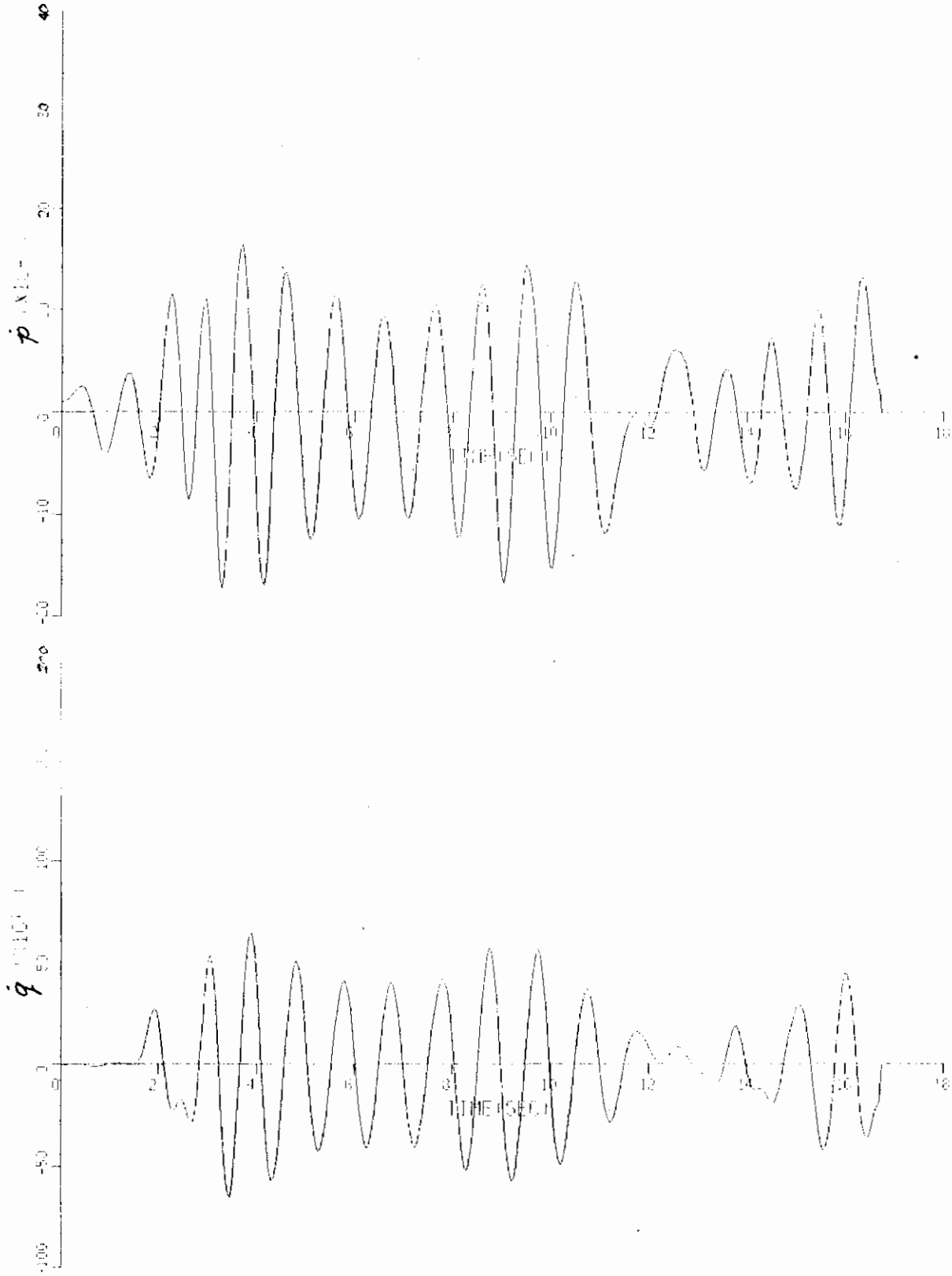

Figure 56 (Continued) RADIO CONTROLLED MODEL TIME HISTORIES - RUN 1

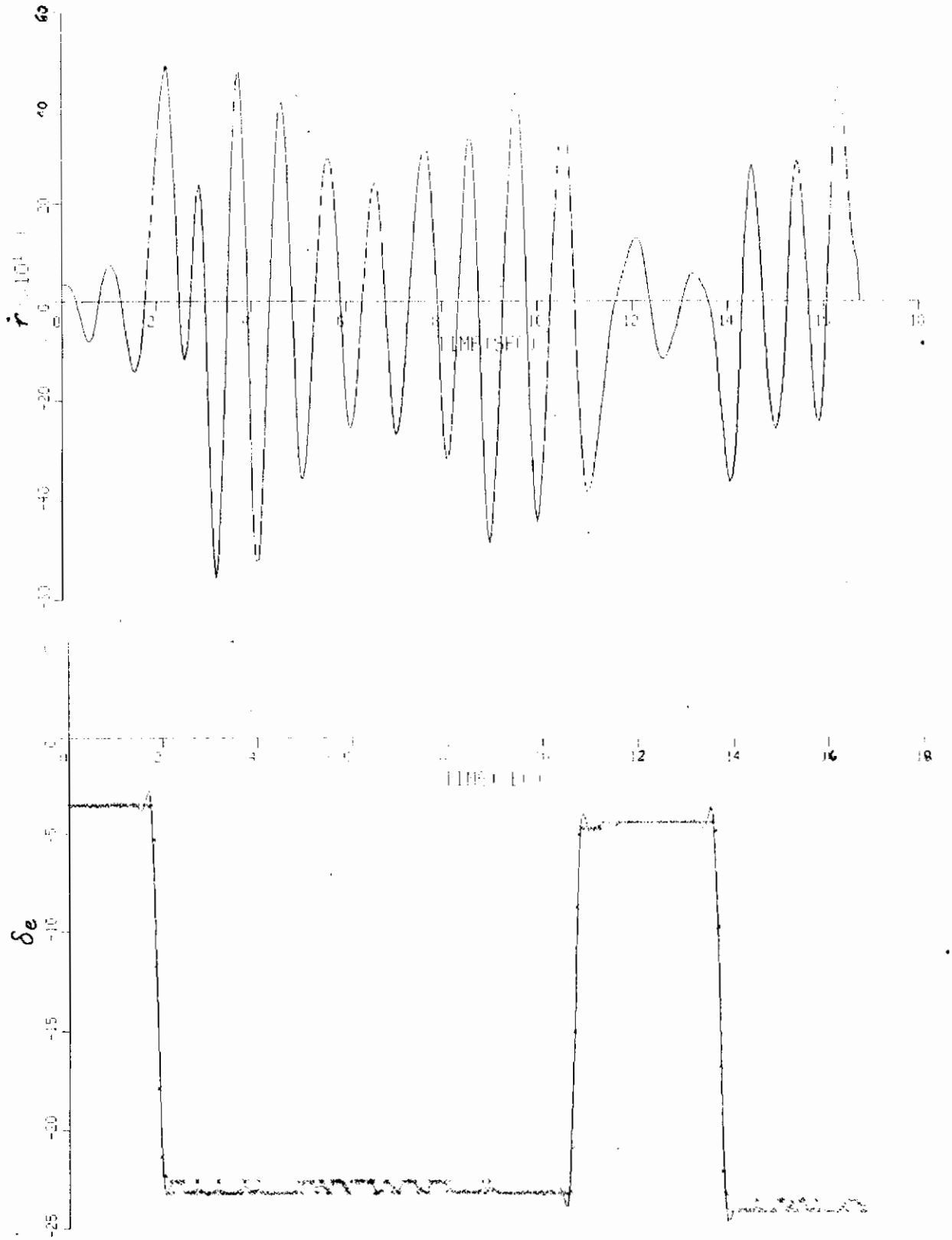

Figure 56 (Continued) RADIO CONTROLLED MODEL TIME HISTORIES - RUN 1

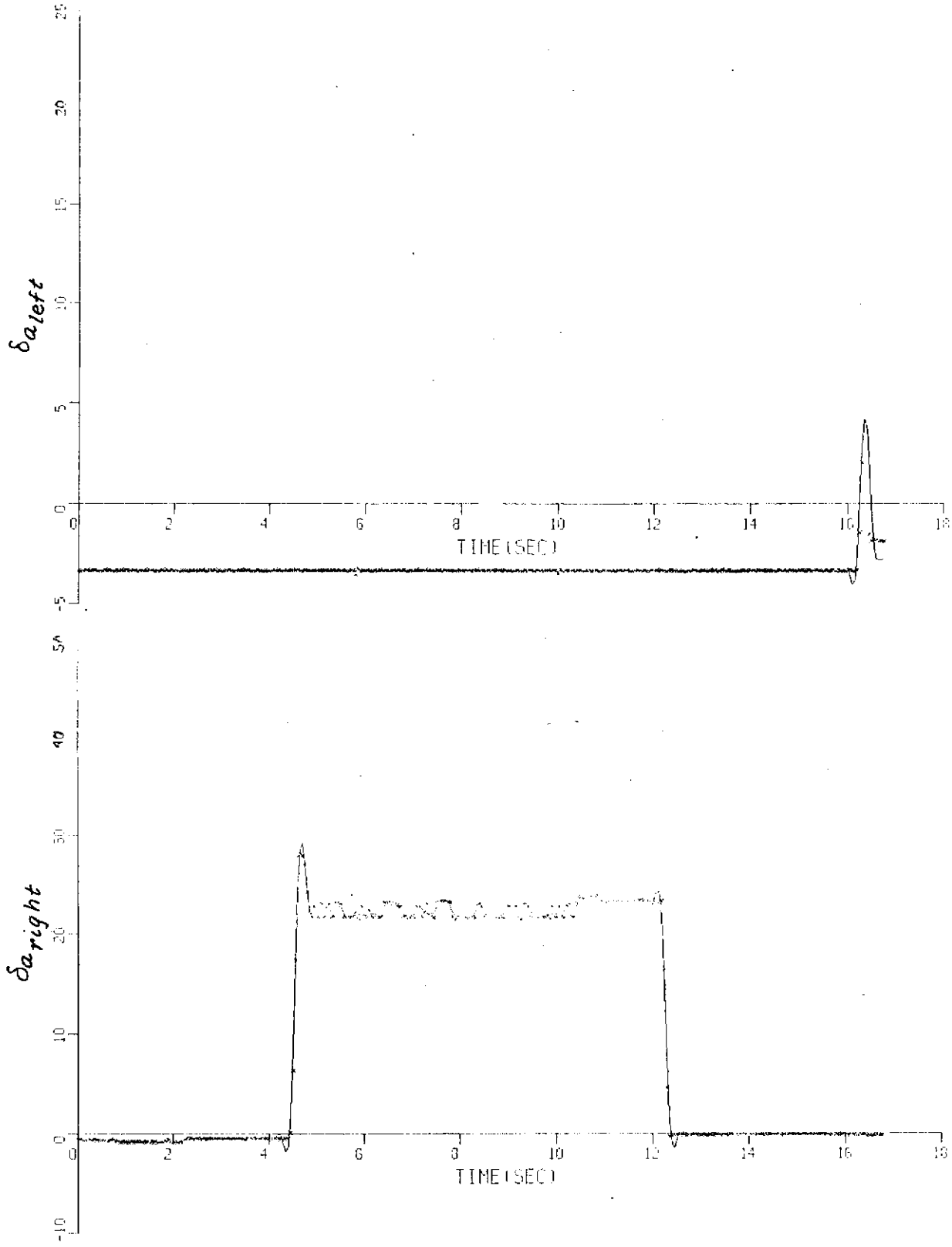

Figure 56 (Continued) RADIO CONTROLLED MODEL TIME HISTORIES - RUN 1

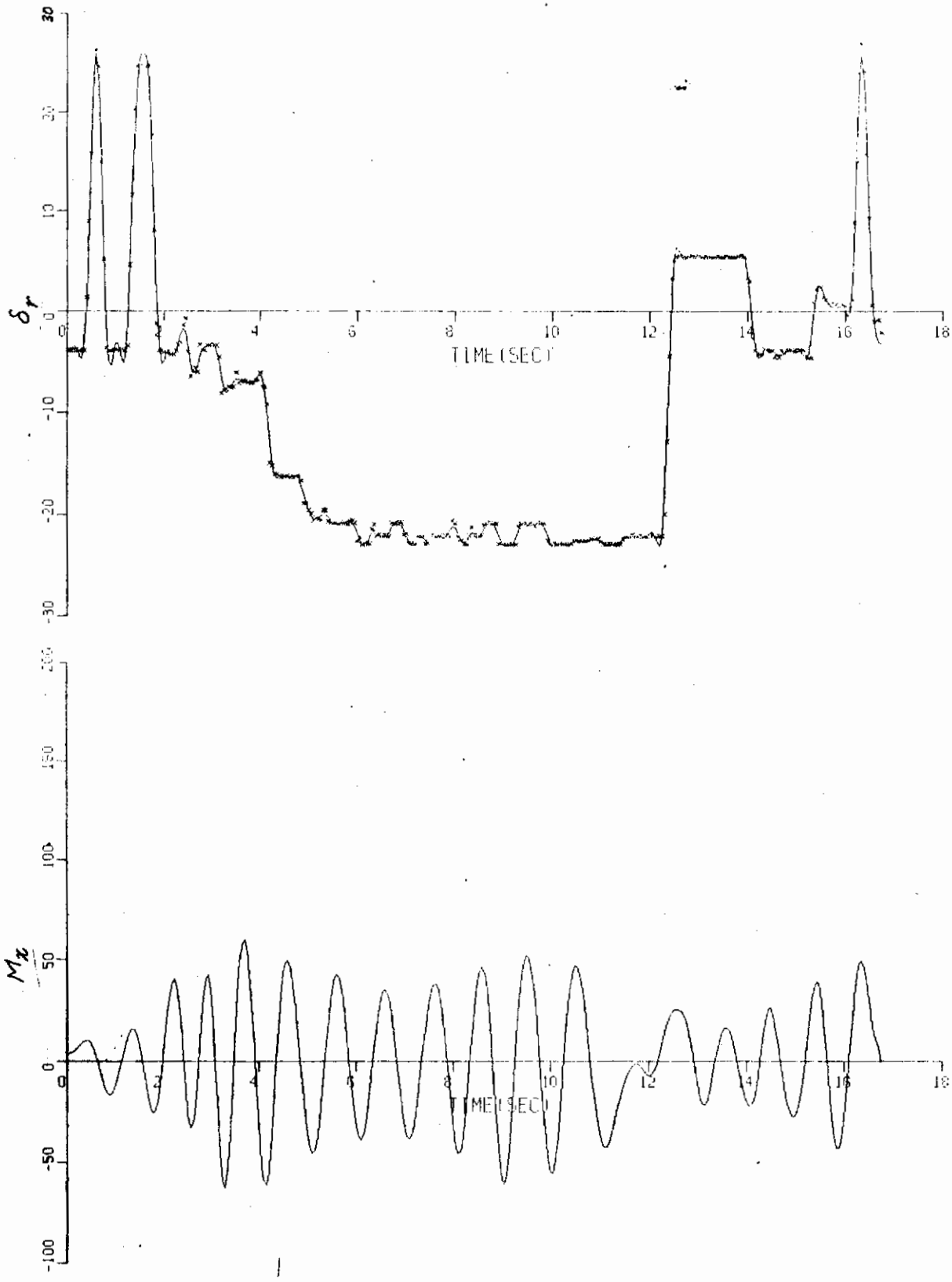

Figure 56 (Continued) RADIO CONTROLLED MODEL TIME HISTORIES - RUN 1

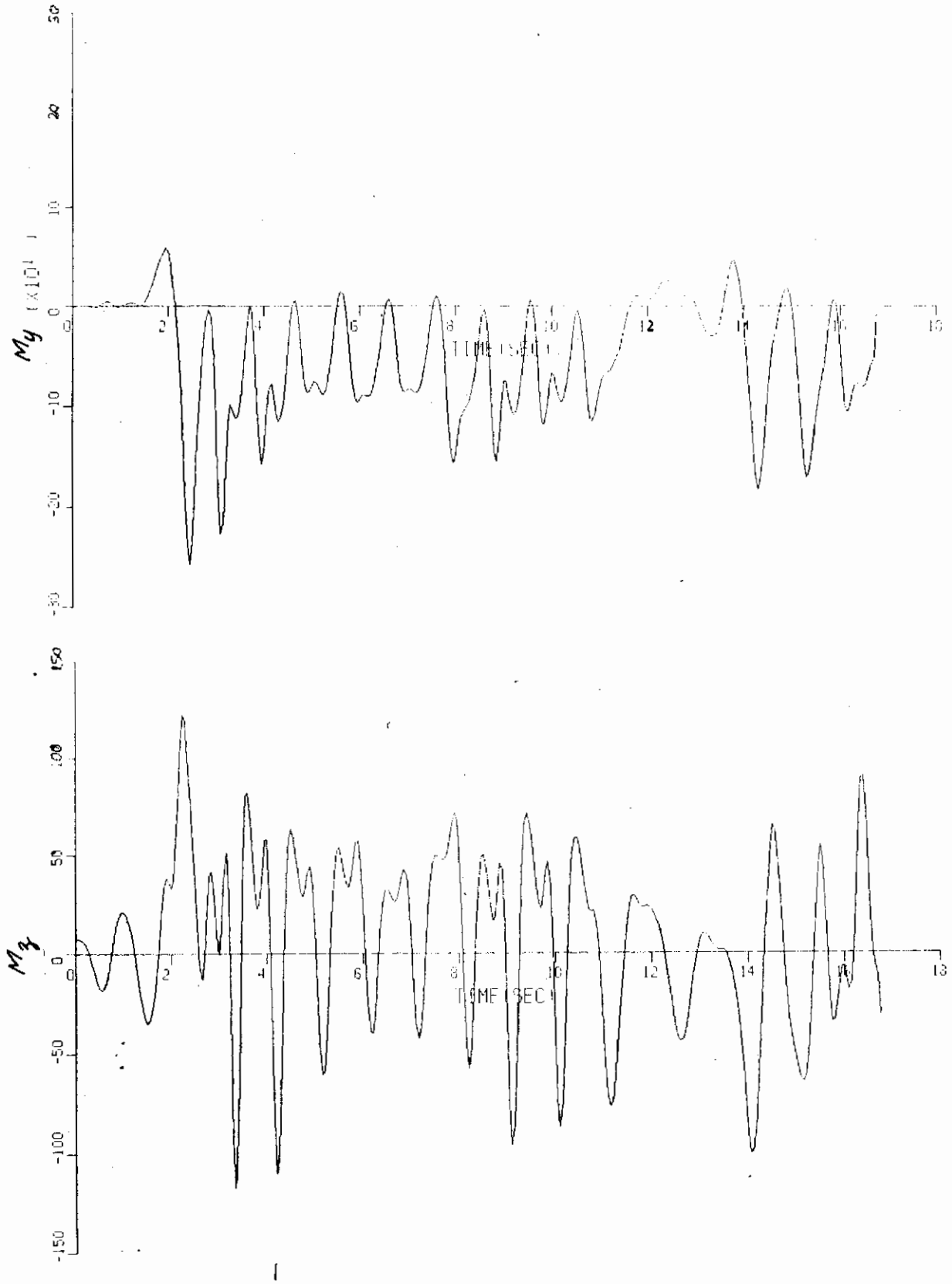

Figure 56 (Concluded) RADIO CONTROLLED MODEL TIME HISTORIES - RUN 1

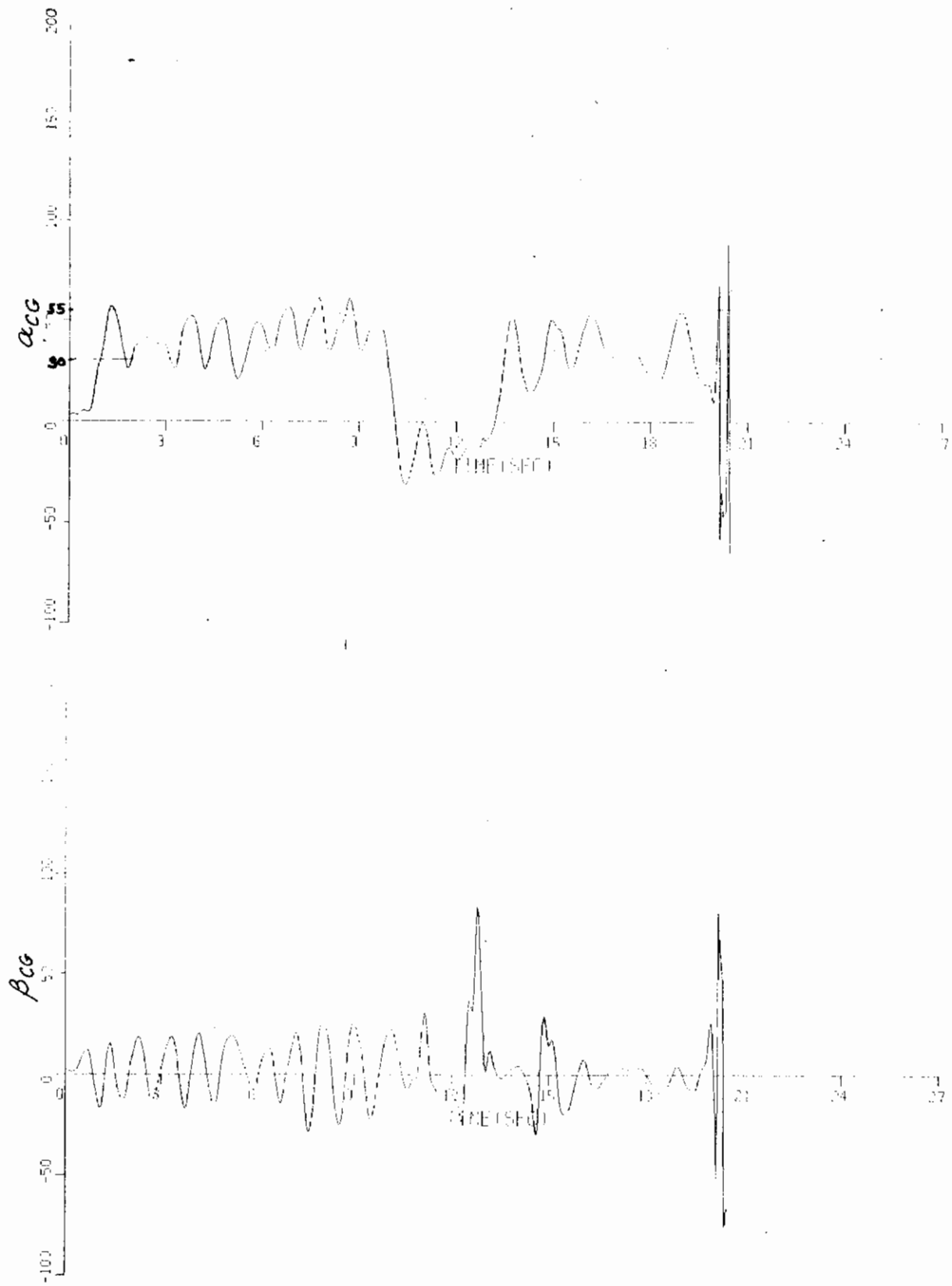

Figure 57 RADIO CONTROLLED MODEL TIME HISTORIES - RUN 3

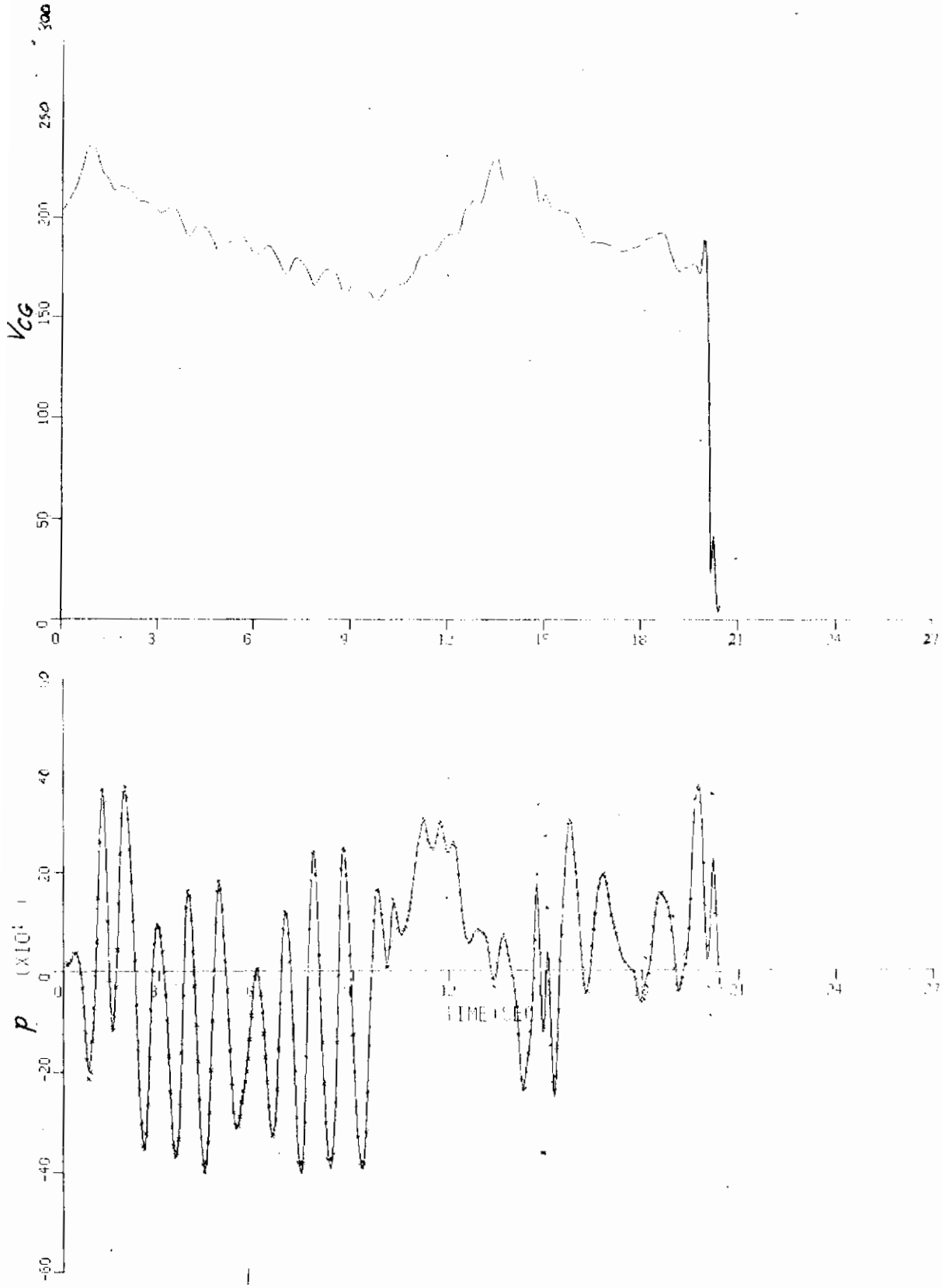

Figure 57 (Continued) RADIO CONTROLLED MODEL TIME HISTORIES - RUN 3

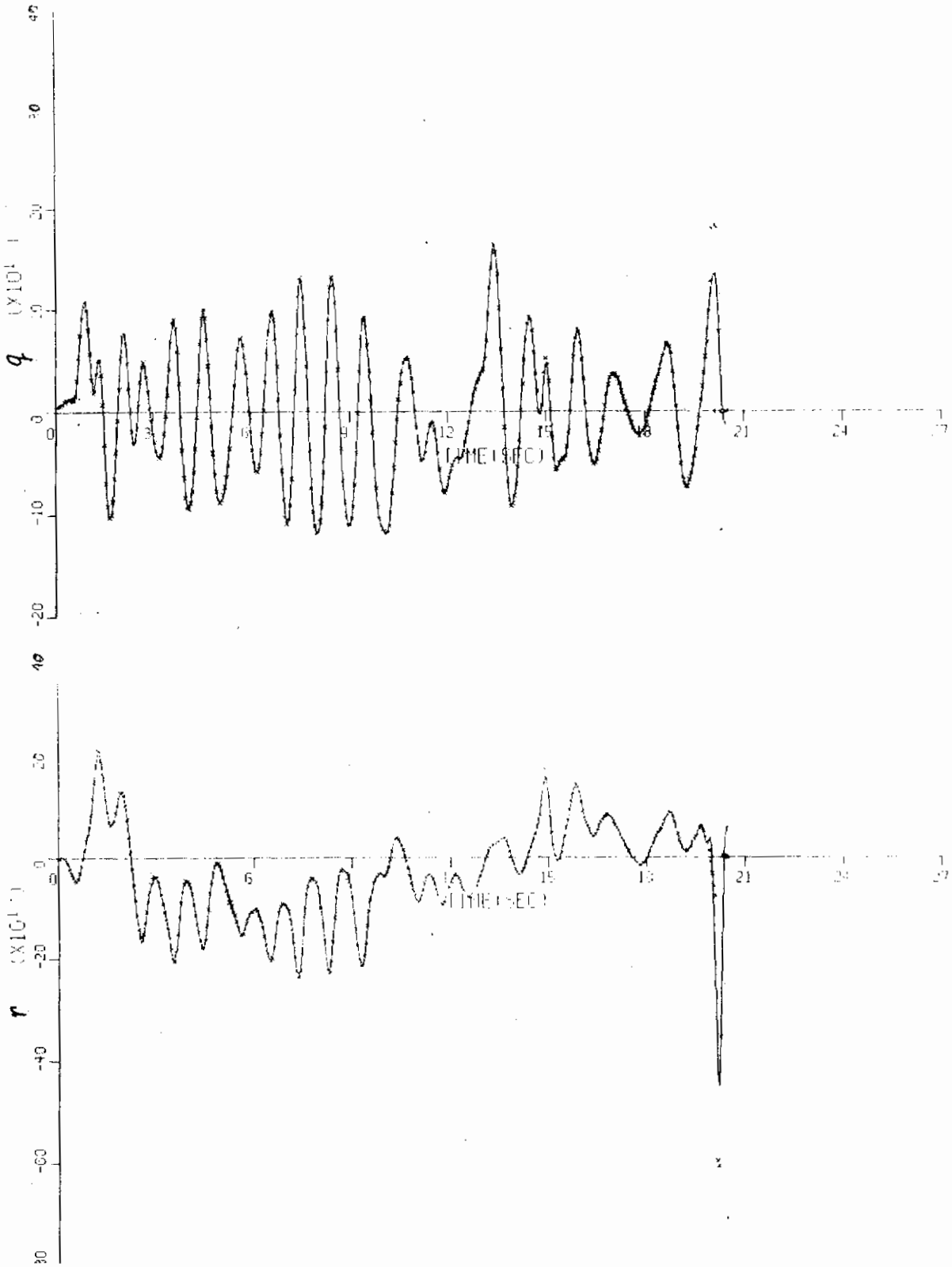

Figure 57 (Continued) RADIO CONTROLLED MODEL TIME HISTORIES - RUN 3

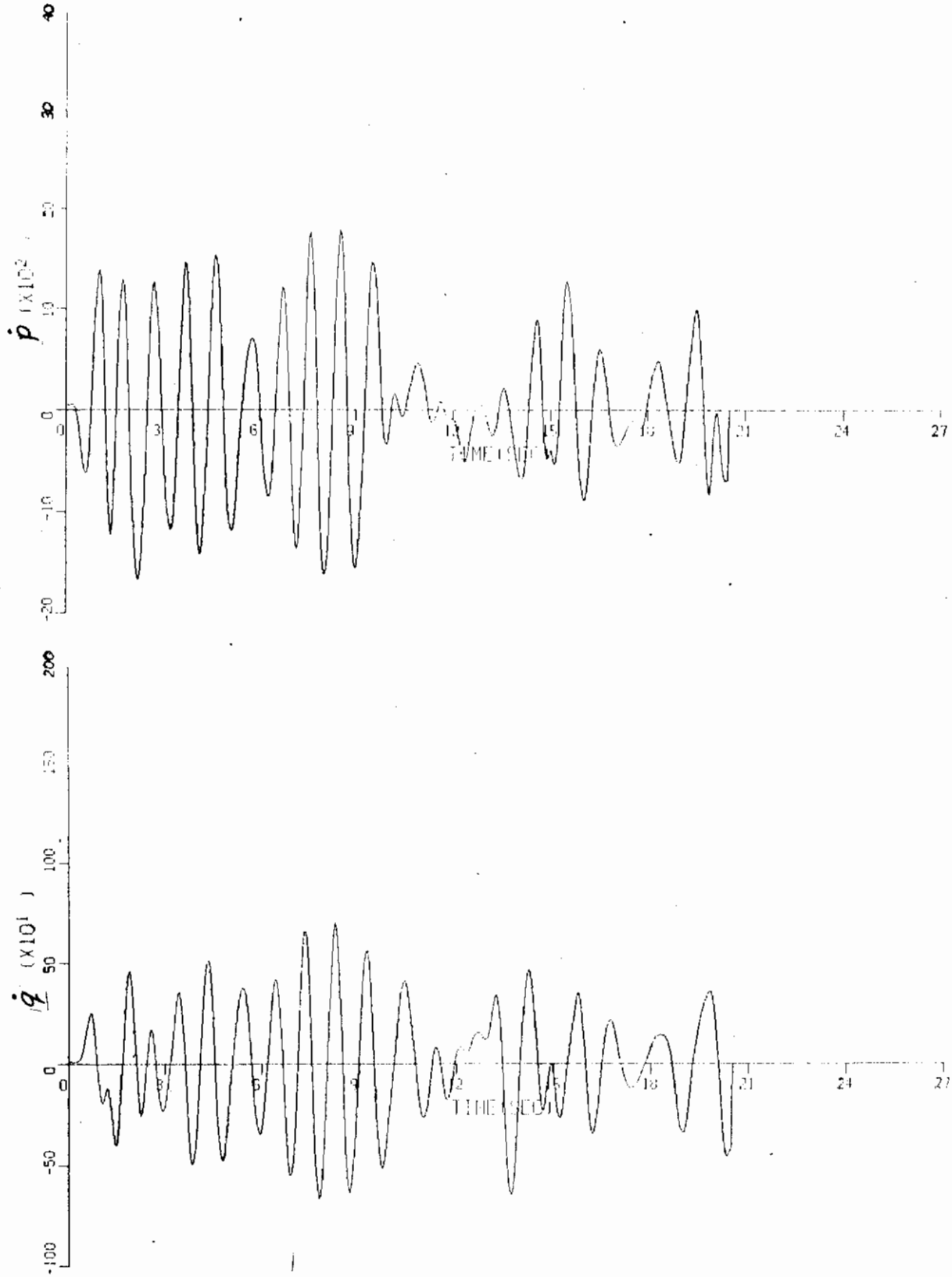

Figure 57 (Continued) RADIO CONTROLLED MODEL TIME HISTORIES - RUN 3

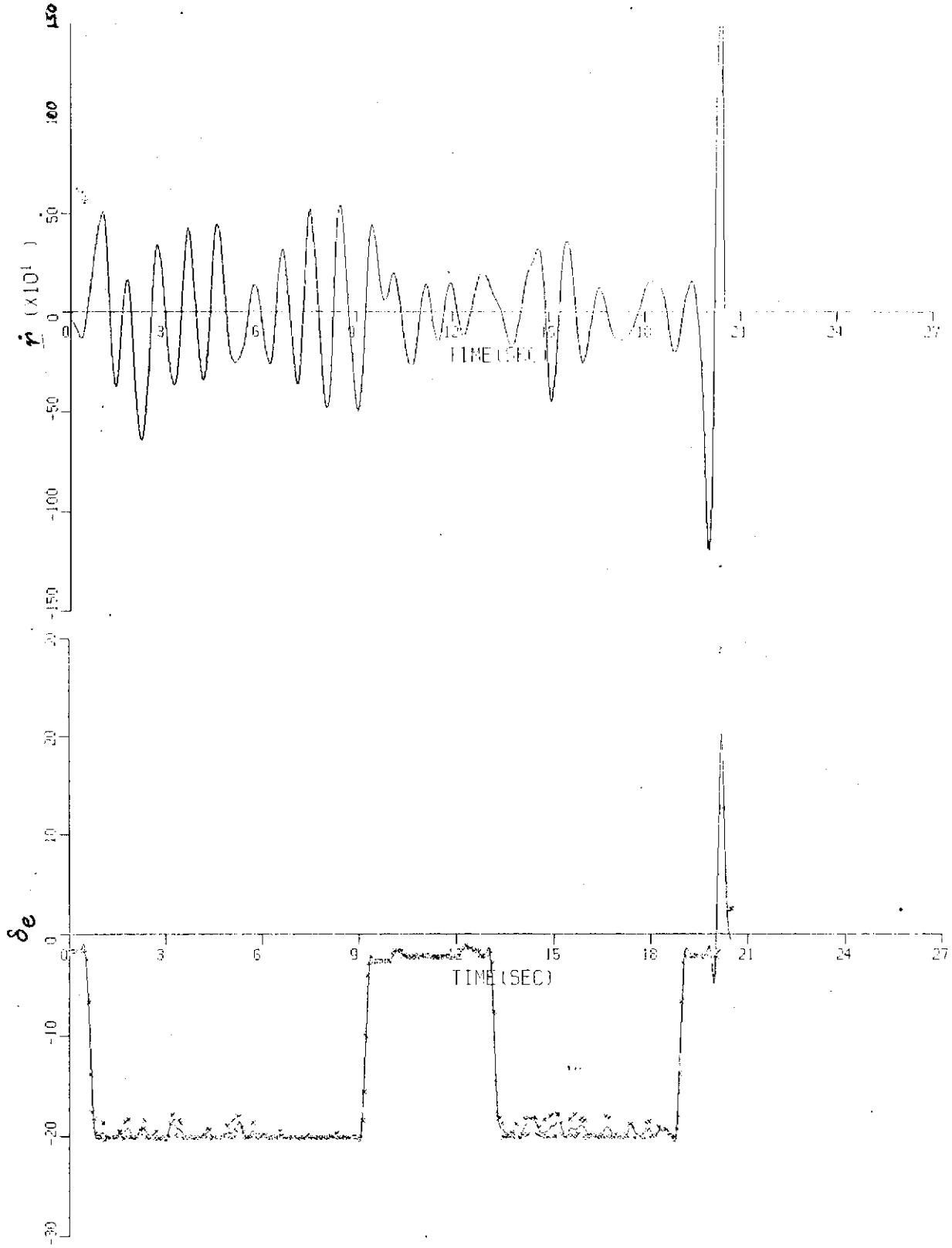

Figure 57 (Continued) RADIO CONTROLLED MODEL TIME HISTORIES - RUN 3

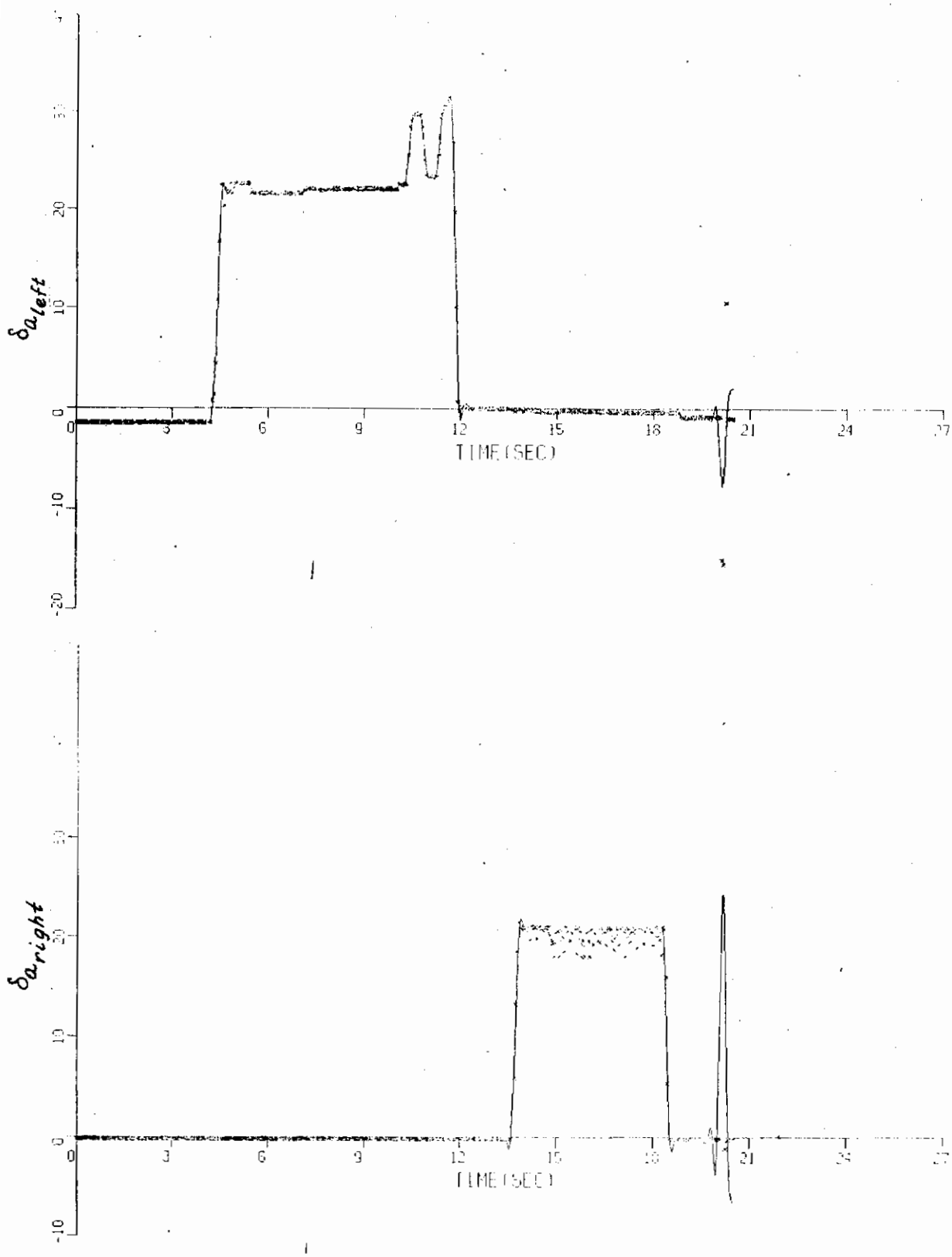

Figure 57 (Continued) RADIO CONTROLLED MODEL TIME HISTORIES - RUN 3

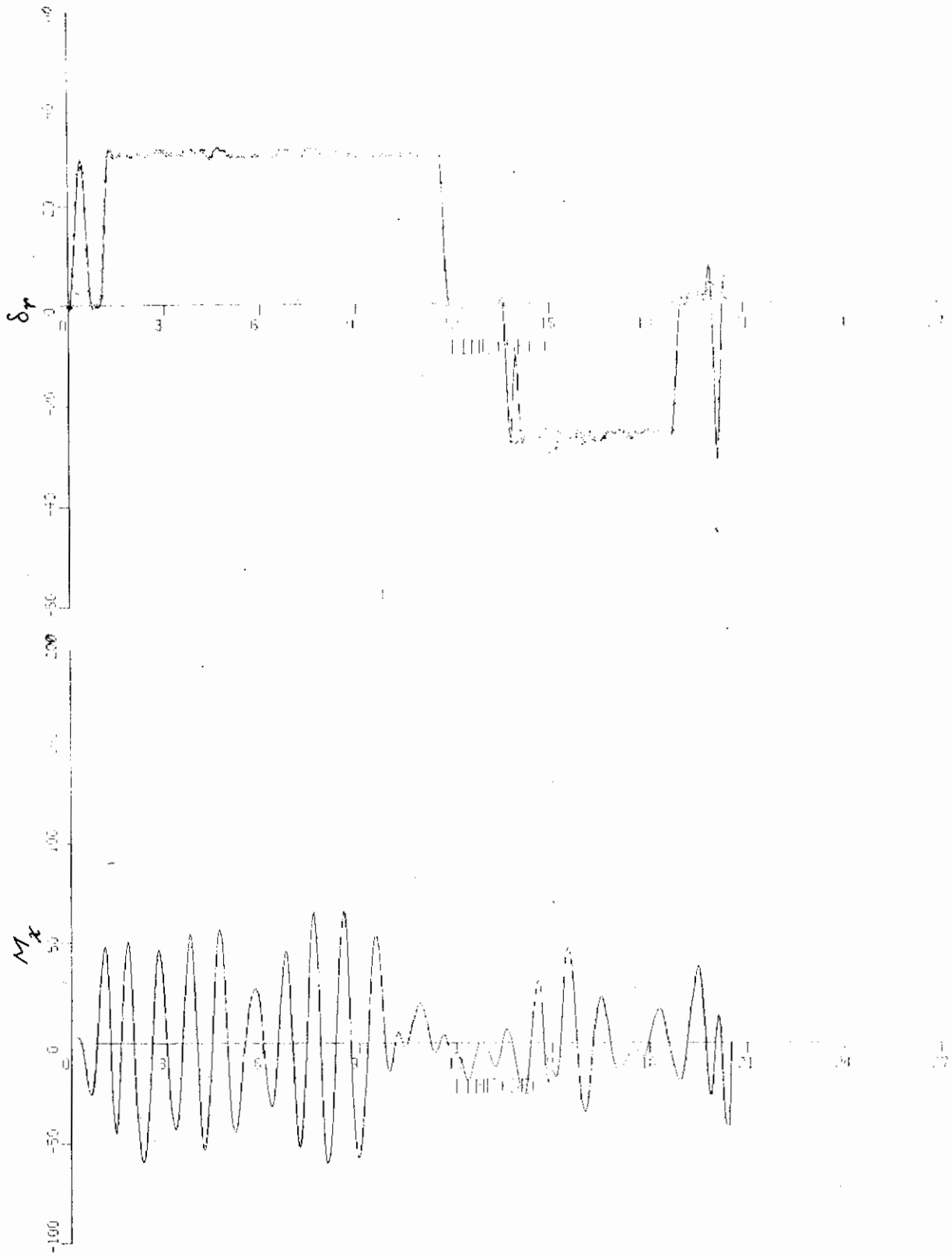

Figure 57 (Continued) RADIO CONTROLLED MODEL TIME HISTORIES - RUN 3

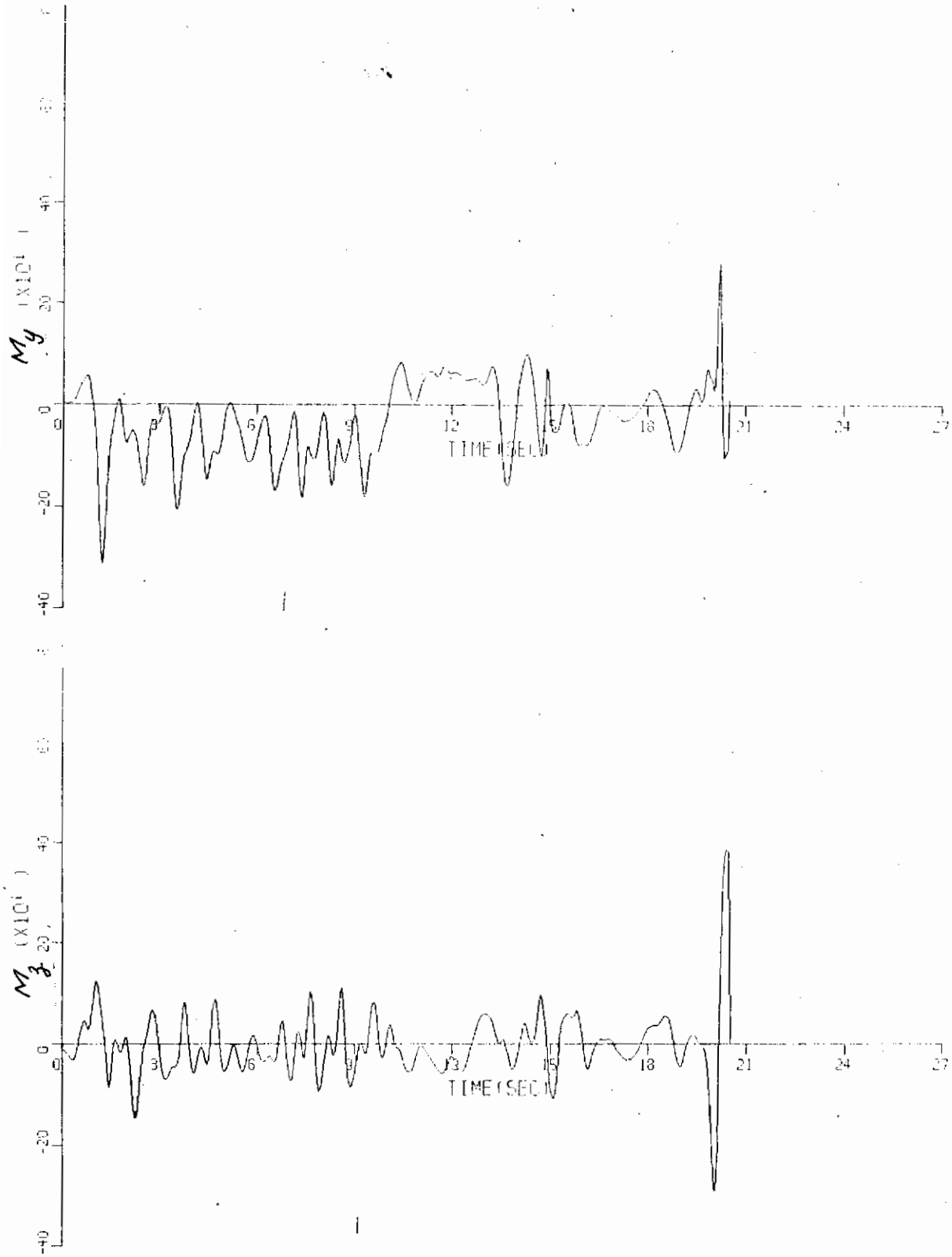

Figure 57 (Concluded) RADIO CONTROLLED MODEL TIME HISTORIES - RUN 3

Table XXIV
AIRCRAFT MASS CHARACTERISTICS AND CENTER OF GRAVITY (CG) LOCATION

RECORD NO.	I_x (slug-ft^2)	I_y (slug-ft^2)	I_z (slug-ft^2)	I_{xz} (slug-ft^2)	GROSS WEIGHT (lb)	CG (% $\bar{c}$)	VERTICAL CG W.L.*(in)
9	25535	168626	188690	6478	43000	32.9	25.1
10	25418	166785	186767	6315	42600	32.5	25.0
11	25100	165725	185461	6196	42000	32.3	24.9
14	24465	162274	181518	5874	40700	31.5	25.1
15	23932	162846	181808	5854	39650	31.0	25.6
17	23638	162865	182020	5555	38400	30.1	24.5
19	23469	158204	177684	4949	37000	29.3	23.3
20	23361	157434	176983	5022	36400	29.4	22.6

*WATER LINE REFERENCE

Table XXV
GEOMETRIC CHARACTERISTICS

b - WING SPAN: 38.4 ft
S - WING AREA: 538.34 ft
$\bar{c}$ - MEAN AERODYNAMIC CHORD: 16.04 ft.

Table XXVI

FLIGHT INSTRUMENTATION CHARACTERISTICS AND LOCATIONS FROM NOMINAL CENTER OF GRAVITY (CG) AT 33% MAC

SENSOR	FULL SCALE RANGE	σ RMS	LOCATION W.R.T. CG AT 33% MAC		
			l_x* (ft)	l_y* (ft)	l_z* (ft)
α -VANE	-30 TO 100 deg	$\pm$ 1.0 deg	38.55	$\approx$ 0.	$\approx$ 0.
β -VANE	$\pm$90 deg	$\pm$ 1.5 deg	38.22	0.	2.2
$n_{x_{cg}}$	$\pm$ 2 g's	$\pm$ 0.05 g's	-0.865	-0.375	0.808
$n_{y_{cg}}$	$\pm$ 2 g's	$\pm$ 0.05 g's	-0.781	-0.375	0.992
$n_{z_{cg}}$	-4 TO 10 g's	$\pm$ 0.13 g's	-0.865	-0.375	1.0
$n_{x_{PS}}$	$\pm$ 2 g's	$\pm$ 0.07 g's	17.14	-0.167	0.667
$n_{y_{PS}}$	$\pm$ 2 g's	$\pm$ 0.07 g's	17.14	-0.167	0.667
$n_{z_{PS}}$	-1 TO 6 g's	$\pm$ 0.1 g's	17.14	-0.092	0.667
p	$\pm$ 200°/sec	$\pm$ 5.2°/sec			
q	$\pm$ 50°/sec	$\pm$ 1.2°/sec			
r	$\pm$ 150°/sec	$\pm$ 4.0°/sec			
ϕ	$\pm$ 180 deg	$\pm$ 2.7 deg			
θ	$\pm$ 85 deg	$\pm$ 1.3 deg			
ψ	$\pm$ 180 deg	$\pm$ 2.7 deg			

* l_x, l_y, l_z - COORDINATES OF SENSOR, MEASURED FROM x, y, z AIRCRAFT BODY AXES AT NOMINAL CG (33% MAC)

TABLE XXVII

MASS CHARACTERISTICS OF THE RADIO CONTROLLED MODEL
(13% FULL SCALE)

S = 8.957 ft^2

b = 4.995 ft

$\bar{c}$ = 2.985 ft

wt = 227.25 lbs

c_g = 33.1% c

I_x = 2.247 $slug\text{-}ft^2$

I_y = 13.317 $slug\text{-}ft^2$

I_{xy} = .560 $slug\text{-}ft^2$

Appendix II

ANALYTICAL REPRESENTATION OF AERODYNAMIC COEFFICIENTS

1. Least Squares Technique

The maximum complexity to which any of the aerodynamic force or moment coefficients for the least squares technique can be written is a formulation of up to 30 of the following 41 types of parameters:

constant	$\dot{\alpha}$	δ_e
α	$\alpha\dot{\alpha}$	$\alpha\delta_e$
α^2	$\alpha^2\dot{\alpha}$	$\alpha^2\delta_e$
β	p	$\beta\delta_e$
β^2	αp	$\beta^2\delta_e$
β^3	$\alpha^2 p$	$\beta^3\delta_e$
$\alpha\beta$	r	$\beta\alpha\delta_e$
$\alpha\beta^2$	αr	$\beta^3\alpha\delta_e$
$\alpha\beta^3$	$\alpha^2 r$	δ_a
$\alpha^2\beta$	$\delta_e r$	δ_a^2
$\alpha^2\beta^2$	$\delta_e\alpha r$	$\alpha\delta_a$
$\alpha^2\beta^3$	$\delta_e\alpha^2 r$	$\alpha^2\delta_a$
q		δ_r
αq		$\alpha\delta_r$
$\alpha^2 q$		

Theoretically this implies that a total of 180 parameters defining the six aerodynamic equations could be attempted to be identified. Realistically this is impossible and a much lower number of parameters can adequately define the aerodynamics.

2. Iterated Kalman Filter/Fixed-Point Smoother Technique

For the Kalman filtering technique the longitudinal and lateral-directional models were treated separately. In the longitudinal cases the maximum complexity that could be identified was a formulation of any number of the following 40 terms. The parameters not being identified were fixed at known values or zero.

C_{m_0}
C_{m_α}
$C_{m_{\alpha^2}}$
$C_{m_{\beta^2}}$
$C_{m_{\alpha\beta^2}}$
$C_{m_{\alpha^2\beta^2}}$
$C_{m_{\delta_e}}$
$C_{m_{\alpha\delta_e}}$
$C_{m_{\alpha^2\delta_e}}$
$C_{m_{\beta^2\delta_e}}$
$C_{m_{\alpha\beta^2\delta_e}}$
$C_{m_{\alpha^2\beta^2\delta_e}}$
$C_{m_{|\delta_a|}}$
C_{m_q}
$C_{m_{\alpha q}}$
$C_{m_{\alpha^2 q}}$
$C_{m_{\alpha^3 q}}$

C_{y_0}
C_{y_α}
$C_{y_{\alpha^2}}$
$C_{y_{\delta_e}}$
$C_{y_{\alpha\delta_e}}$
$C_{y_{\alpha^2\delta_e}}$
$C_{y_{|\delta_a|}}$
C_{y_q}
$C_{y_{\alpha q}}$
$C_{y_{\alpha^2 q}}$
$C_{y_{\alpha^3 q}}$

C_{x_0}
C_{x_α}
$C_{x_{\alpha^2}}$
$C_{x_{\beta^2}}$
$C_{x_{\alpha\beta^2}}$
$C_{x_{\alpha^2\beta^2}}$
$C_{x_{\delta_e}}$
$C_{x_{\alpha\delta_e}}$
$C_{x_{\beta^2\delta_e}}$
C_{x_q}
$C_{x_{\alpha q}}$
$C_{x_{\alpha^2 q}}$

For the lateral-directional cases the maximum complexity available was the identification of a subset of the following 50 parameters. The remainder were fixed at known values or zero.

C_{l_0}

C_{l_β}

$C_{l_{\alpha\beta}}$

$C_{l_{\alpha^2\beta}}$

$C_{l_{\delta_a}}$

$C_{l_{\alpha\delta_a}}$

$C_{l_{\alpha^2\delta_a}}$

$C_{l_{\delta_r}}$

$C_{l_{\alpha\delta_r}}$

C_{l_p}

$C_{l_{\alpha p}}$

$C_{l_{\alpha^2 p}}$

$C_{l_{\alpha^3 p}}$

C_{l_r}

$C_{l_{\alpha r}}$

$C_{l_{\alpha^2 r}}$

C_{n_0}

C_{n_β}

$C_{n_{\alpha\beta}}$

$C_{n_{\alpha^2\beta}}$

$C_{n_{\beta^3}}$

$C_{n_{\alpha\beta^3}}$

$C_{n_{\delta_a}}$

$C_{n_{\alpha\delta_a}}$

$C_{n_{\delta_r}}$

$C_{n_{\alpha\delta_r}}$

$C_{n_{\beta\delta_e}}$

$C_{n_{\alpha\beta\delta_e}}$

$C_{n_{\beta^3\delta_e}}$

$C_{n_{\alpha\beta^3\delta_e}}$

C_{n_p}

$C_{n_{\alpha p}}$

$C_{n_{\alpha^2 p}}$

$C_{n_{\alpha^3 p}}$

C_{n_r}

$C_{n_{\alpha r}}$

$C_{n_{\alpha^2 r}}$

$C_{n_{\delta_e r}}$

$C_{n_{\alpha\delta_e r}}$

C_{y_0}

C_{y_β}

$C_{y_{\alpha\beta}}$

$C_{y_{\delta_r}}$

$C_{y_{\alpha\delta_r}}$

C_{y_p}

$C_{y_{\alpha p}}$

$C_{y_{\alpha^2 p}}$

$C_{y_{\alpha^3 p}}$

C_{y_r}

$C_{y_{\alpha r}}$

Appendix III

SIX-DEGREE-OF-FREEDOM COMPUTER SIMULATION

Integrations of the analytical wind tunnel model or refinements to it for time history matches with the flight data were done on Calspan's six-degree-of-freedom (6 DOF) computer program. This program was modified to include the F-4's nonlinear aerodynamics (Section IV), and engine effects. The equations are written in the body axis system. The differential equations are:

$$[\dot{V}] = \begin{bmatrix} \dot{u} \\ \dot{v} \\ \dot{w} \end{bmatrix} = \frac{1}{m} \cdot [F] - [\omega_x] \cdot [V]$$

$$[\dot{\omega}] = \begin{bmatrix} \dot{p} \\ \dot{q} \\ \dot{r} \end{bmatrix} = [I]^{-1} \cdot ([M] - [\omega_x] \cdot \{[I] \cdot [\omega] + [I_{eng}] \cdot [\omega_{eng}]\})$$

where: $[F] = [F_{Aero}] + [F_{Thrust}] + [F_{Grav}]$

$$[F_{Aero}] = \bar{q} \cdot S \cdot \begin{bmatrix} C_{x_{Aero}} \\ C_{y_{Aero}} \\ C_{z_{Aero}} \end{bmatrix}$$

$$[F_{Thrust}] = \begin{bmatrix} .9958\ (T_R + T_L) \\ .00434\ (T_L - T_R) \\ -.0914\ (T_R + T_L) \end{bmatrix}$$

$$[F_{grav}] = m.g \cdot \begin{bmatrix} -\sin\theta \\ \sin\phi \cdot \cos\theta \\ \cos\phi \cdot \cos\theta \end{bmatrix}$$

$$[\omega_x] = \begin{bmatrix} 0 & -r & q \\ r & 0 & -p \\ -q & p & 0 \end{bmatrix}$$

$$[I] = \begin{bmatrix} I_{xx} & 0 & -I_{xy} \\ 0 & I_{yy} & 0 \\ -I_{xz} & 0 & I_{zz} \end{bmatrix}$$

$$[M] = [M_{Aero}] + [M_{Thrust}]$$

$$[M_{Aero}] = \bar{q} \cdot S \cdot \begin{bmatrix} b & 0 & 0 \\ 0 & \bar{c} & 0 \\ 0 & 0 & b \end{bmatrix} \cdot \begin{bmatrix} C_{\ell_{Aero}} \\ C_{m_{Aero}} - \left(C_{z_{Aero}} \cdot \Delta CG\right) \\ C_{n_{Aero}} + \left(C_{y_{Aero}} \cdot \Delta CG \, \frac{\bar{c}}{b}\right) \end{bmatrix}$$

$$[M_{Thrust}] = \begin{bmatrix} .1833\ (T_L - T_R) \\ (-\ .3894 + .0914\ X_T)\ (T_L + T_R) \\ (\ 1.977 + \ .00434\ X_T)\ (T_L - T_R) \end{bmatrix}$$

$$X_T = .608 + \Delta CG \quad (16.04)$$

$$\Delta CG = CG_{pos} - .33$$

$$[I_{eng}] = \begin{bmatrix} I_{eng} & 0 & 0 \\ 0 & 0 & 0 \\ 0 & 0 & 0 \end{bmatrix}$$

$$[\omega_{eng}] = \begin{bmatrix} \omega_R + \omega_L \\ 0 \\ 0 \end{bmatrix}$$

I_{eng} = engine inertia, 21. slug-ft^2

ω_R, ω_L = engine angular speed, rad/sec

The auxiliary equations for angle of attack and sideslip are:

$$\alpha = \sin^{-1}\left(\frac{w}{V \cos \beta}\right)$$

$$\beta = \sin^{-1}\left(\frac{v}{V}\right)$$

The Euler angles are obtained from the integration of the following equation:

$$\dot{[E]} = \begin{bmatrix} \dot{\phi} \\ \dot{\theta} \\ \dot{\psi} \end{bmatrix} = [c]\ [\omega]$$

where

$$[c] = \begin{bmatrix} 1 & \sin\phi \tan\theta & \cos\phi \tan\theta \\ 0 & \cos\phi & -\sin\phi \\ 0 & \sin\phi \sec\theta & \cos\phi \sec\theta \end{bmatrix}$$

Appendix IV
WIND TUNNEL DATA

1. Wind Tunnel Data

The figures presented in this appendix are hand faired plots of the wind tunnel data used during this investigation. These plots were used to approximate the wind tunnel data when making comparisons between the extracted values from flight data and the wind tunnel values.

The solid curves in these figures are the hand faired plots to the Langley wind tunnel test data (References 10 and 11) and are representative for the $-15^{\circ} \leq \beta \leq 15^{\circ}$. The x's are the actual data points for $\beta = 0^{\circ}$, except for the C_{y_p}, C_{ℓ_β} and C_{n_β} derivatives, and are shown for reference. Because the C_y, C_ℓ and C_n coefficients are approximately linear in β for $|\beta| \lesssim 15^{\circ}$, the x's for the C_{y_β}, C_{ℓ_β} and C_{n_β} derivatives represent a mean value between the data points at $\beta = 10^{\circ}$ and -10°. For example, $C_{\ell_\beta}(\alpha)$ was obtained as follows:

$$C_{\ell_\beta}(\alpha) = \frac{C_\ell(\alpha, \beta = 10^{\circ}) - C_\ell(\alpha, \beta = -10^{\circ})}{20}$$

It should be noted that the faired plots for the $C_{n_{\delta_e}}$, $C_{x_{\delta_e}}$, $C_{\ell_{\delta_a}}$ and $C_{y_{\delta_r}}$ derivatives do not pass through the mean value of the data points. This is because these plots approximate a mean fit to the data for β between $\pm 15^{\circ}$ due to extreme scatter and anomalies in these derivatives as functions of β, especially around $\beta = 0^{\circ}$. Consequently, these plots represent an average value for β between $\pm 15^{\circ}$ and not just for $\beta = 0^{\circ}$.

The solid plots can also be used to approximately describe the equations in Section IV which define the analytical model used to represent the wind tunnel data. However, these equations are much more complex since they take into account β^5 effects not shown on these plots.

Also presented on these figures are data from another set of wind tunnel tests conducted at high angles of attack for comparison purposes. The data is represented by the dashed hand faired plots taken from Reference 15. This data was obtained from a series of Ames/Langley wind tunnel tests and is therefore appropriately labeled Ames.

2. Initial Estimate for Kalman Identification Technique

The bulk of the initial estimates for the iterated Kalman filter/fixed-point smoother identification technique came from polynomial curve fits to the Langley wind tunnel data. These initial estimates are given in the appropriate Tables in Section V, in particular Tables XIV to XXII. However, in some cases, particular control derivatives were held fixed at the Ames wind

tunnel values. Preliminary identification results indicated the Ames control derivatives to be closer to the full scale aircraft in addition to some full scale flight test results from other sources (Reference 27). The values are given below for completeness.

Lateral-Directional Low-α Model:

$$C_{l_{\delta_r}} = -2.2 \times 10^{-4} + 5.0 \times 10^{-6}\,\alpha$$

$$C_{n_{\delta_r}} = 1.4 \times 10^{-3} - 2.5 \times 10^{-5}\,\alpha$$

$$C_{l_{\delta_a}} = 1.05 \times 10^{-3} - 3.5 \times 10^{-5}\,\alpha$$

$$C_{n_{\delta_a}} = -5.24 \times 10^{-5}\,\alpha$$

$$C_{l_r} = -.1 + .02\,\alpha \qquad \text{(Langley data)}$$

Lateral-Directional High - α Model:

$$C_{l_{\delta_r}} = -2.0 \times 10^{-4} + 4.97 \times 10^{-6}\,\alpha \qquad \text{(Langley data)}$$

$$C_{n_{\delta_r}} = 1.60 \times 10^{-3} - 3.5 \times 10^{-5}\,\alpha$$

$$C_{l_{\delta_a}} = 7.75 \times 10^{-4} - 1.9\ 10^{-5}\,\alpha$$

$$C_{n_{\delta_a}} = -9.1 \times 10^{-5} - 3.0 \times 10^{-6}\,\alpha$$

Longitudinal - All Models:

$$C_{m_{|\delta_a|}} = 6.98 \times 10^{-4} \qquad \text{(Reference 16)}$$

$$C_{y_{|\delta_a|}} = .0015 \qquad \text{(Reference 16)}$$

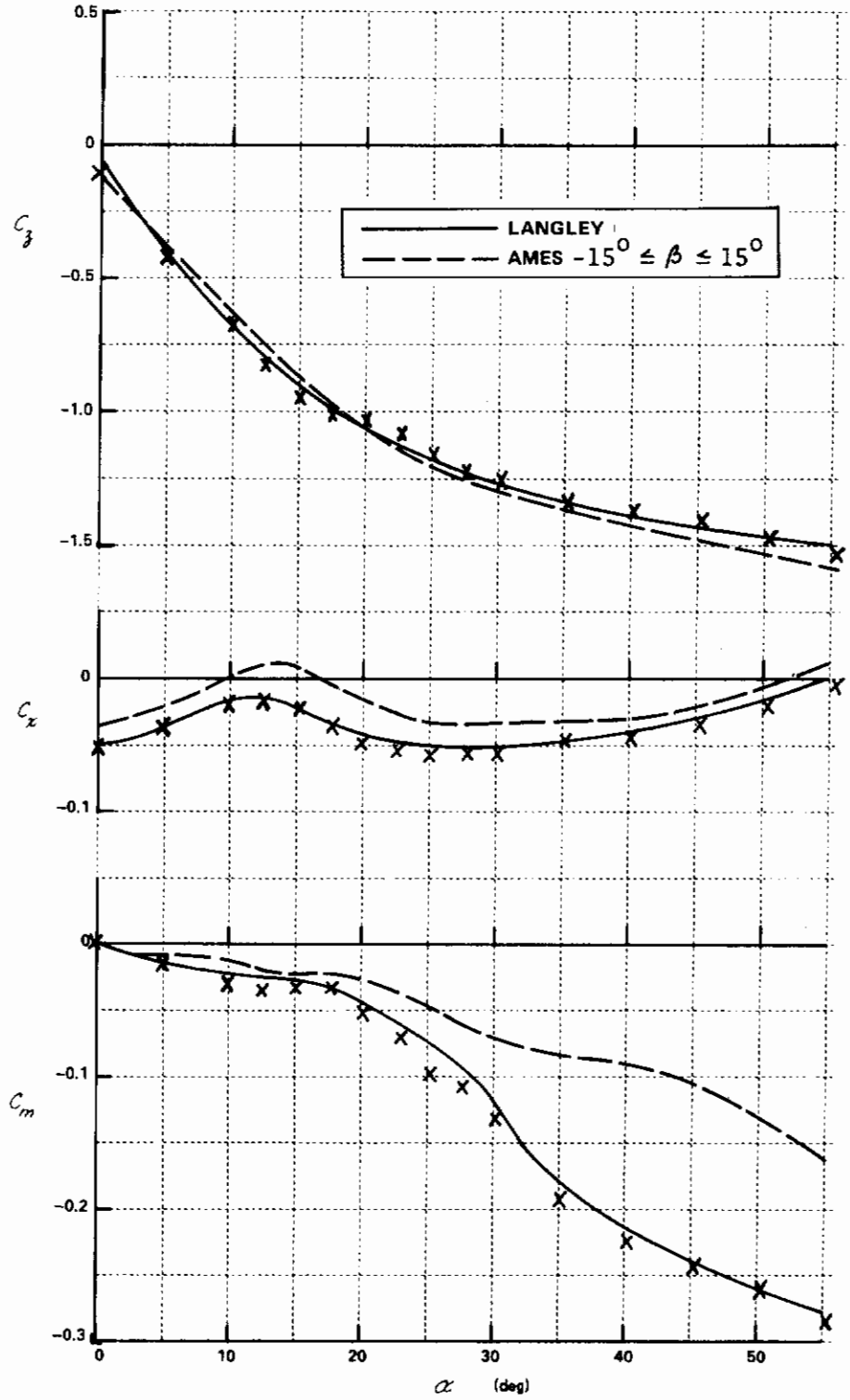

Figure 58 WIND TUNNEL DATA

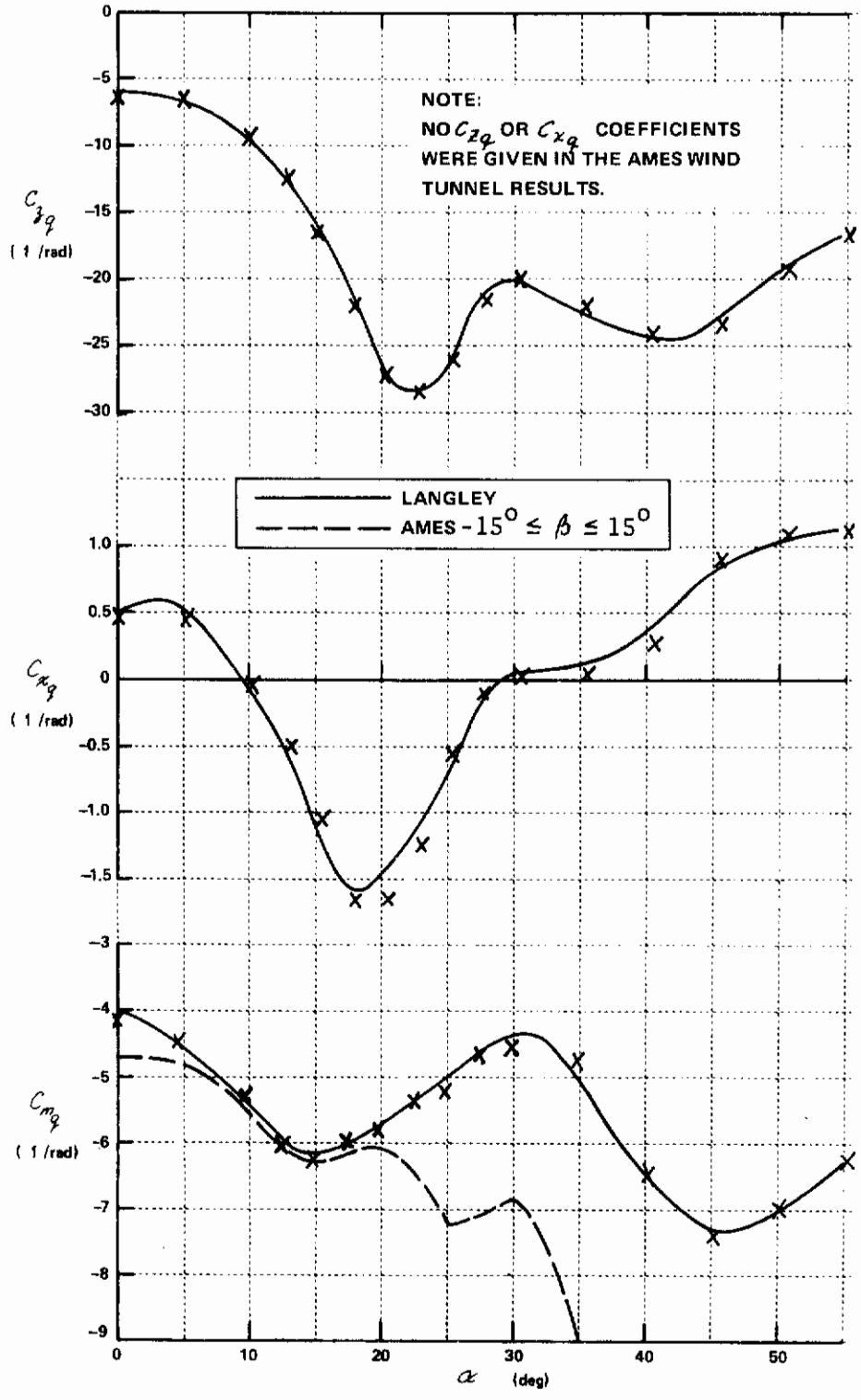

Figure 58 (Continued) WIND TUNNEL DATA

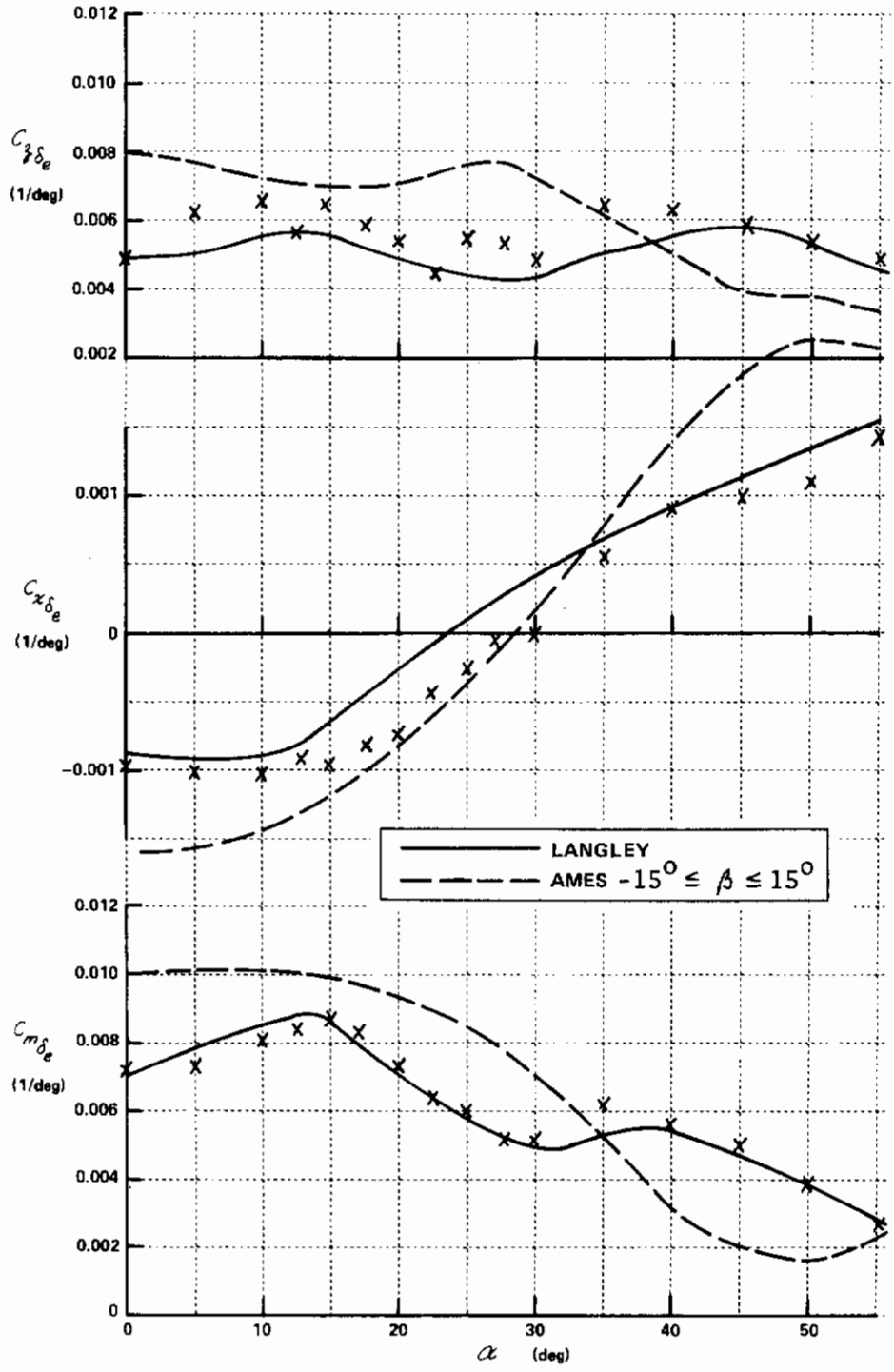

Figure 58 (Continued) WIND TUNNEL DATA

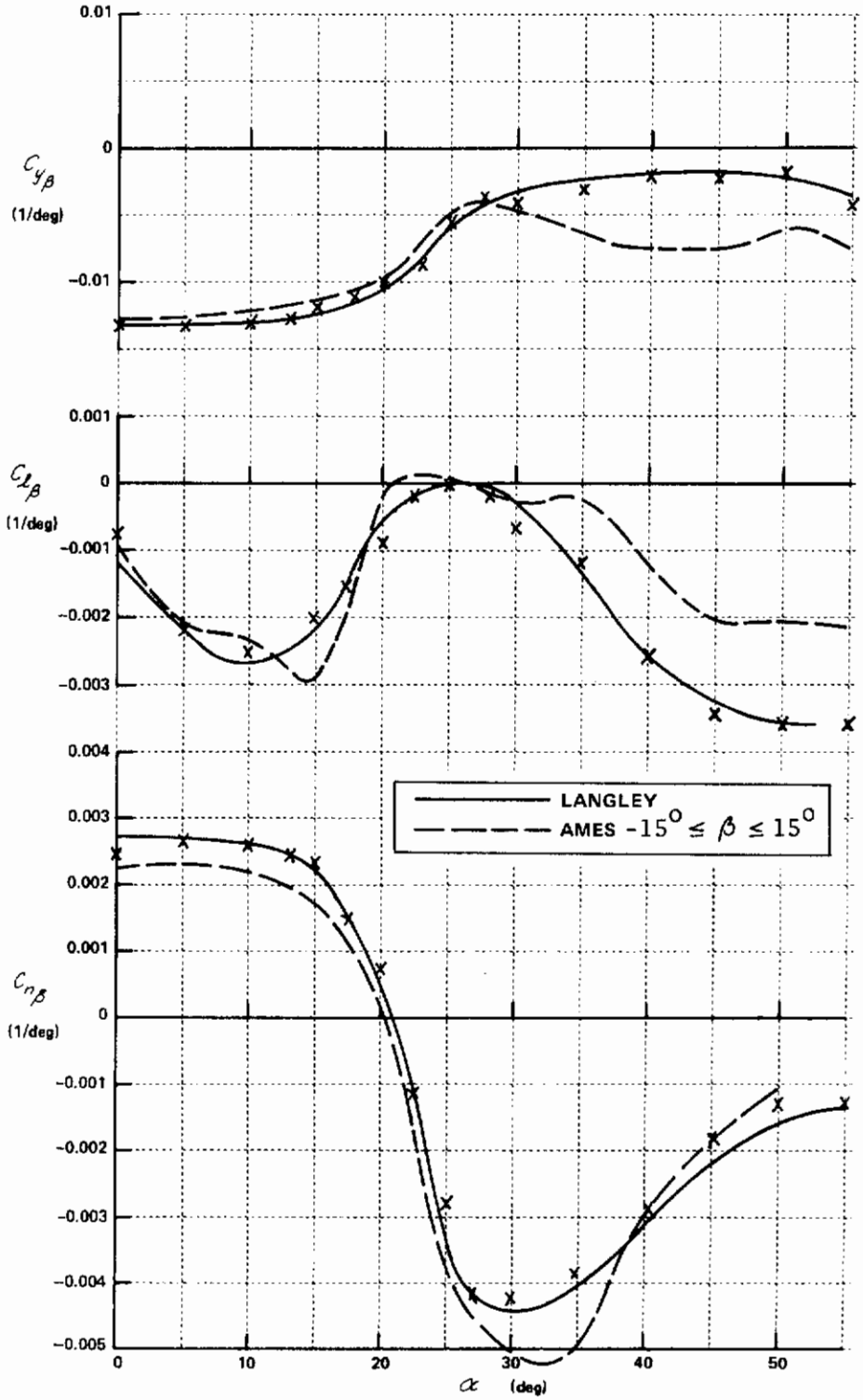

Figure 58 (Continued) WIND TUNNEL DATA

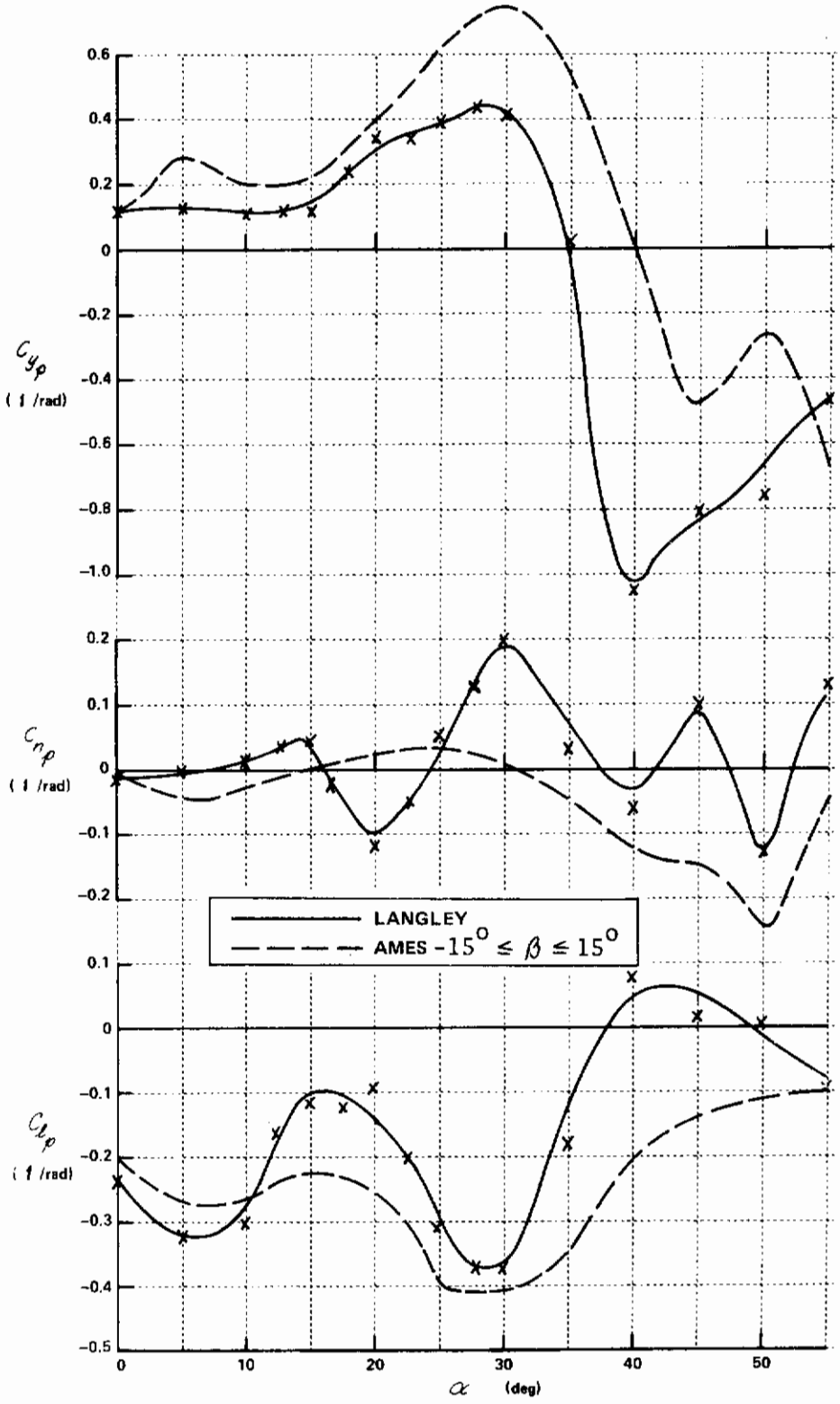

Figure 58 (Continued) WIND TUNNEL DATA

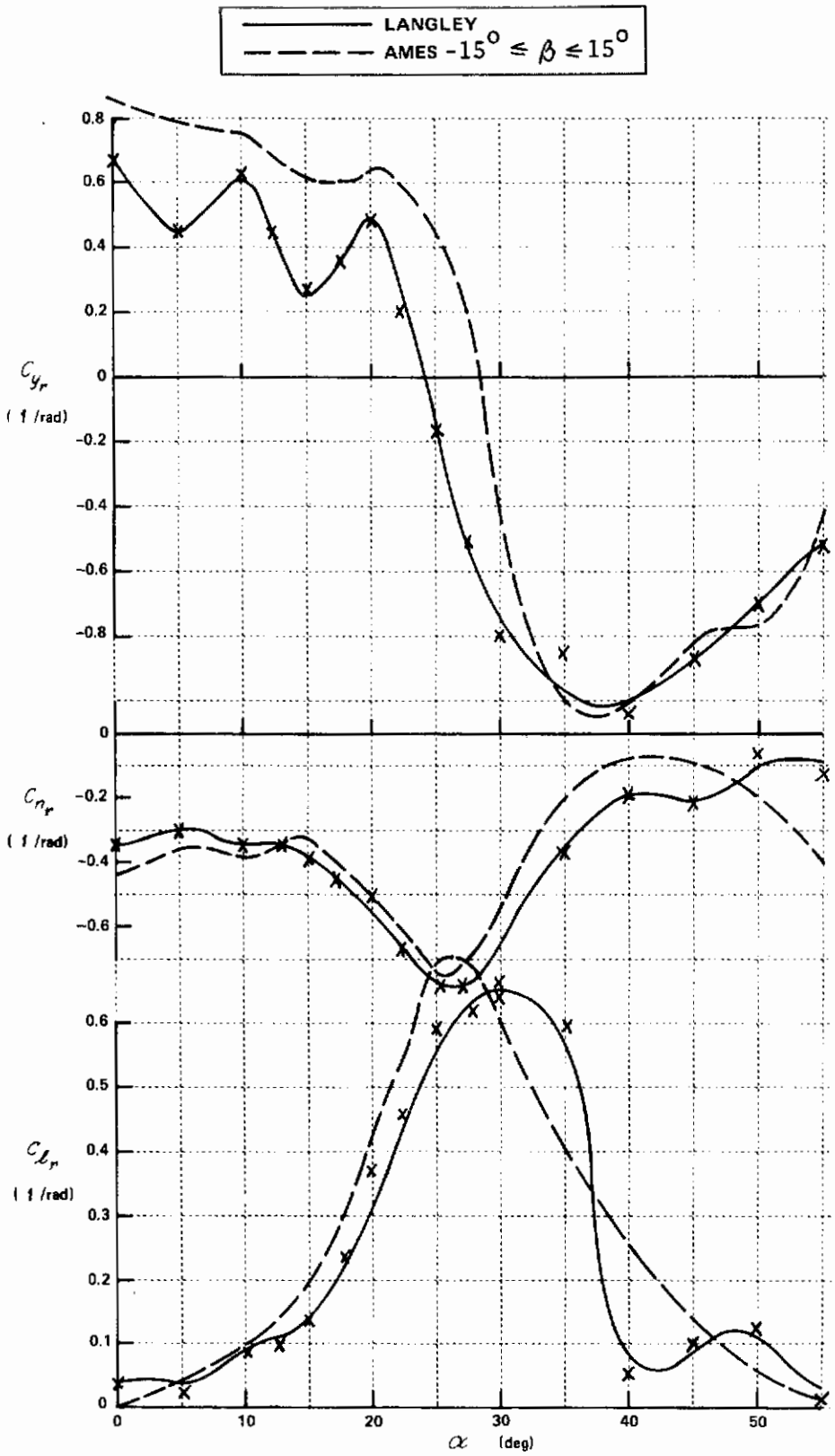

Figure 58 (Continued) WIND TUNNEL DATA

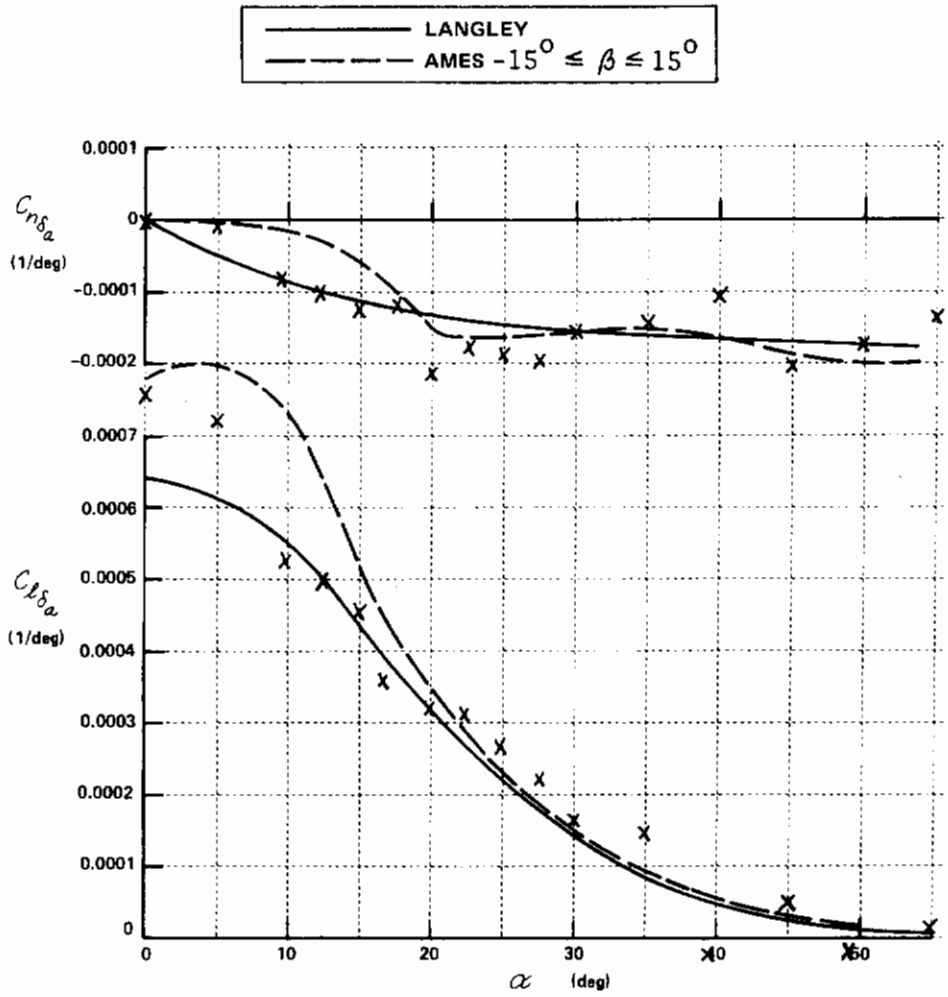

Figure 58 (Continued) WIND TUNNEL DATA

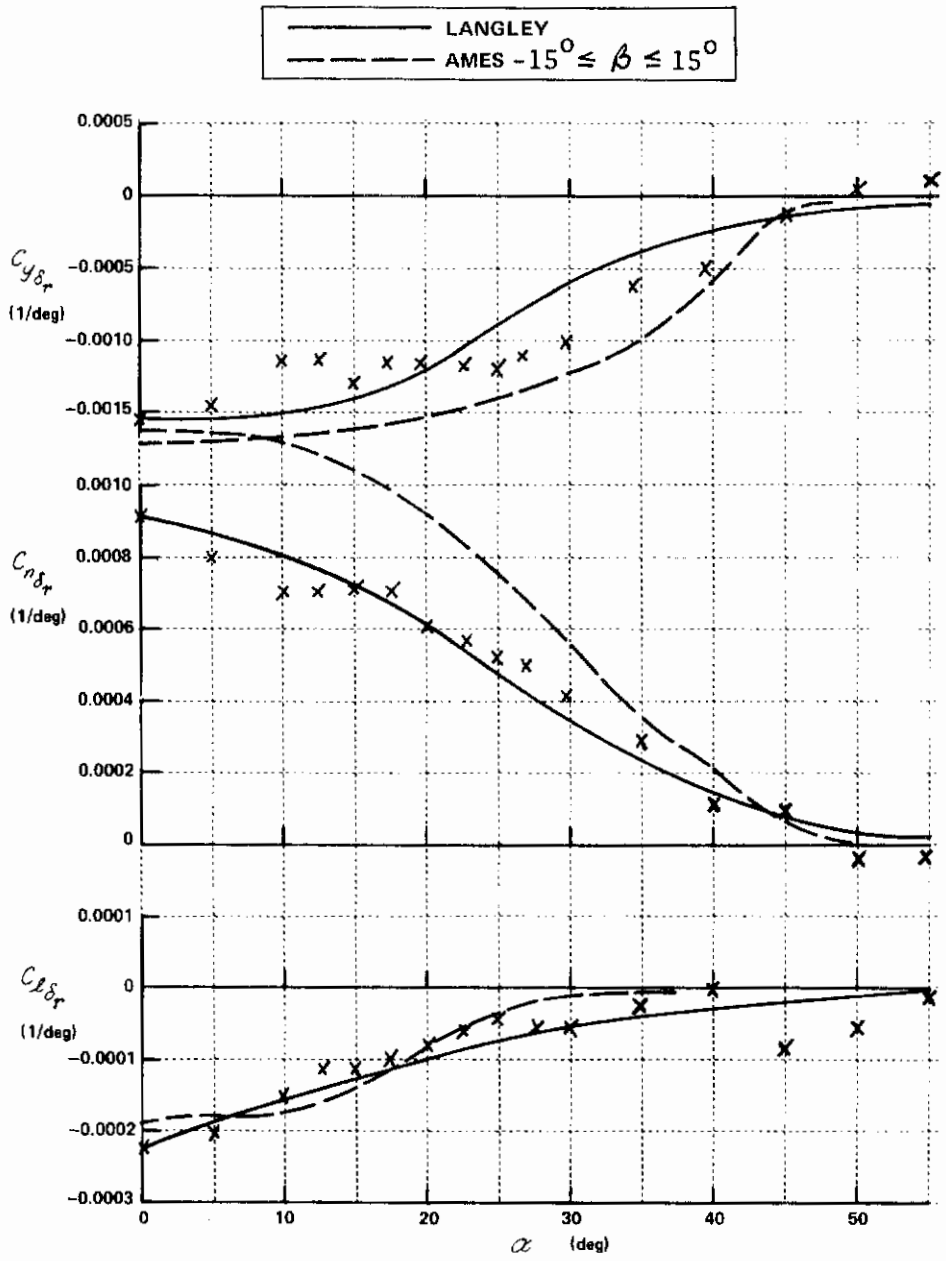

Figure 58 (Concluded) WIND TUNNEL DATA

Appendix V

IDENTIFICATION TECHNIQUES

This appendix reviews the identification technique used during this investigation; a more complete documentation is available in References 17 and 30. The central idea of the technique is to obtain a suboptimal minimum variance (conditional mean) estimate of the parameters and states from the measured data for generally nonlinear systems by extension of Kalman filter theory. This appendix will therefore state this problem formally, describe the least-squares algorithm used to initiate the technique, and discuss the Kalman filter algorithms used and the determination of the input information required by the technique.

V.1 Statement of the Problem

The problem may be stated generally in the following form. Consider a set of nonlinear continuous equations of motion for the aircraft:

$$\dot{x} = f(x, p, u, t) + w(t) \qquad x(0) = x_0 \tag{V-1}$$

where x are the aircraft states such as α, v, p, q, r, etc.

p are the parameters to be identified such as C_{m_α}, C_{l_β}, $C_{l_{\beta\alpha}}$, etc.

u are the control inputs such as δ_e, δ_a, etc.

$w(t)$ is the zero mean Gaussian white noise for approximate gusts or modelling errors.

For the purposes of digital implementation, Equation V-1 is characterized by a difference equation:

$$\begin{aligned} x_i &= f_i(x_{i-1}, p, u_{i-1}) + w_i, \quad x(0) = x_0 \\ E\{w_i\} &= 0 \\ E\{w_i w_j^T\} &= Q_i \delta_{ij} \end{aligned} \tag{V-2}$$

Similarly, a set of noisy discrete measurements is given as

$$\begin{aligned} y_i &= h_i(x_i, p, u_i) + v_i \\ E\{v_i\} &= 0 \\ E\{v_i v_j^T\} &= R_i \delta_{ij} \end{aligned} \tag{V-3}$$

In this form, the identification problem is to obtain the best (e.g., minimum variance, unbiased) estimates for x_o, ρ, and w_i given the measurements y_i, $i = 1, 2....N$. We may also state the problem more simply by considering an augmented state vector:

$$x_a = \begin{bmatrix} x \\ \rho \end{bmatrix} \tag{V-4}$$

Then, Equation V-1 becomes:

$$\dot{x}_{a_i} = \begin{bmatrix} f(x_a, u) \\ 0 \end{bmatrix} + \begin{bmatrix} w \\ 0 \end{bmatrix}, \quad x_a(0) = x_{a_o} \tag{V-5a}$$

or equivalently in discrete form

$$x_{a_i} = f_i(x_{a_{i-1}}, u_{i-1}) + w_i, \quad x_a(0) = x_{a_o} \tag{V-5b}$$

The problem is now seen to be the estimation of x_{a_0} and w_i given y_i, $i = 1,2....N$, where x_{a_0} is a Gaussian random variable such that

$$E\{x_{a_0}\} = \bar{x}_o$$

$$E\{x_{a_0} x_{a_0}^T\} = P_o$$

This problem is solved by using a locally iterated Kalman filter smoother, as will be discussed in Section V.3. To initiate this procedure, however, an initial "guess" of $\bar{x}_o$ and P_o is required, since the filter-smoother is a recursive technique, as is discussed in the next section.

V.2 Least Squares Initial Estimator

The initial estimates of the parameters in x_{a_0} and of the covariance matrix P_o can be obtained by a classical linear regressor; the only restrictions of this technique are that:

(1) Measurements of $\dot{x}$ must be available.

(2) The estimates are biased if the state measurements are noisy.

In practice, the measurements are always noisy, and so the estimates from this equation-error technique are biased; since the parameter vector appears linearly in the state equation, however, the solution for the estimate can be obtained in closed form, and hence this technique provides an effective and efficient means of obtaining an initial guess.

The least squares equation-error estimate is obtained as follows. Writing again the state equation (V-1) at time t_i and breaking the measurement equation (V-3) into measurements of the states and accelerations, we have:

$$\dot{x}(t_i) = f(x(t_i), p, u(t_i)) + w(t_i)$$

or

$$\dot{x}_i = f(x_i, p, u) + w_i \qquad \text{(V-6)}$$

$$y_{1_i} = x_i + v_{1_i} \qquad \text{(V-7)}$$

$$y_{2_i} = h_i(\dot{x}_i, x_i) + v_{2_i} \qquad \text{(V-8)}$$

for $i = 0, 1, 2, \ldots N$.

Substituting V-6 and V-7 into V-8 using all the data ($i = 0, 1, 2, \ldots N$), and noting that the parameter vector appears linearly as a constant for most problem formulations, we obtain the following set of $n(N+1)$ linear equations, where n is the number of state equations and acceleration measurements:

$$Y_2(N) = A_N p + w(N) \qquad \text{(V-9)}$$

Here A_N is a $n(N+1)$ by g matrix consisting of all the state measurements, and g is the dimension of the parameter vector (i.e., the number of parameters to be identified). The estimate of the parameter vector p is obtained by minimizing the "square" of the equation error, that is, $w(N)^T w(N)$ with respect to p. The procedure is precisely valid only if A_N is deterministic (nonstochastic), which can only be true if $v_{1i}(N) = 0$: that is, if the states are measured perfectly. Performing this minimization, the equation-error estimate is seen to be:

$$\hat{p} = (A_N^T A_N)^{-1} A_N^T Y_2(N) \qquad \text{(V-10)}$$

The estimates from equation V-9 are used as the initial estimates for the filter smoother described in the next section.

The covariance of $\hat{p}$, which also needs to be obtained to have an initial estimate for P_0, satisfies the following equation:

$$E\{\hat{p}\,\hat{p}^T\} = \sigma^2 (A_N^T A_N)^{-1} \qquad \text{(V-11)}$$

where

$$E\{w(N)\, w^T(N)\} = \sigma^2 I_{n(N+1)} \qquad \text{(V-12)}$$

The problem is that σ^2, which might be thought of as the variance of the equation error, is not known, and hence it must also be estimated. We may

obtain such an estimate by considering the error of the equation fit with the estimated value of ρ :

$$\hat{\epsilon} = y_2(N) - A_N \hat{\rho} \tag{V-13}$$

Substituting V-9 into V-13, and then substituting for $\hat{\rho}$ from Equation V-10, we obtain:

$$\hat{\epsilon} = \left[I - A_N (A_N^T A_N)^{-1} A_N^T \right] \omega(N) \tag{V-14}$$

Taking $E\{\hat{\epsilon}^T \epsilon\}$ and performing several algebraic and matrix manipulations, the following approximate estimate of σ^2 may be obtained:

$$\hat{\sigma}^2 = \frac{\hat{\epsilon}^T \hat{\epsilon}}{n(N+1) - q} \tag{V-15}$$

Hence, the estimate of the parameter covariance matrix becomes, from V-11:

$$E\{\hat{\rho}\,\hat{\rho}^T\} = \frac{\hat{\epsilon}^T \hat{\epsilon}}{n(N+1)-q} (A_N^T A_N)^{-1} \tag{V-16}$$

Equations V-10 and V-16 represent the desired results from the least squares estimator, and are used to initiate the locally iterated filter smoother. Before proceeding with that discussion, however, it is worthwhile to place the above discussion into the context of the identification of the high angle of attack flight data; for this purpose, an example is presented below.

With the equation-error technique, each equation is essentially considered separately; that is, the $n(N+1)$ equations given by equation V-9 are n independent sets of $N+1$ equations each. Consider, therefore, the pitching moment equation:

$$\begin{aligned} C_m(t) = \frac{\dot{q}_a}{\frac{1}{2}\rho S V^2} = {} & C_{m_0} + C_{m_\alpha}\alpha + C_{m_{\beta^2}}\beta^2 + C_{m_{\alpha\beta^2}}\alpha\beta^2 \\ & + C_{m_{\delta_e}}\delta_e + C_{m_{\delta_e\alpha}}\delta_e\alpha + C_{m_{\delta_e\beta^2}}\delta_e\beta^2 \\ & + C_{m_{\delta_a^2}}\delta_a^2 + C_{m_q}\frac{\bar{c}}{2V}q + C_{m_{q\alpha}}\frac{\bar{c}}{2V}q\alpha \\ & + C_{m_{q\alpha^2}}\frac{\bar{c}}{2V}q\alpha^2 \end{aligned} \tag{V-17}$$

Note that, although equation V-17 is nonlinear in the states (α, q, V) and controls (δ_e , δ_a), the stability and control derivatives which are the parameters to be identified appear linearly. With reference to equation V-9 for data points, we have

$$Y_2(N) = \begin{bmatrix} C_m(t_0) \\ \vdots \\ C_m(t_N) \end{bmatrix} \text{ is } N + 1 \text{ vector}$$

$$p = \begin{bmatrix} C_{m_0} \\ C_{m_\alpha} \\ C_{m_{\beta^2}} \\ \vdots \\ C_{m_{q\alpha^2}} \end{bmatrix} \text{ is 11 by 1 vector}$$

and

$$A_N = \begin{bmatrix} 1 & \alpha(t_0) & \beta^2(t_0) & \alpha(t_0)\beta^2(t_0) & \cdots & q(t_0)\alpha^2(t_0) \\ \vdots & \vdots & \vdots & \vdots & & \vdots \\ 1 & \alpha(t_N) & \beta^2(t_N) & \alpha(t_N)\beta^2(t_N) & \cdots & q(t_N)\alpha^2(t_N) \end{bmatrix}$$

is a N + 1 by 11 matrix.

The estimates of $\hat{p}$ and the covariance of $\hat{p}$ then follow directly by substitution into equations V-10 and V-16.

V.3 Kalman Filter Estimator

The central feature of the identification technique used in this technique is predicated on the fact that the airplane identification problem generally includes both process noise and measurement noise. As was discussed in the last section, equation-error methods, while based on minimizing the process noise $w(t)$, give biased parameter estimates if measurement noise on the states is present, since Λ_N then becomes stochastic. It can also be shown that conventional non-Bayesian output error methods, such as the typical form of quasi-linearization algorithms, give biased estimates in the presence of process noise, since the minimization is performed subject to a set of equations of motion which must be known exactly (Reference 17). For these reasons, a method which can treat both measurement and process noises must be used.

The technique used is based on extension of Kalman filter theory to nonlinear situations. Kalman filter theory is based on Bayesian estimation philosophy, and the estimator seeks the mean of the a posteriori density function. The estimation is performed by minimizing the mean square estimation error $\mathcal{L} = E\,\|\tilde{x}_K\|^2$, where:

$\hat{x}_{K/N} = F\left[y(N)\right]$ is the estimate of x_K and is a function (F [ ]) of the data Y(N); is a random vector (V-18)

$\tilde{x}_K = x_K - \hat{x}_{K/N}$ is a random vector (V-19)

$y(N) \triangleq \left[y_1^T\ y_2^T\ \cdots\ y_N^T\right]^T$

$f\left(x_K \mid y(N)\right)$ is the conditional a posteriori density function of x_K given $y(N)$

So that:

$$\min \mathcal{L} = \min E\,\|\tilde{x}\|^2 = \min E\left\{\left[x_K - F\left[y(N)\right]\right]\right.$$

$$= \min \int_{-\infty}^{\infty}\int_{-\infty}^{\infty}\left[x_K - F\left[y(N)\right]\right]^2 f\left(x_K, y(N)\right) dx_K\, d\,y(N) \qquad \text{(V-20)}$$

It can be shown that the conditional mean is the optimal estimator from equation V-20, that is

$$\hat{x}_{k/N} = E\left(x_k / Y(N)\right)$$

(V-21)

For the case in which equations V-1 and V-3 are linear and the noises are white Gaussian, the state estimation problem leads to the Kalman Bucy filter. In this case, the minimization process of equation V-20 can be performed in an equivalent deterministic fashion, which is shown below as it provides a convenient illustrative model (Reference 31).

Given $\dot{x} = F(t)x + G(t)w$

$y = H(t)x + v$; v, w are white, Gaussian

Minimize with respect to x :

$$\min_x J = \frac{1}{2}\left[x(t_o) - \bar{x}(t_o)\right]^T P_o^{-1}\left[x(t_o) - \bar{x}(t_o)\right]$$

$$+ \frac{1}{2}\int_{t_o}^{t}\left[y(\tau) - H(\tau)x(\tau)\right]^T R^{-1}(\tau)\left[y(\tau) - H(\tau)x(\tau)\right]d\tau$$

$$+ \frac{1}{2}\int_{t_o}^{t} w^T Q^{-1}(\tau)\, w\, d\tau \qquad \text{(V-22)}$$

The solution of V-22 leads to the filter equations for the linear case, which gives the minimum variance (conditional mean) estimates of the states. It is useful to note from equation V-22 that minimization of both the measurement noise v and the process noise w are incorporated in the Kalman filter solution, which is required for the aircraft identification problem.

The extension of this theory to the parameter estimation problem requires some approximation to the optimal nonlinear filter, as equation V-5 is nonlinear in the augmented state even if linear in the original states. To apply the linear theory, the nonlinear system is linearized about a reference condition. The most common such linearization is the extended Kalman filter; it has been shown, however, that the reference trajectory of this approach is not sufficiently accurate to provide unbiased estimates (Reference 17). For this reason, the identification technique used in this program uses a locally iterated filter-smoother, which alternately performs one-stage extended Kalman filtering and smoothing between every two data points and thereby improves the

reference trajectory. It can be shown formally that this procedure reduces the bias in the estimates caused by the nonlinearities. In addition to the improved filter estimates that are thereby obtained, the technique also employs a fixed point smoothing algorithm to obtain the best estimates of the initial conditions of the augmented states.

The derivations of the filter-smoother and fixed point smoother algorithms are given in Reference 17. For completeness, these algorithms are summarized below between the arbitrary data points at time t_{i-1} and t_i.

Locally Iterated Filter-Smoother

$$\hat{x}_{i/i}^{(j+1)} = \hat{x}_{i/i-1}^{(j)} + \psi_i^{(j)} \cdot RES_i^{(j)} \qquad \text{(augmented state estimates)}$$

$$\hat{x}_{i/i-1}^{(j)} = \int_{t_{i-1}}^{t_i} f(x,u)\,dt + \Phi_{i,i-1}^{(j)} \left[\hat{x}_{i-1/i-1} - \hat{x}_{i-1/i}^{(j)} \right] \qquad \text{(predicted state estimate)}$$

$$P_{i/i-1}^{(j)} = \Phi_{i,i-1}^{(j)} P_{i-1} \Phi_{i,i-1}^{(j)\,T} + Q_i \qquad \text{(extrapolated error covariance)}$$

$$\psi_i^{(j)} = P_{i/i-1}^{(j)} H_i^{(j)\,T} \left[H_i^{(j)} P_{i/i-1}^{(j)} H_i^{(j)\,T} + R \right]^{-1} \qquad \text{(gain matrix)}$$

$$\hat{x}_{i-1/i}^{(j+1)} = \hat{x}_{i-1/i-1} + P_{i-1} \Phi_{i,i-1}^{(j)\,T} H_i^{(j)\,T} \left[H_i^{(j)} P_{i/i-1}^{(j)} H_i^{(j)\,T} + R \right]^{-1} \cdot RES_i^{(j)}$$

(one stage smoothed estimate)

$$P_i^{(j)} = \left[I - \psi_i^{(j)} H_i^{(j)} \right] P_{i/i-1}^{(j)} \qquad \text{(covariance matrix of state estimation errors)}$$

where

$$\Phi^{(j)}_{i,i-1} \triangleq I + \frac{\partial f}{\partial x}\Delta t\Big/_{\hat{x}^{(j)}_{i-1/i}} + \frac{1}{2}\left(\frac{\partial f}{\partial x}\right)^2 \Delta t^2 + \cdots \quad \text{(transition matrix)}$$

$$H^{(j)}_i \triangleq \frac{\partial h}{\partial x}\Big/_{\hat{x}^{(j)}_{i/i}} \quad \text{(linearized output matrix)}$$

$$RES^{(j)}_i \triangleq y_i - h_i\left(\hat{x}^{(j)}_{i/i}\right) - H^{(j)}_i\left\{\hat{x}^{(j)}_{i/i-1} - \hat{x}^{(j)}_{i/i}\right\} \quad \text{Residual}$$

Δt = Sample Time

and at the initial or starting conditions

$$\hat{x}^{(1)}_{i-1/i} = \hat{x}_{i-1/i-1}, \quad \hat{x}^{(1)}_{i/i} = \hat{x}^{(1)}_{i/i-1}$$

The iteration scheme starts with $j=1$ and terminates when $x^{(j)}_{i/i} \approx x^{(j-1)}_{i/i}$ or after a prespecified number of iterations, usually one in practice. The converged values of $\hat{x}^{(j)}_{i/i}$, $\hat{x}^{(j-1)}_{i-1/i}$ and $P^{(j-1)}_i$ are taken as the estimates $\hat{x}_{i/i}$, $\hat{x}_{i-1/i}$ and the covariance P_i, respectively, for the next data point.

Fixed Point Smoother

$$\hat{x}_{0/i+1} = \hat{x}_{0/i} + \beta_{i+1} H^{(f)T}_{i+1} R^{-1} RES^{(f)}_{i+1} \quad \text{(fixed point smoother estimate)}$$

$$P_{0/i+1} = P_{0/i} - \beta_{i+1} H^{(f)T}_{i+1} R^{-1} H^{(f)}_{i-1} \beta_i \quad \text{(covariance of fixed point smoothed estimation error)}$$

where

$$\beta_{i+1} = \beta_i \Phi^{(f)T}_{i+1,i} \left[I - \psi^{(f)}_{i+1} H^{(f)}_{i+1} \right]^T$$

$$\beta_0 = P_0$$

and the superscript "(f)" denotes the last local iteration.

V.4 Application of the Kalman Filter Estimator

With reference to equation V-22, it can be seen that the following information is required to perform the identification:

1. Initial estimates of parameters and states at t_0 $x_0(t_0)]$
2. Variances of initial estimates (P_0)
3. Measurement noise variances (R)
4. Process noise variances (Q)

As was discussed in Section V.2, the initial parameter estimates are obtained by a least-squares equation error technique (equation V-10). The initial variances (P_0) may be obtained either from this method (equation V-16) or, as was done primarily on this program, by using a given proportion of the wind tunnel estimates as the initial uncertainty in the parameter estimates. The measurement and process noise statistics are selected to be consistent with the observed state and acceleration measurements, respectively. The selection of the noise statistics in particular is an iterative process which is carried out by observing the residual sequences of the filter operation and adjusting the statistics as required. This "tuning" process is also performed on the initial variances (P_0) of the parameters to ensure that the final parameter estimates are not affected by them.

To ensure that the final parameter estimates are as valid as the data allows, several convergence indications are checked. It is worth noting that this convergence is a strong function of the data record. Both the length of the record and the identifiability of the parameters from the data, which is dependent on the control input time histories and a correct model, may prohibit convergence to the proper parameter values. The checks consist of:

- Inspection of the time histories of the parameter estimates and the covariance matrix evolution ($P_0 \Longrightarrow P_K \Longrightarrow P_f$) with the desired result being visible asymptotic convergence prior to the end of the data record.

- Inspection of the cross-correlation terms in the final covariance matrix P_f . This inspection is aided by normalizing the matrix by the variances (the diagonal terms), in which case off-diagonal terms approaching unity indicate uniqueness and/or identifiability difficulties with the indicated parameters. The desired result is normalized covariances approaching zero for all parameters.

- Inspection of the residual sequences. The desired result is that they appear "white" and that they be consistent with their calculated statistics which indicates that the mathematical model of the system and the measurements used are adequate. The dispersion of these residuals serves as a guide in verifying that the particular values of Q and R (particularly R) were selected correctly. In general, the indication for Q is dominant in the acceleration measurements. Residual drifts from zero indicate modeling errors.

REFERENCES

1. Anon., Ad Hoc Team Report on the F-111 Stall/Post-Stall/Spin Prevention Program, Aeronautical Systems Division, AFSC, USAF, 28 August 1970

2. Hirsch, D.L., Spinning Characteristics of the T-38 Airplane YJ85-GE-1 or YJ85-GE-5 Engines Installed, NOR-61-151, dated November 1961

3. Titiriga, A., et al., F-5 Spin Susceptibility Investigation, NOR-65-33, dated December 1964.

4. Anderson, C.A., Stall/Post-Stall Characteristics of the F-111 Aircraft, paper presented at AGARD cp102 Conference.

5. F-111 Category I Flight Test Progress Report Airplane 4 Stall and Incipient Spin Flight Test Results, General Dynamics Report No. FZM-12-988-45-2, 30 September 1968.

6. McElroy, C.E., et al., Stall/Near Stall Investiagtion of the F-4E Aircraft, FTC-SD-70-20, Air Force Flight Test Center, Edwards AFB, Calif. October 1970

7. Rutan, E.L., et al., Stall/Near Stall Investigation of the F-4E Aircraft, FTC-TR-70-20, Air Force Flight Test Center, Edwards AFB, Calif. August 1970.

8. Clexton, E.W., et al., Evaluation of the Spin and Recovery Characteristics of the F-4E Airplane, NATC-TR-FT-88R-67, Naval Air Test Center, Patuxent River, Maryland. December 1967.

9. Harbaugh, S.P., F-4E Post Stall Flight Test Data, Report No. MDCA197 McDonnell Aircraft Company, 1 November 1972.

10. Anglin, E.L., Static Force Test of a Model of a Twin-Jet Fighter Airplane for Angles of Attack from -10° to 110° and Sideslip Angles from -40° to 40°, NASA TN D-6425, August 1971.

11. Grafton, S.B., and Libbey, C.E., Dynamic Stability Derivatives of A Twin-Jet Fighter Model for Angles of Attack from -10° to 110°, NASA TN D-6091, January 1971

12. Bowman, J.S. and White, W.L., Spin-Tunnel Investigation of a 1/30-Scale Model of the Fighter and Reconnaissance Version of the McDonnell F-4B Airplane, NASA TM SX-1744, April 1969.

13. Chambers, J.R. and Anglin, E.L., Analysis of Lateral-Directional Stability Characteristics of a Twin-Jet Fighter Airplane at High Angles of Attack, NASA TN D-5361, August 1969.

14. Chambers, J.R. and Bowman, J.S., Analysis of the Flat Spin Characteristics of a Twin-Jet Swept-Wing Fighter Airplane, NASA TN D-5409, September 1969.

15. Brady, C.C., Moran, W.A., and Resenstein, M.L., Model F-4 Spin Evaluation Program, Vol. I and II MDC A0005, August 1969.

16. Bonine, W.J., et al., Model F/RF-4B-C Aerodynamic Derivatives MDC-R-9842, December 1971, Revision K.

17. Chen, R., Eulrich, B., Lebacqz, B., Development of Advanced Techniques for the Identification of V/STOL Stability and Control Parameters, CAL Report No. BM-2820-F-1, August 1971.

18. DiFranco, D., In-Flight Parameter Identification by the Equations-of-Motion Technique -- Application to the Variable Stability T-33 Airplane, CAL Report No. TC-1921-F-3, December 1965.

19. Sorenson, John A., Analysis of Instrumentation Error Effects on the Identification Accuracy of Aircraft Parameters, NASA CR-112121, 1972.

20. Wykes, J.H., et al, An Analytic Study of the Dynamics of Spinning Aircraft, WADC-TR-58-381, December 1958.

21. Smith, R.E., Lebacqz, J.V., and Schuler, J.M., Flight Investigation of Various Longitudinal Approach Short Term Dynamics for STOL Landing Approach Using the X-22A Variable Stability Aircraft, Calspan Report No. TB-3011-F-2, January 1973.

22. Larson, D., et al,, Modified Spline Interpolation Function, Contributed Paper given at S.I.A.M. Meeting at Philadelphia, Pa., October, 1968.

23. Buck, T., Instruction for the Use of the General Electric J79-10-17-19 Production Engine Flight Performance Deck, December 1966.

24. Crane, R., and Gentry, J., Major USAF, F-4E Category II Performance Tests, FTC-SD-69-21, August 1969.

25. Chambers, J.R., and Bowman, J.S., "Recent Experience with Techniques for Prediction of Spin Characteristics of Fighter Aircraft," Journal of Aircraft, Vol. 8, No. 7, July 1971.

26. Rutan, E.L. and Gentry, J. R., Category II Stability and Control Evaluation of the F-4E Aircraft, Air Force Flight Test Center Report No. FTC-SD-69-14, July 1969.

27. Carleton, D.L., Stability and Control Derivatives for the F-4E Aircraft, FTC-TD-69-9, September 1969.

28. Libbey, C.E. and Bowman, J.S., Radio-Controlled Free-Flight Spin Tests of a 1/9-Scale Model of the F-111A Airplane, NASA TM SX-2008 May 1970.

29. Smith, R.E., Lebacqz, J.V., and Radford, R.C., Flight Investigation of Lateral-Directional Flying Qualities and Control Power Requirements for STOL Landing Approach Using the X-22A Aircraft, Draft of Final Report, Navy Contract N00019-72-C-0417, Calspan Report AK-5130-F-1, June 1973.

30. Chen, R., and Eulrich, B.J., Parameter and Model Identification of Nonlinear Dynamical Systems Using a Suboptimal Fixed-Point Smoothing Algorithm, Paper presented at JACC, August 1971.

31. Jazwinski, A.H., Stochastic Processes and Filtering Theory, Academic Press, 1970.

32. Anglin, E.L. and Bumer, R.E., Transmittal of Stall Spin Data on the F-4, NASA Langley Research Center, Letter of July 3, 1972.

This page left blank intentionally.

Unclassified

Security Classification

DOCUMENT CONTROL DATA - R & D

(Security classification of title, body of abstract and indexing annotation must be entered when the overall report is classified)

1. ORIGINATING ACTIVITY (Corporate author)	2a. REPORT SECURITY CLASSIFICATION
.Calspan Corporation Box 235 Buffalo, New York 14221	2b. GROUP

3. REPORT TITLE

Identification and Correlation of the F-4E Stall/Post-Stall Aerodynamic Stability and Control Characteristics From Existing Test Data.

4. DESCRIPTIVE NOTES (Type of report and inclusive dates)

Final Report

5. AUTHOR(S) (First name, middle initial, last name)

Bernard J. Eulrich
Norman C. Weingarten

6. REPORT DATE	7a. TOTAL NO. OF PAGES	7b. NO. OF REFS
August 1973	313	32

8a. CONTRACT OR GRANT NO.	9a. ORIGINATOR'S REPORT NUMBER(S)
F33615-72-C-1248 b. PROJECT NO. 8219 c.	BM-3054-F-1
d.	9b. OTHER REPORT NO(S) (Any other numbers that may be assigned this report) AFFDL-TR-73-125

10. DISTRIBUTION STATEMENT

11. SUPPLEMENTARY NOTES	12. SPONSORING MILITARY ACTIVITY
	Air Force Flight Dynamics Laboratory Wright-Patterson AFB, Ohio 45433

13. ABSTRACT

This report documents the results of a study performed for the United States Air Force Flight Dynamics Laboratory to identify the high angle of attack post stall aerodynamic stability and control characteristics of the F-4 aircraft from existing full scale and radio-controlled drop model test data and to correlate these results with similar characteristics obtained from wind tunnel tests. A parameter identification procedure was set up to extract these nonlinear characteristics from flight test records using a nonlinear iterated Kalman filter/fixed-point smoother algorithm and a least square equation error method. Model form is established from wind tunnel data by representing the aerodynamic coefficients by Taylor's series expansions for selected ranges of angle of attack. Although the best flight test data available at high angles of attack were used, aircraft excitation and record length of the flight data were insufficient to enable the extraction of completely accurate and consistent coefficients from the data. Where there was adequate data and consistent instrumentation, the results were good. The results of this study demonstrated feasibility and applicability of the identification approach and techniques utilized, to obtain meaningful results at high angles of attack. Recommendations for future flight test programs are included in this report. Recommendations for the improvement of the identification procedures for the high angle of attack flight regime are also included.

DD FORM 1 NOV 65 1473

Unclassified

Security Classification

14. KEY WORDS	LINK A		LINK B		LINK C	
	ROLE	WT	ROLE	WT	ROLE	WT
stability and control characteristics						
post-stall data						
parameter identification						
iterated Kalman filter						
fixed-point smoother						
F-4E						
high angle of attack						